

HARVARD UNIVERSITY  
Graduate School of Arts and Sciences




DISSERTATION ACCEPTANCE CERTIFICATE

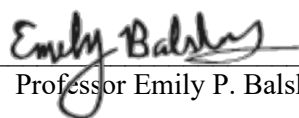
The undersigned, appointed by the  
Department of Chemistry & Chemical Biology  
have examined a dissertation entitled:

Tetracyclines as Antiproliferative Agents for Human Cancers

presented by: Richard Porter Ladley

candidate for the degree of Doctor of Philosophy and hereby  
certify that it is worthy of acceptance.

*Signature*   
*Typed name:* Professor Andrew G. Myers

*Signature*   
*Typed name:* Professor Emily P. Balskus

*Signature*   
*Typed name:* Professor Matthew D. Shair

*Date:* 17 November 2021

# **Tetracyclines as Antiproliferative Agents for Human Cancers**

A dissertation presented

by

Richard Porter Ladley

to

The Department of Chemistry and Chemical Biology

in partial fulfillment of the requirements

for the degree of

Doctor of Philosophy

in the subject of

Chemistry

Harvard University

Cambridge, Massachusetts

November 2021



© 2021 – Richard Porter Ladley

All rights reserved.

## Tetracyclines as Antiproliferative Agents for Human Cancers

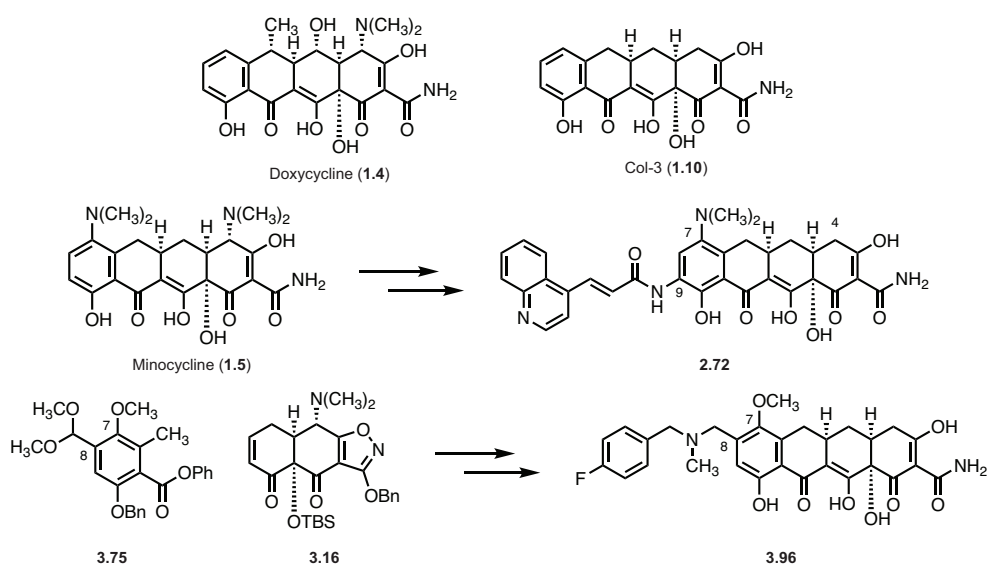
### Abstract

In addition to their antimicrobial properties, the tetracycline class of natural products have demonstrated clinically important effects in the amelioration of human diseases, including cancer and mitochondrial disease. Previously, the Myers group utilized a multidisciplinary strategy featuring proteomics and photoaffinity labeling to identify the eukaryotic 80S ribosome as the target of the tetracyclines in human cells. Our group then established tetracycline derivatives doxycycline (**1.4**) and Col-3 (**1.10**) as inhibitors of cytosolic translation and activators of the general cellular stress monitor, the integrated stress response (ISR). Together, these efforts provided the crucial first steps in elucidating the mechanism by which the tetracyclines exert their antiproliferative effects.

Since this initial discovery, our efforts to better understand the therapeutic potential of the tetracyclines have focused on two areas: novel compound synthesis and mechanistic elucidation. Early on, a medicinal chemistry campaign led to the discovery of a semisynthetic analogue of Col-3 (**2.72**) that displayed improved antiproliferative activity in several human cancer cell lines. We later transitioned to a fully synthetic strategy to enable access to a greater diversity of Col-3 analogues than was allowed by semisynthesis. These efforts resulted in the discovery of a series of C7-methoxy-C8-alkylamino analogues (**3.96**) with improved translation inhibitory potency compared to Col-3. Finally, our mechanistic elucidation efforts focused on investigations of translation inhibition and

signaling pathway activation using a variety of biochemical techniques including polysome profiling, *in vitro* translation experiments, and knockout generation using CRISPR/Cas-9 technology.

Overall, our efforts aim to develop novel tetracycline therapeutics with well-defined activities in human cancer cells with the goal of progressing these compounds to the clinic.



# Tetracyclines as Antiproliferative Agents for Human Cancers

## Table of Contents

<b>Abstract</b>	<b>iii</b>
<b>Table of Contents</b>	<b>v</b>
<b>Acknowledgements</b>	<b>viii</b>
<b>List of Abbreviations</b>	<b>xi</b>
<b>Chapter 1. Introduction and Background</b>	<b>1</b>
1.1 Introduction to the Tetracyclines	2
1.2 Structure of the Tetracyclines and Origins of Antibacterial Activity	5
1.3 Summary of Key Non-Canonical Effects of the Tetracyclines	7
1.4 Mechanistic Elucidation Efforts	11
1.5 Conclusions and Path Forward	22
<b>Chapter 2. Semisynthetic Compound Development Efforts</b>	<b>24</b>
2.1 Introduction to Semisynthetic Compound Development Efforts	25
2.2 History of Tetracycline Semisynthesis	25
2.3 Key Semisynthetic Transformations: C4, C7, and C9	29
2.4 Strategy	35
2.5 Early Compound Development Efforts	38
2.6 Exploration of a Novel Quinoline Analogue	41
2.7 Initial Biological Testing and Pathway Elucidation	47

2.8 Role of the Mitochondria	51
2.9 Conclusions and Path Forward	56
2.10 Chemical Biology Experimental Section	57
2.11 Chemistry Experimental Section	62
<b>Chapter 3. Fully Synthetic Compound Development</b>	<b>143</b>
3.1 Introduction to Fully Synthetic Compound Development Efforts	144
3.2 Overview of Tetracycline Total Synthesis Efforts	144
3.3 Recent Non-Canonical Tetracycline Developments	154
3.4 Strategy	158
3.5 Route Optimization and Compound Development	161
3.6 Biological Evaluations	169
3.7 Conclusions and Path Forward	172
3.8 Chemical Biology Experimental Section	175
3.9 Chemistry Experimental Section	178
<b>Chapter 4. Mechanistic Elucidation Efforts</b>	<b>217</b>
4.1 Introduction to Mechanistic Elucidation Efforts	218
4.2 The Mechanism of Eukaryotic Translation	218
4.3 Small Molecule Modulation of Translation	224
4.4 Early Studies in Translation Inhibition – Polysome Profiling	228
4.5 IRES <i>in vitro</i> Translation Analysis	235
4.6 Ribosome Associated Quality Control System	238
4.7 Ongoing Efforts – Signaling Pathway Analysis	241
4.8 Conclusions and Path Forward	245

4.9 Experimental Section	248
<b>Appendix A: Supplementary Figures</b>	<b>254</b>
<b>Appendix B: Catalogue of Spectra</b>	<b>261</b>

## Acknowledgements

First and foremost, I would like to thank my advisor, Professor Andrew Myers, for his guidance and support over the last four years. From my first days in the lab, Professor Myers has steered the direction of my research progress in a calm and constructive manner, providing space for me and other researchers to try new ideas and make mistakes along the way. I am grateful to have had the opportunity to conduct research in his laboratory and to have worked together during our semesters teaching Chemistry 30. I would also like to thank my committee members, Professors Emily Balskus and Matthew Shair, for their suggestions and guidance during my various committee meetings and exams over the years. I am thankful for the time and effort my committee members dedicated to these sessions and I cannot understate the impact they had on my scientific progress in graduate school. I would also like to thank Professor Robert K. Boeckman Jr., my undergraduate advisor, as well as Dr. Kyle Biegasiewicz and Dr. Justin Niziol, my mentors in the Boeckman group, for their support and encouragement at Rochester. I would not have pursued my graduate degree without their help. I'd also like to thank Professors Joshua Goodman and Thomas Krugh for their encouragement to join the chemistry department at Rochester and for their support during my transition to graduate school

The Myers research group has been a wonderful environment in which to study and engage with chemistry over the past four years. I am grateful for the support and camaraderie from many of my colleagues, namely my rotation mentor Dr. Fan Liu, Dr. Giambattista Testolin, Dr. Aditya Pote, Dr. Sven Hildebrandt, Dr. Senkara Rao Allu, Dr. MD Aatur Rahman, Dr. Thrimurtulu Neetipalli, Dr. Ioana Moga, Mischa Shuttel, Manuel

Schupp, Kelvin Wu, Kelvin Li, and Meiyi Yu. I am extremely grateful to have overlapped in the lab with Dr. Linfeng Chen – a kind mentor and talented biologist whose patience and compassion I will not soon forget. Last but certainly not least, Dr. Amarnath Pisipati, one of the hardest working scientists I have met and a close friend.

I have had the great opportunity to work with a number of collaborators during my time in graduate school – I am grateful to Dr. Maxim Geraschenko and Nadya Makarova for their assistance with polysome profiling, to Dr. Regina Cencic for kindly providing plasmid DNA for translation experiments, and to Professor Eric Bennett and Marylin Leonard for the gift of RQC knockout cell lines. My dissertation would look quite a bit different if it were not for the generosity of these scientists. Thanks also to Dr. Elizabeth Perry and the Puigserver group at Dana-Farber for including the Myers lab in a fascinating collaboration. I would also like to thank Professor Brian Liao and Yumi Koga of the Liao group for their guidance and experimental assistance over the years.

The chemistry department at Harvard is staffed by an incredible group of people, without whom it would be impossible to conduct the types of research that we do. Thanks are owed to our safety team, Dr. Mat Lalonde and Brad Parsons, facilities and building staff, Mike Paterno, Alexa Seney, John Randazzo, and Chris Perry, and office staff, Rhonda Pautler, Marlene Takla, Tracey Schaal, Joe Lavin, Barbara Anderson, and Helen Schwickrath. To the staff of the NMR facility, the recent transformation of which I still find difficult to believe – Dr. Dongtao Cui, Tony Lowe, Dr. Shaw Huang, and Bill Collins. And to the staff at the Bauer core, Kelly Chatman, Claire Reardon, and Jennifer Wang for their help over the years.



I would also like to add, from the Science Center and Bok Center, Dr. Gregg Tucci, Dr. Lu Wang, Dr. Logan McCarty, Dr. Tamara Brenner, and David Rose for their support during my semesters as Head TF for Chemistry 30. I know for certain that I would not have made it through those years without their help.

To my colleagues and mentors at PPG Industries – Dr. Tony Chasser, Dr. Brian Woodworth, Dr. Susan Donaldson, Kevin Dufford, and Katie Schaffer. I recall my time in the powder group so very fondly for the kindness and professionalism of these colleagues and the confidence the research there gave me to pursue graduate work in chemistry. Thanks to Dr. Nils Loewen, Dr. Devora Cohen-Karni, and Dr. Amerdeep Dhaliwal at UPMC Eye and Ear for my first experience in the laboratory – pig eye dissections and all.

Finally, I would like to thank my family for their love and support as I toiled away “in prison” for the past few years. No matter how difficult my research, I always looked forward to my next trip home to reinvigorate my spirits. To Emily Dorian, friend since my earliest days at Rochester.

And, of course, Malia. There is no question that I would not have made it to this point without your support. In the words of George Saunders, “strange to thank the air one breathes – crazy not to.”

## List of Abbreviations

Å	angstrom
A	adenine
Ac	acetyl
acac	acetylacetonate
aq	aqueous
Boc	<i>tert</i> -butylcarbonate
Bu	butyl
C	cytosine
Cbz	carboxybenzyl
<i>cis</i>	<i>Lat.</i> , on the same side
cm <sup>-1</sup>	wavenumber
D	dextrorotatory
DBU	1,8-diazabicyclo[5.4.0]undec-7-ene
de	diastereomeric excess
DIPEA	diisopropylethylamine
DMAP	4- <i>N,N</i> -dimethylaminopyridine
DMF	<i>N,N</i> -dimethylformamide
DMSO	dimethyl sulfoxide
DNA	deoxyribonucleic acid
dr	diastereomeric ratio
<i>E</i>	<i>Ger.</i> , entgegen

ee	enantiomeric excess
ent-	enantiomeric
epi-	epimeric
equiv	equivalent
ESI	electrospray ionization
Et	ethyl
FDA	Food and Drug Administration
FTIR	Fourier transform infrared
G	guanine
g	gram
h	hour
HPLC	high-pressure liquid chromatography
HRMS	high-resolution mass spectrometry
Hz	Hertz
IC <sub>50</sub>	fifty-percent maximal inhibitory
concentration	
<i>J</i>	coupling constant
$\lambda$	wavelength
L	liter; levorotatory
LDA	lithium diisopropylamide
LiHMDS	lithium hexamethyldisilazide
M	molar
mg	milligram

$\mu\text{g}$	microgram
MHz	megahertz
MIC	minimum inhibitory concentration
min	minute
mL	milliliter
$\mu\text{L}$	microliter
mM	millimolar
$\mu\text{M}$	micromolar
<i>m/z</i>	mass to charge ratio
mmol	millimole
$\mu\text{mol}$	micromole
mol	mole
MS	molecular sieves; mass spectrometry
Ms	methanesulfonyl
<i>n</i> -Bu	normal-butyl
NCS	<i>N</i> -chlorosuccinimide
nM	nanomolar
NMR	nuclear magnetic resonance
<i>p</i> -	<i>para</i>
Ph	phenyl
ppm	parts per million
pyr	pyridine

rac-	racemic
<i>R</i>	rectus (Cahn–Ingold–Prelog system)
$R_f$	retention factor
RNA	ribonucleic acid
RP	reverse phase
<i>S</i>	sinister (Cahn–Ingold–Prelog system)
SAR	structure activity relationship(s)
sp.	species
TBS	<i>tert</i> -butyldimethylsilyl
TBSCl	<i>tert</i> -butyldimethylsilyl chloride
<i>t</i> -Bu	<i>tert</i> -butyl
Tet	tetracycline
Tf	trifluoromethanesulfonyl
TFA	trifluoroacetic acid
THF	tetrahydrofuran
TLC	thin-layer chromatography
TMS	trimethylsilyl
$t_R$	retention time
<i>trans</i>	<i>Lat.</i> , across
tRNA	transfer RNA
Ts	tosyl
UV	ultraviolet
<i>Z</i>	<i>Ger.</i> , zusammen

*“What can be asserted without evidence  
can be dismissed without evidence.”*

*Christopher Hitchens*

## **Chapter 1**

### **Introduction and Background**

## 1.1 Introduction to the Tetracyclines

The tetracyclines represent a class of small molecule natural products that have played a central role in human medicine for the past 70 years.<sup>1</sup> The first members of this class of compounds, chlortetracycline (Fig. 1.1A, **1.1**)<sup>2</sup> and oxytetracycline (**1.2**)<sup>3</sup>, were discovered in the 1950s and were immediately set apart for their effective treatment of both Gram-positive and Gram-negative bacterial infections. Shortly thereafter, semisynthetic compound development efforts led to the discovery of novel compounds including tetracycline (**1.3**, 1953,<sup>4</sup> later isolated as a natural product in 1956),<sup>5</sup> doxycycline (**1.4**, 1958),<sup>6</sup> and minocycline (**1.5**, 1967, Fig. 1.1B)<sup>7</sup>. The structural alterations introduced in doxycycline and minocycline were found to minimize a litany of undesirable side-effects associated with tetracycline treatment and these semisynthetic derivatives have since become some of the most widely used antibacterial agents in history. Following these key discoveries, factors including the increasing complexity of semisynthetic transformations

---

<sup>1</sup> Liu, F.; Myers, A. G. *Curr. Opin. Chem. Biol.* **2016**, *32*, 48-57 and references included therein.

<sup>2</sup> Duggar, B. M. *Ann. N. Y. Acad. Sci.* **1948**, *51*, 177-181.

<sup>3</sup> (a) Finlay, A. C.; Hobby, G. L.; P'an, S. Y.; Regna, P. P.; Routein, J. B.; Seeley, D. B.; Shull, G. M.; Sobin, B. A.; Solomons, I. A.; Vinson, J. W.; Kane, J. H. *Science*. **1950**, *111*, 85. (b) Sobin, B. A.; Finlay, A. C.; Terramycin and its Production. U.S. Patent 2,516,080, July 18, 1950.

<sup>4</sup> (a) Booth, J. H.; Morton, J.; Petisi, J. P.; Wilkinson, R. G.; Williams, J. H.; *J. Am. Chem. Soc.* **1953**, *75*, 4621. (b) Conover, L. H.; Moreland, W. T.; English, A. R.; Stephens, C. R.; Pilgrim, F. J.; *J. Am. Chem. Soc.* **1953**, *75*, 4622-4623.

<sup>5</sup> Mineri, P. P.; Sokol, H.; Firman, M. C.; Process for the Preparation of Tetracycline and Chlortetracycline. U.S. Patent 2,734,018, February 7, 1956.

<sup>6</sup> Nelson, M. L.; Levy, S. B. *Ann. N. Y. Acad. Sci.* **2011**, *1241*, 17-32.

<sup>7</sup> Church, R. F. R.; Schaeue, R. E.; Weiss, M. J. *J. Org. Chem.* **1971**, *36*, 723-725.



and the rise of resistance mutations complicated novel compound development efforts and research in the class waned.

Interest in tetracycline discovery efforts was reinvigorated following a seminal publication from the Myers' research group in 2005 that described a highly convergent route to access novel fully synthetic tetracycline analogues (Fig. 1.1D).<sup>8</sup> As a key step, the Myers' synthesis features a sequential Michael addition–Dieckmann condensation reaction between two advanced intermediates: the **D-ring precursor** and the **AB Enone (1.7 and 1.8, Fig. 1.1D)**. Buoyed by excitement surrounding this novel approach, Tetraphase Pharmaceuticals was founded in 2006 to discover and develop novel tetracycline antibiotics.<sup>1</sup> To date, efforts from Tetraphase and the Myers Group have led to an estimated

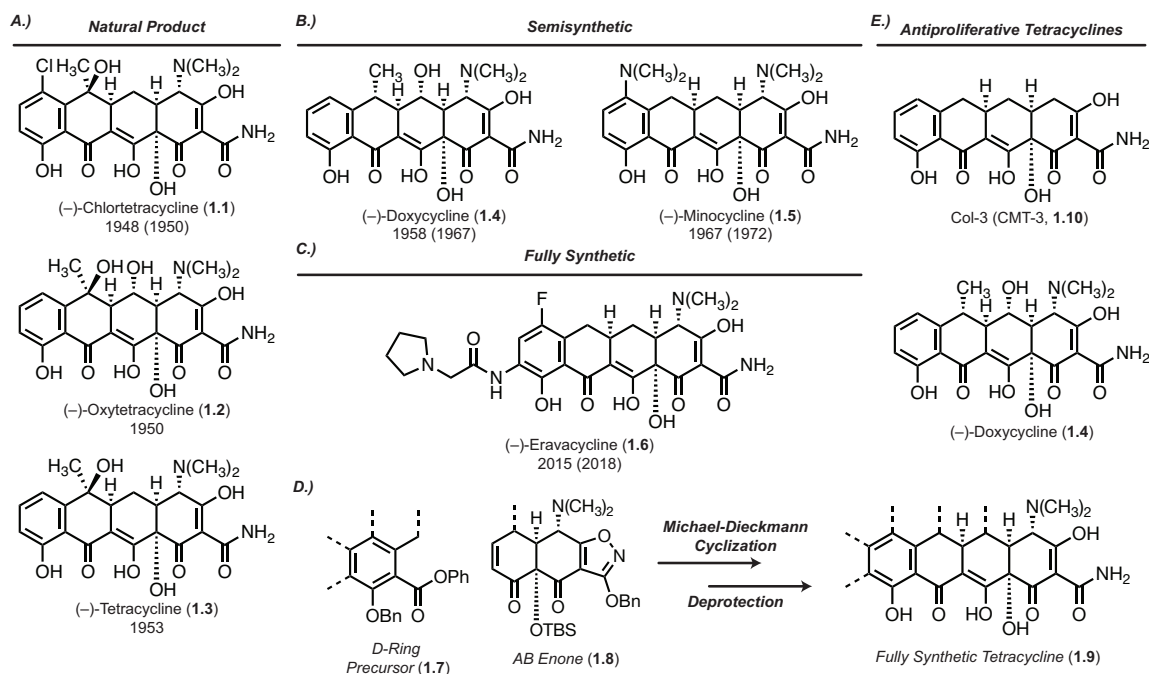


**Figure 1.1 The Tetracyclines.** The tetracycline class of antibacterial agents features natural products (A), semisynthetic analogues (B), and fully synthetic analogues (C), which have been discovered, developed, and synthesized over the past 70 years. In 2005, the Myers Group reported the first practical, scalable synthetic route to access novel tetracyclines (D) which has resulted in the synthesis of over 3,000 novel analogues. Finally, select tetracyclines have displayed antiproliferative effects against human cancers, though further research is needed before moving these compounds to the clinical stage.

<sup>8</sup> (a) Charest, M.; Lerner, C. D.; Brubaker, J. D.; Siegel, D. R.; Myers, A. G. *Science*, **2005**, *308*, 395-398. (b) See also Liu et al., **2016** (Chapter 1, ref. 1).

3,000 novel tetracycline analogues featuring a wide variety of substitution patterns. These efforts were realized in full in 2018 with the FDA-approval of the clinical candidate Eravacycline – the first fully synthetic tetracycline analogue approved for human use (Fig. 1.1C, **1.6**).<sup>1</sup>

Throughout their history, the tetracyclines have consistently shown effects in the amelioration of human disease distinct from their antibacterial properties (Fig. 1.1E). For example, in 2006 a 66-year-old woman was cleared of the rare lung cancer lymphangiomyomatosis (LAM) after a last-ditch treatment effort with doxycycline (**1.4**).<sup>9</sup> Further, the non-antibacterial tetracycline derivative Col-3 (**1.10**) has been the subject of numerous clinical trials related to its antiproliferative properties, including therapeutics for Kaposi's sarcoma and other cancers.<sup>10</sup> Most recently, the tetracyclines have been the subject of several studies related to their effects on human mitochondrial function and doxycycline has been proposed as a novel therapeutic for human mitochondrial disease.<sup>11</sup>

In this chapter, we provide a brief overview of the tetracycline natural products and their history as antibacterial agents. We then transition to the murkier history of non-canonical therapeutic outlets for the tetracyclines and the myriad mechanistic theories advanced in conjunction. We will highlight a landmark publication from the Myers group

---

<sup>9</sup> Moses, M. A.; Harper, J.; Folkman, J. *NEJM*. **2006**, *354*, 2621-2622.

<sup>10</sup> Selected literature: (a) Zhao, L.; Xu, J.; Wang, H.; Fan, S. *Anti-Cancer Drugs*. **2014**, *25*, 1165-1174. (b) Dezube, B. J.; Krown, S. E.; Lee, J. Y.; Bauer, K. S.; Aboulafia, D. M. *J. Clin. Oncology*. **2006**, *24*, 1389-1394. (c) Cianfrocca, M.; Cooley, T. P.; Lee, J. Y.; Rudek, M. A.; Scadden, D. T.; Ratner, L.; Pluda, J. M.; Figg, W. D.; Krown, S. E.; Dezube, B. J. *J. Clin. Oncology*. **2001**, *20*, 153-159.

<sup>11</sup> Perry, E. A.; Bennett, C. F.; Luo, C.; Balsa, E.; Jedrychowski, M.; O'Malley, K. E.; Latorre-Murro, P.; Ladley, R. P.; Reda, K.; Wright, P. M.; Gygi, S. P.; Myers, A. G.; Puigsiver, P. *Nat. Metab.* **2021**, *3*, 33-42.

that identified the human cytosolic ribosome as a target for the tetracyclines, suggesting an origin of the tetracycline's non-canonical effects as well as novel outlets as cancer therapeutics. This study has served as an inspiration for much of the efforts presented through this dissertation, including our subsequent compound development and mechanistic elucidation efforts, both of which will be covered in detail in later chapters.

## 1.2 Tetracycline Structure and Origins of Antibacterial Activity

The name tetracycline derives from the polycyclic core that is shared by all members of this class of natural products. This scaffold features a large amount of oxygenation as well as other functional groups along the so-called “southern hemisphere” of the molecule (Fig. 1.2E). Structure-activity relationship analysis of the antibacterial activity of the tetracyclines has revealed the functional group patterns along the southern hemisphere, including the vinylogous carboxamide structure along the right side of the A-ring, to be critical for antibacterial activity as they form key contacts with the bacterial ribosome during binding (Fig. 1.2D, *vide infra*).<sup>12</sup> The northern hemisphere of the molecule can accommodate a much wider diversity of substitutions, as is demonstrated in the variety of tetracyclines available in the clinic. The sole exception is the dimethylamino group at C4. While this functionality has not been shown to form any key contacts with the bacterial ribosome, removal or alternation of this group typically results in reduction of antibacterial

---

<sup>12</sup> (a) Brodersen, D. E.; Clemons Jr., W. M.; Carter, A. P.; Morgan-Warren, R. J.; Wimberly, B. T.; Ramakrishnan, V. *Cell*. **2000**, *103*, 1143-1154. (b) Piloetti, M.; Schlunzen, F.; Harms, J.; Zarivach, R.; Gluhmann, M.; Avila, H.; Bashan, A.; Bartels, H.; Auerbach, T.; Jacobi, C.; Hartsch, T.; Yonath, A.; Franceschi, F. *EMBO J.* **2001**, *20*, 1829-1839. (c) Nguyen, F.; Starosa, A. L.; Arenz, S.; Sohmen, D.; Donhofer, A.; Wilson, D. N. *Biological Chemistry* **2014**, *395*, 559-575.

activity, suggesting this moiety plays a key role in charge balance, solubility, or any number of other factors governing cell penetrance and target engagement.

Tetracyclines are thought to exert their antibacterial activity through binding of the small subunit of the bacterial ribosome and inhibiting bacterial translation (Fig. 1.2).<sup>1</sup> The first co-crystal structure of the tetracyclines bound to the 30S subunit of the prokaryotic ribosome revealed several different binding locations, with the primary Tet1 binding site near the catalytic core of the ribosome as the primary effector of activity (Fig. 1.2A-D).<sup>12</sup> Tetracycline binding in this location prevents entry of charged aminoacyl tRNAs to the acceptor site (A-site) of the ribosome, thus preventing further progression of the nascent peptide chain and leading to stalling of translation—ultimately resulting in death of the cell.

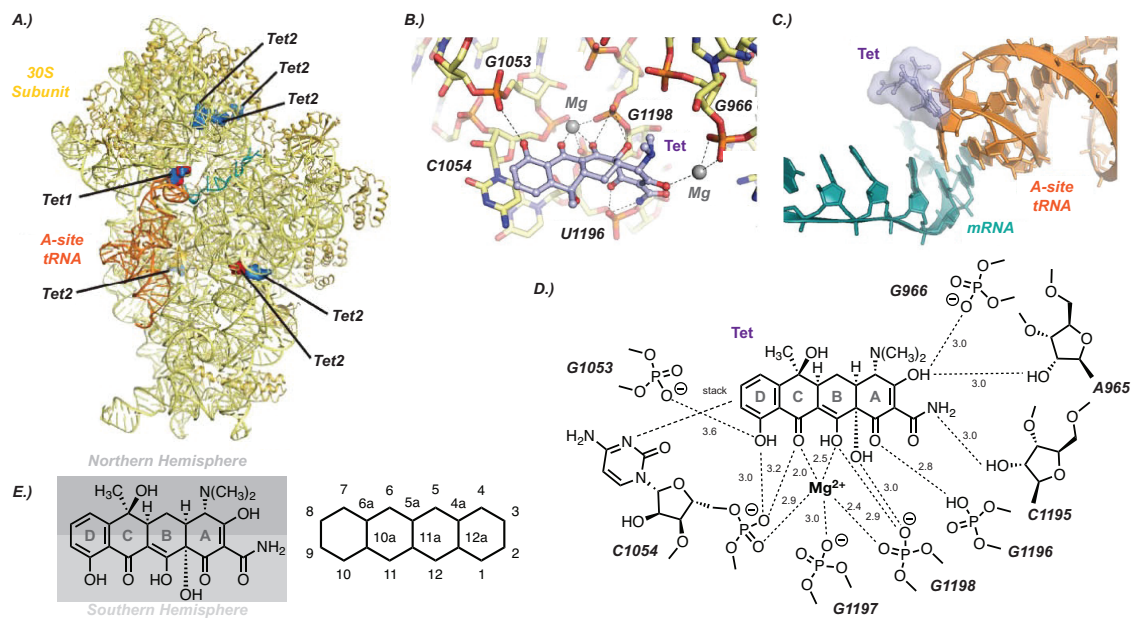


**Figure 1.2 Interaction of Tetracycline with the bacterial 30S ribosome.** (A) Crystal structure of tetracycline bound to the bacterial 30S ribosomal subunit (PDB: 1H9W). (B) Detail of the Tet1 binding site showing tetracycline in purple. Magnesium ions shown in gray. (C) Detail of tetracycline binding as it relates to mRNA and A-site tRNA positioning. (D) Schematic of tetracycline binding in Tet1 binding site. Distances noted in angstroms (Å). (E) Numbering notation for tetracycline carbon atoms. Orientation corresponds to tetracycline shown in (D). Figures A, B, and C adapted from Nguyen, et al., **2014** (Chapter 1, ref. 12c).

The tetracycline-ribosome co-crystal structure also provides a detailed view of the orientation of the compound in its key ribosomal binding pocket (Fig. 1.2B, D).<sup>12</sup> The southern hemisphere of the compound is enmeshed in a complex network of hydrogen bonding and  $\pi$ -stacking interactions that explain the necessity of these functional groups for antibacterial activity. Of primary importance is the magnesium ion situated directly between the oxygen atoms of the C- and B-rings, itself further stabilized through chelation to phosphate residues on C1054, G1197, and G1198. The D-ring is thought to engage in hydrogen bonding interactions with C1054 and G1053 in addition to a  $\pi$ -stacking interaction with the cytosine of C1054. The dense hydrogen bonding network then continues around the A-ring, with the C1-ketone, C2-carboxamide, and C3-enol all engaged in one or more stabilizing interactions. Positions C4 through C9 are directed to relatively uncongested space, with the lack of potential bonding partners here helping to demonstrate why these positions have been so heavily explored throughout the history of semi- and fully synthetic medicinal chemistry campaigns.<sup>1</sup>

While the binding location and molecular orientation of the tetracyclines in human cells will likely differ from those in bacteria, the principles of tetracycline binding gleaned from the bacterial ribosome co-structure provide us with a blueprint for the types of interactions to expect in binding of other RNA-based target biomolecules.

### **1.3 Summary of Key Non-Canonical Effects of the Tetracyclines**

While the non-canonical effects of the tetracyclines have been observed since the outset of their use as antibacterial agents, only recently have studies that seek to understand or exploit these lesser-known applications emerged. In this section we provide a summary

of some of the tetracyclines that have displayed unique and under-investigated therapeutic properties, as well as some of the recent and most promising applications.

Due to its near ubiquity in the clinical setting, doxycycline (**1.4**) has demonstrated perhaps the broadest array of non-canonical effects in treating human diseases. Of particular note, doxycycline has displayed beneficial therapeutic effects in the treatment of a variety of lung conditions. In addition to the aforementioned LAM example, doxycycline was used in the successful treatment of pulmonary capillary hemangiomatosis, a rare disorder categorized by the abnormal growth patterns of capillaries leading to obstruction of pulmonary vasculature.<sup>13, 14</sup> Doxycycline has also been associated with antiproliferative effects *in vitro*, with the compound inducing apoptosis in small cell lung cancer model cell lines (ex. H446) in a dose-dependent manner.<sup>15</sup> The non-antibacterial tetracycline analogue Col-3 (**1.10**) has also been the subject of a variety of clinical applications related to its anticancer effects. Notably, Col-3 was evaluated in Phase I and Phase II clinical trials as a therapeutic for AIDS-related Kaposi's sarcoma.<sup>10</sup> Col-3 has been shown to inhibit the growth of a variety of cancer cell lines, including human cervical and prostate cancers, and has shown promise as an antifungal agent.<sup>16, 17, 18</sup>

---

<sup>13</sup> Ginns, L. C.; Roberts, D. H.; Mark, E. J.; Bruschi, J. L.; Marler, J. J. *Chest*, **2003**, *124*, 2017-2022.

<sup>14</sup> (a) See Moses et al., **2006** (Chapter 1, ref. 9). (b) Wang, Q.; Luo, M.; Xiang, B.; Chen, S.; Ji, Y. *Respiratory Res.* **2020**, *21*, 1-12.

<sup>15</sup> Wang, S.; Zhou, B.; Liu, Y.; Wang, Y.; Liang, Q.; Cai, Y.; Yang, J.; Song, Z.; Li, G. *Int. J. Oncology*, **2016**, *48*, 1353-1360.

<sup>16</sup> Zhao, L.; Xu, J.; Yang, Y.; Chong, Y.; Liu, C.; Jiao, Y.; Fan, S. *Anti-Cancer Drugs* **2013**, *24*, 799-809.

<sup>17</sup> Lokeshwar, B. L.; Houston-Clark, H. L.; Selzer, M. G.; Block, N. L.; Golub, L. M. *Adv. Dent. Res.* **1998**, *12*, 97-102.

<sup>18</sup> Liu, Y.; Ryan, M. E.; Lee, H.-M.; Simon, S.; Tortora, G.; Lauzon, C.; Leung, M. K.; Golub, L. M. *Antimicrob. Ag. Chemother.* **2002**, *46*, 1447-1454.

The semisynthetic analogue tigecycline (**1.11**, Fig. 1.3) has generated excitement in recent years with its application for the treatment of various leukemias.<sup>19</sup> In 2011, Skrtic and colleagues identified tigecycline as a potential therapeutic following a high-throughput screen of FDA-approved small molecules in two human acute myeloid leukemia (AML) cell lines.<sup>20</sup> A secondary genomics screening methodology in yeast pointed to mitochondrial translation as the target of tigecycline in human cells, with shRNA-mediated knockdown of translation factor EF-Tu (equivalent to eIF2 in human cells) mimicking the effects of the tigecycline treatment.<sup>21</sup> The authors posit that the increased reliance of AML cell lines on mitochondrial biogenesis compared to that of standard blood cells provides an explanation for the observed selectivity and sensitivity to tigecycline. In 2016, tigecycline was evaluated in Phase I clinical trials as an intravenous treatment for AML.<sup>22</sup> One recent application takes advantage of tigecycline-induced mitochondrial dysregulation as an adjuvant for standard cancer therapeutics. Therein, AML cells resistant to the Bcl-2 inhibitor venetoclax (**1.13**) were sensitized to the drug following mitochondrial translation inhibition and ISR activation with tigecycline, doxycycline, or the oxazolidinone

---

<sup>19</sup> Selected literature: (a) Xu, Z.; Yan, Y.; Li, Z.; Qian, L.; Gong, Z. *Front. Pharmacol.* **2016**, *7*, 473. (b) Panina, S. B.; Pei, J.; Kirienko, N. V. *Cancer & Metab.* **2021**, *9*, 17. (c) Valli, D.; Gruszka, A. M.; Alcalay, M. J. *Clin. Med.* **2020**, *9*, 1892.

<sup>20</sup> Skrtic, M.; Sriskanthadevan, S.; Jhas, B.; Gebbia, M.; Wang, X.; Wang, Z.; Hurren, R.; Jitkova, Y.; Gronda, M.; Maclean, N.; Lai, C. K.; Eberhard, Y.; Bartoszko, J.; Spagnuolo, P.; Rutledge, A. C.; Datti, A.; Ketela, T.; Moffat, J.; Robinson, B. H.; Cameron, J. H.; Wrana, J.; Eaves, C. J.; Minden, M. D.; Wang, J. C. Y.; Dick, J. E.; Humphries, K.; Nislow, C.; Giaever, G.; Schimmer, A. D. *Cancer Cell* **2011**, *20*, 674-688.

<sup>21</sup> See Chapter 4 for a discussion of the mechanism of translation in eukaryotes.

<sup>22</sup> Reed, G. A.; Schiller, G. J.; Kambhampati, S.; Tallman, M. S.; Douer, D.; Minden, M. D.; Yee, K. W.; Gupta, V.; Brandwein, J.; Jitkova, Y.; Gronda, M.; Hurren, R.; Shamas-Din, A.; Schuh, A. C.; Schimmer, A. D. *Cancer Med.* **2016**, *5*, 3031-3040.

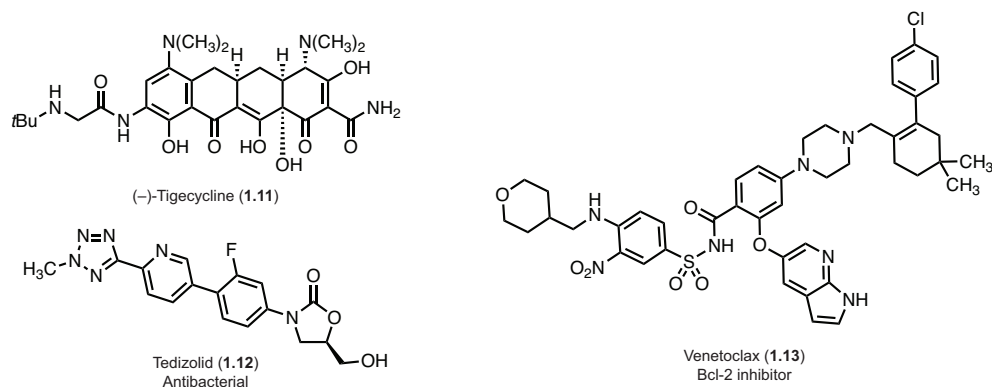


**Figure 1.3 Tigecycline as a Cancer Therapeutic.** Tigecycline (**1.11**) has been investigated as a cancer therapeutic for AML and other leukemias. In one application, tigecycline, doxycycline (**1.4**), and the antibacterial compound tedizolid (**1.12**) were used in combination therapies with the known Bcl-2 inhibitor venetoclax (**1.13**), enabling the latter to overcome resistance mutations in AML cell lines.

antibacterial tedizolid (**1.12**).<sup>23</sup> In short, the disruption of mitochondrial function with tigecycline presents an exciting new therapeutic strategy for the treatment of AML and suggests a potentially broader strategy for the treatment of cancer in general.

Most recently, the tetracyclines have emerged as potential therapeutic agents for a class of rare genetic disorders known as mitochondrial diseases (MD).<sup>11</sup> MD is an umbrella term for a range of conditions caused by mutations in the nuclear or mitochondrial genes that code for mitochondrial proteins, resulting organellar or cellular dysfunction. Due to the ubiquity of mitochondria in human cells these diseases can manifest in a variety of forms and severities for which there are only palliative treatments—no cures exist for mitochondrial disease. In an effort to identify novel therapeutics for MD, researchers at the Dana-Farber Cancer Institute utilized a high-throughput screen on cells containing MD mutations and identified the tetracyclines as a class of small molecules that enable the survival of mitochondrially-deficient cells grown under nutrient stress (low or no glucose) conditions. Further investigation revealed the cell survival observation—termed *rescue*—

<sup>23</sup> Sharon, D.; Cathelin, S.; Mirali, S.; Di Trani, J.; Yanofsky, D. J.; Keon, K. A.; Rubinstein, J. L.; Schimmer, A. D.; Ketela, T.; Chan, S. M. *Science Transl. Med.* **2019**, *11*, eaax2863.



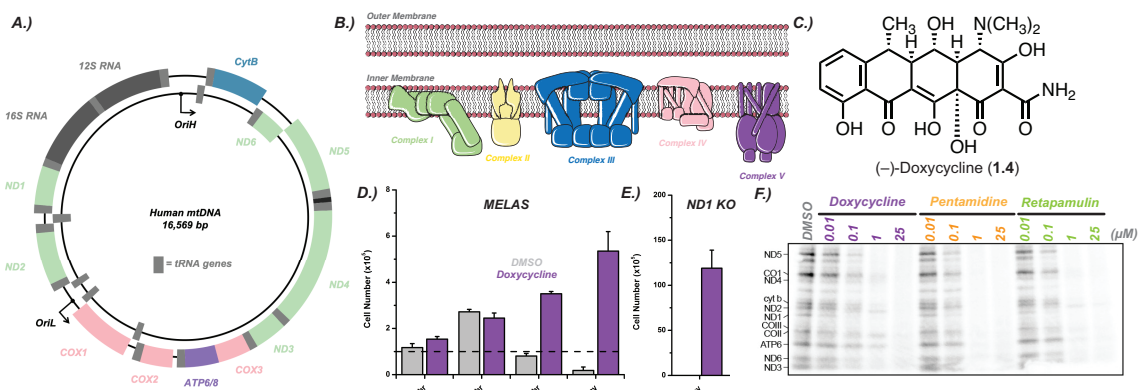


**Figure 1.4 Tetracyclines as Novel Therapeutics for Mitochondrial Disease.** The human mitochondrial genome (A) contains only 13 coding genes, the majority of which code for proteins in the oxidative phosphorylation system (B). Tetracycline antibiotics, including doxycycline (1.4, C), were shown to promote survival of cells containing various mitochondrial deficiencies, including MELAS (mitochondrial encephalomyopathy, lactic acidosis, and stroke-like episodes) featuring non-functional mitochondrial tRNAs and ND1-KO featuring knockout of a subunit of Complex I (D, E). These effects have been linked to moderate inhibition of mitochondrial translation (<sup>35</sup>S-incorporation assay, F) however, the precise mechanism of action remains to be discovered. Figures in D, E, and F adapted from Perry et al., 2021 (Chapter 1, ref. 11).

was linked to a moderate inhibition of mitochondrial translation and reduction of inflammatory and neuroimmune signaling responses following tetracycline treatment.<sup>11</sup> In a striking result, addition of doxycycline to the chow of mice afflicted with a preclinical model of the neurodegenerative MD Leigh syndrome was found to extend mouse lifespan from ~70 days to between 100 and 300 days with significant improvement in neurological function. Together, these findings suggest the tetracyclines could play an important role as novel therapeutics for MD, and further studies are needed to better understand the signaling pathways at play and to explore mitochondrion-specific tetracycline analogues designed to treat MD without antibacterial or antiproliferative side effects.

## 1.4 Mechanistic Elucidation Efforts

Despite the apparent wealth of indications, prior to 2018 no major effort to better understand the origins and mechanism of the non-canonical effects of the tetracyclines in human cells had ever been undertaken.

In the 1990s, a team of researchers led by Lorne M. Golub reported one of the first studies into the non-antimicrobial effects of the tetracyclines.<sup>24</sup> Tetracyclines including doxycycline (**1.4**), minocycline (**1.5**), and tetracycline (**1.3**) were found to inhibit mammalian collagenases as well as several matrix metalloproteinase enzymes (MMPs). MMPs are a class of zinc-dependent proteases involved in an array of cellular growth functions including embryogenesis, tissue remodeling, and tumor progression.<sup>25</sup> MMPs have long been a target of interest in anti-inflammatory and anticancer drug development efforts as disruption of MMP-mediated proteolysis of the extracellular matrix during cell growth could be an effective therapeutic strategy for a variety of human diseases. Golub and colleagues were investigating the application of tetracyclines in treating periodontal diseases and gingival degradation often observed during chronic illnesses like diabetes or rheumatoid arthritis. In a series of reports, researchers discovered *in vivo* administration of minocycline to diabetic rats would decrease collagenase activity by 65% (70% reduction in germ-free rat models).<sup>24</sup> Further experimentation showed that incubation of minocycline with “collagenolytic activity” extracted from rat polymorphonuclear leukocytes or “partially purified” collagenase extracts at or near pharmacologic concentrations resulted in reduction of enzymatic activity. Despite the array of assays performed through these studies, it remains unclear whether the reduction of MMP activity is due to direct inhibition of the enzyme, through inhibition of a broader cellular process (transcription, translation, etc.), or a combination of the two.

---

<sup>24</sup> Golub, L. M.; Ramamurthy, N.S.; McNamara, T. F.; Greenwald, R. A.; Rifkin, B. R. *Crit. Rev. Oral Bio. Med.* **1991**, *2*, 297-322 and references cited therein.

<sup>25</sup> Griffin, M. O.; Fricovsky, E.; Ceballos, G.; Villareal, F. *Am. J. Physiol. Cell Physiol.* **2010**, *299*, 539-548 and references cited therein.

MMP activity is reliant on the presence of zinc and calcium ions both for structural support and proteolytic activity.<sup>25</sup> Given the known reliance of the tetracyclines on magnesium ions for antibacterial activity (Fig. 1.5D), researchers suggested that MMP inhibitory activity stemmed from chelation of zinc and calcium ions by the tetracyclines, destabilizing and/or preventing enzymatic activity. Unfortunately, this hypothesis was never evaluated beyond basic tetracycline/metal ion/collagenase extract co-incubation experiments. While MMP inhibition presents an exciting outlet with the potential to explain a subset of the non-canonical effects of the tetracyclines, the lack of convincing *in vitro* experimentation and the broad array of non-canonical effects in a variety of cancer, tissue, and disease types suggest that a broader theory is needed to provide a full mechanistic picture.

Such a picture was presented in 2018 when the Myers group, led by Professor Andrew Myers and postdoctoral researcher Dr. Jonathan Mortison, utilized a multidisciplinary effort featuring mass spectrometry-coupled proteomics and photo-affinity labeling methodology in the first detailed mechanistic investigation into the antiproliferative effects of the tetracyclines.<sup>26</sup> Firstly, Mortison and colleagues determined the cellular targets of the tetracyclines using affinity isolation and mass spectrometry based SILAC (stable isotopically labeled amino acids in cell culture) methodology.<sup>27</sup> This method utilizes two cell cultures: the first with standard amino acids and the second with “heavy” isotopically labeled amino acids in various treatment states (Fig. 1.5A). The

---

<sup>26</sup> Mortison, J. D.; Schenone, M.; Myers, J. A.; Zhang, Z.; Chen, L. Ciarlo, C.; Comer, E.; Natchair, S. K.; Carr, S. A.; Klaholz, B. P.; Myers, A. G. *Cell Chem. Biol.* **2018**, *25*, 1506-1518.

<sup>27</sup> (a) See Mortison et al., **2018** (Chapter 1, ref. 26). (b) Chen, X.; Wei, S.; Ji, Y.; Guo, X.; Yang, F. *Proteomics.* **2015**, *18*, 3175-3192.

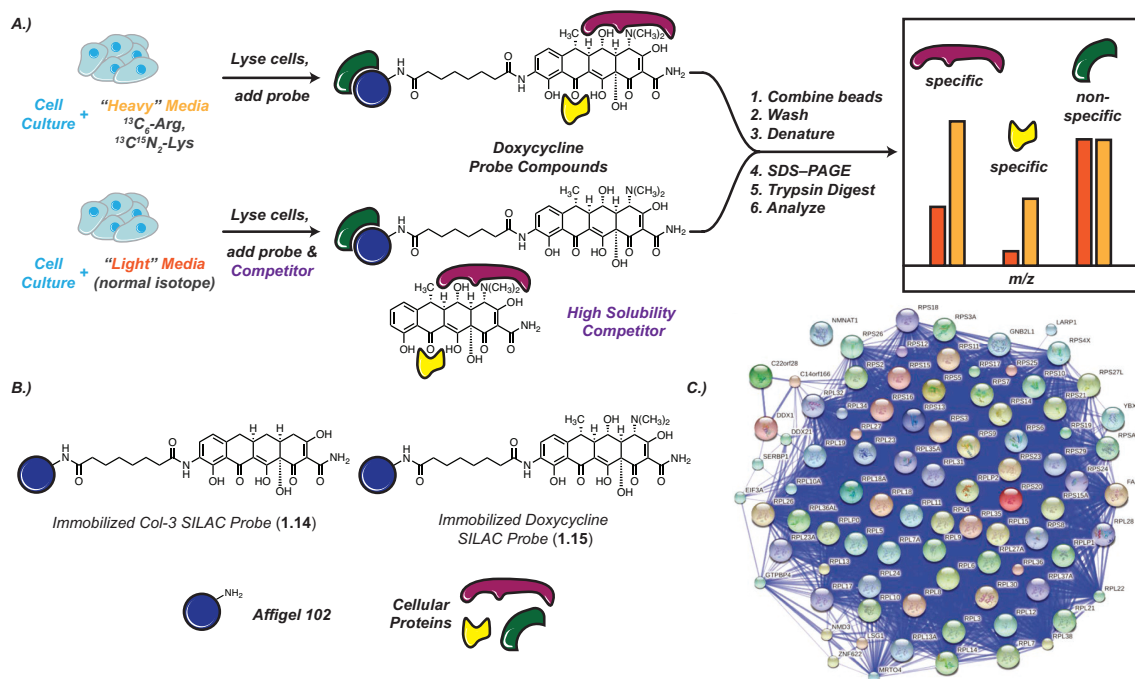


**Figure 1.5 SILAC Experiment Methodology and Results.** Mortison and colleagues employed a SILAC-based methodology as an initial screen for the target(s) of the tetracyclines in human cells. This methodology (A) involves using probe compounds (B) in isotopically labeled cell cultures followed by mass spectrometry analysis of bound proteins to determine cellular targets. Mortison found that ribosomal proteins (C) were overwhelmingly enriched on tetracycline treatment, suggesting eukaryotic translational machinery as the target in human cells. Figure adapted from Mortison et al., **2018** (Chapter 1, ref. 26), with permission.

“heavy” culture of cells is treated with a resin-conjugated tetracycline (**1.14** or **1.15**, Fig. 1.5B) while the normal culture is treated with the same resin probe *and* a soluble competitor compound (doxycycline, **1.4**). The resin beads are then combined and the bound proteins denatured to allow for analysis via mass spectrometry to determine the identity of the proteins bound to the resin probes. In their analysis, Mortison and colleagues found ribosomal proteins were overwhelmingly represented as the targets for both the Col-3 and doxycycline probe compounds – implicating eukaryotic translational machinery as the cellular target.

Following these exciting results, Mortison and colleagues elected to further interrogate the effects of the tetracyclines on the human translational apparatus and developed a novel photo-affinity labeling (PAL) strategy to study ribosomal binding (Fig.

1.6).<sup>28</sup> Toward this end, Mortison developed probe compounds that feature both the tetracycline core structures of interest (Col-3, **1.16**, doxycycline, **1.17**, Fig. 1.6B) and a small handle featuring two key functional groups: a diazirine and an azide. On exposure to ultraviolet light, the diazirine functionality will decompose into nitrogen gas and a reactive carbene species.<sup>29</sup> In a biological context, this carbene is likely to perform a C-H insertion reaction on any nearby residues, thereby covalently crosslinking itself to its biomolecule target. Subsequent cell lysis and isolation of crude RNA allows for pulldown enrichment of tetracycline-RNA crosslinks via click reaction to the pendant azide handle. Finally, the precise binding locations are determined via reverse transcription and deep sequencing as

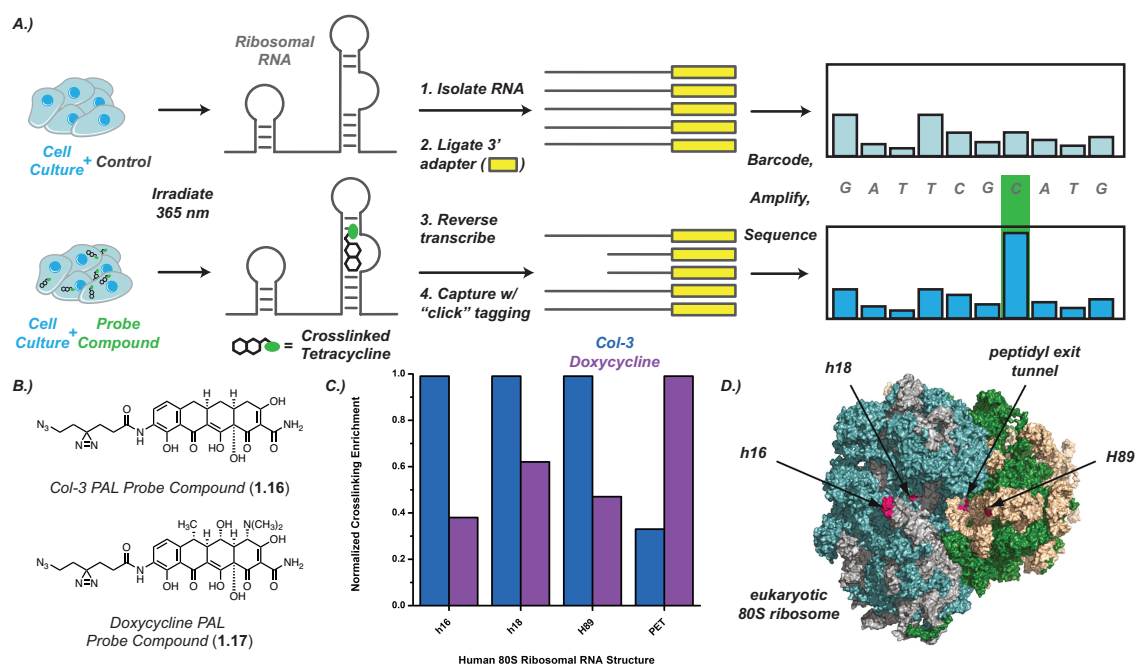


**Figure 1.6 Photoaffinity Labeling (PAL) Experiment.** Mortison utilized a modified PAL strategy to identify the precise binding locations of the tetracyclines on the human 80S ribosome (A). This assay employed probe compounds (B) featuring bifunctional handles for covalent linking to the biomolecule target. Mortison identified four distinct rRNA substructures bound by the tetracyclines (C) which can be visualized using the cryo-EM structure in D. Figure adapted from Mortison et al., **2018** (Chapter 1, ref. 26), with permission.

<sup>28</sup> (a) See Mortison et al., **2018** (Chapter 1, ref. 26). (b) Ge, S.; Chen, B.; Wu, Y.; Long, Q.; Zhao, Y.; Wang, P.; Yang, S. *RSC Adv.* **2018**, *8*, 29428-29454.

<sup>29</sup> West, A. V.; Muncipinto, G.; Wu, H.-Y.; Huang, A. C.; Labenski, M. T.; Jones, L. H.; Woo, C. M. *J. Am. Chem. Soc.* **2021**, *143*, 6691-6700.

crosslinked tetracyclines prevent forward progress of the reverse transcriptase enzyme. DNA sequencing then reveals binding locations as “stops” in DNA synthesis (Fig. S1.1). Through this methodology, Mortison and colleagues enabled unambiguous assignment of the eukaryotic ribosome as the target of the tetracyclines, with Col-3 and doxycycline binding discrete locations across the small and large ribosomal subunits including the peptidyl exit tunnel (PET), and helices h16, h18, and H89 (Fig. 1.6C, D). This finding is perhaps not surprising considering the well-studied target of the tetracyclines in bacteria, however, Mortison’s efforts provided the first evidence that tetracycline interaction with the eukaryotic 80S ribosome could be connected to the array of non-canonical effects that have been associated with the tetracyclines in human cells.

Mortison and colleagues then proceeded to characterize the downstream activity of the tetracyclines in human cancer cells, focusing their efforts on two areas: signaling pathway activation and translation inhibition. RNA sequencing experiments in A375 melanoma cells (Fig. 1.7) revealed a variety of cell salvage and apoptotic signatures broadly linked to activation of a general cell stress pathway, the Integrated Stress Response

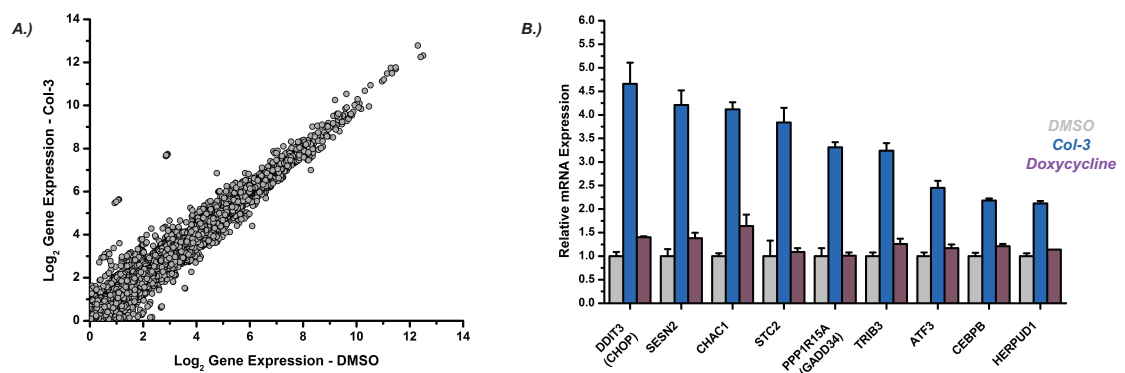


**Figure 1.7 RNA Sequencing.** Mortison conducted RNA sequencing on A375 melanoma cells using both doxycycline and Col-3 (10  $\mu$ M, 6 h), with results from the Col-3 treatment experiment shown in A. Among the activation signatures identified upon subsequent analysis, Mortison identified the integrated stress response as a major signaling pathway activated upon Col-3 treatment (B, blue). Doxycycline (purple) generated only modest activation of the ISR. Samples compared to the DMSO control (gray). Reproduced from Mortison et al., 2018 (Chapter 1, ref. 26), with permission.

(ISR), as well as the central stress regulator Activating Transcription Factor 4 (ATF4). Similar stress signatures were observed in K562 leukemia cells as well as HCT116 colorectal cancer cells, suggesting a general mechanism induced upon tetracycline treatment that contributes to overall antiproliferative activity (Fig. S1.2).

The ISR is a cell stress response pathway that collects a variety of stress signals – from misfolded proteins to potential viral infection – and directs them to a single point: phosphorylation of eukaryotic initiation factor 2 (eIF2, Fig. 1.8A).<sup>30</sup> Briefly, eIF2 plays a critical role in the initiation of translation through the shuttling of the ternary complexes to the 40S preinitiation complex. Phosphorylation of eIF2 inhibits a key GDP/GTP exchange process catalyzed by the guanine nucleotide exchange factor eIF2B, ultimately leading to a decreased concentration of active eIF2 and slowing translation initiation. Inhibition of translation by eIF2 phosphorylation elicits a variety of downstream responses, most notably induction of ATF4, which then organizes either cell salvage or cell death responses. In canonical activation of the ISR, phosphorylation of eIF2 is conducted via protein kinase R-like endoplasmic reticular kinase (PERK), a general sensor for the presence of unfolded or misfolded proteins following translation.<sup>30</sup> Interestingly, Mortison and colleagues identified that while induction of ATF4 and phosphorylation of eIF2 could be readily observed via Western blot shortly following tetracycline treatment, activation of PERK was not observed (Fig. 1.8B). These results suggest that phosphorylation of eIF2 is conducted by another ER-based kinase (ex. HRI, PKR, or GCN2), or another cellular stress signal entirely.

---

<sup>30</sup> (a) Ron, D. and Walter, P. *Nat. Rev. Mol. Cell Biol.* **2007**, *18*, 716-731. (b) See Chapter 4 for a discussion of the mechanism of eukaryotic translation.

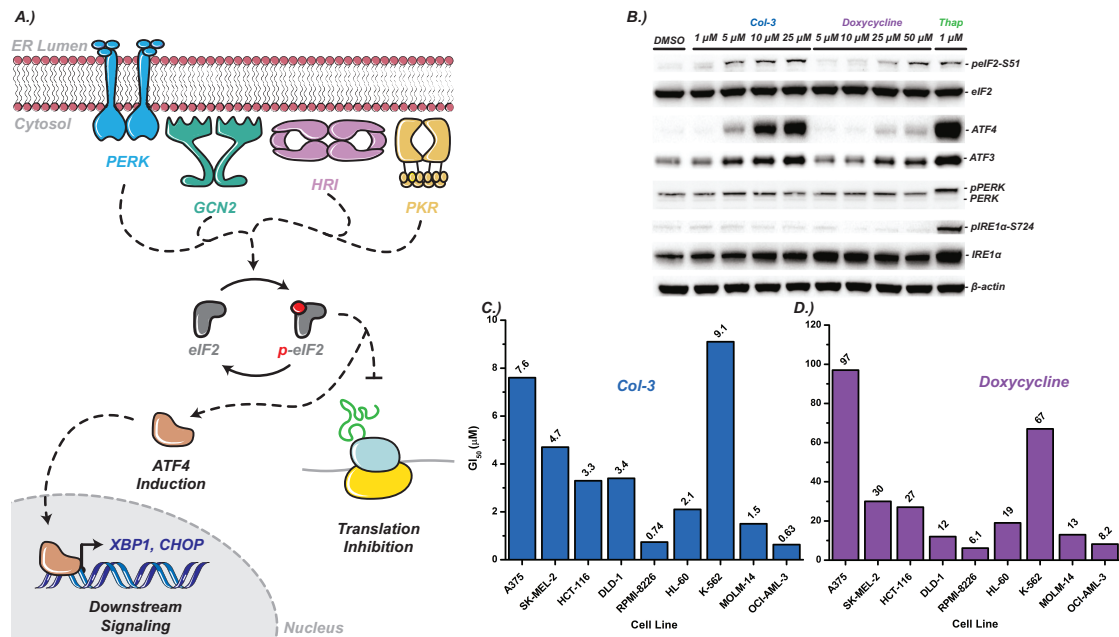


**Figure 1.8 The Integrated Stress Response.** The ISR represents a complex set of signaling pathways that converge to a single point – phosphorylation of the alpha subunit of eIF2 (A). This phosphorylation event triggers a reduction in translational loading as well as activation of downstream signaling modules, particularly ATF4, which in turn is responsible for the activation of cell salvage or cell death pathways. Mortison used immunoblotting to show that while Col-3 induces activation of ATF4, the canonical ISR kinase PERK is not phosphorylated (B). The growth inhibitory values of both Col-3 and doxycycline vary widely based on cell and cancer type (C), perhaps suggesting a variance in sensitivity based on signaling pathway activation. Figures in B and C adapted from Mortison et al., **2018** (Chapter 1, ref. 26).

In addition to signaling pathway analysis, Mortison and colleagues analyzed the effects of the tetracyclines on translation. Translation inhibitory effects were characterized using two assays: HeLa cell-free translation experiments and *O*-propargyl puromycin (OPP) assays (Fig. 1.9).<sup>31, 32</sup> In the former, commercially available HeLa-derived translational systems are programmed with a stock green fluorescent protein (GFP) reporter plasmid and treated with varying concentrations of tetracycline. Translation inhibitory values are then determined after comparison of the fluorescence readout between the

<sup>31</sup> (a) See Mortison et al., **2018** (Chapter 1, ref. 26). (b) Thermo Scientific 1-Step In Vitro Translation (IVT) Systems. Thermo Fisher Scientific.

<sup>32</sup> (a) See Mortison et al, **2018** (Chapter 1, ref. 26). (b) Liu, J.; Xu, Y.; Stoleru, D.; Salic, A. *PNAS*. **2012**, *109*, 413-418.



tetracycline conditions and the untreated control. This high-throughput assay provides a rapid readout of translation inhibitory activities and is often used for initial screening efforts, however major drawbacks include the lack of choice of cell line or cancer type in designing the experiment. This issue is solved with the latter methodology, allowing for a variety of cell types and treatment conditions. Following treatment, cells are treated with OPP, an analogue of the antibacterial compound puromycin which features an alkyne handle on a central hydroxyl group (**1.18** and **1.19**, Fig. 1.9A). Puromycin exerts its cytotoxic effects through binding of the prokaryotic or eukaryotic ribosome in the A-site of the catalytic core, adding to the nascent peptide chain much like a standard amino acid. However, the non-hydrolysable amide bond at the center of the compound prevents addition of further amino acids and the nascent peptide is clipped, terminating translation, subsequently leading to cell death. The OPP assay leverages this mechanism by quantifying the amount of prematurely terminated peptide chains through a fluorescence readout. The alkyne handle of OPP serves as a coupling partner for an azide-functional fluorophore (ex. Alexafluor488) and, following fixation and flow cytometry, the fluorescent signal of each

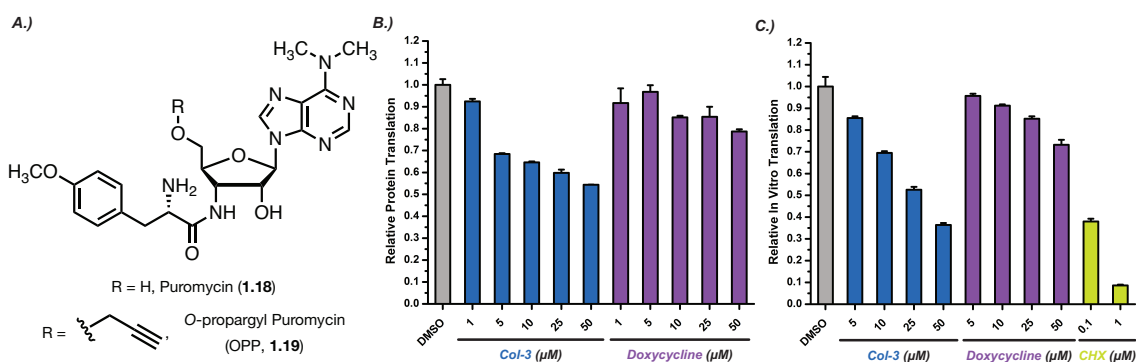


**Figure 1.9 Translation Inhibition Assays.** Translation inhibition was characterized using both HeLa cell free translation assays and OPP incorporation assays. In the latter, a propargyl-analogue of the antibacterial compound puromycin is used to monitor translation in cells, with peptide product subsequently quantified by fluorescence (A). Both OPP assays (B, K562 leukemia cells, 3 h dose) and HeLa lysate assays (C) show dose-dependent inhibition of translation for Col-3 (blue) and, to a lesser extent, doxycycline (purple). The elongation inhibitor cycloheximide (CHX, chartreuse) used as positive control. Figures B and C adapted from Mortison et al., **2018** (Chapter 1, ref. 26), with permission.

treatment condition is compared to the untreated control to calculate translation inhibitory activity. In both the cell-free and OPP assays, Mortison and colleagues found Col-3 to be a potent inhibitor of eukaryotic translation across various cancer cell lines (Fig. 1.9B, C). Doxycycline also demonstrated moderate translation inhibitory effects, though to a much lower extent than Col-3.

Perhaps most interestingly, translation inhibitory effects were found to be independent of ISR activation. The relationship between translation inhibition and signaling pathway activation was interrogated using the recently discovered small molecule ISRIB (**1.20**, Fig. 1.10).<sup>33</sup> ISRIB functions through binding eIF2B, the dedicated guanine nucleotide exchange factor employed by eIF2 for a key GDP/GTP recycling step by locking the enzyme into an active conformation (Fig. 1.10C, D). Typically, ISR-mediated phosphorylation of eIF2 slows the activity of eIF2B and leads to an overall reduction of translational loading. However, with ISRIB functioning as a “molecular staple” and holding eIF2B in an active state, phosphorylation no longer slows recycling of eIF2 and translation is able to continue uninhibited. In short, when analyzing the relationship between ribosomal binding, translation inhibition, and signaling pathway activation, ISRIB provides us with a method to separate translation inhibitory activity caused by ISR activation from inhibitory effects due to ribosomal binding. Upon co-dose with a small amount of ISRIB (200 nM), immunoblotting shows a loss of ATF4 induction (Fig. S1.3), while OPP assays show continued inhibition of translation (Fig. 1.10B). In addition, GI<sub>50</sub> values for most cell lines tested showed no major change for Col-3 or doxycycline (Fig. 1.10E). These results suggest the tetracyclines inhibit translation

---

<sup>33</sup> Zyryanova, A. F.; Weis, F.; Faille, A.; Alard, A. A.; Crespillo-Casado, A.; Sekine, Y.; Harding, H. P.; Allen, F.; Parts, L.; Fromont, C.; Fischer, P. M.; Warren, A. J.; Ron, D. *Science*. **2018**, *359*, 1533-1536.

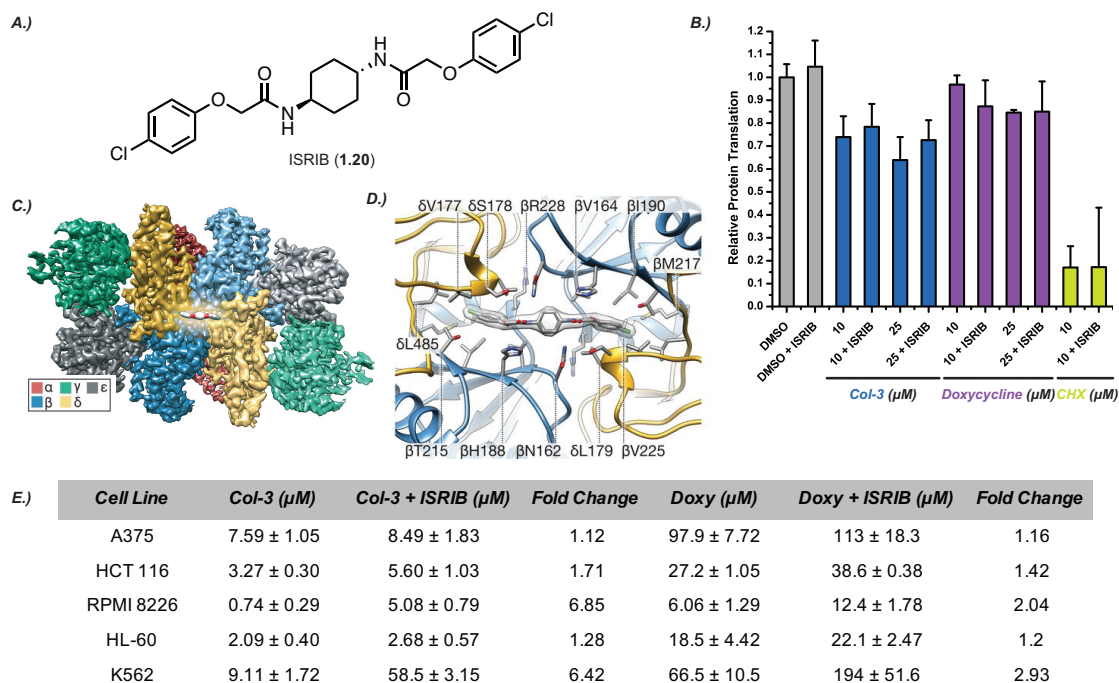


**Figure 1.10 ISRIB and ISR-independent Translation Inhibition.** The small molecule ISRIB (1.20, A) enables assessment of translation inhibitory effects independently of ISR activation. ISRIB co-dose with Col-3 and doxycycline (B) shows insignificant differences in translation inhibitory activities (OPP assay). ISRIB acts through binding of eIF2B, locking the enzyme into an active conformation and rendering phosphorylation of eIF2 an ineffective pathway for translation inhibition (C, D). Growth inhibitory values show a slight variance with ISRIB co-dose, particularly the leukemia cell lines RPMI-8226 and K562. Figures B and E adapted from Mortison et al., 2018 (Chapter 1, ref. 26) with permission. Figures C and D obtained from Zyryanova et al., 2018 (Chapter 1, ref. 33).

independently of ISR activation and provide clues as to the causal relationship between these cellular responses. This is not to say that ISR activation plays no role in the antiproliferative activity of the tetracyclines—ISRIB co-dose conditions lead to minor reductions in  $GI_{50}$  and translation inhibitory values for several cell lines. Further, cessation of ISR activity in the K562 leukemia cell line led to a massive reduction in potency, though a drop of this magnitude has not been observed for any other cancer cell line tested. While ISRIB co-dose experiments provided some interesting findings regarding mechanism of action, many open questions remain regarding the precise nature of signaling progression as well as the various cell-type or cancer-type dependent effects that we observe in select cases.

In total, the efforts of Mortison and colleagues established a strong foundation of chemical and biological experimentation supporting the tetracyclines as potential antiproliferative agents for human cancers, including target identification, binding site elucidation, and initial characterization of downstream activity.

## **1.6 Conclusions and Path Forward**

Once thought to be a well-characterized and benign class of antibacterial agents, recent years have seen the tetracyclines emerge as a highly versatile scaffold that is well suited for a variety of medicinal applications in treating human disease. Through this dissertation, our efforts to further develop the tetracyclines as antiproliferative agents for human cancers have focused on two areas: compound development and mechanistic elucidation.

In Chapter 2, we provide an overview of an early medicinal chemistry effort that utilized semisynthesis to access analogues of Col-3 with improved activity in human cancer cell lines. These efforts quickly identified a novel Col-3 analogue featuring a quinoline moiety with exceptional antiproliferative activity across a range of cancer cell types. We then sought to compare the mechanism of action of this novel analogue to that of Col-3, evaluating effects on signaling progression and translation inhibition as well as mitochondrial toxicity.

Following these results, we elected to transition to a fully synthetic compound development strategy to access a broader selection of substitution patterns around the tetracycline scaffold. In Chapter 3, we detail our efforts to leverage the long history of tetracycline total synthesis in the Myers Group to develop a fully synthetic approach to

Col-3 analogues. These efforts focused on the development of novel C7/C8 substituted analogues which were evaluated for antiproliferative activity and translation inhibitory effects.

Finally, in Chapter 4, we provide a summary of the various experiments used to further our mechanistic understanding of the tetracyclines antiproliferative effects, focusing on translation inhibition and signaling pathway progression. These efforts employed a range of biochemical techniques, including polysome profiling and *in vitro* translation experiments, in an attempt to further illuminate the mechanism tetracycline-induced cell growth inhibition.

While still in early stages, we believe these findings will assist future generations of chemists and biologists in the study of the non-canonical effects of the tetracyclines and may someday contribute to bringing this storied class of compounds to the clinic as novel cancer therapeutics.

## **Chapter 2**

### **Semisynthetic Compound Development Efforts**

## 2.1 Introduction to Semisynthetic Compound Development Efforts

In this chapter, we detail our early efforts to identify analogues of Col-3 featuring improved and well-defined antiproliferative activity using a semisynthetic compound development strategy. We will introduce the concept of semisynthesis as it relates to the tetracyclines, including the key role semisynthesis played in developing novel tetracyclines and some of the reactions that inspired our studies. Our compound development efforts began with the synthesis of several structurally distinct analogues of Col-3 and the discovery of a highly potent derivative featuring an  $\alpha, \beta$ -unsaturated quinoline acid moiety. To further explore this structural element, we developed a short synthetic route to access a range of quinoline-acid compounds for coupling to the tetracycline core. Finally, we describe our efforts to analyze the cellular effects of these compounds through signaling pathway elucidation, translation inhibition analysis, and antibacterial activity testing. In total, these efforts resulted in the discovery of a novel tetracycline with potent anticancer activity and lay the foundation for future development of Col-3 analogues using a fully synthetic strategy.

## 2.2 History of Tetracycline Semisynthesis

The process of semisynthesis has played a key role in the development of many different classes of antibacterial compounds including the macrolides,  $\beta$ -lactams, and tetracyclines.<sup>1</sup> A total synthesis approach seeks to access novel compounds or substitutions by beginning with relatively non-complex, commercially available starting materials and slowly building complexity over the course of a synthetic route. Semisynthesis differs in

---

<sup>1</sup> Wright, P. M.; Seiple, I. B.; Myers, A. G. *Angew. Chem. Int. Ed.*, **2014**, 53, 8840-8869.

that commercially available antibacterial scaffolds are used as the starting point of any given synthetic scheme. Drawbacks of a semisynthetic approach include limitations in the types of reagents available for conducting chemical transformations, as well as the structural positions around the molecular scaffold accessible for derivatization. These limitations are exemplified by the history of tetracycline semisynthetic compound development.<sup>2</sup> Positions C7 and C9, derivatized through aromatic substitution chemistry, have seen extensive exploration while positions C5 and C6, with only a few possible reactions available, were not thoroughly explored until a practical fully synthetic route to the tetracyclines was developed in the early 2000's.<sup>3</sup> Semisynthesis benefits tremendously by offering rapid access to novel natural product derivatives and, for this reason, has played a central role in the early development of many antibacterial compounds used throughout the world today.

Tetracycline (**1.3**) was first discovered through semisynthesis – hydrogenation over palladium on carbon providing the hydrodechlorinated species itself later discovered as a natural product (Fig. 2.1A).<sup>4</sup> Medicinally important compounds such as doxycycline (**1.4**) were discovered during early semisynthetic development efforts at Pfizer (Fig. 2.1B).<sup>5</sup>

---

<sup>2</sup> Hlavka, J. J.; Boothe, J. H. *Experimental Handbook in Pharmacology No. 78: The Tetracyclines*, 1<sup>st</sup> ed.; Springer-Verlag: Berlin, 1985.

<sup>3</sup> (a) See Charest et al., **2005** (Chapter 1, ref. 8) (b) Sun, C.; Wang, Q.; Brubaker, J. D.; Wright, P. M.; Lerner, C. D.; Noson, K.; Charest, M.; Siegel, D. R.; Wang, Y.; Myers, A. G. *JACS*, **2008**, *130*, 17913-17927. (c) Peter M. Wright, Thesis Dissertation, Harvard University, **2012**. (d) Myers, A. G.; Wright, P. M.; Hecker, E. Synthesis of C5-Substituted Tetracyclines, Uses Thereof, and Intermediates Thereof. WO 2012047907 A1. October 4, 2011.

<sup>4</sup> See Chapter 1 for a discussion of the history of tetracycline discovery.

<sup>5</sup> (a) Beereboom, J. J.; Blackwood, R. K.; Rennhard, H. H.; Stephens, J. C. R. alpha-6-deoxytetracycline derivatives and process. 3,200,149, Aug. 10, 1965. (b) Villax, I.; Page, P. R.; Process for the preparation of alpha-6-deoxytetracyclines. 4,500,458, Feb. 19, 1985.



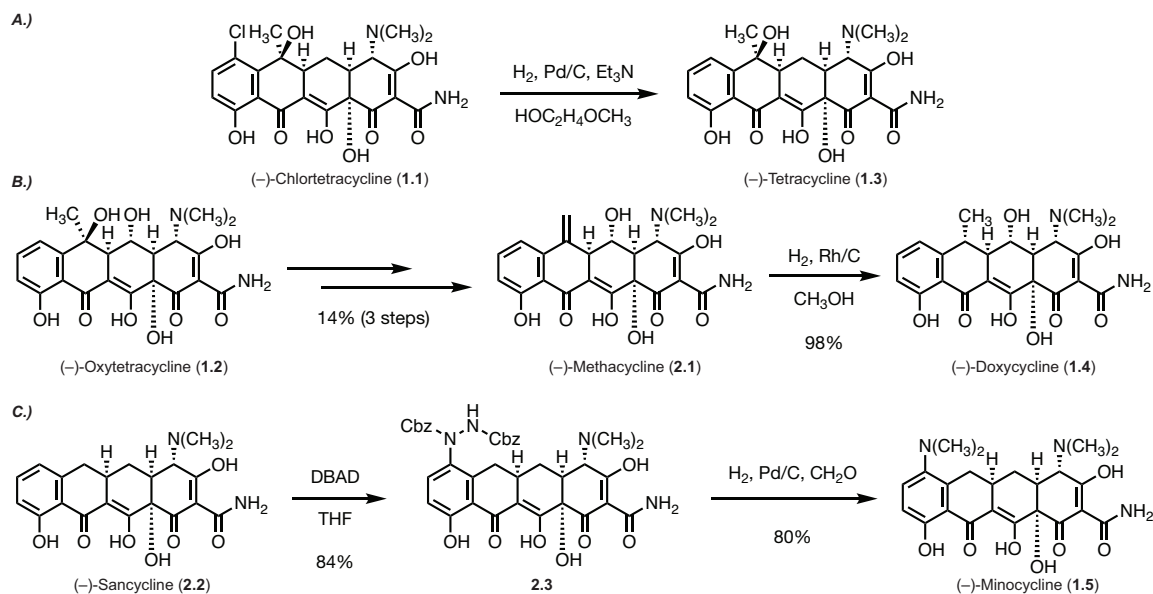


**Figure 2.1 History of Tetracycline Semisynthesis.** Semisynthesis has played an important role in the development of the tetracycline class of antibiotics. Tetracycline itself (**1.3**) was discovered first using semisynthesis (A, later isolated as a natural product). Semisynthetic transformations of the natural product oxytetracycline (**1.2**) provided methacycline (**2.1**) enroute to the popular antibacterial agent doxycycline (**1.4**) (B). The analogue sancycline (**2.2**) can also be used to access minocycline (**1.5**), another key tetracycline antibacterial agent still in use today (C).

Scientists developed a three-step sequence could be used to carry the natural product oxytetracycline (**1.2**) to the C6-alkenyl analogue methacycline (**2.1**) which, following hydrogenation over a rhodium catalyst, would provide the derivative doxycycline in high yield. Similar tactics were employed for the discovery of commonly used tetracyclines minocycline (**1.5**) and tigecycline (**1.11**) in the 1970's and 1990's, respectively. Beginning with sancycline (**2.2**), treatment with dibenzyl azidodicarboxylate provides the C7-substituted compound (**2.3**) which is converted to minocycline following a one-pot reduction/dimethylation step (Fig. 2.1C).<sup>6</sup>

<sup>6</sup> (a) Church, R. F. R.; Schaub, R. E.; Weiss, M. J. *J. Org. Chem.* **1971**, *36*, 723-725. (b) Martell, M.; Booth, J. H. *J. Med. Chem.* **1967**, *10*, 44-46. (c) Zambrano, R. T. Reductive alkylation process. 3,483,251, Dec. 9, 1969.

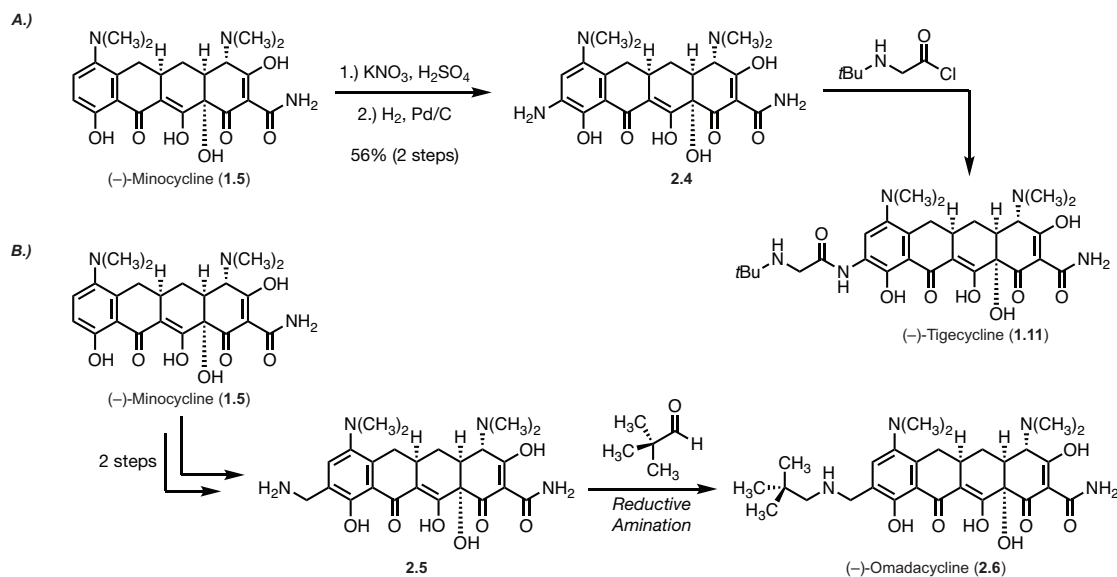


**Figure 2.2 Development of Tigecycline and Omadacycline.** The semisynthetic analogue tigecycline (**1.11**) was developed from minocycline (**1.5**) using a 3-step procedure (A). The recent tetracycline omadacycline (**2.6**) was also developed from minocycline, this time through an aminomethyl intermediate **2.5** (B).

Two decades later, researchers would develop C7, C9-disubstituted tetracyclines in the form of the so-called glycylicyclines: minocycline-type derivatives featuring amide substitution at position C9 (Fig. 2.2A).<sup>7</sup> These efforts were enabled by aromatic nitration and hydrogenation at C9 to provide an amine handle (**2.4**) for substitution with various carboxylic acids or acid chlorides, resulting in the discovery and later approval (2005) of tigecycline (**1.11**).<sup>7</sup> As evidenced by the lengthening gaps between approvals of semisynthetic tetracycline derivatives, the increasing complexity of semisynthetic transformations had slowed development of this class by the 2000s. The next semisynthetic tetracycline approved for human use would not come until 2018 with omadacycline (**2.6**, Fig. 2.2B), a novel C9-methylamino substituted minocycline derivative with a broad range

<sup>7</sup> (a) Sum, P. E.; Lee, V. J.; Testa, R. T.; Hlavka, J. J.; Ellested, G. A.; Bloom, J. D.; Gluzman, Y.; Tally, F. *P. J. Med. Chem.* **1994**, *37*, 184-188. (b) Sum, P. E.; Petersen, P.; *Bioorg. Med. Chem. Lett.* **1999**, *9*, 1459-1462.

of activity across Gram-positive and Gram-negative bacterial strains.<sup>8</sup> The rise of widespread tetracycline resistance in bacteria has also contributed to the decrease in semisynthetic tetracycline development with compounds including doxycycline and minocycline, among the most used antibacterial agents in the world, rendered ineffective against a range of pathogens.<sup>9</sup> Nevertheless, semisynthesis has served as a powerful tool for the development of novel tetracyclines and was a key element of our early efforts to generate tetracyclines with improved antiproliferative activity.

### 2.3 Key Semisynthetic Transformations: C4, C7, and C9

In order to access novel analogues of Col-3, we focused on readily available semisynthetic transformations at positions C7 and C9, as well as the lesser explored C4 position. As displayed in the development of minocycline and tigecycline, nitration and subsequent reduction at C7 and C9 has long served as an important foundation upon which novel tetracyclines could be generated (Fig. 2.2). This methodology was developed further by Nelson and colleagues at Paratek Pharmaceuticals in the early 2000's (Fig. 2.3).<sup>10</sup> Conversion of C7 or C9-amino tetracyclines to the corresponding diazonium salts (**2.7**) enabled access to a variety of alkenyl, aryl, or carbonyl substitution patterns via treatment with the corresponding alkenes/boronic acids in the presence of a palladium catalyst (Fig. 2.3B). This chemistry was tolerated by a number of tetracycline starting materials

---

<sup>8</sup> (a) Honeyman, L.; Ismail, M.; Nelson, M. L.; Bhatia, B.; Bowser, T. E.; Chen, J.; Mechide, R.; Ohemeng, K.; Verma, A. K.; Cannon, E. P.; Macone, A.; Tanaka, S. K.; Levy, S. *Antimicrob. Agents Chemother.* **2014**, *59*, 7044-7053. (b) Tanaka, S. K.; Steenbergen, J.; Villano, S. *Bioorg. Med. Chem.* **2015**, *24*, 6409-6419.

<sup>9</sup> Chopra, I.; Roberts, M. *Microbiol. Mol. Biol. Rev.* **2001**, *65*, 232-260.

<sup>10</sup> Nelson, M. L.; Ismail, M. Y.; McIntyre, L.; Bhatia, B.; Viski, P.; Hawkins, P.; Rennie, G.; Andorsky, D.; Messersmith, D.; Stapleton, K.; Dumornay, J.; Sheahan, P.; Verma, A. K.; Wachol, T.; Levy, S. B. *J. Org. Chem.* **2003**, *68*, 5838-5861.

including doxycycline, minocycline, and sancycline (**1.4**, **1.5**, or **2.2**, Fig. 2.3A). Similar chemistry could be initiated with the C7 and/or C9-iodo compounds (**2.8**, only C9-iodo shown for clarity), accessed as mixtures of mono- and di-iodinated products following treatment with *N*-iodosuccinimide (NIS) in strong acid. These iodinated intermediates were found to allow for a broader diversity of coupling partners during subsequent palladium-

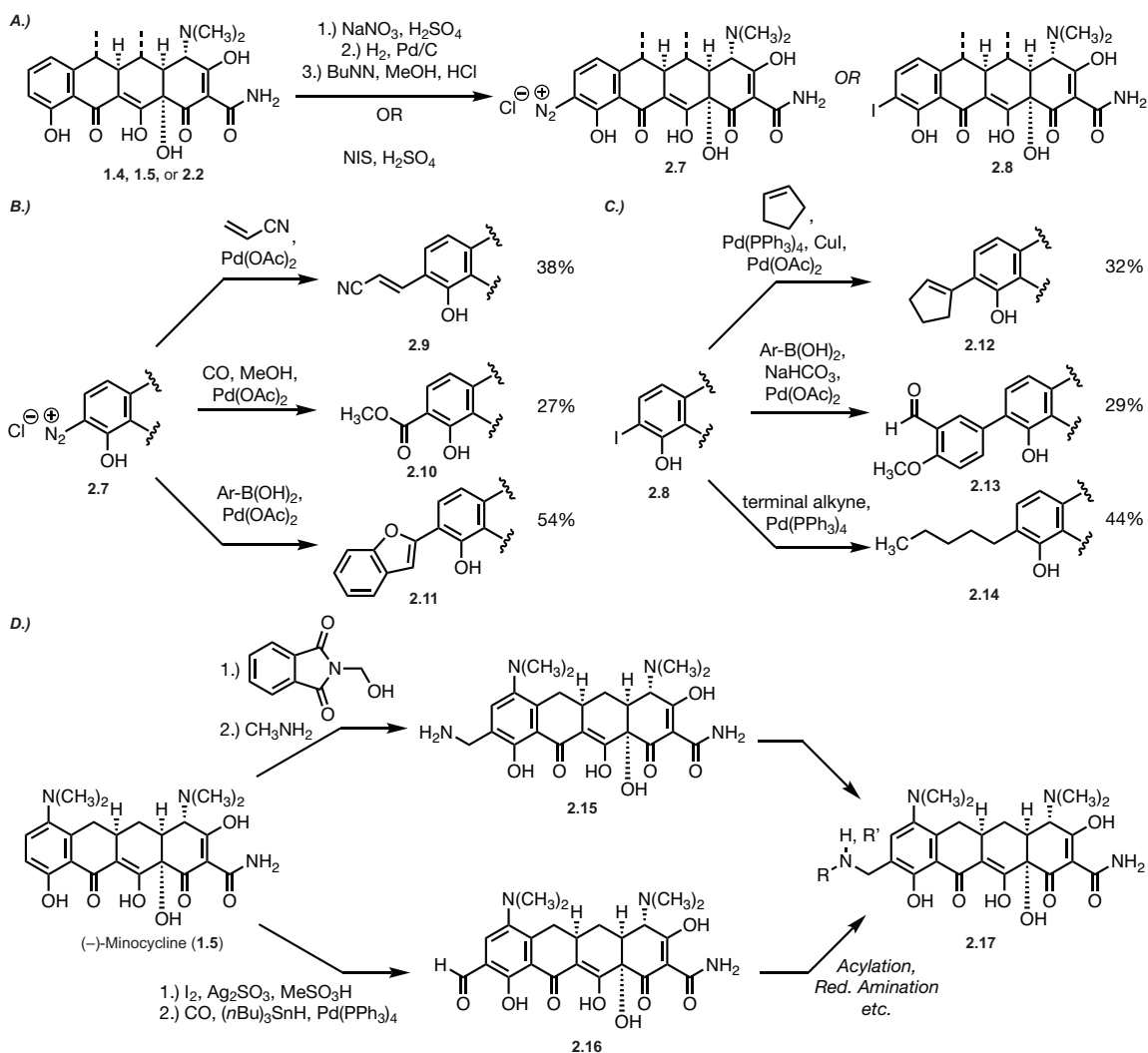


**Figure 2.3 Selection of Modern Semisynthesis Efforts: C7 and C9.** Paratek Pharmaceuticals published a range of semisynthetic transformations at positions C7 and C9. This chemistry utilizes both C7/C9-diazo (**2.7**) and iodo- species (**2.8**) (A) as starting points for palladium-catalyzed cross-coupling chemistry (B, C). Paratek also developed novel C9 substitution chemistry during their discovery and exploration of omadacycline (**2.6**) (D). Here, novel C9-methylamino analogues could be access via the methylamino compound **2.15** or the formyl intermediate **2.16**, both arriving at novel omadacycline analogues via reductive amination or acylation chemistry. Figures A and B adapted from Nelson et al., **2003** (Chapter 2, ref. 10). Yields in B correspond to the doxycycline analogue.

catalyzed cross coupling reactions (Fig. 2.3C). Novel C9 substitution semisynthesis was also on display during Paratek's development of omadacycline (Fig. 2.3D).<sup>8a</sup> Two strategies were employed to access C9-methylamino analogues: phthalimide-based amidomethylation and subsequent deprotection with methylamine (**2.15**) or iodination and organometallic cross-coupling with carbon monoxide to form the 9-formyl minocycline derivative (**2.16**) primed for functionalization via reductive amination. Both strategies enabled access to a variety of novel minocycline/omadacycline-type derivatives, many with expanded antibacterial activity (**2.17**, generic structure).

In contrast to positions along the D-ring, the C4 position on the A-ring has enjoyed only a limited amount of semisynthetic exploration. This is in part due to the increased difficulty surrounding transformations of the C4-dimethylamino group as well as the canonical wisdom holding that any modification of C4 results in complete loss of antibacterial activity.<sup>11</sup> Beginning in the 1960s, semisynthetic transformations at position C4 have covered three major areas: formation of C4-hydroxyl derivatives via a hemiacetal intermediate, generation of C4-amino analogues via an oxime or hydrazone intermediate (Fig. 2.4A), and reduction to 4-dedimethylamino analogues (Fig. 2.5). Successful transformations at C4 rely on conversion of the dimethylamino group into an effective leaving group, typically taking the form of a quaternary ammonium salt species (**2.18**, Fig. 2.4A).<sup>12</sup> For example, scientists at Pfizer discovered that treatment of the tetracycline

---

<sup>11</sup> Selected literature: (a) Mitscher, L. A. *The Chemistry of the Tetracycline Antibiotics*. Marcel Dekker, Inc: New York, 1978. (b) Nelson, M. L. *The Chemistry and Cellular Biology of the Tetracyclines. In Tetracyclines in Biology, Chemistry and Medicine*. Nelson, M., Hillen W., Greenwald, R. A., Eds.; Birkhäuser Verlag: Basel, Switzerland, 2001; 3–63. (c) Esse, R. C.; Lowery, J. A.; Tamorria, C. R.; Sieger, G. M. *J. Am. Chem. Soc.* **1964**, *86*, 3875–3877. (d) Dürkheimer, W. *Angew. Chem. Int. Ed. Engl.* **1975**, *14*, 721–774. (e) Sussman, R. J. Thesis Dissertation, Harvard University, **2015**.

<sup>12</sup> Booth, J. H.; Bonvicino, G. E.; Waller, C. W.; Petisi, J. P.; Wilkinson, R. W.; Broschard, R. B. *J. Am. Chem. Soc.* **1958**, *80*, 1654-1657.

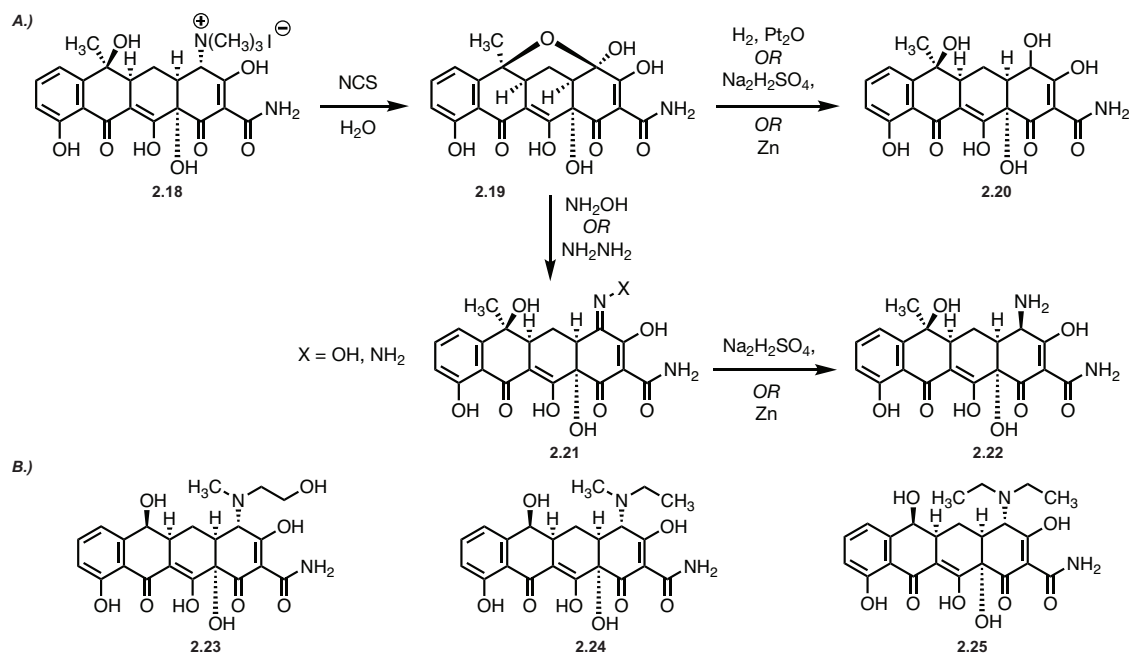


**Figure 2.4 Semisynthetic Access to C4-hydroxy and C4-amino tetracycline analogues.** C4-hydroxyl tetracycline analogues were accessed from tetracycline methiodide (**2.18**) via the C4-C6 hemiketal species **2.19** (A). This intermediate could be reduced to provide the C4-hydroxy analogue **2.20**, or could be used to form the C4-oxime/hydrazone intermediate **2.21**. C4-amino compounds (**2.22**) could then be accessed following reduction under a variety of conditions. A selection of C4-amino compounds developed at Lederle is shown in B.

methiodide salt with *N*-chlorosuccinimide (NCS) would provide the C4-C6 hemiacetal species **2.19**.<sup>13</sup> This intermediate could then be reduced using a number of conditions to provide C4-hydroxyl tetracycline derivatives (**2.20**). The hemiketal intermediate also proved useful for accessing novel C4-amino analogues. Treatment with hydroxylamine or hydrazine would provide the corresponding C4-oxime or C4-hydrazone species (**2.21**) which, following zinc-mediated reduction, provided the unsubstituted amine at C4 (**2.22**).<sup>13</sup> Despite the novelty of these transformations, these C4-hydroxyl and amino derivatives were not thoroughly explored and were given only perfunctory antibacterial evaluations, if any at all. Scientists at Lederle Laboratories would later report analogues of 6-

<sup>13</sup> (a) Blackwood, R. K.; Stephens, C. R. *J. Am. Chem. Soc.* **1964**, *86*, 2736-2727. (b) Blackwood, R. K.; Stephens, C. R. *Can. J. Chem.* **1965**, *43*, 1382-1388.

demethyltetracycline featuring novel alkylation patterns at C4, the result of reductive alkylation strategy using similar C4-amino intermediates (**2.23-2.25**, Fig. 2.4B).<sup>14</sup> Paratek Pharmaceuticals would pick up the torch in the early 2000's, reporting a variety of C4-amino substitutions accessed using similar oxime strategies (structures not shown).<sup>15</sup> After poor results in antibacterial evaluations for both companies, though, these compounds were not pursued further. It would not be until the introduction of fully synthetic capabilities that compounds featuring novel C4-amino substitutions were explored in full.<sup>16</sup>

Of most interest for our research efforts, C4-dedimethylamino analogues were accessed in a two-step sequence from a variety of tetracycline starting materials. First, treatment with iodomethane or a similar methylation reagent would provide the quaternary

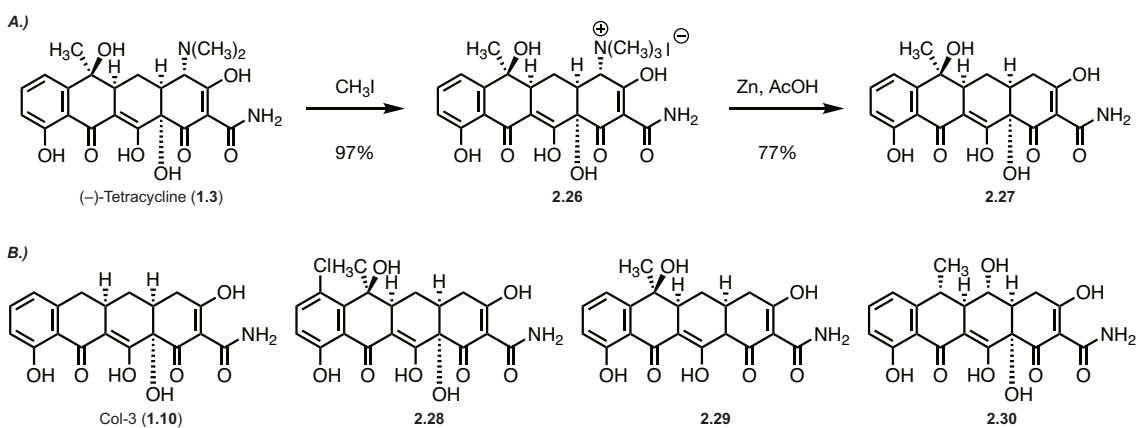


**Figure 2.5 Semisynthetic Access to C4-dedimethylamino Analogues.** Tetracyclines lacking substitution at C4 are accessed via the same methiodide species as above (**2.26**, tetracycline shown) (A). Treatment with zinc in mild acid can then provide the C4-dedimethylamino analogue (**2.27**). A selection of the so-called “chemically modified tetracyclines” (CMTs) are shown in B. These compounds display a diverse set of substitution patterns and an even broader range of utilities.

<sup>14</sup> (a) McCormick, J. R. D.; Sjolander, N. O.; Hirsch, U.; Jensen, E. R.; Doerschuk, A. P. *J. Am. Chem. Soc.* **1957**, *79*, 4561-4563. (b) Esse, R. C.; Lowery, J. A.; Tamorria, C. R.; Sieger, G. M. *J. Am. Chem. Soc.* **1964**, *86*, 3874-3875. (c) Esse, R. C.; Lowery, J. A.; Tamorria, C. R.; Sieger, G. M. *J. Am. Chem. Soc.* **1964**, *86*, 3875-3877.

<sup>15</sup> Berniac, J.; Bhatia, B.; Grier, M.; Nelson, M. L.; Pan, J.; 4-Aminotetracyclines and Methods of Use Thereof. WO 2006047671 A2. October 25, 2005.

<sup>16</sup> See Chapter 3 for discussion on fully synthetic approaches to C4-amino-modified tetracyclines.

ammonium salt **2.26** which, upon treatment with zinc metal in acetic acid, would provide the reduction product **2.27** in decent yield (Fig. 2.5A).<sup>12</sup> C4-dedimethylamino tetracyclines make up the majority of the so-called chemically modified tetracyclines (CMTs, Fig. 2.5B, selected examples).<sup>17</sup> These compounds were evaluated in the early stages of tetracycline semisynthesis but, after poor results, were not pursued much further. CMTs have enjoyed a tepid resurgence in recent years, however, spurred primarily by interest in the non-canonical effects observed for compounds like Col-3 (**1.10**, Fig. 2.5B) and doxycycline (**1.4**), including potential roles as collagenase inhibitors and anti-inflammatory therapeutics.<sup>18</sup> One major study in this area was reported by Abato and colleagues at Paratek Pharmaceuticals in 2010, wherein a range of C4-dedimethylamino analogues of several tetracyclines were evaluated for therapeutic effects in treating rheumatoid arthritis (Fig. 2.6).<sup>19</sup> In addition to providing updated experimental procedures for accessing 4-dedimethylamino analogues of minocycline, doxycycline, and other tetracyclines, Paratek reported an eclectic selection of C7- and C9-substituted “Col-3” analogues using methodology similar to that of Nelson and colleagues in the early 2000’s (Fig. 2.6A, also, *vide supra*). This included Stille and Suzuki-type organometallic coupling reactions, heterocycle synthesis, and C10-dehydroxylation chemistry via a triflate intermediate (**2.33-2.38**, Fig. 2.6B).<sup>20</sup>

---

<sup>17</sup> (a) Gaur, S.; Agnihotri, R. *Indian J. Pharmacol.* **2012**, *44*, 161-167. (b) See Hlavka et al., **1985** (Chapter 2, ref. 2).

<sup>18</sup> See Chapter 1 for discussion of the biological activity of Col-3 and similar analogues.

<sup>19</sup> Abato, P.; Bowser, T.; Higgins, P.; Verma, A. K.; Zhang-Hoover, J. Tetracycline compounds for the treatment of rheumatoid arthritis and related methods of treatment. WO 2010/033939, Mar. 25, 2010.

<sup>20</sup> Kurti, L.; Czako, B. *Strategic Applications of Named Reactions in Organic Synthesis*. Elsevier, Inc.: Amsterdam, 2005.



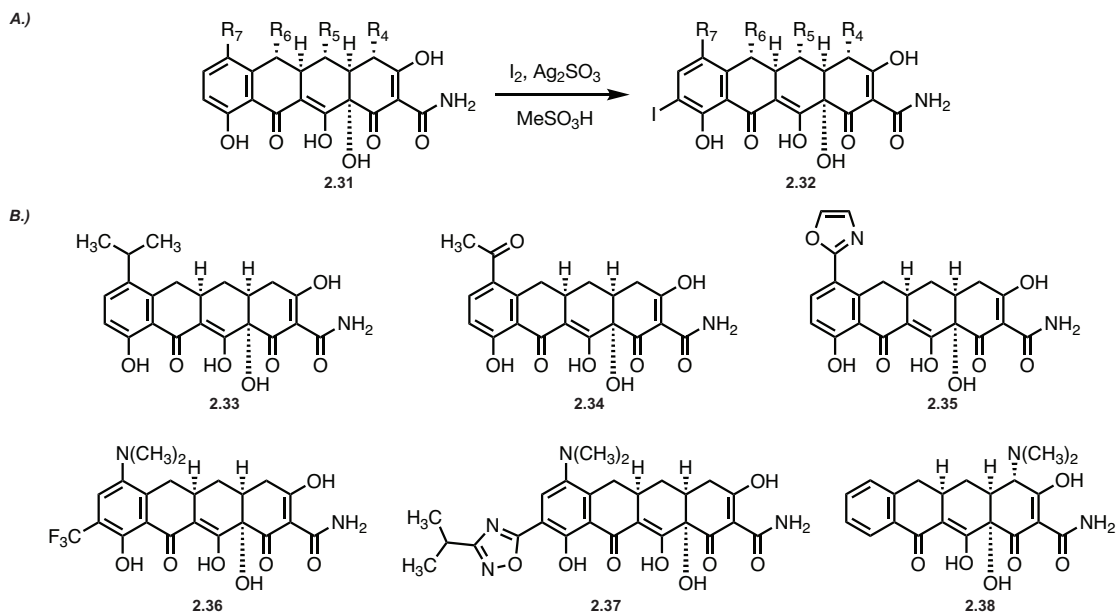


**Figure 2.6 C4-dedimethylamino Compound Development, Paratek Pharmaceuticals.** Paratek Pharmaceuticals utilized their semisynthetic development experience to generate a range of C4-dedimethylamino tetracycline analogues. This was accomplished primarily through C7/C9-iodination chemistry (**2.32**, only C9 shown for clarity) followed by organometallic cross-coupling chemistry (A). A selection of analogues is shown in B. Figure adapted from Abato et al., **2010** (Chapter 2, ref. 19). Numbered R-groups in A refer to standard tetracycline substitution patterns (doxycycline, minocycline, etc.).

In short, the rich history of tetracycline semisynthesis provided us with an enormous repository of chemical transformations and potential analogues of Col-3 accessible for evaluation as antiproliferative agents.

## 2.4 Strategy

At the outset, we were confident in our ability to leverage the history of tetracycline semisynthesis to access a structurally diverse set of Col-3 analogues. Unfortunately, despite the wealth of reported antibacterial activities for tetracycline derivatives, little to no information concerning the antiproliferative activity of these analogues had been published. We therefore began these efforts with a collection of structure-activity relationship data that consisted of the parent compound, Col-3 (**1.10**), and two probe compounds employed in photo-affinity labeling experiments, the active and inactive

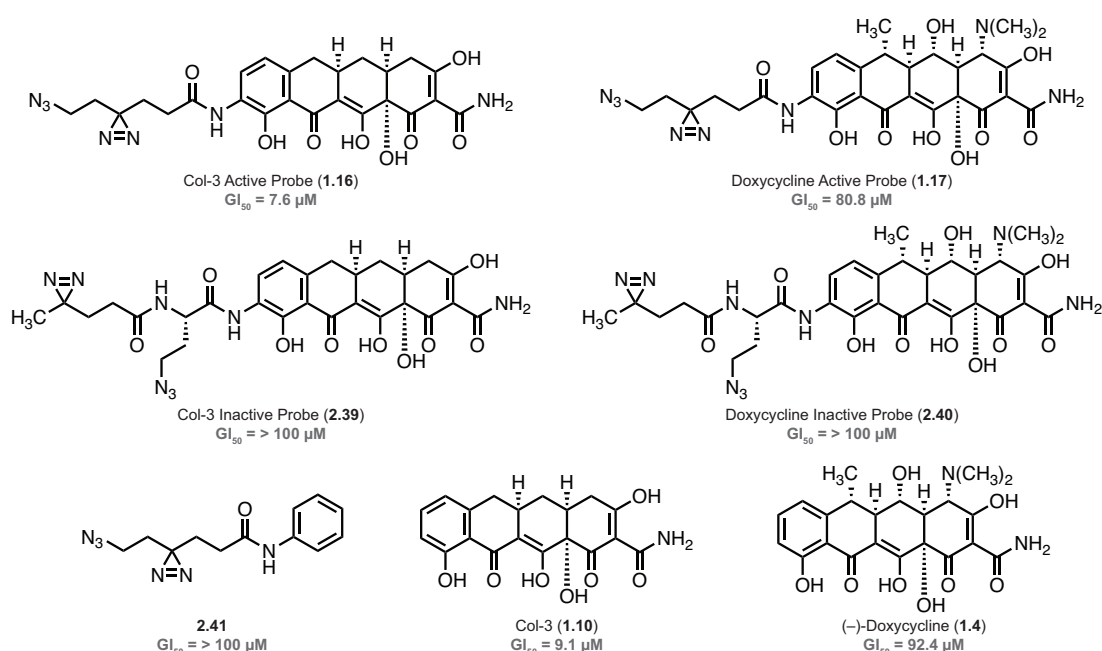


**Figure 2.7 Tetracycline Photoaffinity Labeling Probe Compounds.** Mortison synthesized a variety of probe compounds for use in photoaffinity labeling experiments. Interestingly, Mortison found that certain arrangements of the bifunctional handle (**2.39**, **2.40**) displayed a total loss of activity. Early in our compound development efforts, we used the “active” probe compounds (**1.16**, **1.17**) as starting points for novel Col-3 analogues. GI<sub>50</sub> values obtained in A375 melanoma cells. Figure adapted from Mortison et al., **2018** (Chapter 1, ref. 26).

diazirine/azide probes (Fig. 2.7). Interestingly, Mortison and colleagues reported a small improvement in the activity of the active probe with a GI<sub>50</sub> of 7.6 μM compared to 9.1 μM for Col-3 (**1.16**, Fig. 2.7). Further, the inactive probe showed no activity up to 100 μM in A375 melanoma cells. These data appear to show a strong dependence on substitution at C9 of the tetracycline core, specifically concerning structural elements that feature branching or hydrogen bond-capable motifs. We hypothesized that substitution at C9 with a hydrogen bond donor or acceptor spaced four or five carbon atoms from the tetracycline core and avoiding large, branched elements could yield improvements in activity. We reasoned these short side chains could be obtained from commercial sources or rapidly synthesized and coupled to the tetracycline core through a variety of chemistries (Fig. 2.8A). As discussed in the preceding sections, the C7 and C9 positions can be rapidly

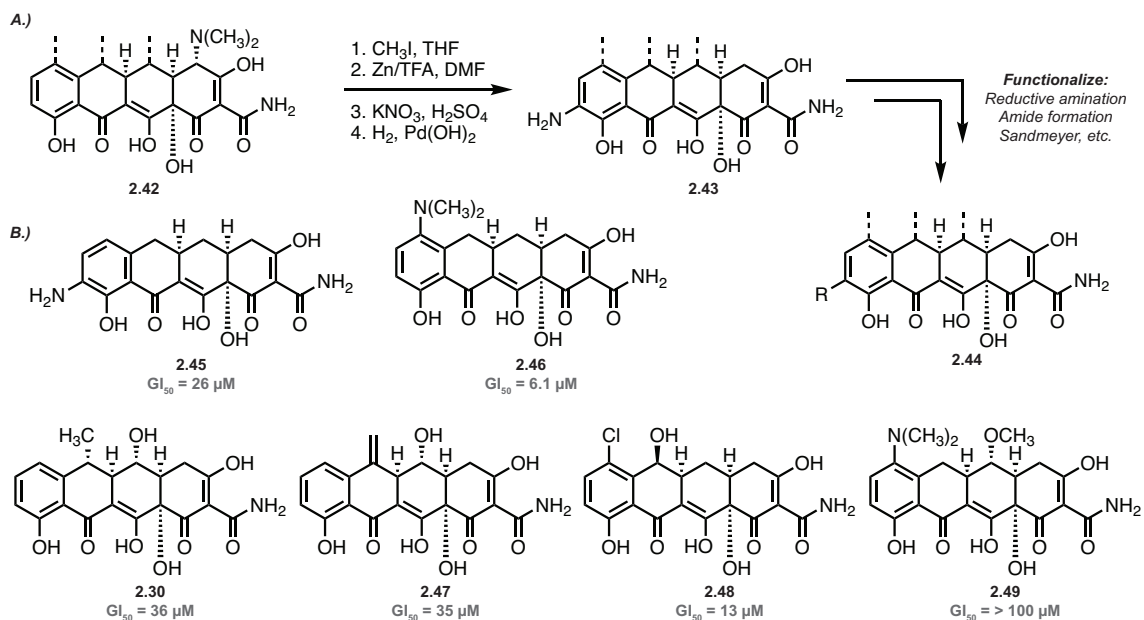


**Figure 2.8 Compound Development Strategy and 4-dedimethylaminotetracyclines.** We envisioned 4-dedimethylamino tetracycline analogues (**2.44**) could be accessed from the tetracycline starting material via the C9-amino intermediate (**2.43**) (A). **2.43** could then be derivatized using reductive amination, amide bond formation, Sandmeyer chemistry, or a variety of other reaction schemes. A rapid screen of 4-dedimethylamino analogues of common tetracyclines (B) showed **2.46** retaining modest potency compared to analogues of doxycycline (**2.30**), methacycline (**2.47**) or other tetracyclines. GI<sub>50</sub> values obtained in K562 leukemia cells.

functionalized with amino groups (**2.43**, only C9-amino shown for clarity) for reductive amination or amide bond formation reactions, or with iodide or diazonium functionalities for organometallic cross coupling reactions. Our options for substitution patterns along the remainder of the tetracycline northern half, C5 through C6, were limited by the availability of tetracycline starting materials. Due to the variance in ribosomal binding behavior between Col-3 and doxycycline, we decided to focus on tetracycline starting materials lacking substitution at C5 and C6 for our initial synthesis efforts. This decision was supported by results from a rapid screen of tetracycline cores showing that compounds like 4-dedimethylamino-doxycycline (**2.30**) and 4-dedimethylamino-demeclocycline (**2.48**) display poor activity in K562 leukemia cells (Fig. 2.8B). The activity of 4-dedimethylamino-minocycline (**2.43**) is essentially equipotent compared to Col-3, our

initial synthesis efforts focused on these compounds for the potential increase in solubility availability of starting materials. In total, this strategy enabled us to generate a range of analogs and further explore the structure-activity relationship surrounding tetracycline antiproliferative activity.

## 2.5 Early Compound Development Efforts

Initially, we utilized a wide range of chemistries to access tetracycline analogues for derivatization and testing. We quickly determined, however, that compounds featuring amide substitution from C9 were displaying exciting improvements in antiproliferative activity and this class of compounds became our primary focus (Fig. 2.9). These analogues were accessed in a two-step sequence from the tetracycline starting material. First, the free-base tetracycline was treated with excess iodomethane at 45 °C overnight to provide the quaternized methiodide salt product and was taken directly to the zinc-mediated reduction step. We performed a series of minor modifications to the reduction procedure developed by Abato and colleagues to enable access to the C4-reduction products of sancycline (**2.2**) and minocycline (**1.5**) in ~60% yield.<sup>21</sup> Briefly, this procedure involves the addition of 1.3 eq. zinc dust in six small portions at 0 °C over the first 2.5 hours of reaction time. The reaction was typically deemed complete after an additional 1 to 1.5 hours at 0 °C, with the portion-wise addition suppressing the formation of many of the side/decomposition products obtained using the procedure of Mortison and colleagues.<sup>22</sup> Amino analogues were then accessed following a nitration/reduction procedure. Here, treatment with

---

<sup>21</sup> See Abato et al., **2010** (Chapter 2, ref. 18).

<sup>22</sup> See Mortison et al., **2018** (Chapter 1, ref. 26).

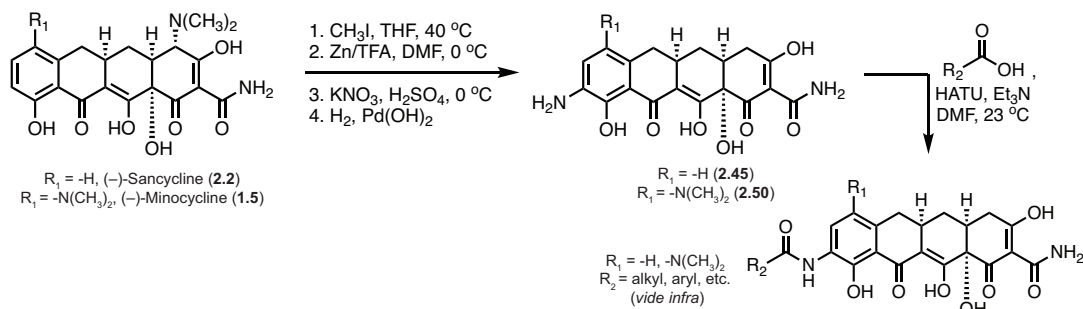


**Figure 2.9** Access to Amide Analogues of Col-3 and 4-dedimethylaminomincycline. Synthetic scheme, as described in Fig. 2.8, that enables access to novel C9-amide analogues of Col-3 and **2.50**. See subsequent figures for specific analogues.

potassium nitrate in strong acid at low temperature would provide the C7/C9-nitro product which was subsequently reduced upon treatment with hydrogen over a palladium hydroxide on carbon catalyst. When sancycline was used as the starting material the nitration/reduction procedure would provide a mixture of C9- and C7-amino products, with C9-amino being the major isomer isolated after purification.<sup>22</sup> Finally, analogues were prepared through standard amide bond formation chemistry with carboxylic acid functional side chains. The tetracycline and carboxylic acid were combined with a peptide coupling agent (ex. HATU) and a weak amine base (Diisopropylethylamine, DIPEA, or triethylamine, TEA) in DMF and stirred at 23 °C for 1-2 hours.<sup>22</sup> Reactions were monitored using analytical LC/MS and, upon completion, the reaction mixture was purified using reverse-phase preparatory HPLC.

A selection of early analogues generated using the above sequence with commercially available acids as well as GI<sub>50</sub> values obtained in K562 leukemia cells is shown in Figure 2.10. We began with a selection of aliphatic compounds such as **2.51**, **2.52**, and **2.55**, containing both linear and branched bonding patterns. We also assessed a variety of different heterocycle substituted compounds including the nicotinic acid

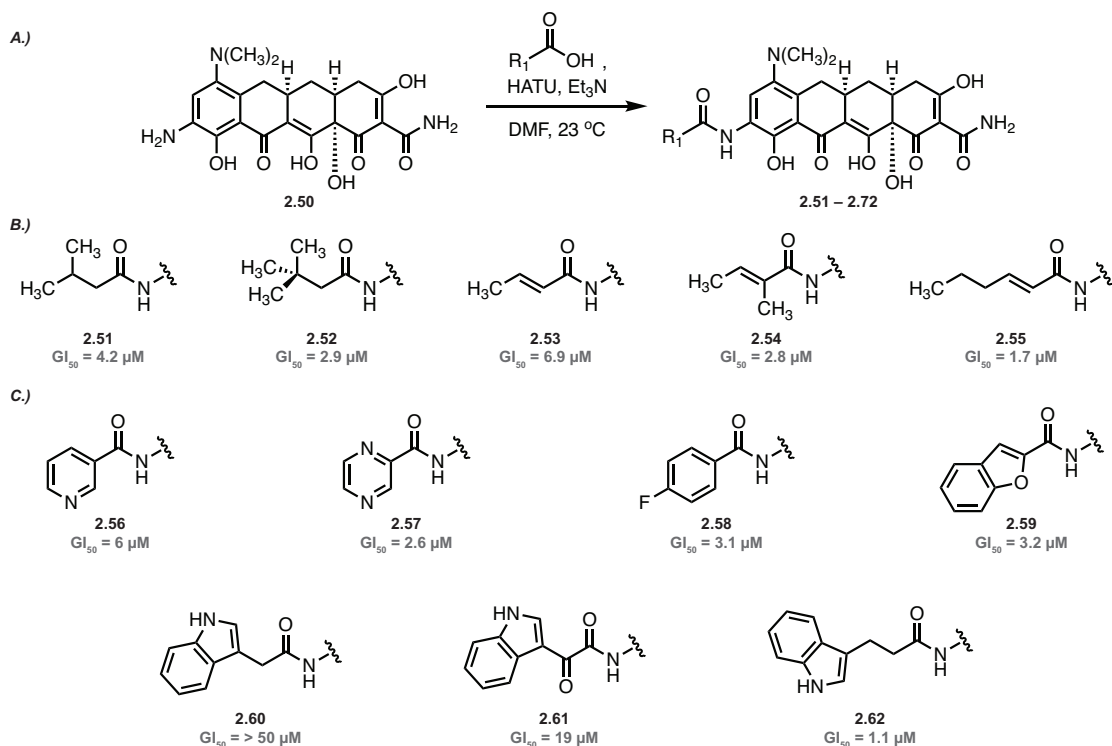


**Figure 2.10 Selected Amide Analogues of Col-3.** A selection of amide analogues of Col-3 are shown in B and C. Novel compounds included alkyl analogues (**2.51** to **2.55**) as well as heterocyclic analogues (**2.56** to **2.62**). Some analogues showed improved activity over the parent compound Col-3 ( $GI_{50} = 9.1 \mu\text{M}$ ).  $GI_{50}$  values obtained in K562 leukemia cells.

analogue **2.56** and the 4-fluorobenzoic acid derivative **2.58**. In a pleasant corroboration of our initial hydrogen bonding/spacer hypothesis, we identified some minor improvements with indole analogue **2.62**, and in the activities of acrylic acid analogues in Figure 2.11, with the initial pyridine analogues **2.69** and **2.70** being the most interesting. Further exploration along this line would identify a quinoline acrylic acid compound, **2.72**, with significantly improved activity over the parent compounds.

The quinoline-substituted analogue, as well as handful of similar pyridine-substituted compounds, were synthesized using the Doebner modification of the Knoevenagel condensation for malonic acid condensation/decarboxylation reactions.<sup>23</sup>

<sup>23</sup> Procedures adapted from: (a) Bian, L.; Cao, S.; Cheng, L.; Nakazaki, A.; Nishikawa, T.; Qi, J. *ChemMedChem* **2018**, *13*, 1972-1977. (b) Ahmed, S. T.; Parmeggiani, F.; Weise, N. J.; Flitsch, S. L.; Turner, N. J. *Org. Lett.* **2016**, *18*, 5468-5471.

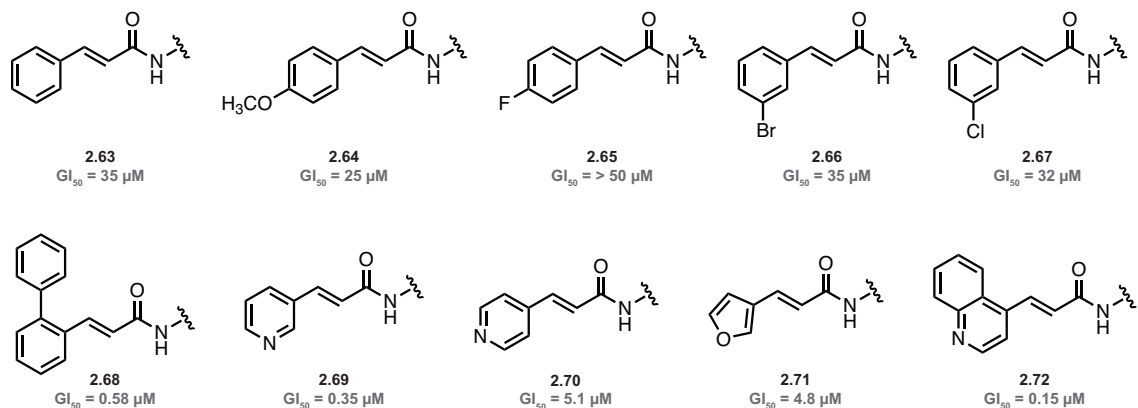


**Figure 2.11 Selected Amide Analogues of Col-3.** A selection of amide analogues of Col-3 featuring heteroaryl groups appended to acrylic acid moieties (**2.63** to **2.72**). Many of these compounds showed improved activity compared to the parent compound, with quinoline analogue **2.72** displaying exceptional potency. Analogues synthesized according to the scheme in Fig. 2.10A.  $GI_{50}$  values obtained in K562 leukemia cells.

Analogue **2.72** displayed activity in the 150 nM range in K562 leukemia cells compared to the 9.1  $\mu\text{M}$   $GI_{50}$  observed for Col-3. A more detailed evaluation of the potency of this analogue revealed increased activity across a range of cancers, including A375 melanoma, HCT116 colorectal, and RPMI-8226 leukemia cell lines (Fig. 2.12B), providing us with our first true hit compound for further exploration.

## 2.6 Exploration of a Novel Quinoline Analogue

Encouraged by these results, we sought to further explore the structure-activity relationship surrounding the quinoline acrylamide appendage by 1.) identifying

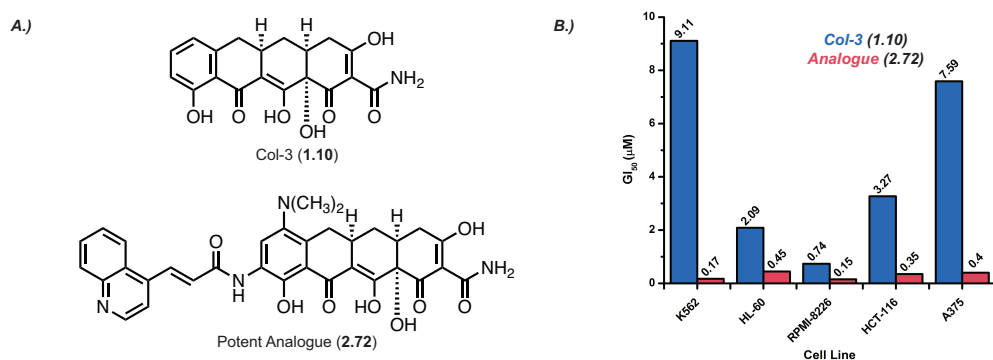


**Figure 2.12 Col-3 and a Potent Analogue.** Parent compound Col-3 (**1.10**) and a novel quinoline analogue (**2.72**) (A). Analogue **2.72** was found to have improved activity across a range of cancer cell lines (B).

components of the structure of **2.72** required for potent activity and 2.) evaluating novel quinoline derivatives to further improve antiproliferative activity.

We began these efforts by pinpointing structural elements of analogue **2.72** that could contribute to the observed increase in antiproliferative effects, including quinoline nitrogen atom, acrylamide alkene, and C7-dimethylamino group. First, we generated analogs with variation in the acrylamide alkene using palladium-catalyzed hydrogenation and Corey-Chaykovsky cyclopropanation reaction conditions to provide the aliphatic (**2.73**) and cyclopropane (**2.74**, mixture of diastereomers) derivatives, respectively (Fig. 2.13).<sup>24</sup> Interestingly, removal of this potential Michael acceptor resulted in moderate loss of activity. However, these compounds remained considerably more potent than the parent compound, Col-3 (GI<sub>50</sub> K562 9.1 μM). We then synthesized a naphthalene derivative **2.75** which lacked the quinoline nitrogen atom of the potent analogue as well as “Col-3” analogue **2.77** lacking a C7-dimethylamino group, both of which also demonstrated

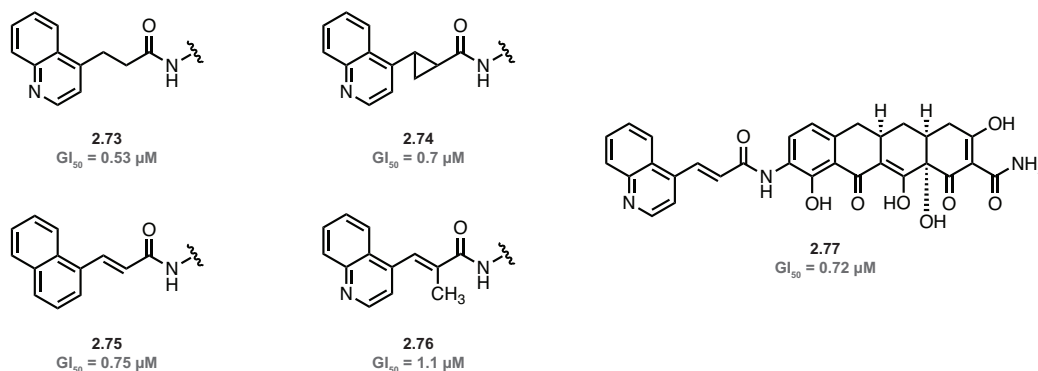


**Figure 2.13 Key Features of Novel Quinoline Analogue 2.76.** We synthesized a handful of analogues of compound **2.74** in an effort to identify key features of this novel scaffold that are contributing to activity. Removal of the alkene in **2.75** or **2.76** resulted in slight loss of activity, as did removal of the C7-dimethylamino group and quinoline nitrogen atom in **2.79** and **2.77**, respectively. The biggest effect on activity was the presence of the methyl group in analogue **2.78**. GI<sub>50</sub> values obtained in K562 leukemia cells.

<sup>24</sup> Corey-Chaykovsky cyclopropanation conditions adapted from: Tadashi, I.; Shuzo, W.; Tatsuya, Y.; Yoshimasa, A.; Mikio, M.; Kaoru, S. Aryl Substituted Carboxamide Derivatives as Calcium or Sodium Channel Blockers. WO 2010137351 A1, May 31, 2010.



moderate loss of activity.<sup>25</sup> The variant that incited the greatest disruption in activity was the methacrylate derivative **2.76**, with a recorded GI<sub>50</sub> near 1  $\mu$ M in K562 leukemia cells. While none of the individual structural elements evaluated in these efforts were found to be critical for activity of analogue **2.72**, we developed a series of broad conclusions regarding the structure-activity relationship at work. The acrylamide alkene does not appear to be acting as a Michael acceptor, as removal of this element does not completely abolish activity. In fact, substitution along the alkene region can have a detrimental effect, as observed in the methacrylate derivative **2.76**. One hypothesis is that the quinoline moiety is participating in a pi-stacking interaction with nearby rRNA nucleotide residues, thus explaining the lack of total reliance on the nitrogen atom. Solubility also appeared as an important factor, with the less potent Col-3 analogue **2.77** showing a decrease in solubility over the parent analogue. Overall, our early efforts to elucidate the structure-activity relationship of potent analogue **2.72** provided critical data and informed future analogue development efforts.

With a general notion of the rules governing the potent activity of **2.72**, we sought to further explore the structure-activity relationship of the quinoline moiety. To generate novel quinoline acids with a range of substitution patterns, we developed a short synthetic route to allow for access to quinoline-acrylic acids from either commercially available quinoline compounds or aniline precursors (Fig. 2.14).<sup>26</sup> Briefly, aniline derivatives were

---

<sup>25</sup> Analogue **2.77** was accessed from 9-amino-Col-3 (**2.45**). See Mortison et al., **2018** (Chapter 1, ref. 26) for synthetic procedures.

<sup>26</sup> Cyclization procedure adapted from: (a) Rotzoll, S.; Reinke, H.; Fischer, C.; Langer, P. *Synthesis* **2009**, *1*, 69-78. (b) Hubschwerlen, C.; Rueedi, G.; Surivet, J.-P.; Zumbunn-Acklin, C. 3-Amino-6-(1-Amino-Ethyl)-Tetrahydropyran Derivatives. WO 2008/15206 A1. June 13, 2008. (c) Baati, R.; Brown, R. C. D.; Dias, J.; Nachon, F.; De Sousa, J. Broad Spectrum Reactivators of OPNA-Inhibition of Human Cholinesterases. WO 2017021319 A1. July 29, 2016.

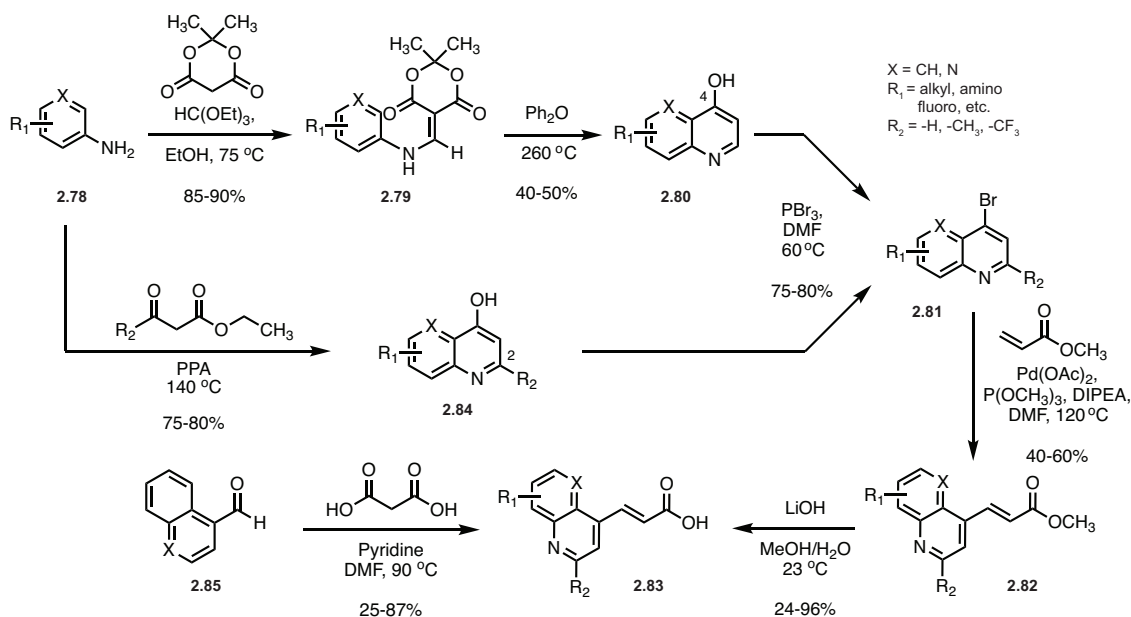


**Figure 2.14 Synthesis of Novel Quinoline Acrylic Acid Compounds.** We developed a series of synthetic routes from the chemical literature which enabled access to novel quinoline acrylic compounds from a variety of starting materials. Substituted anilines (**2.78**, generic structure) could be used to access quinoline compounds with substitution along the “upper” ring system (**2.80**) or “lower” ring system (**2.84**). Acids could also be accessed directly from aldehyde functional quinolines (**2.85**) in one step. PPA = polyphosphoric acid.

first condensed with Meldrum’s acid and triethylorthoformate to provide the adduct **2.79** (general structures shown), typically in high yield. The crude condensation product was then cyclized to the 4-hydroxyquinoline derivative (**2.80**) after brief exposure to high temperature. Treatment with phosphorus tribromide, followed by a Heck reaction and saponification were accomplished using standard conditions and allowed for rapid access to quinoline acid structures with substitution along the “upper” ring system (**2.83**).<sup>27, 28, 29</sup> For analogues with substitution at position 2, we treated various anilines with ethyl

<sup>27</sup> Bromination procedure adapted from: (a) See Hubschwerlen et al., **2008** (Chapter 2, ref. 26b). (b) See Baati et al., **2016** (Chapter 2, ref. 26c).

<sup>28</sup> Heck reaction conditions adapted from Kwok, T. J.; Virgilio, J. A. *Org. Process Res. Dev.* **2005**, *9*, 694-696.

<sup>29</sup> Saponification procedure adapted from Rodriguez, J. G.; Benito, Y. *J. Heterocyclic Chem.* **1988**, *25*, 819-821.

acetoacetate derivatives in polyphosphoric acid at high temperature to access 4-hydroxyquinoline derivatives (**2.84**) via a one-pot condensation/cyclization cascade.<sup>30</sup> In addition, commercially-available brominated quinolines or aldehyde-functional quinolines (**2.85**) could be converted to the desired acid using the Heck/saponification sequence or Knoevenagel conditions, respectively.<sup>23</sup> In combination, these routes allowed for access to a selection novel quinoline acids that were coupled to the tetracycline core and evaluated in cancer cells.

A summary of our quinoline synthesis efforts and resulting antiproliferative activities is shown in Figure 2.15. We accessed quinoline analogues with a variety of substitution patterns, including fluoro- (**2.86**), methoxy- (**2.93**), and amino- (**2.94**) derivatives along with non-polar methyl (**2.88**) or *tert*-butyl (**2.90**) appendages.

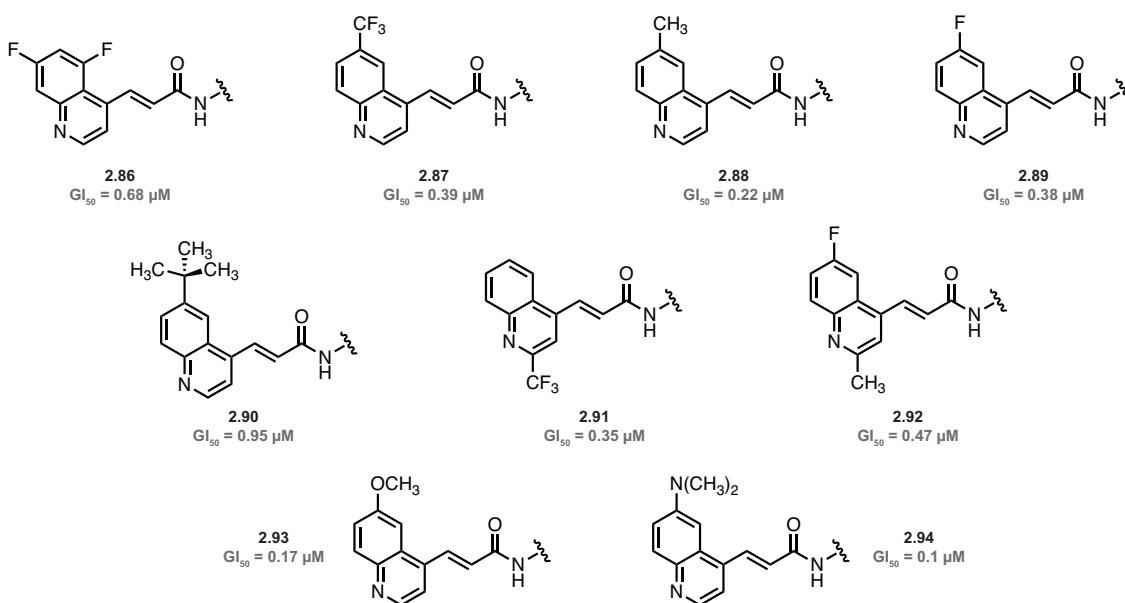


**Figure 2.15 Col-3 Analogues Featuring Novel Quinoline Substitution.** A selection of quinoline analogues synthesized using the schemes in Fig. 2.14, are shown. Novel quinoline acrylic acid compounds were appended to 9-amino-4-dedimethylaminocycline (**2.50**) using amide formation chemistry shown in Fig. 2.10A.  $GI_{50}$  values obtained in K562 leukemia cells.

<sup>30</sup> Cyclization procedure adapted from Xia, C.-L.; Wang, N.; Guo, Q.-L.; Liu, Z.-Q.; Wu, J.Q.; Huang, S.-L.; Ou, T.-M.; Tan, J.-H.; Wang, H.-G.; Li, D.; Huang, Z.-S. *Eur. J. Med. Chem.* **2017**, *130*, 139-153. The resulting 4-hydroxyquinoline products were then carried through the above-mentioned sequence.

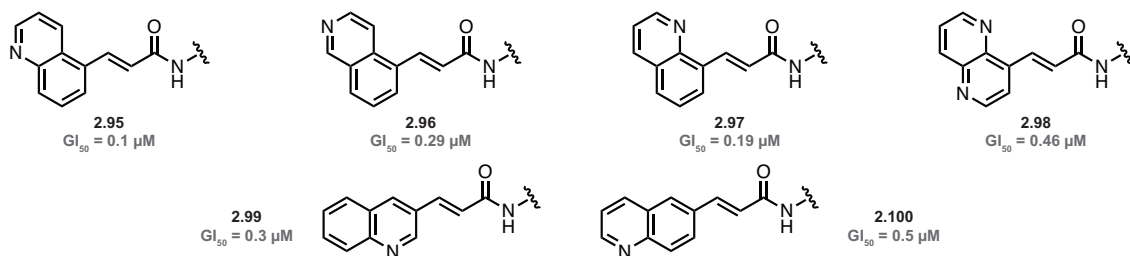


**Figure 2.16 Col-3 Analogues Featuring Novel Quinoline Substitution (cont.).** A selection of quinoline analogues featuring variation in the position of the quinoline nitrogen atom and the orientation of the ring system. Most analogues maintain the majority of the activity observed for analogue **2.72**. Analogues were synthesized using the schemes presented in Figs. 2.10A and 2.14.  $GI_{50}$  values obtained in K562 leukemia cells.

Unfortunately, we did not identify any substituents that garnered significantly improved activity. Compounds featuring polar groups (**2.93**, **2.94**) were often roughly equipotent/possessed slightly improved activity compared to **2.72**, while the fluorinated and hydrocarbon analogues displayed slight loss of activity. Using a variety of commercially available brominated quinolines, we briefly studied the impact of the position of the nitrogen atom around the quinoline scaffold (Fig. 2.16). Interestingly, these analogues all maintained the vast majority of their antiproliferative activity, suggesting the location of this nitrogen in the ring system is not critical.

We identified two analogs, **2.93** and **2.94**, that displayed activity on par with or slightly better than the parent compound. Given the polar nature of the methoxy- and dimethylamino- groups, we hypothesize these increases in activity could be due to improvements in compound solubility similar to that observed with the parent compound and analogue **2.77** (Fig. 2.13). While these potencies were exciting, the lack of major improvement over the parent compound signaled a larger change in direction may be needed to improve activity and better understand cellular effects of these compounds.

## 2.7 Initial Biological Testing and Pathway Elucidation

With our semisynthetic analogue development no longer providing major improvements in activity, we sought to compare the cellular effects of Col-3 and novel analogue **2.72** to try and identify the origins of the improved antiproliferative effects. We pursued this goal first by analyzing signaling pathway activation, including downstream transcription factors and dependence on the integrated stress response (ISR), and then by analysis of translation inhibition.

In their studies, Mortison and colleagues identified the ISR as the primary stress signaling pathway activated upon treatment with tetracyclines.<sup>31</sup> The ISR is comprised of a series of four kinases, PERK, PKR, HRI, and GCN2, which collect a variety of cellular stress signals and transfer them to the phosphorylation of eukaryotic initiation factor 2 (eIF2), triggering a decrease in the rate of translation initiation.<sup>32</sup> This phosphorylation event also triggers activation of the master cell stress regulator ATF4, which controls a range of cell salvage or cell death pathways. In the context of tetracycline-mediated activation of cellular stress, the roles of the various kinases involved in signaling remain a target of current research. However, we can probe induction of ATF4 as a measure of signaling activity using western standard immunoblotting techniques. We analyzed activation of ATF4 upon treatment with Col-3 and analogue **2.72** (Fig. 2.17A).<sup>33</sup> We observed dose-dependent activation of ATF4 in both cases, with analogue **2.72** inducing

---

<sup>31</sup> See Mortison et al., **2018** (Chapter 1, ref. 26).

<sup>32</sup> See Chapter 4 for a discussion of the mechanism of translation in eukaryotes.

<sup>33</sup> Western immunoblot analysis conducted in conjunction with Dr. Linfeng Chen and Kamar Reda in the Myers group.

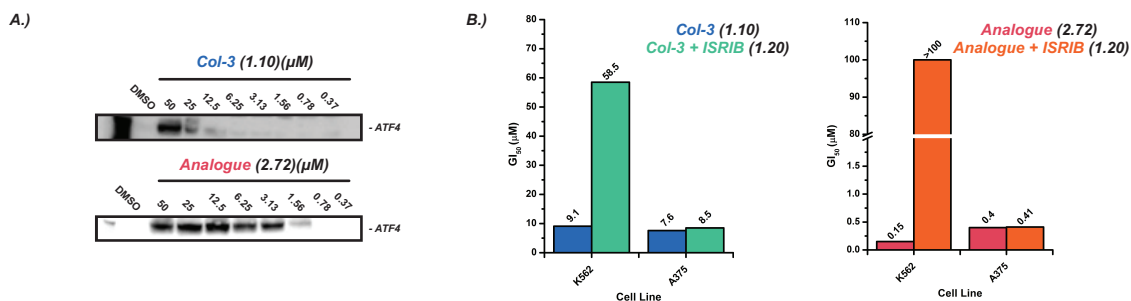


**Figure 2.17 Signaling Pathway Dependence.** Our efforts to better understand the activity of novel quinoline analogue **2.72** focused initially on signaling pathway activation. Western immunoblotting showed analogue **2.72** inducing activation of ATF4 at a far lower concentration than Col-3 (**1.10**) (A). We observe similar patterns of ISR dependence between Col-3 and analogue **2.72**, with both compounds losing the majority of their activity in the K562 leukemia cell line upon ISRIB co-dose. However, the majority of other cell lines maintain similar potencies. Western blot experiments performed with Dr. Linfeng Chen and Kamar Reda in K562 leukemia cells.

activation at  $\sim 3 \mu\text{M}$  concentration and Col-3 at  $25 \mu\text{M}$ . This early finding suggested the increased potency of analogue **2.72** may be due to more effective activation of the ISR. We pursued this hypothesis by exploring the dependence of **2.72**'s potency on ISR activation through co-dosing with ISR-reversal agent ISRIB.<sup>34</sup> Through its binding of the guanine nucleotide exchange factor eIF2B, ISRIB renders phosphorylation of eIF2 an ineffective pathway for reduction of translational loading. On an experimental level, this enables us to disentangle growth inhibitory effects caused by ISR activation from those caused by ribosome-binding induced translation inhibition. When co-dosed with 50 nM ISRIB, Col-3 undergoes a slight loss of growth inhibitory activity in most cell lines (Fig. 2.17B).<sup>35</sup> We observe similar effects for analogue **2.72**, with the  $\text{GI}_{50}$  for A375 melanoma cells shifting only slightly upon ISRIB co-dose. Interestingly, the K562 leukemia cell line shows strong dependence on ISR activation, as the  $\text{GI}_{50}$  of Col-3 drops from  $9 \mu\text{M}$  to nearly  $60 \mu\text{M}$  and the  $\text{GI}_{50}$  of analogue **2.72** from  $0.15 \mu\text{M}$  to greater than  $100 \mu\text{M}$ . This suggests that, in the

<sup>34</sup> See Chapter 1 for a discussion of the mechanism and utility of the small molecule ISRIB.

<sup>35</sup> See Chapter 1 for a discussion of ISRIB and its effects of tetracycline  $\text{GI}_{50}$  values. (b) See Mortison et al., **2018** (Chapter 1, ref. 26).

K562 cell line, activation of the ISR is a critical mechanism through which growth inhibition and cell death signals are communicated.

We then set out to characterize the translation inhibitory effects of analogue **2.72** using an OPP incorporation assay.<sup>36</sup> This assay is founded on the measurement of a fluorescent signal obtained after *in vitro* incorporation and labeling of a puromycin analogue in nascent peptide chains during translation. In A375 melanoma cells, we observe potent, dose-dependent inhibition of translation for both Col-3 and analogue **2.72** (Fig. 2.18).<sup>37</sup> Interestingly, while it appears that analogue **2.72** displays modestly improved translation inhibitory effects compared to Col-3, given the stark differences in growth inhibitory activity, we might expect a greater difference in translation inhibitory activity. Combined with our ISR activation and ISRIB co-dose findings (Fig. 2.17), this suggests the majority of the potency of analogue **2.72** is due to its improved activation of the ISR and not to enhanced efficacy of ribosomal binding.

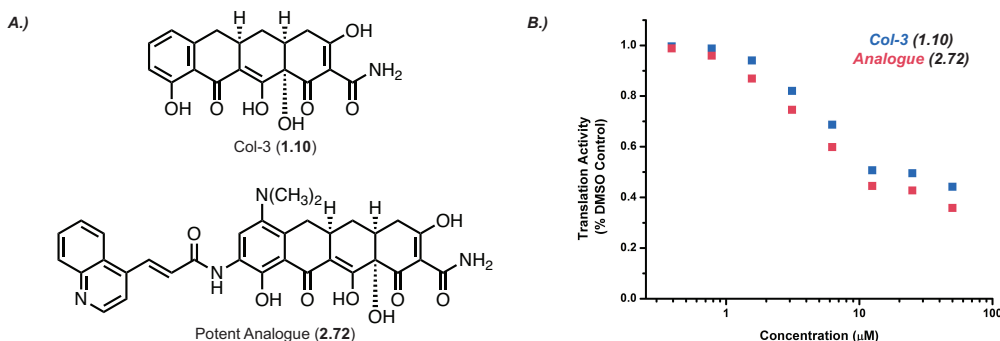


**Figure 2.18 Translation Inhibitory Activity.** Using an OPP incorporation assay, we determined that Col-3 and analogue **2.72** (A) are inhibiting eukaryotic translation to similar degrees (B). These results suggest that the majority of the improvement in antiproliferative activity for analogue **2.72** originates with its increased induction of ATF4 and not translation inhibition efficacy. Experiments performed with Dr. Linfeng Chen and Kamar Reda.

<sup>36</sup> See Chapter 1 for a discussion of the Click-iT™ Plus OPP Alexa Fluor™ Protein Synthesis Assay. Thermo Fisher Scientific.

<sup>37</sup> OPP Assays conducted in conjunction with Dr. Linfeng Chen and Kamar Reda in the Myers group.

As a final biological evaluation during our early stages of analogue development, we sought to better understand the antibacterial activity associated with both Col-3 and analogue **2.72**. The minimization of antibacterial activity is a key property in the creation of effective cancer therapeutics and, given our broad goals of developing tetracycline analogues with well-defined antiproliferative activities, we considered the monitoring of antibacterial activity to be an important piece of biological data. Antibacterial activities for a range of bacterial strains were obtained in-house by Dr. Amarnath Pisipati and are collected in Table 2.1.<sup>38</sup> Col-3 displays moderate potency across a range of Gram-positive and Gram-negative species, bucking the conventional wisdom that compounds lacking the C4-dimethylamino group lack antibacterial activity. While analogue **2.72** lacks all activity in Gram-negative species, it maintains respectable potency in several Gram-positive species. These results suggested that our current lead compounds, Col-3 and analogue **2.72**, continued to display general cytotoxic effects in both eukaryotes and prokaryotes and further development would be necessary to eliminate antibacterial activity all together.

**Table 2.1 Antibacterial Activities.**

	Organism	Strain No.	Genotype	Clindamycin	Minocycline (1.5)	Col-3 (1.10)	Analogue (2.72)
gram positive	<i>S. aureus</i>	HAV # 001	ATCC 29213	0.125	0.25	1	2
	<i>S. aureus</i>	HAV # 002	BAA-977	0.25	0.25	1	NT
	<i>S. aureus</i> (MRSA)	HAV # 016	ATCC BAA-1707	0.125	0.25	1	≤ 0.06
	<i>S. aureus</i> (MRSA)	HAV # 17	Col	0.125	NT	NT	2
	<i>S. pneumoniae</i>	HAV # 003	ATCC 49619	≤ 0.06	NT	NT	1
	<i>S. pyogenes</i>	HAV # 004	ATCC 19615	≤ 0.06	NT	NT	0.5
	<i>E. faecalis</i>	HAV # 005	ATCC 29212	16	4	4	0.5
	<i>E. faecium</i>	HAV # 326	HAV # 326	8	0.125	4	NT
gram negative	<i>E. coli</i>	HAV # 006	ATCC 25922	> 128	0.5	64	> 64
	<i>E. coli</i>	HAV # 038	ΔTolC	8	<0.125	4	> 64
	<i>E. coli</i>	HAV # 040	LptD	4	0.25	0.5	> 64
	<i>H. influenzae</i>	HAV # 007	ATCC 49247	8	NT	NT	> 64
	<i>K. pneumoniae</i>	HAV # 041	KCP	> 128	NT	NT	> 64

<sup>38</sup> Antibacterial activities obtained by Dr. Amarnath Pisipati in the Myers Group.



## 2.8 Role of the Mitochondria

As discussed in Chapter 1, the close homology of the prokaryotic and human mitochondrial ribosomes necessitates antibacterial compounds be evaluated for background toxicity caused by the dysregulation of human mitochondrial function during early cellular screening.<sup>39</sup> On top of this, select tetracyclines have enjoyed resurgent development efforts as cancer therapeutics that is driven primarily by their effects on the mitochondria.<sup>40</sup> Upon discovering the improved activity of analogue **2.72** did not appear to originate with increased translation inhibitory activity, we looked to mitochondrial effects to explain the improved ATF4 induction and growth inhibitory effects that analogue **2.72** displays compared to Col-3. While it has long been known that mitochondrial dysfunction can trigger the activation of a variety of stress responses, including the ISR and ATF4 activation, it was not until a 2020 report that the pathways associated with this communication were uncovered.<sup>41</sup> Using a genome-wise CRISPR knock-out strategy, Guo and colleagues determined that the mitochondrial protease OMA1 and the mitochondrial membrane protein DELE1 work in concert with the eIF2 kinase HRI to relay mitochondrial stress signals to the cytosol.<sup>42</sup> We hypothesized that this pathway could be contributing to the improved ATF4 activation observed for analogue **2.72**, either through direct interaction

---

<sup>39</sup> Kalghathi, S.; Spina, C. S.; Costello, J. C.; Liesa, M.; Morones-Ramirez, J. R.; Slomovic, S.; Molina, A.; Shirihai, O.; Collins, J. J. *Sci. Trans. Med.* **2013**, *5*, 1-11.

<sup>40</sup> See Chapter 1 for a discussion on the tetracyclines and recent mitochondria-based therapeutic strategies.

<sup>41</sup> (a) Fiorese, C. J.; Sculz, A. M.; Lin, Y.-F.; Rosin, N.; Pellegrina, M. W.; Haynes, C. M. *Curr. Biol.* **2016**, *26*, 2037-2043. (b) Munch, C.; Harper, J. W. *Nature*, **2016**, *534*, 710-713. (c) Papa, L.; Germain, D. *J. Cell Sci.* **2011**, *124*, 1396-1402. (d) Papa, L.; Germain, D. *Mol. Cell. Biol.* **2014**, *34*, 699-710. (e) Zhao, Q.; Wang, J.; Levichkin, I. V.; Stasinopoulos, S.; Ryan, M. T.; Hoogenraad, N. J. *EMBO J.* **2002**, *21*, 4411-4419.

<sup>42</sup> Guo, X.; Aviles, G.; Liu, Y.; Tian, R.; Unger, B. A.; Lin, Y.-H. T.; Wiita, A. P.; Xu, K.; Correia, M. A.; Kampmann, M. *Nature* **2020**, *579*, 427-432.

with the mitochondria or through a unique translational dysregulation mechanism involving the cytosolic ribosome.<sup>43</sup>

Toward this end, our first efforts involved the use of a commercially available two-step mitochondrial toxicity assay designed to assess a compound's effect on ATP production and cell viability (Fig. 2.19).<sup>44</sup> In the first step, compounds that have been treated with the small molecule of interest are briefly exposed to a peptide called bis-AAF-R110, which peptide contains a fluorescent reporter, R110 (**2.102**), that is quenched while bound to two Ala-Ala-Phe (AAF) peptides (**2.101**).<sup>45</sup> These quenching peptides are cleaved by dead-cell proteases – proteases released by the cell during apoptosis or membrane disruption – thus providing a rapid fluorescence-based measurement of cell viability. The cells are then exposed to an ATP detection reagent that lyses cells and measures the presence of ATP using a luciferase/luciferin luminescence system (**2.103**). The loss of cell viability with concurrent decrease in ATP concentration suggests the compound is generally cytotoxic, however retention of cell viability with concurrent decrease in ATP concentration suggests mitochondrial toxicity may be at play. Upon evaluation, both Col-3 and analogue **2.72** provided results consistent with generally cytotoxic agents with cell death observed concurrently with loss of ATP production.

---

<sup>43</sup> The close interplay between cytosolic translation control systems and mitochondrial translation control systems has been described by several researchers. Selected example: Couvillion, M. T.; Soto, I. C.; Shipkovenska, G. Churchman, L. S. *Nature* **2016**, *533*, 499-504.

<sup>44</sup> Mitochondrial ToxGlo™ Assay, Promega Corporation.

<sup>45</sup> Jochmans, D.; Leyssen, P.; Neyts, J. *J. Virol. Methods* **2012**, *183*, 176-179.

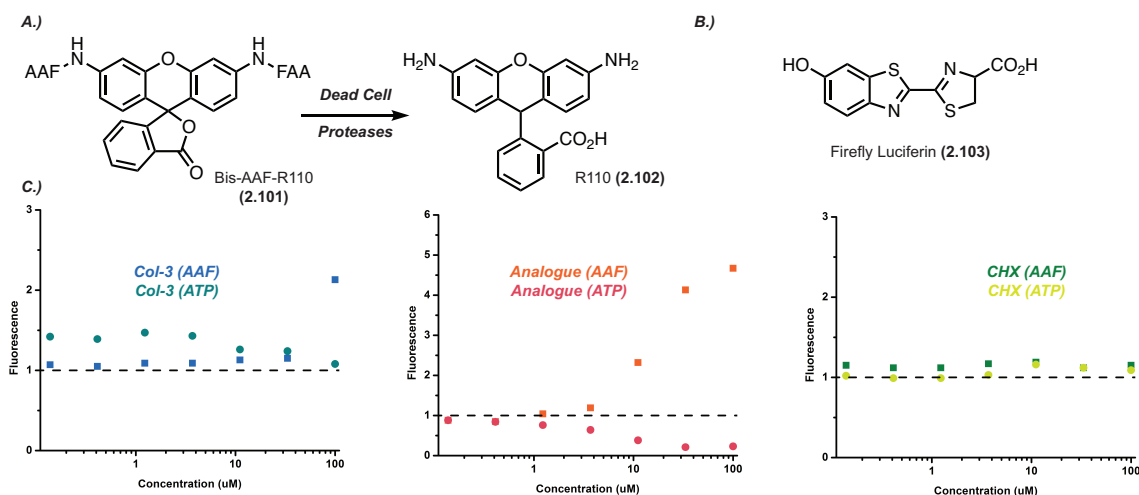


**Figure 2.19 Mitochondrial Toxicity Assays.** Commercially available mitochondrial toxicity assays were used to evaluate the effects of analogue **2.72** on mitochondrial function in HEK293T cells. The mechanism of the assay, using Bis-AAF-R110 (**2.101**) and firefly luciferin (**2.103**) as measures of cell viability and ATP production, respectively, is shown in A and B. The results of the assay (C) were largely inconclusive, we the compounds displaying general cytotoxic effects before effects on ATP product could be observed. Compounds dosed at 50 µM for 4 hours prior to the assay. Cell line: HepG2 hepatocarcinoma cells. CHX = cycloheximide, elongation inhibitor and control (see Chapter 4).

While these assays provided an initial, high-level assessment of mitochondrial behavior on tetracycline treatment, we sought a more detailed picture of mitochondrial translation to further probe the relationship between mitochondrial dysregulation and stress response activation. As a part of the Myers group collaboration with the Puigserver group at the Dana-Farber Cancer Institute, we assessed the effects of a range of tetracycline analogues, including many quinoline analogues, on mitochondrial translation using an  $^{35}\text{S}$ -incorporation assay (Fig. 2.20).<sup>46</sup> This assay relies on the replacement of standard methionine and cysteine amino acids with radioactive counterparts which are then incorporated into peptide chains during translation.<sup>47</sup> To specifically assess effects on mitochondrial translation cycloheximide, a cytosolic ribosome-specific translation

<sup>46</sup> See Chapter 1 for a discussion of the Myers/Puigserver group collaboration.

<sup>47</sup> See Perry et al., **2021** (Chapter 1, ref. 11) and references cited therein.

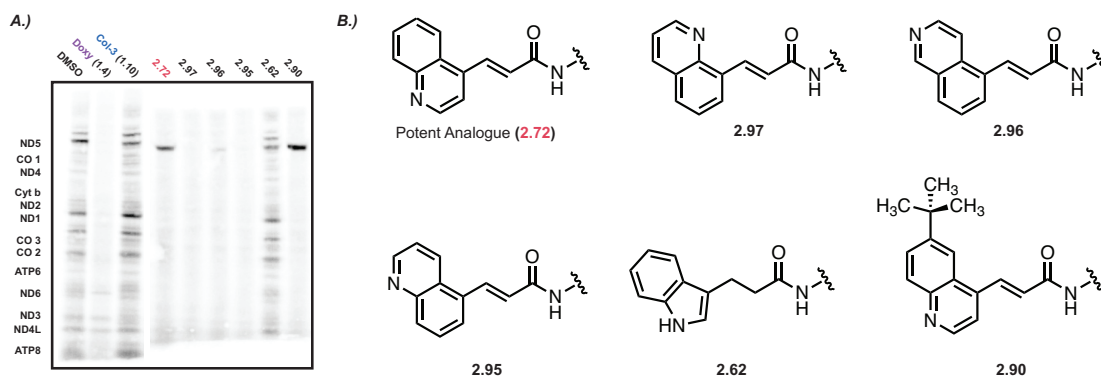


**Figure 2.20 Mitochondrial Translation Assays.** Mitochondrial translation assays conducted at the Puigserver laboratory at the Dana-Farber Cancer Institute showed a selection of the quinoline analogues (B), like doxycycline (**1.4**), potently suppress mitochondrial translation. Col-3 (**1.10**) and indole analogue **2.62**, however, shows little to no effect. This assay provided us with a window into a potential mechanism of these quinoline analogues, suggesting the novel sidechain discovered through these efforts may be improving mitochondrial uptake and translation inhibition. Experiments performed by Dr. Elizabeth Perry at the Dana-Farber Cancer Institute. Data reproduced with permission.

inhibitor is added to stop the production of cytosolic peptides. Following tetracycline treatment, protein isolation and separation allows for visualization of mitochondrially produced proteins via radioactive staining. Interestingly, these assays showed that analogue **2.72**, as well as many other quinoline analogues, potently inhibit mitochondrial translation (with activity similar to that of doxycycline), while Col-3 shows essentially no effect (Fig. 2.20).<sup>48</sup> These results suggest the inhibition of mitochondrial translation, and potential subsequent signaling pathway activation, could be contributing to the ATF4 activation and increased potency observed with analogue **2.72** (*vide supra*).

While still in early stages, our mechanistic elucidation efforts seem to point toward the mitochondria as key players in the increased potency of analogue **2.72**. Further studies are needed to analyze the signaling connections between tetracycline-induced mitochondrial translation inhibition and ISR activation as well as novel interactions between analogue **2.72** and the human mitochondrial ribosome that might be leading to

<sup>48</sup> Unpublished data provided by Dr. Elizabeth Perry in the Puigserver Group. Reproduced with permission.

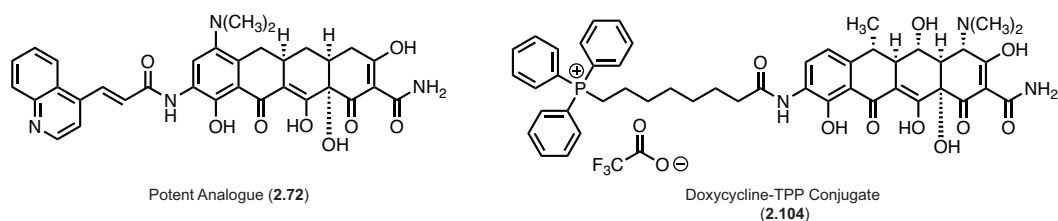


**Figure 2.21 Analogue 2.72 and Mitochondrial Localization.** Cochrane and colleagues investigated the role of TPP ions (**2.104**) in inducing mitochondrial localization for a series of antibacterial compounds including doxycycline. These structural elements could be related to the improved activity seen with our quinoline analogues. Figure adapted from Cochrane et al., **2021** (Chapter 2, ref. 50).

translation attenuation. We are intrigued also by recent publications on the topic of mitochondrial targeting of antibiotics, specifically through the attachment of bulky cations to compounds of interest (Fig. 2.21).<sup>49</sup> This targeting strategy takes advantage of the difference in mitochondrial membrane potential compared to that of the cytosol with lipophilic groups like the triphenylphosphonium (TPP) ion encouraging increased uptake (**2.104**). In 2021, Cochrane and colleagues reported conjugates of the antibiotics azithromycin and doxycycline with TPP ions that displayed improved mitochondrial localization and disruption which they hope to develop further as cancer therapeutics.<sup>50</sup> One potential hypothesis regarding the action of analogue **2.72** centers on this targeting strategy, with bulky, lipophilic groups like quinolines and naphthalenes appended to the tetracycline increasing mitochondrial uptake and leading to the observed inhibition of mitochondrial translation and improved growth inhibitory potencies. Aside from this, mitochondrial targeting presents an exciting outlet for semisynthetic development of the

<sup>49</sup> (a) Zielonka, J.; Joseph, J.; Hardy, M.; Ouari, O.; Vasquez-Vivar, J.; Cheng, G.; Lopez, M.; Kalyanaraman, B. *Chem. Rev.* **2017**, *117*, 10043-10120. (b) Cheng, G.; Hardy, M.; Topchyan, P.; Zander, R.; Volberding, P.; Cui, W.; Kalyanaraman, B. *Sci. Rep.* **2020**, *10*, 17872-17884.

<sup>50</sup> Cochrane, E. J.; Hulit, J.; Lagasse, F. P.; Lechertier, T.; Stevenson, B.; Tudor, C.; Trebicka, D.; Sparey, T.; Ratcliffe, A. J. *ACS Med. Chem. Lett.* **2021**, *12*, 579-584.

tetracyclines and could serve as a useful methodology for the generation of new tetracycline-based cancer therapeutics.

## **2.9 Conclusion and Path Forward**

Our initial stage of antiproliferative tetracycline development utilized semisynthesis to rapidly generate analogues with variation at C7 and C9. Using a photo-affinity labeling probe compound as a guide, we began by pursuing analogues with a broad range of substituents and identified one compound, **2.72**, featuring a quinoline acrylic acid moiety with improved potency over Col-3. We then explored various structural features of the quinoline moiety, including necessary structural elements and differing patterns of substitution, however, we were unable to unearth an analogue with significantly increased potency. As a final stage in these early development efforts, we characterized the downstream signaling pathways and translation inhibition activity associated with analogue **2.72**. While these efforts provided exciting early results, it became abundantly clear that our semisynthetic strategy would be ineffective for exploring different substitution patterns and achieving our grander project goals. In order to develop analogues with greater antiproliferative potency and better-defined cellular properties, we transitioned away from a semisynthetic strategy and toward a fully synthetic approach to access novel Col-3 analogues. Our semisynthetic analogue development and testing efforts laid a strong foundation upon which we were able to build effective analogue synthesis and mechanistic analysis studies.

## 2.10 Chemical Biology Experimental Section

**Mammalian Cell Lines and Cell Culture.** All compounds were dissolved in sterile DMSO to a stock concentration of 20  $\mu$ M and aliquoted prior to freezing at  $-20$  °C. Aliquots were limited to a maximum of 3 freeze–thaw cycles.

**Materials.** A375 (human malignant melanoma; female) cells were cultured in Dulbecco’s Modified Eagle Medium (DMEM) supplemented with 10% fetal bovine serum. K562 (human chronic myelogenous leukemia; female) and HL-60 (human acute promyelocytotic leukemia, female) cells were cultured in Iscove’s Modification of DMEM (IMDM) media supplemented with 10% fetal bovine serum. HCT116 (human colorectal carcinoma; male) cells were cultured in McCoy’s 5a (Iwakata & Grace Modification) media supplemented with 10% fetal bovine serum. HepG2 (human hepatocellular carcinoma; male) cells were cultured in Eagle’s Minimum Essential Medium (EMEM) supplemented with 10% fetal bovine serum. RPMI-8226 (human plasmacytoma, male) cells were cultured in RPMI-1640 supplemented with 10% fetal bovine serum. All cell cultures were maintained in a 5% CO<sub>2</sub> incubator at 37 °C.

**Growth Inhibition Assays.** The growth inhibition assays used to evaluate compound potency in mammalian cells was adapted from Magauer et al., 2013.<sup>51</sup> Briefly, cells were grown to approximately 80% confluence, and then were trypsinized, collected, and pelleted by centrifugation (3 min at 2,000 rpm, 23 °C). The supernatant was discarded

---

<sup>51</sup> Magauer, T.; Smaltz, D. J.; Myers, A. G. *Nat. Chem.* **2013**, *5*, 886-893.

and the cell pellet was resuspended in 10 mL of fresh medium. A sample was diluted 10-fold in fresh medium, and the concentration of cells was determined using a Scepter Cell Sensor automated cell counter. The cell suspension was diluted to a concentration of 5000 cells/mL. Stock solutions of each compound in DMSO were diluted serially with DMSO to provide 7 600X concentrations and one vehicle control for a total of 8 samples/drug. The drug dilutions were then added to a 96-well deep well plate and each mixed with 600  $\mu$ L cell/media solution. The cells/drugs were mixed and 100  $\mu$ L was added to 5 rows of a pre-sterilized 96-well plate. A final column was filled with 100  $\mu$ L culture media to serve as a no cells control. Typical tetracycline concentrations began with 100  $\mu$ M and decreased via a log<sub>2</sub>-scale over 7 total dilutions. Less concentrated dilutions were used for more potent compounds. After incubating at 37 °C for 72 h (5% CO<sub>2</sub>), 20  $\mu$ L of resazurin solution (Promega CellTiter-Blue® Cell Viability Assay) was added to each well. After incubating at 37 °C for 4 h (5% CO<sub>2</sub>), the fluorescence (544 nm excitation/590 nm emission) was recorded using a microplate reader (SpectraMax i3x) as a measure of viable cells. Percent growth inhibition was calculated for each well, based upon the following formula: Percent growth inhibition =  $100 \times (S - B_0) / (B_t - B_0)$  where S is the sample fluorescence, B<sub>t</sub> is the average fluorescence of an untreated population of cells at the completion of the assay, and B<sub>0</sub> is the average fluorescence of an untreated population of cells at the beginning of the assay. Each compound was assayed at seven separate concentrations per experiment. The percent inhibition at each concentration was plotted against log(concentration), and a curve fit was generated using Excel (Microsoft). GI50 values were computed to reflect the concentrations at which the resulting curves pass through 50% inhibition.



**Western Immunoblotting.** Western blot procedure was adapted from Mortison et al., 2018 by Dr. Linfeng Chen.<sup>52</sup> Briefly, samples were prepared with cleared cellular lysates in RIPA buffer containing protease/phosphatase inhibitor cocktail (Pierce) and normalized with a BCA assay kit. The lysates were diluted with 4X LDS loading buffer (Invitrogen) + 10X NuPAGE sample reducing agent, mixed via vortex, and heat denatured at 70 °C for 5 min. The samples were then loaded (10-20 µg protein/lane) onto 4-12% Bis-Tris Gels (Invitrogen) and electrophoresis was carried out at constant voltage: 50 V for 30 min then 150 V for 90 min in 1X MOPS Running Buffer with NuPAGE antioxidant (Invitrogen). The MW standard for visualization was the Biotinylated Protein Ladder Detection Pack (Cell Signaling Technology). The protein bands were then transferred to a 0.2 nitrocellulose (Cell Signaling Technology) membrane at 1.25 A (constant) per gel-membrane sandwich for 12 min on a semi-dry Pierce Power Blotter in Pierce 1-Step Transfer Buffer. The membranes were washed for 5 min in 1X TBS and blocked in 2% nonfat milk in 1X TBST for 1 h at 23 °C. The blocking solution was removed, and the primary antibodies were diluted into in 5% BSA in TBST (see below for typical dilutions), followed by incubation with the membranes overnight (18 h) at 4 °C. Following overnight incubation, primary antibodies were removed, and the blots were washed with 3 x 10 mL 1X TBST for 5 min/wash. The blots were then incubated with the appropriate rabbit or mouse secondary antibody (Promega, Cell Signaling Technologies) in 5% nonfat milk in 1X TBST. The secondary antibody was then removed, and the blots were washed with 3 x 10 mL 1X TBST for 5 min/wash. The blots were then incubated with Immobilon Forte Reagent (Millipore) for 1 min and the chemiluminescent signal was visualized on an Azure

---

<sup>52</sup> See Mortison et al., *Cell Chem. Biol.* 2018 (Chapter 1, ref. 26).

Biosystems Sapphire Biomolecular Imager. Following visualization, the blots were washed with 1X TBS, stripped with Pierce PLUS Western Stripping Buffer, and re-washed with 1X TBS. Blots were then re-blocked and re-probed. Stripping and re-probing was carried out no more than 3 times on a single blot.

- Anti-ATF4 (D4B8) Rabbit mAb (Cell Signaling): 1:1,000
- Anti-Rabbit IgG (H+L), HRP Conjugate (Cell Signaling): 1:2,500
- Biotinylated Protein Ladder Detection Pack (Cell Signaling): 1:1,000

***in vitro* Translation Assay.** O-propargyl puromycin-based translation assays (Thermo Fisher Scientific) were conducted according to the manufacturers protocol. Results were plotted as a percentage of the untreated (DMSO) control using Microsoft Excel and visualized using Origin graphing software.

**Antibacterial Activity and MIC Determination.** Bacterial studies were conducted by Dr. Amarnath Pisipati in the Myers Research Group. Briefly, minimum inhibitory concentrations (MICs) were determined by broth microdilution method or agar dilution method following the Clinical and Laboratory Standards Institute guidelines. Standard bacterial strains were obtained from American Type Culture Collection (ATCC). Before the start of the MIC experiment, standard and test compound stock solutions were prepared in dimethyl sulfoxide (DMSO, Aldrich) at a stock concentration of 5,120 µg/mL. The compound concentration range typically employed for each experiment was 128–0.06 µg/mL (2.5% final DMSO concentration). Minocycline was used as a comparator in all experiments and each experiment was performed in triplicate. All other bacterial strains

were sub-cultured on blood agar plates (tryptic soy agar with 5% sheep blood, Hardy Diagnostics) and incubated overnight at 35 °C. Organisms were suspended in cation-adjusted Mueller–Hinton broth (CaMHB) and optical density was adjusted to 0.5 McFarland standard. Suspensions were further diluted to obtain a final inoculum of  $5 \times 10^5$  CFU/mL for broth microdilution experiments. The minimum concentration of compound required to inhibit visible bacterial growth after 24 h of incubation was recorded as the MIC.

**Mitochondrial Toxicity Assay.** Mitochondrial toxicity assays were conducted using the Mitochondrial ToxGlo assay (Promega) pursuant to the manufacturer’s protocol.

**Mitochondrial Translation Inhibition Assay.** Mitochondrial translation inhibition analysis was conducted by Dr. Elizabeth Perry in the laboratory of Professor Pere Puigserver at the Dana-Farber Cancer Institute.<sup>53</sup>

---

<sup>53</sup> For procedures related to mitochondrial translation inhibition, see Perry et al., **2021** (Chapter 1, ref. 11) and references cited therein.

## 2.11 Chemistry Experimental Section

**General Experimental Procedures.** All reactions were performed in round-bottom flasks fitted with rubber septa under a positive pressure of argon or nitrogen, unless otherwise noted. Air- and moisture-sensitive liquids were transferred via syringe or stainless-steel cannula. Organic solutions were concentrated by rotary evaporation (house vacuum, ca. 25–40 torr) at ambient temperature, unless otherwise noted. Analytical thin-layer chromatography (TLC) was performed using glass plates pre-coated with silica gel (0.25 mm, 60 Å pore-size, 230 400 mesh, Merck KGA) impregnated with a fluorescent indicator (254 nm). TLC plates were visualized by exposure to ultraviolet light, then were stained with either an aqueous sulfuric acid solution of ceric ammonium molybdate (CAM) or an aqueous sodium carbonate solution of potassium permanganate (KMnO<sub>4</sub>) then briefly heated on a hot plate. Flash-column chromatography was performed as described by Still et al., employing silica gel (60 Å, 32–63 μM, standard grade, Dynamic Adsorbents, Inc.) or using the Teledyne ISCO CombiFlash purification system with pre-loaded silica gel columns.<sup>54</sup>

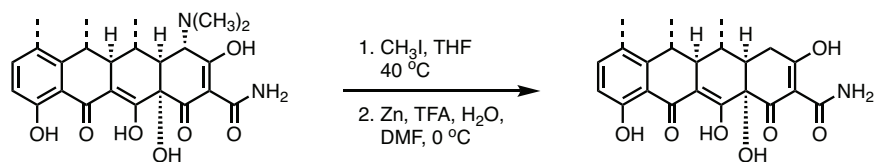
**Materials.** Dry solvents were purchased from the Aldrich Chemical Company in Sure/Seal™ glass bottles and used without further purification. All reagents were purchased and used without purification.

---

<sup>54</sup> Still, W. C.; Kahn, M.; Mitra, A.; *J. Org. Chem.* **1978**, *43*, 2923-2925.

**Instrumentation.** Proton magnetic resonance ( $^1\text{H}$  NMR) spectra were recorded on Varian INOVA 500 (500 MHz) or 600 (600 MHz) NMR spectrometers at 23 °C. Proton chemical shifts are expressed in parts per million (ppm,  $\delta$  scale) and are referenced to residual protium in the NMR solvent ( $\text{CHCl}_3$ ,  $\delta$  7.26;  $\text{D}_2\text{HCO}$ :  $\delta$  3.31). Data are represented as follows: chemical shift, integration, multiplicity (s = singlet, d = doublet, t = triplet, q = quartet, m = multiplet and/or multiple resonances, br = broad, app = apparent), and coupling constant (J) in Hertz. Carbon nuclear magnetic resonance spectra ( $^{13}\text{C}$  NMR) were recorded on a Varian INOVA 500 (125 MHz) NMR spectrometer at 23 °C. Carbon chemical shifts are expressed in parts per million (ppm,  $\delta$  scale) and are referenced to the carbon resonances of the NMR solvent ( $\text{CDCl}_3$ ,  $\delta$  77.0;  $\text{C}_6\text{D}_6$ ,  $\delta$  128.0). High-resolution mass spectra were obtained at the Harvard University Mass Spectrometry Facility. High-performance liquid chromatography–mass spectrometry (LCMS) was performed using an Agilent Technologies 1260-series analytical HPLC system in tandem with an Agilent Technologies 6120 Quadrupole mass spectrometer; a Zorbax Eclipse Plus reverse-phase  $\text{C}_{18}$  column (2.1  $\times$  50 mm, 1.8  $\mu\text{m}$  pore size, 600 bar rating; Agilent Technologies, Santa Clara, CA) was employed as stationary phase. LCMS samples were eluted at a flow rate of 650  $\mu\text{L}/\text{min}$ , beginning with 5% acetonitrile–water containing 0.1% formic acid, grading linearly to 100% acetonitrile containing 0.1% formic acid over 3 minutes, followed by 100% acetonitrile containing 0.1% formic acid for 2 minutes (5 minutes total run time).

For clarity, structures included below that have not appeared in the text are numbered here beginning with **S2.1**.



#### General Procedure A: Synthesis of 4-dedimethylamino tetracycline derivatives.

The desired tetracycline (typically HCl salt, 1 eq.) was suspended in water (0.2M) and stirred. Sodium bicarbonate (2 eq.) was added slowly to the solution. Mild bubbling was observed. The resulting solution was extracted 3X with 20mL dichloromethane. The organic layers were combined, dried over anhydrous sodium sulfate, and concentrated to a yellow/orange solid which was dried on vacuum.<sup>55</sup>

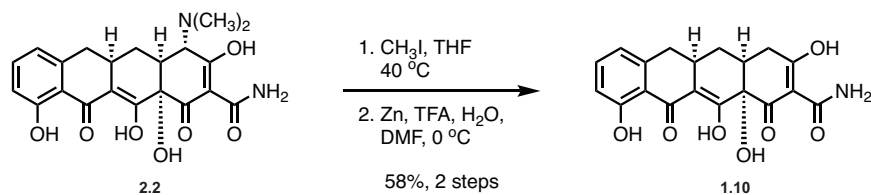
The resulting free-base tetracycline was dissolved in tetrahydrofuran (0.2M) and stirred. Iodomethane (25 eq.) was added, and the reaction was heated to 45 °C for 12 hours, after which the reaction was cooled to 0 °C and diluted with hexanes. The resulting yellow precipitate was collected via filtration, washed with cold hexanes, and dried on vacuum to provide the tetracycline methiodide salt.

The above salt was dissolved in DMF (0.2M) and cooled to 0 °C. Trifluoroacetic acid (5 eq.) and water (4 eq.) were added sequentially. Zinc (activated dust, 1.3 eq.) was added in six equal portions, adding one portion every 20-30 minutes.<sup>56</sup> Following ~3 hours total reaction time, the reaction solution was filtered through a 0.2 μM syringe filter and diluted with water. The pH of the solution was adjusted to 2.5 using ammonium hydroxide solution (25%). The solution was then extracted 3X with dichloromethane. The combined

<sup>55</sup> This step is needed only for those tetracyclines available as the HCl salt.

<sup>56</sup> Activated zinc dust was prepared by treating zinc dust with 1M HCl solution and washing sequentially with water, ethanol, and ether and dried on vacuum.

organic layers were washed 1X with water and 1X with brine, dried over anhydrous sodium sulfate, filtered, and concentrated, typically to a dark yellow/orange residue. The crude product was used in subsequent reactions without further purification. Samples of high purity can be obtained using the following procedure: 30 mg crude product was dissolved in 5 mL 4:1 methanol: DMF. The product was purified by preparative HPLC on an Agilent Prep C18 column [10  $\mu$ m, 250 x 21.2 mm, UV detection at 399 nm, Solvent A: 0.1% formic acid in water, Solvent B: 0.1% formic acid in acetonitrile, injection volume: 5.0 mL (4 mL methanol, 1 mL DMF), gradient elution with 10–70% B over 40 min, flow rate: 15 mL/min]. Fractions were analyzed via analytical LC/MS for purity prior to concentration to provide the desired product, typically as a white or yellow solid.



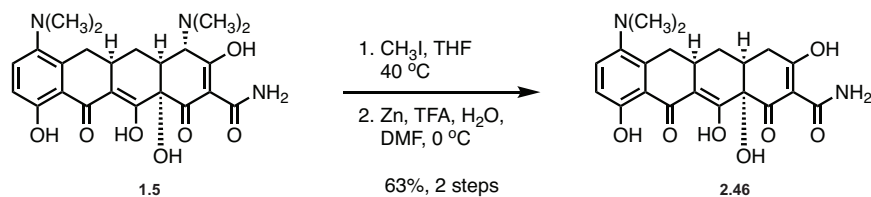
Synthesis of 4-dedimethylamino sancycline (Col-3, **1.10**):

Col-3 (**1.10**) was synthesized according to General Procedure A: Sancycline HCl (**2.2**, 2.5 g, 6 mmol, 1 eq.) was reacted to provide crude Col-3 (**1.10**, 1.3 g, 58%, crude) as an orange residue. Samples of Col-3 could be purified using preparative HPLC, gradient elution with 15–85% B over 40 min, flow rate: 15 mL/min, as described above. Purified Col-3 was obtained as a white solid.

Spectral data obtained for this compound were consistent with those previously reported.<sup>57</sup>

<sup>57</sup> See Mortison et al., **2018** (Chapter 1, ref. 26) and references cited therein.



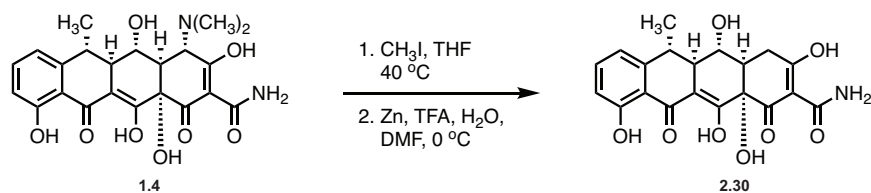


### Synthesis of 4-dedimethylamino minocycline (2.46):

4-dedimethylamino minocycline (**2.46**) was synthesized according to General Procedure A: Minocycline HCl (**1.5**, 3.5 g, 7.65 mmol, 1 eq.) was reacted to provide crude 4-dedimethylamino minocycline (**2.46**, 2 g, 63%, crude) as an orange residue. Samples of 4-dedimethylamino-minocycline could be purified using preparative HPLC, gradient elution with 10–70% acetonitrile over 40 min, flow rate: 15 mL/min, as described above. The formate salt of 4-dedimethylamino-minocycline was obtained as a yellow solid.

<sup>1</sup>H NMR (400 MHz, CD<sub>3</sub>OD) δ 7.37 (d, *J* = 8.9 Hz, 1H), 6.77 (d, *J* = 9.2 Hz, 1H), 3.34 (dd, *J* = 15.6, 4.3 Hz, 1H), 3.24 (dd, *J* = 17.6, 6.3 Hz, 1H), 2.75 (tdd, *J* = 10.1, 7.6, 4.6 Hz, 1H), 2.58 (s, 6H), 2.49 – 2.34 (m, 2H), 2.13 (dd, *J* = 14.3, 13.5 Hz, 1H), 2.03 (ddd, *J* = 13.6, 5.4, 2.7 Hz, 1H), 1.60 (td, *J* = 13.3, 10.8 Hz, 1H).

HRMS (ESI+, *m/z*) [M + H]<sup>+</sup> calc'd for C<sub>21</sub>H<sub>22</sub>N<sub>2</sub>O<sub>7</sub>: 415.1500. Found: 415.1494.

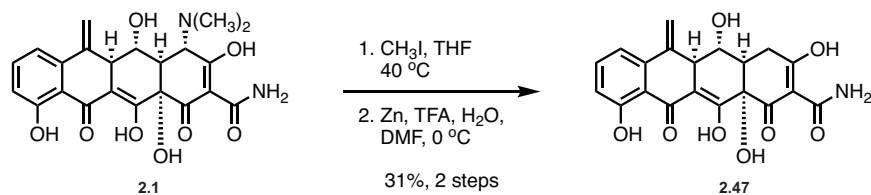


#### Synthesis of 4-dedimethylamino doxycycline (2.30):

4-dedimethylamino doxycycline (**2.30**) was synthesized according to General Procedure A: Doxycycline hyclate (**1.4**) was reacted to provide crude 4-dedimethylamino doxycycline (**2.30**) as a pale residue. Samples of 4-dedimethylamino-doxycycline could be purified using preparative HPLC, gradient elution with 15–85% B over 40 min, flow rate: 15 mL/min, as described above. Purified 4-dedimethylamino-doxycycline was obtained as a yellow solid.

Spectral data obtained for this compound were consistent with those previously reported.<sup>58</sup>

<sup>58</sup> Zhou, Z.-Y.; Wang, H.-T.; Wang, X.-W.; Wang, R.-P.; Du, Y.-S.; Liu, J.-Y. *J. Chinese Pharm. Sci.* **2004**, *13*, 217-220.

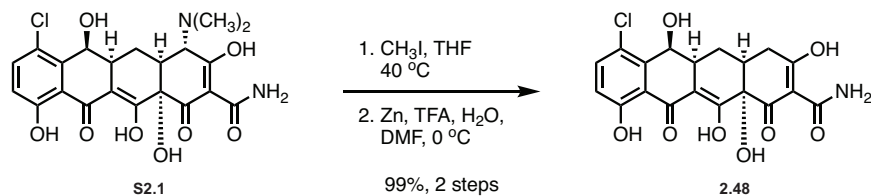


### Synthesis of 4-dedimethylamino methacycline (2.47):

4-dedimethylamino methacycline (**2.47**) was synthesized according to General Procedure A: Methacycline hyclate (**2.1**, 25 mg, 0.057 mmol, 1 eq.) was reacted to provide crude 4-dedimethylamino methacycline (**2.47**) as a pale residue. Samples of 4-dedimethylamino-methacycline could be purified using preparative HPLC, gradient elution with 15–85% B over 40 min, flow rate: 15 mL/min, as described above. Purified 4-dedimethylamino-methacycline was obtained as a yellow solid (6.9 mg, 31%).

$^1\text{H}$  NMR (400 MHz,  $\text{CD}_3\text{OD}$ )  $\delta$  7.48 (dd,  $J = 8.4, 7.6$  Hz, 1H), 7.07 (d,  $J = 7.5$  Hz, 1H), 6.89 (d,  $J = 7.9$  Hz, 1H), 5.52 (d,  $J = 2.4$  Hz, 1H), 5.36 (d,  $J = 2.4$  Hz, 1H), 3.96 (dd,  $J = 11.5, 8.9$  Hz, 1H), 3.40 (dt,  $J = 9.0, 2.4$  Hz, 1H), 3.13 – 2.95 (m, 2H), 2.45 (ddd,  $J = 11.6, 5.4, 1.9$  Hz, 1H).

HRMS (ESI+,  $m/z$ )  $[\text{M} + \text{H}]^+$  calc'd for  $\text{C}_{20}\text{H}_{17}\text{NO}_8$ : 400.1027. Found: 400.1021.

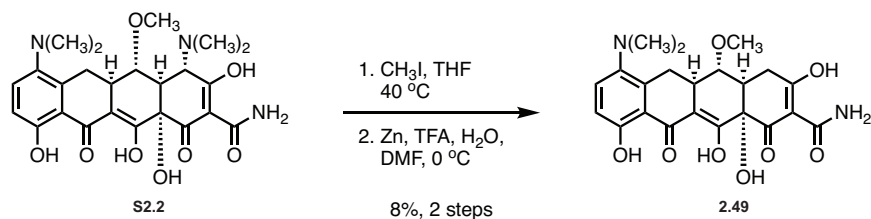


### Synthesis of 4-dedimethylamino-demeclocycline (2.48):

4-dedimethylamino-demeclocycline (**2.48**) was synthesized according to General Procedure A: demeclocycline HCl (**S2.1**, 25 mg, 0.054 mmol, 1 eq.) was reacted to provide crude 4-dedimethylamino demeclocycline (**2.48**) as a pale residue. 4-dedimethylamino demeclocycline was purified using preparative HPLC, gradient elution with 15–85% B over 40 min, flow rate: 15 mL/min, as described above. The product was obtained as a pale yellow/green solid (22.5 mg, 99%).

<sup>1</sup>H NMR (400 MHz, CD<sub>3</sub>OD)  $\delta$  7.52 (d,  $J = 9.0$  Hz, 1H), 6.91 (d,  $J = 8.9$  Hz, 1H), 3.23 (dd,  $J = 18.5, 5.5$  Hz, 1H), 2.92 (ddd,  $J = 10.9, 5.7, 2.9$  Hz, 1H), 2.56 – 2.38 (m, 2H), 2.08 (td,  $J = 13.1, 10.9$  Hz, 1H), 1.90 (ddd,  $J = 13.5, 5.8, 3.1$  Hz, 1H). An additional signal (dd) is hidden beneath the HDO peak ( $\delta$ : 4.80).

HRMS (ESI+,  $m/z$ ) [M + H]<sup>+</sup> calc'd for C<sub>19</sub>H<sub>16</sub>ClNO<sub>8</sub>: 422.0637. Found: 422.0635.

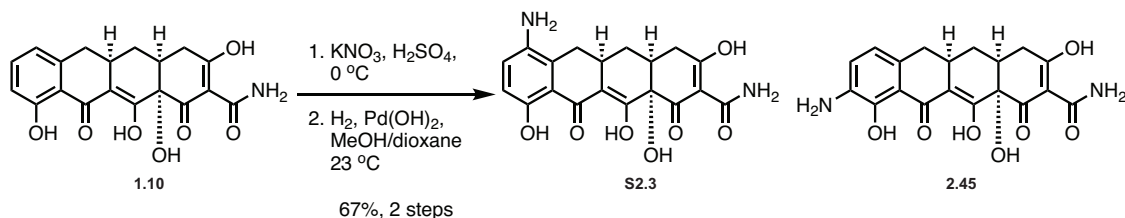


### Synthesis of 4-dedimethylamino-5-methoxy minocycline (2.49):

4-dedimethylamino-5-methoxy minocycline (**2.49**) was synthesized according to General Procedure A: 5-methoxy minocycline HCl (**S2.2**, 25 mg, 0.051 mmol, 1 eq.) was reacted to provide crude 4-dedimethylamino-5-methoxy minocycline (**2.49**) as a pale residue. The product was purified using preparative HPLC, gradient elution with 15–85% B over 40 min, flow rate: 15 mL/min, as described above. Purified 4-dedimethylamino-5-methoxy minocycline was obtained as a yellow solid (1.9 mg, 8 %).

<sup>1</sup>H NMR (400 MHz, CD<sub>3</sub>OD)  $\delta$  7.38 (d,  $J = 8.9$  Hz, 1H), 6.77 (d,  $J = 8.9$  Hz, 1H), 3.72 (dd,  $J = 15.4, 4.3$  Hz, 1H), 3.52 (s, 3H), 3.15 – 3.00 (m, 1H), 2.82 – 2.62 (m, 2H), 2.60 (s, 6H), 2.41 (s, 1H), 2.23 (t,  $J = 14.4$  Hz, 1H). An additional signal (dd) is hidden beneath the MeOH peak ( $\delta$ : 3.31).

HRMS (ESI+,  $m/z$ )  $[M + H]^+$  calc'd for C<sub>22</sub>H<sub>24</sub>N<sub>2</sub>O<sub>8</sub>: 445.1605. Found: 445.1599.



### 7-amino-Col-3 (S2.3) and 9-amino-Col-3 (2.45):

Col-3 (**1.10**, 0.95 g, 2.57 mmol, 1 eq.) was dissolved in 20 mL sulfuric acid and stirred at  $0\text{ }^\circ\text{C}$ . Potassium nitrate (0.35 g, 3.31 mmol, 1.3 eq.) was then added slowly. The resulting yellow/brown solution was stirred at  $0\text{ }^\circ\text{C}$  for 1 hour, at which point LC/MS indicated full consumption of the starting material. The reaction solution was poured slowly over 20 g ice and stirred, forming an off-yellow precipitate. Dichloromethane (30 mL) was added and stirred. The resulting emulsion was filtered through a pad of sand and Celite, washing the pad with excess dichloromethane. The layers were separated, and the aqueous layer washed 3X with (50 mL) dichloromethane. The sand/Celite pad was then washed with 30 mL ethyl acetate. The organics were combined, dried over anhydrous sodium sulfate, filtered, and concentrated to a brown solid. Dry on vacuum.

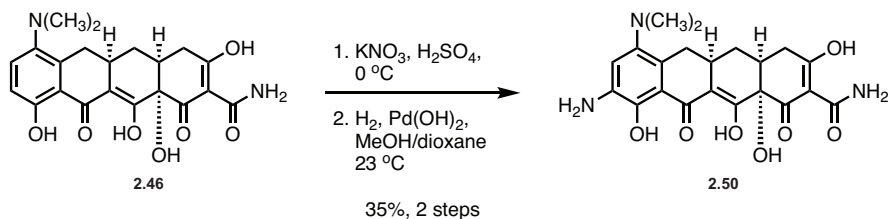
The crude nitrated material was dissolved in 16 mL 1:1 methanol/dioxane and stirred. Palladium hydroxide (20% wt., 0.361 g, 0.514 mmol, 0.2 eq.) was added and the flask was evacuated/backfilled 3X with nitrogen. The flask was then evacuated/backfilled 3X with hydrogen. A hydrogen balloon was fitted with a long needle and inserted into the flask such that the needle reached the level of the solution. Hydrogen was bubbled through the solution for 30 minutes and the needle removed from the solution. The reaction was then allowed to stir under static hydrogen pressure for another 30 minutes. The reaction was then purged with nitrogen and filtered through a pad of Celite, washing the pad with

excess methanol. The filtrate was then concentrated to a dark red solid (0.66 g, 67%, crude mixture of regioisomers).

Samples (~ 30 mg) of the crude product were dissolved in 5 mL 4:1 methanol: *N,N*-dimethylformamide. The product was purified by preparative HPLC on an Agilent Prep C18 column [10 µm, 250 x 21.2 mm, UV detection at 399 nm, Solvent A: 0.1% formic acid in water, Solvent B: 0.1% formic acid in acetonitrile, injection volume: 5.0 mL (4 mL methanol, 1 mL *N,N*-dimethylformamide), gradient elution with 20–80% B over 40 min, flow rate: 15 mL/min]. Fractions were analyzed via analytical LC/MS for purity prior to concentration to provide the desired products (**S.2.1** and **2.45**) as yellow solids. Spectral data obtained for these compounds were consistent with those previously reported.<sup>59</sup>

---

<sup>59</sup> See Mortison et al., **2018** (Chapter 1, ref. 26).



#### 9-amino-4-dedimethylamino-minocycline (2.50):

4-dedimethylamino-minocycline (**2.46**, 1.3 g, 3.14 mmol, 1 eq.) was dissolved in 25 mL sulfuric acid and stirred at  $0\text{ }^\circ\text{C}$ . Potassium nitrate (0.41 g, 4.1 mmol, 1.3 eq.) was then added slowly. The resulting yellow/brown solution was stirred at  $0\text{ }^\circ\text{C}$  for 1 hour, at which point LC/MS indicated full consumption of the starting material. The reaction solution was poured slowly over 20 g ice and stirred, forming an off-yellow precipitate. Dichloromethane (30 mL) was added and stirred. The resulting emulsion was filtered through a pad of sand and Celite, washing the pad with excess dichloromethane. The layers were separated and the aqueous layer washed 3X with (50 mL) dichloromethane. The sand/Celite pad was then washed with 30 mL ethyl acetate. The organics were combined, dried over anhydrous sodium sulfate, filtered, and concentrated to a brown solid. Dry on vacuum.

The crude nitrated material was dissolved in 16 mL 1:1 methanol/dioxane and stirred. Palladium hydroxide (20% wt., 0.088 g, 0.63 mmol, 0.2 eq.) was added and the flask was evacuated/backfilled 3X with nitrogen. The flask was then evacuated/backfilled 3X with hydrogen. A hydrogen balloon was fitted with a long needle and inserted into the flask such that the needle reached the level of the solution. Hydrogen was bubbled through the solution for 30 minutes and the needle removed from the solution. The reaction was then allowed to stir under static hydrogen pressure for another 30 minutes. The reaction

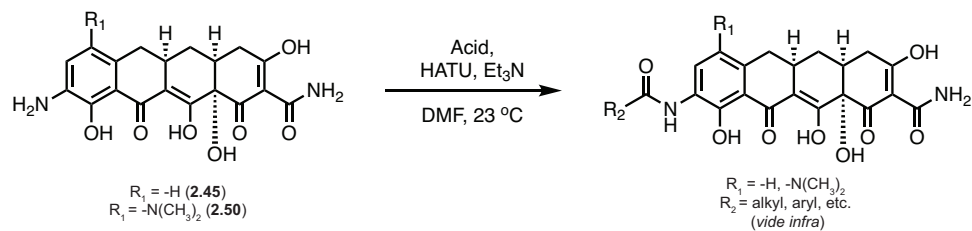


was then purged with nitrogen and filtered through a pad of Celite, washing the pad with excess methanol. The filtrate was then concentrated to a dark red solid (0.48 g, 35 % crude).

Samples (~ 30 mg) of crude product were dissolved in 5 mL 4:1 methanol: *N, N*-dimethylformamide. The product was purified by preparative HPLC on an Agilent Prep C18 column [10  $\mu$ m, 250 x 21.2 mm, UV detection at 399 nm, Solvent A: 0.1% formic acid in water, Solvent B: 0.1% formic acid in acetonitrile, injection volume: 5.0 mL (4 mL methanol, 1 mL *N, N*-dimethylformamide), gradient elution with 10–70% B over 40 min, flow rate: 15 mL/min]. Fractions were analyzed via analytical LC/MS for purity prior to concentration to provide the formate salt of the desired product as a red solid.

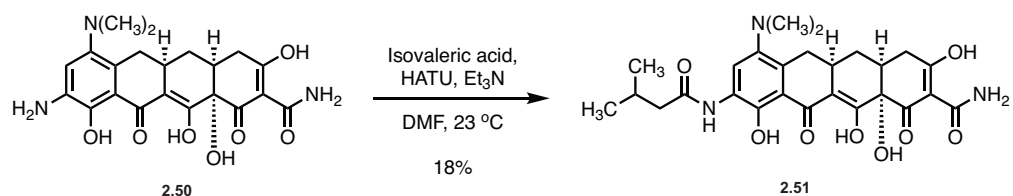
$^1\text{H NMR}$  (400 MHz,  $\text{CD}_3\text{OD}$ )  $\delta$  6.93 (s, 1H), 3.28 – 3.17 (m, 2H), 2.73 (ddt,  $J = 13.3, 10.2, 4.8$  Hz, 1H), 2.58 (s, 6H), 2.49 – 2.33 (m, 2H), 2.11 – 1.96 (m, 2H), 1.58 (td,  $J = 13.3, 10.7$  Hz, 1H).

HRMS (ESI+,  $m/z$ )  $[\text{M} + \text{H}]^+$  calc'd for  $\text{C}_{21}\text{H}_{23}\text{N}_3\text{O}_7$ : 430.1609. Found: 430.1601.



### General Procedure B: Analogue Synthesis via Amide Bond Formation

The 9-amino-4-dedimethylamino tetracycline derivative (**2.45** or **2.50**, 1 eq.) was dissolved in DMF (0.1M) and stirred at 23 °C. HATU (1.5 eq.) was then added, followed by the desired acid (1.5 eq.) and triethylamine (5 eq.). The solution was stirred at 23 °C for 1.5 hours or until completion as monitored by analytical LC/MS. Upon completion, the reaction was diluted with 4 mL methanol and filtered through a 0.2 μM syringe filter. The filtrate was purified by preparative HPLC on an Agilent Prep C18 column [10 μm, 250 x 21.2 mm, UV detection at 399 nm, Solvent A: 0.1% formic acid in water, Solvent B: 0.1% formic acid in acetonitrile, injection volume: 5.0 mL (4 mL methanol + reaction solution), gradient elution with 5–70% B over 40 min, flow rate: 15 mL/min]. Fractions were analyzed via analytical LC/MS for purity prior to concentration to provide the desired product, typically as yellow/brown solids.

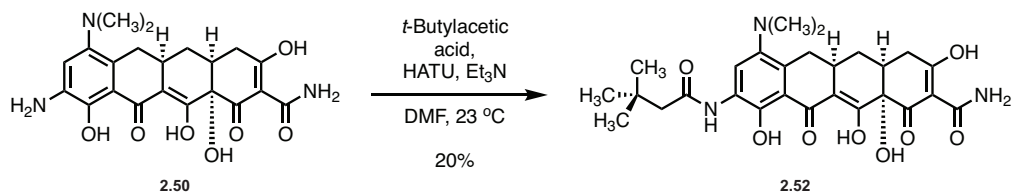


### Analogue 2.51:

Analogue **2.51** was prepared using General Procedure B: 9-amino-4-dimethylamino minocycline (**2.50**, 5 mg, 0.012 mmol) was reacted with isovaleric acid to provide the formate salt of Analogue **2.51** as a yellow solid following preparatory HPLC purification (1.1 mg, 18%).

$^1\text{H NMR}$  (500 MHz,  $\text{CD}_3\text{OD}$ )  $\delta$  8.13 (s, 1H), 3.27 (dd,  $J = 18.5, 5.5$  Hz, 1H), 2.84 – 2.75 (app. m, 1H), 2.60 (s, 6H), 2.51 – 2.38 (m, 2H), 2.34 (d,  $J = 7.3$  Hz, 2H), 2.23 – 2.11 (m, 2H), 2.07 (ddd,  $J = 14.0, 8.1, 2.5$  Hz, 1H), 1.63 (td,  $J = 13.2, 11.4$  Hz, 1H), 1.04 (d,  $J = 6.7$  Hz, 6H). An additional signal (dd) is hidden beneath the MeOH peak ( $\delta$ : 3.31).

LRMS ( $m/z$ )  $[\text{M} + \text{H}]^+$  calc'd for  $\text{C}_{26}\text{H}_{31}\text{N}_3\text{O}_8$ : 514.2189. Found: 514.3.

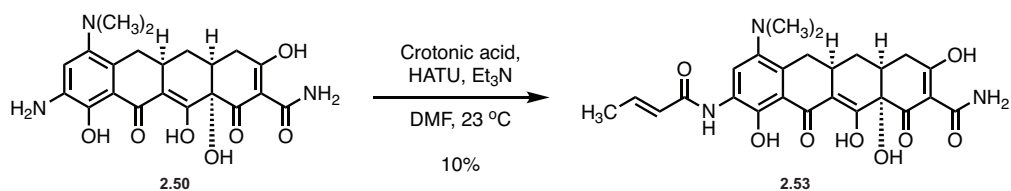


**Analogue 2.52:**

Analogue **2.52** was prepared using General Procedure B: 9-amino-4-dedimethylamino minocycline (**2.50**, 5 mg, 0.012 mmol) was reacted with *t*-butylacetic acid to provide the formate salt of Analogue **2.52** as a yellow solid following preparatory HPLC purification (1.2 mg, 20%).

$^1\text{H}$  NMR (500 MHz,  $\text{CD}_3\text{OD}$ )  $\delta$  8.10 (s, 1H), 3.36 (app. d,  $J = 5.0$  Hz, 1H), 3.27 (dd,  $J = 18.5, 5.2$  Hz, 1H), 2.84 – 2.75 (app. m, 1H), 2.60 (s, 6H), 2.51 – 2.38 (m, 2H), 2.35 (s, 2H), 2.15 (dd,  $J = 15.1, 13.5$  Hz, 1H), 2.06 (ddd,  $J = 13.2, 7.8, 2.7$  Hz, 1H), 1.63 (td,  $J = 13.2, 10.9$  Hz, 1H), 1.12 (s, 9H).

HRMS (ESI+,  $m/z$ )  $[\text{M} + \text{H}]^+$  calc'd for  $\text{C}_{27}\text{H}_{33}\text{N}_3\text{O}_8$ : 528.2340. Found: 528.2334.

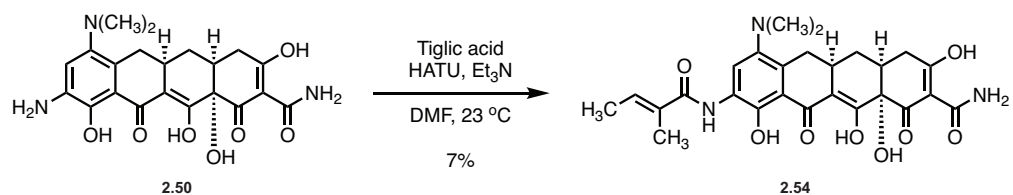


### Analogue 2.53:

Analogue **2.53** was prepared using General Procedure B: 9-amino-4-dedimethylamino minocycline (**2.50**, 5 mg, 0.012 mmol) was reacted with crotonic acid to provide the formate salt of Analogue **2.53** as a yellow solid following preparatory HPLC purification (0.6 mg, 10%).

<sup>1</sup>H NMR (500 MHz, CD<sub>3</sub>OD) δ 8.28 (s, 1H), 7.01 – 6.92 (m, 1H), 6.30 (d, *J* = 15.1 Hz, 1H), 3.37 (app. d, *J* = 4.2 Hz, 1H), 3.25 (app. d, *J* = 6.1 Hz, 1H), 2.84 – 2.75 (app. m, 1H), 2.61 (s, 6H), 2.51 – 2.39 (m, 2H), 2.15 (dd, *J* = 16.2, 14.5 Hz, 1H), 2.07 (ddd, *J* = 12.3, 6.0, 2.4 Hz, 1H), 1.95 (d, *J* = 6.4 Hz, 3H), 1.63 (td, *J* = 12.5, 12.4 Hz, 1H).

LRMS (*m/z*) [M + H]<sup>+</sup> calc'd for C<sub>25</sub>H<sub>27</sub>N<sub>3</sub>O<sub>8</sub>: 498.1876. Found: 498.2.

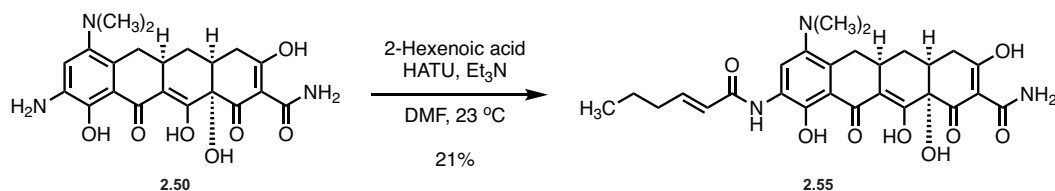


### Analogue 2.54:

Analogue **2.54** was prepared using General Procedure B: 9-amino-4-dimethylamino minocycline (**2.50**, 5 mg, 0.012 mmol) was reacted with tiglic acid to provide the formate salt of Analogue **2.54** as a yellow solid following preparatory HPLC purification (0.4 mg, 7%).

$^1\text{H NMR}$  (500 MHz,  $\text{CD}_3\text{OD}$ )  $\delta$  8.20 (s, 1H), 6.63 (d,  $J = 7.2$  Hz, 1H), 3.25 (app. d,  $J = 7.4$  Hz, 1H), 2.84 – 2.76 (app. m, 1H), 2.61 (s, 6H), 2.51 – 2.38 (m, 2H), 2.16 (dd,  $J = 13.8$ , 13.7 Hz, 1H), 2.07 (ddd,  $J = 14.9$ , 8.8, 3.3 Hz, 1H), 1.97 (s, 3H), 1.87 (d,  $J = 6.9$  Hz, 3H), 1.64 (td,  $J = 13.6$ , 10.4 Hz, 1H). An additional signal (dd) is hidden beneath the MeOH peak ( $\delta$ : 3.31).

LRMS ( $m/z$ )  $[\text{M} + \text{H}]^+$  calc'd for  $\text{C}_{26}\text{H}_{29}\text{N}_3\text{O}_8$ : 512.2033. Found: 512.3.

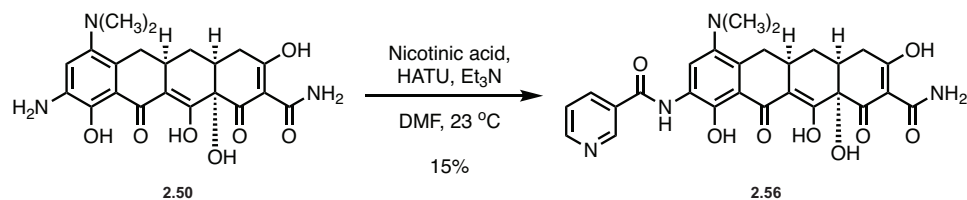


**Analogue 2.55:**

Analogue **2.55** was prepared using General Procedure B: 9-amino-4-dedimethylamino minocycline (**2.50**, 5 mg, 0.012 mmol) was reacted with 2-hexenoic acid to provide Analogue **2.55** as a yellow solid following preparatory HPLC purification (1.3 mg, 21%).

$^1\text{H NMR}$  (500 MHz,  $\text{CD}_3\text{OD}$ )  $\delta$  8.28 (d,  $J = 2.5$  Hz, 1H), 6.96 (dt,  $J = 14.6, 7.0$  Hz, 1H), 6.29 (d,  $J = 15.2$  Hz, 1H), 3.37 (app. d,  $J = 4.3$  Hz, 1H), 3.28 (dd,  $J = 15.2, 7.0$  Hz, 1H), 2.84 – 2.74 (app. m, 1H), 2.61 (s, 6H), 2.51 – 2.38 (m, 2H), 2.28 (q,  $J = 7.2$  Hz, 1H), 2.22 – 2.11 (app. m, 1H), 2.07 (ddd,  $J = 13.1, 6.3, 2.1$  Hz, 1H), 1.65 (td,  $J = 13.3, 10.4$  Hz, 1H), 1.57 (q,  $J = 7.4$  Hz, 1H), 1.09 – 0.97 (m, 5H).

LRMS ( $m/z$ )  $[\text{M} + \text{H}]^+$  calc'd for  $\text{C}_{27}\text{H}_{31}\text{N}_3\text{O}_8$ : 526.2189. Found: 526.2.



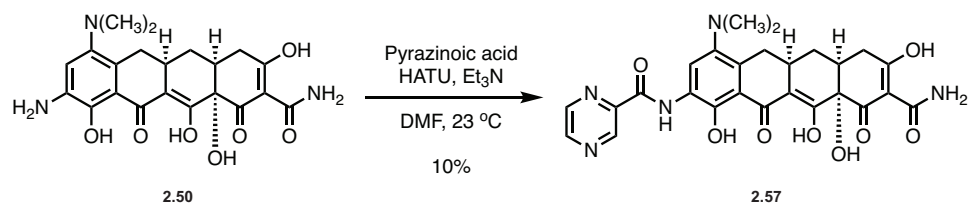
### Analogue 2.56:

Analogue **2.56** was prepared using General Procedure B: 9-amino-4-dedimethylamino minocycline (**2.50**, 5 mg, 0.012 mmol) was reacted with nicotinic acid to provide the product as the formate salt of Analogue **2.56** as a yellow solid following preparatory HPLC purification. (0.9 mg, 14.5 %).

<sup>1</sup>H NMR (400 MHz, CD<sub>3</sub>OD) δ 9.12 (s, 1H), 8.76 (s, 1H), 8.40 (d, *J* = 8.2 Hz, 1H), 8.25 (s, 1H), 7.63 (s, 1H), 3.24 (app. d, *J* = 6.1 Hz, 1H), 2.91 – 2.82 (app. m, 1H), 2.79 (s, 6H), 2.54 – 2.36 (m, 2H), 2.26 (dd, *J* = 13.5, 13.5 Hz, 1H), 2.08 (ddd, *J* = 13.8, 7.6, 2.8 Hz, 1H), 1.64 (td, *J* = 13.4, 11.9 Hz, 1H). An additional signal (dd) is hidden beneath the MeOH peak (δ: 3.31).

HRMS (ESI+, *m/z*) [M + H]<sup>+</sup> calc'd for C<sub>27</sub>H<sub>26</sub>N<sub>4</sub>O<sub>8</sub>: 535.1823. Found: 535.1815.



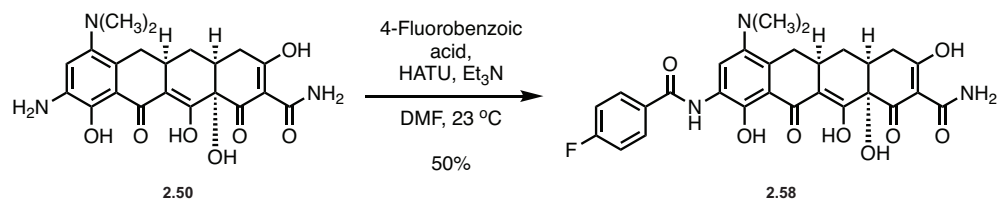


### Analogue 2.57:

Analogue **2.57** was prepared using General Procedure B: 9-amino-4-dedimethylamino minocycline (**2.50**, 5 mg, 0.012 mmol) was reacted with pyrazinoic acid to provide the formate salt of Analogue **2.57** as a yellow solid following preparatory HPLC purification (0.6 mg, 10%).

$^1\text{H NMR}$  (400 MHz,  $\text{CD}_3\text{OD}$ )  $\delta$  9.37 (s, 1H), 8.85 (d,  $J = 2.3$  Hz, 1H), 8.75 (s, 1H), 8.61 (s, 1H), 3.37 (app. d,  $J = 4.2$  Hz, 1H), 3.23 (app. d,  $J = 5.7$  Hz, 1H), 2.86 – 2.73 (app. m, 1H), 2.63 (s, 6H), 2.53 – 2.35 (m, 2H), 2.16 (dd,  $J = 14.5, 14.2$  Hz, 1H), 2.06 (ddd,  $J = 13.8, 6.7, 2.3$  Hz, 1H), 1.63 (td,  $J = 12.0, 10.8$  Hz, 1H).

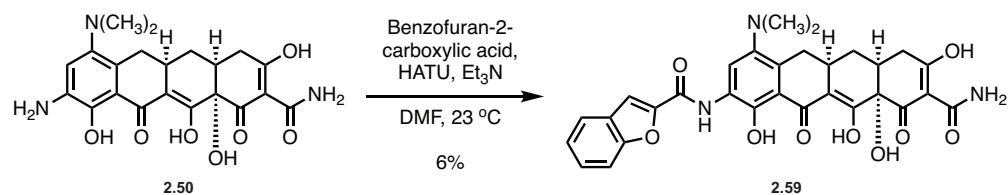
HRMS (ESI+,  $m/z$ )  $[\text{M} + \text{H}]^+$  calc'd for  $\text{C}_{26}\text{H}_{25}\text{N}_5\text{O}_8$ : 536.1776. Found: 536.1771.



Analogue **2.58**:

Analogue **2.58** was prepared using General Procedure B: 9-amino-4-dedimethylamino minocycline (**2.50**, 5 mg, 0.012 mmol) was reacted with 4-fluorobenzoic acid to provide the formate salt of Analogue **2.58** as a yellow solid following preparatory HPLC purification (3.2 mg, 50%).

HRMS (ESI+, *m/z*) [M + H]<sup>+</sup> calc'd for C<sub>28</sub>H<sub>26</sub>FN<sub>3</sub>O<sub>8</sub>: 552.1777. Found: 552.1768.



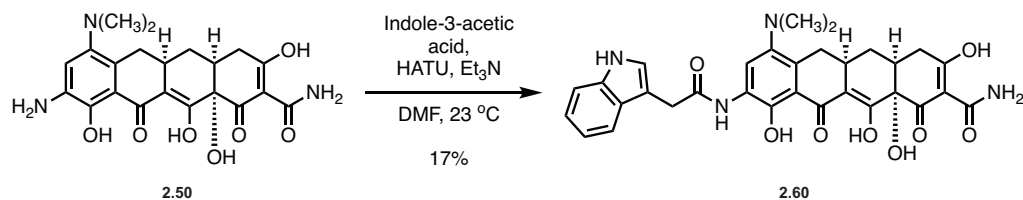
### Analogue 2.59:

Analogue 2.59 was prepared using General Procedure B: 9-amino-4-dedimethylamino minocycline (2.50, 5 mg, 0.012 mmol) was reacted with benzofuran-2-carboxylic acid to provide the formate salt of Analogue 2.59 as a yellow solid following preparatory HPLC purification (0.4 mg, 6%).

<sup>1</sup>H NMR (500 MHz, CD<sub>3</sub>OD) δ 8.39 (d, *J* = 5.6 Hz, 2H), 7.85 – 7.77 (m, 1H), 7.68 (d, *J* = 11.9 Hz, 1H), 7.53 (t, *J* = 8.0 Hz, 1H), 7.49 (s, 1H), 7.38 (t, *J* = 7.4 Hz, 1H), 3.39 (dd, *J* = 15.8, 3.6 Hz, 1H), 2.90 – 2.77 (app. m, 1H), 2.65 (s, 6H), 2.54 – 2.38 (m, 2H), 2.19 (dd, *J* = 13.1, 13.1 Hz, 1H), 2.09 (ddd, *J* = 13.5, 8.7, 1.5 Hz, 1H), 1.67 (td, *J* = 13.0, 11.9 Hz, 1H).

An additional signal (dd) is hidden beneath the MeOH peak (δ: 3.31).

HRMS (ESI+, *m/z*) [M + H]<sup>+</sup> calc'd for C<sub>30</sub>H<sub>27</sub>N<sub>3</sub>O<sub>9</sub>: 574.1820. Found: 574.1811.

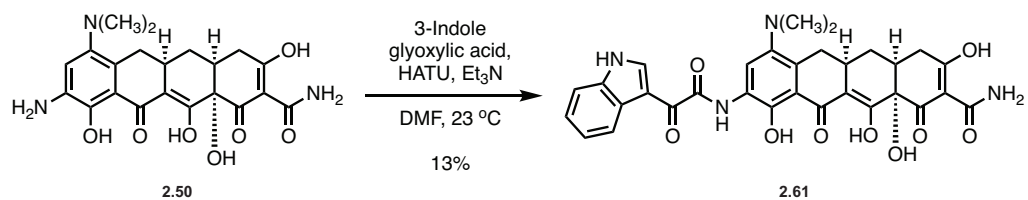


**Analogue 2.60:**

Analogue **2.60** was prepared using General Procedure B: 9-amino-4-dedimethylamino minocycline (**2.50**, 8 mg, 0.019 mmol) was reacted with indole-3-acetic acid to provide the formate salt of Analogue **2.60** as a yellow solid following preparatory HPLC purification (1.9 mg, 17%).

<sup>1</sup>H NMR (400 MHz, CD<sub>3</sub>OD) δ 8.27 (s, 1H), 7.58 (d, *J* = 7.9 Hz, 1H), 7.38 (d, *J* = 8.1 Hz, 1H), 7.30 (s, 1H), 7.13 (t, *J* = 7.6 Hz, 1H), 7.04 (t, *J* = 7.1 Hz, 1H), 3.91 (s, 2H), 3.28 – 3.17 (m, 2H), 2.78 – 2.66 (app. m, 1H), 2.55 (s, 6H), 2.46 – 2.32 (m, 2H), 2.13 – 1.97 (m, 2H), 1.57 (td, *J* = 13.2, 12.8 Hz, 1H). An additional signal (dd) is hidden beneath the MeOH peak (δ: 3.31).

HRMS (ESI+, *m/z*) [M + H]<sup>+</sup> calc'd for C<sub>31</sub>H<sub>30</sub>N<sub>4</sub>O<sub>8</sub>: 587.2136. Found: 587.2124.

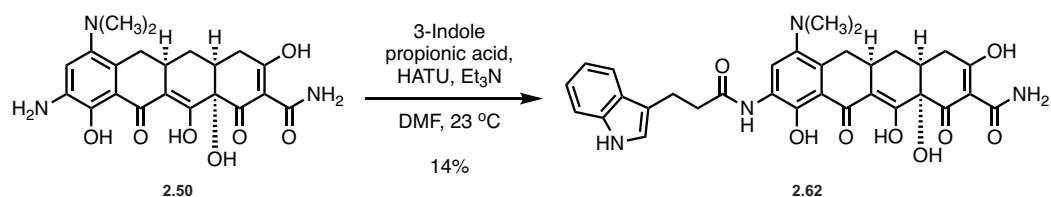


### Analogue **2.61**:

Analogue **2.61** was prepared using General Procedure B: 9-amino-4-dedimethylamino minocycline (**2.50**, 8 mg, 0.019 mmol) was reacted with 3-indoleglyoxylic acid to provide the formate salt of Analogue **2.61** as a yellow solid following preparatory HPLC purification (1.5 mg, 13%).

<sup>1</sup>H NMR (400 MHz, CD<sub>3</sub>OD) δ 9.01 (s, 1H), 8.65 (s, 1H), 8.33 (t, *J* = 4.3 Hz, 1H), 7.53 – 7.45 (m, 1H), 7.32 – 7.24 (m, 2H), 3.26 – 3.16 (app. m, 1H), 2.79 (m, 7H), 2.49 – 2.33 (m, 2H), 2.14 (dd, *J* = 14.5, 14.5 Hz, 1H), 2.01 (app. d, *J* = 13.4 Hz, 1H), 1.59 (td, *J* = 12.6, 12.5 Hz, 1H). An additional signal (dd) is hidden beneath the MeOH peak (δ: 3.31).

HRMS (ESI+, *m/z*) [M + H]<sup>+</sup> calc'd for C<sub>31</sub>H<sub>28</sub>N<sub>4</sub>O<sub>9</sub>: 601.1929. Found: 601.1918.

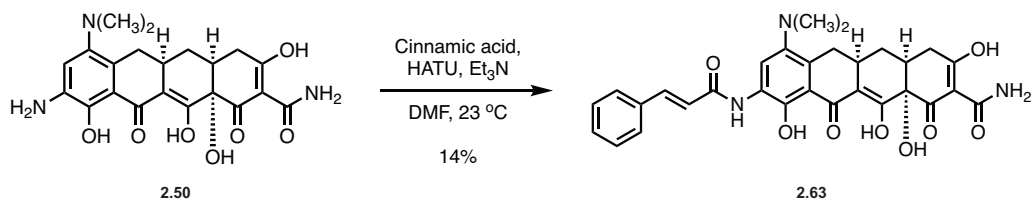


### Analogue 2.62:

Analogue **2.62** was prepared using General Procedure B: 9-amino-4-dedimethylamino minocycline (**2.50**, 10 mg, 0.023 mmol) was reacted with 3-indolepropionic acid to provide the formate salt of Analogue **2.62** as a yellow solid following preparatory HPLC purification (1.9 mg, 14%).

$^1\text{H NMR}$  (400 MHz,  $\text{CD}_3\text{OD}$ )  $\delta$  8.07 (s, 1H), 7.59 (d,  $J = 7.9$  Hz, 1H), 7.31 (d,  $J = 8.1$  Hz, 1H), 7.12 – 7.04 (m, 2H), 6.99 (t,  $J = 7.4$  Hz, 1H), 3.23 (dd,  $J = 17.5, 4.6$  Hz, 1H), 3.16 (t,  $J = 7.5$  Hz, 2H), 2.83 (t,  $J = 8.2$  Hz, 2H), 2.79 – 2.69 (app. m, 1H), 2.56 (s, 6H), 2.49 – 2.33 (m, 2H), 2.11 (dd,  $J = 15.6, 13.6$  Hz, 1H), 2.03 (ddd,  $J = 13.7, 5.4, 2.6$  Hz, 1H), 1.60 (td,  $J = 13.3, 10.8$  Hz, 1H). An additional signal (dd) is hidden beneath the MeOH peak ( $\delta$ : 3.31).

HRMS (ESI+,  $m/z$ )  $[\text{M} + \text{H}]^+$  calc'd for  $\text{C}_{32}\text{H}_{32}\text{N}_4\text{O}_8$ : 601.2293. Found: 601.2282.

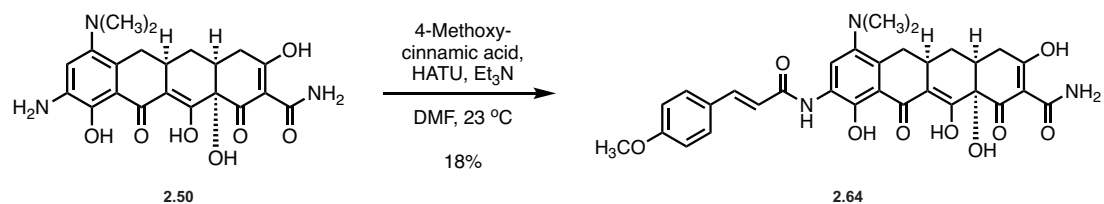


### Analogue 2.63:

Analogue **2.63** was prepared using General Procedure B: 9-amino-4-dedimethylamino minocycline (**2.50**, 10 mg, 0.023 mmol) was reacted with cinnamic acid to provide the formate salt of Analogue **2.63** as a yellow solid following preparatory HPLC purification (1.8 mg, 14%).

<sup>1</sup>H NMR (400 MHz, CD<sub>3</sub>OD) δ 8.36 (s, 1H), 7.70 – 7.59 (m, 3H), 7.46 – 7.35 (m, 3H), 7.00 (d, *J* = 15.7 Hz, 1H), 3.34 (dd, *J* = 16.4, 4.3 Hz, 1H), 3.24 (dd, *J* = 18.0, 5.2 Hz, 1H), 2.78 (ddt, *J* = 14.8, 10.2, 4.9 Hz, 1H), 2.61 (s, 5H), 2.50 – 2.35 (m, 2H), 2.13 (dd, *J* = 15.5, 13.6 Hz, 1H), 2.05 (ddd, *J* = 13.5, 5.4, 2.7 Hz, 1H), 1.62 (td, *J* = 13.4, 10.8 Hz, 1H).

HRMS (ESI+, *m/z*) [M + H]<sup>+</sup> calc'd for C<sub>30</sub>H<sub>29</sub>N<sub>3</sub>O<sub>8</sub>: 560.2027. Found: 560.2020.



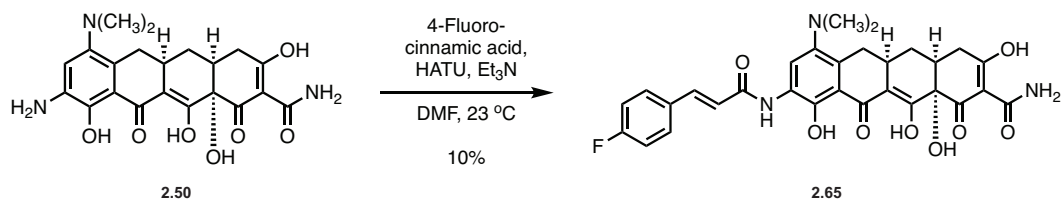
**Analogue 2.64:**

Analogue **2.64** was prepared using General Procedure B: 9-amino-4-dedimethylamino minocycline (**2.50**, 10 mg, 0.023 mmol) was reacted with 4-methoxycinnamic acid to provide the formate salt of Analogue **2.64** as a yellow solid following preparatory HPLC purification (2.5 mg, 18%).

<sup>1</sup>H NMR (400 MHz, CD<sub>3</sub>OD) δ 8.36 (s, 1H), 7.66 – 7.54 (m, 3H), 6.96 (d, *J* = 8.5 Hz, 2H), 6.84 (d, *J* = 15.6 Hz, 1H), 3.83 (s, 3H), 3.39 – 3.33 (app. m, 1H), 3.23 (app. d, *J* = 5.5 Hz, 1H), 2.78 (ddt, *J* = 15.9, 8.5 Hz, 1H), 2.61 (s, 6H), 2.50 – 2.34 (m, 2H), 2.14 (dd, *J* = 14.5, 0.9 Hz, 1H), 2.05 (ddd, *J* = 13.1, 8.3, 3.0 Hz, 1H), 1.62 (td, *J* = 13.0, 11.4 Hz, 1H).

HRMS (ESI+, *m/z*) [M + H]<sup>+</sup> calc'd for C<sub>31</sub>H<sub>31</sub>N<sub>3</sub>O<sub>9</sub>: 590.2133. Found: 590.2122.



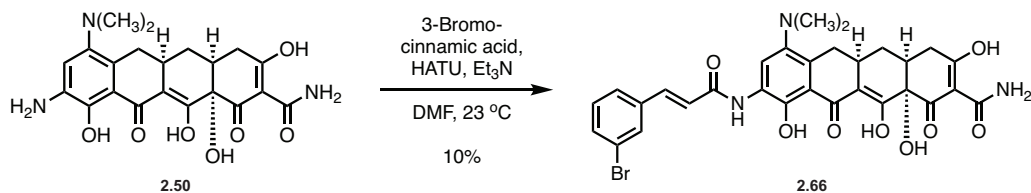


**Analogue 2.65:**

Analogue **2.65** was prepared using General Procedure B: 9-amino-4-dedimethylamino minocycline (**2.50**, 8 mg, 0.019 mmol) was reacted with 4-fluorocinnamic acid to provide the formate salt of Analogue **2.65** as a yellow solid following preparatory HPLC purification (1.1 mg, 10%).

<sup>1</sup>H NMR (400 MHz, CD<sub>3</sub>OD) δ 8.36 (s, 1H), 7.71 – 7.61 (m, 3H), 7.16 (t, *J* = 8.7 Hz, 2H), 6.95 (d, *J* = 15.6 Hz, 1H), 3.35 (app. d, *J* = 3.9 Hz, 1H), 3.23 – 3.17 (app. m, 1H), 2.83 – 2.72 (app. m, 1H), 2.60 (s, 6H), 2.49 – 2.33 (m, 2H), 2.14 (dd, *J* = 13.5, 11.7 Hz, 1H), 2.05 (ddd, *J* = 13.3, 7.4, 2.7 Hz, 1H), 1.63 (td, *J* = 12.9, 10.3 Hz, 1H).

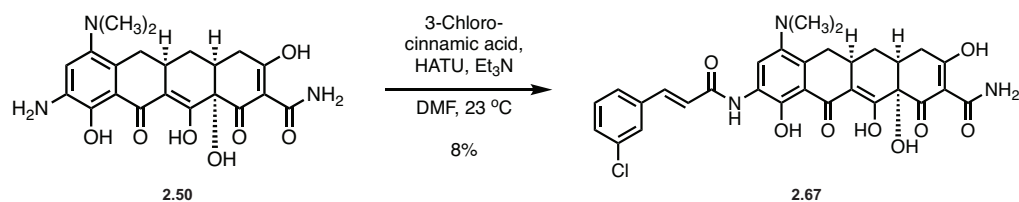
HRMS (ESI+, *m/z*) [M + H]<sup>+</sup> calc'd for C<sub>30</sub>H<sub>28</sub>FN<sub>3</sub>O<sub>8</sub>: 578.1933. Found: 578.1922.



**Analogue 2.66:**

Analogue **2.66** was prepared using General Procedure B: 9-amino-4-dedimethylamino minocycline (**2.50**, 8 mg, 0.019 mmol) was reacted with 3-bromocinnamic acid to provide the formate salt of Analogue **2.66** as a yellow solid following preparatory HPLC purification (1.2 mg, 10%).

<sup>1</sup>H NMR (400 MHz, CD<sub>3</sub>OD) δ 8.36 (s, 1H), 7.81 (d, *J* = 1.8 Hz, 1H), 7.64 – 7.52 (m, 3H), 7.34 (t, *J* = 7.9 Hz, 1H), 7.03 (d, *J* = 15.6 Hz, 1H), 3.36 (app. d, *J* = 4.3 Hz, 1H), 3.23 (app. d, *J* = 5.1 Hz, 1H), 2.84 – 2.72 (app. m, 1H), 2.61 (s, 6H), 2.52 – 2.35 (m, 2H), 2.14 (dd, *J* = 15.4, 13.8 Hz, 1H), 2.05 (ddd, *J* = 13.3, 7.9, 2.9 Hz, 1H), 1.62 (td, *J* = 13.4, 10.8 Hz, 1H). HRMS (ESI+, *m/z*) [M + H]<sup>+</sup> calc'd for C<sub>30</sub>H<sub>28</sub>BrN<sub>3</sub>O<sub>8</sub>: 638.1133. Found: 638.1118.

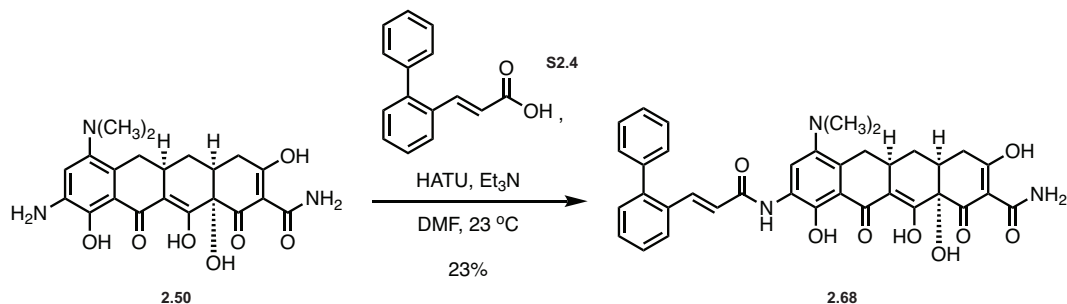


**Analogue 2.67:**

Analogue **2.67** was prepared using General Procedure B: 9-amino-4-dedimethylamino minocycline (**2.50**, 8 mg, 0.019 mmol) was reacted with 3-chlorocinnamic acid to provide the formate salt of Analogue **2.67** as a yellow solid following preparatory HPLC purification (0.9 mg, 8%).

<sup>1</sup>H NMR (400 MHz, CD<sub>3</sub>OD) δ 8.36 (d, *J* = 2.5 Hz, 1H), 7.67 – 7.51 (m, 3H), 7.44 – 7.33 (m, 2H), 7.03 (d, *J* = 15.6 Hz, 1H), 3.36 (app. d, *J* = 4.3 Hz, 1H), 3.24 (dd, *J* = 13.1, 5.5 Hz, 1H), 2.84 – 2.72 (app. m, 1H), 2.60 (s, 6H), 2.51 – 2.34 (m, 2H), 2.14 (dd, *J* = 15.6, 13.6 Hz, 1H), 2.05 (ddd, *J* = 14.3, 8.1, 2.7 Hz, 1H), 1.62 (td, *J* = 13.5, 10.8 Hz, 1H).

HRMS (ESI+, *m/z*) [M + H]<sup>+</sup> calc'd for C<sub>30</sub>H<sub>28</sub>ClN<sub>3</sub>O<sub>8</sub>: 594.1638. Found: 594.1629.

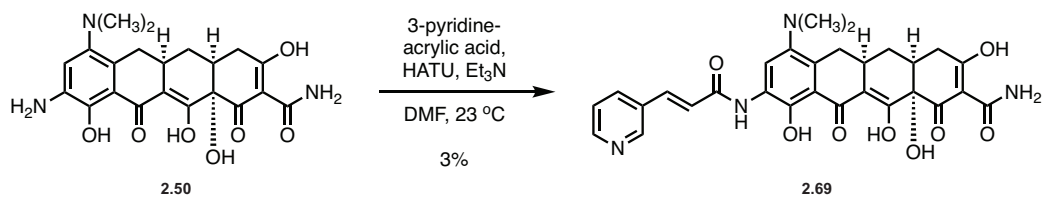


### Analogue 2.68:

Analogue **2.68** was prepared using General Procedure B: 9-amino-4-dedimethylamino minocycline (**2.50**, 10 mg, 0.023 mmol) was reacted with 1,1'-biphenyl-2-acrylic acid (**S2.5**) to provide the formate salt of Analogue **2.68** as a yellow solid following preparatory HPLC purification (3.4 mg, 23%).

<sup>1</sup>H NMR (500 MHz, 1:1 CDCl<sub>3</sub> : CD<sub>3</sub>OD) δ 7.80 (d, *J* = 7.5 Hz, 1H), 7.74 (d, *J* = 15.6 Hz, 1H), 7.47 – 7.25 (m, 9H), 6.84 (d, *J* = 15.5 Hz, 1H), 3.28 – 3.16 (m, 2H), 2.87 – 2.65 (m, 7H), 2.50 – 2.33 (m, 2H), 2.22 (app. t, *J* = 14.6 Hz, 1H), 2.04 (ddd, *J* = 13.5, 7.6, 2.3 Hz, 1H), 1.65 (td, *J* = 13.4, 10.9 Hz, 1H).

HRMS (ESI+, *m/z*) [M + H]<sup>+</sup> calc'd for C<sub>36</sub>H<sub>33</sub>N<sub>3</sub>O<sub>8</sub>: 636.2340. Found: 636.2331.

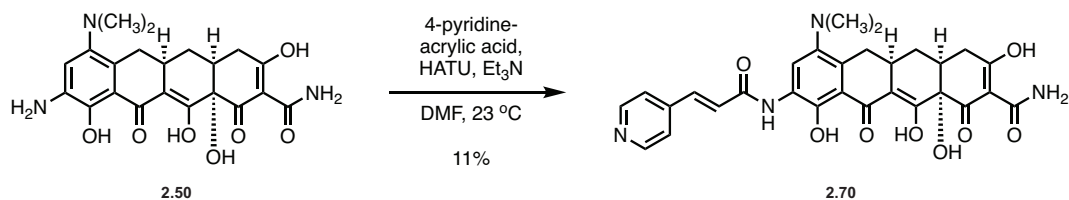


### Analogue 2.69:

Analogue **2.69** was prepared using General Procedure B: 9-amino-4-dedimethylamino minocycline (**2.50**, 8 mg, 0.019 mmol) was reacted with 3-pyridineacrylic acid to provide the formate salt of Analogue **2.69** as a yellow solid following preparatory HPLC purification (0.3 mg, 3%).

<sup>1</sup>H NMR (400 MHz, CD<sub>3</sub>OD) δ 8.78 (s, 1H), 8.54 (d, *J* = 4.8 Hz, 1H), 8.38 (s, 1H), 8.12 (d, *J* = 7.9 Hz, 1H), 7.69 (d, *J* = 15.8 Hz, 1H), 7.50 (dd, *J* = 8.1, 4.9 Hz, 1H), 7.15 (d, *J* = 15.8 Hz, 1H), 3.37 (app. d, *J* = 4.4 Hz, 1H), 3.24 (app. d, *J* = 6.2 Hz, 1H), 2.86 – 2.73 (app. m, 1H), 2.61 (s, 6H), 2.51 – 2.35 (m, 2H), 2.15 (dd, *J* = 15.6, 14.1 Hz, 1H), 2.05 (ddd, *J* = 13.1, 8.3, 1.7 Hz, 1H), 1.63 (td, *J* = 13.3, 10.7 Hz, 1H).

HRMS (ESI+, *m/z*) [M + H]<sup>+</sup> calc'd for C<sub>39</sub>H<sub>28</sub>N<sub>4</sub>O<sub>8</sub>: 561.1980. Found: 561.1971.

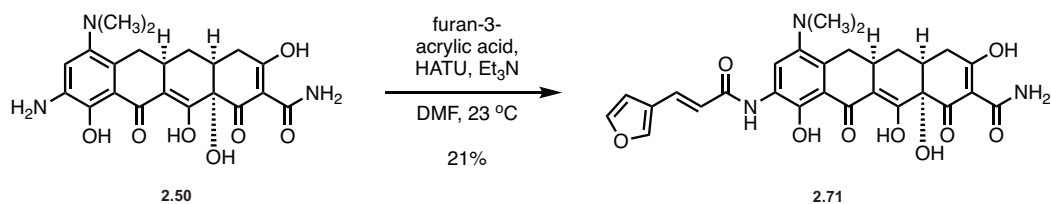


### Analogue 2.70:

Analogue **2.70** was prepared using General Procedure B: 9-amino-4-dedimethylamino minocycline (**2.50**, 8 mg, 0.019 mmol) was reacted with 4-pyridineacrylic acid to provide the formate salt of Analogue **2.70** as a yellow solid following preparatory HPLC purification (1.1 mg, 11%).

<sup>1</sup>H NMR (400 MHz, CD<sub>3</sub>OD) δ 8.59 (d, *J* = 5.2 Hz, 2H), 8.37 (s, 1H), 7.67 – 7.58 (m, 3H), 7.26 (d, *J* = 15.7 Hz, 1H), 3.36 (dd, *J* = 15.6, 4.6 Hz, 1H), 3.23 (app. d, *J* = 5.5 Hz, 1H), 2.79 (ddt, *J* = 15.2, 10.5, 5.0 Hz, 1H), 2.61 (s, 6H), 2.51 – 2.35 (m, 2H), 2.16 (dd, *J* = 14.3, 14.1 Hz, 1H), 2.06 (ddd, *J* = 15.2, 6.2, 3.3 Hz, 1H), 1.62 (td, *J* = 13.5, 10.7 Hz, 1H).

HRMS (ESI+, *m/z*) [M + H]<sup>+</sup> calc'd for C<sub>39</sub>H<sub>28</sub>N<sub>4</sub>O<sub>8</sub>: 561.1980. Found: 561.1971.

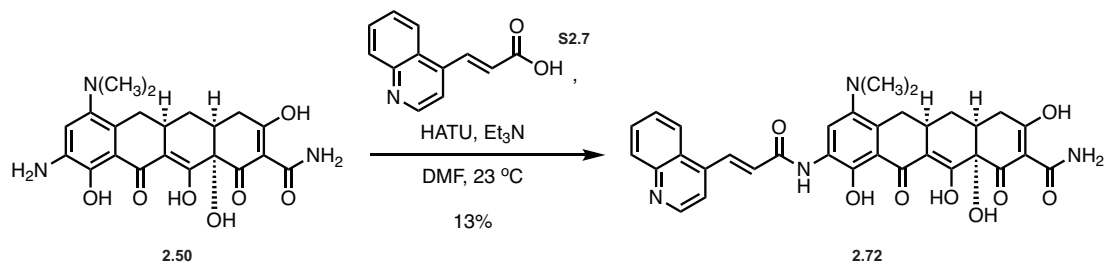


### Analogue 2.71:

Analogue **2.71** was prepared using General Procedure B: 9-amino-4-dedimethylamino minocycline (**2.50**, 8 mg, 0.019 mmol) was reacted with furan-3-acrylic acid to provide the formate salt of Analogue **2.71** as a yellow solid following preparatory HPLC purification (2.2 mg, 21%).

<sup>1</sup>H NMR (400 MHz, CD<sub>3</sub>OD) δ 8.34 (s, 1H), 7.84 (s, 1H), 7.62 – 7.52 (m, 2H), 6.76 (d, *J* = 1.9 Hz, 1H), 6.70 (d, *J* = 15.5 Hz, 1H), 3.35 (app. d, *J* = 4.3 Hz, 1H), 3.24 (app. d, *J* = 6.3 Hz, 1H), 2.78 (ddt, *J* = 15.1, 10.7, 4.8 Hz, 1H), 2.60 (s, 6H), 2.51 – 2.34 (m, 2H), 2.13 (dd, *J* = 15.5, 13.6 Hz, 1H), 2.05 (ddd, *J* = 13.5, 5.4, 2.7 Hz, 1H), 1.62 (td, *J* = 13.3, 10.8 Hz, 1H).

HRMS (ESI+, *m/z*) [M + H]<sup>+</sup> calc'd for C<sub>28</sub>H<sub>27</sub>N<sub>3</sub>O<sub>9</sub>: 550.1820. Found: 550.1811.



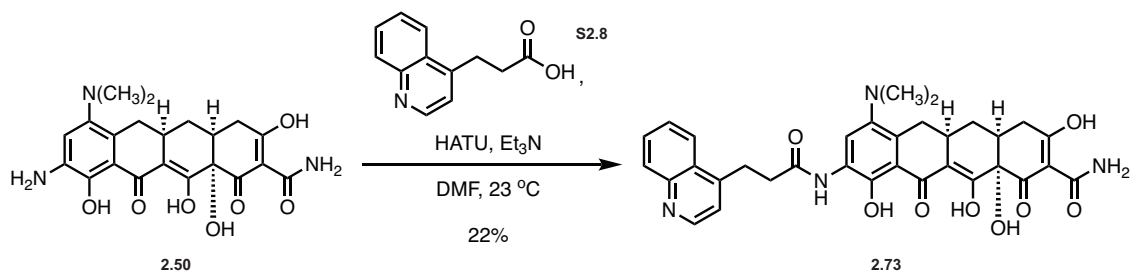
### Analogue 2.72:

Analogue **2.72** was prepared using General Procedure B: 9-amino-4-dedimethylamino minocycline (**2.50**, 8 mg, 0.019 mmol) was reacted with quinoline-4-acrylic acid (**S2.7**) to provide the formate salt of Analogue **2.72** as a yellow solid following preparatory HPLC purification (1.5 mg, 13%).

<sup>1</sup>H NMR (400 MHz, CD<sub>3</sub>OD) δ 8.89 (d, *J* = 4.6 Hz, 1H), 8.46 (m, 2H), 8.34 (d, *J* = 8.4 Hz, 1H), 8.09 (d, *J* = 8.5 Hz, 1H), 7.88 – 7.79 (m, 2H), 7.73 (t, *J* = 7.6 Hz, 1H), 7.30 (d, *J* = 15.5 Hz, 1H), 3.37 (app. d, *J* = 4.3 Hz, 1H), 3.23 (app. d, *J* = 5.7 Hz, 1H), 2.79 (ddt, *J* = 15.0, 10.2, 4.8 Hz, 1H), 2.63 (s, 6H), 2.51 – 2.35 (m, 2H), 2.16 (dd, *J* = 14.8, 13.8 Hz, 1H), 2.07 (ddd, *J* = 13.8, 8.0, 2.6 Hz, 1H), 1.63 (td, *J* = 13.0, 10.5 Hz, 1H).

HRMS (ESI+, *m/z*) [M + H]<sup>+</sup> calc'd for C<sub>33</sub>H<sub>30</sub>N<sub>4</sub>O<sub>8</sub>: 611.2136. Found: 611.2121.

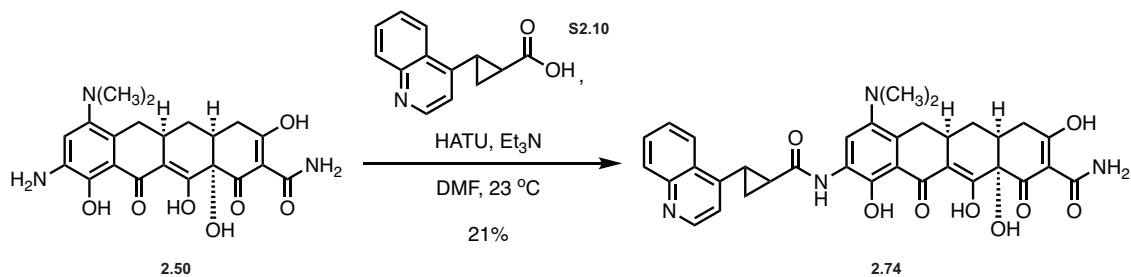




### Analogue 2.73:

Analogue **2.73** was prepared using General Procedure B: 9-amino-4-dedimethylamino minocycline (**2.50**, 8 mg, 0.019 mmol) was reacted with 4-quinolinepropanoic acid (**S2.8**) to provide the formate salt of Analogue **2.73** as a yellow solid following preparatory HPLC purification (2.5 mg, 22%).

<sup>1</sup>H NMR (400 MHz, CD<sub>3</sub>OD) δ 8.74 (d, *J* = 4.6 Hz, 1H), 8.27 (d, *J* = 8.4 Hz, 1H), 8.07 – 8.01 (m, 2H), 7.77 (t, *J* = 7.6 Hz, 1H), 7.67 (t, *J* = 7.6 Hz, 1H), 7.49 (d, *J* = 4.6 Hz, 1H), 3.56 (t, *J* = 7.6 Hz, 2H), 3.33 (app. d, *J* = 4.9 Hz, 1H), 3.22 (app. d, *J* = 5.8 Hz, 1H), 2.96 (t, *J* = 7.8 Hz, 2H), 2.80 – 2.69 (app. m, 1H), 2.57 (s, 6H), 2.48 – 2.34 (m, 1H), 2.11 (dd, *J* = 14.7, 14.3 Hz, 1H), 2.03 (ddd, *J* = 13.3, 7.8, 2.8 Hz, 1H), 1.61 (td, *J* = 13.6, 10.2 Hz, 1H). HRMS (ESI+, *m/z*) [M + H]<sup>+</sup> calc'd for C<sub>33</sub>H<sub>32</sub>N<sub>4</sub>O<sub>8</sub>: 613.2293. Found: 613.2280.

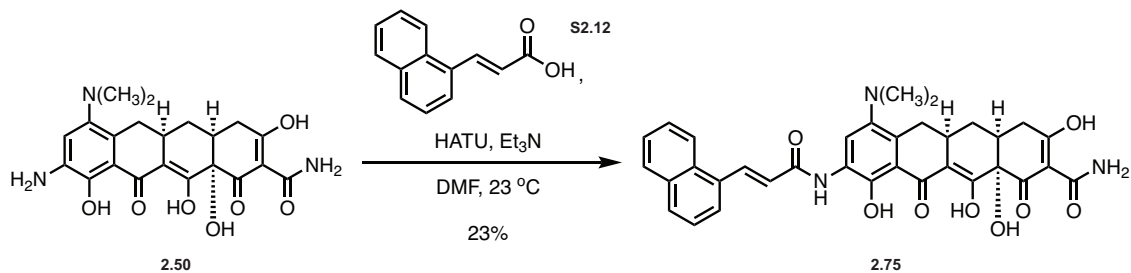


#### Analogue 2.74:

Analogue 2.74 was prepared using General Procedure B: 9-amino-4-dedimethylamino minocycline (**2.50**, 8 mg, 0.019 mmol) was reacted with cyclopropane quinoline derivative **S2.10** to provide the formate salt of Analogue 2.74 as a yellow solid as a mixture of diastereomers following preparatory HPLC purification (2.5 mg, 21%).

<sup>1</sup>H NMR (400 MHz, CD<sub>3</sub>OD) δ 8.77 (d, *J* = 4.6 Hz, 1H), 8.34 (d, *J* = 8.4 Hz, 1H), 8.26 (d, *J* = 3.8 Hz, 1H), 8.11 – 8.01 (m, 1H), 7.80 (dd, *J* = 8.5, 6.9 Hz, 1H), 7.70 (dt, *J* = 10.8, 5.3 Hz, 1H), 7.35 (d, *J* = 4.7 Hz, 1H), 3.36 (app. d, *J* = 4.3 Hz, 1H), 3.22 (app. d, *J* = 5.8 Hz, 1H), 3.16 – 3.05 (m, 1H), 2.82 – 2.72 (app. m, 1H), 2.61 (s, 6H), 2.50 – 2.35 (m, 3H), 2.14 (dd, *J* = 15.5, 13.7 Hz, 1H), 2.06 (ddd, *J* = 13.4, 7.7, 2.5 Hz, 1H), 1.85 – 1.75 (m, 1H), 1.68 – 1.55 (m, 2H).

HRMS (ESI+, *m/z*) [M + H]<sup>+</sup> calc'd for C<sub>34</sub>H<sub>32</sub>N<sub>4</sub>O<sub>8</sub>: 625.2293. Found: 625.2280.

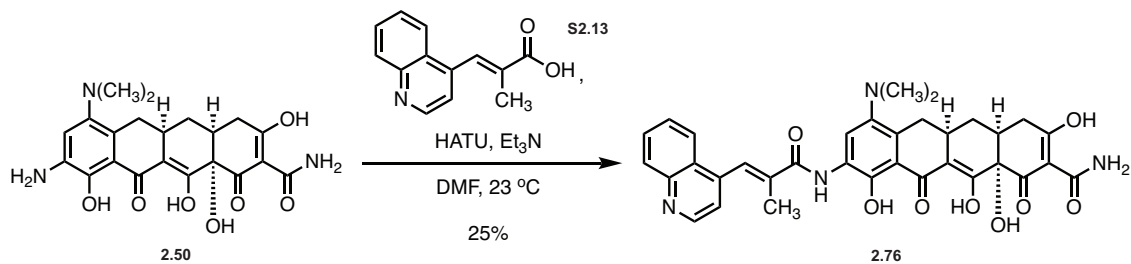


### Analogue 2.75:

Analogue **2.75** was prepared using General Procedure B: 9-amino-4-dedimethylamino minocycline (**2.50**, 5 mg, 0.012 mmol) was reacted with naphthalene-1-acrylic acid (**S2.12**) to provide the formate salt of Analogue **2.75** as a yellow solid following preparatory HPLC purification (1.6 mg, 23%).

<sup>1</sup>H NMR (500 MHz, CD<sub>3</sub>OD) δ 8.56 (d, *J* = 15.4 Hz, 1H), 8.44 (s, 1H), 8.29 (d, *J* = 8.5 Hz, 1H), 8.00 – 7.90 (m, 3H), 7.65 – 7.52 (m, 3H), 7.10 (d, *J* = 15.4 Hz, 1H), 3.36 (dd, *J* = 15.6, 4.5 Hz, 1H), 3.28 (dd, *J* = 18.3, 5.7 Hz, 1H), 2.79 (ddt, *J* = 15.2, 10.3, 4.7 Hz, 1H), 2.65 (s, 6H), 2.52 – 2.39 (m, 2H), 2.16 (dd, *J* = 15.1, 13.7 Hz, 1H), 2.07 (ddd, *J* = 13.2, 7.9, 2.6 Hz, 1H), 1.64 (td, *J* = 13.9, 11.5 Hz, 1H).

HRMS (ESI+, *m/z*) [M + H]<sup>+</sup> calc'd for C<sub>34</sub>H<sub>31</sub>N<sub>3</sub>O<sub>8</sub>: 610.2184. Found: 610.2172.

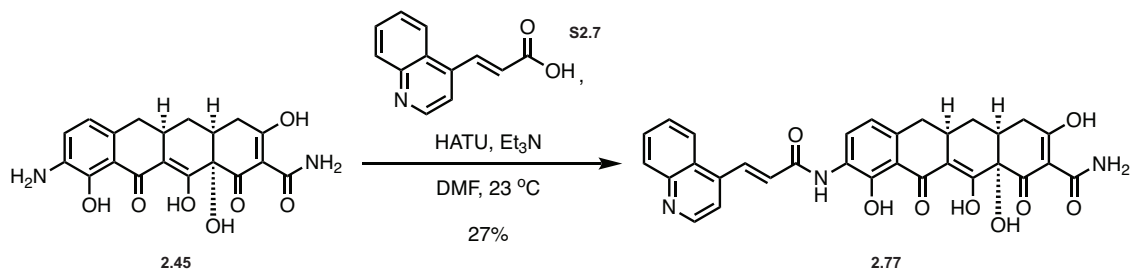


### Analogue 2.77:

Analogue 2.77 was prepared using General Procedure B: 9-amino-4-dedimethylamino minocycline (**2.50**, 5 mg, 0.012 mmol) was reacted with quinoline methacrylate derivative **S2.13** to provide the formate salt of Analogue 2.77 as a yellow solid following preparatory HPLC purification (1.8 mg, 25%).

<sup>1</sup>H NMR (400 MHz, CD<sub>3</sub>OD) δ 8.89 (d, *J* = 4.5 Hz, 1H), 8.20 (s, 1H), 8.09 (d, *J* = 8.4 Hz, 2H), 7.89 (s, 1H), 7.83 (t, *J* = 7.7 Hz, 1H), 7.68 (t, *J* = 7.6 Hz, 1H), 7.51 (d, *J* = 4.5 Hz, 1H), 3.36 (dd, *J* = 16.1, 3.6 Hz, 1H), 3.23 (app. d, *J* = 5.0 Hz, 1H), 2.84 – 2.75 (app. m, 1H), 2.63 (s, 6H), 2.51 – 2.34 (m, 2H), 2.17 (dd, *J* = 14.5, 14.0 Hz, 1H), 2.12 – 2.02 (m, 4H), 1.64 (td, *J* = 12.6, 10.5 Hz, 1H).

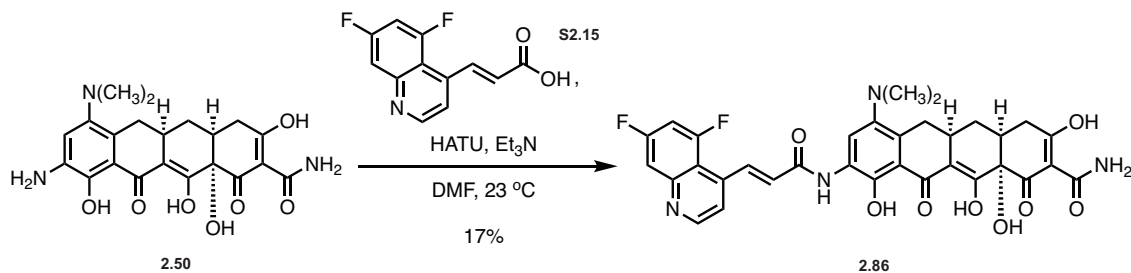
HRMS (ESI+, *m/z*) [M + H]<sup>+</sup> calc'd for C<sub>34</sub>H<sub>32</sub>N<sub>4</sub>O<sub>8</sub>: 625.2293. Found: 625.2285.



**Analogue 2.77:**

Analogue **2.77** was prepared using General Procedure B: 9-amino-Col-3 (**2.45**, 5 mg, 0.013 mmol) was reacted with quinoline-4-acrylic acid (**S2.7**) to provide Analogue **2.77** as a yellow solid following preparatory HPLC purification (2 mg, 27%).

HRMS (ESI+,  $m/z$ )  $[M + H]^+$  calc'd for C<sub>31</sub>H<sub>25</sub>N<sub>3</sub>O<sub>8</sub>: 568.1714. Found: 568.1704.

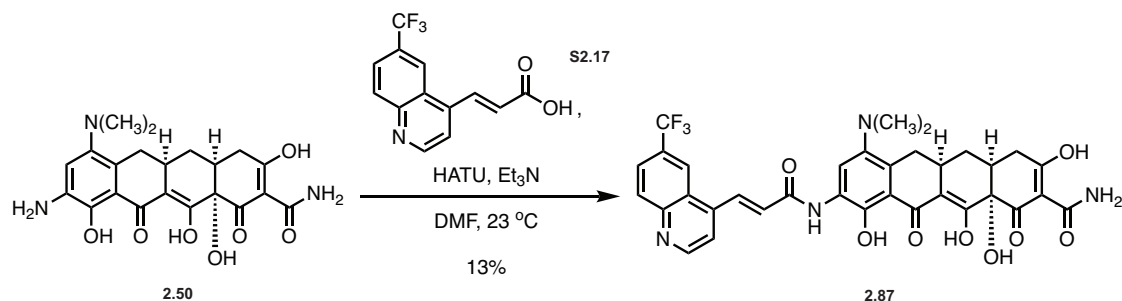


### Analogue 2.86:

Analogue **2.86** was prepared using General Procedure B: 9-amino-4-dedimethylamino minocycline (**2.50**, 10 mg, 0.023 mmol) was reacted with 5,7-difluoroquinoline acrylic acid derivative **S2.15** to provide the formate salt of Analogue **2.86** as a yellow solid following preparatory HPLC purification (2.5 mg, 17%).

<sup>1</sup>H NMR (500 MHz, 1:1 CDCl<sub>3</sub> : CD<sub>3</sub>OD) δ 8.88 (d, *J* = 5.0 Hz, 1H), 8.57 – 8.45 (m, 2H), 7.67 – 7.56 (m, 2H), 7.22 (t, *J* = 9.9 Hz, 1H), 6.96 (d, *J* = 15.2 Hz, 1H), 3.28 (app. s, 1H), 2.86 – 2.77 (app. m, 1H), 2.63 (s, 6H), 2.52 – 2.33 (m, 2H), 2.18 (dd, *J* = 15.0, 12.8 Hz, 1H), 2.06 (ddd, *J* = 13.0, 11.9, 3.0 Hz, 1H), 1.69 (td, *J* = 13.0, 12.7 Hz, 1H). An additional signal (dd) is hidden beneath the MeOH peak (δ: 3.31).

HRMS (ESI+, *m/z*) [M + H]<sup>+</sup> calc'd for C<sub>33</sub>H<sub>28</sub>F<sub>2</sub>N<sub>4</sub>O<sub>8</sub>: 647.1948. Found: 647.1935.



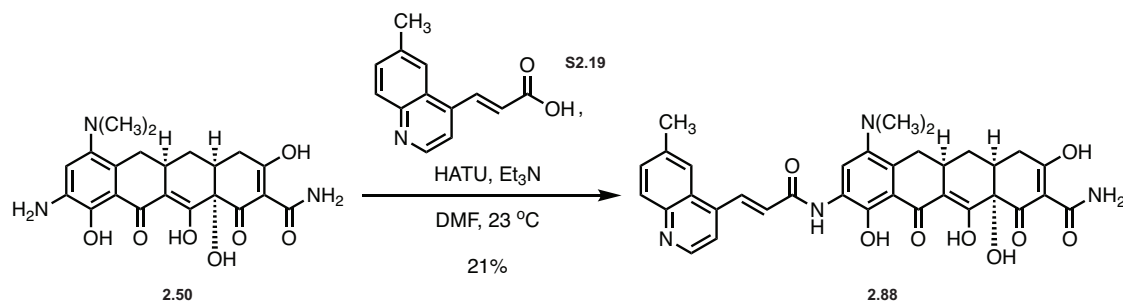
**Analogue 2.87:**

Analogue **2.87** was prepared using General Procedure B: 9-amino-4-dedimethylamino minocycline (**2.50**, 10 mg, 0.023 mmol) was reacted with 6-trifluoromethylquinoline acrylic acid derivative **S2.17** to provide the formate salt of Analogue **2.87** as a yellow solid following preparatory HPLC purification (2 mg, 13%).

<sup>1</sup>H NMR (500 MHz, 1:1 CDCl<sub>3</sub> : CD<sub>3</sub>OD) δ 9.02 (s, 1H), 8.61 (s, 1H), 8.48 (d, *J* = 15.5 Hz, 1H), 8.25 (d, *J* = 8.9 Hz, 1H), 7.99 (d, *J* = 8.9 Hz, 2H), 7.87 (s, 1H), 7.29 (d, *J* = 15.3 Hz, 1H), 3.26 (app. d, *J* = 15.6 Hz, 1H), 2.85 (br. s, 7H), 2.53 – 2.36 (m, 2H), 2.29 (dd, *J* = 15.6, 11.3 Hz, 1H), 2.07 (ddd, *J* = 14.3, 4.6, 2.1 Hz, 1H), 1.71 (td, *J* = 12.2, 11.3 Hz, 1H).

An additional signal (dd) is hidden beneath the MeOH peak (δ: 3.31).

HRMS (ESI+, *m/z*) [M + H]<sup>+</sup> calc'd for C<sub>34</sub>H<sub>29</sub>F<sub>3</sub>N<sub>4</sub>O<sub>8</sub>: 679.2010. Found: 679.1994.

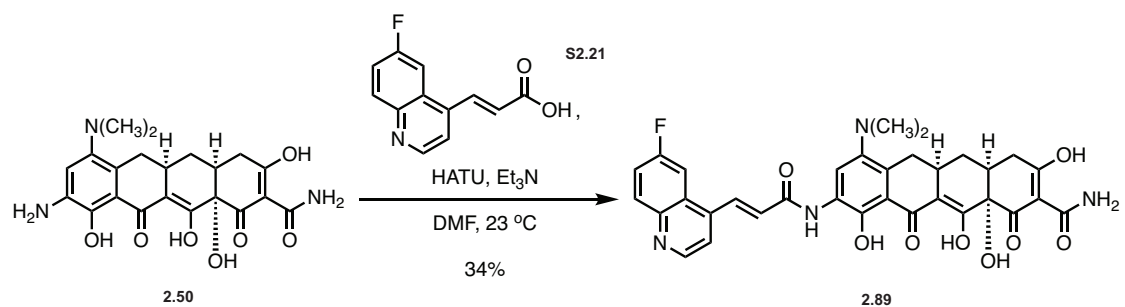


### Analogue 2.88:

Analogue **2.88** was prepared using General Procedure B: 9-amino-4-dedimethylamino minocycline (**2.50**, 5 mg, 0.012 mmol) was reacted with 6-methylquinoline acrylic acid derivative **S2.19** to provide the formate salt of Analogue **2.88** as a yellow solid following preparatory HPLC purification (1.5 mg, 21%).

<sup>1</sup>H NMR (500 MHz, 1:1 CDCl<sub>3</sub> : CD<sub>3</sub>OD) δ 8.95 (d, *J* = 5.3 Hz, 1H), 8.57 (s, 1H), 8.51 (d, *J* = 15.5 Hz, 1H), 8.27 (s, 1H), 8.11 – 8.02 (m, 2H), 7.90 (d, *J* = 8.5 Hz, 1H), 7.43 (d, *J* = 15.4 Hz, 1H), 2.90 – 2.82 (app. m, 1H), 2.75 (s, 6H), 2.68 (s, 3H), 2.53 – 2.36 (m, 2H), 2.25 (dd, *J* = 13.6, 13.6 Hz, 1H), 2.08 (ddd, *J* = 13.8, 8.4, 1.8 Hz, 1H), 1.70 (td, *J* = 13.9, 11.0 Hz, 1H). An additional two signals (dd) are hidden beneath the MeOH peak (δ: 3.31). HRMS (ESI+, *m/z*) [M + H]<sup>+</sup> calc'd for C<sub>34</sub>H<sub>32</sub>N<sub>4</sub>O<sub>8</sub>: 625.2293. Found: 625.2284.



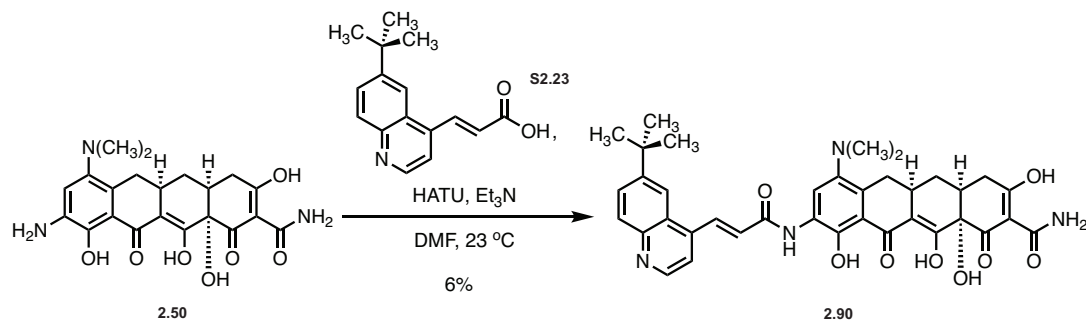


### Analogue 2.89:

Analogue **2.89** was prepared using General Procedure B: 9-amino-4-dedimethylamino minocycline (**2.50**, 5 mg, 0.012 mmol) was reacted with 6-fluoroquinoline acrylic acid derivative **S2.21** to provide the formate salt of Analogue **2.89** as a yellow solid following preparatory HPLC purification (2.5 mg, 34%).

<sup>1</sup>H NMR (500 MHz, CD<sub>3</sub>OD) δ 8.98 (d, *J* = 4.9 Hz, 1H), 8.82 (s, 1H), 8.44 (d, *J* = 15.5 Hz, 1H), 8.22 (dd, *J* = 9.3, 5.2 Hz, 1H), 8.11 (dd, *J* = 9.9, 2.7 Hz, 1H), 7.97 (d, *J* = 5.0 Hz, 1H), 7.79 (t, *J* = 8.0 Hz, 1H), 7.41 (d, *J* = 15.5 Hz, 1H), 3.19 (dd, *J* = 15.1, 4.8 Hz, 1H), 3.14 (s, 6H), 3.00 – 2.92 (app. m, 1H), 2.52 (ddd, *J* = 11.8, 8.4, 2.7 Hz, 1H), 2.48 – 2.39 (m, 2H), 2.13 (ddd, *J* = 13.2, 8.3, 2.6 Hz, 1H), 1.69 (td, *J* = 14.1, 11.9 Hz, 1H). An additional signal (dd) is hidden beneath the MeOH peak (δ: 3.31).

HRMS (ESI+, *m/z*) [M + H]<sup>+</sup> calc'd for C<sub>33</sub>H<sub>29</sub>FN<sub>4</sub>O<sub>8</sub>: 629.2042. Found: 629.2029.

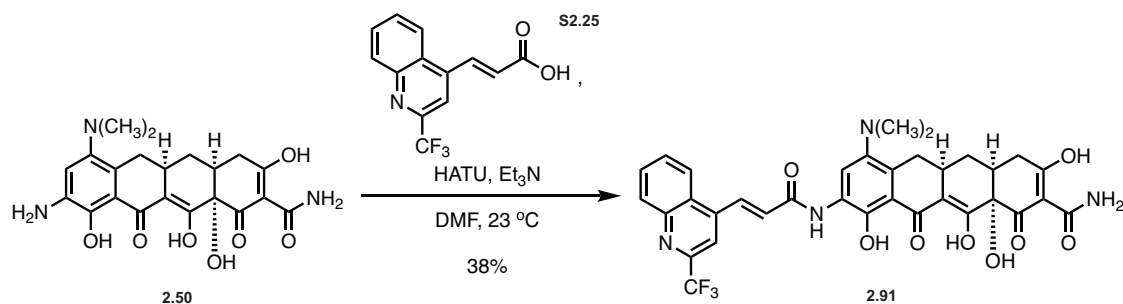


### Analogue 2.90:

Analogue **2.90** was prepared using General Procedure B: 9-amino-4-dedimethylamino minocycline (**2.50**, 8 mg, 0.019 mmol) was reacted with 6-*t*-butylquinoline acrylic acid derivative **S2.23** to provide the formate salt of Analogue **2.90** as a yellow solid following preparatory HPLC purification (0.7 mg, 6%).

<sup>1</sup>H NMR (400 MHz, CD<sub>3</sub>OD)  $\delta$  8.82 (d,  $J = 4.7$  Hz, 1H), 8.50 (d,  $J = 15.5$  Hz, 1H), 8.44 (s, 1H), 8.23 (s, 1H), 8.06 – 7.94 (m, 2H), 7.79 (d,  $J = 4.8$  Hz, 1H), 7.30 (d,  $J = 15.5$  Hz, 1H), 3.38 (app. d,  $J = 4.4$  Hz, 1H), 3.25 (app. d,  $J = 5.4$  Hz, 1H), 2.84 – 2.73 (app. m, 1H), 2.63 (s, 6H), 2.51 – 2.35 (m, 2H), 2.16 (dd,  $J = 15.9, 13.6$  Hz, 1H), 2.06 (ddd,  $J = 13.4, 8.5, 3.1$  Hz, 1H), 1.63 (td,  $J = 13.6, 10.5$  Hz, 1H), 1.48 (s, 9H).

HRMS (ESI+,  $m/z$ ) [M + H]<sup>+</sup> calc'd for C<sub>37</sub>H<sub>38</sub>N<sub>4</sub>O<sub>8</sub>: 667.2762. Found: 667.2750.

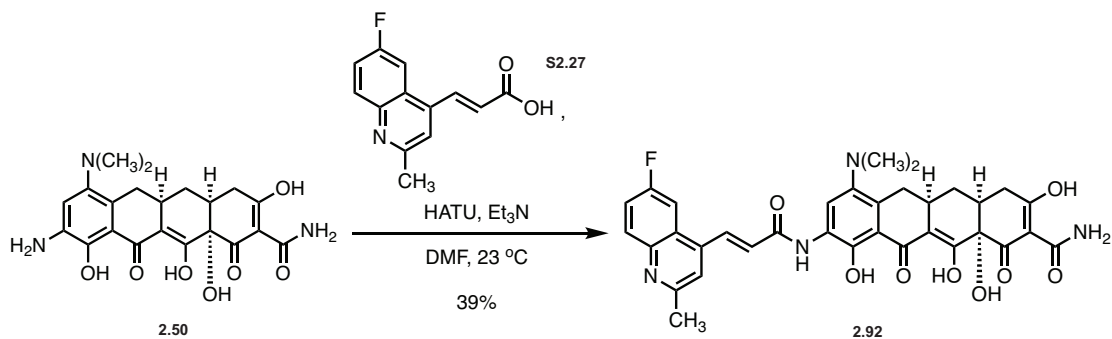


### Analogue 2.91:

Analogue **2.91** was prepared using General Procedure B: 9-amino-4-dedimethylamino minocycline (**2.50**, 5 mg, 0.012 mmol) was reacted with 2-trifluoromethylquinoline acrylic acid derivative **S2.25** to provide the formate salt of Analogue **2.91** as a yellow solid following preparatory HPLC purification (3 mg, 38%).

<sup>1</sup>H NMR (500 MHz, CD<sub>3</sub>OD) δ 8.78 (s, 1H), 8.54 (d, *J* = 15.5 Hz, 1H), 8.42 (d, *J* = 8.5 Hz, 1H), 8.25 (d, *J* = 8.5 Hz, 1H), 8.14 (s, 1H), 7.97 (t, *J* = 7.9 Hz, 1H), 7.88 (t, *J* = 7.6 Hz, 1H), 7.44 (d, *J* = 15.5 Hz, 1H), 3.28 (app. d, *J* = 5.9 Hz, 1H), 3.20 (dd, *J* = 15.5, 4.4 Hz, 1H), 3.08 (s, 6H), 2.98 – 2.89 (app. m, 1H), 2.52 (ddd, *J* = 12.7, 5.5, 1.7 Hz, 1H), 2.48 – 2.34 (m, 2H), 2.12 (ddd, *J* = 13.4, 6.2, 1.7 Hz, 1H), 1.68 (td, *J* = 13.6, 10.9 Hz, 1H).

HRMS (ESI+, *m/z*) [M + H]<sup>+</sup> calc'd for C<sub>34</sub>H<sub>29</sub>F<sub>3</sub>N<sub>4</sub>O<sub>8</sub>: 679.2010. Found: 679.1992.

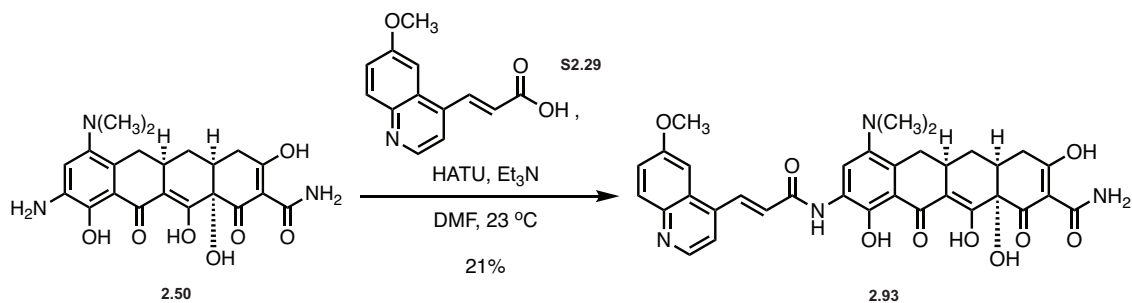


### Analogue 2.92:

Analogue **2.92** was prepared using General Procedure B: 9-amino-4-dedimethylamino minocycline (**2.50**, 5 mg, 0.012 mmol) was reacted with 2-methyl-6-fluoroquinoline acrylic acid derivative **S2.27** to provide the formate salt of Analogue **2.92** as a yellow solid following preparatory HPLC purification (2.9 mg, 39%).

<sup>1</sup>H NMR (500 MHz, CD<sub>3</sub>OD) δ 8.75 (s, 1H), 8.42 (d, *J* = 15.6 Hz, 1H), 8.24 – 8.16 (m, 2H), 8.08 (s, 1H), 7.91 (t, *J* = 9.8 Hz, 1H), 7.47 (d, *J* = 15.4 Hz, 1H), 3.24 (dd, *J* = 15.2, 4.5 Hz, 1H), 3.04 (s, 6H), 2.96 (s, 3H), 2.51 (ddd, *J* = 10.7, 5.4, 2.4 Hz, 1H), 2.47 – 2.34 (m, 2H), 2.13 (ddd, *J* = 13.1, 8.7, 3.3 Hz, 1H), 1.68 (td, *J* = 14.0, 10.7 Hz, 1H). An additional signal (dd) is hidden beneath the MeOH peak (δ: 3.31).

HRMS (ESI+, *m/z*) [M + H]<sup>+</sup> calc'd for C<sub>34</sub>H<sub>31</sub>FN<sub>4</sub>O<sub>8</sub>: 643.2199. Found: 643.2188.

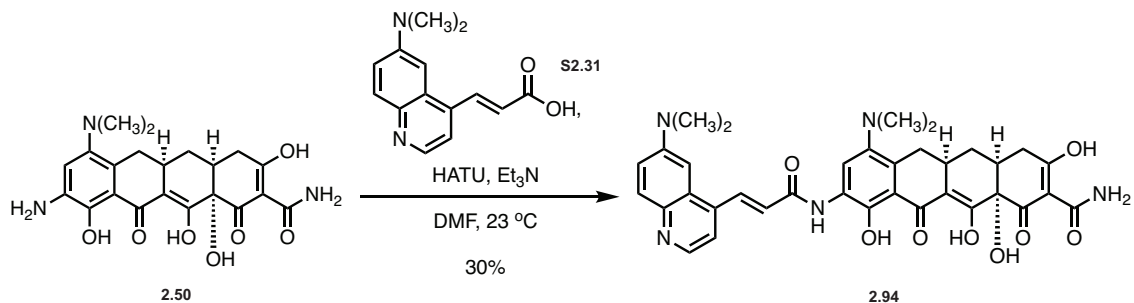


### Analogue 2.93:

Analogue **2.93** was prepared using General Procedure B: 9-amino-4-dedimethylamino minocycline (**2.50**, 5 mg, 0.012 mmol) was reacted with 6-methoxyquinoline acrylic acid derivative **S2.29** to provide the formate salt of Analogue **2.93** as a yellow solid following preparatory HPLC purification (1.6 mg, 21%).

<sup>1</sup>H NMR (500 MHz, 1:1 CDCl<sub>3</sub> : CD<sub>3</sub>OD) δ 8.86 (d, *J* = 5.4 Hz, 1H), 8.59 (d, *J* = 1.3 Hz, 1H), 8.47 (d, *J* = 15.4 Hz, 1H), 8.14 – 8.05 (m, 2H), 7.74 – 7.69 (m, 2H), 7.45 (d, *J* = 15.5 Hz, 1H), 4.08 (s, 3H), 2.93 – 2.82 (app. m, 1H), 2.78 (s, 6H), 2.52 – 2.36 (m, 2H), 2.26 (dd, *J* = 14.6, 13.8 Hz, 1H), 2.08 (ddd, *J* = 13.6, 8.3, 2.8 Hz, 1H), 1.70 (td, *J* = 11.8, 10.3 Hz, 1H). An additional two signals (dd) are hidden beneath the MeOH peak (δ: 3.31).

HRMS (ESI+, *m/z*) [M + H]<sup>+</sup> calc'd for C<sub>34</sub>H<sub>32</sub>N<sub>4</sub>O<sub>9</sub>: 641.2242. Found: 641.2230.

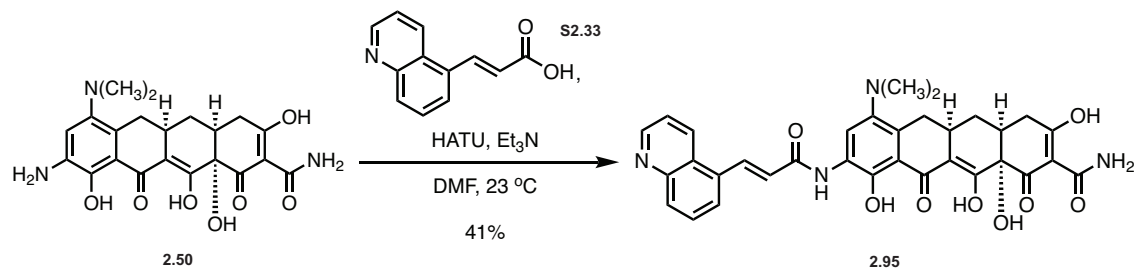


### Analogue 2.94:

Analogue **2.94** was prepared using General Procedure B: 9-amino-4-dedimethylamino minocycline (**2.50**, 5 mg, 0.012 mmol) was reacted with 6-dimethylaminoquinoline acrylic acid derivative **S2.31** to provide the formate salt of Analogue **2.94** as a yellow solid following preparatory HPLC purification (2.3 mg, 30%).

<sup>1</sup>H NMR (500 MHz, CD<sub>3</sub>OD) δ 8.67 (d, *J* = 8.2 Hz, 2H), 8.46 (d, *J* = 15.5 Hz, 1H), 8.09 – 8.03 (m, 2H), 7.91 – 7.85 (m, 1H), 7.50 (d, *J* = 15.2 Hz, 1H), 7.26 (s, 1H), 3.29 – 3.25 (m, 7H), 2.94 – 2.85 (m, 7H), 2.54 – 2.39 (m, 2H), 2.31 (dd, *J* = 14.0, 13.7 Hz, 1H), 2.11 (ddd, *J* = 12.7, 7.0, 2.5 Hz, 1H), 1.67 (dd, *J* = 13.0, 10.5 Hz, 1H). An additional signal (dd) is hidden beneath the MeOH peak (δ: 3.31).

HRMS (ESI+, *m/z*) [M + H]<sup>+</sup> calc'd for C<sub>35</sub>H<sub>35</sub>N<sub>5</sub>O<sub>8</sub>: 654.2558. Found: 654.2546.

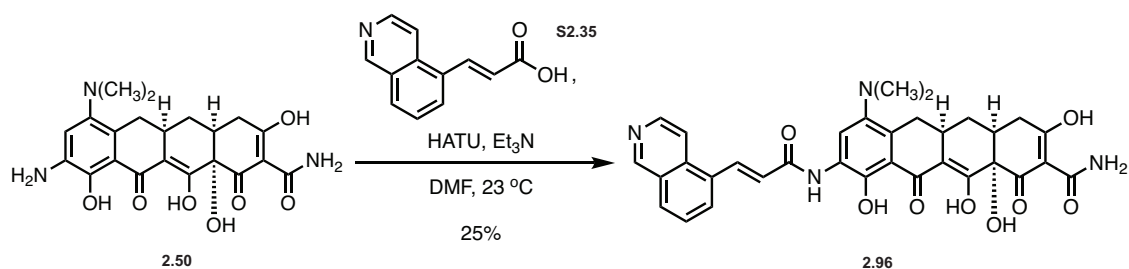


### Analogue 2.95:

Analogue **2.95** was prepared using General Procedure B: 9-amino-4-dedimethylamino minocycline (**2.50**, 5 mg, 0.012 mmol) was reacted with quinoline-5-acrylic acid derivative **S2.33** to provide the formate salt of Analogue **2.95** as a yellow solid following preparatory HPLC purification (2.9 mg, 41%).

<sup>1</sup>H NMR (500 MHz, 1:1 CDCl<sub>3</sub> : CD<sub>3</sub>OD) δ 9.13 (d, *J* = 8.7 Hz, 1H), 9.06 (dd, *J* = 4.8, 1.5 Hz, 1H), 8.67 (s, 1H), 8.49 (d, *J* = 15.4 Hz, 1H), 8.22 – 8.13 (m, 2H), 8.02 (dd, *J* = 8.5, 7.4 Hz, 1H), 7.90 (dd, *J* = 8.7, 4.8 Hz, 1H), 7.17 (d, *J* = 15.4 Hz, 1H), 3.30 – 3.22 (m, 2H), 2.93 – 2.90 (m, 7H), 2.53 – 2.36 (m, 2H), 2.31 (dd, *J* = 13.7, 13.7 Hz, 1H), 2.08 (ddd, *J* = 12.6, 6.3, 3.1 Hz, 1H), 1.69 (td, *J* = 13.4, 11.4 Hz, 1H).

HRMS (ESI+, *m/z*) [M + H]<sup>+</sup> calc'd for C<sub>33</sub>H<sub>30</sub>N<sub>4</sub>O<sub>8</sub>: 611.2136. Found: 611.2124.



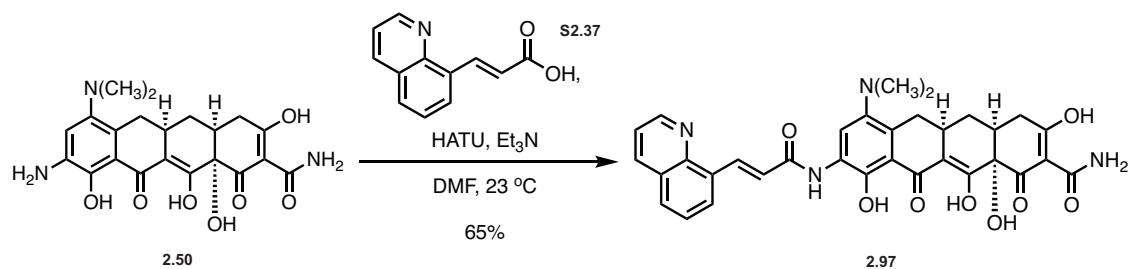
### Analogue 2.96:

Analogue **2.96** was prepared using General Procedure B: 9-amino-4-dedimethylamino minocycline (**2.50**, 5 mg, 0.012 mmol) was reacted with isoquinoline-5-acrylic acid derivative **S2.35** to provide the formate salt of Analogue **2.96** as a yellow solid following preparatory HPLC purification (1.8 mg, 25%).

<sup>1</sup>H NMR (500 MHz, 1:1 CDCl<sub>3</sub> : CD<sub>3</sub>OD) δ 9.57 (s, 1H), 8.62 – 8.57 (m, 2H), 8.53 (d, *J* = 6.6 Hz, 1H), 8.46 (d, *J* = 15.4 Hz, 1H), 8.41 (d, *J* = 7.3 Hz, 1H), 8.37 (d, *J* = 8.3 Hz, 1H), 7.96 (t, *J* = 7.8 Hz, 1H), 7.19 (d, *J* = 15.4 Hz, 1H), 3.28 (app. d, *J* = 4.6 Hz, 1H), 2.92 – 2.85 (app. m, 1H), 2.82 (s, 6H), 2.53 – 2.35 (m, 2H), 2.27 (dd, *J* = 13.6, 12.4 Hz, 1H), 2.08 (ddd, *J* = 12.1, 6.8, 1.1 Hz, 1H), 1.70 (td, *J* = 14.0, 11.3 Hz, 1H). An additional signal (dd) is hidden beneath the MeOH peak (δ: 3.31).

HRMS (ESI+, *m/z*) [M + H]<sup>+</sup> calc'd for C<sub>33</sub>H<sub>30</sub>N<sub>4</sub>O<sub>8</sub>: 611.2136. Found: 611.2125.



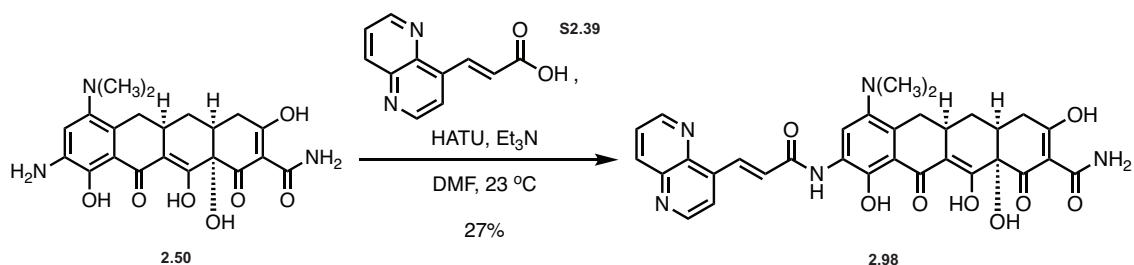


### Analogue 2.97:

Analogue **2.97** was prepared using General Procedure B: 9-amino-4-dedimethylamino minocycline (**2.50**, 5 mg, 0.012 mmol) was reacted with quinoline-8-acrylic acid derivative **S2.37** to provide the formate salt of Analogue **2.97** as a yellow solid following preparatory HPLC purification (4.6 mg, 65%).

$^1\text{H}$  NMR (500 MHz, 1:1  $\text{CDCl}_3$  :  $\text{CD}_3\text{OD}$ )  $\delta$  9.01 – 8.96 (m, 1H), 8.91 (d,  $J = 15.9$  Hz, 1H), 8.83 (s, 1H), 8.40 (dt,  $J = 8.3, 1.6$  Hz, 1H), 8.18 (d,  $J = 7.3$  Hz, 1H), 8.01 (d,  $J = 8.1$  Hz, 1H), 7.68 (d,  $J = 7.3$  Hz, 1H), 7.61 (ddd,  $J = 8.3, 4.3, 1.5$  Hz, 1H), 7.30 (dd,  $J = 16.1, 1.3$  Hz, 1H), 3.17 (app. d,  $J = 5.0$  Hz, 1H), 3.13 (s, 6H), 2.99 – 2.89 (m, 1H), 2.51 (ddd,  $J = 13.0, 8.0, 3.0$  Hz, 1H), 2.45 – 2.34 (m, 2H), 2.10 (ddd,  $J = 11.9, 5.3, 1.9$  Hz, 1H), 1.69 (td,  $J = 13.0, 11.1$  Hz, 1H). An additional signal (dd) is hidden beneath the MeOH peak ( $\delta$ : 3.31).

HRMS (ESI+,  $m/z$ )  $[\text{M} + \text{H}]^+$  calc'd for  $\text{C}_{33}\text{H}_{30}\text{N}_4\text{O}_8$ : 611.2136. Found: 611.2122.

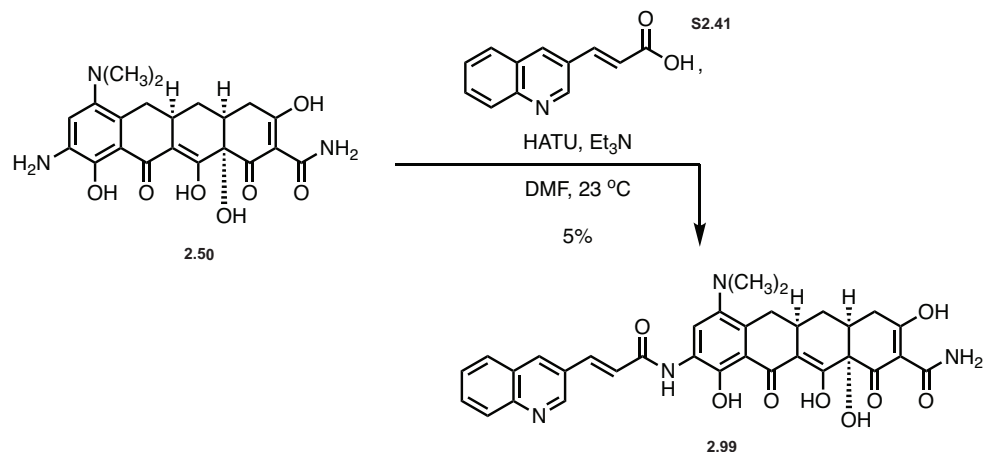


### Analogue **2.98**:

Analogue **2.98** was prepared using General Procedure B: 9-amino-4-dedimethylamino minocycline (**2.50**, 5 mg, 0.012 mmol) was reacted with 1,5-naphthyridine-4-acrylic acid derivative **S2.39** to provide the formate salt of Analogue **2.98** as a yellow solid following preparatory HPLC purification (1.9 mg, 27%).

<sup>1</sup>H NMR (500 MHz, 1:1 CDCl<sub>3</sub> : CD<sub>3</sub>OD) δ 9.07 (dd, *J* = 4.0, 1.6 Hz, 1H), 8.98 (d, *J* = 4.6 Hz, 1H), 8.82 (d, *J* = 15.9 Hz, 1H), 8.64 (s, 1H), 8.43 (dd, *J* = 8.9, 1.7 Hz, 2H), 8.00 (d, *J* = 4.6 Hz, 1H), 7.79 (dd, *J* = 8.6, 4.0 Hz, 1H), 7.51 (d, *J* = 15.9 Hz, 1H), 3.29 (app. d, *J* = 4.3 Hz, 1H), 2.91 – 2.79 (m, 6H), 2.53 – 2.35 (m, 2H), 2.28 (dd, *J* = 14.6, 13.6 Hz, 1H), 2.06 (ddd, *J* = 13.6, 7.7, 1.9 Hz, 1H), 1.68 (td, *J* = 13.6, 9.8 Hz, 1H). An additional signal (dd) is hidden beneath the MeOH peak (δ: 3.31).

HRMS (ESI+, *m/z*) [M + H]<sup>+</sup> calc'd for C<sub>32</sub>H<sub>29</sub>N<sub>5</sub>O<sub>8</sub>: 612.2089. Found:612.2080.

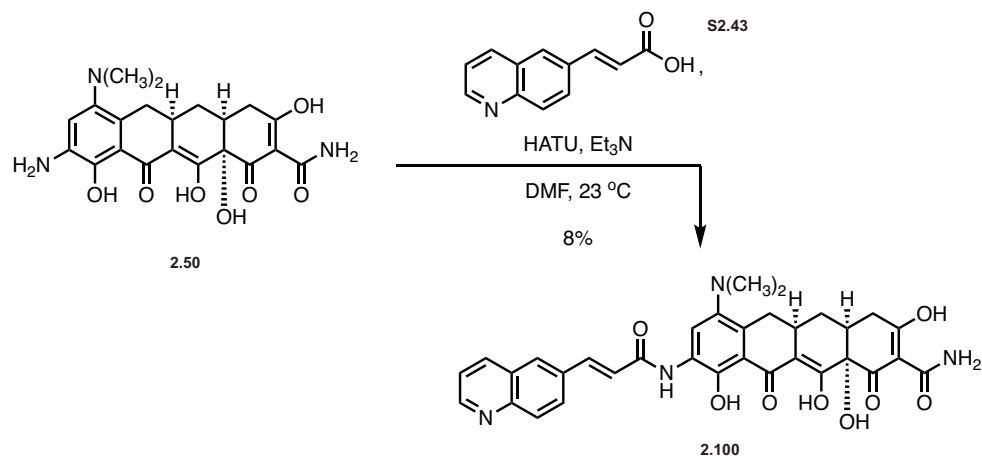


### Analogue 2.99:

Analogue **2.99** was prepared using General Procedure B: 9-amino-4-dedimethylamino minocycline (**2.50**, 8 mg, 0.019 mmol) was reacted with quinoline-3-acrylic acid derivative **S2.41** to provide the formate salt of Analogue **2.99** as a yellow solid following preparatory HPLC purification (0.6 mg, 5%).

<sup>1</sup>H NMR (400 MHz, CD<sub>3</sub>OD) δ 9.15 (s, 1H), 8.55 (s, 1H), 8.43 (d, *J* = 19.8 Hz, 1H), 8.03 (dd, *J* = 16.1, 8.3 Hz, 2H), 7.91 – 7.77 (m, 2H), 7.66 (t, *J* = 7.6 Hz, 1H), 7.30 (d, *J* = 15.8 Hz, 1H), 3.37 (app. d, *J* = 4.3 Hz, 1H), 3.23 (app. d, *J* = 5.5 Hz, 1H), 2.85 – 2.73 (app. m, 1H), 2.62 (s, 6H), 2.51 – 2.35 (m, 2H), 2.15 (dd, *J* = 15.4, 14.0 Hz, 1H), 2.06 (ddd, *J* = 14.2, 8.0, 2.5 Hz, 1H), 1.63 (td, *J* = 13.3, 10.6 Hz, 1H).

HRMS (ESI+, *m/z*) [M + H]<sup>+</sup> calc'd for C<sub>33</sub>H<sub>30</sub>N<sub>4</sub>O<sub>8</sub>: 611.2136. Found: 611.2124.

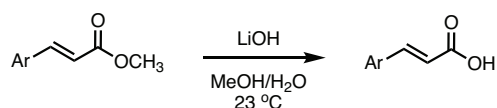


### Analogue 2.100:

Analogue **2.100** was prepared using General Procedure B: 9-amino-4-dedimethylamino minocycline (**2.50**, 8 mg, 0.019 mmol) was reacted with quinoline-6-acrylic acid derivative **S2.43** to provide the formate salt of Analogue **2.100** as a yellow solid following preparatory HPLC purification (0.9 mg, 8%).

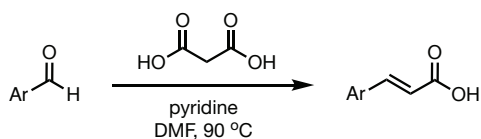
<sup>1</sup>H NMR (400 MHz, CD<sub>3</sub>OD) δ 8.86 (d, *J* = 4.1 Hz, 1H), 8.45 – 8.37 (m, 2H), 8.16 – 8.03 (m, 3H), 7.86 (d, *J* = 15.6 Hz, 1H), 7.58 (dd, *J* = 8.3, 4.3 Hz, 1H), 7.19 (d, *J* = 15.7 Hz, 1H), 3.37 (app. d, *J* = 4.3 Hz, 1H), 3.24 (app. d, *J* = 4.9 Hz, 1H), 2.84 – 2.74 (app. m, 1H), 2.62 (s, 6H), 2.52 – 2.36 (m, 2H), 2.15 (dd, *J* = 13.7, 13.7 Hz, 1H), 2.06 (ddd, *J* = 12.7, 6.4, 2.4 Hz, 1H), 1.63 (td, *J* = 13.7, 11.3 Hz, 1H).

HRMS (ESI+, *m/z*) [M + H]<sup>+</sup> calc'd for C<sub>33</sub>H<sub>30</sub>N<sub>4</sub>O<sub>8</sub>: 611.2136. Found: 611.2124.



### General Procedure C: Acrylate Synthesis via Saponification

Aryl methacrylate derivative (1 eq.) was dissolved in 5:1 methanol/water (0.1 M) and stirred at 23 °C. Lithium hydroxide (3 eq.) was added and the reaction was stirred for 18 hours at 23 °C. The resulting cloudy solution was concentrated to a white/tan solid. The solid was dissolved in water and acidified with conc. HCl solution until a precipitate formed. The solution was extracted 3X with dichloromethane and 1X with ethyl acetate and the combined organics were washed 1X with brine. The organics were then dried on anhydrous sodium sulfate, filtered, and concentrated to a white/tan solid. The crude product was typically obtained in high purity and could be used in subsequent reactions without further purification.

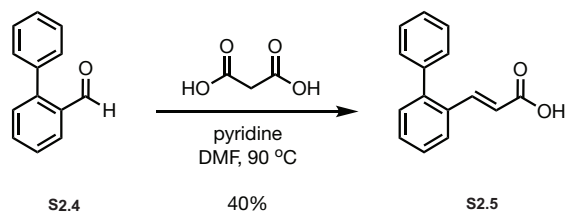


**General Procedure D: Acrylate synthesis via Malonic Acid Condensation**<sup>60</sup>

Aryl aldehyde derivative (1 eq.), malonic acid (3 eq.), and pyridine (1 eq.) were combined in DMF (0.5 M) and stirred. The solution was heated to 90 °C for 5 hours. The solution was cooled to 23 °C and 3 volumes of water were added. The solution was acidified to pH 2 with concentrated aqueous HCl solution leading to formation of a white precipitate. The precipitate was collected via filtration and the resulting solid dried on vacuum to provide the product acrylic acid derivative as a white solid. The crude product was typically obtained in high purity and could be used in subsequent reactions without further purification.

---

<sup>60</sup> This procedure was adapted from: Li, X.; Sheng, J.; Huang, G.; Ma, R.; Yin, F.; Song, D.; Zhao, C.; Ma, S. *Eur. J. Med. Chem.* **2015**, *97*, 32-41.



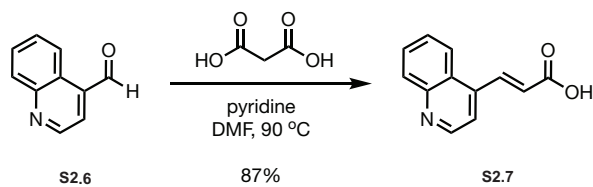
(E)-3-([1,1'-biphenyl]-2-yl)acrylic acid (S2.5):

(E)-3-([1,1'-biphenyl]-2-yl)acrylic acid (**S2.5**) was prepared using General Procedure C: [1,1'-biphenyl]-2-carbaldehyde (**S2.4**, 0.4 g, 2.195 mmol, 1 eq.) was reacted as described to provide the product as a light brown solid. The product was used in subsequent reactions without further purification (0.192 g, 40%).

Spectral data obtained for this compound were consistent with those previously reported.<sup>61</sup>

---

<sup>61</sup> Passos, G. F. S.; Gomes, M. G. M.; de Aquino, T. M.; de Araujo-Junior, J. X.; de Souza, S. J. M.; Cavalecante, J. P. M.; dos Santos, E. C.; Bassi, E. J.; da Silva-Junior, E. F. *Pharmaceuticals* **2020**, *13*, 141-164.



(E)-3-(quinolin-4-yl)acrylic acid (S2.7):

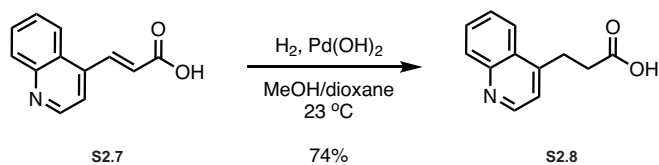
(E)-3-(quinolin-4-yl)acrylic acid (S2.7) was prepared using General Procedure C: quinoline-4-carbaldehyde (S2.6, 1.0 g, 6.36 mmol, 1 eq.) was reacted as described to provide the product as a light brown solid. The product was used in subsequent reactions without further purification (1.1 g, 87%).

$^1\text{H}$  NMR (400 MHz, DMSO- $d_6$ )  $\delta$  8.94 (d,  $J$  = 4.5 Hz, 1H), 8.33 (d,  $J$  = 15.9 Hz, 1H), 8.26 (dd,  $J$  = 8.5, 1.3 Hz, 1H), 8.08 (dd,  $J$  = 8.4, 1.3 Hz, 1H), 7.86 (d,  $J$  = 4.5 Hz, 1H), 7.83 (ddd,  $J$  = 8.4, 6.8, 1.4 Hz, 1H), 7.70 (ddd,  $J$  = 8.3, 6.9, 1.4 Hz, 1H), 6.80 (d,  $J$  = 15.8 Hz, 1H).

$^{13}\text{C}$  NMR (101 MHz, DMSO- $d_6$ )  $\delta$  167.34, 150.84, 148.61, 139.64, 138.27, 130.24, 130.16, 127.89, 126.43, 125.85, 123.97, 119.04.

HRMS (ESI+,  $m/z$ )  $[\text{M} + \text{H}]^+$  calc'd for  $\text{C}_{12}\text{H}_9\text{NO}_2$ : 198.0561. Found: 198.0555.





3-(quinolin-4-yl)propanoic acid (S2.8):

(*E*)-3-(quinolin-4-yl)acrylic acid (S2.7, 0.2 g, 1.004 mmol, 1 eq.) was dissolved in 6 mL 1:1 methanol/dioxane and stirred at 23 °C. Palladium hydroxide (25 wt. %, 0.028 g, 0.201 mmol, 0.2 eq.) was added and the reaction vessel was evacuated and backfilled 3X with nitrogen. The vessel was then evacuated and backfilled 3X with hydrogen. The reaction was stirred for 1.5 hours under static hydrogen pressure at 23 °C. Following this, the reaction was purged with nitrogen and filtered through a pad of Celite, washing the pad with excess methanol. The filtrate was concentrated to an off-white solid which was then dried on vacuum. The crude product was used in subsequent reactions without further purification (0.150 g, 74% yield).

$^1\text{H}$  NMR (400 MHz, DMSO)  $\delta$  8.79 (d,  $J = 4.4$  Hz, 1H), 8.16 (dd,  $J = 8.5, 1.4$  Hz, 1H), 8.02 (dd,  $J = 8.5, 1.3$  Hz, 1H), 7.76 (ddd,  $J = 8.3, 6.8, 1.4$  Hz, 1H), 7.64 (ddd,  $J = 8.3, 6.8, 1.4$  Hz, 1H), 7.38 (d,  $J = 4.4$  Hz, 1H), 3.33 (t,  $J = 7.6$  Hz, 2H), 2.69 (t,  $J = 7.6$  Hz, 2H).

$^{13}\text{C}$  NMR (101 MHz, DMSO)  $\delta$  174.13, 150.69, 148.21, 147.18, 130.18, 129.61, 127.37, 127.04, 124.22, 121.06, 34.19, 26.89.

HRMS (ESI+,  $m/z$ )  $[\text{M} + \text{H}]^+$  calc'd for  $\text{C}_{12}\text{H}_{11}\text{NO}_2$ : 200.0717. Found: 200.0711.



2-(quinolin-4-yl)cyclopropane-1-carboxylic acid (S2.10):<sup>62</sup>

Sodium hydride (0.042 g, 1.056 mmol, 1.2 eq.) was added to 4 mL dimethylsulfoxide and stirred at 23 °C. Trimethylsulfoxonium iodide (0.232 g, 1.056 mmol, 1.2 eq.) was added and the reaction was stirred at 23 °C for 20 minutes. ethyl (*E*)-3-(quinolin-4-yl)acrylate (S2.9, 0.2 g, 0.88 mmol, 1 eq.) was added and the reaction was heated to 60 °C for 18 hours.<sup>63</sup> Following overnight stirring, TLC analysis revealed a 1:1 ratio of starting material to product. Another 1.2 equivalents of sulfur ylide (prepared as above, Sodium hydride (0.042 g, 1.056 mmol, 1.2 eq.) was added to 4 mL dimethylsulfoxide and stirred at 23 °C. Trimethylsulfoxonium iodide (0.232 g, 1.056 mmol, 1.2 eq.) was added and the reaction was stirred at 23 °C for 20 minutes) was added to the reaction solution and the reaction was stirred for an additional 10 hours at 60 °C, at which time the reaction was deemed complete by TLC and LC/MS analysis. The reaction was cooled to 23 °C and poured into 50 mL water. The solution was extracted 2X with 20 mL ethyl acetate. The organic layers were combined, dried over anhydrous sodium sulfate, and concentrated to a pale-yellow solid.

The crude product was hydrolyzed according to General Procedure D: Ethyl 2-(quinolin-4-yl)cyclopropane-1-carboxylate (0.2 g, 0.829 mmol, 1 eq.) was reacted as

<sup>62</sup> Procedure adapted from Tadashi et al., **2010** (Chapter 2, ref. 24).

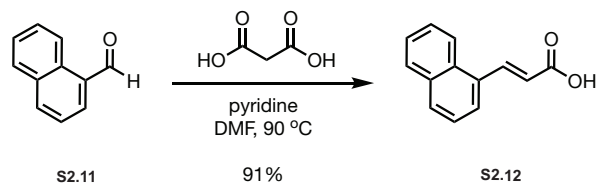
<sup>63</sup> Ethyl (*E*)-3-(quinolin-4-yl)acrylate (S2.9) was prepared from (*E*)-3-(quinolin-4-yl)acrylic acid (S2.7) using standard ester formation conditions.

described to provide the product as a brown solid. The product was used in subsequent reactions without further purification (0.177 g, 93%, mixture of diastereomers).

$^1\text{H}$  NMR (400 MHz, DMSO)  $\delta$  9.10 (d,  $J = 5.5$  Hz, 1H), 8.55 – 8.44 (m, 2H), 8.10 (ddd,  $J = 8.4, 6.9, 1.3$  Hz, 1H), 7.95 (ddd,  $J = 8.4, 6.9, 1.2$  Hz, 1H), 7.67 (d,  $J = 5.5$  Hz, 1H), 3.20 (ddd,  $J = 11.0, 5.7, 2.5$  Hz, 1H), 2.29 (ddd,  $J = 8.2, 6.2, 4.4$  Hz, 1H), 1.76 (ddt,  $J = 8.6, 6.0, 3.1$  Hz, 2H).

$^{13}\text{C}$  NMR (101 MHz, DMSO)  $\delta$  173.41, 133.69, 129.73, 128.34, 125.31, 118.31, 25.21, 22.35, 17.39.

HRMS (ESI+,  $m/z$ )  $[\text{M} + \text{H}]^+$  calc'd for  $\text{C}_{13}\text{H}_{11}\text{NO}_2$ : 214.0863. Found: 214.0864.



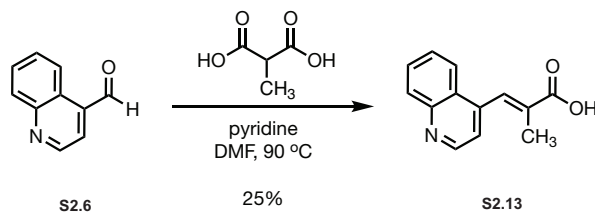
(E)-3-(naphthalen-1-yl)acrylic acid (S2.12):

(E)-3-(naphthalen-1-yl)acrylic acid (S2.12) was prepared using General Procedure C: 1-naphthaldehyde (S2.11, 0.3 g, 0.261 mL, 1.921 mmol, 1 eq.) was reacted as described to provide the product as a light brown solid. The product was used in subsequent reactions without further purification (0.3449 g, 91%).

$^1\text{H}$  NMR (400 MHz, DMSO)  $\delta$  8.38 (d,  $J = 15.8$  Hz, 1H), 8.20 (dd,  $J = 8.5, 1.3$  Hz, 1H), 8.05 – 7.96 (m, 2H), 8.00 – 7.91 (m, 1H), 7.68 – 7.51 (m, 3H), 6.60 (d,  $J = 15.7$  Hz, 1H).

$^{13}\text{C}$  NMR (101 MHz, DMSO)  $\delta$  167.93, 140.46, 133.77, 131.51, 131.22, 130.80, 129.19, 127.61, 126.77, 126.21, 125.68, 123.46, 122.63.

HRMS (ESI+,  $m/z$ )  $[\text{M} + \text{H}]^+$  calc'd for  $\text{C}_{13}\text{H}_{10}\text{O}_2$ : 197.0608. Found: 197.0604.



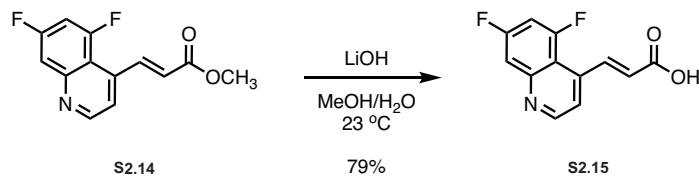
**(E)-2-methyl-3-(quinolin-4-yl)acrylic acid (S2.13):**

(E)-2-methyl-3-(quinolin-4-yl)acrylic acid (S2.13) was prepared using General Procedure C: quinoline-4-carbaldehyde (S2.6, 0.63 g, 4.01 mmol, 1 eq.) was reacted with methylmalonic acid as described to provide the product as a light brown solid. The product was used in subsequent reactions without further purification (0.210 g, 25%).

$^1\text{H}$  NMR (400 MHz, DMSO)  $\delta$  12.95 (s, 1H), 8.94 (d,  $J = 4.4$  Hz, 1H), 8.14 – 8.04 (m, 1H), 7.99 (t,  $J = 1.4$  Hz, 1H), 7.91 (dd,  $J = 8.3, 1.4$  Hz, 1H), 7.81 (ddd,  $J = 8.4, 6.8, 1.4$  Hz, 1H), 7.75 – 7.61 (m, 1H), 7.45 (d,  $J = 4.5$  Hz, 1H), 1.87 (d,  $J = 1.4$  Hz, 3H).

$^{13}\text{C}$  NMR (101 MHz, DMSO)  $\delta$  168.91, 150.59, 148.23, 141.74, 134.21, 133.62, 130.20, 130.11, 127.59, 126.20, 125.03, 121.40, 14.71.

HRMS (ESI+,  $m/z$ )  $[\text{M} + \text{H}]^+$  calc'd for  $\text{C}_{13}\text{H}_{11}\text{NO}_2$ : 212.0717. Found: 212.0713.



**(E)-3-(5,7-difluoroquinolin-4-yl)acrylic acid (S2.15):**

(E)-3-(5,7-difluoroquinolin-4-yl)acrylic acid (**S2.15**) was prepared using General Procedure D: Methyl (E)-3-(5,7-difluoroquinolin-4-yl)acrylate (**S2.14**, 0.2 g, 0.803 mmol, 1 eq.) was reacted as described to provide the product as a light brown solid. The product was used in subsequent reactions without further purification (0.15 g, 79%).<sup>64</sup>

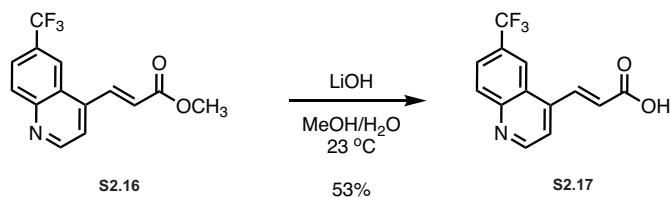
<sup>1</sup>H NMR (400 MHz, DMSO)  $\delta$  8.96 (d,  $J = 4.6$  Hz, 1H), 8.31 (dd,  $J = 15.7, 5.5$  Hz, 1H), 7.75 (d,  $J = 4.6$  Hz, 1H), 7.73 – 7.60 (m, 2H), 6.57 (dd,  $J = 15.8, 1.8$  Hz, 1H).

<sup>13</sup>C NMR (101 MHz, DMSO)  $\delta$  167.19, 162.97 (d,  $J = 15.4$  Hz), 160.60 (dd,  $J = 18.9, 15.0$  Hz), 158.13 (d,  $J = 14.7$  Hz), 152.94, 149.87 (dd,  $J = 14.3, 3.9$  Hz), 141.57 (d,  $J = 12.8$  Hz), 139.46 (t,  $J = 2.8$  Hz), 126.12, 120.58 (d,  $J = 2.5$  Hz), 113.85 (dd,  $J = 11.2, 2.2$  Hz), 110.39 (dd,  $J = 20.3, 4.7$  Hz), 104.70 (dd,  $J = 29.7, 27.1$  Hz).

<sup>19</sup>F NMR (376 MHz, DMSO)  $\delta$  -106.36, -108.10.

HRMS (ESI+,  $m/z$ )  $[M + H]^+$  calc'd for C<sub>12</sub>H<sub>7</sub>F<sub>2</sub>NO<sub>2</sub>: 234.0372. Found: 234.0368.

<sup>64</sup> Methyl (E)-3-(5,7-difluoroquinolin-4-yl)acrylate (**S2.14**) was prepared in three steps from commercially available 3,5-difluoroaniline using the scheme outlined in Figure 2.14.



(E)-3-(6-(trifluoromethyl)quinolin-4-yl)acrylic acid (S2.17):

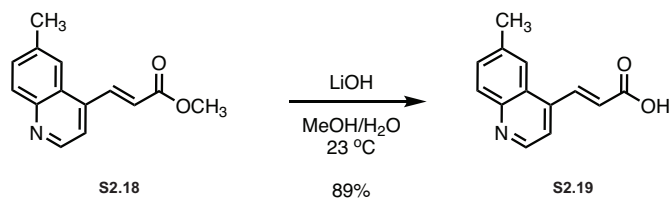
(E)-3-(6-(trifluoromethyl)quinolin-4-yl)acrylic acid (**S2.17**) was prepared using General Procedure D: Methyl (E)-3-(6-(trifluoromethyl)quinolin-4-yl)acrylate (**S2.16**, 0.2 g, 0.711 mmol, 1 eq.) was reacted as described to provide the product as a light brown solid. The product was used in subsequent reactions without further purification (0.1 g, 53%).<sup>65</sup>

<sup>1</sup>H NMR (400 MHz, DMSO)  $\delta$  9.09 (d,  $J = 4.6$  Hz, 1H), 8.61 (s, 1H), 8.39 (d,  $J = 15.8$  Hz, 1H), 8.28 (d,  $J = 8.8$  Hz, 1H), 8.08 (dd,  $J = 8.9, 2.0$  Hz, 1H), 8.00 (d,  $J = 4.6$  Hz, 1H), 6.84 (d,  $J = 15.8$  Hz, 1H).

<sup>19</sup>F NMR (376 MHz, DMSO)  $\delta$  -60.60.

HRMS (ESI+,  $m/z$ )  $[M + H]^+$  calc'd for C<sub>13</sub>H<sub>8</sub>F<sub>3</sub>NO<sub>2</sub>: 268.0580. Found: 268.0580.

<sup>65</sup> Methyl (E)-3-(6-(trifluoromethyl)quinolin-4-yl)acrylate (**S2.16**) was prepared in three steps from commercially available 4-trifluoromethylaniline using the scheme outlined in Figure 2.14.



(E)-3-(6-methylquinolin-4-yl)acrylic acid (S2.19):

(E)-3-(6-methylquinolin-4-yl)acrylic acid (S2.19) was prepared using General Procedure D: Methyl (E)-3-(6-methylquinolin-4-yl)acrylate (S2.18, 0.300 g, 1.320 mmol, 1 eq.) was reacted as described to provide the product as a light brown solid. The product was used in subsequent reactions without further purification (0.250 g, 89%).<sup>66</sup>

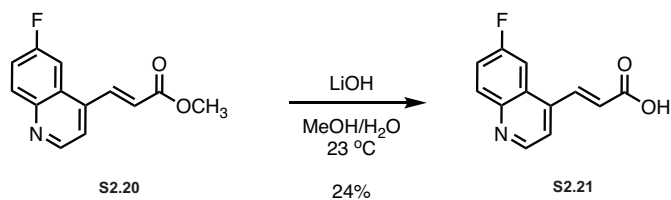
<sup>1</sup>H NMR (400 MHz, DMSO)  $\delta$  8.82 (d,  $J$  = 4.6 Hz, 1H), 8.26 (d,  $J$  = 15.8 Hz, 1H), 8.00 (s, 1H), 7.93 (d,  $J$  = 8.6 Hz, 1H), 7.79 (d,  $J$  = 4.6 Hz, 1H), 7.62 (dd,  $J$  = 8.6, 1.8 Hz, 1H), 6.74 (d,  $J$  = 15.8 Hz, 1H), 2.50 (s, 3H).

<sup>13</sup>C NMR (101 MHz, DMSO)  $\delta$  167.36, 149.40, 146.53, 139.59, 138.25, 137.89, 132.71, 129.31, 126.45, 125.92, 122.75, 119.03, 21.82.

HRMS (ESI+,  $m/z$ )  $[M + H]^+$  calc'd for C<sub>13</sub>H<sub>11</sub>NO<sub>2</sub>: 214.0863. Found: 214.0863.

<sup>66</sup> Methyl (E)-3-(6-methylquinolin-4-yl)acrylate (S2.18) was prepared in three steps from commercially available 4-methylaniline using the scheme outlined in Figure 2.14.





(E)-3-(6-fluoroquinolin-4-yl)acrylic acid (S2.21):

(E)-3-(6-fluoroquinolin-4-yl)acrylic acid (S2.21) was prepared using General Procedure D: . Methyl (E)-3-(6-fluoroquinolin-4-yl)acrylate (S2.20, 0.167 g, 0.721 mmol, 1 eq.) was reacted as described to provide the product as a light brown solid. The product was used in subsequent reactions without further purification (0.04 g, 24%).<sup>67</sup>

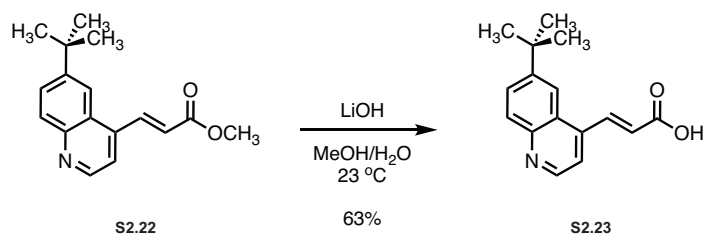
<sup>1</sup>H NMR (400 MHz, DMSO)  $\delta$  8.92 (d,  $J$  = 4.6 Hz, 1H), 8.25 (d,  $J$  = 15.8 Hz, 1H), 8.15 (dd,  $J$  = 9.2, 5.7 Hz, 1H), 8.04 (dd,  $J$  = 10.5, 2.8 Hz, 1H), 7.91 (d,  $J$  = 4.6 Hz, 1H), 7.75 (td,  $J$  = 8.8, 2.8 Hz, 1H), 6.81 (d,  $J$  = 15.8 Hz, 1H).

<sup>13</sup>C NMR (101 MHz, DMSO)  $\delta$  167.28, 161.93, 159.48, 150.26 (d,  $J$  = 2.7 Hz), 145.88, 139.65 (d,  $J$  = 5.5 Hz), 137.96, 133.01 (d,  $J$  = 9.6 Hz), 126.72, 120.40 (d,  $J$  = 25.5 Hz), 119.70, 107.98 (d,  $J$  = 23.0 Hz).

<sup>19</sup>F NMR (376 MHz, DMSO)  $\delta$  -73.88.

HRMS (ESI+,  $m/z$ ) [M + H]<sup>+</sup> calc'd for C<sub>12</sub>H<sub>8</sub>F<sub>2</sub>NO<sub>2</sub>: 218.0612. Found: 218.0613.

<sup>67</sup> Methyl (E)-3-(6-fluoroquinolin-4-yl)acrylate (S2.20) was prepared in three steps from commercially available 4-fluoroaniline using the scheme outlined in Figure 2.14.



(E)-3-(6-(tert-butyl)quinolin-4-yl)acrylic acid (S2.23):

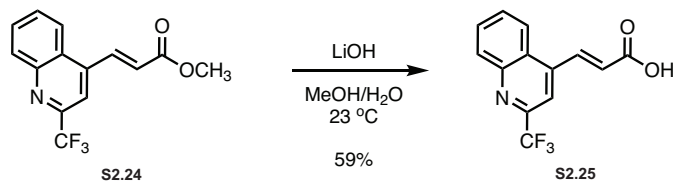
(E)-3-(6-(tert-butyl)quinolin-4-yl)acrylic acid (**S2.23**) was prepared using General Procedure D: Methyl (E)-3-(6-(tert-butyl)quinolin-4-yl)acrylate (**S2.22**, 0.5 g, 1.856 mmol, 1 eq.) was reacted as described to provide the product as a light brown solid. The product was used in subsequent reactions without further purification (0.3 g, 63%).<sup>68</sup>

<sup>1</sup>H NMR (400 MHz, DMSO)  $\delta$  8.85 (d,  $J = 4.5$  Hz, 1H), 8.28 (d,  $J = 15.8$  Hz, 1H), 8.06 – 7.99 (m, 2H), 7.94 (dd,  $J = 8.9, 2.1$  Hz, 1H), 7.78 (d,  $J = 4.5$  Hz, 1H), 6.78 (d,  $J = 15.8$  Hz, 1H), 1.41 (s, 9H).

<sup>13</sup>C NMR (101 MHz, DMSO)  $\delta$  167.67, 150.16, 150.04, 147.21, 139.94, 137.15, 129.85, 129.05, 125.44, 119.03, 118.27, 35.48, 31.34.

HRMS (ESI+,  $m/z$ )  $[M + H]^+$  calc'd for C<sub>16</sub>H<sub>17</sub>NO<sub>2</sub>: 256.1332. Found: 256.1334.

<sup>68</sup> Methyl (E)-3-(6-(tert-butyl)quinolin-4-yl)acrylate (**S2.22**) was prepared in three steps from commercially available 4-*tert*-butylaniline using the scheme outlined in Figure 2.14.



(E)-3-(2-(trifluoromethyl)quinolin-4-yl)acrylic acid (S2.25):

(E)-3-(2-(trifluoromethyl)quinolin-4-yl)acrylic acid (S2.25) was prepared using General Procedure D: Methyl (E)-3-(2-(trifluoromethyl)quinolin-4-yl)acrylate (S2.24, 0.33 g, 1.173 mmol, 1 eq.) was reacted as described to provide the product as a light brown solid. The product was used in subsequent reactions without further purification (0.185 g, 59%).<sup>69</sup>

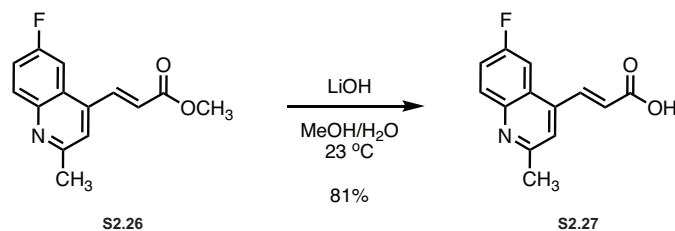
<sup>1</sup>H NMR (400 MHz, DMSO)  $\delta$  12.94 (s, 1H), 8.39 (d,  $J = 8.5$  Hz, 1H), 8.35 (d,  $J = 15.9$  Hz, 1H), 8.29 (s, 1H), 8.22 (d,  $J = 8.4$  Hz, 1H), 7.98 (dd,  $J = 8.4, 6.9$  Hz, 1H), 7.86 (dd,  $J = 8.5, 6.9$  Hz, 1H), 7.02 (d,  $J = 15.9$  Hz, 1H).

<sup>13</sup>C NMR (101 MHz, DMSO)  $\delta$  167.19, 147.49, 143.11, 137.02, 131.98, 130.53, 130.21, 128.54, 126.75, 124.41, 123.33, 120.59, 114.75.

<sup>19</sup>F NMR (376 MHz, DMSO)  $\delta$  -65.98.

HRMS (ESI+,  $m/z$ )  $[M + H]^+$  calc'd for C<sub>13</sub>H<sub>8</sub>F<sub>3</sub>NO<sub>2</sub>: 266.0434. Found: 266.0435.

<sup>69</sup> Methyl (E)-3-(2-(trifluoromethyl)quinolin-4-yl)acrylate (S2.24) was prepared in three steps from commercially available aniline using the scheme outlined in Figure 2.14.



**(E)-3-(6-fluoro-2-methylquinolin-4-yl)acrylic acid (S2.27):**

(E)-3-(6-fluoro-2-methylquinolin-4-yl)acrylic acid (S2.27) was prepared using General Procedure D: Methyl (E)-3-(6-fluoro-2-methylquinolin-4-yl)acrylate (S2.26, 0.56 g, 2.283 mmol, 1 eq.) was reacted as described to provide the product as a light brown solid. The product was used in subsequent reactions without further purification (0.43 g, 81%).<sup>70</sup>

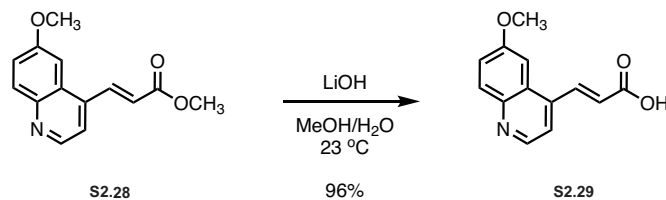
<sup>1</sup>H NMR (400 MHz, DMSO, crude)  $\delta$  12.64 (s, 1H), 8.03 (d,  $J = 15.8$  Hz, 1H), 7.86 (dd,  $J = 9.2, 5.7$  Hz, 1H), 7.79 (dd,  $J = 10.4, 2.8$  Hz, 1H), 7.68 (s, 1H), 7.58 – 7.46 (m, 1H), 7.09 (s, 1H), 6.96 (s, 1H), 6.84 (s, 1H), 6.63 (d,  $J = 15.8$  Hz, 1H), 3.72 (s, 7H), 2.50 (s, 3H).

<sup>13</sup>C NMR (101 MHz, DMSO)  $\delta$  167.29, 161.46, 158.59 (d,  $J = 2.8$  Hz), 145.15, 139.95, 137.97, 131.80 (d,  $J = 9.7$  Hz), 126.63, 125.13 (d,  $J = 9.5$  Hz), 120.53, 120.21 (d,  $J = 25.6$  Hz), 107.85 (d,  $J = 23.4$  Hz), 24.88.

<sup>19</sup>F NMR (376 MHz, DMSO)  $\delta$  -73.89

HRMS (ESI+,  $m/z$ )  $[M + H]^+$  calc'd for C<sub>13</sub>H<sub>10</sub>FNO<sub>2</sub>: 230.0623. Found: 230.0623.

<sup>70</sup> Methyl (E)-3-(6-fluoro-2-methylquinolin-4-yl)acrylate (S2.26) was prepared in three steps from commercially available 4-fluoroaniline using the scheme outlined in Figure 2.14.



(E)-3-(6-methoxyquinolin-4-yl)acrylic acid (S2.29):

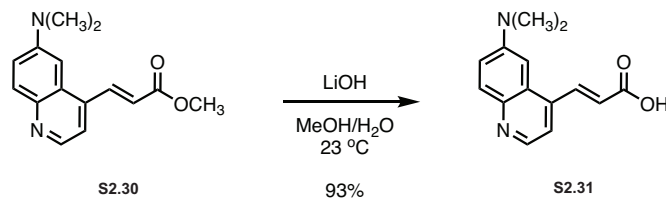
(E)-3-(6-methoxyquinolin-4-yl)acrylic acid (S2.29) was prepared using General Procedure D: Methyl (E)-3-(6-methoxyquinolin-4-yl)acrylate (S2.28, 0.100 g, 0.411 mmol, 1 eq.) was reacted as described to provide the product as a light brown solid. The product was used in subsequent reactions without further purification (0.094 g, 96%).<sup>71</sup>

<sup>1</sup>H NMR (400 MHz, DMSO)  $\delta$  8.75 (d,  $J = 4.5$  Hz, 1H), 8.30 (d,  $J = 15.7$  Hz, 1H), 7.98 (d,  $J = 9.4$  Hz, 1H), 7.79 (d,  $J = 4.6$  Hz, 1H), 7.46 (s, 2H), 6.78 (d,  $J = 15.7$  Hz, 1H), 3.97 (s, 3H).

<sup>13</sup>C NMR (101 MHz, DMSO)  $\delta$  167.52, 158.32, 148.06, 144.84, 138.47, 138.40, 131.73, 127.12, 126.23, 122.72, 119.30, 101.91, 56.12.

HRMS (ESI+,  $m/z$ )  $[M + H]^+$  calc'd for C<sub>13</sub>H<sub>11</sub>NO<sub>3</sub>: 228.0666. Found: 228.0663.

<sup>71</sup> Methyl (E)-3-(6-methoxyquinolin-4-yl)acrylate (S2.28) was prepared in three steps from commercially available 4-methoxyaniline using the scheme outlined in Figure 2.14.



**(E)-3-(6-(dimethylamino)quinolin-4-yl)acrylic acid (S2.31):**

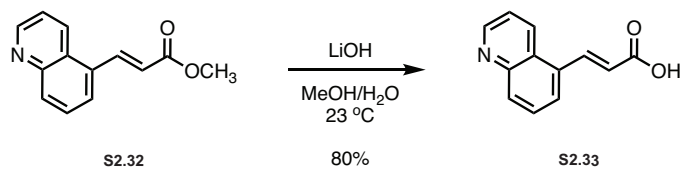
(E)-3-(6-(dimethylamino)quinolin-4-yl)acrylic acid (**S2.31**) was prepared using General Procedure D: Methyl (E)-3-(6-(dimethylamino)quinolin-4-yl)acrylate (**S2.30**, 0.400 g, 1.561 mmol, 1 eq.) was reacted as described to provide the product as a light brown solid. The product was used in subsequent reactions without further purification (0.350 g, 93%).<sup>72</sup>

<sup>1</sup>H NMR (400 MHz, DMSO)  $\delta$  8.55 (d,  $J = 4.5$  Hz, 1H), 8.21 (d,  $J = 15.7$  Hz, 1H), 7.87 (d,  $J = 9.3$  Hz, 1H), 7.64 (d,  $J = 4.5$  Hz, 1H), 7.49 (dd,  $J = 9.4, 2.7$  Hz, 1H), 6.94 (d,  $J = 2.7$  Hz, 1H), 6.72 (d,  $J = 15.8$  Hz, 1H), 3.08 (s, 6H).

<sup>13</sup>C NMR (101 MHz, DMSO)  $\delta$  167.74, 149.15, 145.68, 142.86, 138.50, 136.78, 130.88, 127.59, 125.52, 119.92, 119.20, 99.83, 40.64.

HRMS (ESI+,  $m/z$ )  $[M + H]^+$  calc'd for C<sub>14</sub>H<sub>14</sub>N<sub>2</sub>O<sub>2</sub>: 241.0983. Found: 241.0982.

<sup>72</sup> Methyl (E)-3-(6-(dimethylamino)quinolin-4-yl)acrylate (**S2.30**) was prepared in three steps from commercially available 4-(Dimethylamino)aniline using the scheme outlined in Figure 2.14.



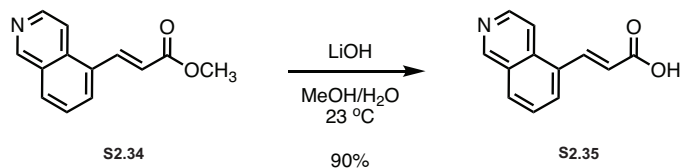
(E)-3-(quinolin-5-yl)acrylic acid (S2.33):

(E)-3-(quinolin-5-yl)acrylic acid (**S2.33**) was prepared using General Procedure D: Methyl (*E*)-3-(quinolin-5-yl)acrylate (**S2.32**, 0.200 g, 0.938 mmol, 1 eq.) was reacted as described to provide the product as a light brown solid. The product was used in subsequent reactions without further purification (0.150 g, 80%).<sup>73</sup>

Spectral data obtained for this compound were consistent with those previously reported.<sup>74</sup>

<sup>73</sup> Methyl (*E*)-3-(quinolin-5-yl)acrylate (**S2.32**) was prepared in one step from commercially available 5-bromoquinoline and methyl acrylate using standard Heck reaction conditions.

<sup>74</sup> Finn, P. W.; Kalvinsh, I.; Loza, E.; Andrianov, V.; Habrova, O.; Lolya, D.; Piskunova, I. Carbamic Acid Compounds Comprising a Bicyclic Heteroaryl Group as HDAC Inhibitors. WO 2004/076386 A1. February 24, 2004.



(E)-3-(isoquinolin-5-yl) acrylic acid (S2.35):

(E)-3-(isoquinolin-5-yl) acrylic acid (S2.35) was prepared using General Procedure D: Methyl (E)-3-(isoquinolin-5-yl)acrylate (S2.34, 0.25 g, 1.172 mmol, 1 eq.) was reacted as described to provide the product as a light brown solid. The product was used in subsequent reactions without further purification (0.21 g, 90%).<sup>75</sup>

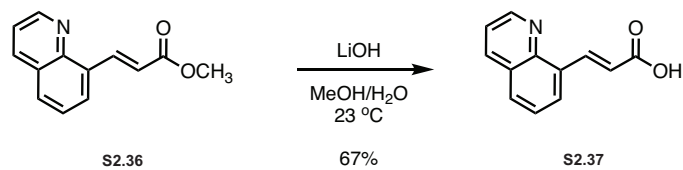
<sup>1</sup>H NMR (400 MHz, DMSO)  $\delta$  12.66 (s, 1H), 9.37 (s, 1H), 8.58 (d,  $J = 5.9$  Hz, 1H), 8.31 (d,  $J = 15.6$  Hz, 1H), 8.22 (app. t,  $J = 9.0$  Hz, 2H), 8.08 (d,  $J = 6.1$  Hz, 1H), 7.73 (app. t,  $J = 7.6$  Hz, 1H), 6.69 (d,  $J = 15.6$  Hz, 1H).

<sup>13</sup>C NMR (101 MHz, DMSO)  $\delta$  167.73, 153.62, 144.34, 138.91, 133.69, 130.57, 130.45, 129.69, 128.88, 127.76, 123.24, 116.53.

HRMS (ESI+,  $m/z$ )  $[M + H]^+$  calc'd for C<sub>12</sub>H<sub>9</sub>NO<sub>2</sub>: 198.0561. Found: 198.0556.

<sup>75</sup> Methyl (E)-3-(isoquinolin-5-yl) acrylate (S2.34) was prepared in one step from commercially available 5-bromoisoquinoline and methyl acrylate using standard Heck reaction conditions.





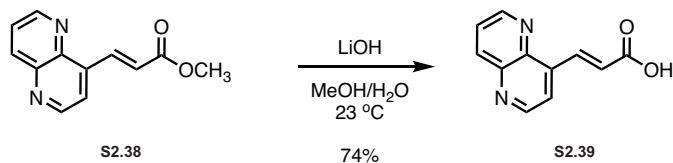
(E)-3-(quinolin-8-yl) acrylic acid (S2.37):

(E)-3-(quinolin-8-yl) acrylic acid (**S2.37**) was prepared using General Procedure D: Methyl (*E*)-3-(quinolin-8-yl) acrylate (**S2.36**, 0.6 g, 2.81 mmol, 1 eq.) was reacted as described to provide the product as a light brown solid. The product was used in subsequent reactions without further purification (0.378 g, 67%).<sup>76</sup>

Spectral data obtained for this compound were consistent with those previously reported.<sup>77</sup>

<sup>76</sup> Methyl (*E*)-3-(quinolin-8-yl) acrylate (**S2.36**) was prepared in one step from commercially available 8-bromoquinoline and methyl acrylate using standard Heck reaction conditions.

<sup>77</sup> Wahler, K.; Kraling, K.; Steuber, H.; Meggers, E. *ChemistryOpen* **2013**, 2, 180-185.



(E)-3-(1,5-naphthyridin-4-yl)acrylic acid (S2.39):

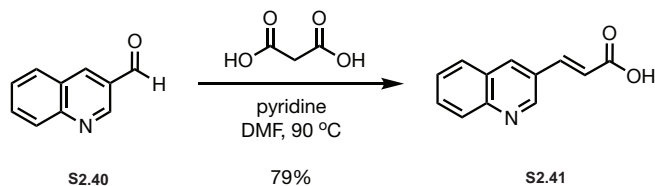
(E)-3-(1,5-naphthyridin-4-yl)acrylic acid (S2.39) was prepared using General Procedure D: Methyl (E)-3-(1,5-naphthyridin-4-yl)acrylate (S2.38, 0.100 g, 0.467 mmol, 1 eq.) was reacted as described to provide the product as a light brown solid. The product was used in subsequent reactions without further purification (0.07 g, 74%).<sup>78</sup>

<sup>1</sup>H NMR (400 MHz, DMSO)  $\delta$  12.76 (s, 1H), 9.07 (dd,  $J = 15.6, 4.3$  Hz, 2H), 8.70 (d,  $J = 16.3$  Hz, 1H), 8.48 (d,  $J = 8.5$  Hz, 1H), 8.18 (d,  $J = 4.5$  Hz, 1H), 7.87 (dd,  $J = 8.5, 4.1$  Hz, 1H), 7.08 (d,  $J = 16.2$  Hz, 1H).

<sup>13</sup>C NMR (101 MHz, DMSO)  $\delta$  167.63, 151.87, 151.72, 144.19, 141.00, 139.83, 137.93, 137.41, 125.96, 125.70, 121.50.

HRMS (ESI+,  $m/z$ )  $[M + H]^+$  calc'd for C<sub>11</sub>H<sub>8</sub>N<sub>2</sub>O<sub>2</sub>: 199.0513. Found: 199.0509.

<sup>78</sup> Methyl (E)-3-(1,5-naphthyridin-4-yl)acrylate (S2.38) was prepared in three steps from 3-aminopyridine using the scheme outlined in Figure 2.14.



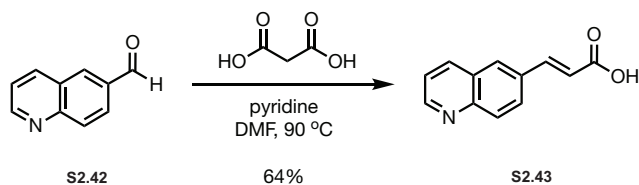
**(E)-3-(quinolin-3-yl)acrylic acid (S2.41):**

(E)-3-(quinolin-3-yl)acrylic acid (**S2.41**) was prepared using General Procedure C: quinoline-3-carbaldehyde (**S2.40**, 0.5 g, 3.18 mmol, 1 eq.) was reacted as described to provide the product as a light brown solid. The product was used in subsequent reactions without further purification (0.5 g, 76%).

<sup>1</sup>H NMR (400 MHz, DMSO) δ 12.60 (s, 1H), 9.23 (d, *J* = 2.2 Hz, 1H), 8.68 (d, *J* = 2.2 Hz, 1H), 8.02 (m, 2H), 7.85 – 7.74 (m, 2H), 7.65 (app. t, *J* = 7.5 Hz, 1H), 6.85 (d, *J* = 16.1 Hz, 1H).

<sup>13</sup>C NMR (101 MHz, DMSO) δ 167.81, 150.34, 148.34, 141.22, 135.95, 131.04, 129.30, 129.14, 127.97, 127.80, 121.82.

HRMS (ESI+, *m/z*) [*M* + H]<sup>+</sup> calc'd for C<sub>12</sub>H<sub>9</sub>NO<sub>2</sub>: 198.0561. Found: 198.0555.



**(E)-3-(quinolin-6-yl)acrylic acid (S2.43):**

(E)-3-(quinolin-6-yl)acrylic acid (**S2.43**) was prepared using General Procedure C: quinoline-6-carbaldehyde (**S2.42**, 0.5 g, 3.18 mmol, 1 eq.) was reacted as described to provide the product as a light brown solid. The product was used in subsequent reactions without further purification (0.41 g, 64%).

$^1\text{H}$  NMR (400 MHz, DMSO)  $\delta$  12.53 (s, 1H), 8.92 (dd,  $J = 4.2, 1.7$  Hz, 1H), 8.37 (dd,  $J = 8.4, 1.7$  Hz, 1H), 8.26 (d,  $J = 1.9$  Hz, 1H), 8.18 – 8.09 (m, 1H), 8.01 (d,  $J = 8.8$  Hz, 1H), 7.77 (d,  $J = 16.0$  Hz, 1H), 7.57 (dd,  $J = 8.3, 4.2$  Hz, 1H), 6.71 (d,  $J = 16.0$  Hz, 1H).

$^{13}\text{C}$  NMR (101 MHz, DMSO)  $\delta$  167.96, 151.93, 148.83, 143.54, 137.00, 132.89, 130.03, 130.00, 128.36, 128.22, 122.65, 121.11.

HRMS (ESI+,  $m/z$ )  $[\text{M} + \text{H}]^+$  calc'd for  $\text{C}_{12}\text{H}_9\text{NO}_2$ : 198.0561. Found: 198.0556.

## **Chapter 3**

### **Fully Synthetic Compound Development Efforts**

### **3.1 Introduction to Fully Synthetic Compound Development Efforts**

In this chapter, we discuss our transition away from semisynthesis and toward full synthesis as a strategy for accessing a broader diversity of analogues for evaluation as antiproliferative agents. These efforts were inspired in part by the improvements in activity achieved through our semisynthetic medicinal chemistry campaign, as well as by recent reports from Tetrphase Pharmaceuticals and others regarding the discovery of novel tetracyclic compounds with potential as cancer therapeutics. We begin with a detailed history of tetracycline total synthesis efforts, focusing primarily on the landmark publication from the Myers group in 2005 and its various evolutions through updated synthetic routes published in years since. We then provide a summary of recent tetracycline synthesis reports, mainly from Tetrphase Pharmaceuticals, that served as a foundation for our ongoing compound development efforts. Finally, we describe our synthesis strategy, provide an overview of our novel Col-3 analogues, and summarize the assays performed to better understand the biological activity of these compounds. In total, these efforts not only yielded a set of novel tetracycline analogues with antiproliferative activity, but also provide a roadmap for future development of fully synthetic analogues of Col-3.

### **3.2 Overview of Tetracycline Total Synthesis Efforts**

Owing to their structural complexity and exciting therapeutic properties, the tetracycline natural products have been a target of total synthesis chemists since their discovery in the 1960s. Indeed, the next 40 years would see total synthesis efforts from many of the finest synthetic chemists of the era, Woodward (1962 and 1968), Shemaykin

(1967), Muxfeldt (1979), and Stork (1996), to name a few.<sup>1, 2, 3, 4</sup> These syntheses all followed the same broad strategy: building the tetracycline core in a linear sequence of steps beginning with the D-ring and working “right” toward the A-ring. While these efforts enabled access to a variety of tetracycline or tetracycline-like compounds, the lengthy linear sequence of steps made effective scale-up and derivatization challenging. As a result, exploration of the tetracycline scaffold was limited to semisynthesis for much of its history.<sup>5</sup>

This changed in 2005 with a landmark publication from the Myers group at Harvard University. The Myers synthesis utilized a novel convergent step to join two late-stage precursors, the D-ring precursor (**1.7**) and the AB Enone (**3.1**, generic structure), in a single, high-yielding transformation to provide the protected tetracycline scaffold (**3.2**, Fig. 3.1).<sup>6</sup> This key step represents an anionic cyclization: deprotonation of the D-ring methyl group at low temperature initiates a Michael addition into the enone moiety of the AB Enone to provide the addition product as the enolate. Subsequent warming to room temperature then allows for enolate attack into the nearby phenyl ester of the D-ring precursor in a Dieckmann condensation mechanism, with expulsion of the phenolate providing the C-ring

---

<sup>1</sup> (a) Conover, L. H.; Butler, K.; Johnston, J. D.; Korst, J. J.; Woodward, R. B. *J. Am. Chem. Soc.* **1962**, *84*, 3222-3224. (b) Korst, J. J.; Johnston, J. D.; Butler, K. E.; Bianco, E. J.; Conover, L. H.; Woodward, R. B. *J. Am. Chem. Soc.* **1968**, *90*, 439-457.

<sup>2</sup> Gurevich, A. I.; Karapetyan, M. N.; Kolosov, M. N.; Korobko, V. G.; Onoprienko, V. V.; Popravko, S. A.; Shemyakin, M. M. *Tet. Lett.* **1967**, *8*, 131-134.

<sup>3</sup> Muxfeldt, H.; Hass, G.; Hardtman, G.; Kathawala, F.; Mooberry, J. B.; Vedejs, E. *J. Am. Chem. Soc.* **1979**, *101*, 698-701.

<sup>4</sup> Stork, G.; La Clair, J. J.; Spargo, P.; Nargund, R. P.; Totah, N. *J. Am. Chem. Soc.* **1996**, *118*, 5304-5305.

<sup>5</sup> See Chapter 2 for a summary of selected tetracycline semisynthesis efforts.

<sup>6</sup> See Charest et al., **2005** (Chapter 1, ref. 8a).

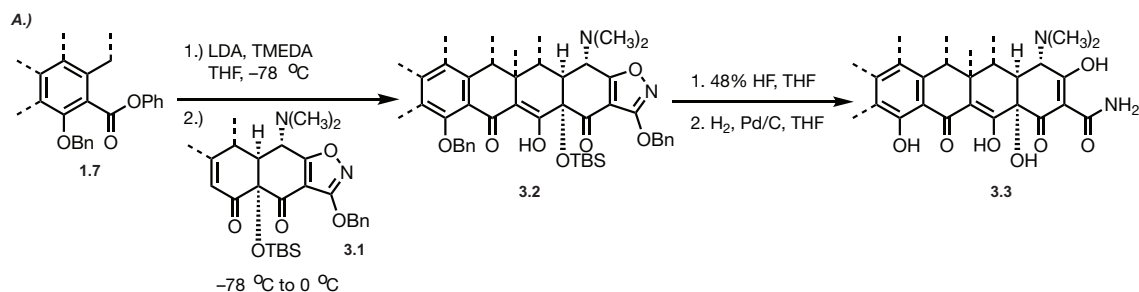


**Figure 3.1 The Myers' Tetracycline Synthesis.** The Myers route to the tetracyclines features a key step involving the coupling of two advanced intermediates, the D-ring precursor (**1.7**, generic structure) and the AB Enone (**3.1**, generic structure). This reaction proceeds via an anionic cyclization procedure consisting of Michael addition followed by Dieckmann condensation to provide the C-ring of the scaffold in **3.2**. A two-step deprotection sequence is then employed to access the final tetracycline analogue (**3.3**, generic structure). This route has been used to access tetracycline analogues with variation at position C5, C5a, C6, and C7-C9.

of the tetracycline scaffold. To access the tetracycline product, compounds were typically exposed to hydrofluoric acid to enact desilylation of the C12a-hydroxyl group, followed by hydrogenation over palladium on carbon to cleave the C10-benzyl group and open the isoxazole protecting group to reveal the vinylogous carboxamide structure of the A-ring. In sharp contrast to the previously developed total synthesis routes, the Myers route combined a highly convergent synthesis with scalable intermediates to enable late-stage modification and diversification—the Myers synthesis has been used to install novel substituents at positions C4, C5, C5a, C6, C7, C8, and C9.<sup>7, 8, 9</sup> This synthesis route served as the foundation for the creation of Tetrphase Pharmaceuticals in 2006 and has since

<sup>7</sup> Selected examples of C4-modulation: (a) Xiao, X.-Y.; Dumas, J. P.; Hunt, D. K.; Sun, C.; Zhao, P. Tetracycline compounds and methods of treatment. WO 2018/045084 A1. Aug. 30, 2017. (b) Xiao, X.-Y.; Clark, R. B.; Hunt, D. K.; Sun, C. Tetracycline Compounds. WO 2014/036502 A2. August 30, 2013.

<sup>8</sup> Selected examples of C5- and C5a-modulation: (a) See Charest et al., **2005** (Chapter 1, ref. 8a). (b) Wright, P. M.; Myers, A. G. *Tetrahedron*, **2011**, *67*, 9853-9869. (c) Wright, P. M. Ph. D. Thesis; Harvard University, 2015. (d) Liu, F.; Wright, P. M.; Myers, A. G. *Org. Lett.* **2017**, *19*, 206-209. (e) Myers, A. G.; Wright, P. M.; Hecker, E. Synthesis of C5-Substituted Tetracyclines, Uses Thereof, and Intermediates Thereof. WO 2012/047907 A1. October 4, 2011.

<sup>9</sup> Selected examples of C7, C8, and C9-modulation: (a) See Charest et al., **2005** (Chapter 1, ref. 8a). (b) Sun, C.; Wang, Q.; Brubaker, J. D.; Wright, P. M.; Lerner, C. D.; Noson, K.; Charest, M.; Siegel, D. R.; Wang, Y.-M.; Myers, A. G. *J. Am. Chem. Soc.* **2008**, *130*, 17913-17927. (c) *Topics in Medicinal Chemistry: Antibacterials*, Sun, C.; Xiao, X. Y. Springer Verlag – Berlin, Germany, **2017**, *26*, 55-96.



generated an estimated 3,000 novel tetracycline analogues for evaluation as antibacterial agents.<sup>10</sup>

The simpler of the two Michael-Dieckmann reaction precursors, the D-ring precursor is typically prepared from substituted benzene derivatives in a handful of steps (precise step-count depends on substituents).<sup>11</sup> The more challenging coupling partner, the AB Enone, has experienced several revised synthesis efforts over the years to enable scalable and convergent access. The 2005 synthesis relied on the large-scale production of the protected epoxy-ester intermediate **3.7** from benzoic acid, accomplished through an enzymatic dihydroxylation procedure and epoxidation/rearrangement sequence (Fig. 3.2).<sup>6</sup> Subsequent introduction of the lithiated isoxazole intermediate **3.8** resulted in the ketone product **3.9** in good yield. Treatment with lithium trifluoromethanesulfonate followed by trifluoroacetic acid (TFA) then provided the closed A-ring product **3.10**. This intermediate served as a branching point for accessing C5-hydroxyl substituted analogues or those lacking C5-substitution. In the former, the hydroxyl group was converted to the bromide under Appel conditions, then further transformed to sulfide **3.11** with thiophenol, setting up for an oxidation/Mislow-Evans rearrangement sequence to provide the C5-hydroxyl intermediate **3.13**. The C5-functionalized AB Enone (**3.14**) was then accessed after benzoyl protection at C5 and a C12-desilylation/oxidation and C12a-protection sequence. The standard AB Enone (**3.16**) was accessed in a similar manner following reductive

---

<sup>10</sup> (a) See Liu et al., **2016** (Chapter 1, ref. 1) (b) Liu, F., PhD Thesis, Harvard University, 2017.

<sup>11</sup> Selected examples of diverse D-ring precursor substitutions: (a) Chen, C.-L.; Clark, R. B.; Deng, Y.; Plamondon, L.; Sun, C.; Xiao, X.-Y. *Tetracycline Analogs*. WO 2012/021712 A1. Aug. 11, 2011. (b) Clark, R. B.; He, M.; Deng, Y.; Sun, C.; Chen, C.-L.; Hunt, D. K.; O'Brien, W. J.; Fyfe, C.; Grossman, T. H.; Sutcliffe, J. A.; Achorn, C.; Hogan, P. C.; Katz, C. E.; Niu, J.; Zhang, W.-Y.; Zhu, Z.; Ronn, M.; Xiao, X.-Y. *J. Med. Chem.* **2013**, *56*, 8112-8138. (c) Sun, C.; Hunt, D. K.; Chen, C.-L.; Deng, Y.; He, M.; Clark, R. B.; Fyfe, C.; Grossman, T. H.; Sutcliffe, J. A.; Xiao, X.-Y. *J. Med. Chem.* **2015**, *58*, 4703-4712.

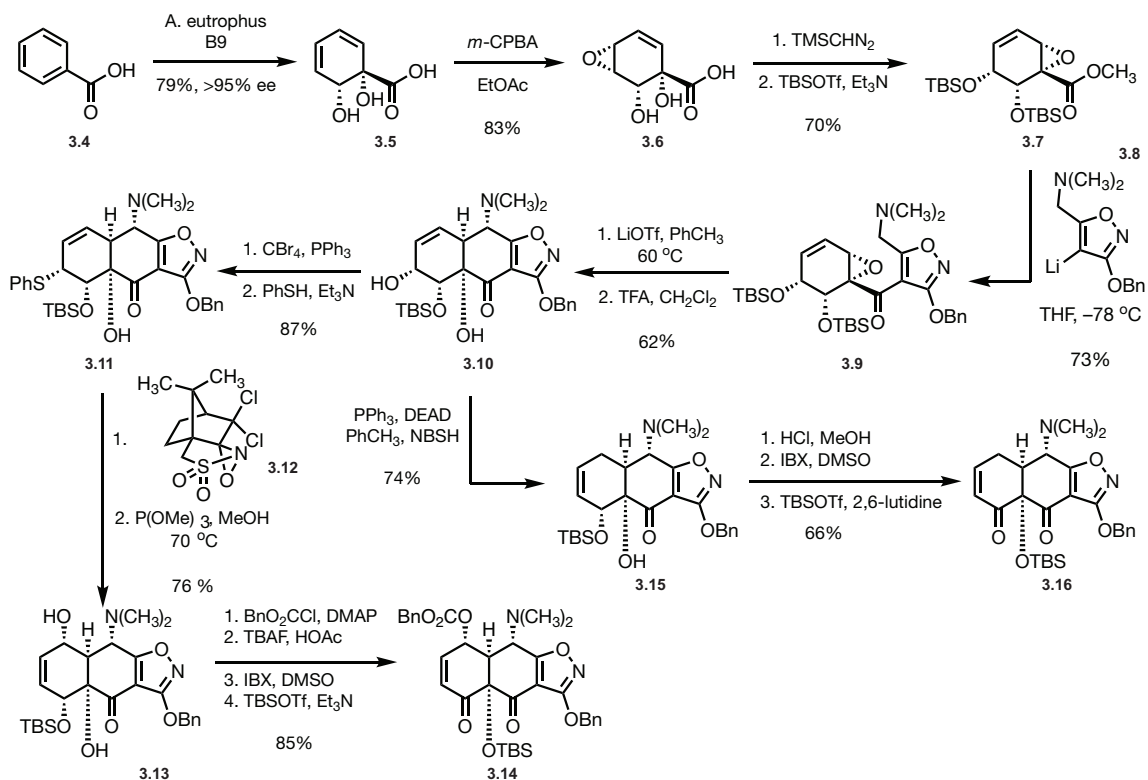


**Figure 3.2 Myers' Group First Generation Access to the AB Enone (1.6).** The first-generation synthesis of the AB Enone consisted of a lengthy route beginning with benzoic acid. This route served as a branching point to access the standard AB Enone (1.6) as well as a C5-hydroxylated AB Enone (3.14) useful for accessing analogues of doxycycline. During attempts to scale this route, researchers encountered difficulties surrounding the enzymatic dihydroxylation step (3.4 to 3.5) which, among other issues, inspired a redesigned synthesis. Figure adapted from Charest et al., 2005 (Chapter 1, ref. 8).

transposition of the hydroxyl group to yield 3.15, enabling the same desilylation/oxidation/silylation procedure as above.

In an updated route reported in 2007, Brubaker and Myers presented a major redesign in synthesis of this key intermediate – one that would eventually become the foundation for the industrial scale-up routes used at Tetraphase Pharmaceuticals (Fig. 3.3).<sup>12</sup> This route was designed around another key convergent reaction: the coupling of 3-methoxyfuraldehyde (3.22) and allylic amine isoxazole 3.21 to provide the intermediate hydroxyl compound 3.23 which, after intramolecular furan Diels-Alder reaction and

<sup>12</sup> Brubaker, J. D.; Myers, A. G. *Org. Lett.* 2007, 9, 3523-3525.

oxidation at C1, provided the general AB Enone core structure (**3.24**). This route was completed following demethylation of the C12-methylether and rearrangement on the B-ring using boron trichloride ( $\text{BCl}_3$ ), followed by protection of the resulting C12a-hydroxyl group as the silyl ether (AB Enone, **3.16**). The 3-methoxyfuraldehyde starting material was originally accessed from 3-methoxyfuran, itself a product of a scalable 4-step sequence starting with 3-chloro-1,2-propane (an updated synthesis from Tetraphase Pharmaceuticals would enable access from 3-bromofuran in a 2-step sequence).<sup>13, 14</sup> Access to allylic amine precursor **3.21** proved more challenging. Brubaker eventually settled on enantioselective addition of a vinyl group to aldehyde-functional isoxazole **3.18** using divinyl zinc and norephedrine-derived lithium alkoxide **3.19**. This unique reaction relied on chelation of both the aldehyde and isoxazole oxygen atoms by lithium, enabling the vinyl zinc moiety, itself chelated to the nearby ephedrine oxygen, to deliver the vinyl nucleophile directly to

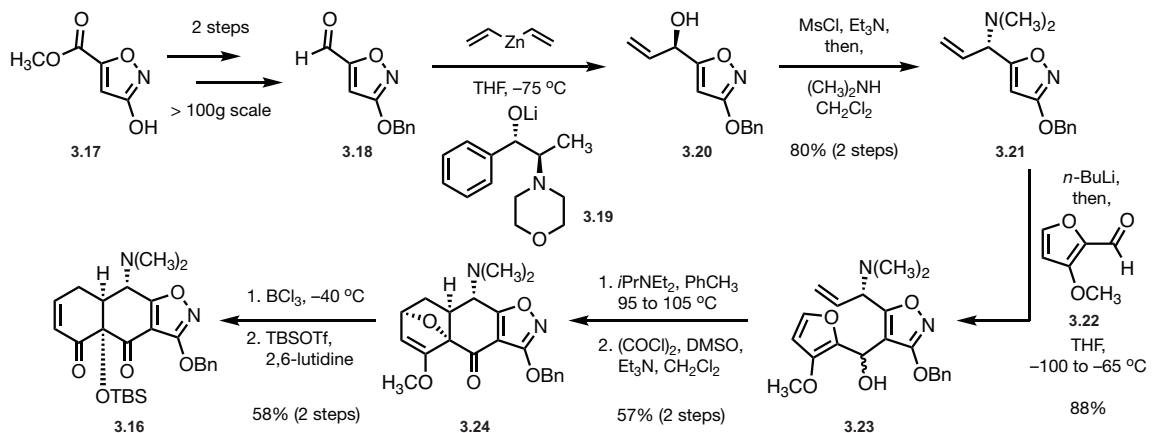


**Figure 3.3 A Second-Generation Synthesis of the AB Enone: The Brubaker/Myers Route.** In 2007, a redesigned route to the AB Enone employed a convergent coupling step between allylic amine **3.21** and 3-methoxyfuraldehyde **3.22**. Following coupling, treatment with DIPEA at high temperature would provide the furan Diels-Alder product. From there, three steps would provide the AB Enone product (**3.16**) in good yield. Figure adapted from Brubaker et al., **2007** (Chapter 3, ref. 12).

<sup>13</sup> Meister, C.; Scharf, H.-D. *Synthesis* **1981**, 737-738.

<sup>14</sup> Ronn, M.; Lim, N.-K.; Hogan, P.; Zhang, W.-Y.; Zhu, Z.; Dunwoody, N. *Synlett* **2012**, 23, 134-136.

one face. This reaction provided the alcohol product in 93% ee and 90% yield. From there, allylic amine precursor **3.21** was accessed following mesylation of the hydroxyl group in **3.20** and S<sub>N</sub>2 displacement with dimethylamine in DCM.

Over subsequent years, Tetrphase would build and expand on the Brubaker route to access both the AB Enone as well as final tetracyclines in high yield and purity following large-scale synthesis (Fig. 3.4, 3.5).<sup>15</sup> Tetrphase would report an updated synthesis of the aldehyde isoxazole intermediate **3.18** from dimethylmaleate (**3.25**), as well as an optimized procedure to access allylic amine **3.21** via a similar ephedrine-mediated enantioselective vinyl addition and mesylation/displacement strategy (Fig. 3.4A). While this procedure lent itself well to scale-up efforts, Tetrphase would go on to report a second-generation route that instead relied on *tert*-butyl sulfinylamine auxiliaries developed by Ellman for the selective vinyl addition (Fig. 3.4B). In this iteration, the Ellman auxiliary was condensed onto aldehyde **3.18** to form sulfinylimine **3.29**. Diastereoselective addition was then achieved using vinylmagnesium chloride with catalytic amounts of methyllithium and zinc (II) chloride. This transformation is thought to proceed via formation of a dimethyl vinyl zincate species that conducts the delivery of the vinyl group to the imine, allowing dimethylzinc to recycle following each addition and providing the product (**3.30**) in high yield and diastereoselectivity. The allylic amine product (**3.21**) was then accessed following hydrolysis of the auxiliary to provide the intermediate amine and subsequent reductive amination using formaldehyde and 2-picoline borane complex (2-PB, **3.31**) as a

---

<sup>15</sup> (a) Zhang, W.-Z.; Chen, C.-L.; He, M.; Zhu, Z.; Hogan, P.; Gilicky, O.; Dunwoody, N.; Ronn, M. *Org. Proc. Res. Dev.* **2017**, *21*, 377-386. (b) Zhang, W.-Y.; Hogan, P. C.; Chen, C.-L.; Niu, J.; Wang, Z.; Lafrance, D.; Gilicky, O.; Dunwoody, N.; Ronn, M. *Org. Proc. Res. Dev.* **2015**, *19*, 1784-1795. (c) Zhang, W.-Y.; Sun, C.; Hunt, D.; He, M.; Deng, Y.; Zhu, Z.; Chen, C.-L.; Katz, C. E.; Niu, J.; Hogan, P. C.; Xiao, X.-Y.; Dunwoody, N.; Ronn, M. *Org. Proc. Res. Dev.* **2016**, *20*, 284-296.

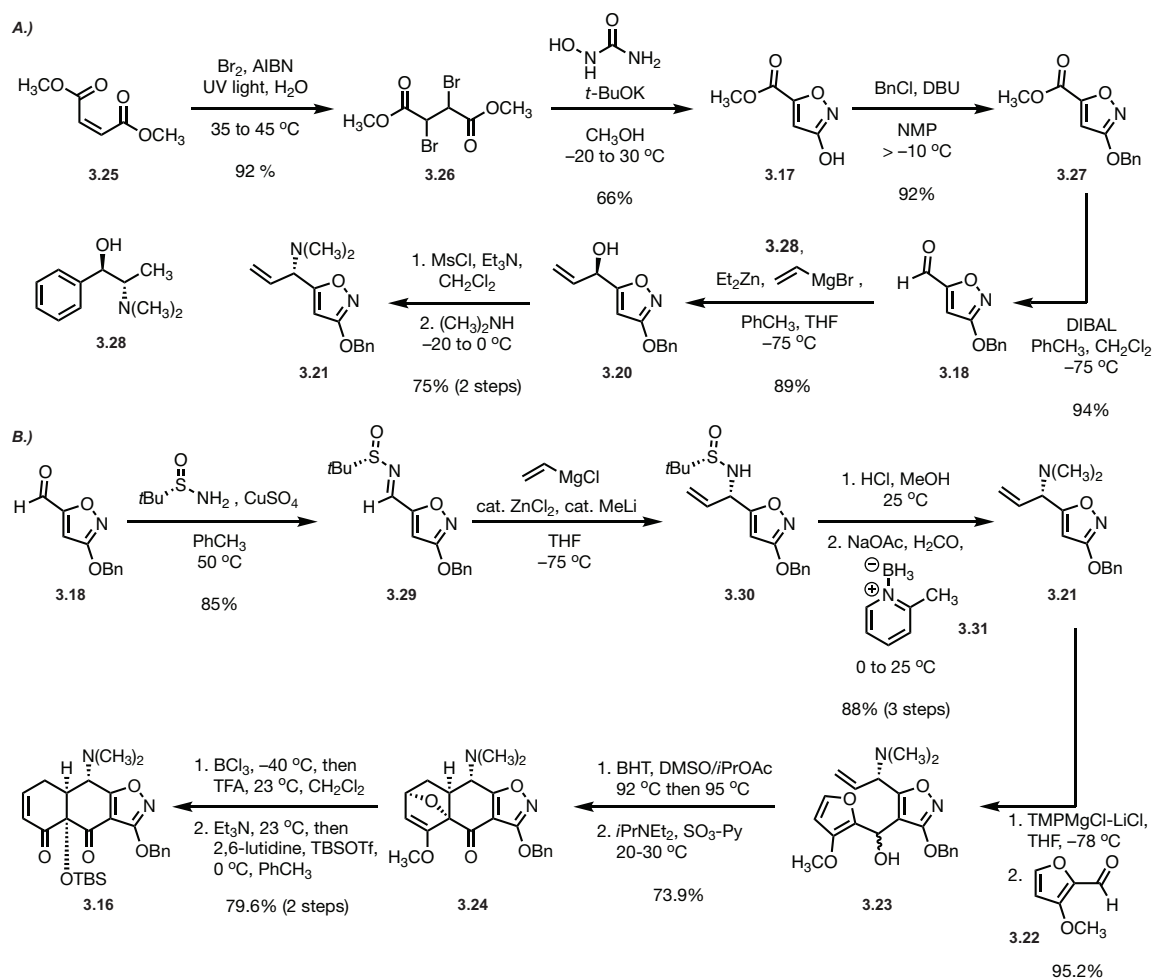


**Figure 3.4 Updated Access to the AB Enone: Tetraphase Developments.** Tetraphase would optimize the Brubaker/Myers route to the AB Enone for large-scale production. Two routes were reported, the first featuring an ephedrine-mediated vinyl addition to aldehyde **3.18** (A), and the second employing Ellman auxiliary-type chemistry (**3.30**) (B). The latter was used for scale-up procedures to support compound development efforts. Figure adapted from Zhang et al., **2017**, Zhang et al., **2017**, and Zhang et al., **2016** (Chapter 3, refs 15a, 15b, 15c).

weak reducing agent. Tetraphase' access to the AB Enone remained relatively unchanged, with a handful of alterations to base choice for the initial coupling reaction and optimized conditions for the furan Diels-Alder reaction presented in their final route (Fig. 3.4B). Tetraphase also presented optimized Michael-Dieckmann reaction conditions in their

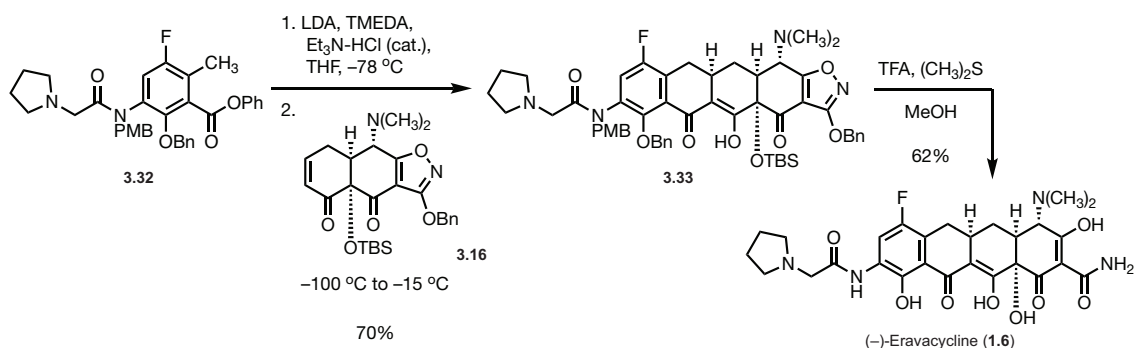


**Figure 3.5 Large-Scale Production of Eravacycline.** Tetraphase would employ minor modifications of the Myers' route to access the clinical candidate Eravacycline (**1.6**) from D-ring **3.32** on large-scale. Figure adapted from Ronn et al., **2013** and Zhang et al., **2017** (Chapter 3, refs. 16a-b).

synthesis of eravacycline (**1.6**), enabling access to large quantities of the cyclized product in a single batch to support clinical studies (Fig. 3.5).<sup>16</sup>

A final redesigned route was presented by researchers in the Myers group in 2011 (Fig. 3.6).<sup>17</sup> Inspired by the utility of the Michael-Dieckmann reaction in forming the C-ring of the tetracycline scaffold, the group sought to employ this methodology in formation of the A-ring as a method for circumventing the furan Diels-Alder reaction typically used. This route employed masked cyclohexenone **3.35** as a coupling partner for isoxazole ester **3.34**. Michael-Dieckmann procedure would provide the cyclized product **3.36** in 62% yield with the stereochemistry of the dimethylamino group at C4 opposite of desired. Exposure of **3.36** to high temperature would initiate a retro-Diels-Alder reaction to expel phenyldimethylcyclopentadiene (**3.37**, mixture of isomers) and reveal the masked enone (**3.38**) of the B-ring. Treatment of **3.38** with lithium *tert*-butoxide would provide an enolate at C12a which could be trapped with a nitro-variant of Davis' oxaziridine (**3.39**) to provide

<sup>16</sup> (a) Ronn, M.; Zhu, Z.; Hogan, P. C.; Zhang, W.-Y.; Niu, J.; Katz, C. E.; Dunwoody, N.; Gilicky, O.; Deng, Y.; Hunt, D. K.; He, M.; Chen, C.-L.; Sun, C.; Clark, R. B.; Xiao, X.-Y. *Org. Proc. Res. Dev.* **2013**, *17*, 838-845. (b) Zhang, W.-Y.; Che, Q.; Crawford, S.; Ronn, M.; Dunwoody, N. *J. Org. Chem.* **2017**, *82*, 936-943.

<sup>17</sup> Kummer, D. A.; Li, D.; Dion, A.; Myers, A. G. *Chem. Sci.* **2011**, *2*, 1710-1718.

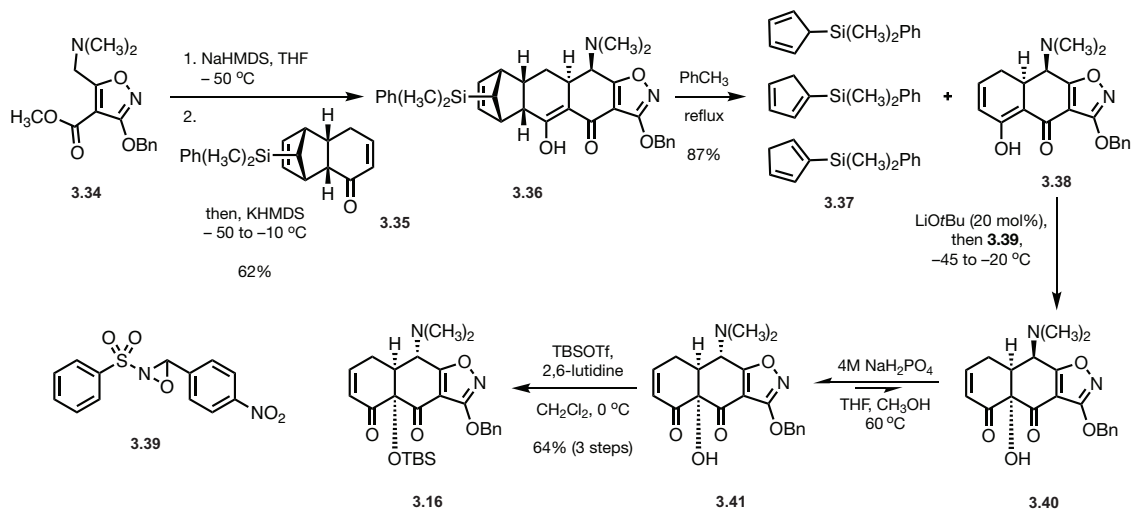


**Figure 3.6 Final Redesigned Route to Access the AB Enone.** In 2011, the Myers group reported a final redesigned route to access the AB Enone (**3.16**). This route employed a novel Michael-Dieckmann cyclization procedure between isoxazole **3.34** and masked cyclohexanone **3.35**. Following coupling, the “masked” Enone was revealed after retro-Diels-Alder reaction at high temperature to provide **3.38**. Face-selective oxidation with Davis’ oxazridine **3.39** then provided the C12a-hydroxyl group (**3.40**). The AB Enone was access following epimerization at C4 and TBS protection. Figure adapted from Kummer et al., **2011** (Chapter 3, ref. 17).

the C12a-hydroxyl group (**3.40**). The selectivity of this reaction is thought to rely upon the incorrect stereochemistry of the C4-dimethylamino group providing steric occlusion of the upper face of the molecule. Finally, the AB Enone was accessed following epimerization at C4 (**3.41**) and protection of the C12a-hydroxyl group as the silyl ether (AB Enone, **3.16**). This route was optimized for laboratory synthesis and reliably produced upwards of 50 grams of AB Enone in a single run. Despite the novelty of the Michael-Dieckmann cyclization strategy on display, this route has not seen much application outside of the Myers group.

The 2005 Myers synthesis of the tetracyclines represents a watershed moment in the history of tetracycline development, with efforts during the following years generating numerous optimized and redesigned syntheses. Through these efforts, chemists can now access tetracycline analogues with a variety of substitution patterns and at any scale.

### 3.3 Recent Non-Canonical Tetracycline Developments

In this section, we provide a summary of efforts in recent years to develop novel tetracyclines with non-canonical activities, primarily those from Tetraphase Pharmaceuticals. Tetraphase was acquired by La Jolla Pharmaceuticals in 2020, leading a cessation of their tetracycline research efforts.<sup>18</sup> Prior to this, however, Tetraphase had evaluated a subset of their compound library for antileukemic effects and identified a series of compounds with intriguing activity, with a selection shown in Figure 3.7.<sup>19</sup> Tetraphase had utilized their second-generation manufacturing route, which accessed allylic amine precursor **3.21** via Ellman auxiliary and reductive amination (Fig. 3.4), as a method for exploring novel substitution patterns at C4. This was accomplished through introduction of diallylamino isoxazole **3.42** and generation of the corresponding diallyl AB Enone **3.43** (Fig. 3.7A). Following elaboration to the tetracycline scaffold, bisdeallylation was achieved after treatment with dimethylbarbituric acid and a palladium catalyst, enabling functionalization via reductive amination (**3.47**).<sup>20</sup> Alternatively, allylic amine **3.42** could be functionalized earlier in the sequence and carried to the full scaffold. Coupled with a C7-methoxy-C8-pyrrolidino D-ring precursor (**3.44**), originally identified for its exceptional antibacterial activity, these alternations generated tetracycline analogues with exceptional antiproliferative activities in human leukemia cell lines, including the lead

---

<sup>18</sup> La Jolla Pharmaceutical Company announces the closing of acquisition of Tetraphase Pharmaceuticals, Inc. *Intrado GlobeNewsWire*. (Accessed August 28, 2021).

<sup>19</sup> Sun, C.; Zhao, P.; Hunt, D.; Kerstein, K.; McKellip, S.; Bostwick, R.; Dumas, J.; Xiao, X.-Y. Discovery and Structure-Activity Relationship of TP-2846: A Novel Tetracycline Antileukemia Agent. Poster presented at: American Association for Cancer Research Annual Conference (#3857); March 29-April 3, 2019; Atlanta, GA.

<sup>20</sup> Xiao, X.-Y.; Dumas, J. P.; Hunt, D. K.; Sun, C.; Zhao, P. Tetracycline Compounds and Methods of Treatment. U. S. Patent Number WO 2018045084. August 3, 2017.



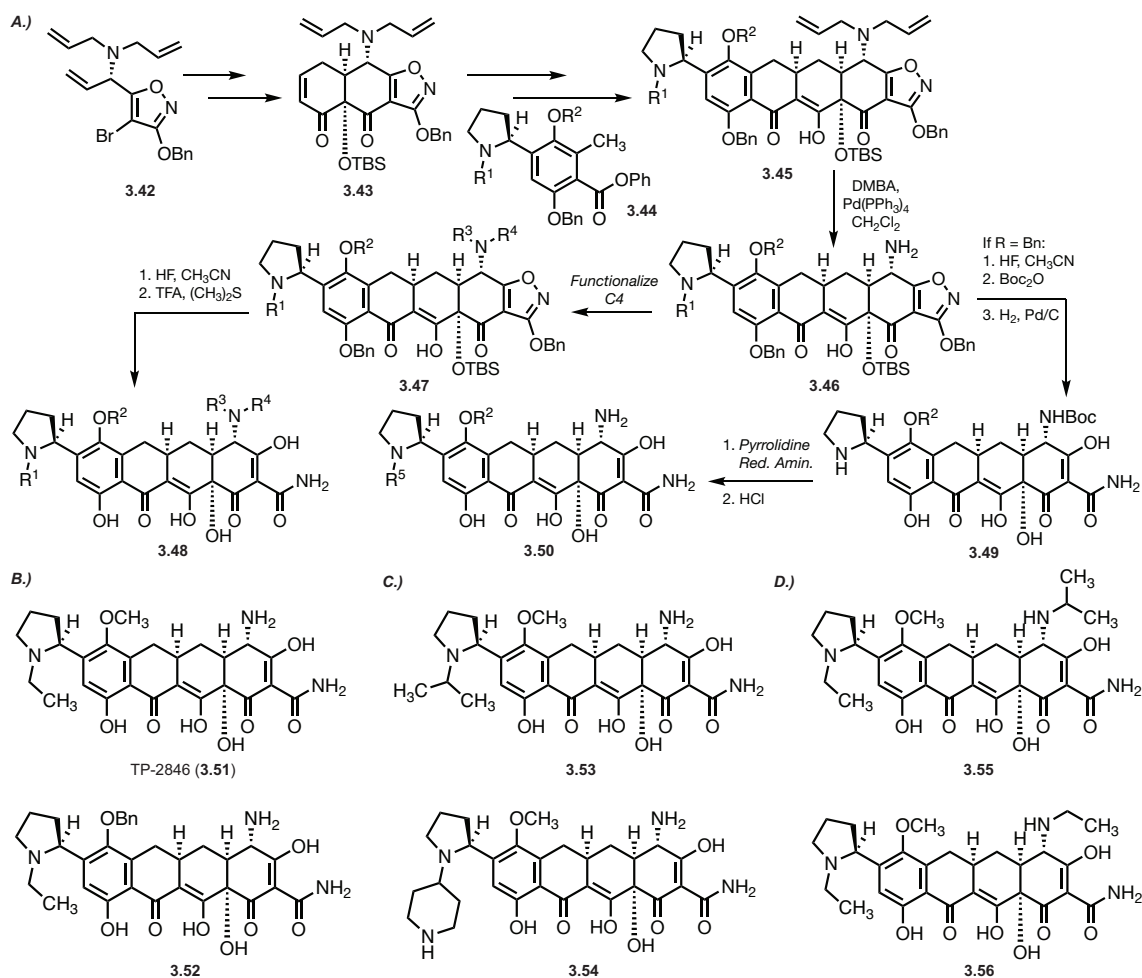


**Figure 3.7 Development of Novel C4-amino Tetracyclines with Antileukemia Activity.** Tetraphase utilized a diallyl isoxazole intermediate (**3.42**) to access AB Enone **3.43** (A, see B-D for R groups). This species was coupled with D-ring **3.44** to provide the tetracycline scaffold which could then be derivatized into analogues using a number of similar routes (See **3.48** and **3.50**). A selection of novel analogues featuring C7 variation (B) pyrrolidine nitrogen variation (C), and alkyl variation at C4 (D). The lead compound, TP-2846 (**3.51**) is shown in C. Figures adapted from Sun et al., **2019** (Chapter 3, ref. 19).

compound TP-2846 (**3.51**, Fig. 3.7B).<sup>21</sup> The researchers would continue to explore novel substitution patterns, primarily at C4, C7, and the pyrrolidine nitrogen atom, however, no major improvements were uncovered (selected analogues, Fig. 3.7B-D). Subsequent *in vitro* analyses revealed mitochondrial translation as a target of TP-2846 in human cells,

<sup>21</sup> (a) Sun, C.; Deng, Y.; Hunt, D. K.; Fyfe, C.; Chen, C.-L.; Clark, R. B.; Grossman, T. H.; Sutcliffe, J. A.; Xiao, X.-Y. *J. Antibiot.* **2018**, *71*, 287-297. (b) Zhang, W.-Y.; Sun, C.; Hunt, D. K.; He, M.; Deng, Y.; Zhu, Z.; Chen, C.-L.; Katz, C. E.; Niu, J.; Hogan, P. C.; Xiao, X.-Y.; Dunwoody, N.; Ronn, M. *Org. Proc. Res. Dev.* **2015**, 284-296.

with the compound showing strong inhibition of mitochondrially produced proteins and only moderate inhibition of cytosolic proteins (COX-1 vs. COX-4, immunoblot, Fig. 3.8).<sup>22</sup> Further, gene expression analysis using RT-qPCR revealed signatures consistent with loss of mitochondrial function and cell cycle inhibition. In *in vivo* testing, TP-2846 displayed good pharmacokinetic properties and potent activity in acute myeloid leukemia mouse xenograft models, with > 50% tumor reduction in most animals treated.<sup>23</sup> These studies provided exciting initial data regarding a relatively novel application of the tetracyclines: mitochondrially targeted cancer therapeutics.<sup>24</sup> While further efforts are needed to

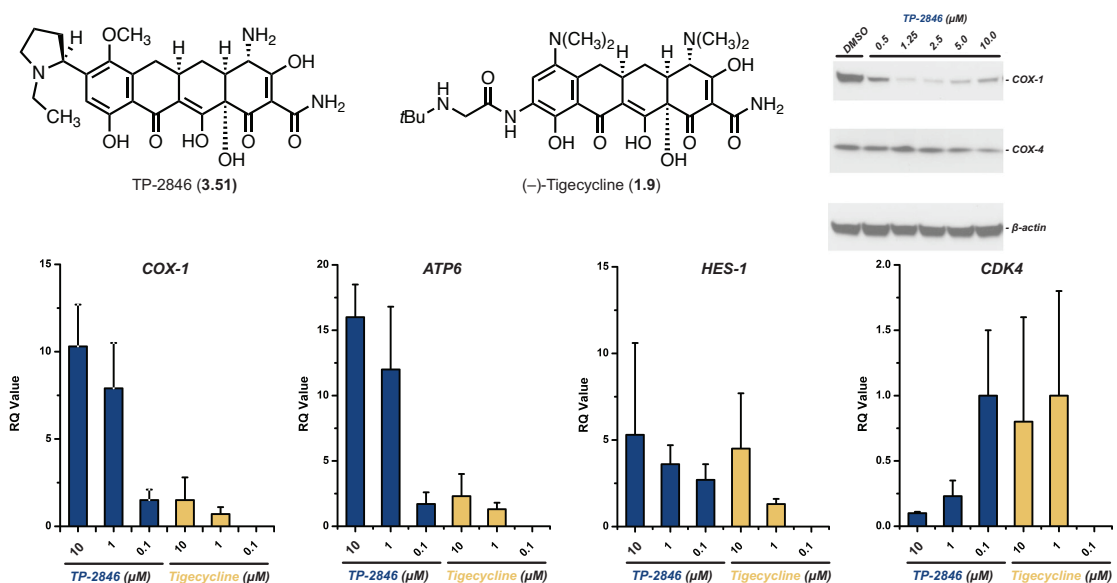


**Figure 3.8 Early Biological Evaluation of TP-2846 (3.51).** Tetrachase determined that the novel antileukemia tetracycline TP-2846 (3.51) was targeting mitochondrial translation. Western blot analysis shows inhibition of the mitochondrially produced COX1, while the cytosolically produced COX4 is unaffected. Further, RT-qPCR analysis of several gene signatures revealed TP-2846 was dysregulating mitochondrial function and inhibiting cell cycle progression (COX-1, ATP6, HES-1, and CDK4). Figures adapted from Fyfe et al, 2019 (Chapter 3, ref. 22).

<sup>22</sup> Fyfe, C.; Bhargava, A.; Ballesteros, J.; Robles, A.; MacKee, E. E.; Sun, C.; Xiao, X.-Y. Dumas, J. *In Vitro* Characterization of TP-2846: A Novel Tetracycline Antileukemia Agent. Poster presented at: American Association for Cancer Research Annual Conference (#4802); March 29-April 3, 2019; Atlanta, GA.

<sup>23</sup> Xiao, X.-Y.; Sun, C.; Zhou, J.; Tatsuta, N.; Newman, J.; White, D.; Hibner, B.; Chakravarty, A.; Dumas, J. *In Vivo* Activities of TP-2846: A Novel Tetracycline Antileukemia Agent. Poster presented at: American Association for Cancer Research Annual Conference (#3880); March 29-April 3, 2019; Atlanta, GA.

<sup>24</sup> See Chapter 1 for a review of the tetracyclines and recent mitochondria-based therapeutic applications.

characterize the antibacterial activity, as well as the effects on cytosolic translation and signaling pathways, the discovery of TP-2846 represents a significant step forward in the application of non-canonical tetracyclines.

In 2020, researchers from the laboratory of Daniel Wilson reported a mechanistic analysis of the tetracycline-like antibacterial natural product tetracenomycin X (TcmX, **3.58**, Fig. 3.9A).<sup>25</sup> TcmX, which bears structural relationships to both tetracycline and doxorubicin (**3.59**), shows both antibacterial activity against Gram-positive strains as well as cytotoxic effects in a variety of human cells. Through their studies, Osterman and colleagues determined TcmX binds to the peptide exit tunnel of the human cytosolic ribosome – a location nearly identical to that of doxycycline (Fig. 3.9B-D).<sup>26</sup> The

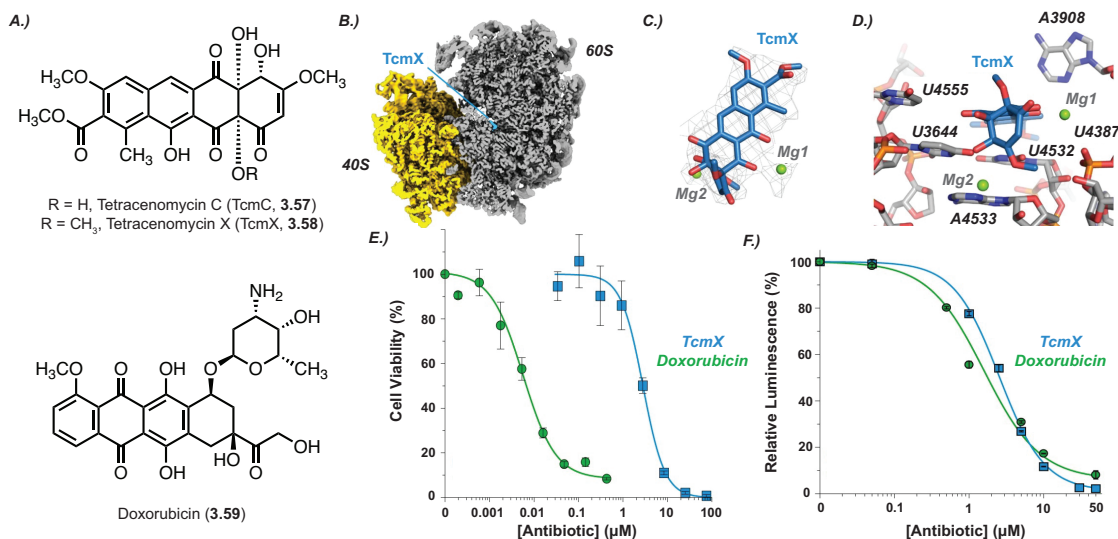


**Figure 3.9 Tetracenomycin X and Ribosomal Binding Locations.** An exciting 2020 report discussed the tetracycline-like antibacterial compound Tetracenomycin X (TcmX, **3.58**) and its cytotoxic properties (A). The compound, structurally similar to both the tetracyclines and known anthracycline cancer therapeutic doxorubicin (**3.59**), was shown to the peptide exit tunnel of the human cytosolic ribosome (B-D). TcmX was also found to inhibit cell growth and cytosolic translation (E, F, respectively), particularly of short peptide sequences. Figures adapted from Osterman et al., **2020** (Chapter 3, ref. 25).

<sup>25</sup> Osterman, I. A.; Wieland, M.; Maviza, T. P.; Lashkevich, K. A.; Lukianov, D. A.; Komarova, E. S.; Zakalyukina, Y. V.; Buschauer, R.; Shiriaev, D. I.; Leyn, S. A.; Zlamal, J. E.; Biryukov, M. V.; Skvortsov, D. A.; Tashlitsky, V. N.; Polshakov, V. I.; Cheng, J.; Polikanov, Y.; Bogdanov, A. A.; Osterman, A. L.; Dmitriev, S. E.; Roland, B.; Dontsova, O. A.; Wilson, D. N.; Sergiev, P. V. *Nat. Chem. Biol.* **2020**, *16*, 1071-1077.

<sup>26</sup> See Mortison et al., **2018** (Chapter 1, ref. 26).

researchers went on to report these cytotoxic agents ( $GI_{50}$  2.5  $\mu$ M, HEK293T cells) also inhibited human cytosolic translation. Subsequent ribosomal toeprinting analysis would reveal these compounds target the elongation stage of translation: the synthesis of short oligopeptides was permitted; however, the occlusion of the peptide exit tunnel by TcmX would prevent generation of longer peptides. While TcmX differs from the tetracyclines in a variety of ways, including the overall “flat” shape of the compound, this report provides us with yet another example of tetracycline-like compounds in non-canonical applications and lends further confidence to our efforts to develop novel Col-3 analogues as cancer therapeutics.

### 3.4 Strategy

We sought to leverage the long history of tetracycline development in the Myers group as well as the exciting recent efforts from Tetrphase and others (*vide supra*) to inform our analogue synthesis strategy. These efforts would require the synthesis of D-ring precursors with novel substitutions as well as an AB Enone-like structure lacking substitution at C4. Our semisynthetic compound development efforts suggested that substitutions at positions C5 and C6 have a deleterious effect on antiproliferative activity.<sup>27</sup> Further, the history of tetracycline synthesis in the Myers group and at Tetrphase ensured a large repository of procedures for accessing a variety of D-ring precursors. As a result, our early efforts focused on the development of a new AB Enone-like compound to enable convergent access to novel fully synthetic Col-3 analogues. One of the later iterations of the Myers AB Enone synthesis developed by Kummer and colleagues in 2011 appeared

---

<sup>27</sup> See Chapter 2 for a discussion of 4-dedimethylamino tetracycline analogues and their activities.

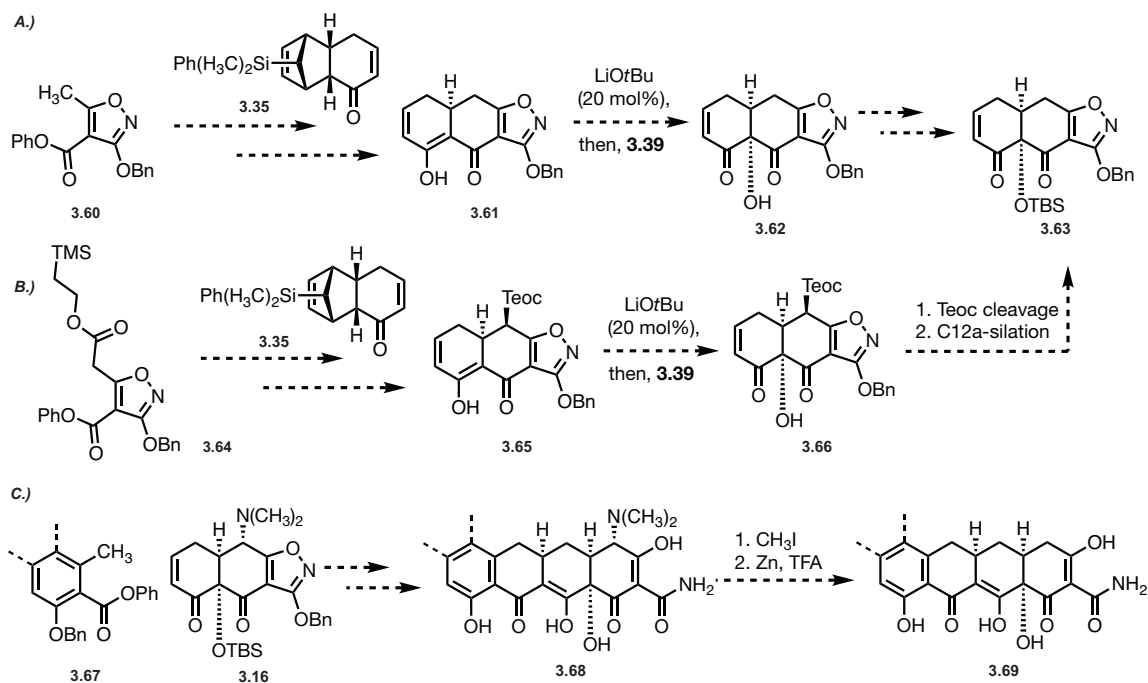


**Figure 3.10 Strategy Overview: Fully Synthetic Analogues of Col-3.** During planning stages, we considered a variety of routes for accessing novel, fully synthetic analogues of Col-3. We initially considered using routes similar to those developed by Kummer et al. to access a novel “Col-3” AB Enone (**3.63**) which lacked substitution at C4. After initial evaluations, though, we elected to utilize our semisynthetic methodology to cleave the C4-dimethylamino group as a final step in our synthesis, enabling access to novel Col-3 analogues while still employing the majority of the tetracycline synthesis route.

particularly well-suited for this synthesis (Fig. 3.6), as the C4-dimethylamino group is known to play a key role in the product ratio of the furan-Diels-Alder reaction used in the Brubaker/Tetraphase syntheses.<sup>28, 29</sup> Along these lines, we hypothesized that an isoxazole precursor (**3.60**, Fig. 3.10A) could be introduced to cyclohexenone **3.35** for Michael-Dieckmann cyclization, then carried through the remainder of the route to access the “Col-3” AB Enone **3.63**. One potential roadblock involved the diastereoselective hydroxylation reaction with lithium *tert*-butoxide and Davis oxaziridine derivative **3.39** (**3.61** to **3.62**, Fig. 3.10A). As discussed above, the steric blocking provided by the C4-dimethylamino group

<sup>28</sup> See Brubaker et al., **2007** (Chapter 3, ref. 7).

<sup>29</sup> See Zhang et al., **2015**, Zhang et al., **2016**, and Zhang et al., **2017** (Chapter 3, refs 15a, 15b, 15c).

in “upward-facing” stereochemistry is thought to be critical for the bottom-face selectivity of this hydroxylation reaction (see Fig. 3.6). Our proposed solution involved the introduction of a cleavable protecting group at C4 such as a trimethylsilylethoxycarbonyl (Teoc) group (**3.64**, Fig. 3.10B), enabling late stage deprotection via fluoride treatment to reveal the unsubstituted AB Enone **3.63**.<sup>30</sup> In theory, this group would provide the necessary steric presence to enable a selective hydroxylation reaction. The majority of the synthesis in this route proceeded smoothly, however, we encountered difficulties during the Michael-Dieckmann reaction between isoxazole **3.64** and cyclohexenone **3.35**. These challenges, coupled with the general challenges associated with novel route optimization and scale-up, led us to reevaluate our compound development priorities and pursue a different route towards novel Col-3 analogues. We elected to take a page from our semisynthesis handbook and utilize the methylation/reduction procedure for cleavage of the C4-dimethylamino group (Fig. 3.10C). This strategy would allow us to utilize the majority of the tetracycline total synthesis route to access analogues, then we would employ our optimized C4-dedimethylation procedure, which provided Col-3 in upwards of 60% yield, to access final analogues.<sup>31</sup> This methodology ultimately proved successful and, after optimization, enabled us to access a variety of full synthetic Col-3 analogues for evaluation.

---

<sup>30</sup> Our Teoc-based protecting group strategy was based on a report of a tetracycline-like antibacterial agent from the Nicolaou group: Nicolaou, K. C.; Hale, C. R. H.; Nilewski, C.; Ioannidou, H. A.; ElMarrouni, A.; Nilewski, L. G.; Beabout, K.; Wang, T. T.; Shamoo, Y. *J. Am. Chem. Soc.* **2014**, *136*, 12137-12160.

<sup>31</sup> See Chapter 2 for a discussion of our tetracycline semisynthesis procedures.

### 3.5 Route Optimization and Compound Development

After screening a handful of potential D-ring precursors, including C7-fluoro-analogues, we settled on utilizing a C7-methoxy-C8-methylamino scaffold similar to those developed by Tetraphase Pharmaceuticals for both its antibacterial and anticancer properties.<sup>21</sup> This scaffold would allow us to compare activities with Tetraphase's lead compounds (see Fig. 3.7) and expand their synthesis efforts to develop novel analogues. Access to novel Col-3 analogues began with preparation of a C7-methoxy-C8-acetal D-ring precursor (**3.75**, Fig. 3.11) for coupling to the AB Enone (**3.16**).<sup>32</sup> This short sequence begins with the dibromination of 1,4-dimethoxybenzene (**3.70**) with molecular bromine, followed by magnesiation and carboxylation with isopropyl magnesium chloride-lithium chloride complex and carbon dioxide, respectively, to provide the carboxylic acid derivative **3.71**. The phenyl ester was then formed via the acid chloride following treatment

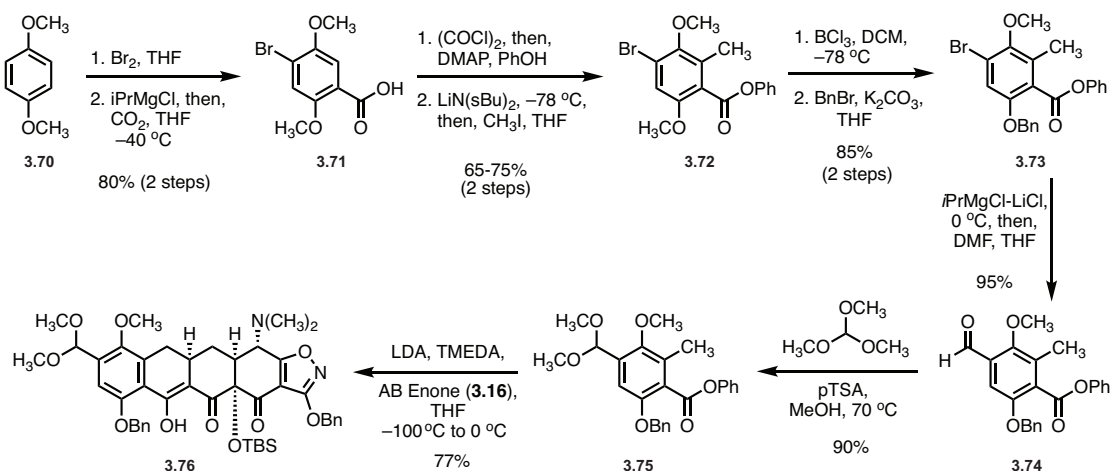


**Figure 3.11 Access to C7-methoxy-C8-acetal functionalized D-ring Precursors.** We utilized published routes to access D-ring precursors for use in our tetracycline synthesis. This route begins with 1,4-dimethoxybenzene (**3.70**), and carries it through a series of carboxylation, methylation, and deprotection/protection steps to access the D-ring precursor **3.75** primed for Michael-Dieckmann reaction with the AB Enone (**3.16**). Route and figure adapted from Zhang et al., **2015** (Chapter 3, ref. 21b) and Chen et al., **2010** (Chapter 3, ref. 32b).

<sup>32</sup> (a) See Sun et al., **2018** and Zhang et al., **2015** (Chapter 3, ref. 21a, b). (b) Chen, C.-L.; Clark, R. B.; Deng, Y.; He, M.; Plamondon, L.; Sun, C.; Xiao, X.-Y.; Tetracycline Compounds. WO 2010/129057. May 7, 2010.





handle which was then functionalized with standard reductive amination chemistry (ex. sodium triacetoxyborohydride) (**3.77**, Fig. 3.77). The reductive amination product **3.77** was then carried through a four-step “deprotection” sequence: C12a-desilylation with HF, C10-benzyl cleavage and isoxazole opening with H<sub>2</sub> and Pd/C, protection of the amine with Boc-anhydride, and finally methylation and Zn-mediated reduction of the C4-dimethylamino group to provide the desired Col-3 analogs for evaluation (**3.78**). On execution, this route provided several challenges that slowed analogue synthesis. The placement of the reductive amination step meant that derivatized scaffolds required a series of 5 to 6 steps before accessing analogues for testing. More importantly, the aliphatic amine groups located off C8 would be readily quaternized during iodomethane treatment. As a result, secondary amines required a Boc-protection step prior to methylation, and tertiary amines were not accessible through this route. While this route could provide analogues for evaluation, these challenges inspired us to develop a different approach.

Our second-generation route revolved around the placement of the reductive amination derivatization step as the last step of the synthesis, enabling easier stockpiling

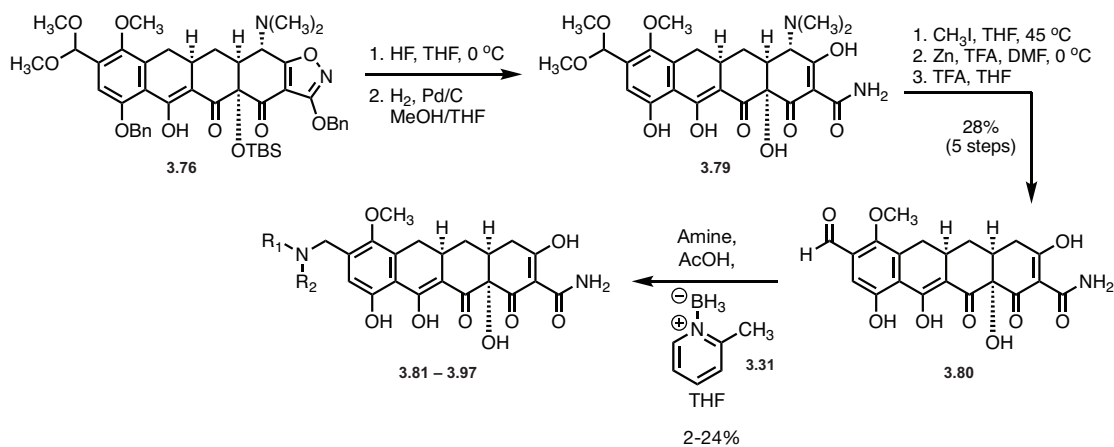


**Figure 3.13 Second Generation Route to Access Novel Col-3 Analogues.** In our redesigned effort, the protected tetracycline scaffold (**3.76**) was fully deprotected to provide C8-aldehyde functional precursor **3.80**. This material served as an excellent starting place for analogue synthesis via reductive amination.

of material and rapid conversion to analogues. This route begins with the same protected tetracycline scaffold (**3.76**, Fig. 3.13) as above. Treatment of **3.76** with excess HF solution for 1 hour at 0 °C followed by hydrogenation over a palladium on carbon catalyst would provide deprotection product **3.79** featuring an intact acetal protecting group at C8. **3.79** was then subjected to methylation conditions to provide the intermediate quaternary methiodide salt, the product of which was taken directly to the zinc-mediated reduction step to enact cleavage of the C4-ammonium group. We found that this final zinc reduction step would provide varying mixtures of the desired aldehyde (**3.80**) and the acetal-protected product. To avoid over-reduction products often observed in longer reaction times during the zinc-mediated reduction step, we elected to bring the crude product of this step through a short treatment with strong acid (ex. TFA, 6M HCl) to provide the acetal deprotection product **3.80**. To access novel analogues, we employed reductive amination conditions developed at Tetraphase that employed 2-picoline-borane complex (**3.31**) as a weak reducing agent.<sup>34</sup> We found these conditions, combined with an amine of choice and acetic acid, would provide Col-3 analogues in good yield following HPLC purification. This route provided us with a range of fully synthetic Col-3 analogues for evaluation.

In our early screening efforts (Fig. 3.14), we sought to evaluate a wide variety of substitution patterns on the C8 position including aryl and heteroaryl (**3.81**, **3.83**) groups, polar amino functionalities (**3.84**, **3.85**), and long chain alkyl/hydroxyl groups (**3.87**). Our semisynthetic compound development efforts described in Chapter 2 suggested polar functionalities might help improve the activity for the otherwise non-polar Col-3 scaffold, however, our evaluations in K562 leukemia cells and HCT116 colorectal cancer cells

---

<sup>34</sup> (a) See Zhang et al., **2015** (Chapter 3, ref. 15b). (b) Kulkarni, A. S.; Ramachandran, P. V.; *Org. Synth.* **2017**, *94*, 332-345.

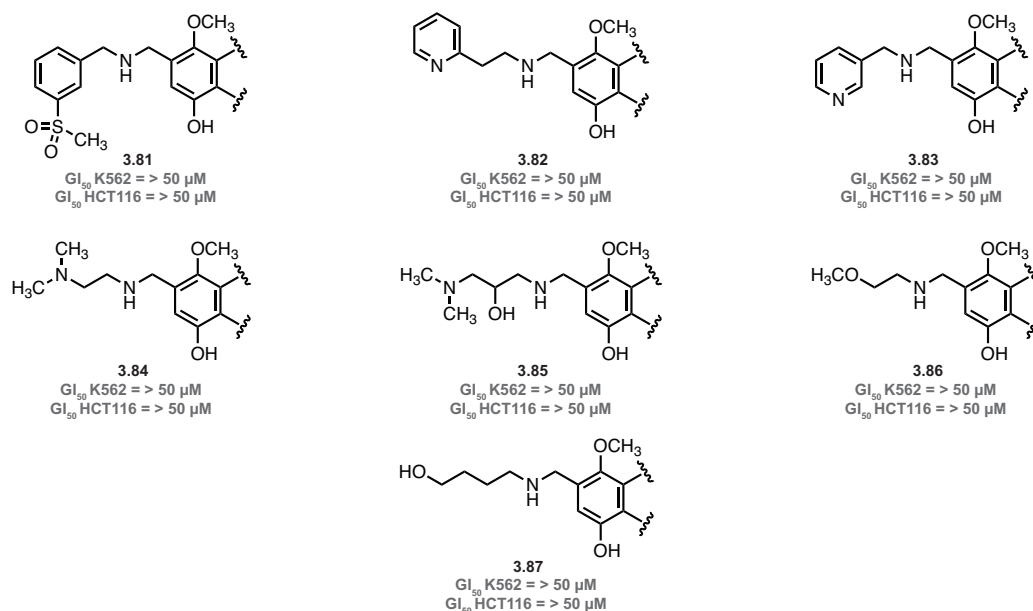


**Figure 3.14 Selected Fully Synthetic Col-3 Analogues: Early Screening.** A selection of early analogues from our synthesis efforts. While we attempted to synthesize compounds with a range of functionalities, these compounds showed no activity against K562 leukemia cells or HCT116 colorectal cancer cells (up to 50  $\mu$ M). Growth assays conducted with Meiyi Yu.

showed precisely the opposite. Many of the analogues synthesized early in our efforts showed a complete loss of activity in both K562 and HCT116 cancer cell lines. While disappointing, these results provided some interesting evidence that these novel Col-3 analogues were potentially activating a different mechanism than that of our semisynthetic quinoline analogues. A small selection of these early analogues, shown in Figure 3.15, displayed modest activity against the two cell lines. In general, these compounds featured cyclic morpholine (**3.88**, **3.89**) or azepane (**3.89**) ring systems, or shorter chain alkyl groups (**3.91**). While these compounds were barely in the ballpark of the parent compound Col-3 ( $GI_{50}$  K562 = 9.1  $\mu$ M,  $GI_{50}$  HCT116 = 3.3  $\mu$ M), our findings suggested that hydrophobic substituents could potentially be beneficial for improving the activity of these analogues. This inspired our synthesis of a selection of compounds (Fig. 3.16) featuring hydrophobic (**3.92**, **3.95**) or fluorinated groups (**3.93**, **3.94**). We were excited to find these compounds displayed improved activities over the aforementioned Col-3 analogues, with two

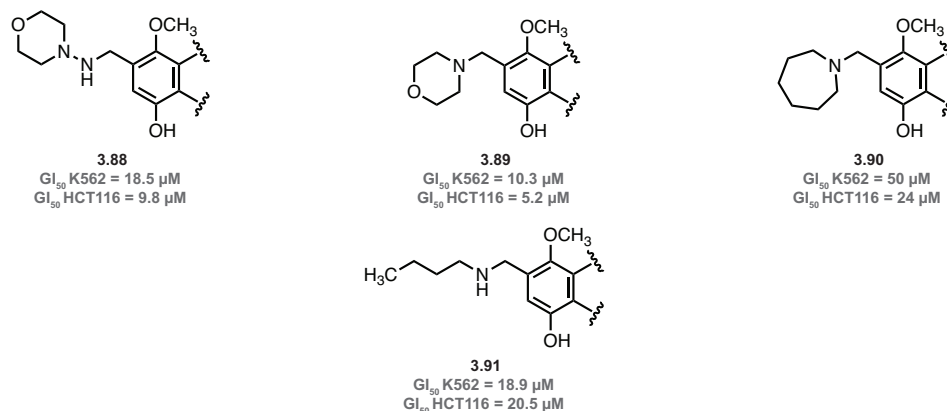


**Figure 3.15 Selected Fully Synthetic Analogues: Early Screening (cont).** While the majority of the compounds synthesized during our initial efforts displayed little to no activity, a selection of morpholine (**3.88**, **3.89**) and azepane (**3.90**) substituted compounds displayed modest growth inhibitory activity. Growth assays conducted with Meiyi Yu.

examples, **3.93** and **3.94**, providing growth inhibitory potencies equal to that or slightly improved over Col-3.

Excited by these results, we sought to further explore these hydrophobic analogues using two methodologies. First, we evaluated the role of intramolecular hydrogen bonding and its effect on growth inhibitory potency. Upon analysis of the structures in Figure 3.16, we identified a hydrogen bonding interaction via a six-membered ring formed between the hydrogen atom of the C8-methylamine and the lone pairs of the C7-methoxy group. Seeing

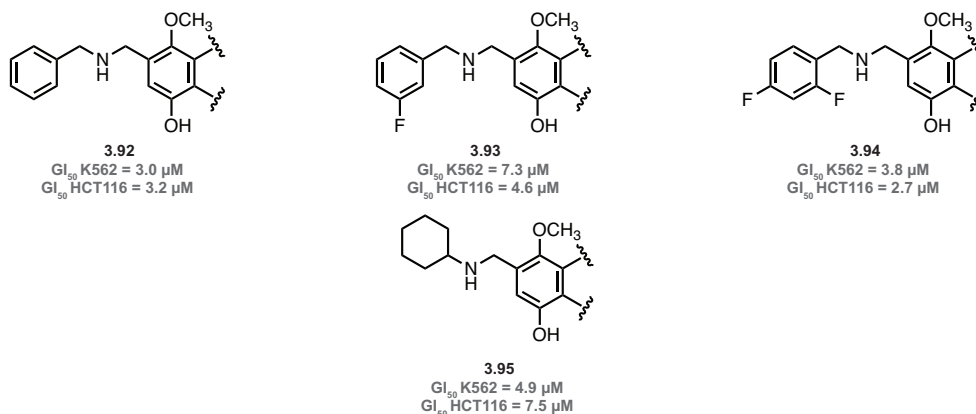


**Figure 3.16 A Selection of Col-3 Analogues Showing Improved Antiproliferative Activity.** Substitution of our scaffold with hydrophobic groups, such as benzyl (**3.92**) or cyclohexyl (**3.95**) moieties, or fluorinated groups including fluorinated benzylamines **3.93** and **3.94** provided modest improvements in activity. These analogues displayed potencies near or improved over the parent compound Col-3. Growth assays conducted with Meiyi Yu.

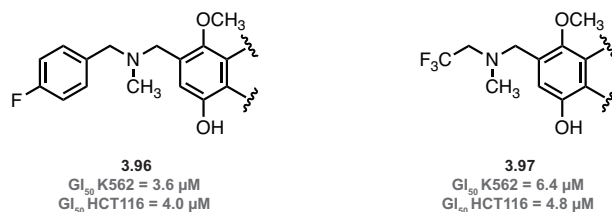


**Figure 3.17 Methylamino Analogues.** To investigate the role intramolecular hydrogen bonding might be playing in attenuating the activity of our novel Col-3 analogues, we synthesized two compounds, **3.96** and **3.97**, that featuring methyl substitution at the benzylamine nitrogen atom. These compounds maintained potencies similar to those of the hydrophobic analogues in Fig. 3.16. Growth assays conducted with Meiyi Yu.

as this strong interaction could potentially be preventing interactions with our biomolecule target, we synthesized two analogues, **3.96** and **3.97**, featuring methyl groups on the C8-methylamine nitrogen atom to prevent hydrogen bond formation (Fig. 3.16). These analogues were accessed via reductive amination of **3.80** with 4-fluoro-*N*-methylbenzylamine and *N*-methyl-2,2,2-trifluoroethylamine, respectively. While these analogues retained much of their potency (as compared to non-methylated analogues), they did not display any major gains in activity that would warrant further exploration.

In a second attempt to improve on the activity of our C7-methoxy analogues, we pursued analogues featuring a trifluoromethoxy group at C7. Given the improvement in activity observed with our fluorinated analogues, we theorized additional hydrophobicity or steric occlusion at C7 might be beneficial for antiproliferative activity. C7-trifluoromethoxy analogues were accessed in a manner similar to that used in our C7-methoxy synthesis.<sup>35</sup> This route begins with 4-trifluoromethoxyanisole (**3.98**, Fig. 3.18) and proceeds via a series of 10 steps to the highly substituted D-ring precursor **3.99**. The methodology to access C7-methoxy analogues was then employed to carry the protected tetracycline scaffold **3.100** to the aldehyde-functional Col-3 analogue **3.102**, which was

<sup>35</sup> C7-trifluoromethoxy substituted D-ring precursors were accessed using chemistry developed at Tetrphase Pharmaceuticals: See Xiao et al., **2014** (Chapter 3, ref. 7b).

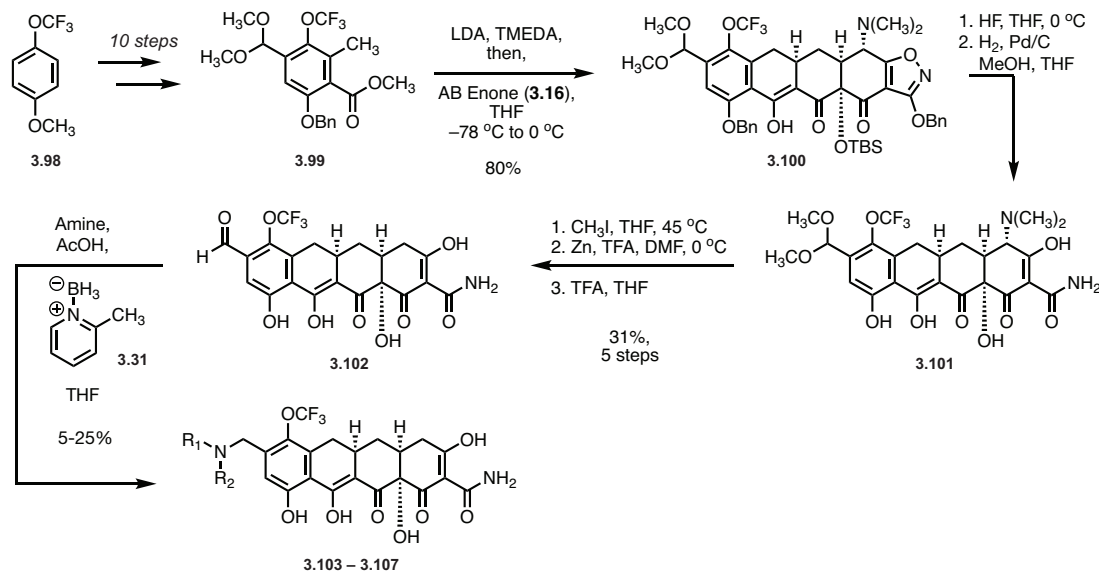


**Figure 3.18 Synthetic Access to C7-trifluoromethoxy Col-3 Analogues.** To further investigate the role of fluorination on the antiproliferative activity of our compounds, we utilized chemistry developed at Tetraphase Pharmaceuticals to generate a C7-trifluoromethoxy-functional D-ring precursor (**3.99**). This compound was coupled to the AB Enone and carried to the aldehyde functional Col-3 analogue **3.102** in a manner identical to that presented in Figure 3.13. Novel analogues were accessed using reductive amination chemistry with a variety of commercially available amines.

finally functionalized using reductive amination chemistry. A selection of analogues C7-trifluoromethoxy analogues is shown in Figure 3.19. Interestingly, while these analogues did not provide any major improvements in activity, we do note a broader disparity in activities between K562 leukemia cells and HCT116 colorectal cancer cells. While many of our synthetic analogues, including quinoline analogue **2.72** and the selection of potent C7-methoxy compounds (**3.92 – 3.95**), displayed non-specific activity across the majority of cancer cell lines tested, our C7-trifluoromethoxy analogues (Fig. 3.19) may be providing us with a different mechanism or selectivity that could be exploited further for treating certain types of cancer.<sup>36</sup>

<sup>36</sup> See Chapter 2 for a summary of potencies for Col-3 and analogue **2.72**.

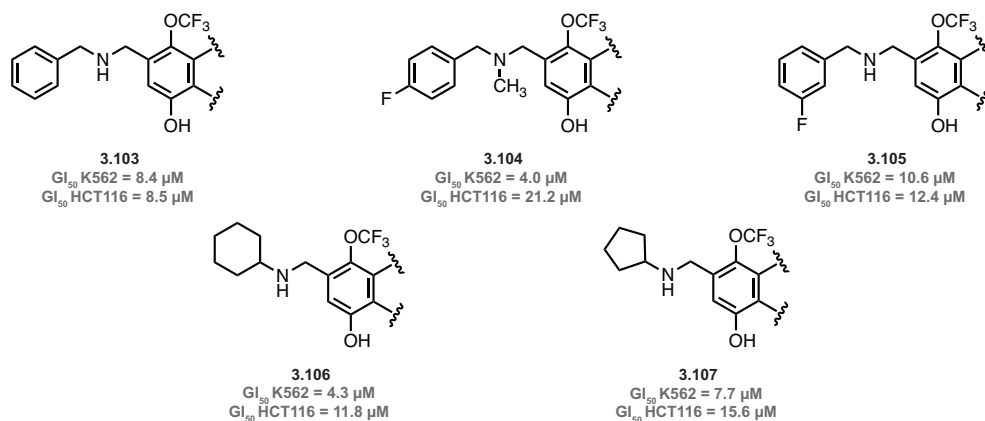


**Figure 3.19 Selected C7-trifluoromethoxy Col-3 Analogues.** Using the procedures presented in Fig. 3.18, we synthesized a selection of C7-trifluoromethoxy analogues. These compounds feature C8-substitution similar to that identified in Fig. 3.16 for their improved antiproliferative activity. Interestingly, while these analogues do not display any dramatically improved activity, we do note broader disparities between the potencies in K562 leukemia cells and HCT116 colorectal cancer cells. Growth assays conducted with Meiyi Yu.

### 3.6 Biological Evaluations

With our analogue synthesis efforts providing us with an interesting range of activities in human cancer cell lines, we sought to perform a set of foundational biological evaluations to understand if and how the mechanism of these novel analogues differs from that of the parent compound, Col-3, and our potent semisynthetic analogue, **2.72**. As in Chapter 2, these efforts focused on downstream signaling effects and translation inhibitory potency.

We first utilized an ISRIB co-dose assay to assess how and to what degree the ISR is contributing to overall cytotoxic effects of our novel compounds.<sup>37</sup> As described above, ISRIB functions through binding of eIF2B, the dedicated guanine nucleotide exchange factor involved in recycling eIF2 during the initiation stage of translation.<sup>38</sup> Binding of ISRIB is proposed to lock eIF2B into an active conformation, preventing phosphorylation

<sup>37</sup> See Chapter 1 for a discussion of ISRIB and its uses.

<sup>38</sup> See Chapter 4 for an overview of the mechanism of translation initiation in eukaryotes.

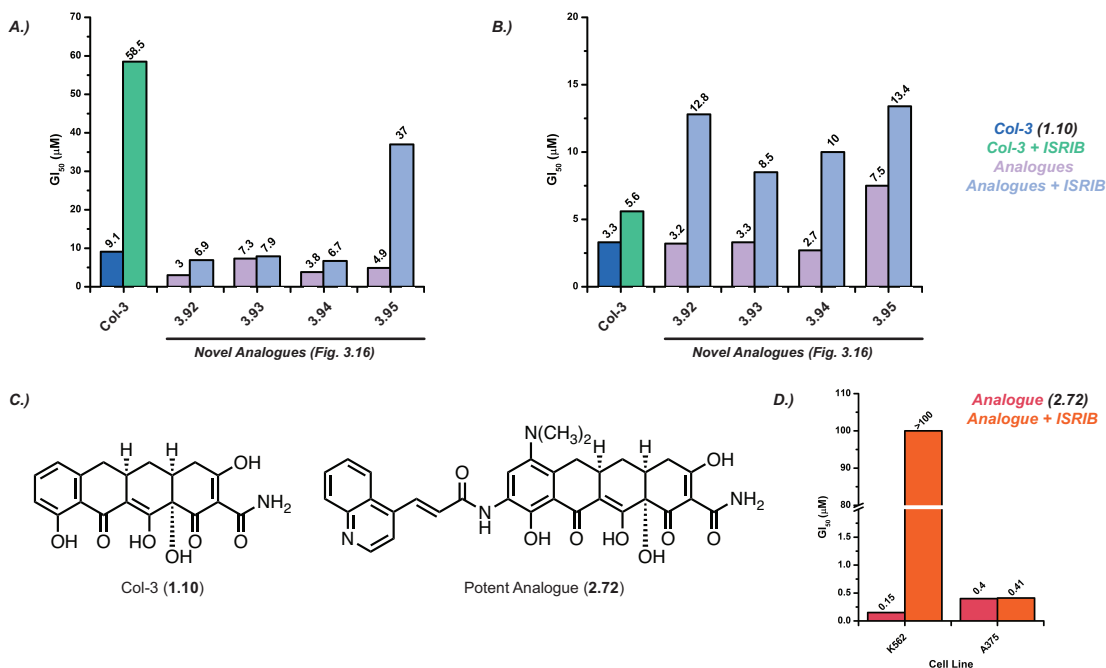


**Figure 3.20 ISRIB Co-Dose Experiments.** One of our first biological evaluations with our fully synthetic analogues was a standard ISRIB co-dose experiment. This experiment allows us to control for activation of the ISR upon tetracycline treatment, thus providing an idea of the relative contributions of ISR activation and ribosomal binding/translation inhibition to overall antiproliferative activity. A selection of our most potent compounds shows varying effects upon ISRIB co-dose in K562 leukemia cells, with only analogue **3.95** (cyclohexyl-) showing a loss of activity similar to that observed for Col-3 and semisynthetic analogue **2.72** (A, C, D). Our compounds show a greater dependence on ISR activation in HCT116 colorectal cancer cells (B), though, showing again the differences in cellular responses based on cell/cancer type.

of eIF2 from slowing the recycling process. ISRIB thus enables us to separate antiproliferative effects caused by ISR activation from those stemming from translation inhibition, ribosome binding, or inhibition/activation of another cellular process. Both Col-3 and our novel semisynthetic analogue **2.72** display peculiar cell line-specific effects in ISRIB co-dose experiments, with the GI<sub>50</sub> of both compounds shifting drastically upon co-dose in K562 leukemia cells. In other cell lines, however, the differences are less stark: analogue **2.72** maintains the majority of its activity upon ISRIB co-dose in A375 melanoma cells and Col-3 shows only modest shifts in activity across a variety of cell lines (Fig. 3.20, see also Chapter 1, Fig. 1.10). We evaluated a series of our more potent fully synthetic analogues (**3.92** to **3.96**, see Figs. 3.16, 3.17) in the same manner to look for shifts in GI<sub>50</sub>



value (Fig. 3.20). Interestingly, these compounds appear to show less dependence on ISR activation than Col-3 or analogue **2.74**. In K562 leukemia cells, our fully synthetic analogues show only minor decreases in antiproliferative activity, particularly when compared to Col-3. We see slightly larger shifts in HCT116 colorectal cancer cells, a difference that was not observed with Col-3, once again highlighting the cell line-specific effects for our compounds. While still in early stages of evaluation, our ISRIB co-dose results suggest that our fully synthetic C7-methoxy-C8-methylamino analogues are generating a greater percentage of their antiproliferative activity from ribosomal binding and translation inhibition.

Excited by these early findings, we set about quantifying the translation inhibitory potencies of a selection of our most potent fully synthetic analogues. We elected to utilize an *in vitro* translation assay based on HeLa cell lysates for these experiments as it provided a rapid and easily scalable methodology quantifying general translation inhibition.<sup>39</sup> This

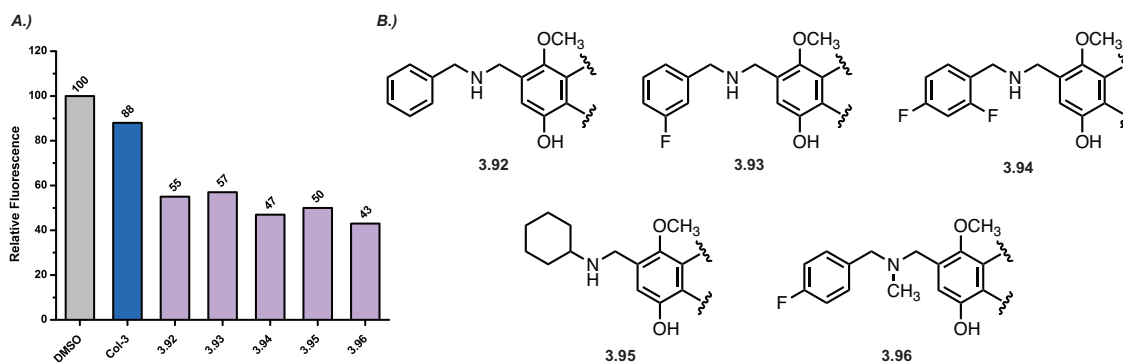


**Figure 3.21 Initial Evaluation of Translation Inhibitory Potencies.** An initial experiment using HeLa cell lysates (A) showed that our fully synthetic analogues (B) were inhibiting cytosolic translation at a slightly increased level compared to Col-3 (**1.10**). These interesting results corroborate our ISRIB co-dose experiment findings. These early results, however, only represent *in vitro* experimentation on HeLa lysates – further studies will be required in a variety of cell lines using more detailed translation inhibition assays (ex. OPP assay) to fully characterize the translation inhibitory potencies of these compounds. Results averaged from two experiments.

<sup>39</sup> 1-Step Human Coupled IVT Kit, Thermo Fisher Scientific. See Chapter 1 for discussion and use in Mortison et al., **2018** (Chapter 1, ref. 26).

assay functions through the introduction of plasmid DNA coding for GFP to a HeLa cervical cancer cell lysate along with accessory proteins and a small molecule of interest. Following incubation, translation inhibitory values are determined by comparing GFP production to the DMSO control. The results of this assay for a selection of our more potent analogues (**3.92** to **3.96**) are shown in Fig. 3.21. We note that each of our analogues, with growth inhibitory potencies on par or slightly improved over Col-3 (Figs. 3.16, 3.17), are showing improved translation inhibitory activity in our HeLa lysate experiment. These results provide a pleasant corroboration of our ISRIB co-dose experiments and the hypothesis that, despite showing similar  $GI_{50}$  values, our fully synthetic analogues may be exhibiting improved translation inhibitory effects. It is important to note that these experiments represent only the beginning of a series of key biological experiments to better understand the cellular mechanism of our novel analogues. Further experiments are needed to assess ATF4 activation and mitochondrial dysregulation, while a more in-depth translation inhibition experiment is needed to screen multiple cell lines and dosing regimens before making any conclusions about the origins of the antiproliferative activities of our novel analogues. Overall, our initial evaluations suggest that the cellular mechanism of our fully synthetic analogues differs slightly from those identified for Col-3 and analogue **2.72** and further studies are needed to characterize and exploit this mechanism for improved therapeutic function.

### **3.7 Conclusion and Path Forward**

The semisynthetic compound development efforts presented in Chapter 2 inspired us to expand the diversity of analogues accessible for evaluation using a fully synthetic

approach. We leveraged the extensive history of tetracycline total synthesis in the Myers group to develop a scalable and diversifiable route to access novel analogues of Col-3 featuring a variety of substitution patterns. After some early evaluation, we settled on a series of C7-methoxy-C8-methylamino analogues that, when substituted with fluorinated aryl substituents or cyclic aliphatic groups, displayed potencies on par or slightly improved over that of Col-3. Our initial biological evaluations provided a series of interesting findings: while analogue **2.72** appears to be generating its improved activity through more efficient activation of the ISR through mitochondrial dysregulation, it appears that a greater percentage of the activity of our novel fully synthetic analogues originates with improved translation inhibitory effects. Further studies are needed to assess the role of translation inhibition, ISR activation, and mitochondrial dysregulation for these compounds, both as a comparison to Col-3 and analogue **2.72** and as key steps in improving our understanding of the cellular effects of the tetracyclines.

In total, our synthesis efforts have succeeded in identifying analogues of Col-3 with improved antiproliferative activities and unique cellular effects. These efforts have also put on display the broad polypharmacology associated with this class of natural products, as minor alterations to structure, solubility, and charge state result in a variety of different biological effects. As efforts to develop novel antiproliferative tetracyclines continue in the Myers' group, we believe it will be critical to pursue structural information in the form of cryogenic electron microscopy (cryo-EM) co-structures of the tetracyclines bound to the human cytosolic and human mitochondrial ribosomes. We believe this type of information will be indispensable as ongoing synthesis efforts attempt to disentangle the array of biological effects associated with these compounds. In addition, the utilization of high

throughput, multiplexed cellular screening methodologies like PRISM at the Broad Institute would enable identification of specific cancers or cell lines with unique sensitivities to tetracycline antiproliferative agents. Coupled with continued synthesis efforts, we are confident that the combination of cryo-EM structural information and large-scale cellular screening could continue to push antiproliferative tetracyclines to the clinical stage.

### 3.8 Chemical Biology Experimental Section

**Mammalian Cell Lines and Cell Culture.** All compounds were dissolved in sterile DMSO to a stock concentration of 20  $\mu$ M and aliquoted prior to freezing at  $-20$  °C. Aliquots were limited to a maximum of 3 freeze–thaw cycles.

**Materials.** K562 (human chronic myelogenous leukemia; female) cells were cultured in Iscove’s Modification of DMEM (IMDM) media supplemented with 10% fetal bovine serum. HCT116 (human colorectal carcinoma; male) cells were cultured in McCoy’s 5a (Iwakata & Grace Modification) media supplemented with 10% fetal bovine serum. All cell cultures were maintained in a 5% CO<sub>2</sub> incubator at 37 °C.

**Growth Inhibition Assay.** The growth inhibition assays used to evaluate compound potency in mammalian cells was adapted from Magauer et al., **2013**.<sup>40</sup> Briefly, cells were grown to approximately 80% confluence, and then were trypsinized, collected, and pelleted by centrifugation (3 min at 2,000 rpm, 23 °C). The supernatant was discarded and the cell pellet was resuspended in 10 mL of fresh medium. A sample was diluted 10-fold in fresh medium, and the concentration of cells was determined using a Scepter Cell Sensor automated cell counter. The cell suspension was diluted to a concentration of 5000 cells/mL. Stock solutions of each compound in DMSO were diluted serially with DMSO to provide 7 600X concentrations and one vehicle control for a total of 8 samples. The drug dilutions were then added to a 96-well deep well plate and each mixed with 600  $\mu$ L

---

<sup>40</sup> Magauer, T.; Smaltz, D. J.; Myers, A. G. *Nat. Chem.* **2013**, 5, 886-893.

cell/media solution. The cells/drugs were mixed well and 100  $\mu$ L was added to 5 rows of a pre-sterilized 96-well plate. A final column was filled with 100  $\mu$ L culture media to serve as a no cells control. Typical tetracycline concentrations began with 100  $\mu$ M and decreased via a log<sub>2</sub>-scale over 7 total dilutions. Less concentrated dilutions were used for more potent compounds. After incubating at 37 °C for 72 h (5% CO<sub>2</sub>), 20  $\mu$ L of resazurin solution (Promega CellTiter-Blue® Cell Viability Assay) was added to each well. After incubating at 37 °C for 4 h (5% CO<sub>2</sub>), the fluorescence (544 nm excitation/590 nm emission) was recorded using a microplate reader (SpectraMax PLUS384) as a measure of viable cells. Percent growth inhibition was calculated for each well, based upon the following formula: Percent growth inhibition =  $100 \times (S - B_0) / (B_t - B_0)$  where S is the sample fluorescence, B<sub>t</sub> is the average fluorescence of an untreated population of cells at the completion of the assay, and B<sub>0</sub> is the average fluorescence of an untreated population of cells at the beginning of the assay. Each compound was assayed at seven separate concentrations per experiment. The percent inhibition at each concentration was plotted against log(concentration), and a curve fit was generated using Excel (Microsoft). GI50 values were computed to reflect the concentrations at which the resulting curves pass through 50% inhibition.

***in vitro* Translation Assay.** Translation inhibition assays were conducted using the 1-Step Human Coupled *In Vitro* Protein Expression Kit (Thermo Fisher Scientific) using the methodology developed in Mortison et al., **2018** with minor alteration.<sup>41</sup> Briefly, the translation reactions were prepared by first pre-mixing the HeLa lysate, accessory proteins,

---

<sup>41</sup> See Mortison et al., **2018** (Chapter 1, ref. 11).

reaction mix, nuclease-free water. Then, the indicated concentrations of Col-3, doxycycline, cycloheximide, or DMSO (vehicle control) was added into the reaction mixture. After a 5 min incubation at room temperature, pCFE-GFP plasmid DNA was added to the reaction. The reaction was the incubated for 4 h at 30 °C. The samples were then directly transferred to a blackbottom 96-well plate and read using a fluorescence plate reader at Ex/Em (482/512 nm).

### 3.9 Chemistry Experimental Section

**General Experimental Procedures.** All reactions were performed in round-bottom flasks fitted with rubber septa under a positive pressure of argon or nitrogen, unless otherwise noted. Air- and moisture-sensitive liquids were transferred via syringe or stainless-steel cannula. Organic solutions were concentrated by rotary evaporation (house vacuum, ca. 25–40 torr) at ambient temperature, unless otherwise noted. Analytical thin-layer chromatography (TLC) was performed using glass plates pre-coated with silica gel (0.25 mm, 60 Å pore-size, 230 400 mesh, Merck KGA) impregnated with a fluorescent indicator (254 nm). TLC plates were visualized by exposure to ultraviolet light, then were stained with either an aqueous sulfuric acid solution of ceric ammonium molybdate (CAM) or an aqueous sodium carbonate solution of potassium permanganate (KMnO<sub>4</sub>) then briefly heated on a hot plate. Flash-column chromatography was performed as described by Still et al., employing silica gel (60 Å, 32–63 μM, standard grade, Dynamic Adsorbents, Inc.) or using the Teledyne ISCO CombiFlash purification system with pre-loaded silica gel columns.<sup>42</sup>

**Materials.** Dry solvents were purchased from the Aldrich Chemical Company in Sure/Seal™ glass bottles and used without further purification. All reagents were purchased and used without purification with the following exceptions: Tetramethylethylenediamine and diisopropylamine were distilled from calcium hydride

---

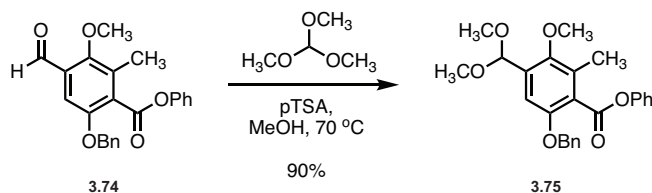
<sup>42</sup> Still, W. C.; Kahn, M.; Mitra, A.; *J. Org. Chem.* **1978**, *43*, 2923-2925.



under an argon atmosphere. Benzyl bromide was filtered neat through a column of oven-dried basic alumina immediately prior to use.

**Instrumentation.** Proton magnetic resonance ( $^1\text{H}$  NMR) spectra were recorded on Varian INOVA 500 (500 MHz) or 600 (600 MHz) NMR spectrometers at 23 °C. Proton chemical shifts are expressed in parts per million (ppm,  $\delta$  scale) and are referenced to residual protium in the NMR solvent ( $\text{CHCl}_3$ ,  $\delta$  7.26;  $\text{D}_2\text{HCO}$ :  $\delta$  3.31). Data are represented as follows: chemical shift, integration, multiplicity (s = singlet, d = doublet, t = triplet, q = quartet, m = multiplet and/or multiple resonances, br = broad, app = apparent), and coupling constant (J) in Hertz. Carbon nuclear magnetic resonance spectra ( $^{13}\text{C}$  NMR) were recorded on a Varian INOVA 500 (125 MHz) NMR spectrometer at 23 °C. Carbon chemical shifts are expressed in parts per million (ppm,  $\delta$  scale) and are referenced to the carbon resonances of the NMR solvent ( $\text{CDCl}_3$ ,  $\delta$  77.0;  $\text{C}_6\text{D}_6$ ,  $\delta$  128.0). High-resolution mass spectra were obtained at the Harvard University Mass Spectrometry Facility. High-performance liquid chromatography–mass spectrometry (LCMS) was performed using an Agilent Technologies 1260-series analytical HPLC system in tandem with an Agilent Technologies 6120 Quadrupole mass spectrometer; a Zorbax Eclipse Plus reverse-phase  $\text{C}_{18}$  column (2.1  $\times$  50 mm, 1.8  $\mu\text{m}$  pore size, 600 bar rating; Agilent Technologies, Santa Clara, CA) was employed as stationary phase. LCMS samples were eluted at a flow rate of 650  $\mu\text{L}/\text{min}$ , beginning with 5% acetonitrile–water containing 0.1% formic acid, grading linearly to 100% acetonitrile containing 0.1% formic acid over 3 minutes, followed by 100% acetonitrile containing 0.1% formic acid for 2 minutes (5 minutes total run time).

**Synthetic Procedures.** For clarity, compounds that have not been assigned numbers in the text are numbered sequentially beginning with **S3.1**.



C7-Methoxy-C8-acetal functionalized D-Ring Precursor (**3.75**)<sup>43</sup>:

Aldehyde **3.74** (3.75 g, 9.9 mmol, 1 eq.) was dissolved in 30 mL anhydrous methanol in a flame dried 100 mL round-bottom flask.<sup>44</sup> Trimethylorthoformate (3.3 mL, 29.9 mmol, 3 eq.) was added, followed by *p*-TSA (0.057 g, 0.29 mmol, 0.3 eq.). The resulting yellow solution was heated to 70 °C and allowed to stir at that temperature for 19 hours. Following stirring, the reaction was cooled to 23 °C and concentrated. The resulting yellow residue was redissolved in dichloromethane and washed sequentially with water and brine (30 mL each), dried over sodium sulfate, and concentrated to a yellow oil. The crude material was purified using flash column chromatography (0 to 15% EtOAc / hexanes) to provide the desired product as an off-white solid (3.77 g, 90%).

<sup>1</sup>H NMR (400 MHz, CDCl<sub>3</sub>) δ 7.48 – 7.40 (m, 2H), 7.40 – 7.20 (m, 5H), 7.15 – 7.05 (m, 3H), 5.61 (s, 1H), 5.15 (s, 2H), 3.76 (s, 3H), 3.36 (s, 6H), 2.39 (s, 3H).

<sup>13</sup>C NMR (101 MHz, CDCl<sub>3</sub>) δ 166.37, 151.69, 150.78, 150.50, 136.58, 133.45, 130.18, 129.48, 128.50, 128.01, 127.66, 126.02, 125.16, 121.73, 109.02, 99.42, 77.24, 70.94, 61.74, 53.72.

HRMS (ESI+, *m/z*) [M + H]<sup>+</sup> calc'd for C<sub>20</sub>H<sub>24</sub>O<sub>6</sub>: 399.1204. Found: 399.1201.

<sup>43</sup> Procedure modeled after that reported in Chen et al., **2010** (Chapter 3, ref. 32b).

<sup>44</sup> Aldehyde **3.74** was synthesized according to the procedures in Zhang et al., **2016** (Chapter 3, ref. 15c).

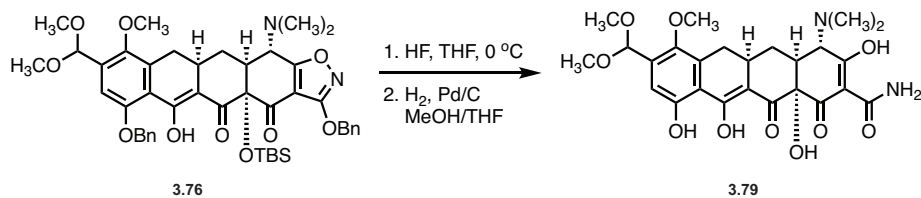


solid. The crude product was purified using flash column chromatography (0 to 30 % EtOAc/hexanes) to provide the desired product as bright yellow foam (0.65 g, 77%).

$^1\text{H}$  NMR (400 MHz,  $\text{CDCl}_3$ )  $\delta$  16.05 (s, 1H), 7.42 (m, 4H), 7.35 – 7.14 (m, 6H), 7.04 (s, 1H), 5.48 (s, 1H), 5.29 (s, 2H), 5.17 (d,  $J = 12.4$  Hz, 1H), 5.11 (d,  $J = 12.4$  Hz, 1H), 3.94 (d,  $J = 10.5$  Hz, 1H), 3.64 (s, 3H), 3.28 (s, 3H), 3.20 (dd,  $J = 15.7, 4.6$  Hz, 1H), 3.19 (s, 3H), 2.92 – 2.81 (m, 1H), 2.52 – 2.33 (m, 2H), 2.42 (s, 6H), 2.06 (dt,  $J = 14.5, 1.7$  Hz, 1H), 0.76 (s, 9H), 0.76 (d,  $J = 5.8$  Hz, 1H), 0.21 (s, 3H), 0.08 (s, 3H).

$^{13}\text{C}$  NMR (101 MHz,  $\text{CDCl}_3$ )  $\delta$  190.05, 186.78, 184.26, 183.50, 170.13, 157.78, 150.75, 139.51, 139.18, 137.60, 131.02, 130.98, 130.95, 130.23, 129.51, 123.73, 114.47, 110.98, 109.80, 101.56, 84.37, 79.74, 75.03, 73.69, 64.27, 63.83, 56.77, 55.61, 49.18, 44.37, 35.08, 30.91, 28.55, 25.45, 21.55, -1.14.

HRMS (ESI+,  $m/z$ )  $[\text{M} + \text{H}]^+$  calc'd for  $\text{C}_{45}\text{H}_{54}\text{N}_2\text{O}_{10}\text{Si}$ : 811.3620. Found: 811.3622.

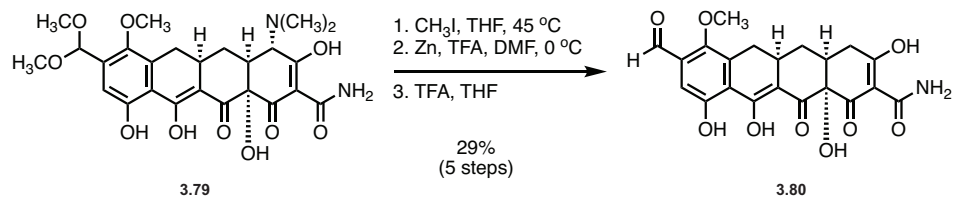


Deprotected C7-methoxy-C8-acetal Tetracycline (**3.79**)<sup>46</sup>:

Protected tetracycline **3.76** (0.2 g, 0.25 mmol, 1 eq.) was dissolved in 2 mL THF and stirred at 0 °C in a polypropylene tube. Hydrofluoric acid (48% solution, 0.09 mL, 10 eq.) was then added dropwise. The solution turned from a pale-yellow color to a light bright following the addition. The reaction was allowed to stir for 1 hour at 0 – 10 °C with progress monitored by LC/MS. Upon completion, the reaction was poured into a solution of potassium phosphate (0.5 M aq., 15 mL) and stirred. The solution was then extracted 3X with ethyl acetate (10 mL each) and the combined organics dried over sodium sulfate, filtered, and concentrated to a yellow/brown solid.

The crude solid was dissolved in 6 mL 1:1 THF:methanol and stirred at 23 °C. Palladium on carbon (10%, 0.052 g, 0.05 mmol, 0.2 eq.) was then added to give a black suspension. The flask was evacuated and backfilled 3X with nitrogen, then evacuated and backfilled 3X with hydrogen using a balloon. The reaction was then allowed to stir for 1 hour under static hydrogen pressure. Upon completion, the reaction flask was flushed with nitrogen for 10 minutes, then filtered through a pad of celite. The pad was washed with 50 mL methanol and the filtrate was concentrated to a light brown solid. Dry on vacuum. The crude product **3.79** was typically taken directly to the next step without further purification.

<sup>46</sup> Procedure modeled after that reported in Chen et al., **2010** (Chapter 3, ref. 32b).



### Aldehyde **3.80**:

Tetracycline **3.79** (0.3 g, 0.56 mmol, 1 eq.) was dissolved in 2 mL THF and stirred. Iodomethane (0.9 mL, 14.5 mmol, 25 eq.) was added dropwise and the reaction was heated to 45 °C and stirred at that temperature for 19 hours. Following stirring, the reaction solution was concentrated to a bright yellow solid.

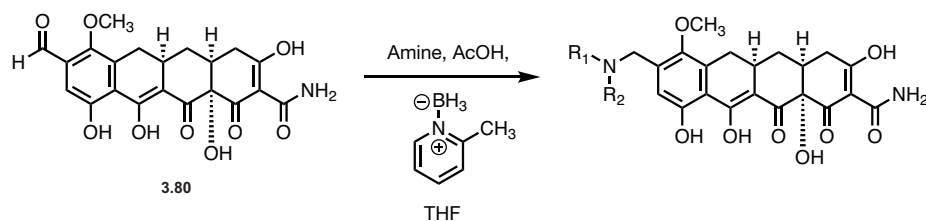
The solid was dissolved in 2 mL DMF and stirred at 0 °C. Water (0.052 mL, 2.9 mmol, 5 eq.) and TFA (0.18 mL, 2.3 mmol, 4 eq.) were then added sequentially to provide a bright yellow solution. Zinc (0.049 g, 0.76 mmol, 1.3 eq.) was then added in 5-6 small portions every 25 minutes. Following completion of the zinc additions, the reaction was stirred for another 1.5 to 2 hours at 0 °C, or until LC/MS indicated consumption of the methylated starting material. The reaction solution was filtered through a 0.2  $\mu\text{M}$  syringe filter to remove the unreacted zinc and the reaction was diluted with water. The pH was adjusted to 2.5 with 25% ammonium hydroxide solution, then extracted 3X with DCM (20 mL each). The organics were combined and washed with water and brine (30 mL each). The organic layer was then dried over sodium sulfate, filtered, and concentrated to an orange/brown residue. Dry on vacuum.

Following drying, the residue was redissolved in THF and TFA (2 mL) was added. The dark orange solution was allowed to stir for 19 hours at 23 °C. Following stirring, the solution was concentrated to a flaky orange solid and dried on vacuum. The crude product was typically used in subsequent reactions without further purification (0.07 g, 29%,

crude). Samples of high purity can be obtained using the following procedure: 30 mg crude product was dissolved in 5 mL 4:1 methanol: DMF. The product was purified by preparative HPLC on an Agilent Prep C18 column [10  $\mu$ m, 250 x 21.2 mm, UV detection at 399 nm, Solvent A: 0.1% formic acid in water, Solvent B: 0.1% formic acid in acetonitrile, injection volume: 5.0 mL (4 mL methanol, 1 mL DMF), gradient elution with 10–75% B over 40 min, flow rate: 15 mL/min]. Fractions were analyzed via analytical LC/MS for purity prior to concentration to provide the desired product, typically as a yellow solid.

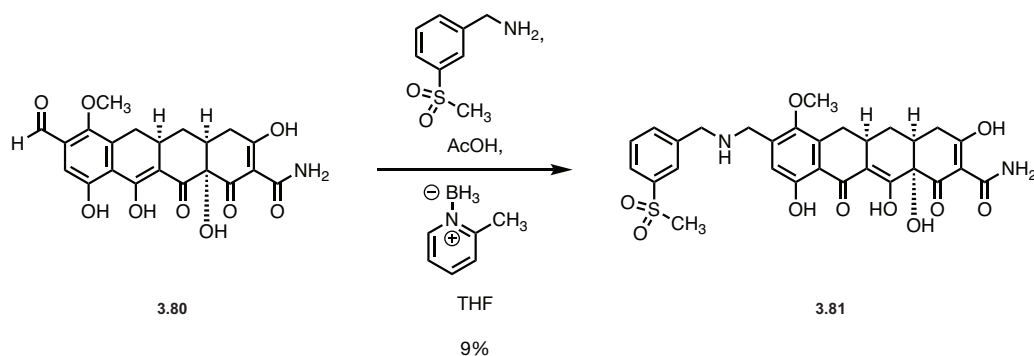
HRMS (ESI+,  $m/z$ )  $[M + H]^+$  calc'd for  $C_{21}H_{19}NO_9$ : 430.1133. Found: 430.1135.





**General Procedure A: Reductive Amination with Aldehyde 3.80:**

Aldehyde **3.80** (10 mg, 0.023 mmol, 1 eq.) was dissolved in 1 mL THF and stirred at 23 °C. Amine (5 eq.) was added, followed by acetic acid (5 eq.) and 2-picoline-borane (4 eq.). The solution typically turned from light orange to deep red in color following amine addition. The reaction was typically allowed to stir at 23 °C for 1 to 2 hours, or until LCMS indicated consumption of the starting material. Upon completion, the reaction solution was concentrated to an orange/red residue and dried on vacuum. The residue was then redissolved in methanol and purified by preparative HPLC on an Agilent Prep C18 column [10 μm, 250 x 21.2 mm, UV detection at 399 nm, Solvent A: 0.1% formic acid in water, Solvent B: 0.1% formic acid in acetonitrile, injection volume: 5.0 mL (4 mL methanol + reaction solution), gradient elution with 5–65% B over 40 min, flow rate: 15 mL/min]. Fractions were analyzed via analytical LC/MS for purity prior to concentration to provide the desired product, typically as a yellow solid.

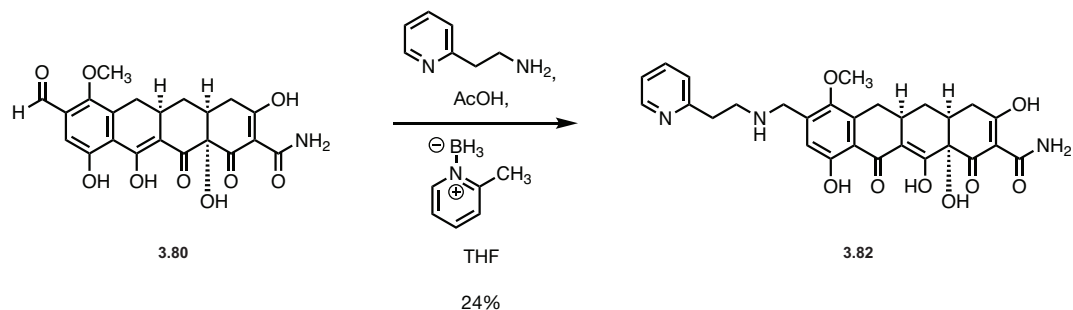


**Analogue 3.81:**

Analogue **3.81** was prepared using General Procedure A: Aldehyde **3.80** (10 mg, 0.023 mmol, 1 eq., crude) was reacted with 3-(methylsulfonyl)benzylamine to provide Analogue **3.81** following preparatory HPLC purification. (1 mg, 9 %).

$^1\text{H}$  NMR (400 MHz,  $\text{CD}_3\text{OD}$ )  $\delta$  8.11 (d,  $J = 1.9$  Hz, 1H), 8.07 – 8.03 (m, 1H), 7.83 (dt,  $J = 7.8, 1.5$  Hz, 1H), 7.73 (t,  $J = 7.8$  Hz, 1H), 6.89 (s, 1H), 4.40 (s, 2H), 4.22 (AB q,  $J = 13.4$  Hz, 2H), 3.62 (s, 3H), 3.23 (app. d,  $J = 5.8$  Hz, 1H), 3.14 (s, 3H), 2.82 (ddt,  $J = 15.0, 10.2, 5.5$  Hz, 1H), 2.51 – 2.25 (m, 3H), 2.07 (ddd,  $J = 13.5, 5.4, 2.8$  Hz, 1H), 1.62 (td,  $J = 13.4, 11.5$  Hz, 1H).

HRMS (ESI+,  $m/z$ )  $[\text{M} + \text{H}]^+$  calc'd for  $\text{C}_{29}\text{H}_{30}\text{N}_2\text{O}_{10}\text{S}$ : 599.1694. Found: 599.1691.

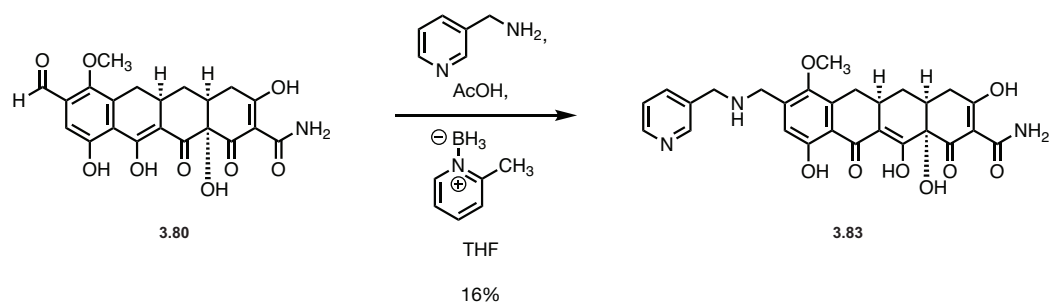


### Analogue 3.82:

Analogue **3.82** was prepared using General Procedure A: Aldehyde **3.80** (10 mg, 0.023 mmol, 1 eq., crude) was reacted with 2-pyridylethylamine to provide Analogue **3.82** following preparatory HPLC purification. (3 mg, 24 %).

$^1\text{H}$  NMR (400 MHz,  $\text{CD}_3\text{OD}$ )  $\delta$  8.55 – 8.50 (m, 1H), 7.79 (td,  $J = 7.7, 1.8$  Hz, 1H), 7.37 – 7.29 (m, 2H), 6.93 (s, 1H), 4.27 (q,  $J = 13.4$  Hz, 2H), 3.74 (s, 3H), 3.47 (t,  $J = 6.9$  Hz, 2H), 3.19 (t,  $J = 6.3$  Hz, 2H), 3.15 (app. d,  $J = 4.4$  Hz, 1H), 2.83 (ddt,  $J = 15.0, 12.3, 7.3$  Hz, 1H), 2.50 – 2.28 (m, 3H), 2.08 (ddd,  $J = 14.1, 8.0, 3.2$  Hz, 1H), 1.64 (td,  $J = 13.4, 11.0$  Hz, 1H).

HRMS (ESI+,  $m/z$ )  $[\text{M} + \text{H}]^+$  calc'd for  $\text{C}_{28}\text{H}_{29}\text{N}_3\text{O}_8$ : 536.2027. Found: 536.2024.

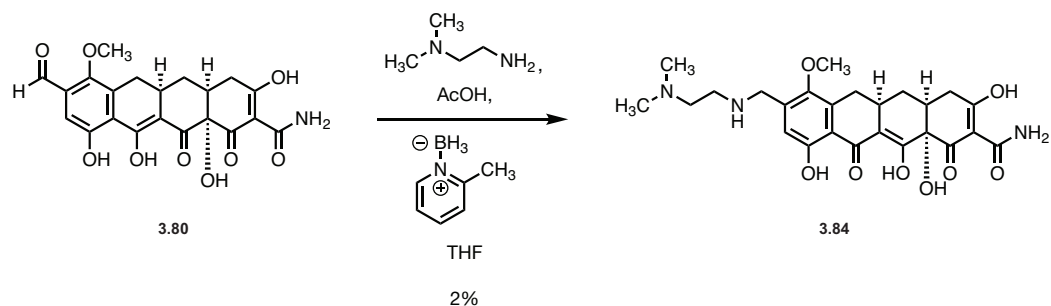


### Analogue 3.83:

Analogue **3.83** was prepared using General Procedure A: Aldehyde **3.80** (10 mg, 0.023 mmol, 1 eq., crude) was reacted with 3-picolylamine to provide Analogue **3.83** as the formate salt following preparatory HPLC purification. (2 mg, 16 %).

<sup>1</sup>H NMR (400 MHz, CD<sub>3</sub>OD) δ 8.66 (s, 1H), 8.60 (d, *J* = 5.0 Hz, 1H), 7.97 (dt, *J* = 8.0, 1.9 Hz, 1H), 7.52 (dd, *J* = 7.9, 4.9 Hz, 1H), 6.90 (s, 1H), 4.32 – 4.08 (m, 4H), 3.63 (s, 3H), 3.23 (dd, *J* = 17.5, 6.2 Hz, 1H), 3.13 (dd, *J* = 15.8, 4.3 Hz, 1H), 2.84 – 2.76 (app. m, 1H), 2.52 – 2.25 (m, 3H), 2.07 (ddd, *J* = 13.6, 5.4, 2.7 Hz, 1H), 1.62 (td, *J* = 13.3, 10.8 Hz, 1H).

HRMS (ESI+, *m/z*) [M + H]<sup>+</sup> calc'd for C<sub>27</sub>H<sub>27</sub>N<sub>3</sub>O<sub>8</sub>: 522.1871. Found: 522.1864.

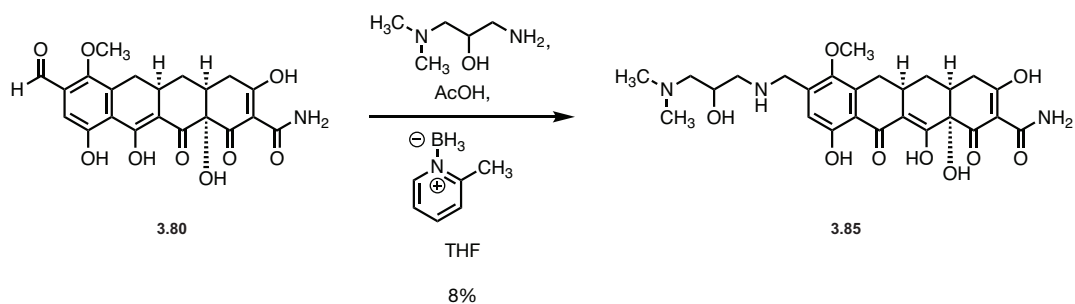


Analogue **3.84**:

Analogue **3.84** was prepared using General Procedure A: Aldehyde **3.80** (10 mg, 0.023 mmol, 1 eq., crude) was reacted with *N,N*-dimethylethylenediamine to provide Analogue **3.84** following preparatory HPLC purification. (0.2 mg, 2 %).

<sup>1</sup>H NMR (400 MHz, CD<sub>3</sub>OD) δ 6.92 (s, 1H), 4.15 (AB q, *J* = 13.1 Hz, 2H), 3.71 (s, 3H), 3.23 (app. d, *J* = 5.7 Hz, 1H), 3.15 (dd, *J* = 16.7, 4.9 Hz, 1H), 2.86 (s, 6H), 2.84 – 2.75 (app. m, 1H), 2.51 – 2.25 (m, 3H), 2.07 (ddd, *J* = 13.6, 5.4, 2.8 Hz, 1H), 1.63 (td, *J* = 13.3, 10.8 Hz, 1H).

HRMS (ESI+, *m/z*) [M + H]<sup>+</sup> calc'd for C<sub>25</sub>H<sub>31</sub>N<sub>3</sub>O<sub>8</sub>: 502.2184. Found: 502.2178.

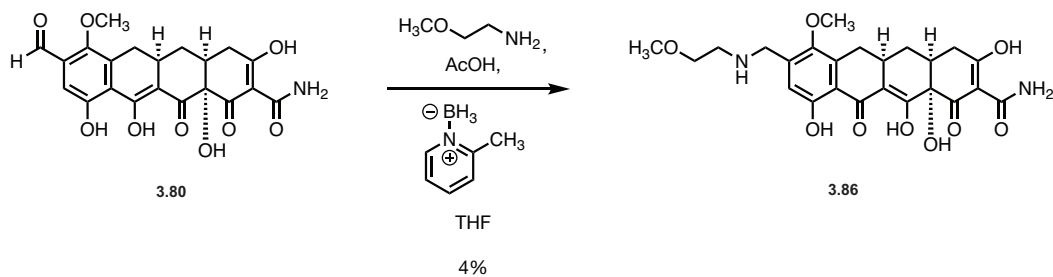


### Analogue 3.85:

Analogue **3.85** was prepared using General Procedure A: Aldehyde **3.80** (10 mg, 0.023 mmol, 1 eq., crude) was reacted with 1-amino-3-(dimethylamino)-2-propanol to provide Analogue **3.85** following preparatory HPLC purification. (1.0 mg, 8 %).

$^1\text{H}$  NMR (400 MHz,  $\text{CD}_3\text{OD}$ )  $\delta$  6.94 (s, 1H), 4.40 – 4.17 (m, 4H), 3.73 (d,  $J = 1.3$  Hz, 3H), 3.26 – 3.11 (m, 4H), 3.08 – 2.99 (app. m, 1H), 2.93 (s, 6H), 2.83 (ddt,  $J = 14.8, 10.4, 4.8$  Hz, 1H), 2.52 – 2.29 (m, 3H), 2.07 (ddd,  $J = 13.6, 5.5, 2.7$  Hz, 1H), 1.63 (td,  $J = 13.3, 10.7$  Hz, 1H).

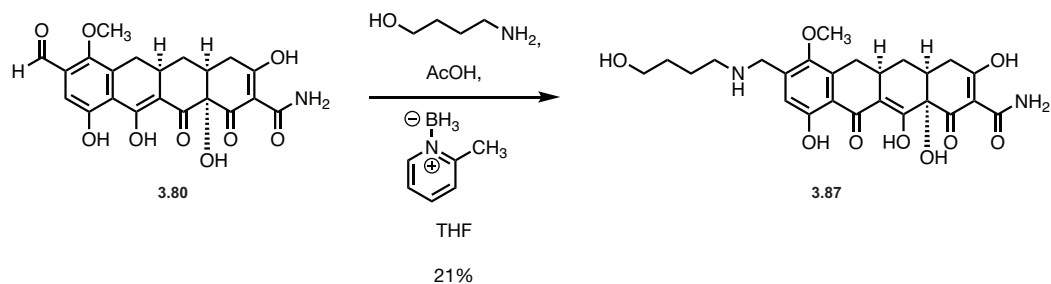
HRMS (ESI+,  $m/z$ )  $[\text{M} + \text{H}]^+$  calc'd for  $\text{C}_{26}\text{H}_{33}\text{N}_3\text{O}_9$ : 532.2290. Found: 532.2280.



Analogue **3.86**:

Analogue **3.86** was prepared using General Procedure A: Aldehyde **3.80** (10 mg, 0.023 mmol, 1 eq., crude) was reacted with 1-amino-2-methoxyethane to provide Analogue **3.86** following preparatory HPLC purification. (0.4 mg, 4 %).

HRMS (ESI+,  $m/z$ )  $[M + H]^+$  calc'd for  $C_{25}H_{28}N_2O_9$ : 489.1868. Found: 489.1865.



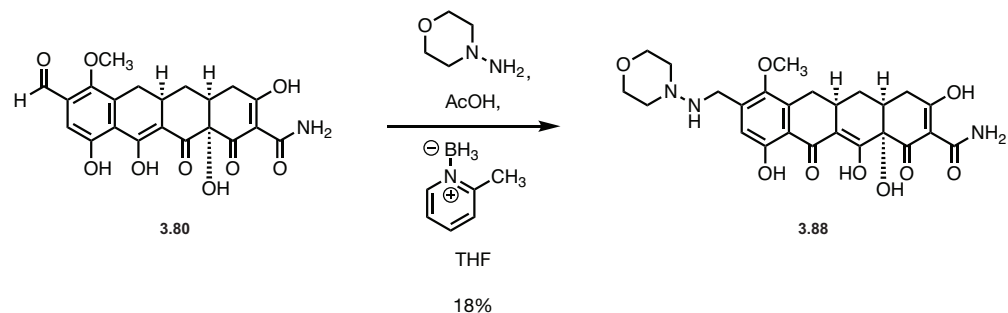
### Analogue **3.87**:

Analogue **3.87** was prepared using General Procedure A: Aldehyde **3.80** (10 mg, 0.023 mmol, 1 eq., crude) was reacted with 1-amino-4-butanol to provide Analogue **3.87** following preparatory HPLC purification. (2.5 mg, 21 %).

$^1\text{H}$  NMR (400 MHz,  $\text{CD}_3\text{OD}$ )  $\delta$  6.91 (s, 1H), 4.21 (AB q,  $J = 50.8, 13.6$  Hz, 2H), 3.72 (s, 3H), 3.63 – 3.54 (m, 2H), 3.23 (app. d,  $J = 5.6$  Hz, 1H), 3.16 (dd,  $J = 15.6, 4.4$  Hz, 1H), 3.13 – 3.05 (m, 2H), 2.83 (ddt,  $J = 15.0, 10.2, 4.9$  Hz, 1H), 2.52 – 2.27 (m, 3H), 2.07 (ddd,  $J = 13.7, 5.4, 2.7$  Hz, 1H), 1.87 – 1.76 (m, 2H), 1.69 – 1.50 (m, 3H).

HRMS (ESI+,  $m/z$ )  $[\text{M} + \text{H}]^+$  calc'd for  $\text{C}_{25}\text{H}_{30}\text{N}_2\text{O}_9$ : 503.2024. Found: 503.2018.



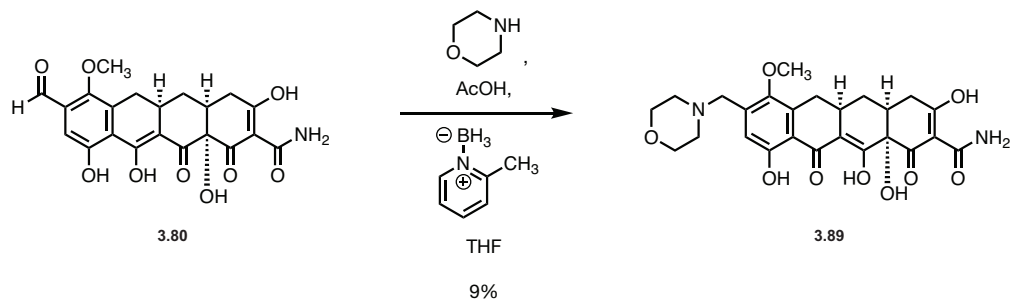


**Analogue 3.88:**

Analogue **3.88** was prepared using General Procedure A: Aldehyde **3.80** (10 mg, 0.023 mmol, 1 eq., crude) was reacted with 4-aminomorpholine to provide Analogue **3.88** following preparatory HPLC purification. (2.2 mg, 18 %).

$^1\text{H NMR}$  (400 MHz,  $\text{CD}_3\text{OD}$ )  $\delta$  6.93 (s, 1H), 4.28 (AB q,  $J = 13.0$  Hz, 2H), 3.87 – 3.79 (m, 4H), 3.71 (s, 3H), 3.21 (dd,  $J = 20.6, 5.8$  Hz, 1H), 3.17 – 3.09 (m, 5H), 2.82 (ddt,  $J = 14.9, 10.1, 4.9$  Hz, 1H), 2.51 – 2.26 (m, 3H), 2.07 (ddd,  $J = 13.6, 5.5, 2.7$  Hz, 1H), 1.63 (td,  $J = 13.0, 11.4$  Hz, 1H).

HRMS (ESI+,  $m/z$ )  $[\text{M} + \text{Na}]^+$  calc'd for  $\text{C}_{25}\text{H}_{29}\text{N}_3\text{O}_9$ : 538.1796. Found: 513.1790.

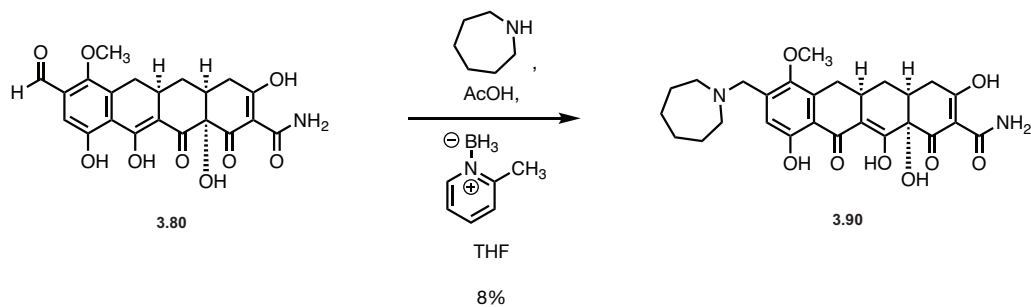


**Analogue 3.89:**

Analogue **3.89** was prepared using General Procedure A: Aldehyde **3.80** (10 mg, 0.023 mmol, 1 eq., crude) was reacted with morpholine to provide Analogue **3.89** as the formate salt following preparatory HPLC purification. (1 mg, 9 %).

<sup>1</sup>H NMR (400 MHz, CD<sub>3</sub>OD) δ 6.98 (s, 1H), 4.30 (AB q, *J* = 14.0 Hz, 2H), 3.86 (br. s, 4H), 3.71 (s, 3H), 3.28 – 3.21 (m, 5H), 3.17 (dd, *J* = 15.6, 4.4 Hz, 1H), 2.84 (ddt, *J* = 15.0, 10.2, 4.9 Hz, 1H), 2.52 – 2.29 (m, 3H), 2.08 (ddd, *J* = 13.7, 5.4, 2.7 Hz, 1H), 1.64 (td, *J* = 13.8, 12.1 Hz, 1H).

HRMS (ESI+, *m/z*) [M + H]<sup>+</sup> calc'd for C<sub>25</sub>H<sub>28</sub>N<sub>2</sub>O<sub>9</sub>: 501.1868. Found: 501.1862.

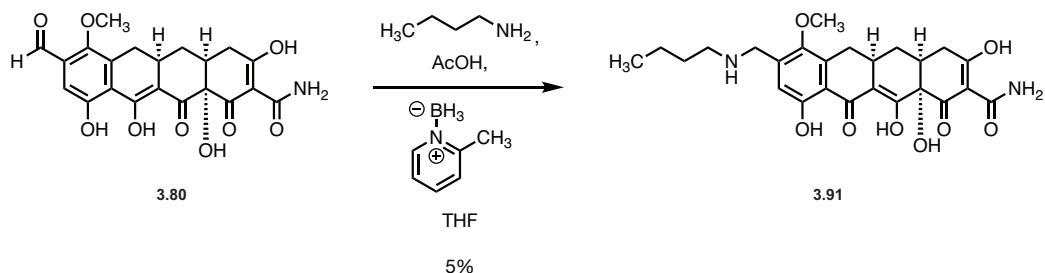


Analogue **3.90**:

Analogue **3.90** was prepared using General Procedure A: Aldehyde **3.80** (10 mg, 0.023 mmol, 1 eq., crude) was reacted with azepane to provide Analogue **3.90** following preparatory HPLC purification. (1 mg, 8 %).

$^1\text{H}$  NMR (400 MHz,  $\text{CD}_3\text{OD}$ )  $\delta$  6.98 (s, 1H), 4.33 (AB q,  $J = 14.1$  Hz, 2H), 3.72 (s, 3H), 3.23 (app. d,  $J = 6.9$  Hz, 1H), 3.16 (dd,  $J = 14.1, 4.1$  Hz, 1H), 2.85 (ddt,  $J = 13.9, 9.4, 4.1$  Hz, 1H), 2.52 – 2.29 (m, 3H), 2.08 (ddd,  $J = 12.9, 7.2, 2.2$  Hz, 1H), 2.03 – 1.78 (m, 7H), 1.77 – 1.57 (m, 6H).

HRMS (ESI+,  $m/z$ )  $[\text{M} + \text{H}]^+$  calc'd for  $\text{C}_{27}\text{H}_{32}\text{N}_2\text{O}_8$ : 513.2231. Found: 513.2229.

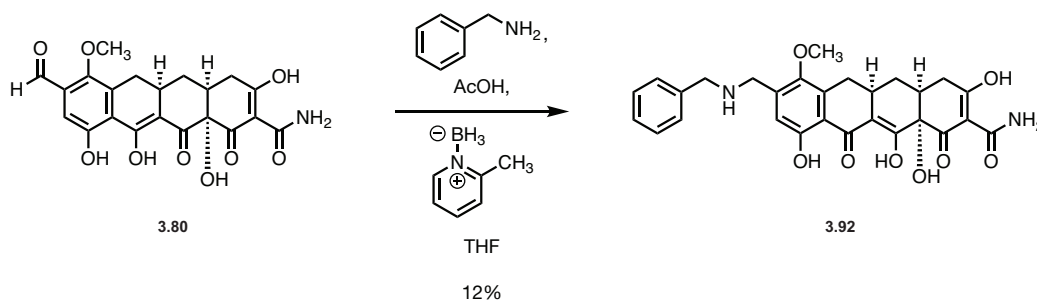


### Analogue 3.91:

Analogue **3.91** was prepared using General Procedure A: Aldehyde **3.80** (10 mg, 0.023 mmol, 1 eq., crude) was reacted with *n*-butylamine to provide Analogue **3.91** as the formate salt following preparatory HPLC purification. (0.5 mg, 5 %).

$^1\text{H}$  NMR (400 MHz,  $\text{CD}_3\text{OD}$ )  $\delta$  6.89 (s, 1H), 4.14 (AB q,  $J = 15.8$  Hz, 2H), 3.71 (s, 3H), 3.20 (dd,  $J = 19.7, 6.8$  Hz, 1H), 3.02 – 2.93 (m, 2H), 2.87 – 2.77 (app. m, 1H), 2.51 – 2.27 (m, 3H), 2.07 (ddd,  $J = 13.2, 7.9, 3.9$  Hz, 1H), 1.73 – 1.56 (m, 3H), 1.42 (m, 2H), 0.97 (t,  $J = 7.4$  Hz, 3H).

HRMS (ESI+,  $m/z$ )  $[\text{M} + \text{H}]^+$  calc'd for  $\text{C}_{25}\text{H}_{30}\text{N}_2\text{O}_8$ : 487.2075. Found: 487.2071.

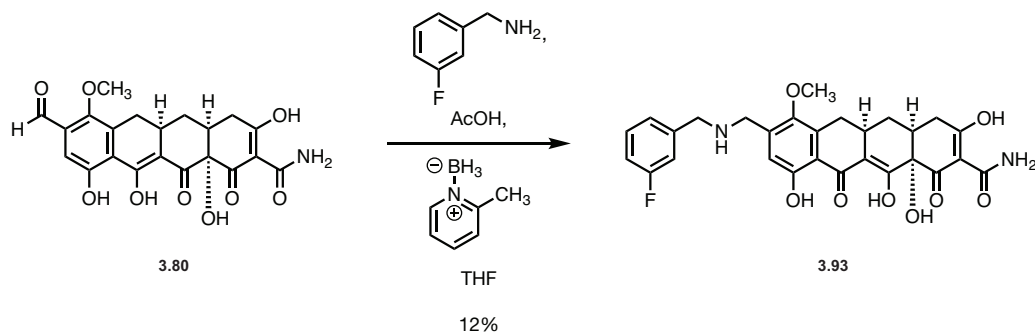


**Analogue 3.92:**

Analogue **3.92** was prepared using General Procedure A: Aldehyde **3.80** (10 mg, 0.023 mmol, 1 eq., crude) was reacted with benzylamine to provide Analogue **3.92** as the formate salt following preparatory HPLC purification. (1.4 mg, 12 %).

$^1\text{H}$  NMR (400 MHz,  $\text{CD}_3\text{OD}$ )  $\delta$  7.48 – 7.31 (m, 5H), 6.86 (s, 1H), 4.12 – 3.87 (m, 4H), 3.57 (s, 3H), 3.23 (dd,  $J = 18.7, 5.6$  Hz, 1H), 3.13 (dd,  $J = 16.3, 4.9$  Hz, 1H), 2.81 (ddt,  $J = 14.7, 10.1, 4.4$  Hz, 1H), 2.50 – 2.22 (m, 3H), 2.06 (ddd,  $J = 13.6, 5.4, 2.7$  Hz, 1H), 1.61 (td,  $J = 13.3, 10.7$  Hz, 1H).

HRMS (ESI+,  $m/z$ )  $[\text{M} + \text{H}]^+$  calc'd for  $\text{C}_{28}\text{H}_{28}\text{N}_2\text{O}_8$ : 521.1918. Found: 521.1915.

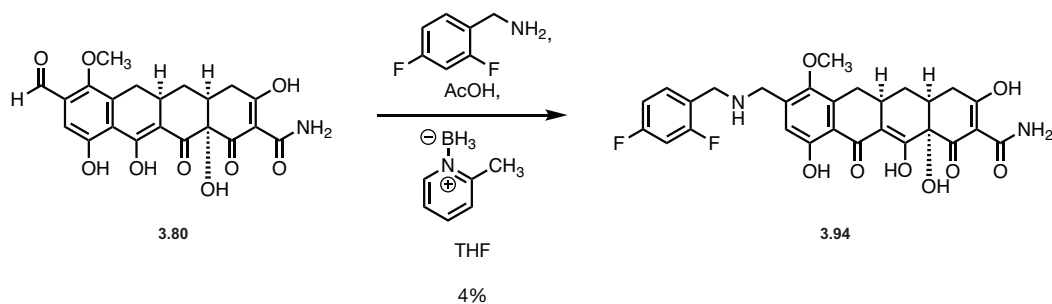


**Analogue 3.93:**

Analogue **3.93** was prepared using General Procedure A: Aldehyde **3.80** (10 mg, 0.023 mmol, 1 eq., crude) was reacted with 3-fluorobenzylamine to provide Analogue **3.93** following preparatory HPLC purification. (12 mg, 12 %).

$^1\text{H NMR}$  (400 MHz,  $\text{CD}_3\text{OD}$ , crude)  $\delta$  7.58 – 7.44 (m, 1H), 7.36 – 7.15 (m, 3H), 6.89 (s, 1H), 4.33 – 4.09 (m, 4H), 3.61 (s, 3H), 3.23 (app. d,  $J = 5.7$  Hz, 1H), 3.17 (app. d,  $J = 4.5$  Hz, 1H), 2.88 – 2.80 (app. m, 1H), 2.51 – 2.26 (m, 3H), 2.07 (ddd,  $J = 11.4, 7.5, 2.8$  Hz, 1H), 1.63 (dd,  $J = 13.2, 12.2$  Hz, 1H).

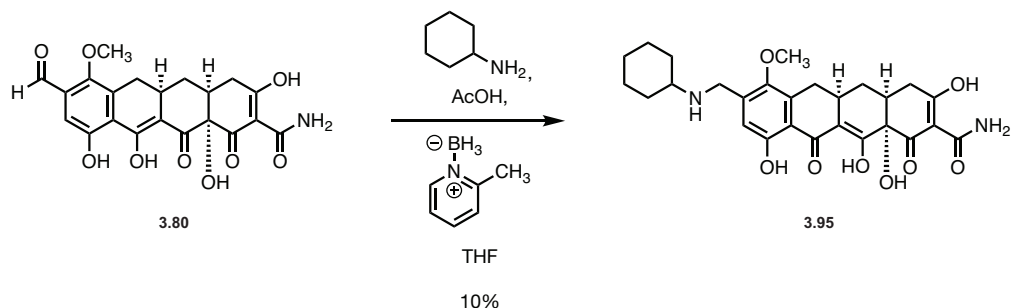
HRMS (ESI+,  $m/z$ )  $[\text{M} + \text{H}]^+$  calc'd for  $\text{C}_{28}\text{H}_{27}\text{FN}_2\text{O}_8$ : 539.1824. Found: 539.1814.



Analogue **3.94**:

Analogue **3.94** was prepared using General Procedure A: Aldehyde **3.80** (10 mg, 0.023 mmol, 1 eq., crude) was reacted with 2,4-difluorobenzylamine to provide Analogue **3.94** following preparatory HPLC purification. (0.5 mg, 4 %).

HRMS (ESI+,  $m/z$ )  $[M + H]^+$  calc'd for  $C_{28}H_{26}F_2N_2O_8$ : 557.1730. Found: 557.1732.



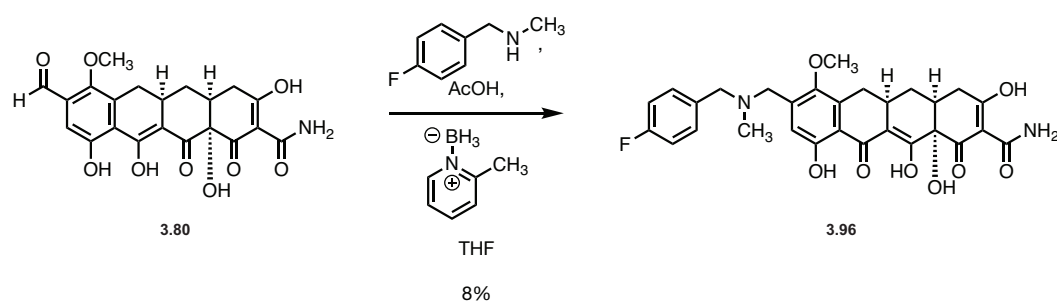
**Analogue 3.95:**

Analogue **3.95** was prepared using General Procedure A: Aldehyde **3.80** (10 mg, 0.023 mmol, 1 eq., crude) was reacted with cyclohexylamine to provide Analogue **3.95** as the formate salt following preparatory HPLC purification. (1.2 mg, 10 %).

$^1\text{H}$  NMR (400 MHz,  $\text{CD}_3\text{OD}$ )  $\delta$  6.89 (s, 1H), 4.18 (AB q,  $J = 15.2$  Hz, 2H), 3.71 (s, 3H), 3.23 (dd,  $J = 17.9, 6.1$  Hz, 1H), 3.14 (dd,  $J = 16.0, 3.9$  Hz, 1H), 3.09 (br. s, 1H), 2.82 (ddt,  $J = 15.0, 10.1, 4.7$  Hz, 1H), 2.51 – 2.27 (m, 3H), 2.16 (br. s, 1H), 2.06 (ddd,  $J = 11.9, 7.2, 3.0$  Hz, 1H), 1.91 (br. s, 1H), 1.77 – 1.56 (m, 2H), 1.48 – 1.17 (m, 7H).

HRMS (ESI+,  $m/z$ )  $[\text{M} + \text{H}]^+$  calc'd for  $\text{C}_{27}\text{H}_{32}\text{N}_2\text{O}_8$ : 513.2231. Found: 513.2228.



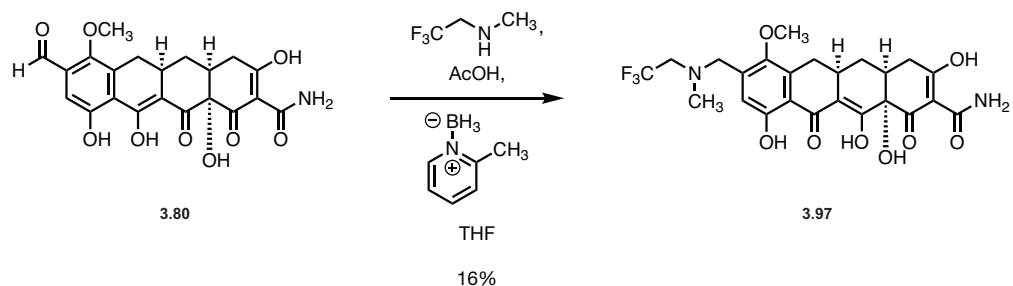


### Analogue **3.96**:

Analogue **3.96** was prepared using General Procedure A: Aldehyde **3.80** (10 mg, 0.023 mmol, 1 eq., crude) was reacted with 4-fluoro-*N*-methylbenzylamine to provide Analogue **3.96** following preparatory HPLC purification. (0.5 mg, 8 %).

<sup>1</sup>H NMR (400 MHz, CD<sub>3</sub>OD) δ 7.46 (s, 2H), 7.20 – 7.09 (m, 1H), 6.94 (s, 1H), 3.89 (br. s, 4H), 3.52 (s, 3H), 3.15 (app. d, *J* = 4.0 Hz, 1H), 2.86 – 2.76 (app. m, 1H), 2.53 – 2.39 (m, 5H), 2.27 (dd, *J* = 14.5, 14.5 Hz, 1H), 2.06 (ddd, *J* = 13.2, 6.9, 2.3 Hz, 1H), 1.61 (td, *J* = 13.2, 10.9 Hz, 1H).

HRMS (ESI+, *m/z*) [M + H]<sup>+</sup> calc'd for C<sub>29</sub>H<sub>29</sub>FN<sub>2</sub>O<sub>8</sub>: 553.1981. Found: 553.1975.

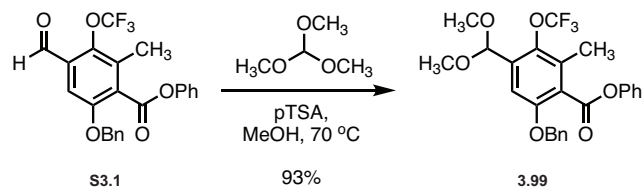


### Analogue 3.97:

Analogue **3.97** was prepared using General Procedure A: Aldehyde **3.80** (10 mg, 0.023 mmol, 1 eq., crude) was reacted with *N*-methyl-*N*-(2,2,2-trifluoroethyl)amine HCl to provide Analogue **3.97** as the formate salt following preparatory HPLC purification. (1 mg, 16 %).

$^1\text{H}$  NMR (400 MHz,  $\text{CD}_3\text{OD}$ )  $\delta$  6.90 (s, 1H), 3.76 (s, 2H), 3.63 (s, 3H), 3.25 – 3.16 (m, 2H), 2.85 – 2.77 (app. m, 1H), 2.49 – 2.43 (app. m, 1H), 2.41 (s, 3H), 2.25 (dd,  $J = 14.7$ , 14.7 Hz, 1H), 2.06 (ddd,  $J = 13.9$ , 8.7, 3.2 Hz, 1H), 1.61 (td,  $J = 13.9$ , 11.6 Hz, 1H).

HRMS (ESI+,  $m/z$ )  $[\text{M} + \text{H}]^+$  calc'd for  $\text{C}_{24}\text{H}_{25}\text{F}_3\text{N}_2\text{O}_8$ : 527.1636. Found: 527.1629.



C7-Methoxy-C8-acetal functionalized D-Ring Precursor (**3.99**)<sup>47</sup>:

Aldehyde **S3.1** (3 g, 6.97 mmol, 1 eq.) was dissolved in 30 mL anhydrous methanol in a flame dried 100 mL round-bottom flask.<sup>48</sup> Trimethylorthoformate (3.1 mL, 27.9 mmol, 4 eq.) was added, followed by *p*-TSA (0.04 g, 0.21 mmol, 0.3 eq.). The resulting yellow solution was heated to 70 °C and allowed to stir at that temperature for 19 hours. Following stirring, the reaction was cooled to 23 °C and concentrated. The resulting yellow residue was redissolved in dichloromethane and washed sequentially with water and brine (30 mL each), dried over sodium sulfate, and concentrated to a yellow oil. The crude material was purified using flash column chromatography (0 to 15% EtOAc / hexanes) to provide the desired product as an off-white solid (3.1 g, 93 %).

<sup>1</sup>H NMR (400 MHz, CDCl<sub>3</sub>) δ 7.48 – 7.35 (m, 8H), 7.20 (s, 1H), 7.13 – 7.01 (m, 2H), 5.51 (s, 1H), 5.18 (s, 2H), 3.37 (s, 6H), 2.42 (s, 3H).

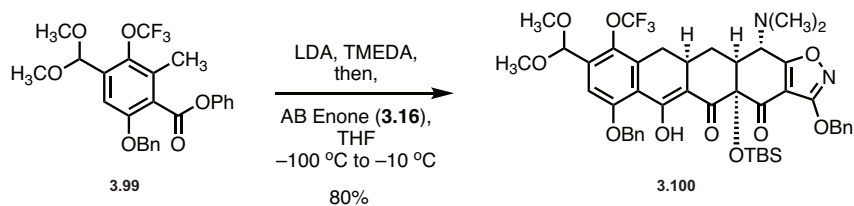
<sup>19</sup>F NMR (376 MHz, CDCl<sub>3</sub>) δ -56.17.

<sup>13</sup>C NMR (101 MHz, CDCl<sub>3</sub>) δ 165.52, 154.16, 150.60, 139.32, 135.97, 135.13, 131.29, 129.54, 128.60, 128.27, 128.24, 127.80, 127.71, 126.19, 125.44, 122.19, 121.61, 121.58, 119.62, 109.15, 99.48, 70.99, 68.00, 54.40, 25.63.

HRMS (ESI+, *m/z*) [M + H]<sup>+</sup> calc'd for C<sub>20</sub>H<sub>21</sub>F<sub>3</sub>O<sub>6</sub>: 437.1182. Found: 437.1197.

<sup>47</sup> Procedure modeled after that reported in Chen et al., **2010** (Chapter 3, ref. 32b).

<sup>48</sup> Aldehyde **S3.1** synthesized according to procedures reported in Xiao et al., **2014** (Chapter 3, ref. 7b) and Zhang et al., **2016** (Chapter 3, ref. 15c).



C7-Methoxy-C8-acetal functionalized tetracycline scaffold (**3.100**)<sup>49</sup>:

15mL anhydrous THF was added to a flame-dried round bottom flask and stirred at  $-78\text{ }^{\circ}\text{C}$ . Diisopropylamine (0.279 mL, 1.9 mmol, 1.35 eq.) and TMEDA (0.57 mL, 3.8 mmol, 2.6 eq.) were added, followed by *n*-butyllithium solution (2.47 M in THF, 0.79 mL, 1.9 mmol, 1.35 eq.). The solution was allowed to stir at  $-78\text{ }^{\circ}\text{C}$  for 30 minutes. D-ring precursor **3.99** (0.83 mg, 1.74 mmol, 1.2 eq.) was dissolved in a separate flame-dried round bottom flask and dissolved in 3 mL anhydrous THF. The D-ring solution was then added to the LDA solution in a dropwise manner at  $-78\text{ }^{\circ}\text{C}$ . The solution rapidly turned a deep red color during the addition. The solution was allowed to stir at  $-78\text{ }^{\circ}\text{C}$  for 30 minutes. The solution was then cooled to  $-100\text{ }^{\circ}\text{C}$  using a pentanes/liquid nitrogen bath. AB Enone (**3.16**, 0.7 mg, 1.5 mmol, 1 eq., dissolved in 3 mL anhydrous THF) was itself cooled to  $-78\text{ }^{\circ}\text{C}$  and added via cannula to the above anion solution at  $-100\text{ }^{\circ}\text{C}$  with vigorous stirring. The solution became a pale orange/red color following the addition. The solution was allowed to warm from  $-100\text{ }^{\circ}\text{C}$  to  $-78\text{ }^{\circ}\text{C}$  over 30 minutes. LiHMDS solution (1M solution in THF, 1.59 mL, 1.59 mmol, 1.1 eq.) was then added dropwise and the solution was allowed to warm to  $-10\text{ }^{\circ}\text{C}$  over 40 minutes. Following warming, the reaction was quenched with 20 mL 1:1 saturated aqueous  $\text{NH}_4\text{Cl}$  solution : 1X phosphate buffered saline (PBS) solution and diluted with ethyl acetate (10 mL). The layers were separated and the

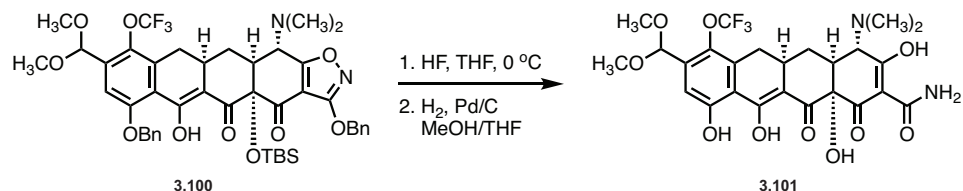
<sup>49</sup> Procedure modeled after that reported in Xiao et al., **2014** (Chapter 3, ref. 7b).

organics were washed with water and brine (20 mL each), dried on sodium sulfate, and concentrated to a dark yellow foamy solid. The crude product was purified using flash column chromatography (0 to 30 % EtOAc/hexanes) to provide the desired product as bright yellow foam (1.0 g, 80 %).

$^1\text{H}$  NMR (400 MHz,  $\text{CDCl}_3$ )  $\delta$  15.94 (s, 1H), 7.53 – 7.46 (m, 4H), 7.42 – 7.27 (m, 6H), 7.22 (s, 1H), 5.47 (s, 1H), 5.38 (s, 2H), 5.26 (dd,  $J = 12.4, 7.4$  Hz, 2H), 4.00 (d,  $J = 10.6$  Hz, 1H), 3.36 (s, 3H), 3.32 (s, 3H), 3.23 (dd,  $J = 16.0, 4.5$  Hz, 1H), 2.99 – 2.85 (m, 1H), 2.60 – 2.42 (m, 9H), 2.15 (dt,  $J = 14.4, 1.7$  Hz, 1H), 0.84 (s, 9H), 0.29 (s, 3H), 0.16 (s, 3H).

$^{19}\text{F}$  NMR (376 MHz,  $\text{CDCl}_3$ )  $\delta$  -56.59.

HRMS (ESI+,  $m/z$ )  $[\text{M} + \text{H}]^+$  calc'd for  $\text{C}_{45}\text{H}_{51}\text{F}_2\text{N}_2\text{O}_{10}\text{Si}$ : 865.3383. Found: 865.3359.

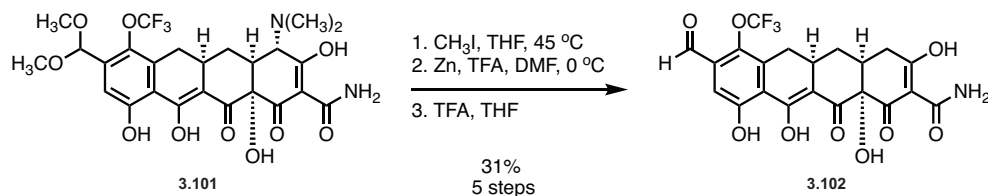


Deprotected C7-methoxy-C8-acetal Tetracycline (**3.101**)<sup>50</sup>:

Protected tetracycline **3.100** (0.6 g, .69 mmol, 1 eq.) was dissolved in 2 mL THF and stirred at 0 °C in a polypropylene tube. Hydrofluoric acid (48% solution, 0.25 mL, 10 eq.) was then added dropwise. The solution turned from a pale-yellow color to a light bright following the addition. The reaction was allowed to stir for 1 hour at 0 – 10 °C with progress monitored by LC/MS. Upon completion, the reaction was poured into a solution of potassium phosphate (0.5 M aq., 15 mL) and stirred. The solution was then extracted 3X with ethyl acetate (10 mL each) and the combined organics dried over sodium sulfate, filtered, and concentrated to a yellow/brown solid.

The crude solid was dissolved in 5 mL 1:1 THF : methanol and stirred at 23 °C. Palladium on carbon (10%, 0.15 g, 0.14 mmol, 0.2 eq.) was then added to give a black suspension. The flask was evacuated and backfilled 3X with nitrogen, then evacuated and backfilled 3X with hydrogen using a balloon. The reaction was then allowed to stir for 1 hour under static hydrogen pressure. Upon completion, the reaction flask was flushed with nitrogen for 10 minutes, then filtered through a pad of celite. The pad was washed with 50 mL methanol and the filtrate was concentrated to a light brown solid. Dry on vacuum. The crude product (~0.4 g) was typically taken directly to the next step without further purification.

<sup>50</sup> Procedure modeled after that reported in Chen et al., **2010** (Chapter 3, ref. 32b).



### Aldehyde 3.102:

Tetracycline SM (0.35 g, 0.61 mol, 1 eq.) was dissolved in 2 mL THF and stirred. Iodomethane (1.4 mL, 21.4 mmol, 35 eq.) was added dropwise and the reaction was heated to 45 °C and stirred at that temperature for 19 hours. Following stirring, the reaction solution was concentrated to a bright yellow solid.

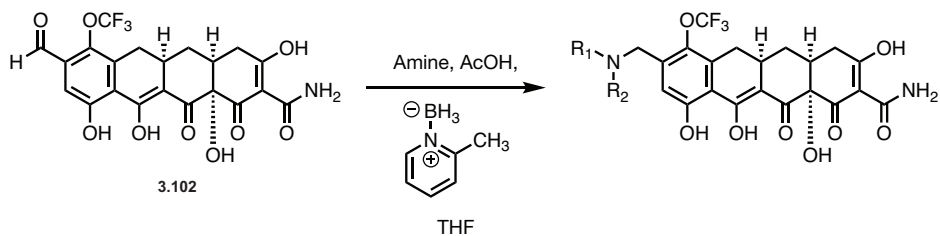
The solid was dissolved in 0.5 mL DMF and stirred at 0 °C. Water (0.06 mL, 3.1 mmol, 5 eq.) and TFA (0.19 mL, 2.5 mmol, 4 eq.) were then added sequentially to provide a bright yellow solution. Zinc (0.052 g, 0.8 mmol, 1.3 eq.) was then added in 5-6 small portions every 25 minutes. Following completion of the zinc additions, the reaction was stirred for another 1.5 to 2 hours at 0 °C, or until LC/MS indicated consumption of the methylated starting material. The reaction solution was filtered through a 0.2 μM syringe filter to remove the unreacted zinc and the reaction was diluted with water. The pH was adjusted to 2.5 with 25% ammonium hydroxide solution, then extracted 3X with DCM (20 mL each). The organics were combined and washed with water and brine (30 mL each). The organic layer was then dried over sodium sulfate, filtered, and concentrated to an orange/brown residue. Dry on vacuum.

Following drying, the residue was redissolved in THF and TFA (2 mL) was added. The dark orange solution was allowed to stir for 19 hours at 23 °C. Following stirring, the solution was concentrated to a flaky orange solid and dried on vacuum. The crude product was typically used in subsequent reactions without further purification (0.09 g, 31%).

Samples of high purity can be obtained using the following procedure: 30 mg crude product was dissolved in 5 mL 4:1 methanol: DMF. The product was purified by preparative HPLC on an Agilent Prep C18 column [10  $\mu$ m, 250 x 21.2 mm, UV detection at 399 nm, Solvent A: 0.1% formic acid in water, Solvent B: 0.1% formic acid in acetonitrile, injection volume: 5.0 mL (4 mL methanol, 1 mL DMF), gradient elution with 10–75% B over 40 min, flow rate: 15 mL/min]. Fractions were analyzed via analytical LC/MS for purity prior to concentration to provide the desired product, typically as a yellow solid.

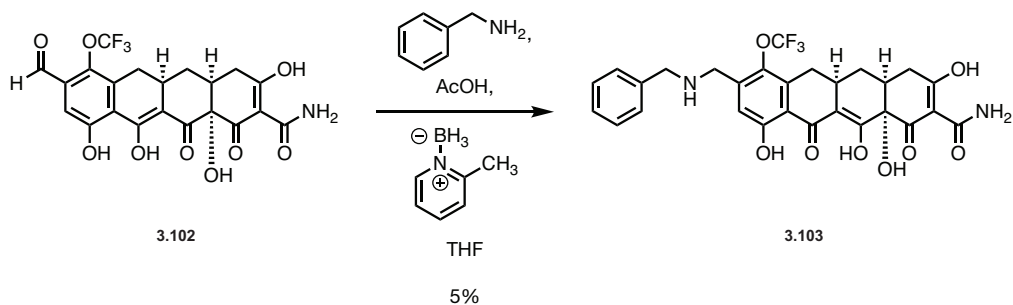
HRMS (ESI+,  $m/z$ ) [M + H]<sup>+</sup> calc'd for C<sub>21</sub>H<sub>16</sub>F<sub>3</sub>NO<sub>9</sub>: 484.0850. Found: 484.0860.





**General Procedure B: Reductive Amination with Aldehyde 3.102:**

Aldehyde **3.102** (10 mg, 0.021 mmol, 1 eq.) was dissolved in 1 mL THF and stirred at 23 °C. Amine (5 eq.) was added, followed by acetic acid (5 eq.) and 2-picoline-borane (4 eq.). The solution typically turned from light orange to deep red in color following amine addition. The reaction was typically allowed to stir at 23 °C for 1 to 2 hours, or until LCMS indicated consumption of the starting material. Upon completion, the reaction solution was concentrated to an orange/red residue and dried on vacuum. The residue was then redissolved in methanol and purified by preparative HPLC on an Agilent Prep C18 column [10 μm, 250 x 21.2 mm, UV detection at 399 nm, Solvent A: 0.1% formic acid in water, Solvent B: 0.1% formic acid in acetonitrile, injection volume: 5.0 mL (4 mL methanol + reaction solution), gradient elution with 5–70% B over 40 min, flow rate: 15 mL/min] over two runs. Fractions were analyzed via analytical LC/MS for purity prior to concentration to provide the desired product, typically as a yellow solid.



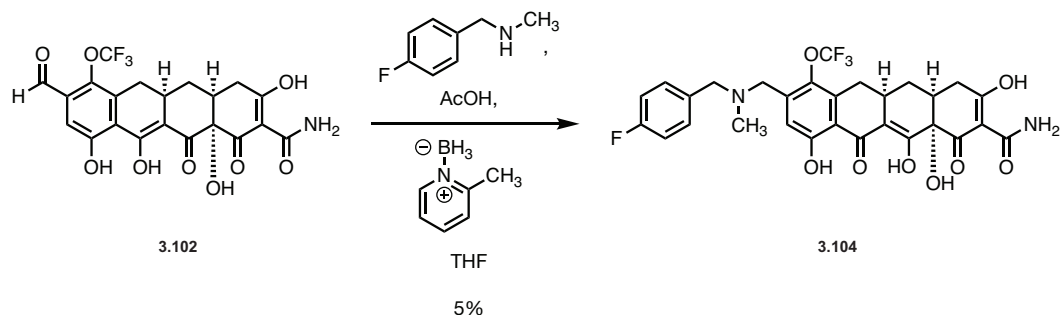
### Analogue 3.103:

Analogue **3.103** was prepared using General Procedure B: Aldehyde **3.102** (10 mg, 0.021 mmol, 1 eq., crude) was reacted with benzylamine to provide Analogue **3.103** as the formate salt following preparatory HPLC purification. (0.5 mg, 5%).

<sup>1</sup>H NMR (400 MHz, CD<sub>3</sub>OD) δ 7.36 – 7.20 (m, 5H), 7.06 (s, 1H), 3.77 (br. s, 4H), 3.22 (dd, *J* = 18.5, 5.7 Hz, 1H), 3.08 (dd, *J* = 15.6, 4.2 Hz, 1H), 2.87 – 2.75 (app. m, 1H), 2.49 – 2.33 (m, 2H), 2.27 (dd, *J* = 14.8, 14.8 Hz, 1H), 2.05 (ddd, *J* = 12.8, 6.1, 2.8 Hz, 1H), 1.59 (td, *J* = 13.5, 10.9 Hz, 1H).

<sup>19</sup>F NMR (376 MHz, CD<sub>3</sub>OD) δ -58.54.

HRMS (ESI+, *m/z*) [M + H]<sup>+</sup> calc'd for C<sub>28</sub>H<sub>25</sub>F<sub>3</sub>N<sub>2</sub>O<sub>8</sub>: 575.1636. Found: 575.1644.



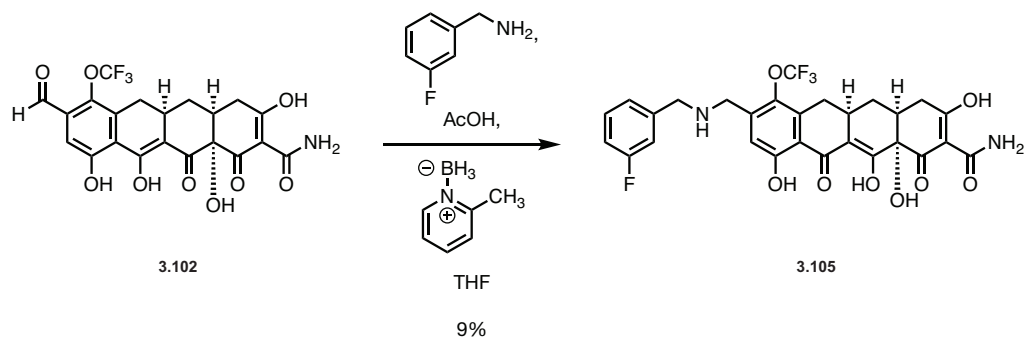
### Analogue 3.104:

Analogue **3.104** was prepared using General Procedure B: Aldehyde **3.102** (10 mg, 0.021 mmol, 1 eq., crude) was reacted with 4-fluoro-*N*-methylbenzylamine to provide Analogue **3.104** as the formate salt following preparatory HPLC purification. (0.6 mg, 5%).

$^1\text{H}$  NMR (400 MHz,  $\text{CD}_3\text{OD}$ )  $\delta$  7.36 (dd,  $J = 8.4, 5.5$  Hz, 2H), 7.17 (s, 1H), 7.04 (t,  $J = 8.7$  Hz, 2H), 3.59 – 3.50 (m, 4H), 3.21 (app. d,  $J = 5.5$  Hz, 1H), 3.10 (dd,  $J = 15.7, 4.3$  Hz, 1H), 2.87 – 2.77 (m, 1H), 2.50 – 2.35 (m, 2H), 2.27 (dd,  $J = 14.9, 14.9$  Hz, 1H), 2.18 (s, 3H), 2.05 (ddd,  $J = 13.7, 7.4, 4.3$  Hz, 1H), 1.58 (td,  $J = 13.7, 11.5$  Hz, 1H).

$^{19}\text{F}$  NMR (376 MHz,  $\text{CD}_3\text{OD}$ )  $\delta$  -58.49, -117.80.

HRMS (ESI+,  $m/z$ )  $[\text{M} + \text{H}]^+$  calc'd for  $\text{C}_{29}\text{H}_{26}\text{F}_4\text{N}_2\text{O}_8$ : 607.1698. Found: 607.1688.



### Analogue 3.105:

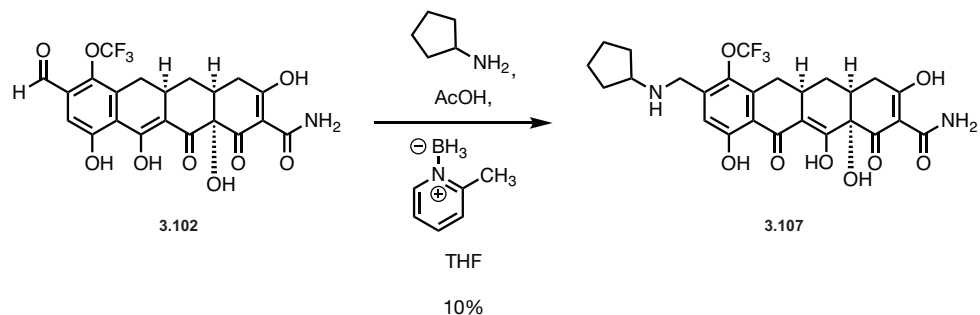
Analogue **3.105** was prepared using General Procedure B: Aldehyde **3.102** (10 mg, 0.021 mmol, 1 eq., crude) Aldehyde **3.102** was reacted with 3-fluorobenzylamine to provide Analogue **3.105** as the formate salt following preparatory HPLC purification. (1.1 mg, 9%).

$^1\text{H}$  NMR (400 MHz,  $\text{CD}_3\text{OD}$ )  $\delta$  7.32 (td,  $J = 7.9, 5.9$  Hz, 1H), 7.17 – 7.05 (m, 3H), 6.97 (td,  $J = 8.6, 2.5$  Hz, 1H), 3.91 – 3.71 (m, 4H), 3.23 (dd,  $J = 18.1, 5.4$  Hz, 1H), 3.08 (dd,  $J = 15.8, 4.2$  Hz, 1H), 2.88 – 2.77 (app. m, 1H), 2.50 – 2.34 (m, 2H), 2.27 (dd,  $J = 14.8, 14.1$  Hz, 1H), 2.05 (ddd,  $J = 11.9, 6.5, 2.1$  Hz, 1H), 1.59 (td,  $J = 13.1, 11.9$  Hz, 1H).

$^{19}\text{F}$  NMR (376 MHz,  $\text{CD}_3\text{OD}$ )  $\delta$  -58.55, -115.64.

HRMS (ESI+,  $m/z$ )  $[\text{M} + \text{H}]^+$  calc'd for  $\text{C}_{28}\text{H}_{24}\text{F}_4\text{N}_2\text{O}_8$ : 593.1542. Found: 593.1529.





**Analogue 3.107:**

Analogue **3.107** was prepared using General Procedure B: Aldehyde **3.102** (10 mg, 0.021 mmol, 1 eq., crude) was reacted with cyclopentylamine to provide Analogue **3.107** as the formate salt following preparatory HPLC purification. (1.1 mg, 10%).

$^1\text{H}$  NMR (400 MHz,  $\text{CD}_3\text{OD}$ )  $\delta$  6.98 (s, 1H), 4.04 (s, 2H), 3.22 (dd,  $J = 18.3, 5.0$  Hz, 1H), 3.07 (dd,  $J = 16.0, 5.0$  Hz, 1H), 2.85 (app. s, 1H), 2.50 – 2.24 (m, 3H), 2.11 – 1.97 (m, 2H), 1.78 (br. s, 3H), 1.70 – 1.49 (m, 6H).

$^{19}\text{F}$  NMR (376 MHz,  $\text{CD}_3\text{OD}$ )  $\delta$  -58.58.

HRMS (ESI+,  $m/z$ )  $[\text{M} + \text{H}]^+$  calc'd for  $\text{C}_{26}\text{H}_{27}\text{F}_3\text{N}_2\text{O}_8$ : 553.1792. Found: 553.1786.

## **Chapter 4**

### **Mechanistic Elucidation Efforts**

#### **4.1 Introduction to Mechanistic Elucidation Efforts**

In this chapter we provide a summary of our efforts to better understand the mechanism by which the tetracyclines exert their antiproliferative activity in human cancer cells. These efforts are divided into two broad areas of study: translation inhibition and signaling pathway progression. As a primer for these efforts, we provide a brief introduction to the mechanism of eukaryotic translation as well as a review of small molecule translation inhibitors and their mechanisms of action. We then detail our research efforts into the mechanism of translation inhibition, focusing primarily on our progression from polysome profiling to *in vitro* translation experiments, and an investigation into the ribosome-associated quality control system and its role in tetracycline-mediated cell death. Finally, we provide a summary of our efforts to better understand the signaling pathways activated on tetracycline treatment and how these relate to the inhibition of translation and growth arrest. While many of these efforts are still underway, we believe the foundation provided in this chapter will provide future biologists important information for further studies.

#### **4.2 The Mechanism of Eukaryotic Translation**

As in all domains of life on earth, translation in eukaryotes refers to the mechanism by which genetic information encoded in RNA is transitioned into functionalized protein by a macromolecular machine called the ribosome.<sup>1</sup> Translation can be broken down into four major steps: Initiation, Elongation, Termination, and Recycling. While core features of translation are conserved across the three kingdoms of life, translation in eukaryotes is

---

<sup>1</sup> Parsyan, A. *Translation and its Regulation in Cancer Biology and Medicine*; Springer, 2014.



the most complex by far, requiring dozens of unique protein cofactors to orchestrate this complex and energy-intensive process.<sup>1</sup> Here, we will briefly discuss the core elements of the four stages of eukaryotic translation, their relationship to human disease, and the mechanism of several small molecules which exert their inhibitory effects on one or more of the stages of translation.

The initiation stage of translation represents the most complex and highly regulated of the four stages, requiring the greatest number of protein and RNA cofactors.<sup>2</sup> As a result, initiation is the stage of translation most often associated with development and progression of cancer. Broadly, initiation involves the separate preparation of mRNA, an initiator tRNA, and the 40S (small) subunit of the ribosome. These units are joined by a series of eukaryotic initiation factors (eIFs), enabling the recognition of a start codon and, as a final step, the association of the 60S (large) subunit to form a competent 80S ribosome complex that is ready to begin the production of nascent peptides in the elongation stage. This process is shown as a series of steps in Figure 4.1. Beginning on one arm of this convergent process, an initiator tRNA is joined with an eIF2 cofactor and GTP molecule to form the Ternary Complex (TC) (see *eIF2 Activation*, Fig. 4.1). The TC, along with eIF5, can then be joined to the 40S ribosomal subunit, itself decorated with eIFs 1, 1A, and 3, to form the 43S complex typically referred to as the pre-initiation complex (PIC) (see *PIC Formation*, Fig. 4.1). Several variations of this mechanism exist, with one major alternate pathway involving the addition of the TC with eIFs 1, 3, and 5 to form the multifunctional complex (MFC) and later joining both the 40S subunit and eIF1A to form the competent 43S complex. Simultaneously, a series of similar steps are being used to

---

<sup>2</sup> (a) See Parsyan, A., **2014**, Part 1, Chapter 2 (Chapter 4, ref. 1). (b) Merrick, W. C.; Pavitt, G. D. *Cold Spring Harb. Perspect. Biol.* **2018**, *10*, a033092 and references cited therein.

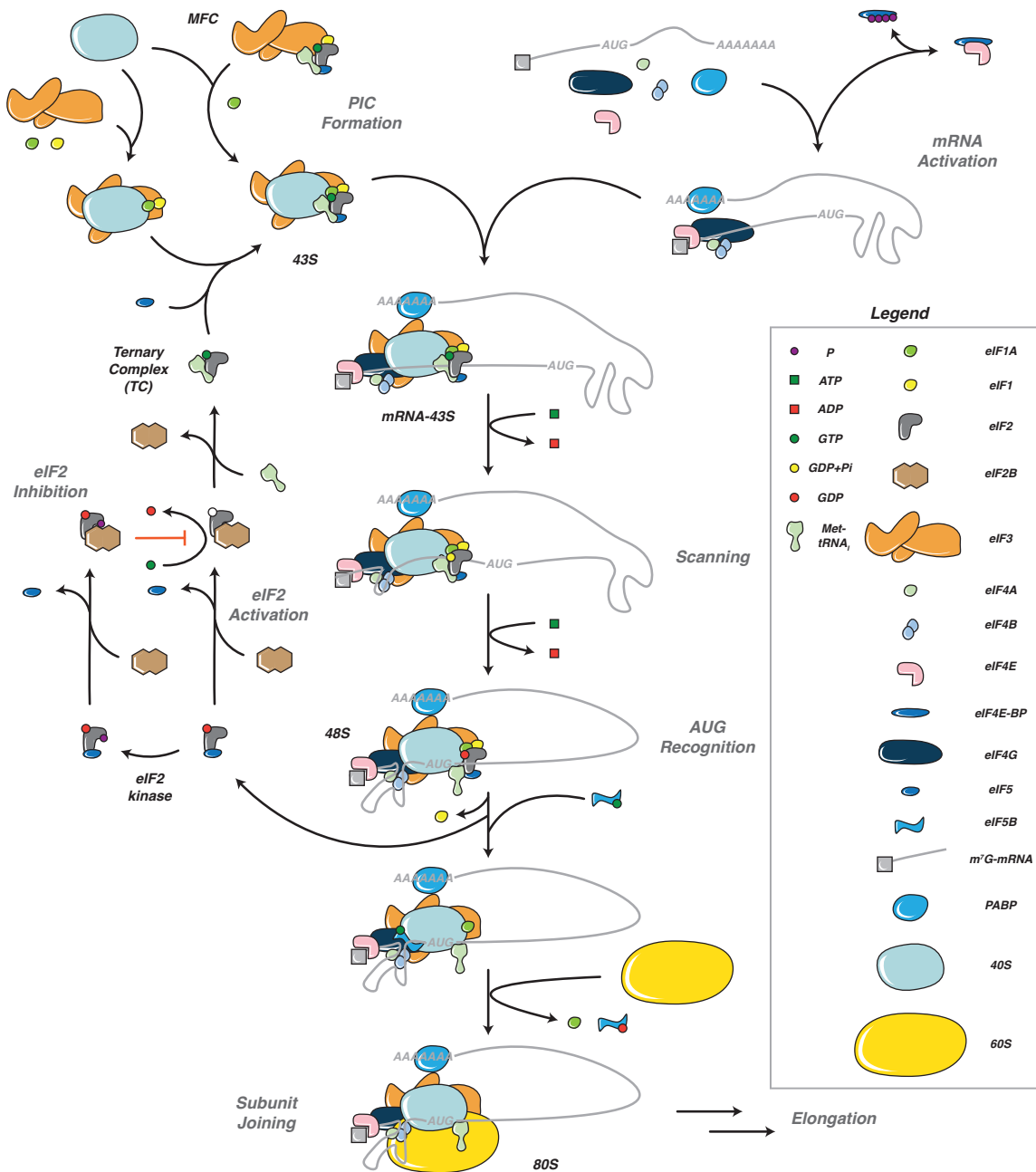


**Figure 4.1 Translation Initiation in Eukaryotes.** A broad overview of the initiation stage of eukaryotic translation is shown. The scheme can be broadly classified into six key areas (dark gray): PIC Formation, mRNA Activation, Scanning, AUG Recognition, eIF2 Activation, and Subunit Joining. Broadly, the 40S subunit and associated cofactor proteins are prepared (PIC Formation), resulting in formation of the 43S complex. mRNA transcripts are similarly prepared with a series of initiation cofactors (mRNA Activation) and subsequently joined with the 43S complex to form the 43S-mRNA species. This complex then enters the Scanning phase, slowly progressing through the 5'-UTR of the mRNA until a start codon (AUG) is recognized by the initiation tRNA. This recognition initiates a series of associations and dissociations, the precise mechanism for some of which is not yet known, ultimately resulting in the joining of the 60S subunit. This competent 80S complex is then ready for the elongation stage. A key area of translation initiation is the recycling of eIF2 (eIF2 Activation). This process is highly regulated via phosphorylation through the integrated stress response (ISR, see Chapter 1). Figure adapted from Merrick et al., 2018 (Chapter 4, ref. 2b).

combine mRNA with eIFs 4A, 4B, 4E, and 4G, as well as the poly-A binding protein (PABP) (see *mRNA activation*, Fig. 4.1). The components of this activated mRNA complex play a number of key roles: eIF4A and 4B display helicase activity to aid in unwinding mRNA helices, eIF4E anchors the complex to the m<sup>7</sup>-guanosine cap structure present on all eukaryotic transcripts, and the PABP binds to the poly-adenosine tail structure that is added to mRNA strands as a way to loop the RNA structure back to the main complex. A key regulatory mechanism in translation initiation involves the sequestration of eIF4E by the 4E binding protein (4E-BP). A variety of regulatory pathways used to modify translational loading end with 4E-BP, as phosphorylation of this cofactor leads to release of bound eIF4E and allows for translation to proceed unencumbered. The eIF4E/4E-BP relationship is our first example of the interplay between regulatory pathways and the progression of translation.

Assembly proceeds with the joining of the activated mRNA and the 43S complexes, a process thought to be orchestrated by interactions between eIF3 and eIF4G, as well as several positions along the 40S subunit. The next step—scanning—involves the slow movement of the 43S complex down the mRNA strand in the 5'-untranslated region (UTR)—the region between the m<sup>7</sup>-G cap and the closest start codon (typically AUG) in an ATP-dependent manner (see *Scanning and AUG recognition*, Fig. 4.1). This process is completed upon recognition of a start codon, initiating the liberation of eIF1 as well as a spent ternary complex (eIF2/5/GDP). In a final series of steps, eIF5B/GTP joins the complex and assists in the joining of the 60S (large) ribosomal subunit, after which both eIF1A and eIF5B/GDP are liberated and a competent 80S complex is formed and ready to begin the elongation stage. While recycling of most of the cofactors involved in initiation

is straightforward, the regeneration of the ternary complex is perhaps the most highly regulated. This process involves the replenishment of GTP by the dedicated guanine nucleotide exchange factor eIF2B, which joins the complex and spurs the release of eIF5. The ternary complex is then reformed following exchange of eIF2B for a new initiator tRNA. This GDP/GTP reprocessing step is subject to regulatory control from a variety of signaling pathways including the Integrated Stress Response (ISR). These pathways function through phosphorylation of the  $\alpha$ -subunit of eIF2 which results in a decrease in the rate of GDP/GTP exchange by eIF2B. This process ultimately results in a diminished concentration of ternary complex, thus decreasing translational loading in a manner similar to that which results from sequestration of eIF4E by 4E-BP (*vide supra*).

Relative to the initiation stage, the remaining stages of translation are straightforward. The elongation stage can be visualized as a cyclical progression of aminoacyl-tRNAs through three sites at the catalytic core of the ribosome, commonly referred to as the A-, P-, and E-sites.<sup>3</sup> Like initiation, the movements associated with elongation are often assisted by eukaryotic elongation factors (eEFs). At the beginning of this cycle, the 80S complex features an aminoacyl-tRNA in the P site holding a nascent peptide as well as a spent tRNA in the E site ready for ejection. The first step in elongation consists of release of the spent tRNA and introduction of the next tRNA to the A-site, a process assisted by the cofactor eEF1A. Recognition of the appropriate anticodon on an incoming tRNA initiates GTP hydrolysis and release of eEF1A. With a new aminoacyl-tRNA situated in the A site, the peptidyl transferase center (PTC) catalyzes formation of a new peptide bond and transfers the nascent peptide chain to the A-site tRNA. As a final

---

<sup>3</sup> Dever, T. E.; Green, R. *Cold Spring Harb. Perspect. Biol.* **2012**, *4*, a013706 and references cited therein.

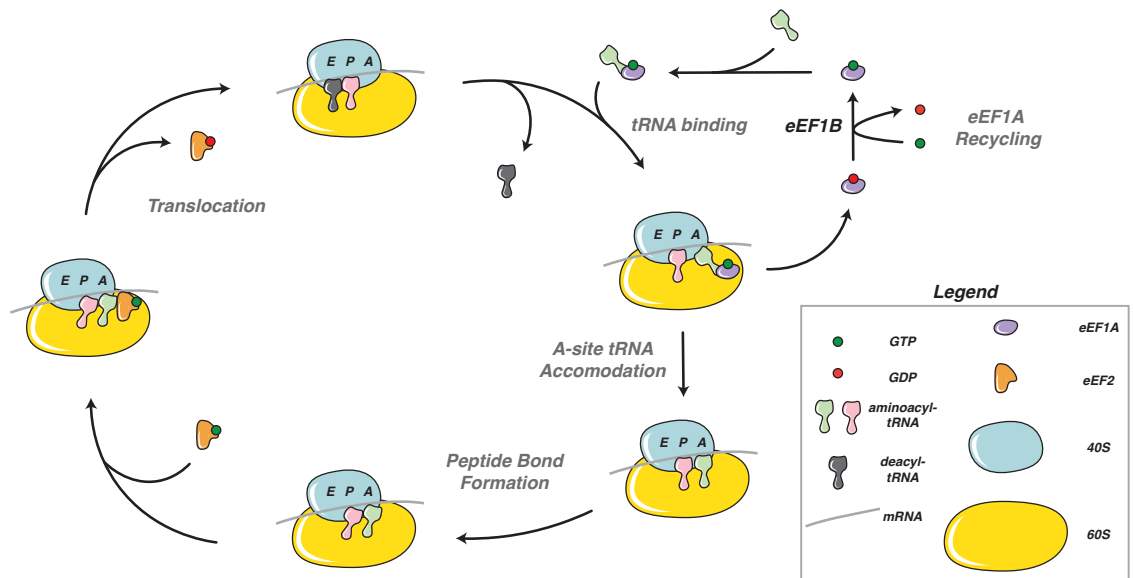


**Figure 4.2 The Elongation Stage of Eukaryotic Translation** Straightforward in comparison, the elongation stage of translation represents the method by which the sequence of nucleotides on an mRNA transcript are converted into a chain of amino acids in a nascent peptide. Broad steps involved in this process are shown in dark gray: tRNA Binding, A-site tRNA Accommodation, Peptide Bond Formation, and Translocation. In general, protein cofactors eEF1A and B work to prepare incoming tRNAs for binding to the ribosome. In a series of large conformational changes, the binding sites at the catalytic core of the ribosome shift tRNA positioning and nascent peptide location to allow for new tRNAs to enter. This process is completed cyclically until a stop codon is reached. Figure adapted from Dever et al., **2012** (Chapter 4, ref. 3).

step, the transition of the tRNAs from the A/P sites to P/E is initiated during a ratcheting of the ribosomal subunits to generate hybrid A/P and P/E locations. Full translocation is then completed after association eEF2 which, after assisting in the tRNA site transition, undergoes GTP hydrolysis and is released. This step leaves the tRNAs in appropriate positions in the catalytic core to accept a new tRNA and begin the elongation cycle again, doing so until a stop codon is reached and translation enters the final two stages: termination and recycling.

The final two steps of translation utilize a relatively simple mechanism for the separation of the 80S ribosome from its mRNA transcript and subsequent recycling of the components.<sup>4</sup> The arrival of a stop codon in the catalytic core of the ribosome initiates

<sup>4</sup> See Dever et al., **2012** (Chapter 4, ref. 3) and references cited therein.

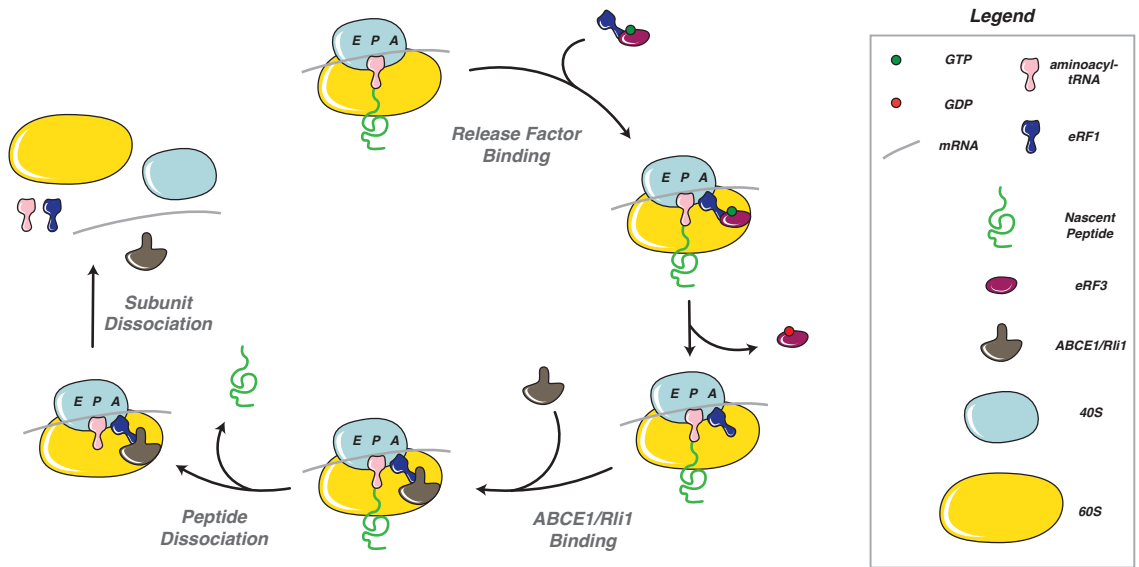


**Figure 4.3 The Termination/Recycling Stages of Eukaryotic Translation.** The final stages of translation consist primarily of a method for removing ribosomes from a given mRNA transcript and recycling them for use in initiation. Broad steps are noted in dark gray: Release Factor Binding, ABCE1/Rli Binding, Peptide Dissociation, and Subunit Dissociation. Binding of tRNA-mimic eRF1 initiates recruitment of ABCE1/Rli, which behaves like a crowbar during its prying apart of the 40 and 60S ribosomal complexes. Figure adapted from Dever et al., **2012** (Chapter 4, ref. 3).

recruitment of a release factor complex featuring recycling factors (eRFs) 1 (high-fidelity stop codon recognition) and 3 (GTPase activity) bound to a GTP molecule. eRF3 is released following GTP hydrolysis, allowing for the recruitment of the release factor ABCE1/Rli which in turn assists first with cleavage of the nascent peptide followed by subunit dissociation. While many of the steps involved in the four stages of translation have yet to be uncovered, the schematics presented in Figures 4.1, 4.2, and 4.3 provide a summary the current understanding of these complex processes and will undoubtedly require updates and refreshments as research continues.

### 4.3 Small Molecule Modulation of Translation

Its centrality to all cellular processes has established translation as a common target for chemists seeking to disrupt cellular growth or protein production, particularly those studying oncogene-based translational dysregulation and cancer progression. Over the

years, a number of natural products and related synthetic analogues have been developed as eukaryote-specific translation inhibitors for treating human cancers, with many showing promise in early clinical stages. Homoharringtonine (HHT, **4.1**, brand name Omacetexine, Fig. 4.4) is currently the only eukaryotic translation inhibitor approved for human use, primarily for the treatment of certain types of chronic myeloid leukemia (CML).<sup>5</sup> HHT is thought to inhibit translation through the binding of the 80S ribosome near the A-site and inhibiting peptide bond formation and elongation of the nascent chain.<sup>6</sup> Cycloheximide (**4.2**), another well-known eukaryotic translation inhibitor, has played a key role in the study of protein synthesis for decades.<sup>7</sup> While a similar glutarimide analogue, lactimidomycin (**4.3**), inhibits the initiation stage of translation through blocking progression of the start codon, cycloheximide has been shown to bind to the E-site of elongating ribosomes and freeze their movement along a given mRNA transcript.<sup>8</sup> Similarly to cycloheximide, the natural products anisomycin (**4.4**) and agelastatin A (**4.5**)

---

<sup>5</sup> (a) Chen, Y.; Li, S. *Onco. Targets Ther.* **2014**, *7*, 177-186. (b) Kantarjian, H. M.; Talpaz, M.; Santini, V.; Murgo, A.; Cheson, B.; O'Brian, S. M. *Cancer*, **2001**, *92*, 1591-1605. (c) Kim, T. D.; Frick, M.; Le Coutre, P. *Exp. Opin. Pharmacother.* **2011**, *12*, 2381-2392.

<sup>6</sup> See the following for a selection of mechanistic studies regarding homoharringtonine: (a) Gurel, G.; Blaha, G.; Moore, P. B.; Steitz, T. A. *JMB* **2009**, *389*, 146-156. (b) Robert, F.; Carrier, M.; Rawe, S.; Chen, S.; Lowe, S.; Pelletier, J. *PLoS One* **2009**, *4*, e5428. (c) Tang, R.; Faussat, A.-M.; Majdak, P.; Marzac, C.; Dubrulle, S.; Marjanovic, Z.; Legrand, O.; Marie, J.-P. *Mol. Cancer. Ther.* **2006**, *5*, 723-731.

<sup>7</sup> Park, Y.; Koga, Y.; Su, C.; Waterbury, A. L.; Johnny, C. L.; Liau, B. B. *Angew. Chem. Int. Ed.* **2019**, *58*, 5387-5391.

<sup>8</sup> Schneider-Poetsch, T.; Ju, J.; Eyler, D. E.; Dang, Y.; Bhat, S.; Merrick, W. C.; Green R.; Shen, B.; Liu, J. *O. Nat. Chem. Biol.* **2010**, *6*, 209-217.

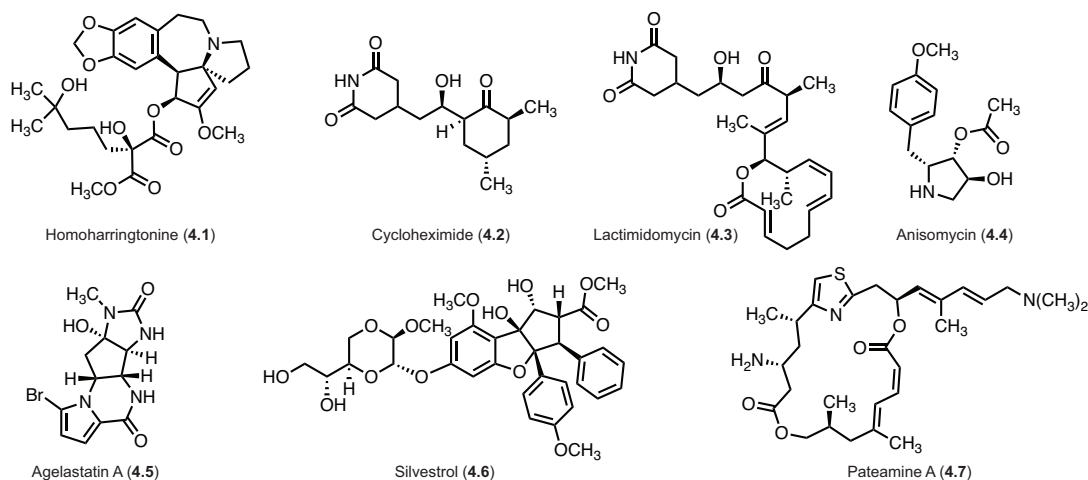


**Figure 4.4 A Selection of Small Molecule Translation Inhibitors.** Eukaryotic translation inhibitors are found in many different classes of natural product. While many compounds are currently under research or in clinical trials, the only translation inhibitor approved as a cancer therapeutic is homoharringtonine (**4.1**). The compound cycloheximide (**4.2**) is used throughout biochemistry laboratories as a reliable inhibitor of elongating ribosomes (see Polysome Profiling section below). Many other translation inhibitors have been identified as potential cancer therapeutics and are in various stages of investigation.

also bind locations in the PTC, disrupting elongation progression.<sup>9, 10</sup> Perhaps the most promising amongst pre-clinical eukaryotic translation inhibitors are those that target initiation co-factors involved in specific oncogenic translation programs.<sup>11</sup>

Compounds such as those discussed above tend to display broad off-target toxicities as their translation inhibitory effects span both cancerous and non-cancerous cells, presenting challenges associated with canonical chemotherapeutic drugs. Compounds in current development stages include the rocaglates, a class of synthetic translation inhibitors based on the natural products silvestrol and rocaglamide (**4.6**, Fig.

<sup>9</sup> McClary, B.; Zinshteyn, B.; Meyer, M.; Jouanneau, M.; Pellegrina, S.; Yusupova, G.; Schuller, A.; Reyers, J. C. P.; Liu, J.; Gou, Z.; Ayinde, S.; Luo, C.; Dang, Y.; Romo, D.; Yusupov, M.; Green, R.; Liu, J. O. *Cell Chem. Biol.* **2017**, *24*, 605-613.

<sup>10</sup> de Loubresse, N. G.; Prokhorova, I.; Holtkamp, W.; Rodnina, M. V.; Yusupova, G.; Yusupov, M. *Nature* **2014**, *513*, 517-522.

<sup>11</sup> (a) Chu, J.; Pelletier, J. *Cold Spring Harb. Perspect. Biol.* **2018**, *10*, a032995. (b) Manier, S.; Huynh, D.; Shen, Y. J.; Zhou, J.; Yusufzai, T.; Salem, K. Z.; Ebright, R. Y.; Shi, J.; Park, J.; Glavey, S. V.; Devine, W. G.; Liu, C.-J.; Leleu, X.; Quesnel, B.; Roche-Lestienne, C.; Snyder, J. K.; Brown, L. E.; Gray, N.; Bradner, J.; Whitesell, L.; Porco Jr., J. A.; Ghobrial, I. M. *Sci. Transl. Med.* **2017**, *9*, 1-13.



4.4).<sup>12</sup> These compounds have been shown to bind eIF4A, the DEAD-box helicase tasked with unwinding the densely structured 5'-untranslated regions of a given mRNA during translation initiation, preventing effective scanning of the 43S complex and inhibiting the initiation stage of translation.<sup>13</sup> The rocaglates have been identified as a potential therapeutic for B-cell lymphomas, specifically those featuring dysregulation of the oncogenic transcription factor MYC.<sup>14</sup> Among its myriad mechanisms for increasing protein synthesis and cell growth, MYC stimulates expression of subunits of the cap-binding complex involved in translation initiation, including eIF4A, as well as the mTOR signaling pathway, which plays a role in upregulating translation initiation through phosphorylation of 4E-BP. By disrupting these specific oncogenic pathways, the rocaglates display improved specificity for lymphomas compared to other cancer types and non-cancerous cells, differing by a wide margin from blanket elongation inhibitors. The marine natural product pateamine A (**4.7**) represents another eIF4A inhibitor, this time increasing the protein's affinity for the closely associated eIF4B and eIF4G and subsequently inducing stalling of initiation complexes.<sup>15</sup>

As we seek to better understand the mechanism underlying the anticancer effects of the tetracyclines and to develop these compounds further in the clinical stage, it is clear

---

<sup>12</sup> Chu, J.; Zhang, W.; Cencic, R.; Devine, W. G.; Beglov, D.; Henkel, T.; Brown, L. E.; Vajda, S.; Porco Jr., J. A.; Pelletier, J. *Cell Chem. Biol.* **2019**, *26*, 1-8 and references cited therein.

<sup>13</sup> (a) Iwasaki, S.; Floor, S. N.; Ingolia, N. T. *Nature* **2016**, *534*, 558-561. (b) Iwasaka, S.; Iwasaka, W.; Takahashi, M.; Sakamoto, A.; Watanabe, C.; Shichino, Y.; Floor, S. N.; Fujiwara, K.; Mito, M.; Dodo, K.; Sodeoka, M.; Imataka, H.; Honma, T.; Fukuzawa, K.; Ito, T.; Ingolia, N. T. *Mol. Cell* **2019**, *73*, 738-748. (C) Chu, J.; Cencic, R.; Wang, W.; Porco Jr., J. A.; Pelletier, J. *Mol. Cancer Ther.* **2016**, *15*, 136-141.

<sup>14</sup> Zhang, X.; Bi, C.; Lu, T.; Zhang, W.; Yue, T.; Wang, C.; Tian, T.; Zhang, X.; Huang, Y.; Lunning, M.; Hao, X.; Brown, L. E.; Devine, W. G.; Vose, J.; Porco Jr., J. A.; Fu, K. *Lymphoma* **2020**, *34*, 138-150.

<sup>15</sup> Low, W.-K.; Dang, Y.; Schneider-Poetsch, T.; Shi, Z.; Choi, N. S.; Merrick, W. C.; Romo, D. T.; Liu, J. O. *Mol. Cell* **2005**, *20*, 709-722.

we need to focus not only on translation inhibitory effects but on the identification and optimization of the disruption of certain oncogenic translation programs to target particular cancer types. Recent discoveries, both in our research and elsewhere, have suggested mitochondrial translation as a potential target for the tetracyclines in human cells.<sup>16</sup> However, at this stage of our studies, it is clear that translation inhibitory potency stands as an important foundation upon which other cellular effects could be investigated and exploited.

#### **4.4 Early Studies in Translation Inhibition – Polysome Profiling**

Early on in our mechanistic elucidation efforts, we utilized polysome profiling to gain a deeper understanding of the interaction between the tetracyclines and translating ribosomes. We envisioned these efforts helping to expand our knowledge of the mechanics behind tetracycline-induced translation inhibition as well as inspiring additional paths of inquiry for subsequent studies.

Polysome profiling, an old biochemical method used to analyze the behavior of translating ribosomes, is particularly useful when assessing the cellular effects of small molecules.<sup>17</sup> Briefly, this methodology involves the culturing and treatment of a large number of cells with a small molecule of interest. In a key step following treatment, the cells are washed with a buffer solution containing the translation inhibitor cycloheximide (CHX). CHX is used for its ability to stop elongating ribosomes and secure them to a given mRNA strand, ensuring that ribosomes remain roughly in place during subsequent

---

<sup>16</sup> See Chapter 1 for a discussion of the tetracyclines and mitochondrial dysregulation. See also Chapter 2 for the discovery of analogue **2.72** and a summary its mitochondrial effects.

<sup>17</sup> Chasse, H.; Boulben, S.; Costache, V.; Cormier, P.; Morales, J. *Nucleic Acids Res.* **2016**, *45*, e15.

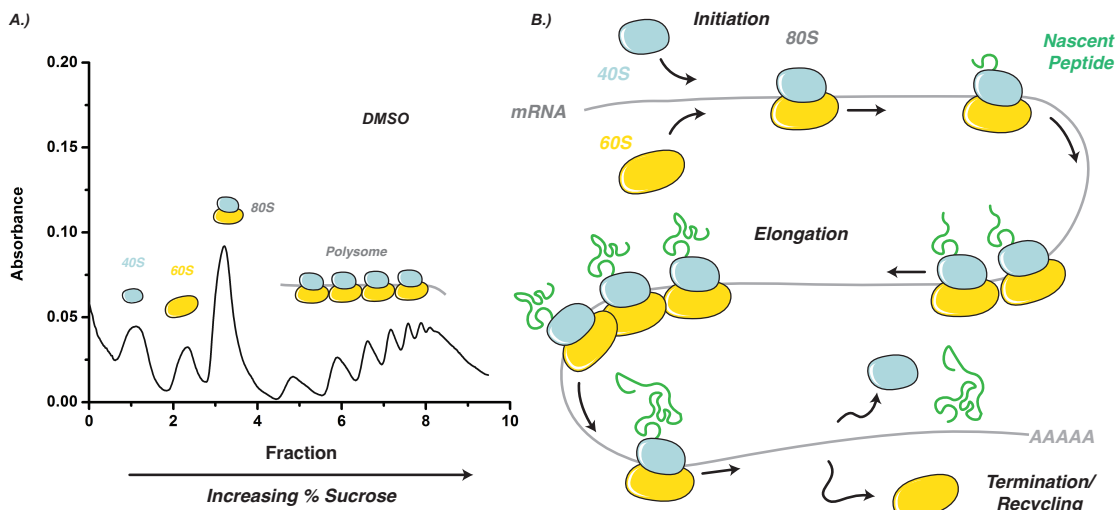


**Figure 4.5 Polysome Profiling Schematic.** A generic polysome profile is shown in A, with components labeled following stratification with sucrose gradient ultracentrifugation. These components comprise the three stages of translation (B, also Figs. 4.1, 4.2, and 4.3) and the relative differences in absorbance allow us to comment on the status of translation during small molecular treatment.

cell lysis and manipulation steps.<sup>7</sup> Cells are then lysed and the resulting crude lysates—a mixture of ribosomal RNA, proteins, and other biomolecules—loaded onto 10-50% sucrose gradients prepared in centrifuge tubes. The process of ultracentrifugation then enables the stratification of the components of the lysates by density for subsequent visualization via UV absorbance. In a typical polysome profile, the lower density components, including the 40S and 60S ribosomal subunits, elute in the earliest fractions and are followed by a large peak representing the 80S ribosome (monosome, Fig. 4.5A). The final series of peaks comprise the polysome region—the highest density components of the lysate that represent multiple ribosomes attached to a single mRNA transcript. This snapshot of ribosomal behavior (Fig. 4.5B) enables us to compare the relative quantities of ribosomal components and form broad hypotheses regarding the effects of the tetracyclines on the mechanism of translation.

To gain a general understanding of the effects of Col-3 and analogue **2.72** on translation, we conducted time course experiments in the HEK293T cell line (Fig. 4.6).

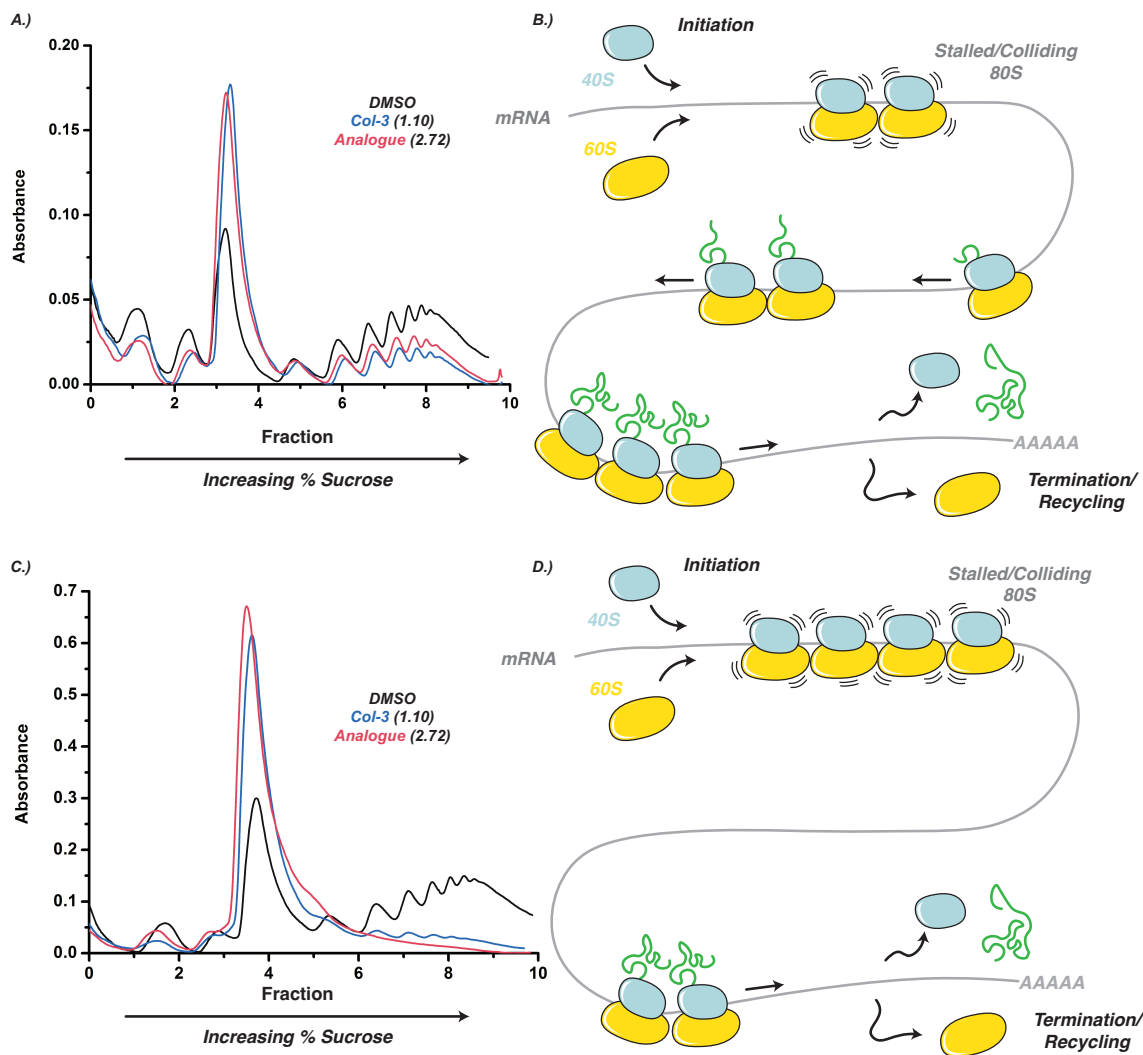


**Figure 4.6 Time Course Experiment: Col-3 and Analogue 2.72.** Polysome profiles for HEK293T cells treated with Col-3 and analogue 2.72 for 2 hours (A) and 12 hours (C). Schematics representing the suggested translational response shown in B (2 hours) and D (12 hours). Compounds dosed at 50  $\mu$ M. Experiments performed at the Gladyshev Laboratory with the assistance of Dr. Maxim Geraschenko and Nadya Makarova.

Following two hours of treatment, we note a sharp increase in the proportion of 80S monosome for both Col-3 and analogue 2.72 compared to the DMSO control (Fig. 4.6A). This is accompanied by moderate depletion of the polysome region for both compounds. This signature suggests our compounds are exerting their inhibitory effects on the initiation stage of translation, as ribosomes that are already translating (polysome region) can continue unencumbered. However, at the completion of a given mRNA transcript, these

ribosomes cycle back to the initiation stage only to encounter a blockade at the 80S monosome stage as they try to begin elongation (Fig. 4.6B). This signature is more pronounced in the 12-hour treatment condition (Fig. 4.6C), in which we again note a strong 80S monosome peak and near total depletion of the polysome region (Fig. 4.6D). Similar to the results from our in vitro translation assays, the polysome profile signatures showed little to no dependence on ISR activation after evaluation with an ISRIB co-dose experiment (Fig. S4.1). As discussed above, the initiation stage of translation is by far the most complex and energy intensive of the four stages of translation, so it is perhaps not surprising that the tetracyclines appear to be affecting this stage in human cells. Regardless, these results helped to focus our mechanistic studies to one specific stage of translation.

While we enjoyed access to polysome profiling equipment we elected to evaluate a handful of other hypotheses concerning the roles of the tetracyclines' ribosomal binding sites in translation inhibition. One hypothesis that lent itself well to evaluation by polysome profiling was ribosome-mRNA stability upon Col-3 binding. The four ribosomal binding sites identified by Mortison and colleagues all play key roles during translation, with the disruption of any one potentially leading to inhibitory effects.<sup>18</sup> We became interested in the helix h16 binding site, targeted primarily by Col-3, as it has been reported to make a number of key contacts with mRNA as it feeds into the catalytic core of the ribosome during translation initiation and elongation.<sup>19</sup> Binding of Col-3 or analogue **2.72** in this location could lead to destabilization of the incoming mRNA and cause the 80S complex

---

<sup>18</sup> See Mortison et al., **2018** (Chapter 1, ref. 26) and references cited therein.

<sup>19</sup> Martin, F.; Menetret, J.-F.; Simonette, A.; Myasnikov, A. G.; Vicens, Q.; Fix-Prongidi, L.; Natchair, S. K.; Klaholz, B. P.; Eriani, G. *Nat. Commun.* **2016**, *7*, 12622.

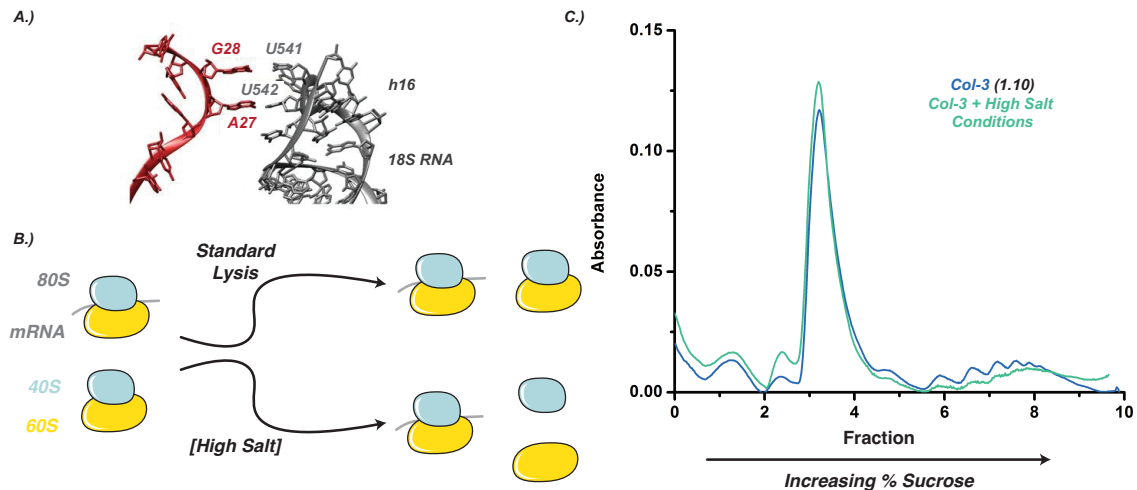


**Figure 4.7 Ribosome Stability Experiment.** Helix h16 of the eukaryotic ribosome is known to form a number of contacts with mRNA as it is fed into the peptidyl transferase center during translation (A). Given Col-3 and doxycycline binding at this location of the ribosome, we were interested in using our polysome profiling method to screen for disruptions of ribosome/mRNA binding using varying salt concentrations (B). Unfortunately, no major changes were observed in the polysome profile for Col-3 (C) or analogue **2.72** (Supplementary Fig. S4.2). Figure in A adapted from Martin et al., **2016** (Chapter 4, ref. 19).

or preinitiation complexes to split prior to elongation (Fig. 4.7A). In theory, the 80S monosome peak observed on the polysome profile could represent both competent 80S complexes (RNA-bound) and simply 40S/60S pairs that are not ready to initiate translation, but have snapped together nonetheless following mRNA disruption (Fig. 4.7B). We evaluated this hypothesis using an experimental technique for the isolation 80S ribosomes, whereby a higher concentration of NaCl and KCl is used in the wash, lysis, and sucrose buffers (250 mM vs. 50 mM) to force non-mRNA bound 80S complexes to dissociate prior to analysis.<sup>20, 21</sup> In theory, this would enable us to visualize a depletion of the 80S monosome peak and increase of the 40S and 60S subunit peaks. Unfortunately, upon

<sup>20</sup> Khatter, H.; Myasnikov, A. G.; Mastio, L.; Billas, I. M. L.; Birck, C.; Stella, S.; Klaholz, B. P. *Nucleic Acids Res.* **2014**, *42*, e49.

<sup>21</sup> Procedure developed with Dr. Maxim Geraschenko, Gladyshev Laboratory, Brigham and Womens Hospital in Boston, MA.

evaluation in high-salt conditions, we observed no major change in the ratio of the subunit peaks to the monosome peak for either Col-3 (Fig. 4.7C) or analogue **2.72** (Fig. S4.2).

In a second attempt evaluate the role of the tetracyclines' ribosomal binding sites, we utilized a crosslinking strategy to screen for the presence of stalled pre-initiation complexes or protein cofactors on the 40S or 60S subunits.<sup>22</sup> This experiment was based on several reports that describe the interaction of ribosomal helices h16 and h18 with protein cofactors during the initiation stage. For example, in addition to forming base-pairs with incoming mRNA transcripts, helix h16 has been shown to form contacts with helicase eIF4B (Fig. 4.8A), as well as eIF3 and the scanning factor DHX29.<sup>23, 24</sup> Helix h18 has been shown to form similar connections with subunits of eIF3, as well as various recycling factors (eRFs) during termination/recycling.<sup>23, 25</sup> Finally, helix H89 plays a critical role in the arrangement of ribosomal proteins during construction of the 60S subunit prior to 80S assembly.<sup>26</sup> In most cases, destabilization of these protein cofactors could lead to stalling of the 43S, 48S, or 80S complexes during the initiation stage leading to the observed polysome results (Fig. 4.8B). Under typical polysome profiling conditions, low-density proteins like stalled initiation cofactors would likely not survive the ultracentrifugation

---

<sup>22</sup> Valasek, L.; Szamecz, B.; Hinnebusch, A. G.; Nielsen, K. H. *Methods in Enzymology*, **2007**, *429*, 163-183 and references included therein.

<sup>23</sup> Eliseev, B.; Yeramala, L.; Leitner, A.; Keruppasamy, M.; Raimondeau, E.; Huard, K.; Alkalaeva, R.; Aebersold, R.; Schaffitzel, C. *Nucleic Acids Res.* **2018**, *46*, 2678-2689.

<sup>24</sup> (a) Pisarev, A. V.; Kolupaeva, V. G.; Yusupov, M. M.; Hellen, C. U. T.; Pestova, T. V. *EMBO J.* **2008**, *27*, 1609-1621. (b) Hashem, Y.; de Georges, A.; Dhote, V.; Langlois, R.; Liao, H. Y.; Grassucci, R. A.; Hellen, C. U. T.; Pestova, T. V.; Frank, J. *Cell* **2013**, *153*, 1108-1119.

<sup>25</sup> Bulygin, K. N.; Burtuli, Y. S.; Malygin, A. A.; Graifer, D. M.; Frolova, L. Y.; Karpova, G. G. *RNA* **2015**, *22*, 278-289.

<sup>26</sup> Zhou, Y.; Musalgaonkar, S.; Johnson, A. W.; Taylor, D. W. *Nat. Commun.* **2019**, *10*, 958.

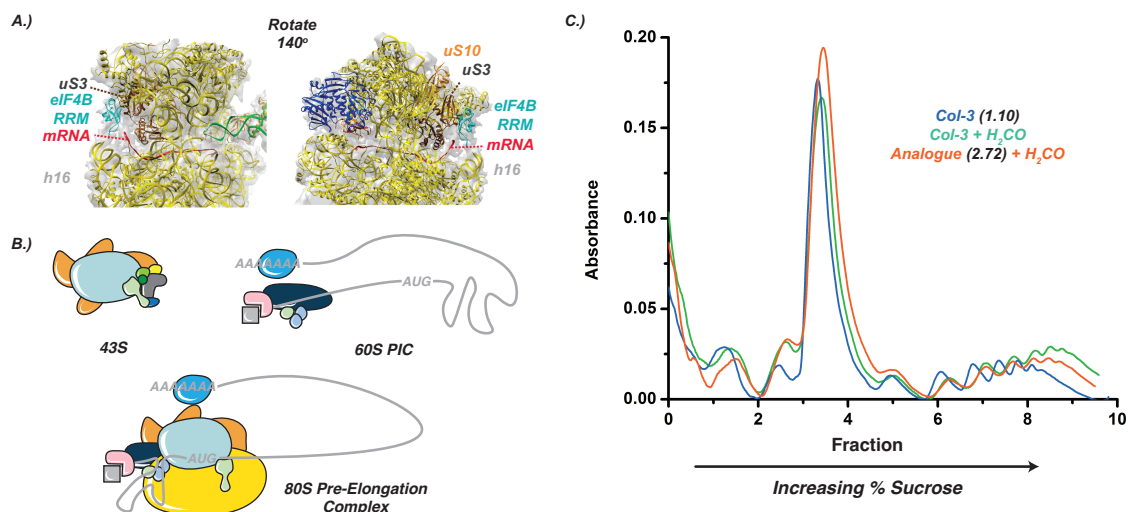


**Figure 4.8 Formaldehyde Crosslinking Experiment.** Due to the proximity of a Col-3's binding locations to ribosomal locations known to interact with initiation cofactors during translation (helix h16 example, A), we were interested in screening for protein cofactors stalled on ribosomal subunits during translation inhibition (a selection of preinitiation complexes shown in B, also, see Fig. 4.1). This experiment involved the addition of a short treatment with formaldehyde solution as a crosslinking step prior to standard polysome profiling. Sadly, we did not see any major differences in the polysome profile (C) for the un-crosslinked (blue) and crosslinked (green, orange) profiles, suggesting protein cofactors are not involved in Col-3's mechanism of ribosomal destabilization. PIC = pre-initiation complex. Figure in A adapted from Eliseev et al., **2018** (Chapter 4, ref. 23).

conditions, explaining why these effects could not be observed in our standard experiments (*vide supra*). To stabilize any pendant cofactors for centrifugation, we incorporated a formaldehyde-based crosslinking methodology into our polysome profiling experiments that should allow for visualization and characterization of these cofactors following profiling.<sup>27</sup> Procedurally, post-treatment cells were collected and exposed to 0.1% formaldehyde solution for 10 minutes prior to lysis. Excess formaldehyde was then quenched and the samples lysed and carried through the standard polysome profiling methodology. Upon evaluation of Col-3, doxycycline, and analogue **2.72**, we were disappointed to see no major differences between the crosslinked and non-crosslinked polysome profiles (Fig. 4.8C, Fig. S4.3). These results suggest that either the tetracyclines

<sup>27</sup> (a) See Valasek et al. **2007** (Chapter 4, ref. 21) and references included therein. (b) Shi, Z.; Fujii, K.; Kovary, K. M.; Genuth, N. R.; Rost, H. L.; Teruel, M. N.; Barna, M. *Mol. Cell* **2017**, *67*, 71-83 and references included therein.



are not inducing stalling of initiation cofactors on pre-initiation ribosomal complexes or whatever disruption is occurring is simply not severe enough to result in outright stalling that could be observed on the polysome trace.

In total, polysome profiling provided us with a useful methodology for evaluating the effects of our compounds on translation, particularly in identifying the initiation stage as an area for further evaluation and characterization.

#### **4.5 IRES *in vitro* Translation Analysis**

Despite our lack of results from our polysome profiling efforts, we sought to continue our analyses of the role specific protein cofactors might be playing in the inhibitory effects of the tetracyclines using dual-luciferase *in vitro* translation experiments.

These experiments utilized bicistronic reporter complexes that contain two luminescent constructs: a firefly luciferase controlled by a standard cap-dependent initiation structure and a renilla luciferase controlled by an internal ribosomal entry site (IRES). IRES's are unique RNA secondary structures that circumvent the need for select initiation cofactors, allowing for the initiation of translation on uncapped or otherwise foreign RNA transcripts (Fig. 4.9).<sup>28</sup> These RNA structures were first discovered in viruses, as a method for bypassing the standard cohort of accessory proteins involved in eukaryotic translation is central to viral pathology, and several IRESs have since been identified in eukaryotic mRNAs.<sup>29</sup> For example, an IRES element first isolated from the

---

<sup>28</sup> Komar, A. A.; Hatzoglou, M. *Cell Cycle* **2011**, *10*, 229-240.

<sup>29</sup> (a) See Komar et al., **2011** (Chapter 4, ref. 28). (b) Lee, K.-M.; Chen, C.-J.; Shih, S.-R. *Trends Microbiol.* **2017**, *25*, 546-561. (c) Komar, A. A.; Masumder, B.; Merrick, W. C. *Gene* **2012**, *502*, 75-86.

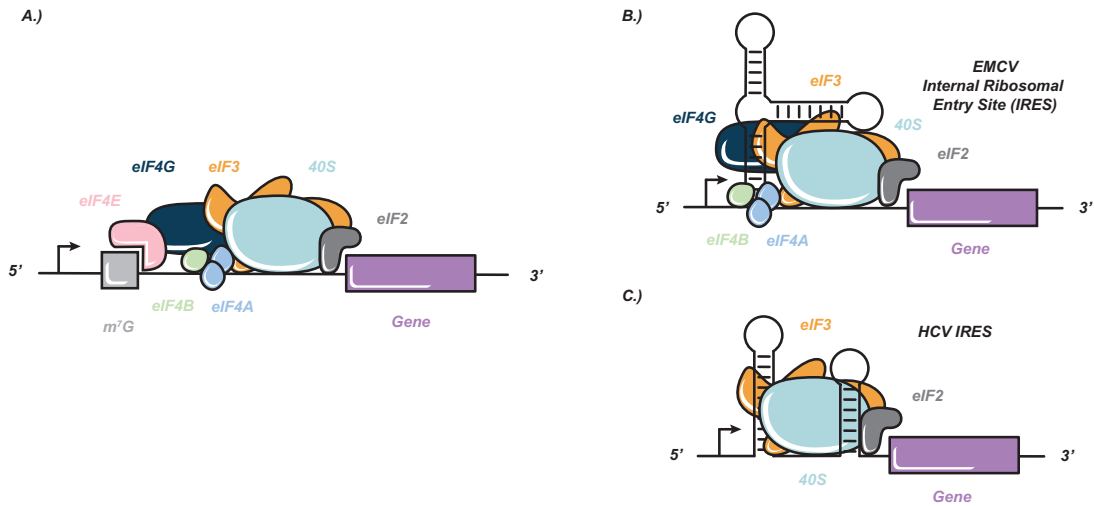


**Figure 4.9 Cap-Dependent and IRES Dependent Translation.** For most genes, translation is organized by a number of protein cofactors, largely directed by an  $m^7$ -guanosine cap structure (A, also, see Fig. 4.1). However, translation has been observed to begin without the complete assortment of initiation cofactors when a unique RNA secondary structural element is present: the internal ribosomal entry site (IRES, B, C). Several IRES's exist, each lacking one or more initiation cofactors typically required for cap-dependent translation. We utilize DNA constructs containing these plasmids to study how Col-3 effect the initiation stage of translation. Figures are cartoons not meant to represent actual RNA secondary structural information.

encephalomyocarditis virus (EMCV, Fig. 4.9B) can initiate translation without the cap-binding protein eIF4E.<sup>30</sup> In an assay format, IRESs allow us to screen for resistance to tetracycline-induced translation inhibition: should the mechanism of the tetracyclines involve disruption of a specific protein cofactor, removal of that cofactor would confer resistance. These assays have been used in the mechanistic analysis of a variety of small molecule translation inhibitors and, when compared to polysome profiling, provided us with a more precise methodology for studying cofactor involvement.<sup>31</sup> We obtained IRES reporter constructs containing the EMCV IRES (*vide supra*) as well as the hepatitis C virus (HCV) IRES (Fig. 4.9C), which obviates the need for the entire cap-binding complex

<sup>30</sup> Bochkov, Y. A.; Palmenberg, A. C.; *Biotechniques* **2006**, *41*, 286-288.

<sup>31</sup> Selected examples: (a) See Schneider-Poetsch et al., **2020** (Chapter 4, ref. 8). (b) McClary et al., **2017** (Chapter 4, ref. 9). (c) Low et al., **2005** (Chapter 4, ref. 15).

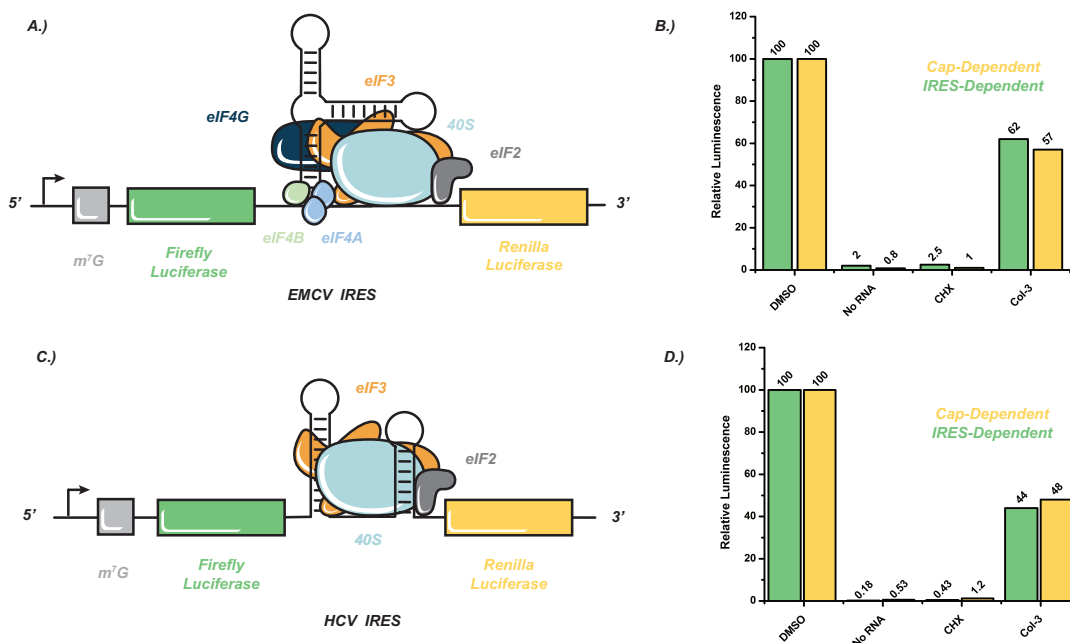


**Figure 4.10 Dual-Luciferase *In Vitro* Translation Assays.** We obtained plasmids containing bicistronic reporter complexes for both the EMCV (A) and the HCV (C) IRES structural elements. Following transcription and translation, the commercially available dual-luciferase assay kit was used to quantify the translation products for both luminescent proteins (Firefly, cap-dependent, and Renilla, IRES-dependent). Unfortunately, no major differences were noted in the translation inhibitory efficacy for the cap-dependent and IRES-dependent translation conditions for the EMCV (B) or HCV (D) systems. Compounds dosed at 50  $\mu$ M for  $\sim$ 2 hours prior to read. CHX = cycloheximide (4.2), negative control. Figures in A and C are cartoons not meant to represent actual RNA secondary structural information.

(eIF4F, containing eIFs 4A, 4B, 4E, and 4G).<sup>32, 33</sup> The plasmids were first linearized via restriction digest, then *in vitro* transcribed to the corresponding RNA. The RNA was then introduced to rabbit reticulocyte lysate translational systems and treated with the compound of interest. The translation activity was assessed using the commercially available dual-luciferase assay kit, enabling quantification of translation via luminescence on a plate reader.

Unfortunately, our results showed no major difference in the translation inhibitory efficacy of Col-3 against the EMCV or HCV IRES systems (Fig. 4.10). Col-3 would induce

<sup>32</sup> Dual-Luciferase reporter constructs were obtained as a kind gift from the laboratory of Professor Jerry Pelletier at McGill University.

<sup>33</sup> (a) See Bochkov et al., 2006 (Chapter 4, ref. 30). (b) Otto, G. A.; Puglisi, J. D. *Cell* 2004, 119, 396-380.

inhibition of both the cap-dependent and IRES-dependent reporter for both IRESs, suggesting that none of the cofactors modulated by the structures are involved in the mechanism of tetracycline-induced translation inhibition. Combining these results with those from our polysome crosslinking experiment, we began to suspect that the mechanism of tetracycline-induced translation inhibition stemmed from subtle, cooperative effects at multiple binding sites on the ribosome rather than the outright inhibition or disruption of a specific initiation cofactor(s).

#### 4.6 Ribosome Associated Quality Control System

As a final portion of our studies of translation inhibition, we sought to identify a cellular process that combined a method for monitoring subtle disruptions in translational progress with subsequent inhibition of translation and ISR activation. We identified the so-called ribosome-associated quality control complex (RQC) as one pathway for further investigation.<sup>34</sup> Broadly, the RQC represents a collection of proteins which monitor the movement of ribosomes during translation (Fig. 4.11). Should a disruption to ribosomal progress arise, the RQC recruits a series of proteins to ubiquitinate both the nascent peptide chain and the stalled ribosomal subunits, targeting them for proteasomal degradation. For many years, research focused only on RQC activity present following stalls during the elongation stage of translation, with ubiquitin ligases ZNF598 and listerin (LTN1) initiating site specific ubiquitination on the nascent peptide and subunits (Fig. 4.11A).<sup>35</sup>

---

<sup>34</sup> Joazeiro, C. A. P. *Nat. Rev. Mol. Cell Biol.* **2019**, *20*, 368-383.

<sup>35</sup> (a) See Joazeiro et al., **2019** (Chapter 4, ref. 34). (b) Brandman, O.; Hegde R. S.; *Nat. Struct. Mol. Biol.* **2016**, *23*, 7-15. (c) Inada, T. *Nuc. Acids. Res.* **2020**, *48*, 1084-1096.

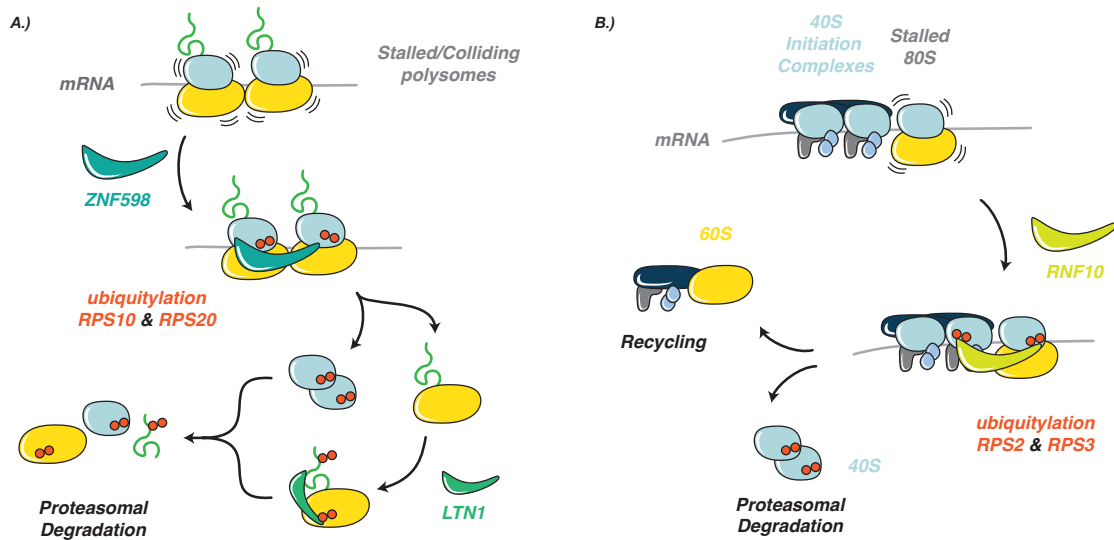


**Figure 4.11 Overview of Ribosome Associated Quality Control (RQC).** The RQC is a series of cell signaling pathways that have been identified as critical regulators of cell stress and translational control. In the case of translational aberrations, the elongation stage, ribosomal proteins S10 and S20 are ubiquitinated, along with the nascent peptide and 60S subunit (A). In the case of disruptions during the initiation stage, the RQC organizes ubiquitination of ribosomal proteins S2 and S3, targeting only the 40S subunit for proteasomal degradation (B). Figures adapted from Brandman et al., **2016** (Chapter, ref. 35b). and Garshott et al., **2021** (Chapter 4, ref. 36).

However, recent evidence has been uncovered to suggest that separate systems operate for ribosomal subunits stalled in the initiation stage of translation (Fig. 4.11B).<sup>36</sup> Here, the ligase RNF10 organizes ubiquitination of ribosomal proteins S2 and S3, targeting stalled preinitiation complexes for destruction. The RQC has also been linked to activation of the ISR, with the two processes working synergistically to maintain proteostasis and, if necessary, decrease translational loading in the event of high-frequency translational abnormalities.<sup>37</sup> For example, the close interplay between GCN2 activation and the RQC has been characterized in yeast with GCN1, the effector protein linked to GCN2 activation, forming contacts with stalled ribosomal subunits and leading to ISR activation through

<sup>36</sup> Garshott, D. M.; An, G.; Sundaramoorthy, E.; Leonard, M.; Vicary, A.; Harper, J. W.; Bennett, E. J. *Cell Rep.* **2021**, *36*, 109642.

<sup>37</sup> Garshott, D. M.; Sundaramoorthy, E.; Leonard, M.; Bennett, E. J. *eLife* **2020**, *9*, e54023 and references cited therein.

phosphorylation of eIF2.<sup>38</sup> Furthermore, a variety of dynamic feedback loops have been uncovered, including evidence that the eIF2 kinase PERK can initiate site specific regulatory ubiquitination of the 40S subunit, stimulating further RQC activation and decreasing translational loading.<sup>39</sup> In short, with its proximity to a number of cellular process associated with the mechanism of the tetracyclines, the RQC presented an exciting new target in our efforts to elucidate the mechanism of the tetracyclines in human cells.

While we have only just initiated our investigation of the RQC, our early evidence suggests that this system does indeed play a role during tetracycline-induced translation inhibition and stress response activation. Immunoblots conducted on protein lysates obtained from treated HEK293T cells show Col-3 inducing ubiquitylation of both RPS2 and RPS3 (Fig. 4.12A). Interestingly, we note this ubiquitylation appears to be strongest at

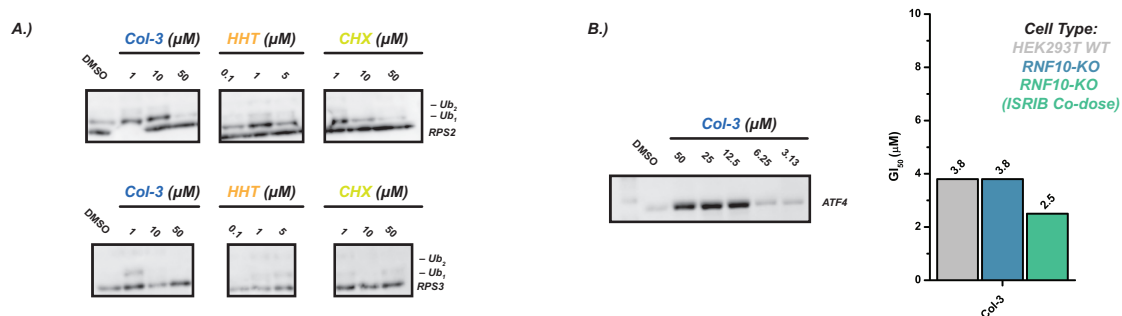


**Figure 4.12 Initial RQC Investigations.** In our early studies into the role of the RQC in surveilling translation inhibition and coordinated ISR activation, we evaluated HEK293T cells for ubiquitylation of ribosomal proteins S2 and S3 (A). Col-3 (**1.10**) was found to induce ubiquitylation at low concentrations, while higher concentrations appear to reduce ubiquitylation levels. The known translation inhibitors homoharringtonine (HHT, **4.1**) and cycloheximide (CHX, **4.2**) are included as controls. Knockout of ubiquitin ligase RNF10, however, did not attenuate ATF4 induction or growth inhibitory potency (B). Further studies are needed with this knockout cell line to fully characterize RQC activation on tetracycline treatment. The RNF10-KO cell line provided by Professor Eric Bennett was reported in Garshott et al., **2021** (Chapter 4, ref. 36). Ub = ubiquitin. ISRIB Co-Dose = 200 nM ISRIB.

<sup>38</sup> (a) Pochopien, A. A.; Beckert, B.; Kasvandik, S.; Berninghausen, O.; Beckmann, R.; Tenson, T.; Wilson, D. N. *PNAS* **2021**, *118*, e2022756118. (b) Yan, L. L.; Zaher, H. S. *Mol. Cell* **2021**, *81*, 614-628. (c) Lee, S. J.; Swanson, M.; Sattlegger, E. *Biochem. J.* **2015**, *466*, 547-559.

<sup>39</sup> Higgins, R.; Gendron, J. M.; Rising, L.; Mak, R.; Webb, K.; Kaiser, S. E.; Zuzow, N.; Riviere, P.; Yang, B.; Fenech, E.; Tang, X.; Lindsay, S. A.; Christianson, J. C.; Hampton, R. Y.; Wasserman, S. A.; Bennett, E. *J. Mol. Cell* **2015**, *59*, 35-49.

lower concentrations of Col-3. Similar concentration dependent effects were observed by Garshott and colleagues in their studies of RPS2/RPS3 ubiquitylation following translation inhibitor treatment and could suggest a number of different results, including rapid clearance of stalled ribosomes upon extended and robust stress response activation at higher inhibitor concentrations.<sup>36</sup> We also began to assess the effects of Col-3 on HEK293T cells engineered with a knockout of RNF10, the ubiquitin ligase recruited as a part of RQC activation following initiation stalling.<sup>40</sup> In our early assessments of this cell line, we do not observe any major changes in growth inhibitory potency when compared to HEK293T wild type cells, nor do we observe abrogation of ATF4 induction (Fig. 4.12B). Both readouts of signaling activity represent cumulative effects of a variety of different cellular processes, however, and further studies will be needed to fully interrogate the role the RQC is playing in mediating translation inhibition and ISR activation following Col-3 treatment.

Our investigation into the mechanism of translation inhibition has provided us with fascinating insights into the cellular responses to tetracycline treatment. Several key questions remain, including the role of the RQC and the interplay between ribosomal binding, translation inhibition, and ISR activation.

#### **4.7 Ongoing Efforts – Signaling Pathway Analysis**

While the investigation of the mechanism of translation inhibition has been our primary focus, we have also aided a series of studies into the various signaling pathways activated on tetracycline treatment and how these pathways contribute to the overall potency of the compounds. At the time of the publication of this dissertation, these efforts

---

<sup>40</sup> HEK293T Flp-In cell line containing RNF10 knockout was obtained as a kind gift from the laboratory of Professor Eric Bennett at the University of California at San Diego.

remained ongoing. As a result, in this section we hope to provide both background and a summary of our current efforts to assist future researchers in continuing these studies.

As discussed in Chapter 1, Mortison and colleagues utilized RNA sequencing, supplemented with western immunoblotting analysis, to identify and confirm activation of the ISR following tetracycline treatment through induction of ATF4 and phosphorylation of eIF2.<sup>41</sup> Interestingly, the typical kinase involved in ISR activation, PERK, was found not to be activated upon tetracycline treatment in A375 melanoma cells. Furthermore, a similar cell stress regulator, inositol-requiring enzyme 1 (IRE1) was also found to be inactive following tetracycline treatment. Combined, these results suggest Col-3 and the tetracyclines are activating a non-canonical series of signaling pathways related to the inhibition of translation and cell growth arrest. We have investigated one of these pathways—the RQC (*vide supra*)—but we remain interested in the role other eIF2 kinases may be playing in ATF4 induction and translation inhibition, particularly as they relate to potentially exploitable weaknesses in certain types of cancer.

As a part of their initial analysis, Mortison and colleagues assessed changes to the translome with and without Col-3 treatment using tandem-mass-tag (TMT)-mediated proteomics.<sup>42</sup> Renewed analysis of this raw data with updated databases did not provide any novel insights into signaling pathway progression, nor did assessment of broader

---

<sup>41</sup> See Chapter 1 for a discussion of signaling pathway analyses conducted for the tetracyclines. See also Mortison et al., **2018** (Chapter 1, ref. 26).

<sup>42</sup> Experiments performed by Dr. Jonathan Mortison of the Myers Group. Unpublished data reproduced with permission.



cellular pathways through gene ontology or KEGG pathway mapping (Fig. 4.13).<sup>43, 44</sup> Disappointed with this direction, we sought a more detailed investigation of ATF4 induction and set about characterizing the roles of other eIF2 kinases, particularly HRI, GCN2, and PKR, and their potential role in tetracycline-induced cell growth arrest. These efforts were conducted by Kamar Reda, research technician in the Myers Group, and spanned several different methodologies. We initially explored probing the role of each eIF2 kinase with standard immunoblotting techniques and siRNA-mediated knockdown in an attempt to correlate loss of certain kinases with attenuation of ATF4 induction.<sup>45</sup> Unfortunately, we encountered challenges in generating knockdowns of effective strength and in sourcing antibodies that would reproducibly enable visualization of eIF2 kinases like HRI and GCN2. We also explored pharmacologic disruption of eIF2 kinases as a

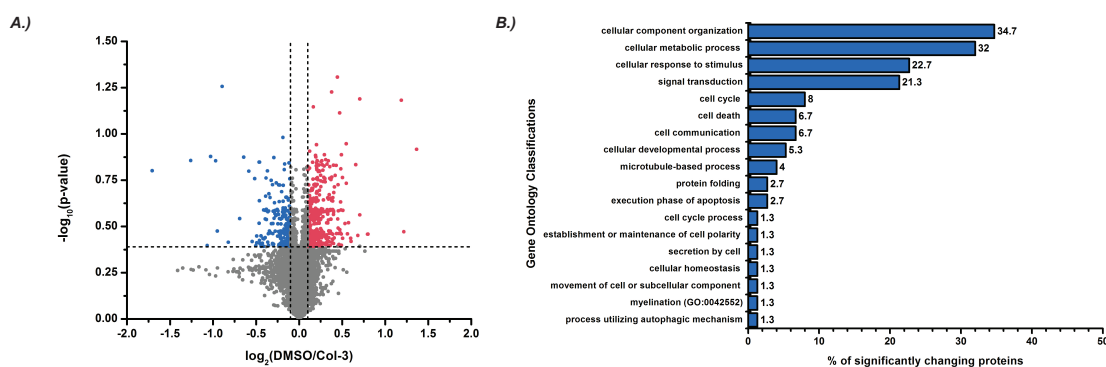


**Figure 4.13 Proteomics Analysis Reveals No New Information.** As an early part of our signaling pathway analysis, we resubjected proteomics data obtained by Dr. Jonathan Mortison to scrutiny in updated databases. Mortison and colleagues had conducted proteomics experiments on A375 melanoma and HCT116 colorectal cancer cell lines at 6 and 24 h treatment timepoints (A375, 6 h experiment shown in A). Renewed analysis of these data, including gene ontology mapping (B, A375 6 h, upregulated proteins) revealed stress signatures similar to those observed in the initial analysis. HCT116 data not shown. Raw data provided by Dr. Jonathon Mortison.

<sup>43</sup> Gene ontology analysis was conducted using PantherGO software: Mi, H.; Muruganujan, A.; Huang, X.; Ebert, D.; Mills, C.; Guo, X.; Thomas, P. D. *Nat. Protoc.* **2019**, *14*, 703-721.

<sup>44</sup>KEGG Pathway Mapping conducted using the KEGG online database: <https://www.genome.jp/kegg/pathway.html>. (Accessed November 2021).

<sup>45</sup> Experiments performed by Dr. Linfeng Chen and Kamar Reda in the Myers Group. Unpublished data.

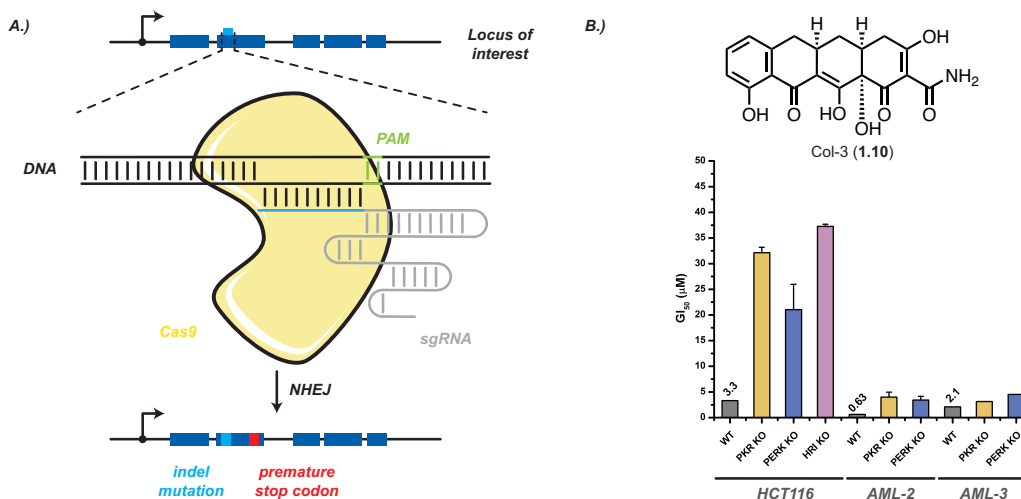


**Figure 4.14 CRISPR-mediated Knockout of ISR Kinases.** As a method for further evaluating the role of the various ISR kinases in mediating stress response activation following tetracycline treatment, efforts lead by Kamar Reda in the Myers Group produced a series of cell lines harboring knockouts of the kinases PERK, PKR, GCN2, and HRI. These cell lines were generated using CRISPR/Cas9 technology (A). While our investigation of these cell lines is ongoing, initial growth inhibitory data shows that knockout of these kinases alters growth patterns for certain cells. Knockout cell lines generated by Kamar Reda.

method to screen for involvement in tetracycline induced ATF4 activation, however difficulties related to specificity of binding and the lack of known inhibitors targeting HRI soured these efforts.<sup>46</sup> We ultimately settled on the generation of a series of knockout cell lines using CRISPR/Cas9 methodology. These efforts remain underway, however Kamar Reda succeeded in generating knockouts of PERK, PKR, GCN2, and HRI in a variety of different cancer cell lines including HCT116 colorectal cancer, K562 leukemia, and OCI-AML-2/3 leukemia models. We have only begun evaluation of signaling responses in these cell lines, however early results have shown that the lack of certain kinases can produce a

<sup>46</sup> A selection of literature discussing kinase inhibitors for eIF2 kinases. **PERK**: Mahameed, M.; Wilhelm, T.; Darawshi, O.; Obiedat, A.; Tommy, W.-S.; Chintla, C.; Schubert, T.; Samali, A.; Chevet, E.; Eriksson, L. A.; Hubert, M.; Tirosh, B. *Cell Death & Disease* **2019**, *10*, 300. (b) Axten, J. M.; Romerli, S. P.; Shu, A.; Ralph, J.; Medina, J. R.; Feng, Y.; Li, W. H. H.; Grant, S. W.; Heering, D. A.; Minthorn, E.; Mencken, T.; Gaul, N.; Goetz, A.; Stanley, T.; Hassell, A. M.; Gampe, R. T.; Atkins, C.; Kumar, R. *ACS Med. Chem. Lett.* **2013**, *4*, 964-968. **GCN2**: Nakamura, A.; Nambu, T.; Ebara, S.; Hasegawa, Y.; Toyoshima, K.; Tsuchiya, Y.; Tomita, D.; Fujimoto, J.; Kurasawa, O.; Takahara, C.; Ando, A.; Nishigaki, R.; Satoma, Y.; Hata, A.; Hara, T. *PNAS* **2018**, *115*, 7776-7785. **PKR**: Jammi, N. V.; Whitby, L. R.; Beal, P. A. *Biochem. Biophys. Res. Commun.* **2003**, *308*, 50-57. **HRI**: Zhang, Q.; Du, R.; dos Santos, G. R. R. M.; Yefidoff-Freedman, R.; Bohm, A.; Halperin, J.; Chorev, M.; Aktas, B. H. *Eur. J. Med. Chem.* **2020**, *187*, 111973.

range of effects on cell growth patterns (Fig. 4.14B). We note an increase in growth inhibitory activity for Col-3 in all HCT116 knockouts tested while the knockouts of PERK and PKR in OCI-AML-2 and -3 show little difference compared to the wild type controls. These cell lines present an exciting start to an important line of inquiry in our signaling pathway analysis efforts with further studies needed to evaluate ATF4 activation and translation inhibitory effects in each knockout.

Our signaling pathway investigations have spanned several different methodologies, however, we believe our efforts have left open a variety of interesting areas of study for future chemical biologists interested in signaling pathway interrogation.

#### **4.8 Conclusions and Path Forward**

In addition to our synthetic studies, we were interested continuing the efforts started by Dr. Jonathan Mortison to examine and better understand the origin of the non-canonical effects of the tetracyclines in human cells, particularly regarding their potential as cancer therapeutics. The majority of our efforts focused on ribosomal binding and translation inhibition and we employed a variety of biochemical techniques to explore the effects of Col-3 treatment on ribosomal behavior. Polysome profiling experiments suggested Col-3 was exerting its inhibitory effects during the initiation stage of translation, but subsequent polysome experiment and *in vitro* translation experiments failed to uncover specific protein cofactors involved in this mechanism. We then pivoted our investigation to a translation monitoring system known as the RQC and identified activation of this system following Col-3 treatment that could be contributing to ISR activation following translation inhibition. Several lines of inquiry remain open in these efforts, both focused on the RQC

and translation inhibition and with our more general signaling pathway analysis efforts. In total, we believe our mechanistic studies have contributed to our understanding of the origins of the tetracyclines antiproliferative effects on human cells and have taken another step toward the development of the tetracyclines as therapeutics with well-defined activities in human cells.

As discussed in Chapter 3, there are several key outlets that could be explored in future studies. Related to structural understanding and further analogue development, cryo-EM co-structures of the tetracyclines bound to eukaryotic cytosolic and mitochondrial ribosomes would be instrumental for generating tetracyclines for specific disease applications. In the short term, we believe these compounds would benefit from a large, multiplexed screening assay to identify certain cell lines or cancers predisposed to growth inhibition by the tetracyclines and aid in establishing therapeutic index for certain diseases.<sup>47</sup> While our mechanistic studies have uncovered some useful information, it has also become clear that the tetracyclines are intimately involved in a dense network of signaling responses related to a number of translational surveillance and protective systems, including the RQC, the ISR, and others. Disentanglement of these pathways remains a formidable challenge and, while interesting from a basic research point of view, may not assist in the development of the tetracyclines as therapeutics for specific types of cancer. Combining further mechanistic studies with profiling efforts focused on identification of effective therapeutic index would provide a holistic mechanistic understand that can also play a central role in progressing antiproliferative tetracyclines to the clinical stage. The tetracyclines represent a class of natural product small molecules

---

<sup>47</sup> An example assay: PRISM: Multiplexed Cell Line Profiling, Broad Institute. URL: [www.theprismlab.org](http://www.theprismlab.org) (Accessed November 5, 2021).

with considerable untapped potential for treating a variety of human diseases and we believe that with continued studies in both the synthesis of novel tetracyclines and mechanistic elucidation efforts that these compounds could, one day, make an impact in the clinic.

## 4.9 Experimental Section

**Mammalian Cell Lines and Cell Culture.** All compounds were dissolved in sterile DMSO (Millipore) to a stock concentration of 20  $\mu$ M and aliquoted prior to freezing at  $-20$  °C. Aliquots were limited to a maximum of 3 freeze–thaw cycles.

**Materials.** K562 (human chronic myelogenous leukemia; female) cells were cultured in Iscove’s Modification of DMEM (IMDM) media supplemented with 10% fetal bovine serum. HCT116 (human colorectal carcinoma; male) cells were cultured in McCoy’s 5a (Iwakata & Grace Modification) media supplemented with 10% fetal bovine serum. HEK293T (human embryonic kidney) and HEK293FlpIn RNF10-KO cells were cultured in DMEM media supplemented with 10% fetal bovine serum. All cell cultures were maintained in a 5% CO<sub>2</sub> incubator at 37 °C.

**Polysome Profiling: General Procedure.** Polysome profiling experiments were conducted in the laboratory of Professor Vadim Gladyshev at Brigham and Women’s Hospital in Boston, MA and the following procedure was adapted from that developed by Dr. Maxim Geraschenko.<sup>48</sup> HEK293T cells were cultured to near confluence (80-90%) in 15-cm culture plates (Thermo-Fisher). The culture medium was replaced, and the tetracycline was added for the desired dosing time. Upon completion of the treatment, the media was aspirated, and the cells were washed once with the ice-cold buffer: 20 mM Tris-HCl, 50 mM NaCl, 50 mM KCl, 10 mM MgCl<sub>2</sub>, 0.1 mg/ml cycloheximide while attached

---

<sup>48</sup> Personal conversation and experimental guidance from Dr. Maxim Geraschenko, Gladyshev Group, Brigham and Women’s Hospital, Boston, MA.

to the cell culture plate. Lysis was conducted in the same buffer as above supplemented with 1% Triton X100, protease inhibitors without EDTA (Roche), 1 mM DTT, and 40 U/ml RNAsin® Plus Ribonuclease Inhibitor (Promega). Cell debris was removed by the centrifugation at 12,000 g for 4 min. Cleared lysates were loaded on 10–50 sucrose gradients and spun for 3 hours at 35,000 g. The centrifuge tubes were then analyzed using a Bio-Rad UV analysis system and the UV absorption data visualized using LoggerPro software. The raw data was then processed and analyzed using Microsoft Excel and RStudio. Plots were generated using Origin graphing software.

**Polysome Profiling: ISRIB Co-Dose Experiments.** For ISRIB co-dose conditions, ISRIB was added to the chosen tetracycline treatment at a final concentration of 200 nM. The cell treatment, lysis, and polysome analysis was completed in the same manner as above.

**Polysome Profiling: Ribosomal Stability Experiments.** For the ribosomal stability experiments (high-salt), identical experimental conditions were used as described above, with the exception that the 50 mM concentrations of NaCl and KCl in the wash, lysis, and sucrose buffers were replaced with 250 mM NaCl and KCl.

**Polysome Profiling: Crosslinking Experiments.** The formaldehyde crosslinking experiments were conducted using procedures similar to those described by Shi et al., *Mol. Cell* **2017**.<sup>49</sup> Briefly, immediately following tetracycline treatment, cells were washed with

---

<sup>49</sup> See Shi et al., **2017** (Chapter 4, ref. 27b) and references cited therein.

the aforementioned buffers and collected. The cells were then treated with wash buffer supplemented with 0.1% formaldehyde for 10 minutes at 23 °C. Cells were then treated with 1/10<sup>th</sup> volume of quenching buffer (2.5M glycine, 25mM Tris base) and mixed slowly. The cells were then centrifuged briefly and lysed according to the above procedure.

**IRES Dual-Luciferase Reporter Assays.** Plasmids corresponding to the desired dual-luciferase reporter vectors were obtained from the laboratory of Professor Jerry Pelletier at McGill University. The following procedure was adapted from procedures developed by Professor Jerry Pelletier and the laboratory of Professor Jun Liu (Johns Hopkins University).<sup>50, 51</sup> The reporter plasmids were first linearized with BamH1 and visualized via gel electrophoresis. *In vitro* translation kits featuring SP6 polymerase (HCV vector) and T3 polymerase (EMCV vector) were obtained from Thermo-Fisher Scientific and used according to the manufacturer's instructions for the incorporation of the m<sup>7</sup>-guanosine cap structure. Transcripts were then isolated using an RNeasy RNA isolation kit (Qiagen). The resulting transcript (~200 ng) was then added to 25 µL rabbit reticulocyte lysate (RRL) *in vitro* translation system reactions (Promega) and incubated with the desired concentration of small molecule for 30 min to 2 hours. Aliquots of the reaction mixtures were then analyzed for the expression of luciferase and renilla luminescence using a Dual-Luciferase Reporter Assay System (Promega) and the resulting signal measured using a

---

<sup>50</sup> Selected example: Cencic, R.; Carrier, M.; Galicia-Vasquez, G.; Bordeleau, M.-E.; Sukarieh, R.; Bourdeau, A.; Brem, B.; Teodoro, J. G.; Greger, H.; Tremblay, M. L.; Porco Jr., J. A.; Pelletier, J. *PLoS One* **2009**, *4*, eS223.

<sup>51</sup> See Schneider-Poetsch et al., **2010** (Chapter 4, ref. 8) and references cited therein.



SpectraMax i3x plate reader (Molecular Devices). The raw data was processed using Microsoft Excel and plots were generated using Origin graphing software.

**Growth Inhibition Assays.** The growth inhibition assays used to evaluate compound potency in mammalian cells was adapted from Magauer et al., **2013**.<sup>52</sup> Briefly, cells were grown to approximately 80% confluence, and then were trypsinized, collected, and pelleted by centrifugation (3 min at 2,000 rpm, 23 °C). The supernatant was discarded and the cell pellet was resuspended in 10 mL of fresh medium. A sample was diluted 10-fold in fresh medium, and the concentration of cells was determined using a Scepter Cell Sensor automated cell counter. The cell suspension was diluted to a concentration of 5000 cells/mL. Stock solutions of each compound in DMSO were diluted serially with DMSO to provide 7 600X concentrations and one vehicle control for a total of 8 samples/drug. The drug dilutions were then added to a 96-well deep well plate and each mixed with 600  $\mu$ L cell/media solution. The cells/drugs were mixed and 100  $\mu$ L was added to 5 rows of a pre-sterilized 96-well plate. A final column was filled with 100  $\mu$ L culture media to serve as a no cells control. Typical tetracycline concentrations began with 100  $\mu$ M and decreased via a log<sub>2</sub>-scale over 7 total dilutions. Less concentrated dilutions were used for more potent compounds. After incubating at 37 °C for 72 h (5% CO<sub>2</sub>), 20  $\mu$ L of resazurin solution (Promega CellTiter-Blue® Cell Viability Assay) was added to each well. After incubating at 37 °C for 4 h (5% CO<sub>2</sub>), the fluorescence (544 nm excitation/590 nm emission) was recorded using a microplate reader (SpectraMax i35x) as a measure of viable cells. Percent growth inhibition was calculated for each well, based upon the following formula: Percent

---

<sup>52</sup> Magauer, T.; Smaltz, D. J.; Myers, A. G. *Nat. Chem.* **2013**, *5*, 886-893.

growth inhibition =  $100 \times (S - B_0) / (B_t - B_0)$  where S is the sample fluorescence, B<sub>t</sub> is the average fluorescence of an untreated population of cells at the completion of the assay, and B<sub>0</sub> is the average fluorescence of an untreated population of cells at the beginning of the assay. Each compound was assayed at seven separate concentrations per experiment. The percent inhibition at each concentration was plotted against log(concentration), and a curve fit was generated using Excel (Microsoft). GI50 values were computed to reflect the concentrations at which the resulting curves pass through 50% inhibition.

**Western Immunoblotting.** Western blot procedure was adapted from Mortison et al., 2018 by Dr. Linfeng Chen.<sup>53</sup> Briefly, samples were prepared with cleared cellular lysates in RIPA buffer containing protease/phosphatase inhibitor cocktail (Pierce) and normalized with a BCA assay kit. The lysates were diluted with 4X LDS loading buffer (Invitrogen) + 10X NuPAGE sample reducing agent, mixed via vortex, and heat denatured at 70 °C for 5 min. The samples were then loaded (10-20 µg protein/lane) onto 4-12% Bis-Tris Gels (Invitrogen) and electrophoresis was carried out at constant voltage: 50 V for 30 min then 150 V for 90 min in 1X MOPS Running Buffer with NuPAGE antioxidant (Invitrogen). The MW standard for visualization was the Biotinylated Protein Ladder Detection Pack (Cell Signaling Technology). The protein bands were then transferred to a 0.2 nitrocellulose (Cell Signaling Technology) membrane at 1.25 A (constant) per gel-membrane sandwich for 12 min on a semi-dry Pierce Power Blotter with Pierce 1-Step Transfer Buffer. The membranes were washed for 5 min in 1X TBS and blocked in 2% nonfat milk in 1X TBST for 1 h at 23 °C. The blocking solution was removed, and the

---

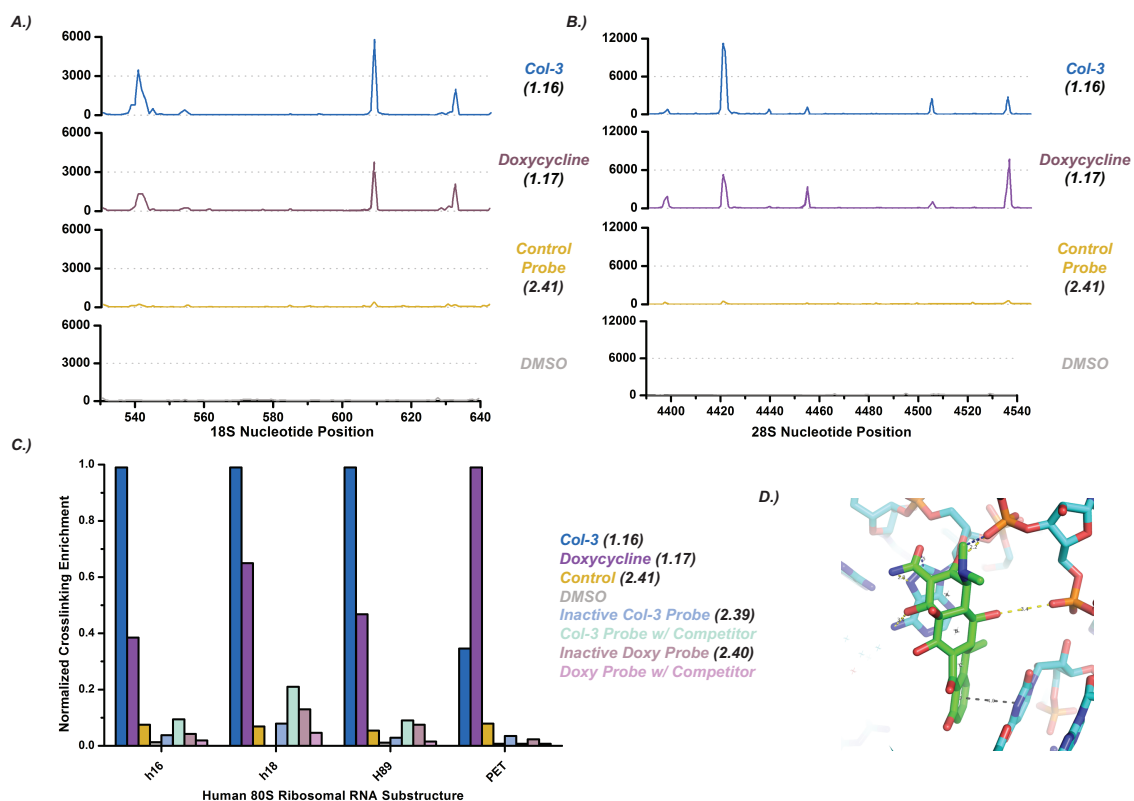
<sup>53</sup> See Mortison et al., 2018 (Chapter 1, ref. 26).

primary antibodies were diluted into in 5% BSA in TBST (see below for typical dilutions), followed by incubation with the membranes overnight (18 h) at 4 °C. Following overnight incubation, primary antibodies were removed, and the blots were washed with 3 x 10 mL 1X TBST for 5 min/wash. The blots were then incubated with the appropriate rabbit or mouse secondary antibody (Promega, Cell Signaling Technologies) in 5% nonfat milk in 1X TBST. The secondary antibody was then removed, and the blots were washed with 3 x 10 mL 1X TBST for 5 min/wash. The blots were then incubated with Immobilon Forte Reagent (Millipore) for 1 min and the chemiluminescent signal was visualized on an Azure Biosystems Sapphire Biomolecular Imager. Following visualization, the blots were washed with 1X TBS, stripped with Pierce PLUS Western Stripping Buffer, and re-washed with 1X TBS. Blots were then re-blocked and re-probed. Stripping and re-probing was carried out no more than 3 times on a single blot.

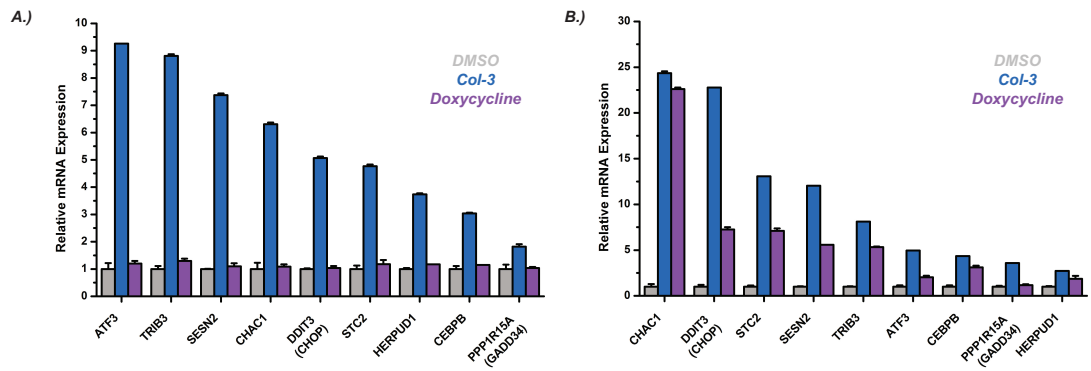
- Rabbit monoclonal anti-RPS2 (Bethyl Laboratories): 1:1,000
- Rabbit monoclonal anti-RPS3 (Bethyl Laboratories): 1:1,000
- Anti-ATF4 (D4B8) Rabbit mAb (Cell Signaling): 1:1,000
- Anti-Rabbit IgG (H+L), HRP Conjugate (Cell Signaling): 1:2,500
- Biotinylated Protein Ladder Detection Pack (Cell Signaling): 1:1,000

## **Appendix A**

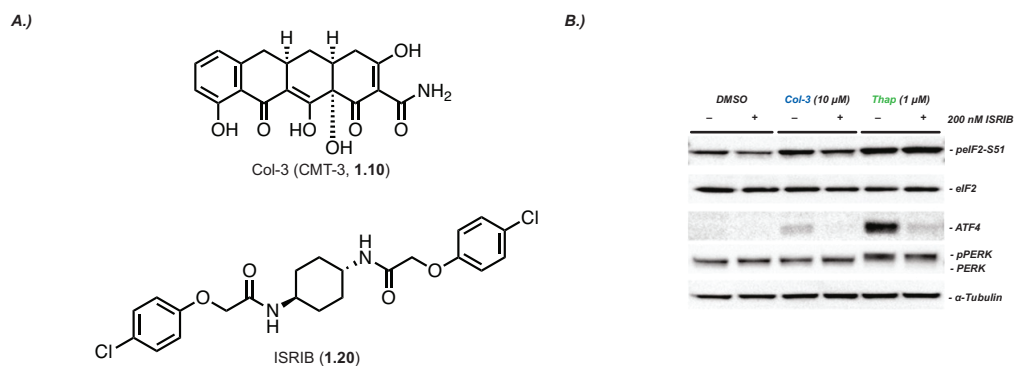
### **Supplementary Figures**



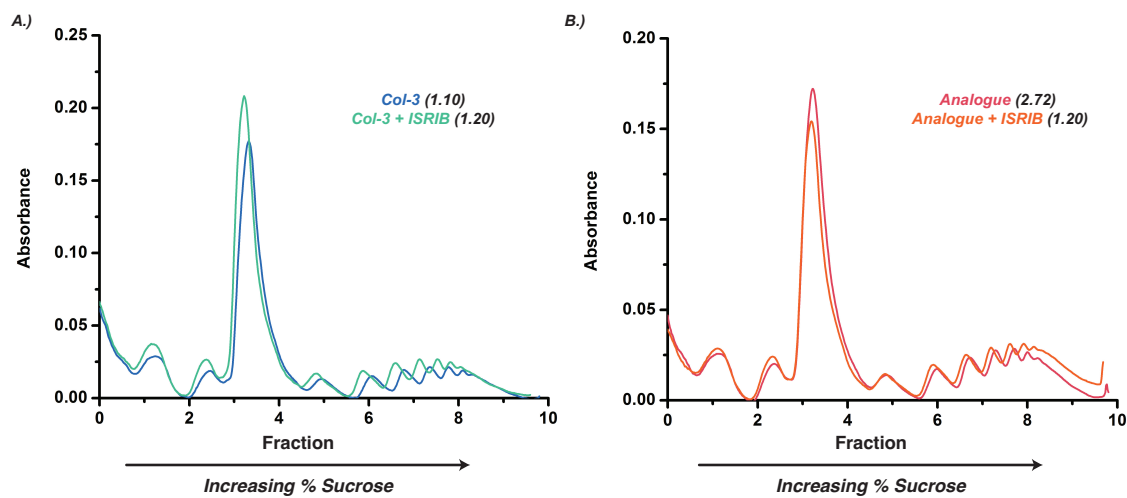
**Figure S1.1 Photoaffinity Labeling Experiment – Additional Figures.** These additional figures show the complete scale of the photoaffinity labeling experiments conducted by Mortison and colleagues during the target identification studies. The figures in A and B show the “stops” in reverse transcription caused by crosslinked tetracyclines (or control compounds) encountered during sample processing. These stops were then mapped to the ribosomal RNA sequence and the RNA substructures quantified (C). Various control compounds were used in these experiments (see also Fig. 2.7 for structures). These studies were later corroborated by structural data obtained by the Klaholz group at the University of Strasbourg in France. Prof. Bruno Klaholz and colleagues obtained a co-structure of doxycycline (**1.4**) bound to the human 80S ribosome in the peptide exit tunnel at the precise location predicted in Mortison’s PAL studies. Figs. A, B, and C adapted from Mortison et al., **2018** (Chapter 1, ref. 26) with permission. Image in D courtesy of Prof. Bruno Klaholz, unpublished data.



**Figure S1.2 RNA Sequencing Results – Additional Figures.** In addition to the RNA sequencing results shown in Fig. 1.7, Mortison and colleagues utilized NanoString technologies to visualize ISR activation in K562 leukemia (A) and HCT116 colorectal cancer (B) cell lines. Combined with the results from the A375 melanoma cells, these experiments show that activation of the ISR as a common pathway in human cells following tetracycline treatment. Figures adapted from Mortison et al., **2018** (Chapter 1, ref. 26).

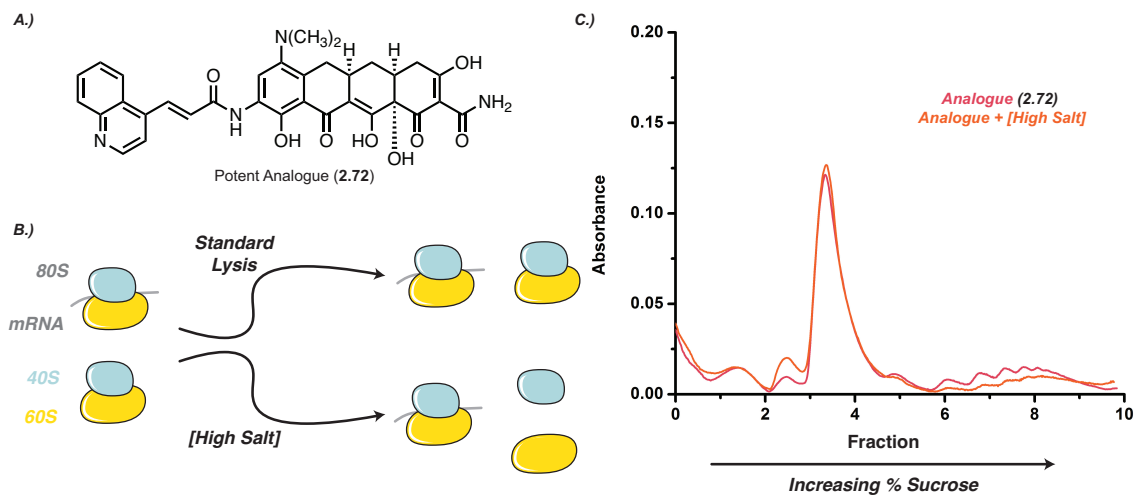


**Figure S1.3 ISR Activation and ISRIB Co-Dose.** Immunoblotting experiments show clear reduction of ATF4 activation upon co-dose with 200 nM ISRIB (1.20). As expected, phosphorylation of eIF2 remains unchanged. Thap = Thapsigargin, blanket ISR activator and positive control.

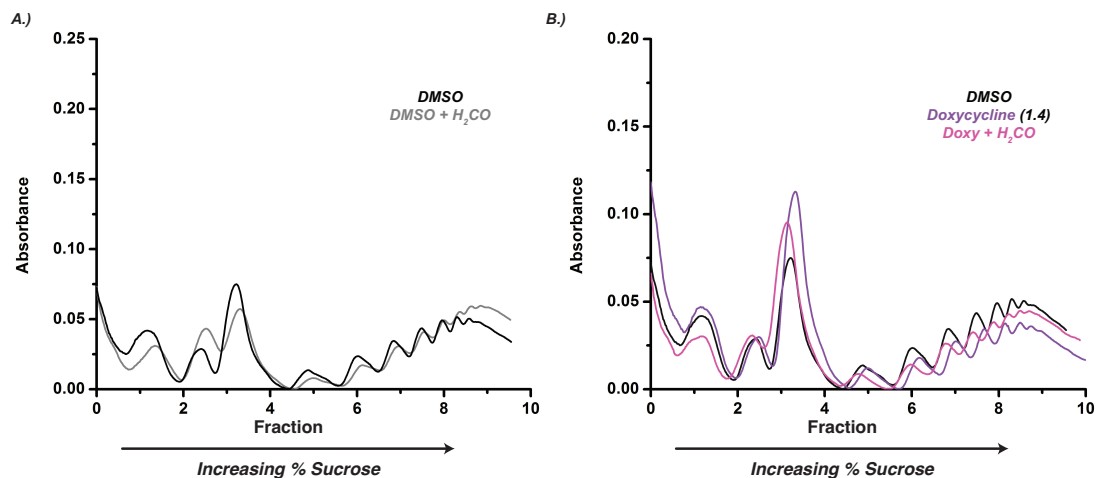


**Figure S4.1 Polysome Profiling Results – ISRIB Co-Dose Experiment.** Similar to our results in standard translation inhibition experiments, our polysome profiling results show no dependence on ISR activation during ISRIB co-dose experiments. HEK293T cell line dosed for 2 hours with 50  $\mu$ M Col-3 (**1.10**) or analogue **2.72** with or without 200 nM ISRIB (**1.20**). Experiments performed at the Gladyshev Laboratory with the assistance of Dr. Maxim Geraschenko.





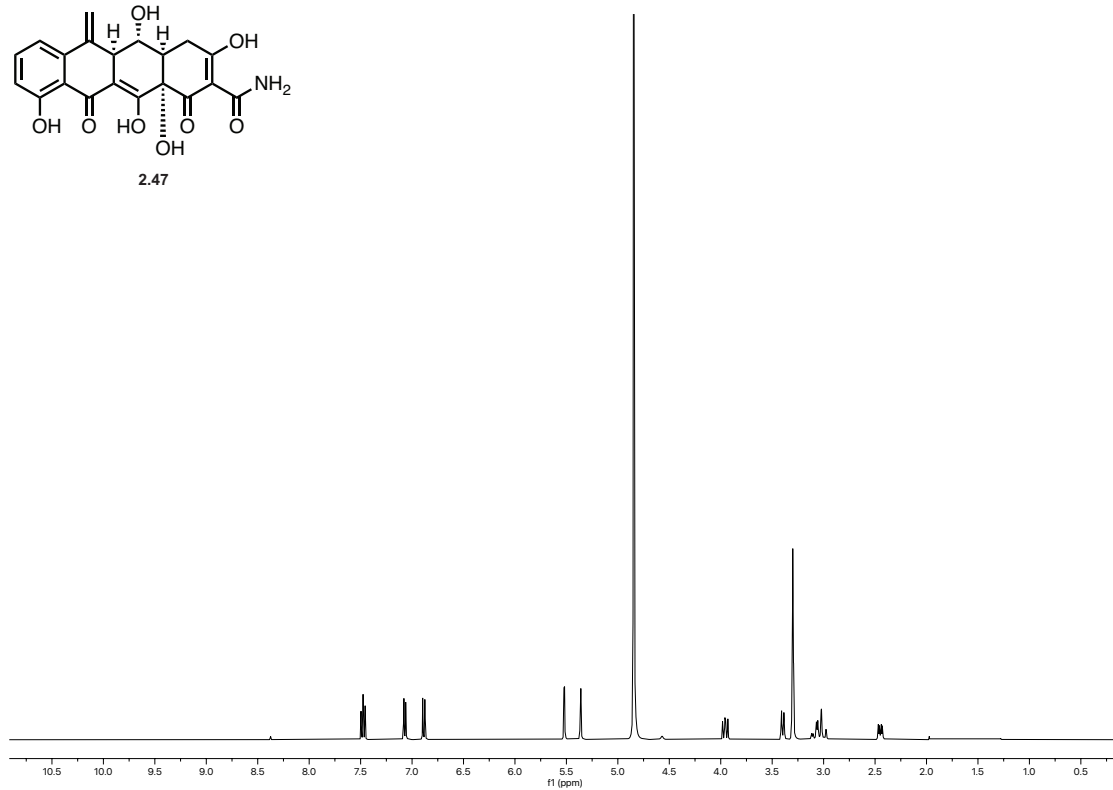
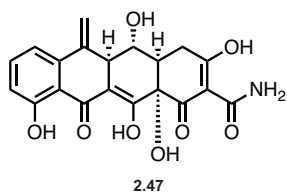
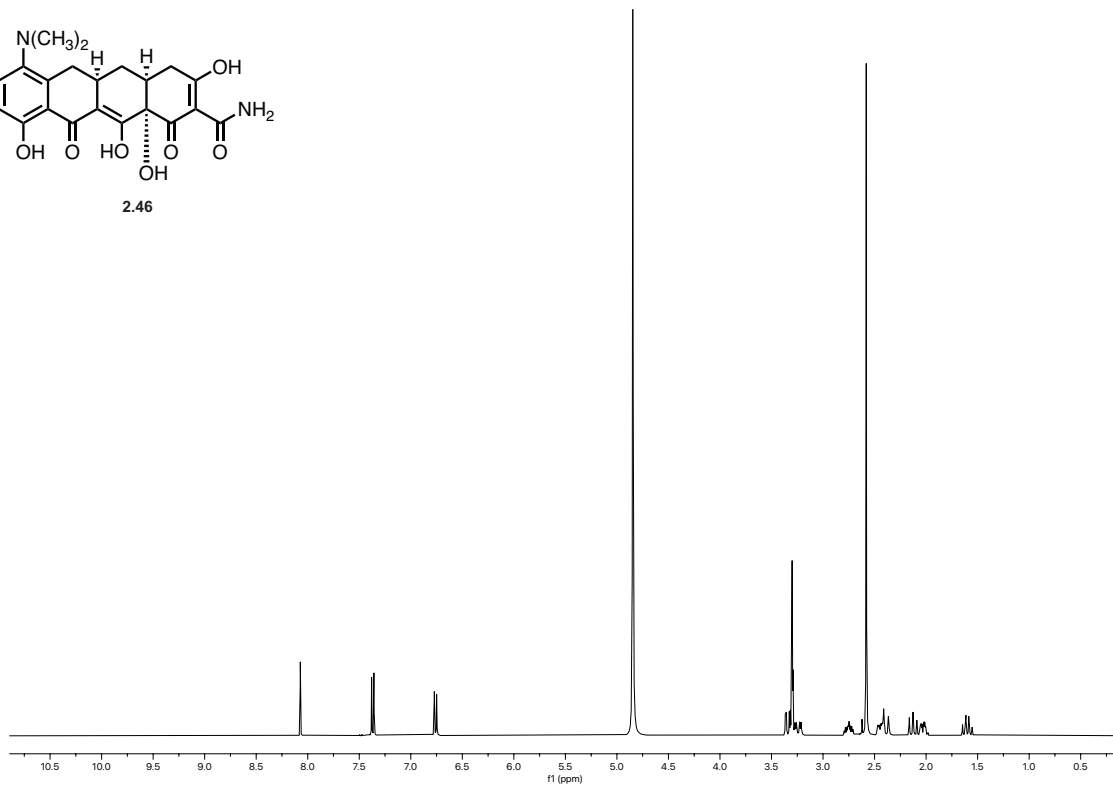
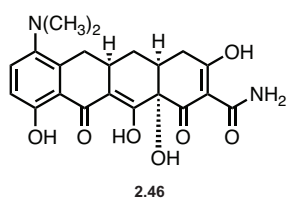
**Figure S4.2 Polysome Profiling Results – Analogue 2.72 and High Salt.** As described for our Col-3 experiment (Fig. 4.7), polysome profiling with analogue 2.72 in high salt concentration did not show any signs of instability of the RNA/ribosome complex. These findings suggest the tetracyclines Col-3 and analogue 2.72 are not destabilizing incoming RNA transcripts during translation initiation or elongation. Experiments performed at the Gladyshev Laboratory with the assistance of Dr. Maxim Geraschenko.

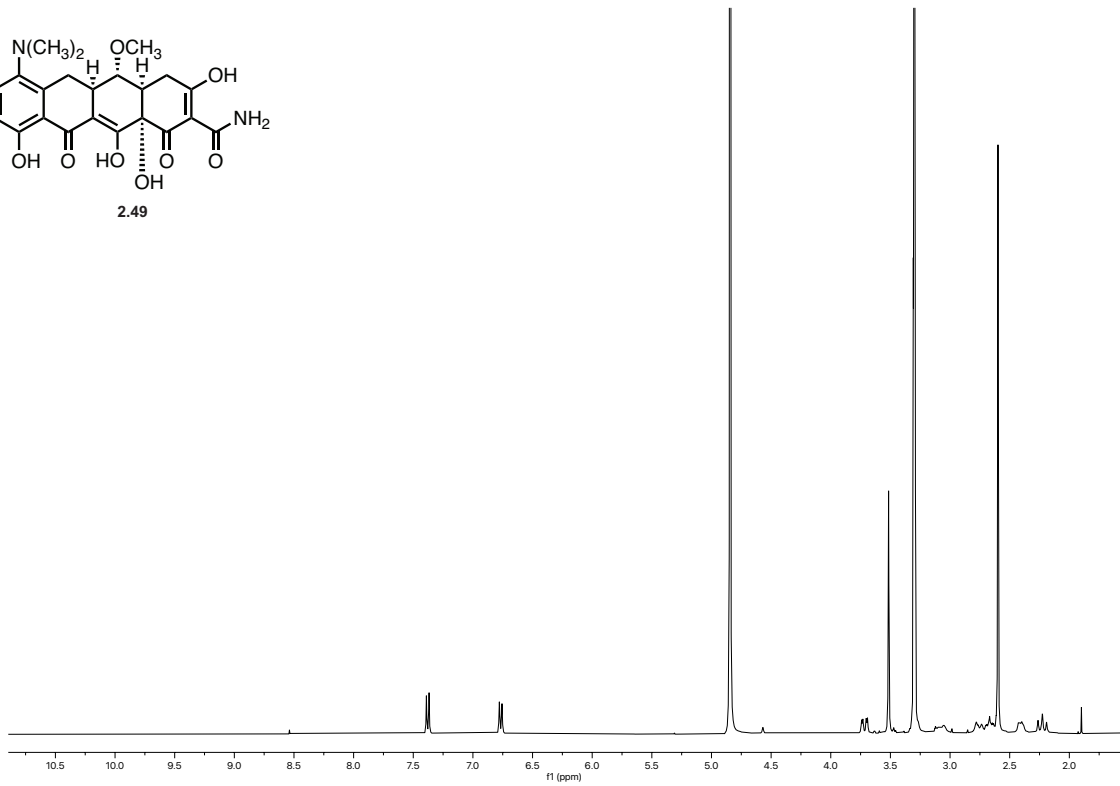
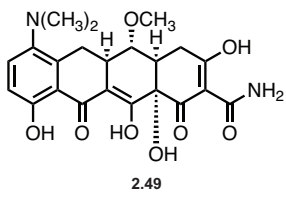
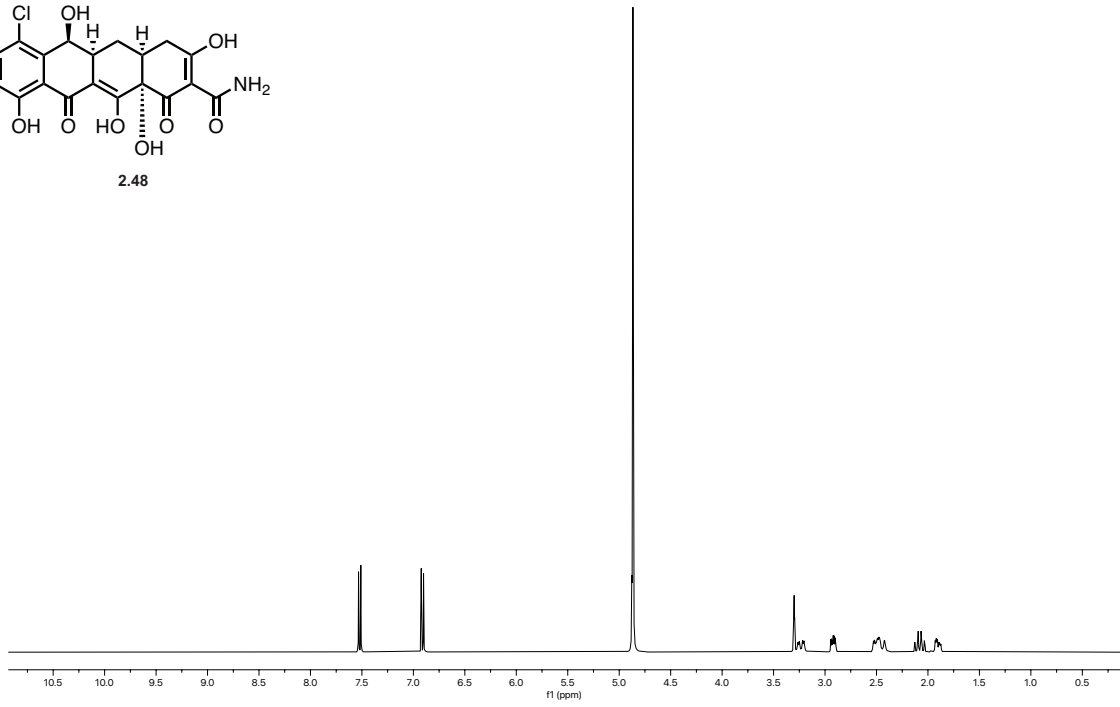
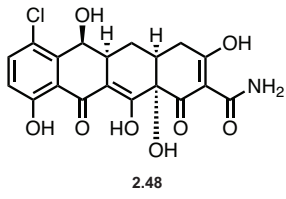


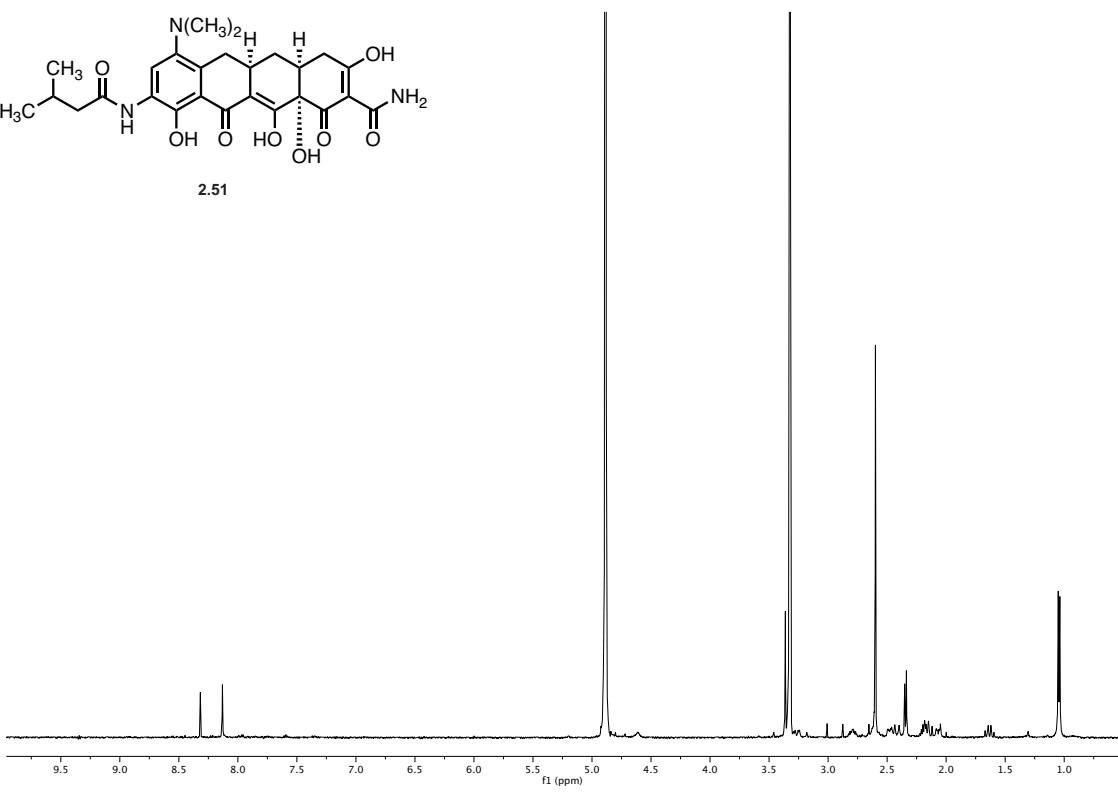
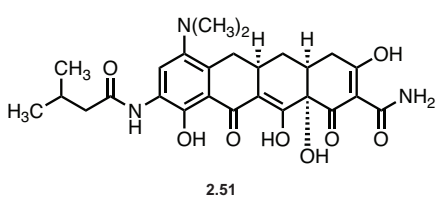
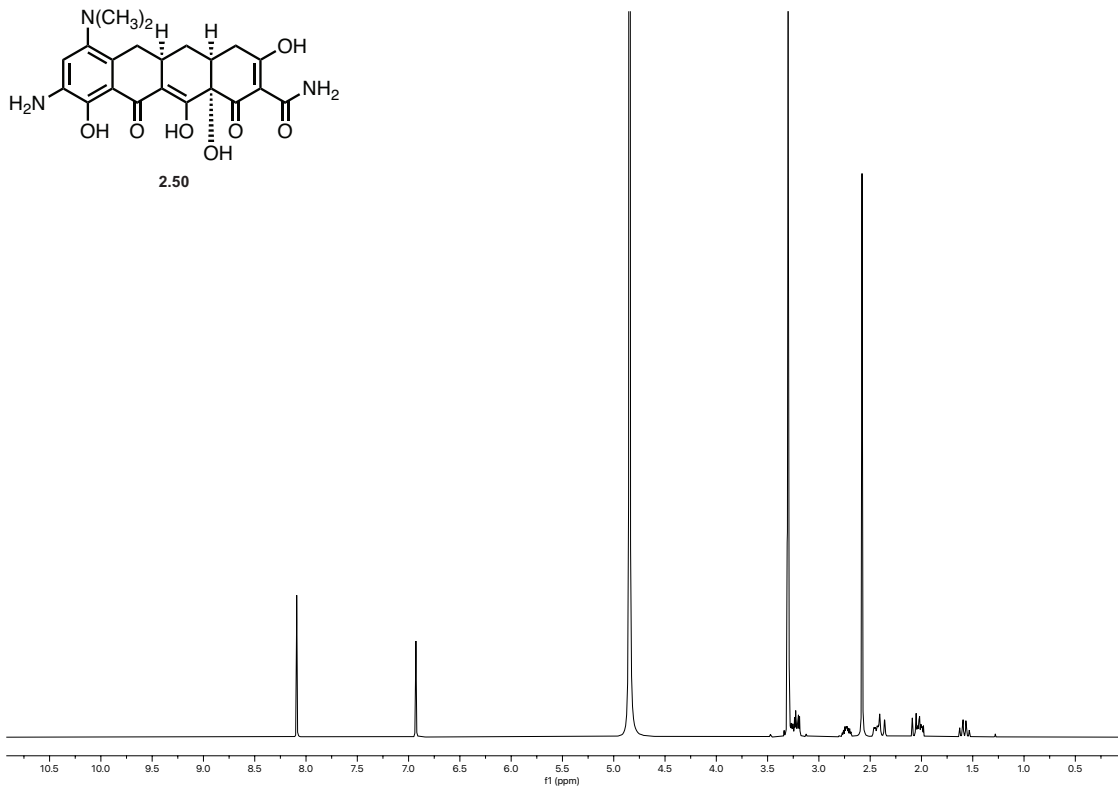
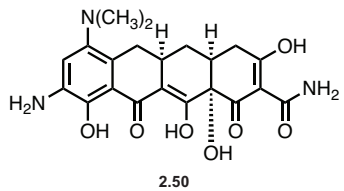
**Figure S4.3 Polysome Profiling Results – DMSO and Doxycycline with Formaldehyde Crosslinking.** As control experiments for Col-3 and analogue **2.72** (Fig. 4.8), we analyzed polysome profiles for both DMSO (A) and doxycycline (**1.4**, B) in crosslinking conditions. As observed for the other tetracyclines, we do not observe any major differences in the profiles for these compounds. Experiments performed at the Gladyshev Laboratory with the assistance of Dr. Maxim Geraschenko.

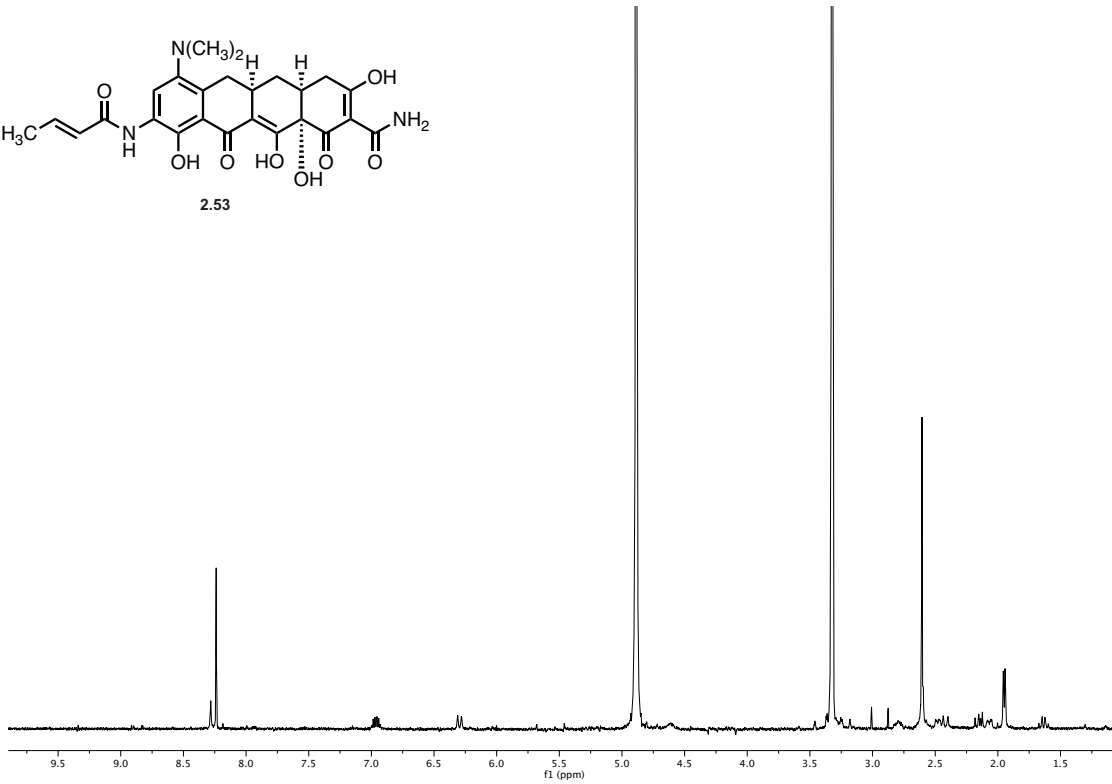
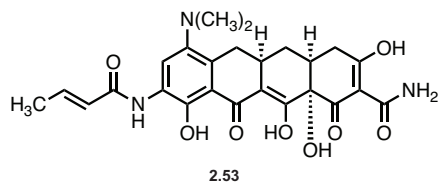
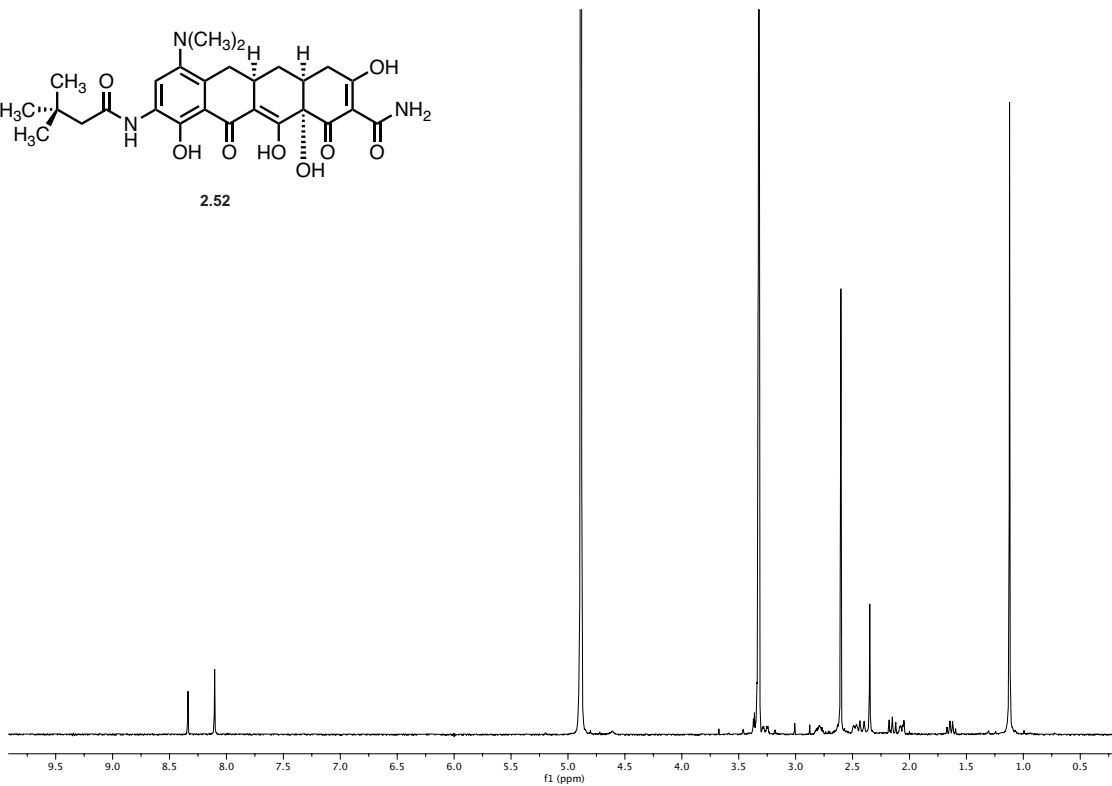
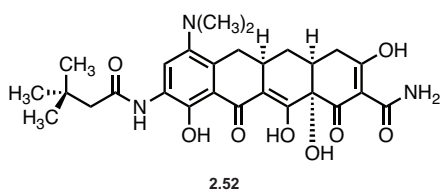
## **Appendix B**

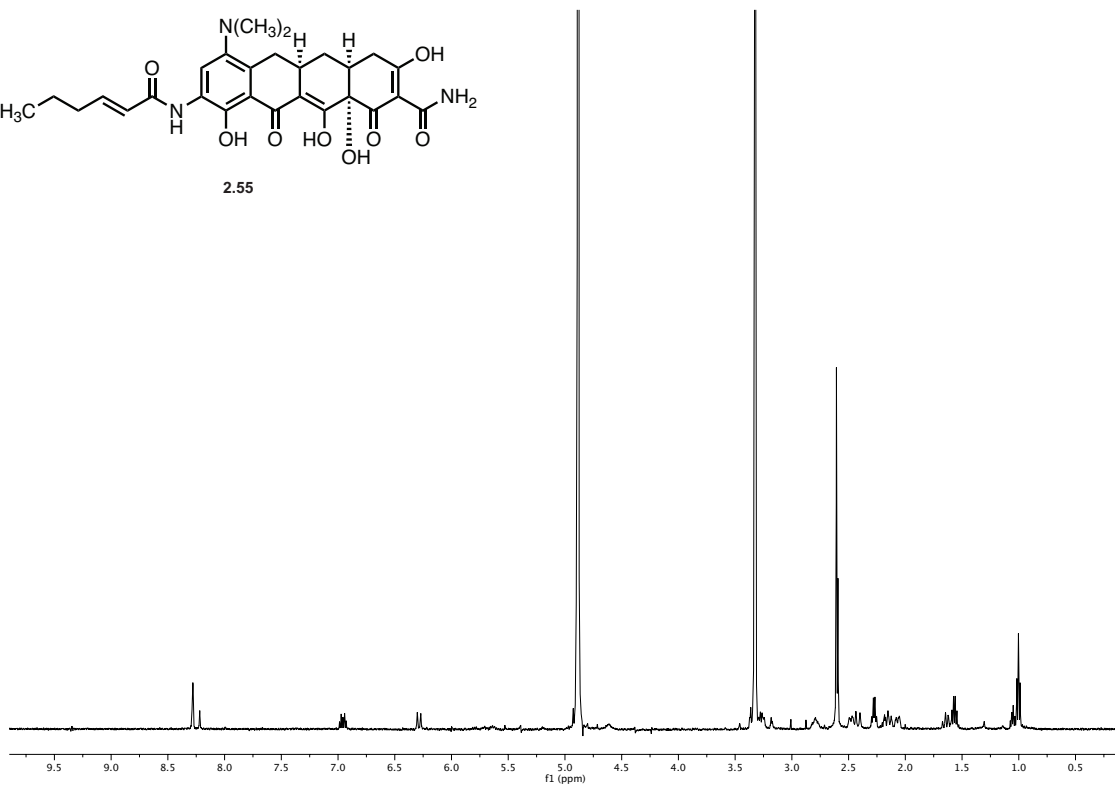
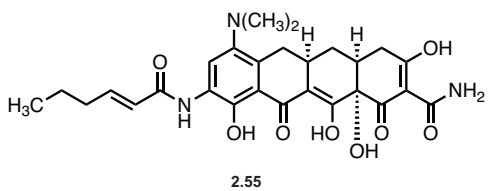
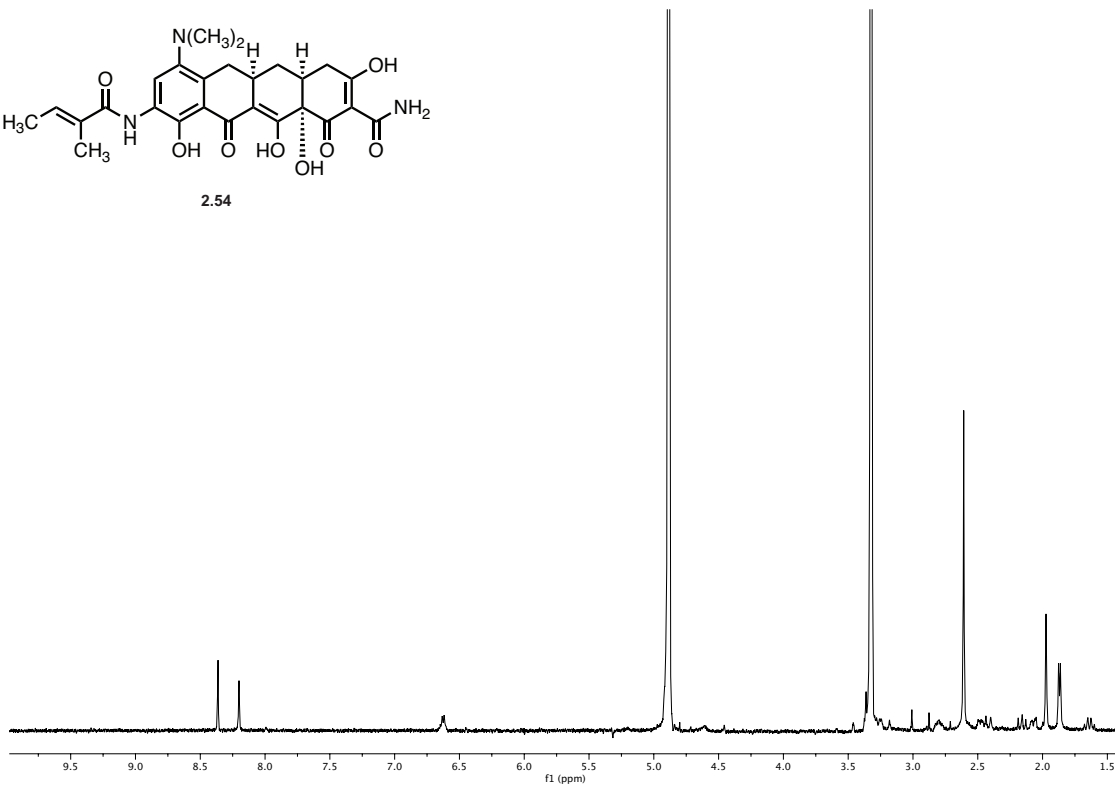
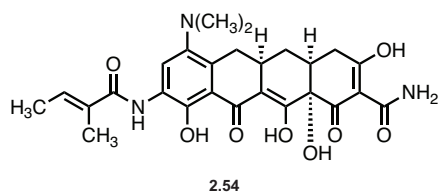
### **Catalogue of Spectra**



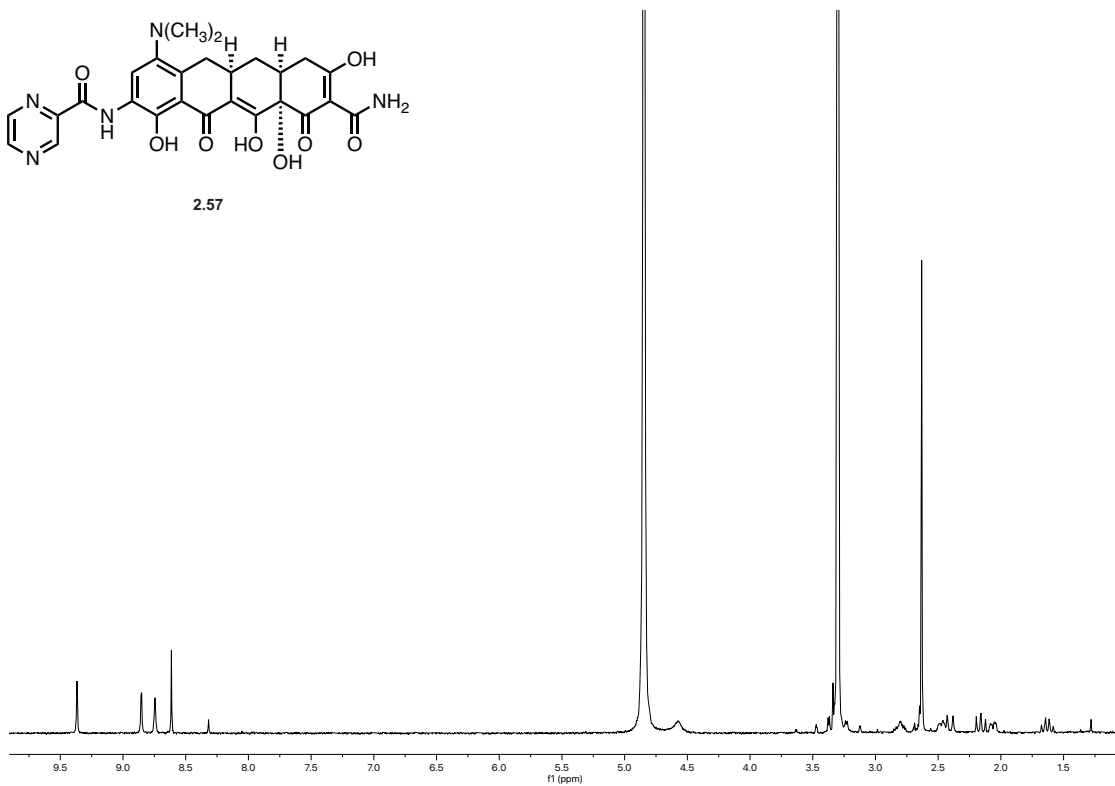
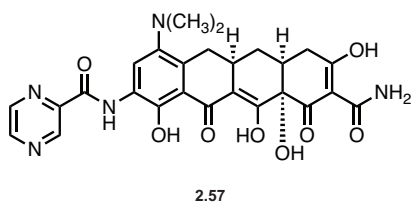
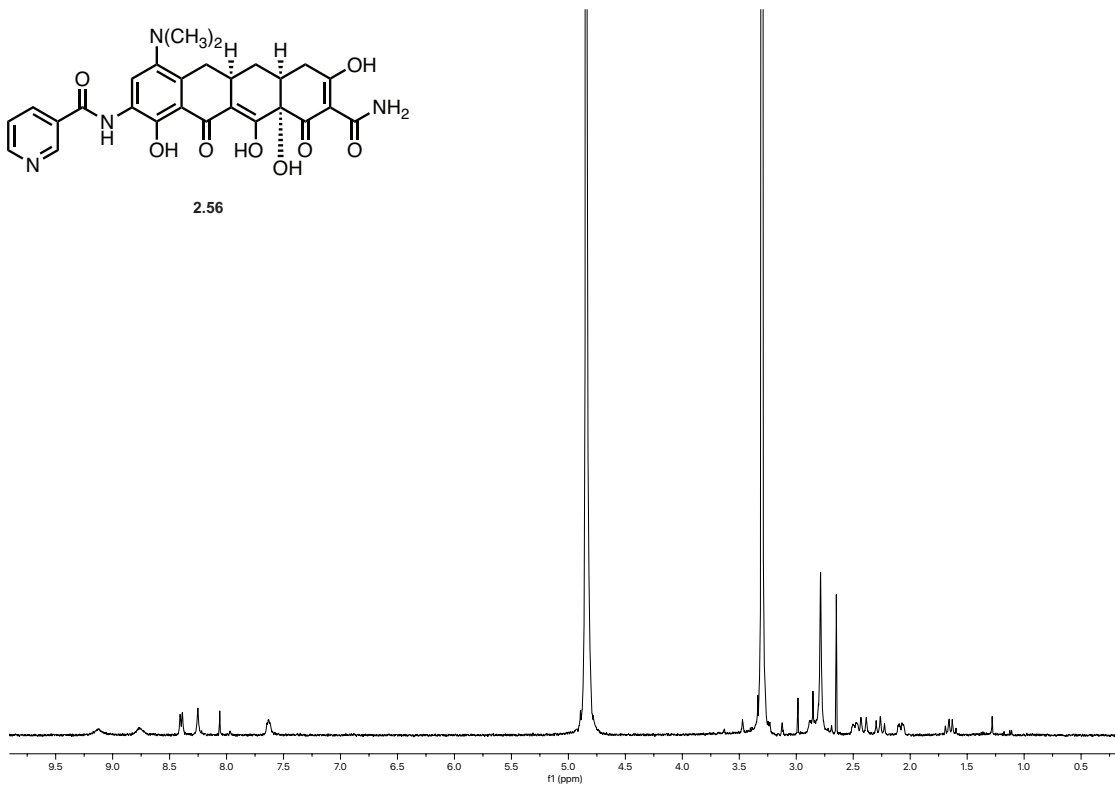
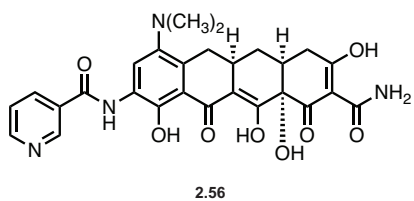


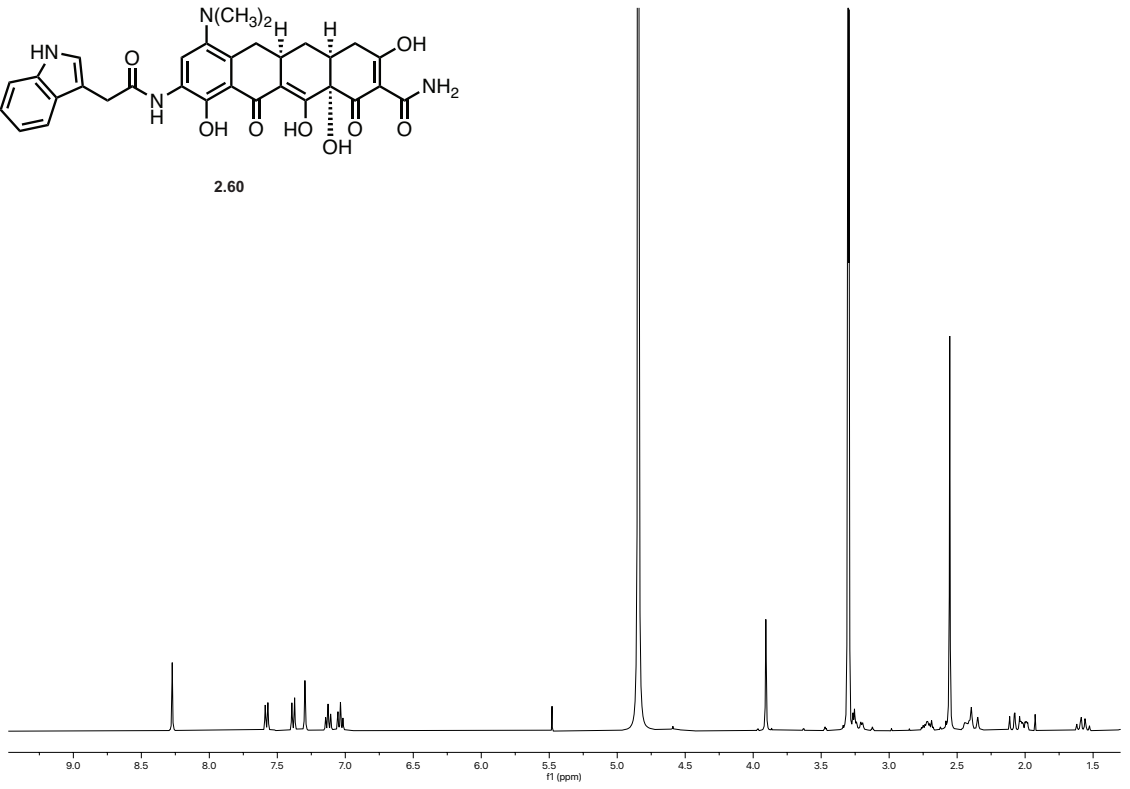
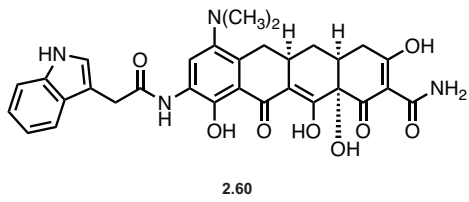
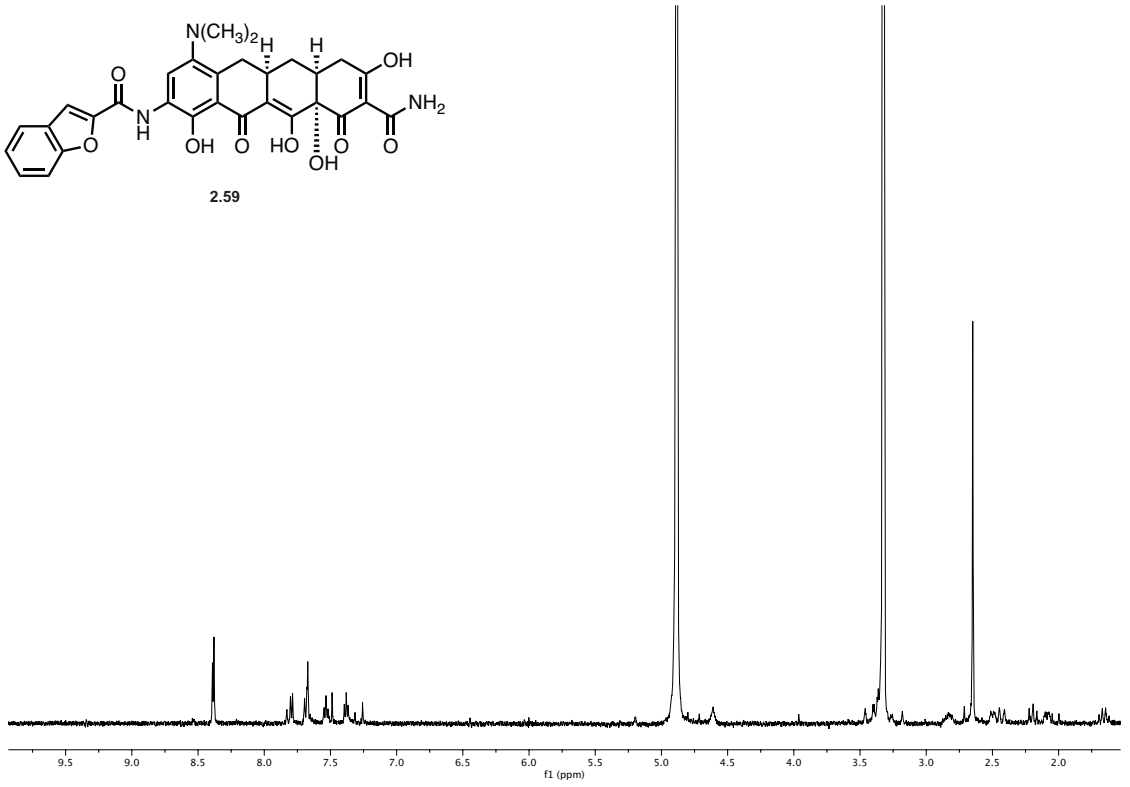
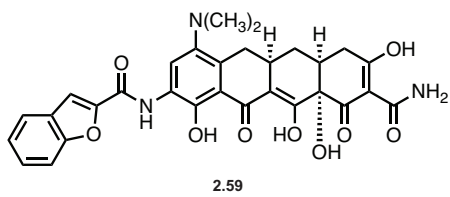


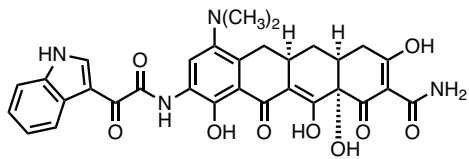




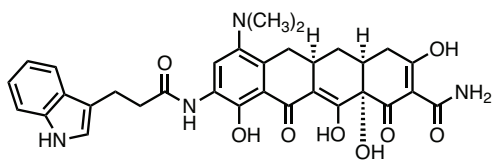
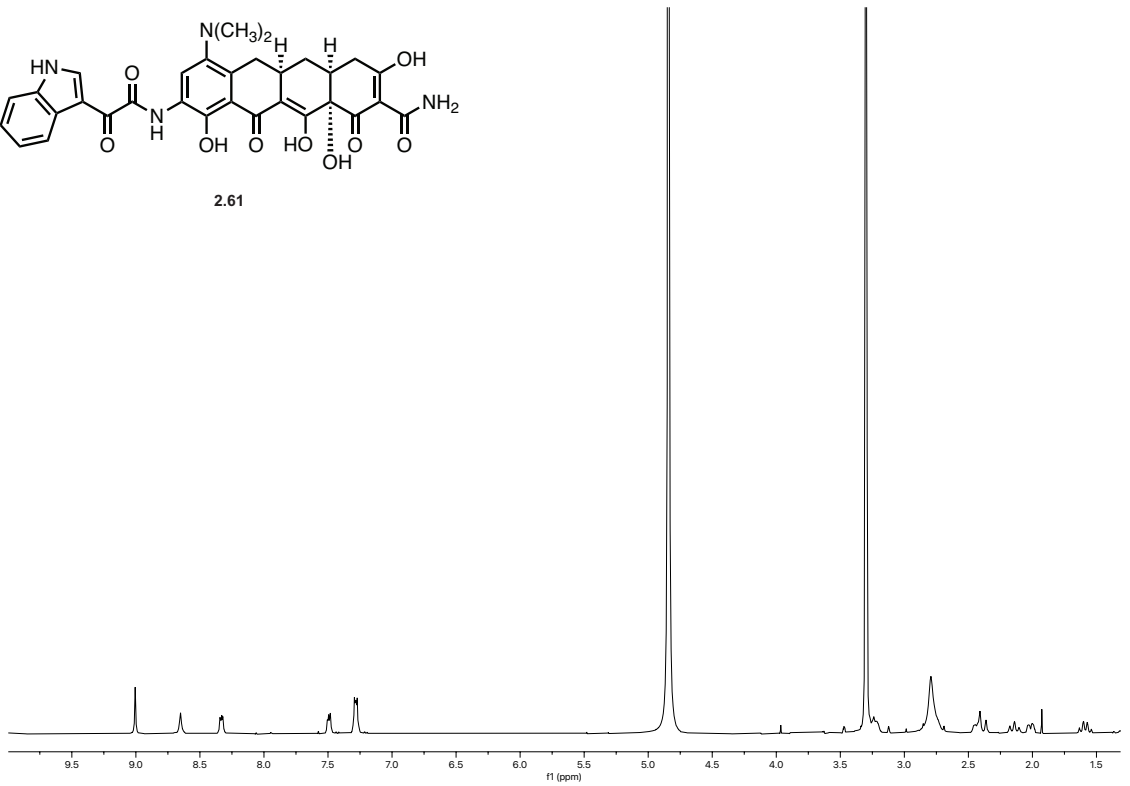




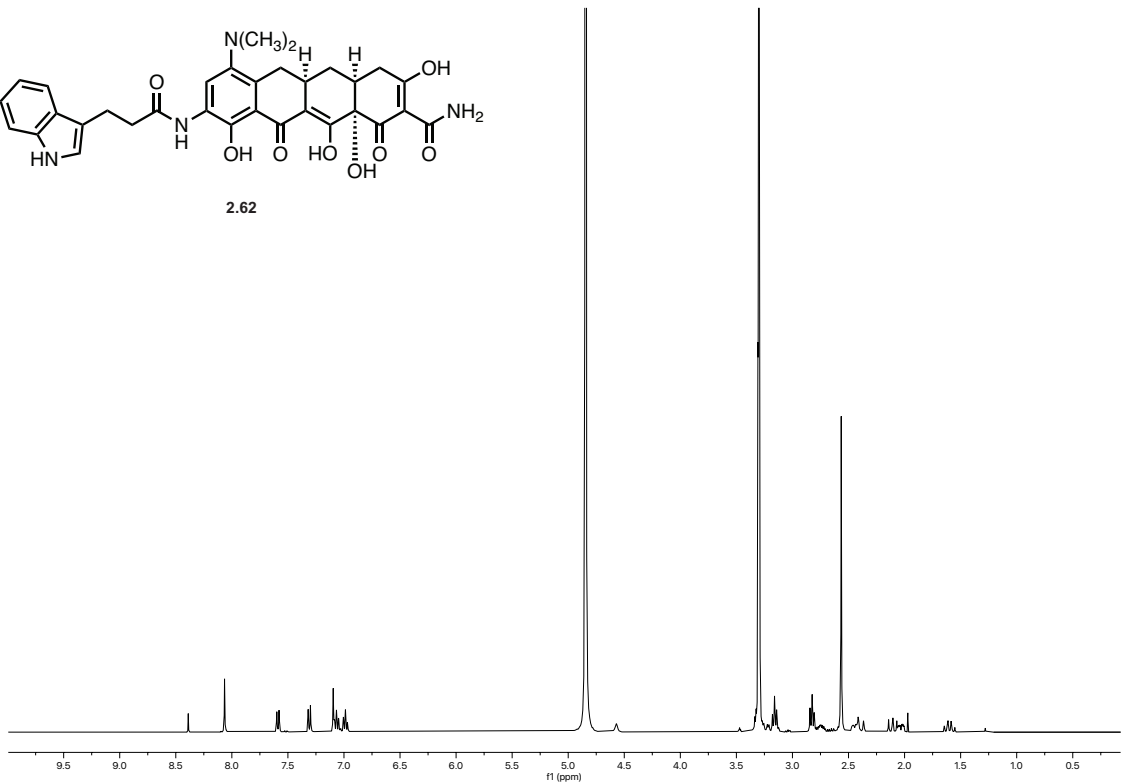


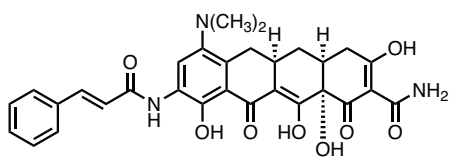


2.61

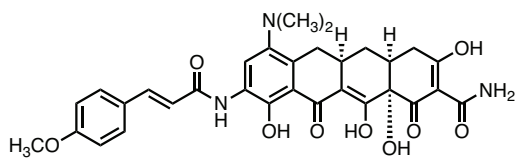
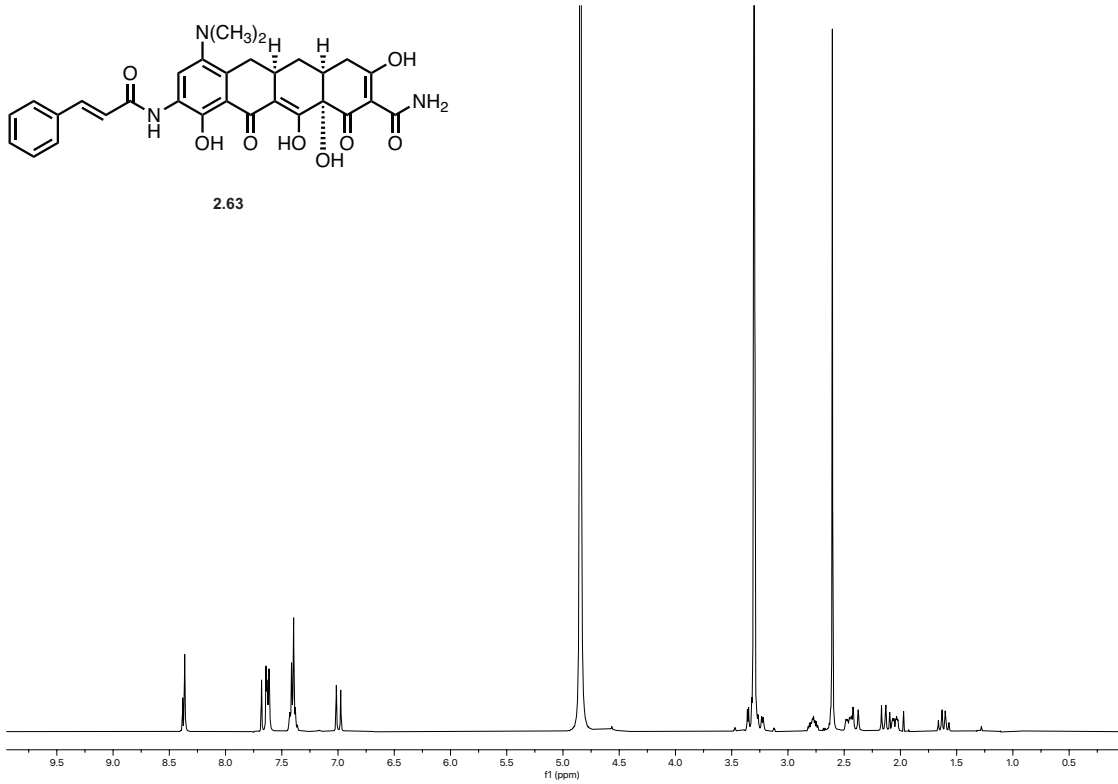


2.62

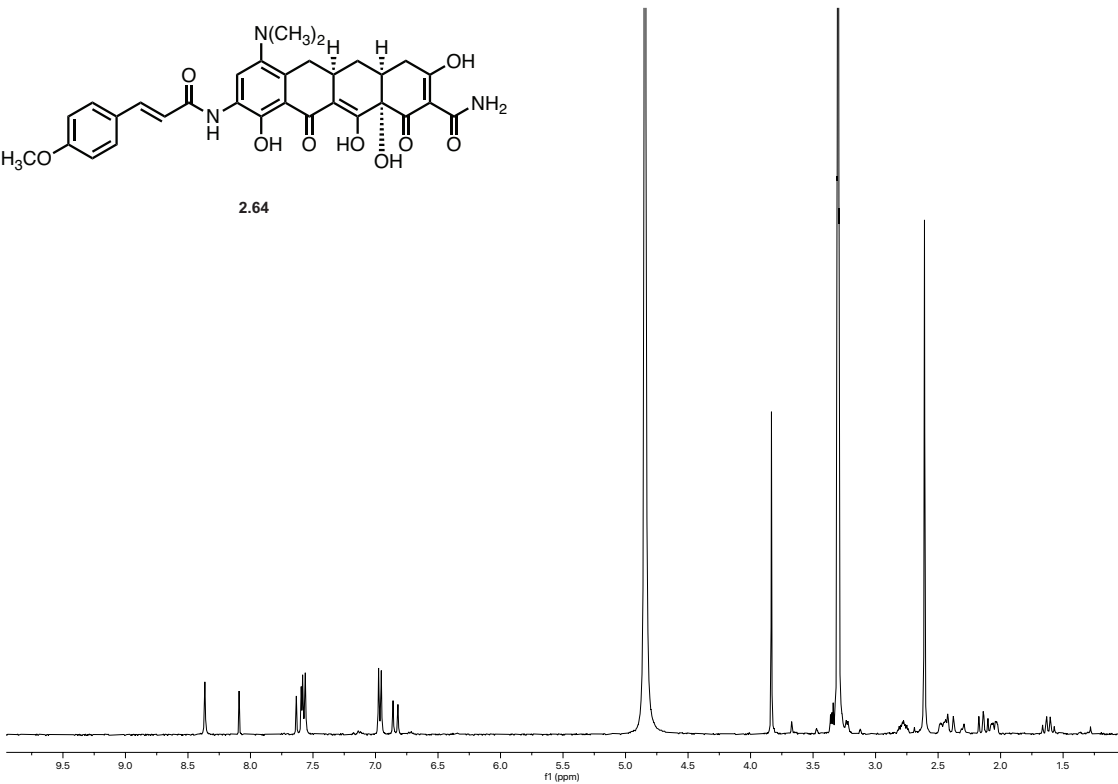


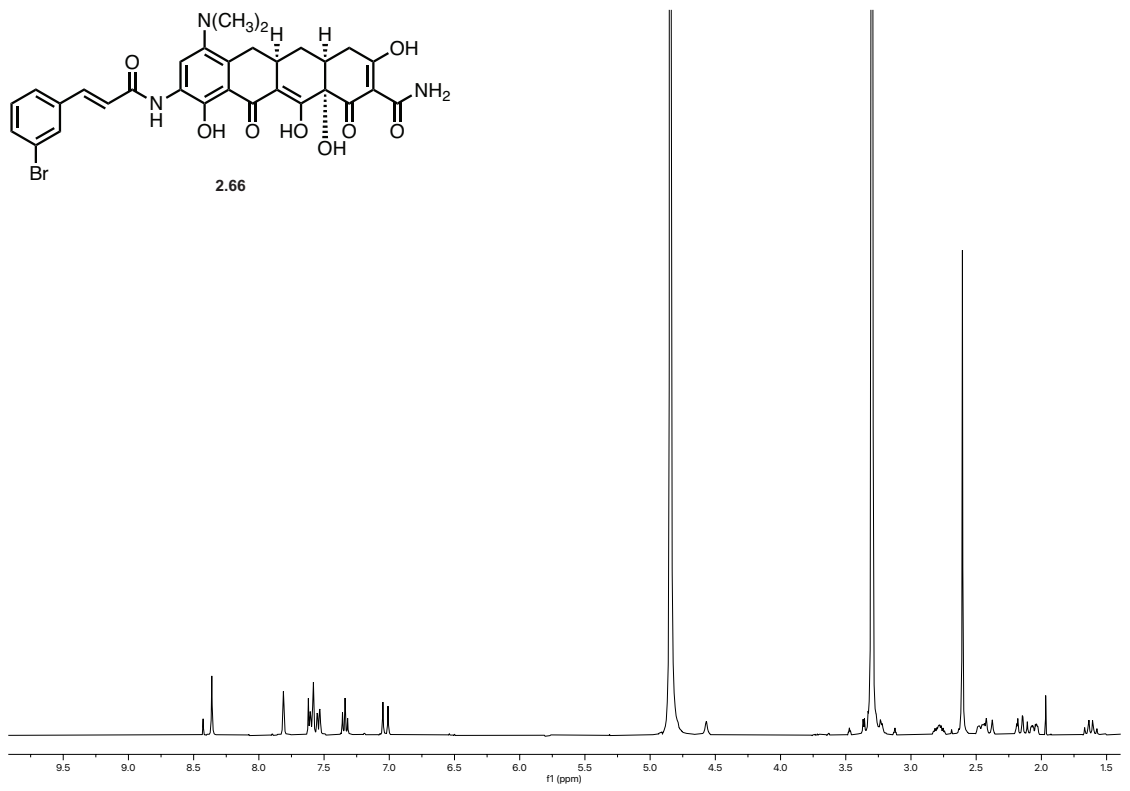
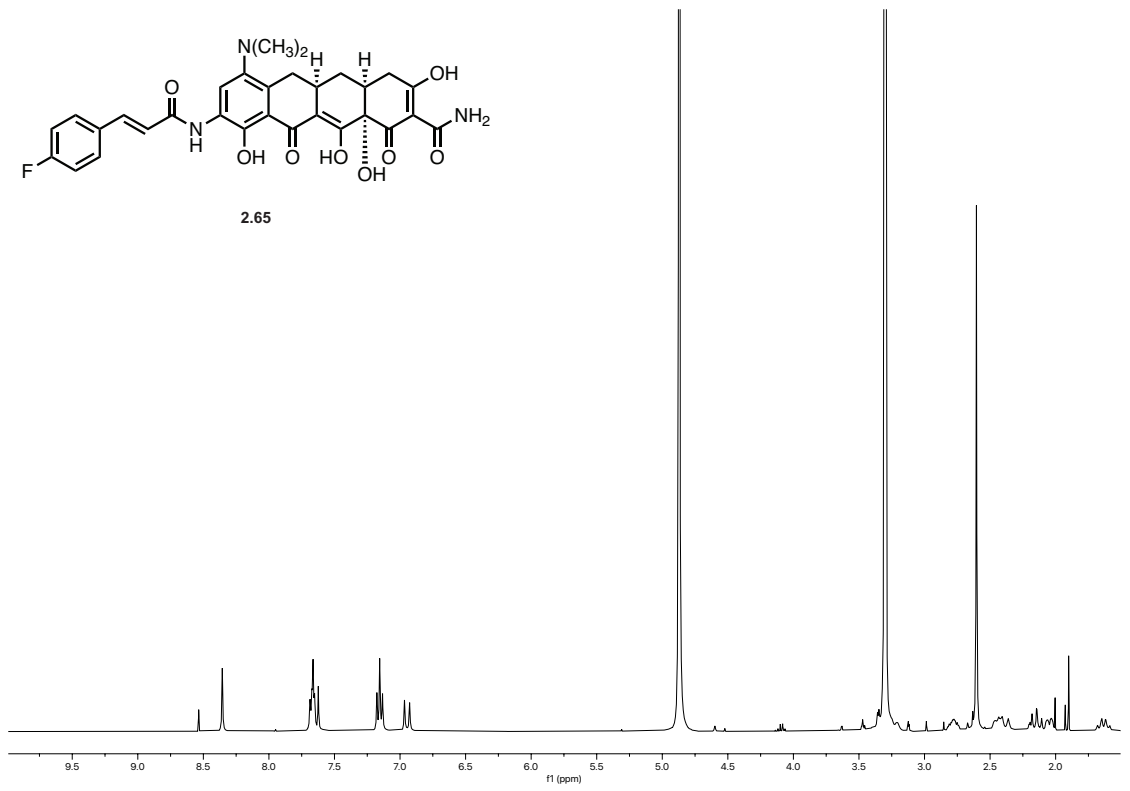


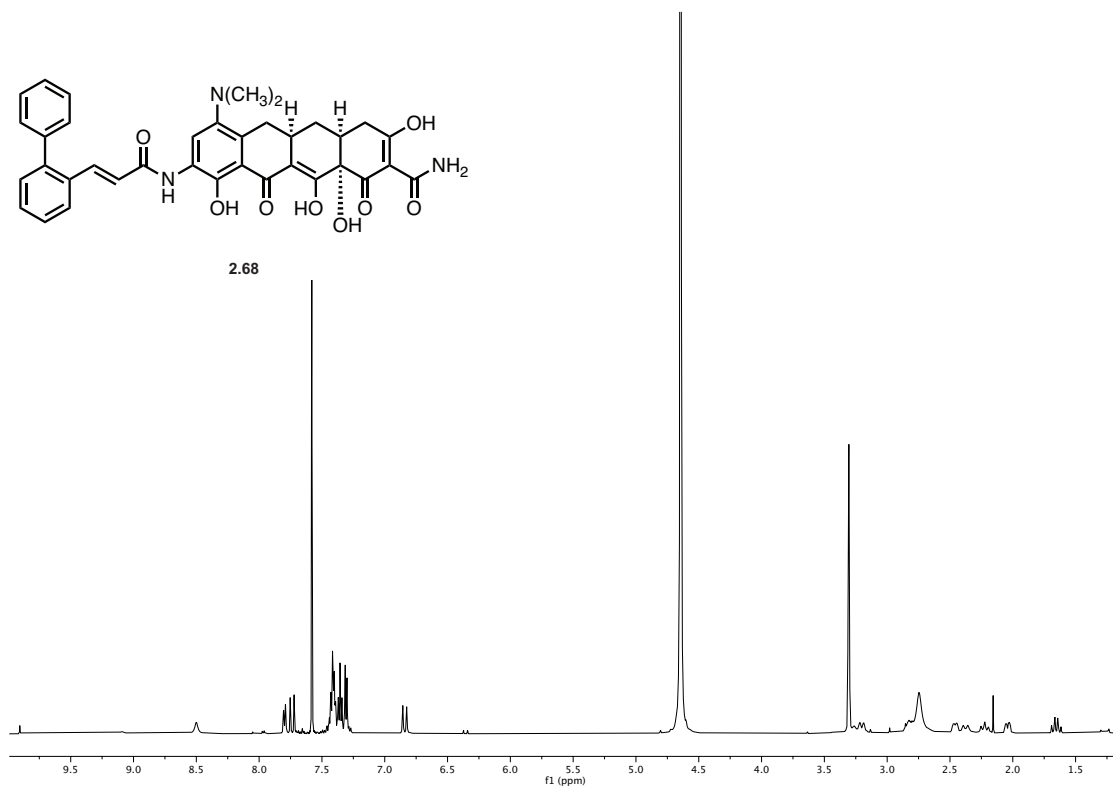
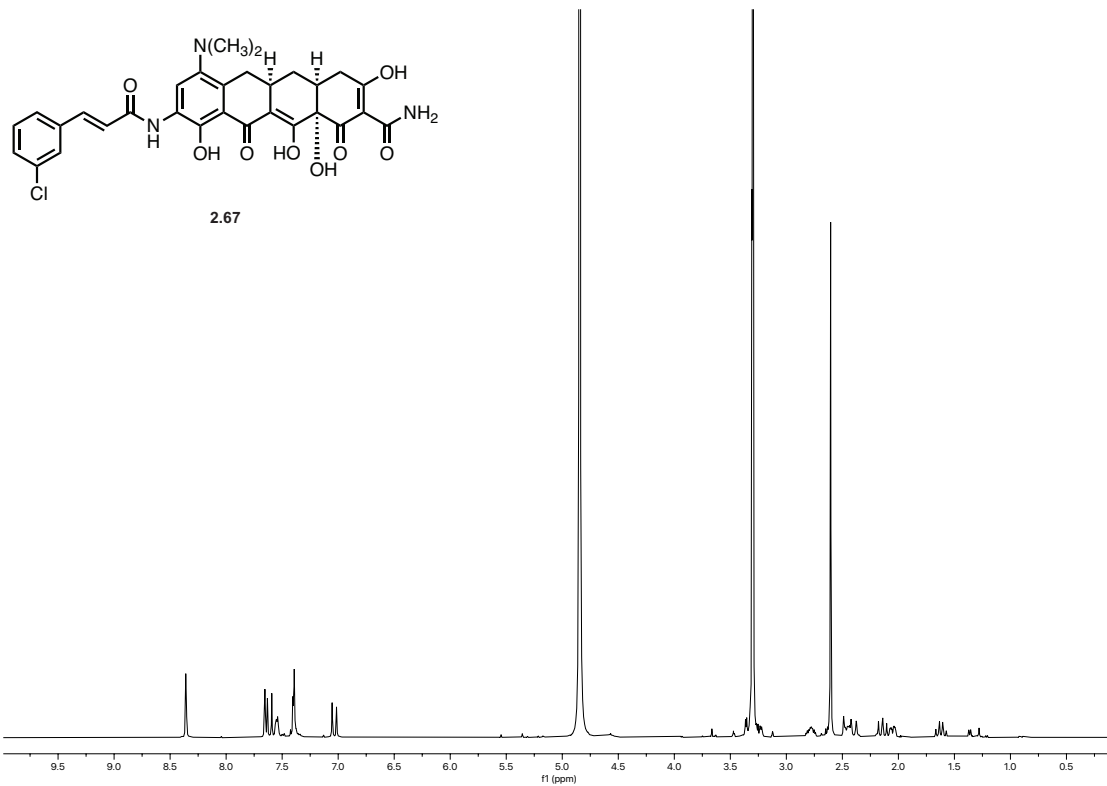
2.63



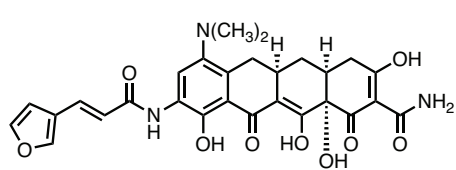
2.64



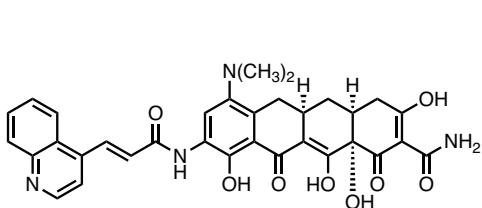
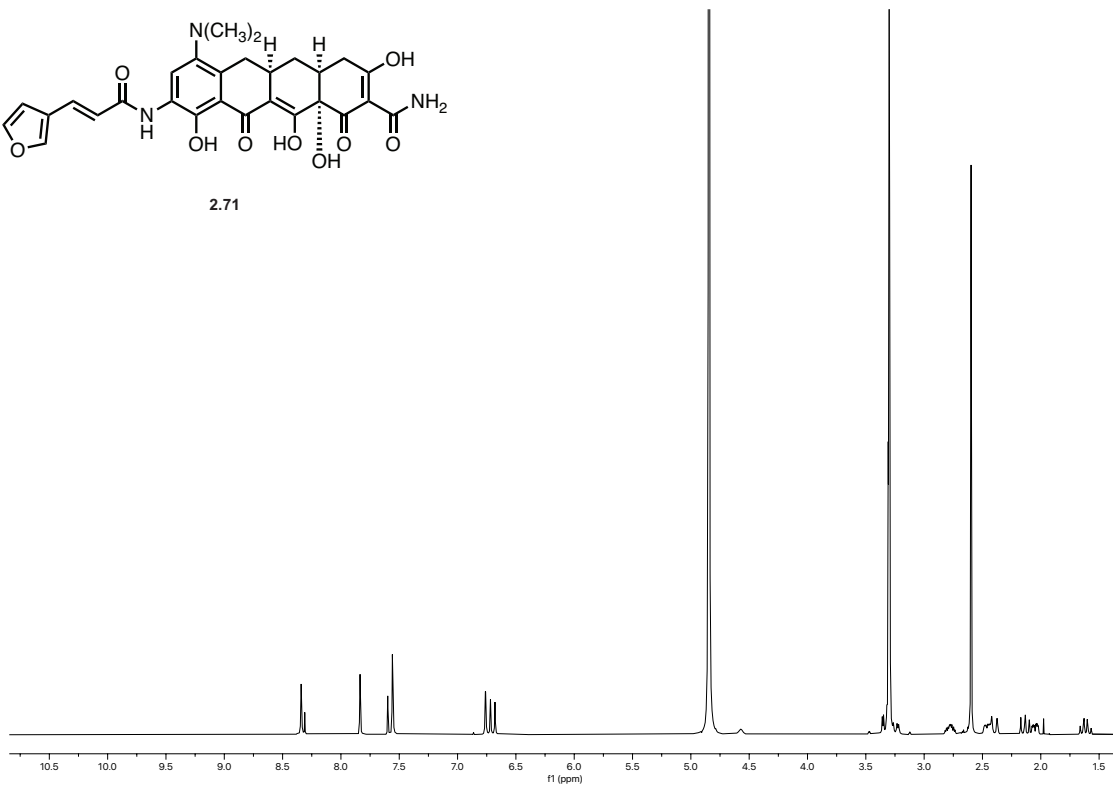




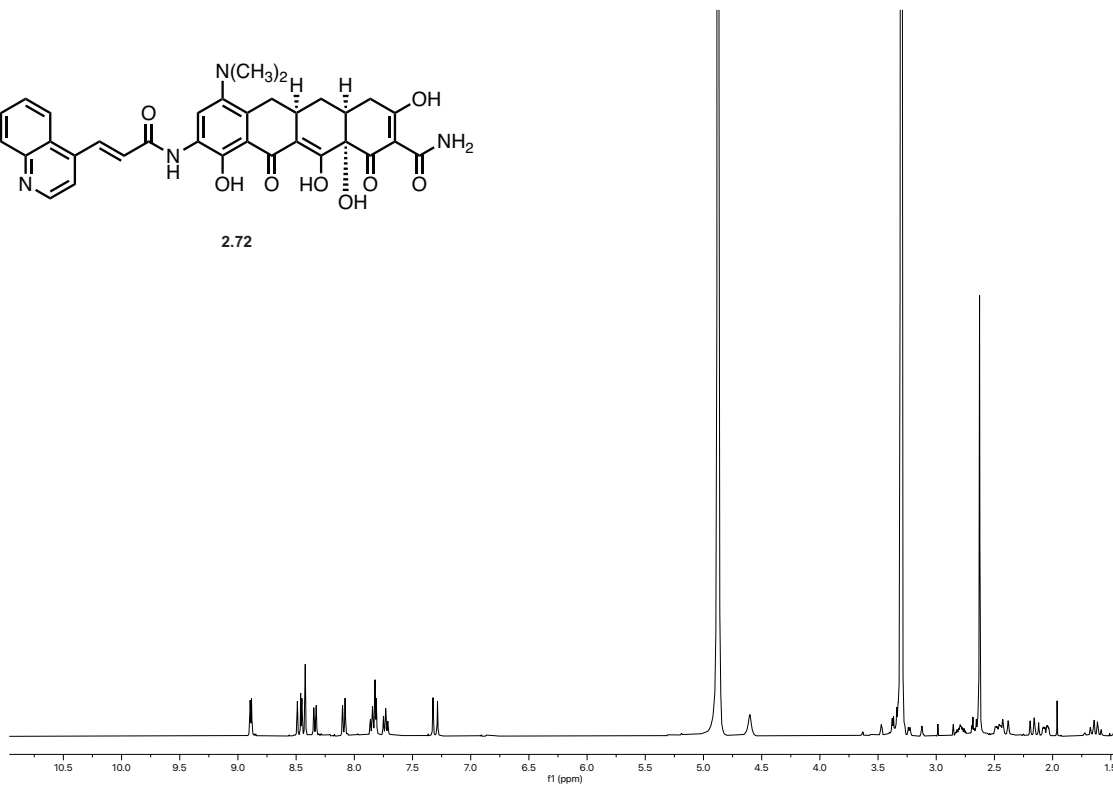




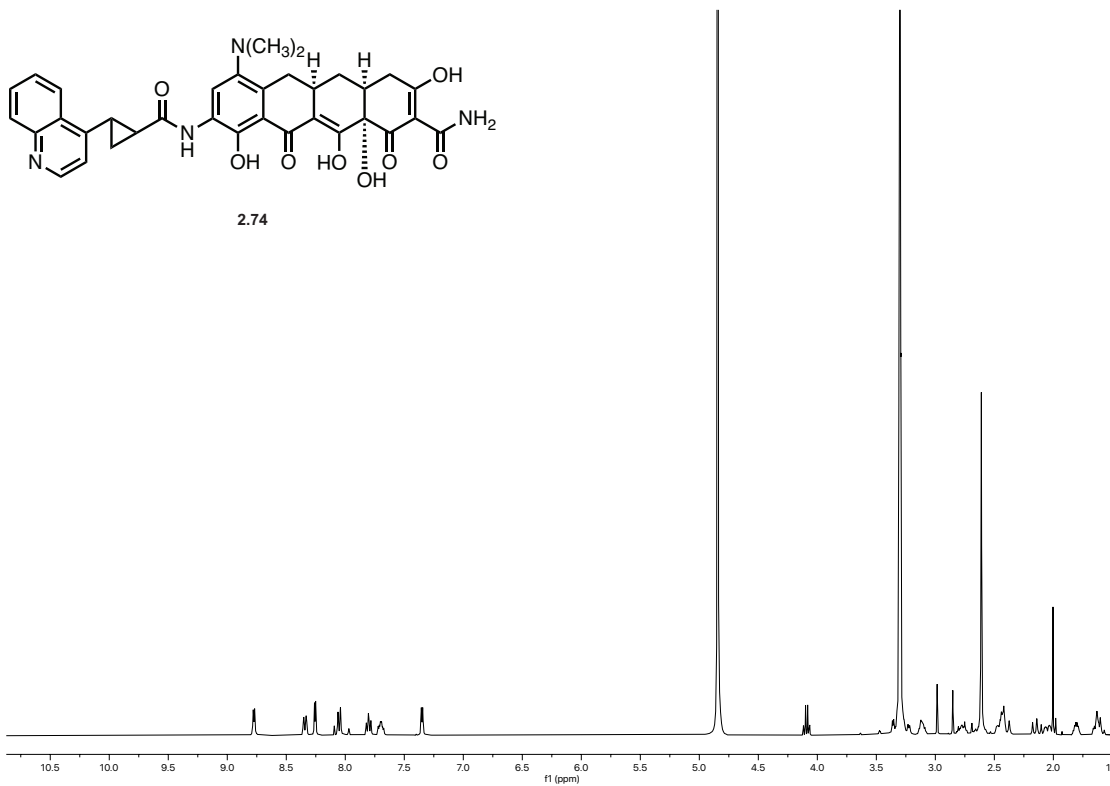
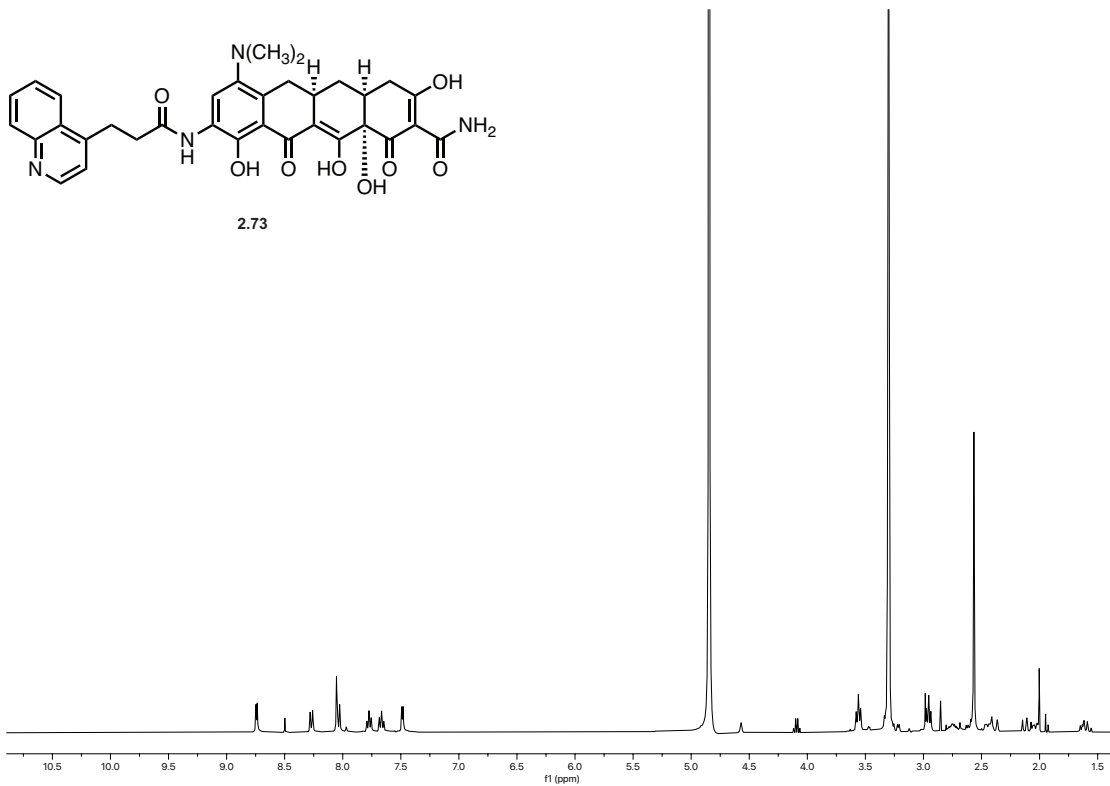
2.71

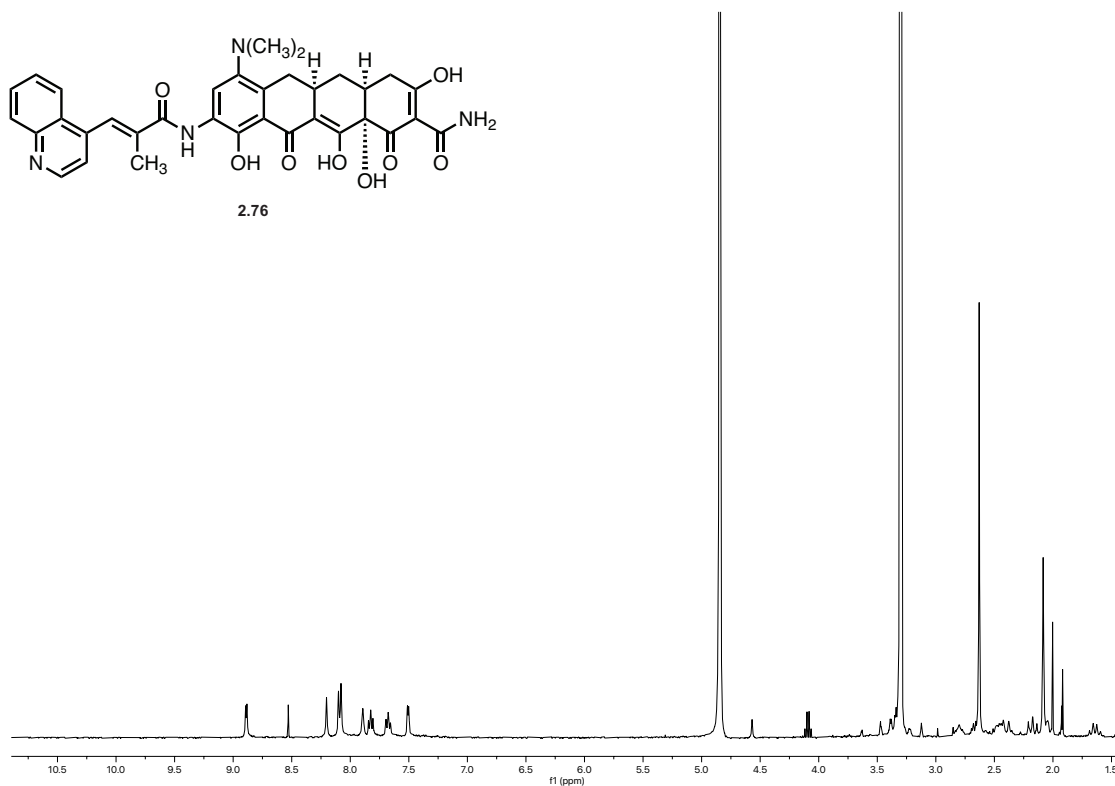
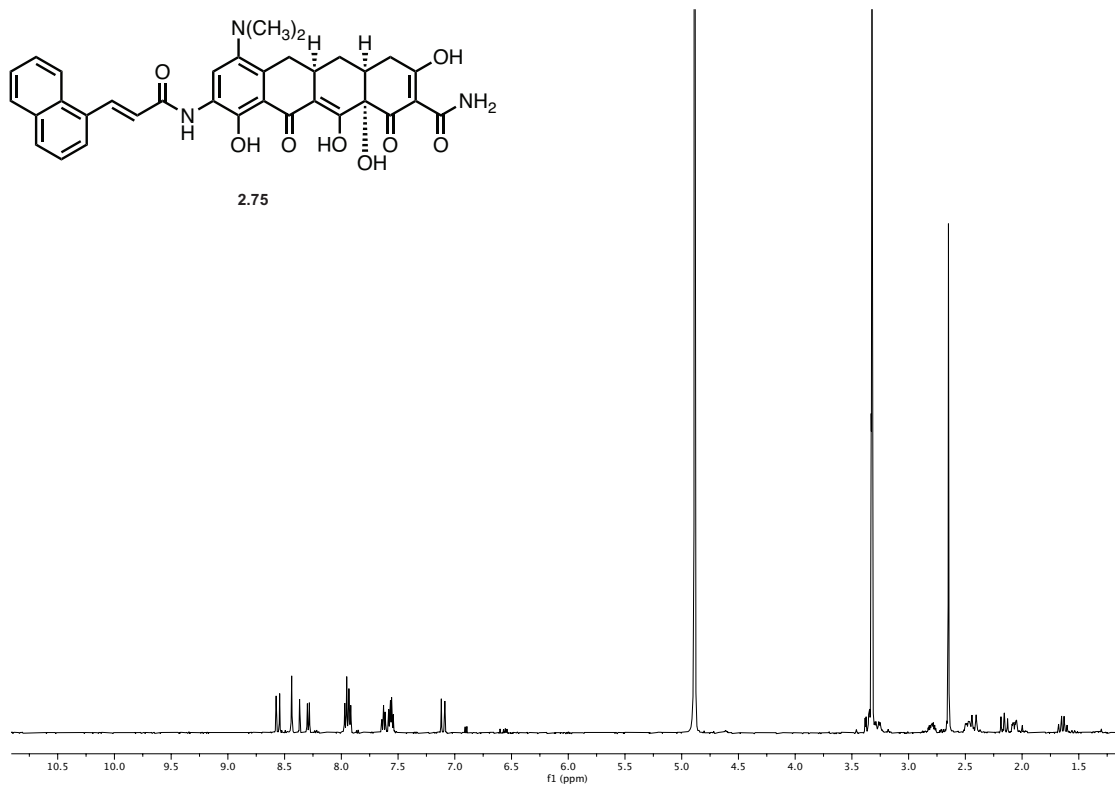


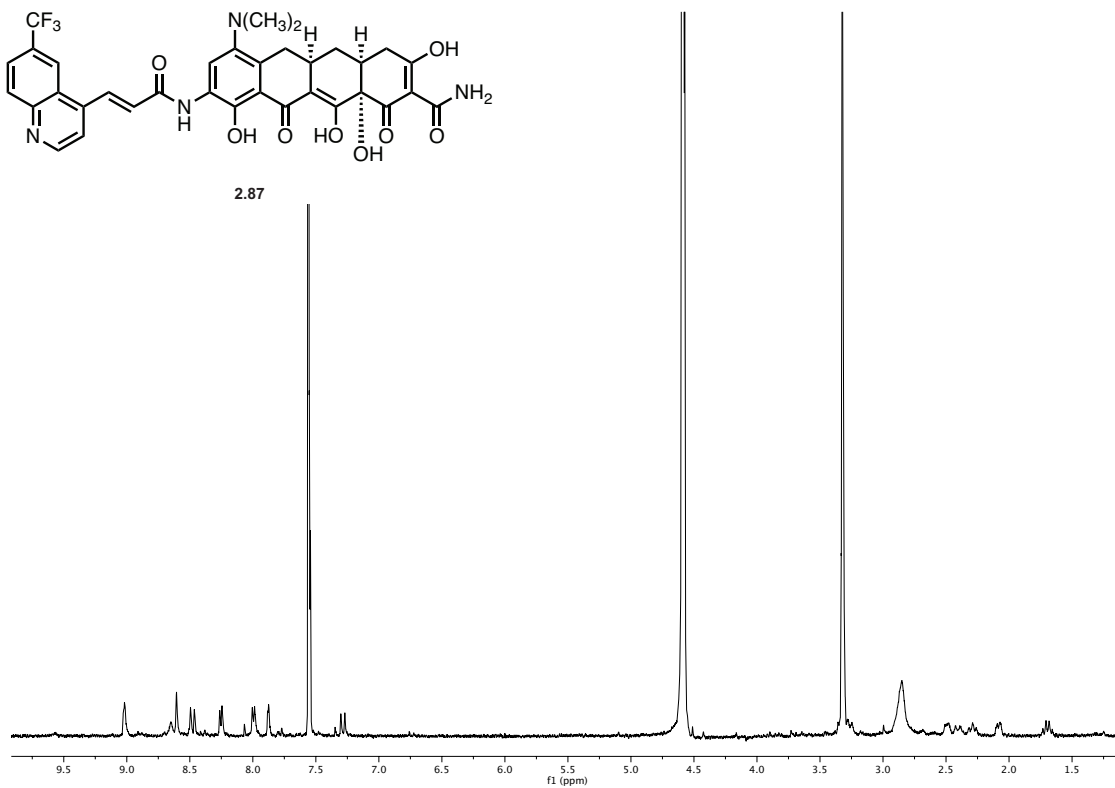
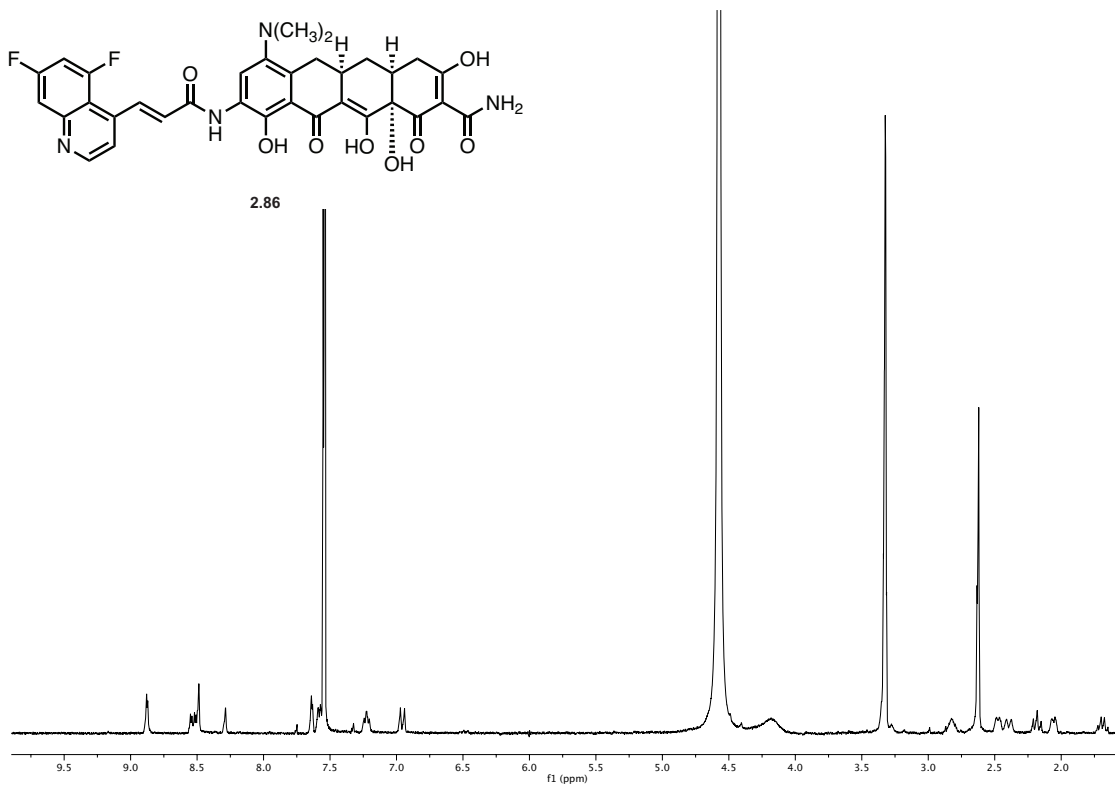
2.72

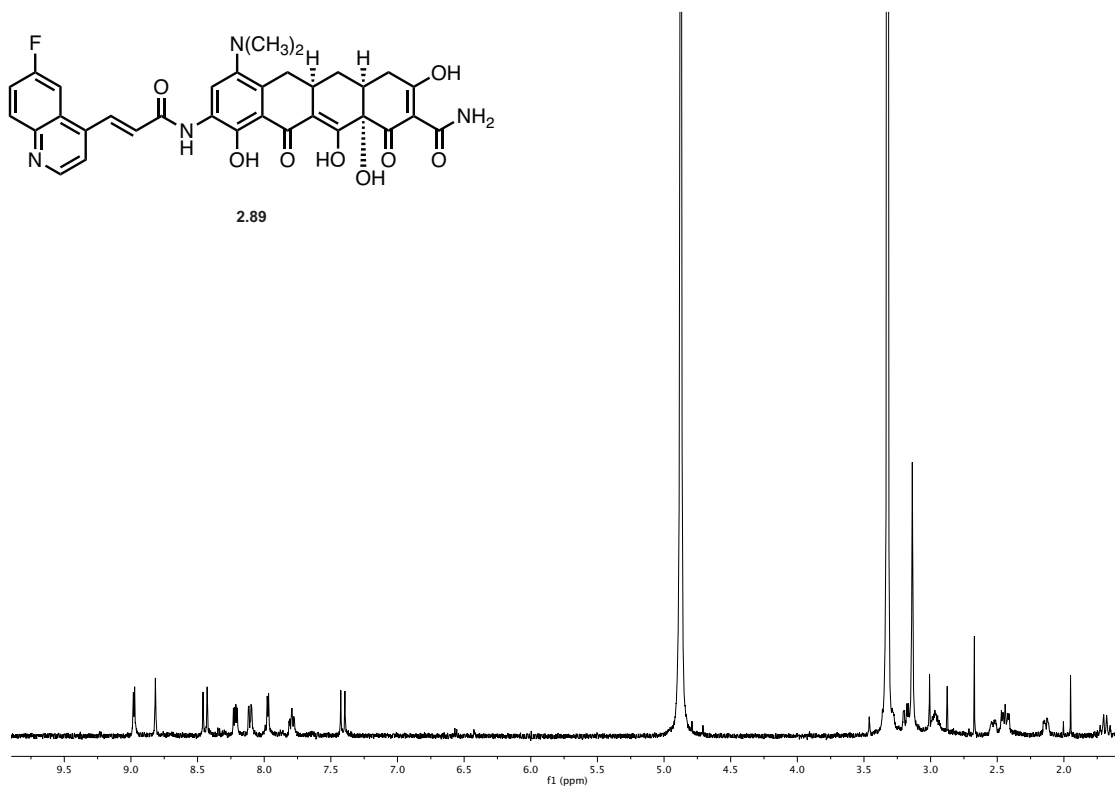
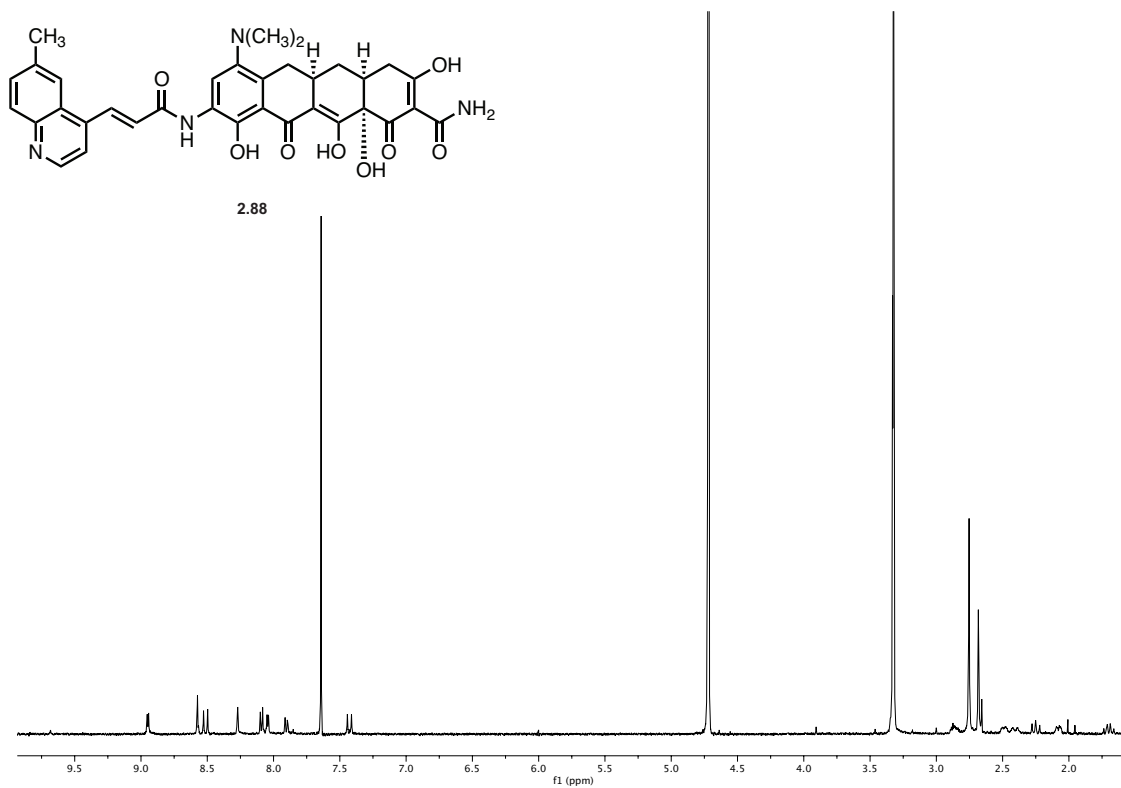


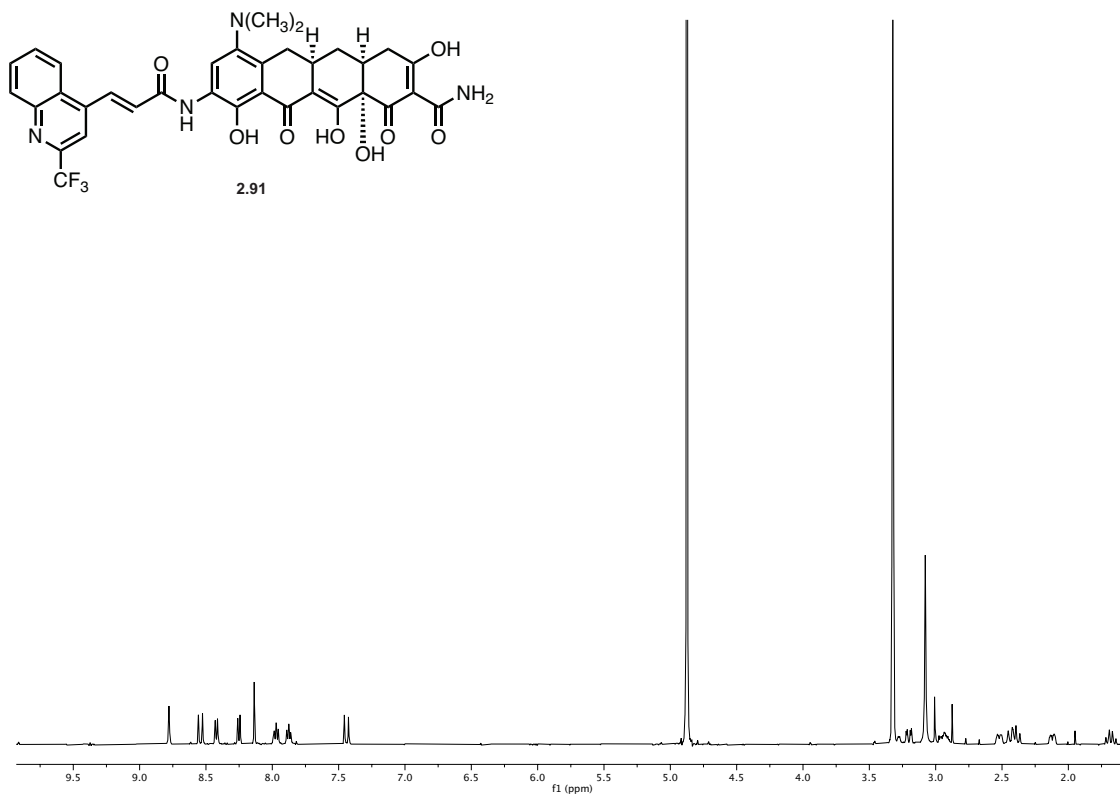
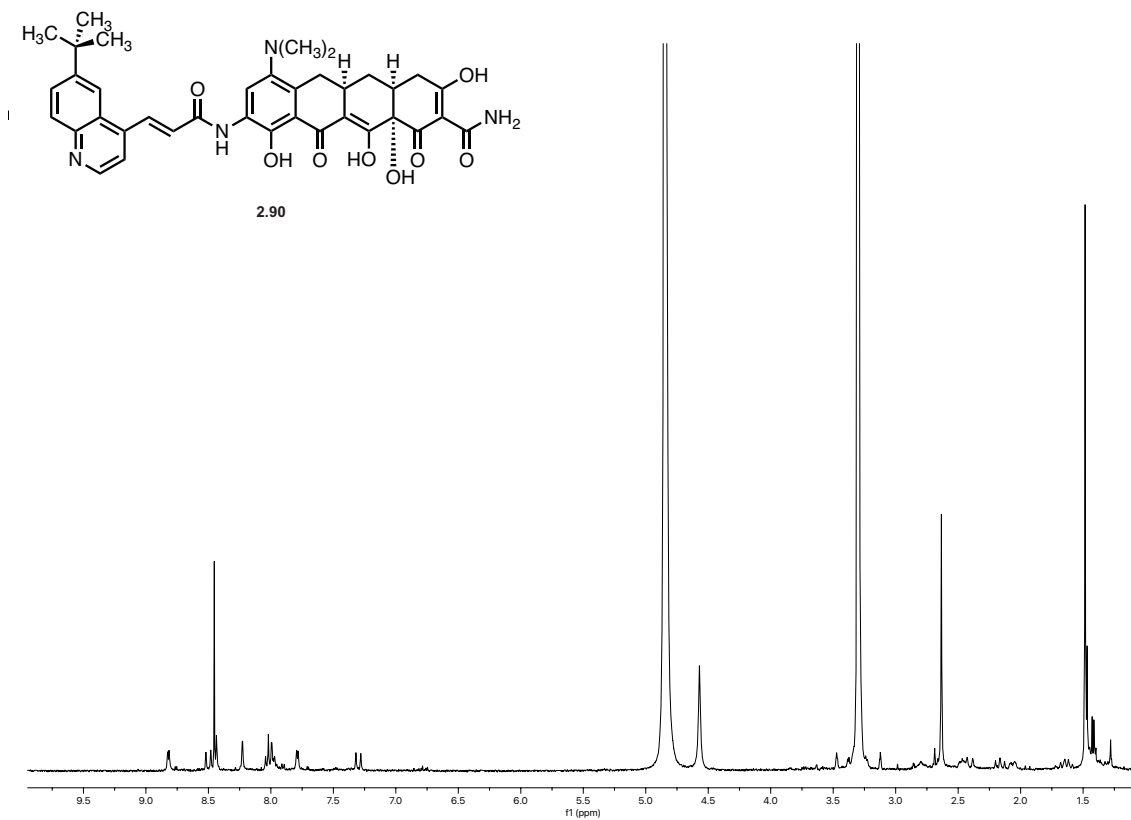


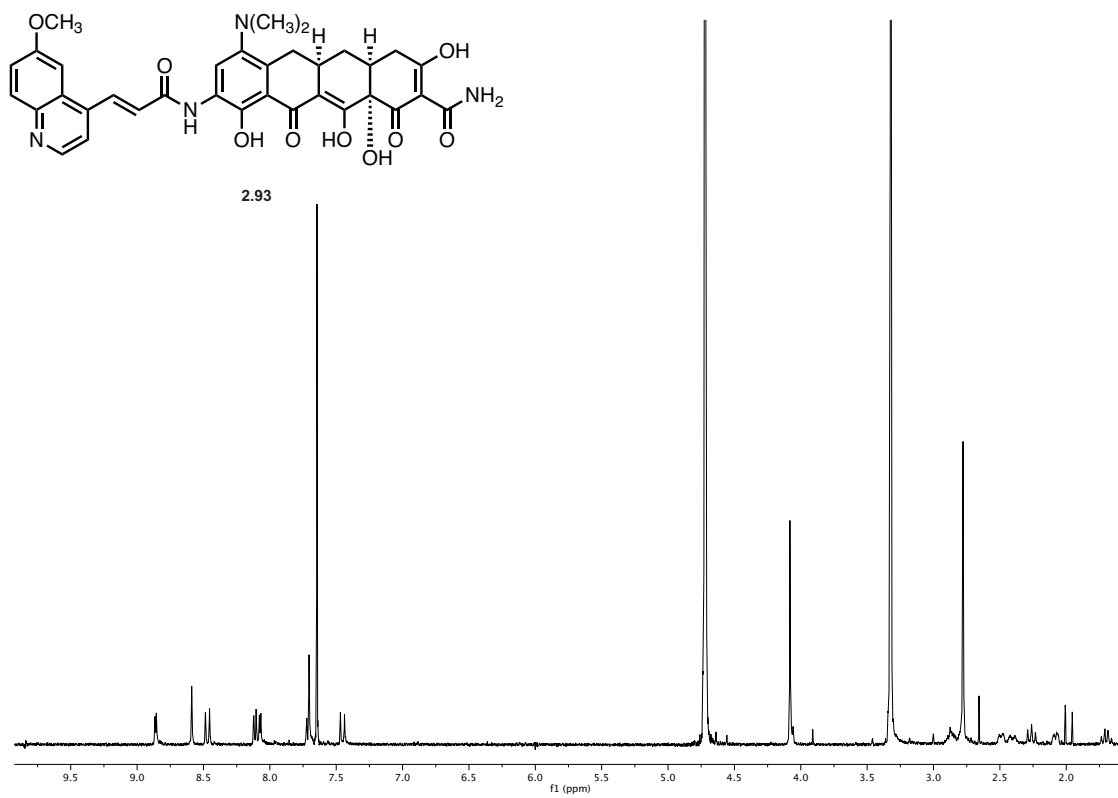
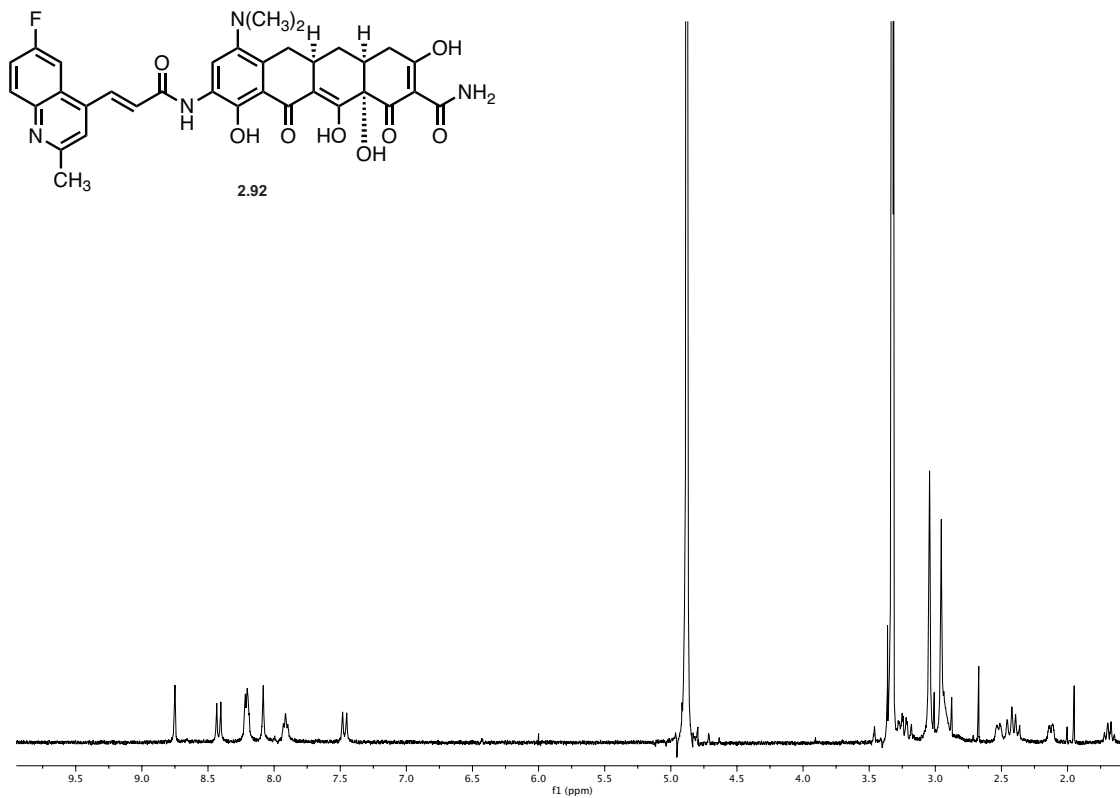


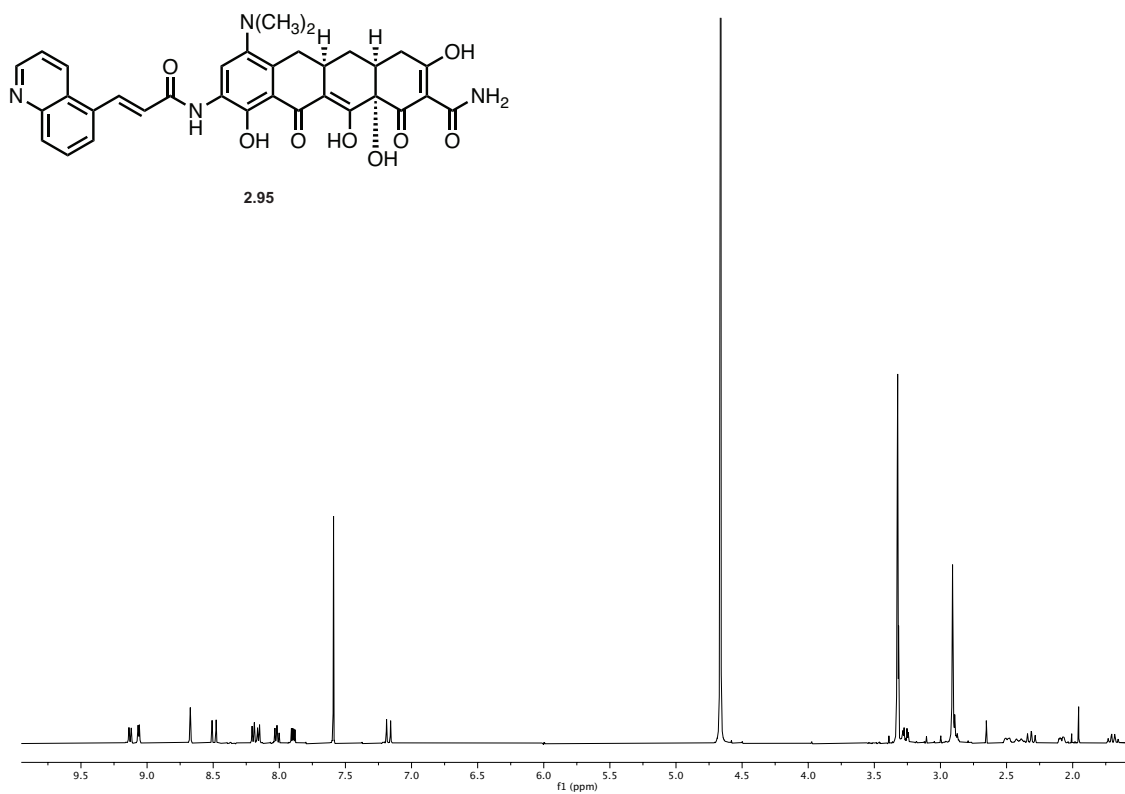
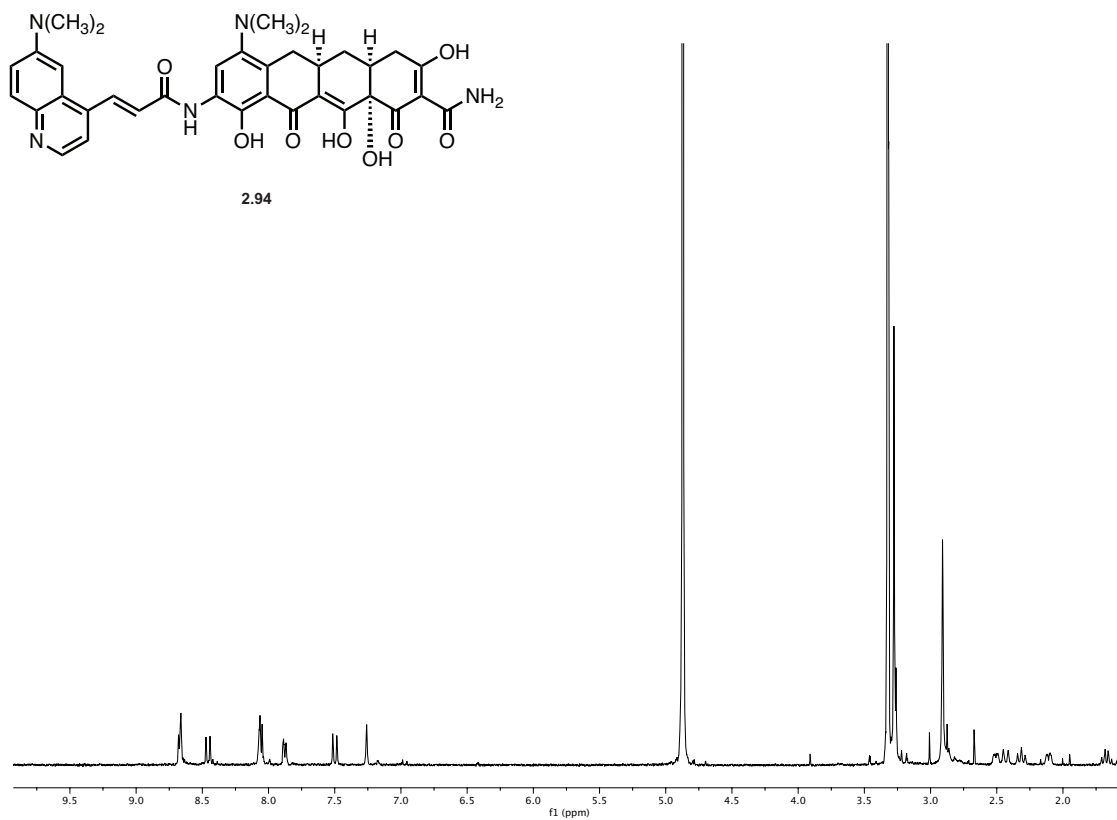


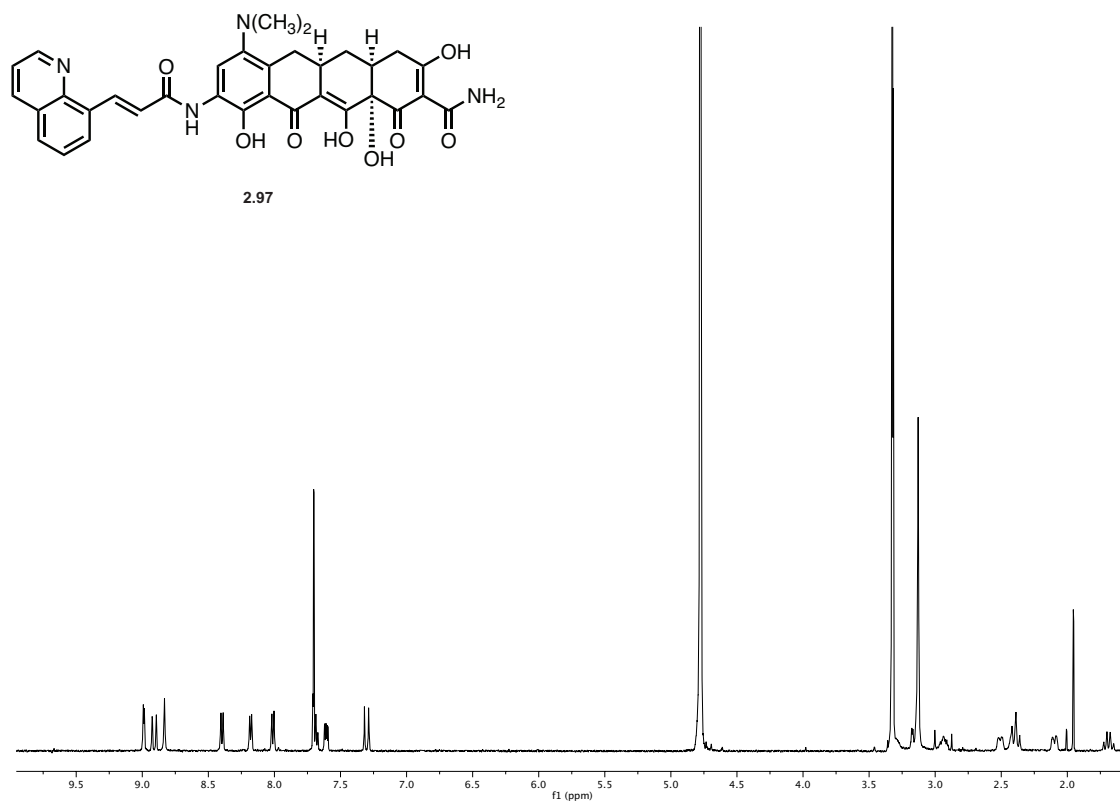




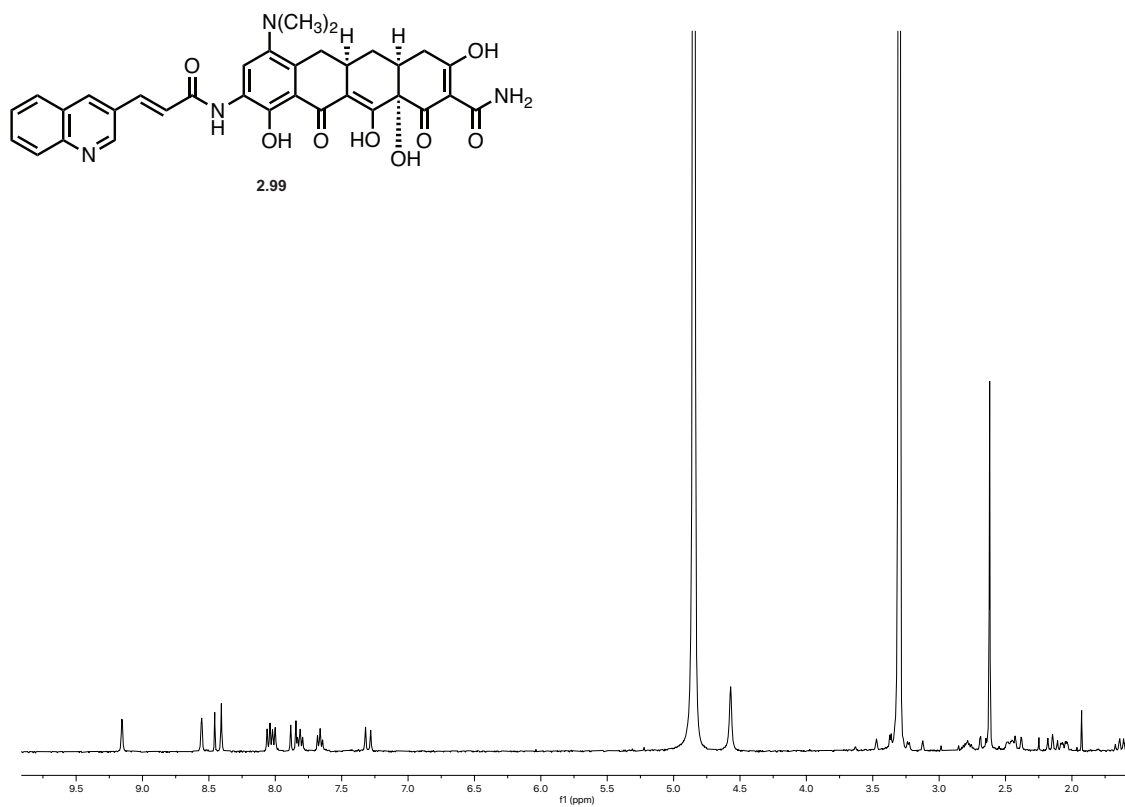
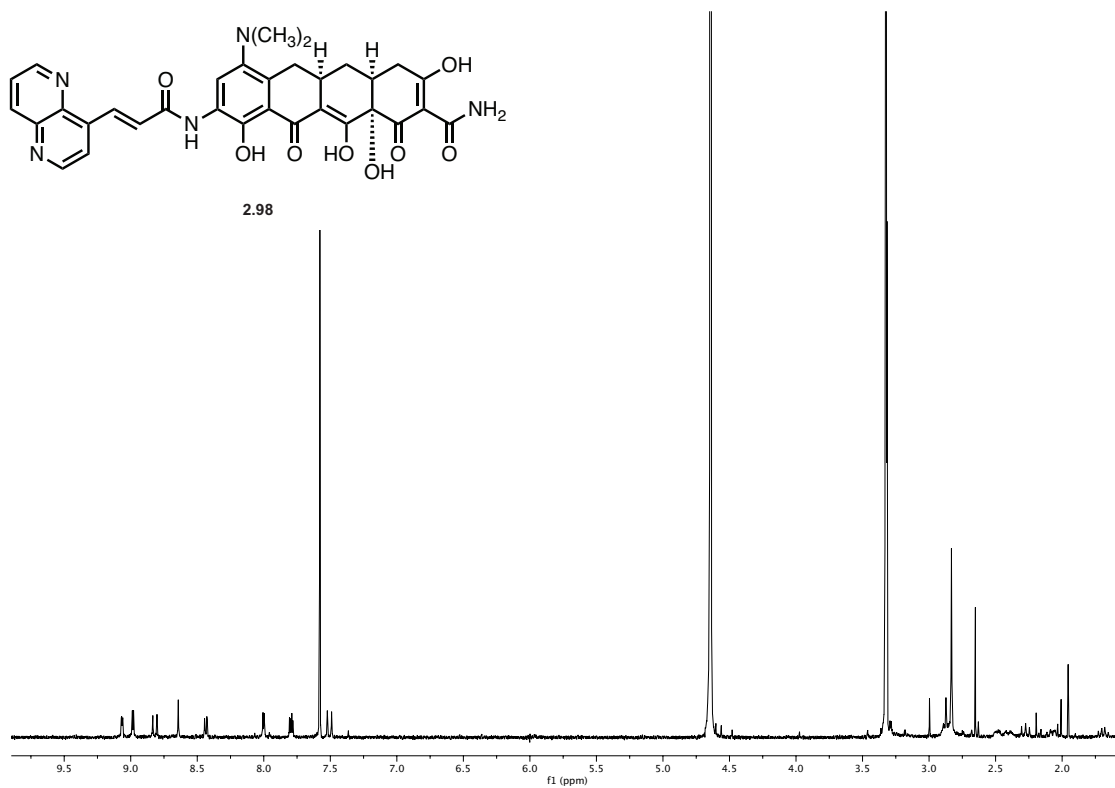


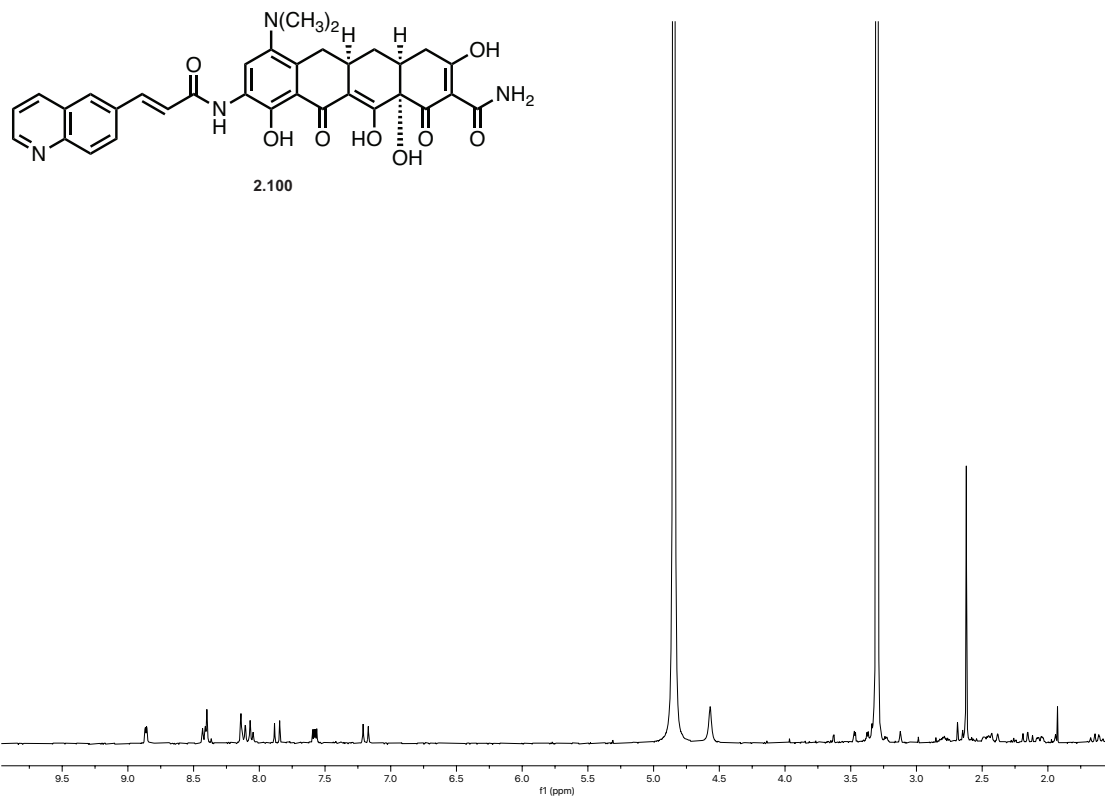


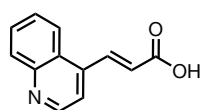




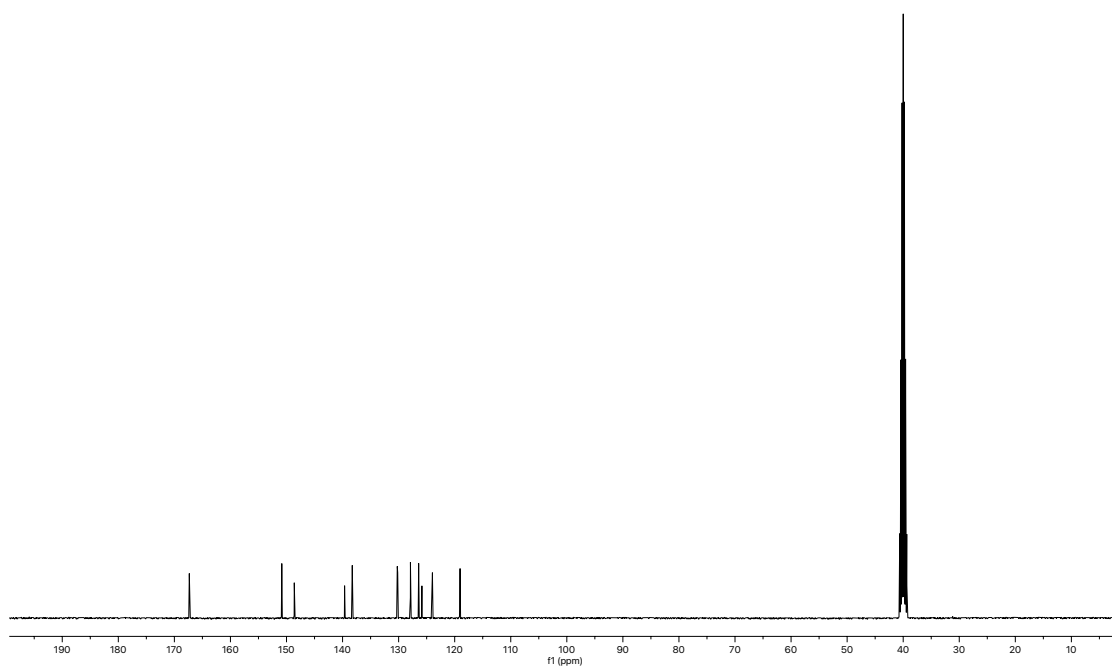
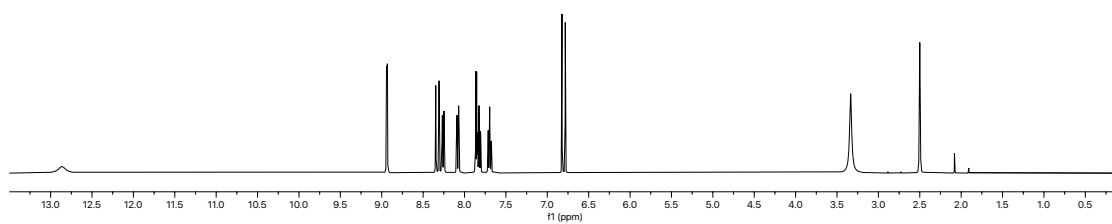


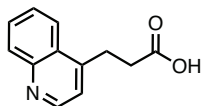




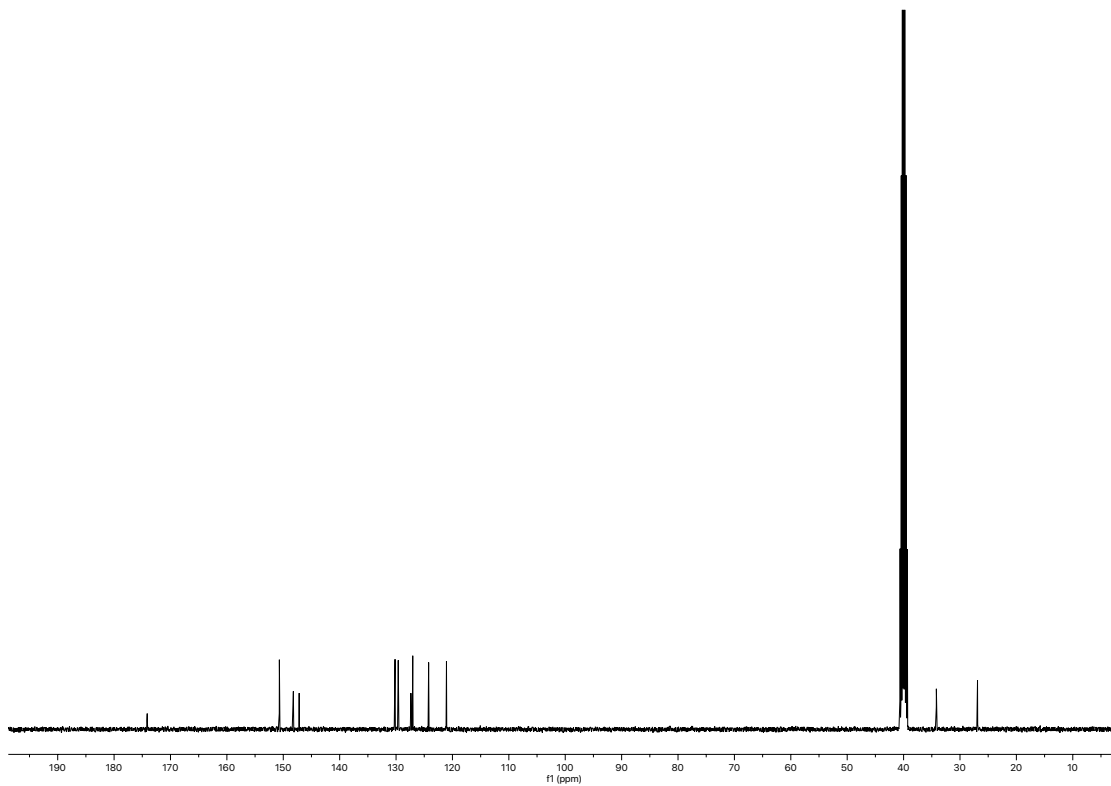
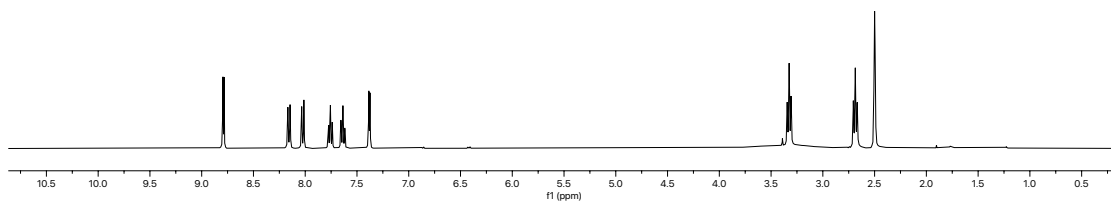


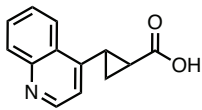
S2.7



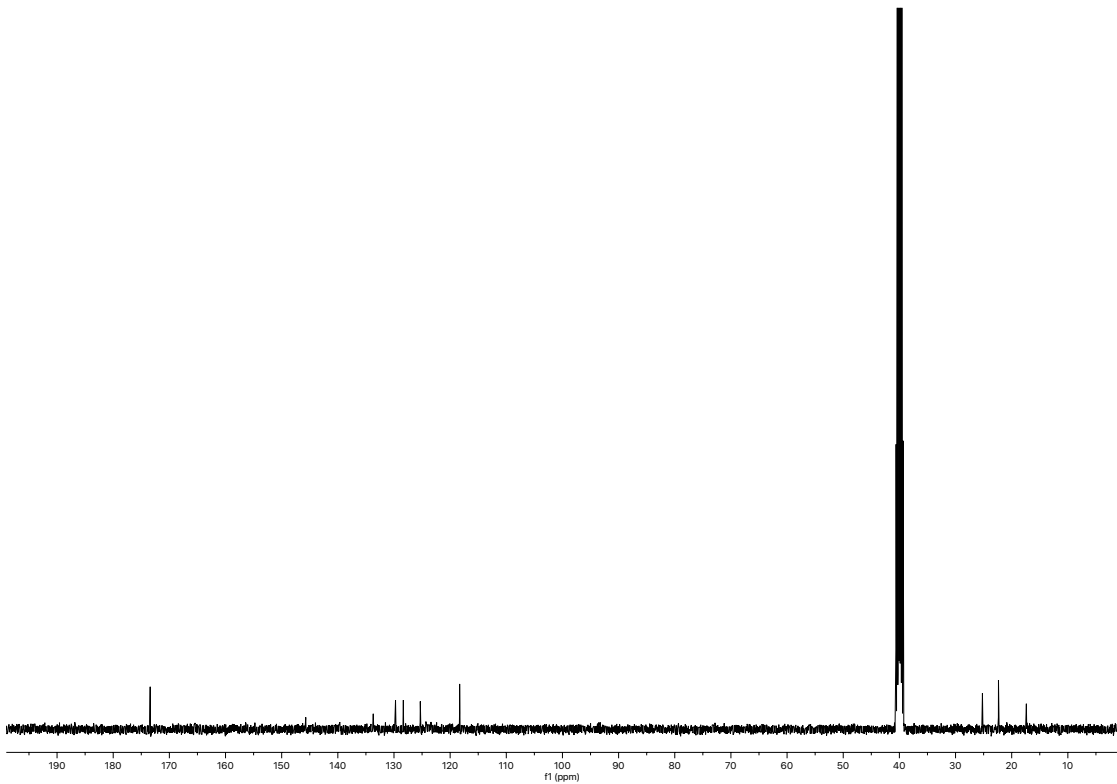
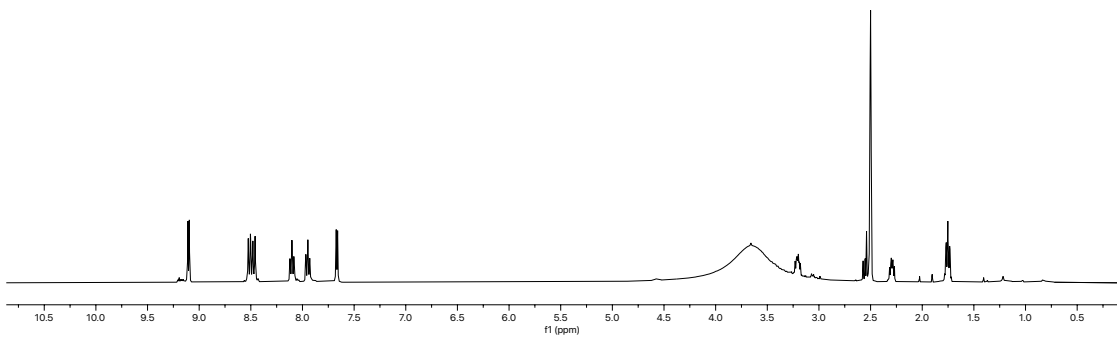


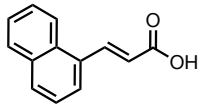
S2.8



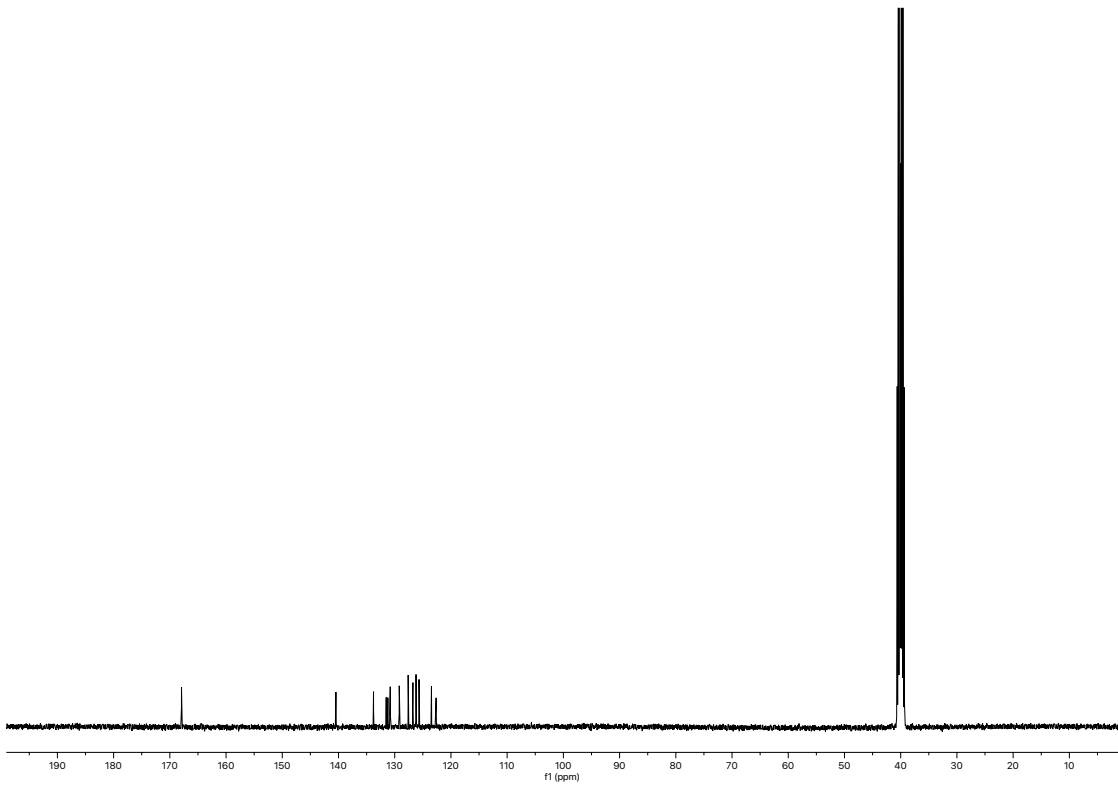
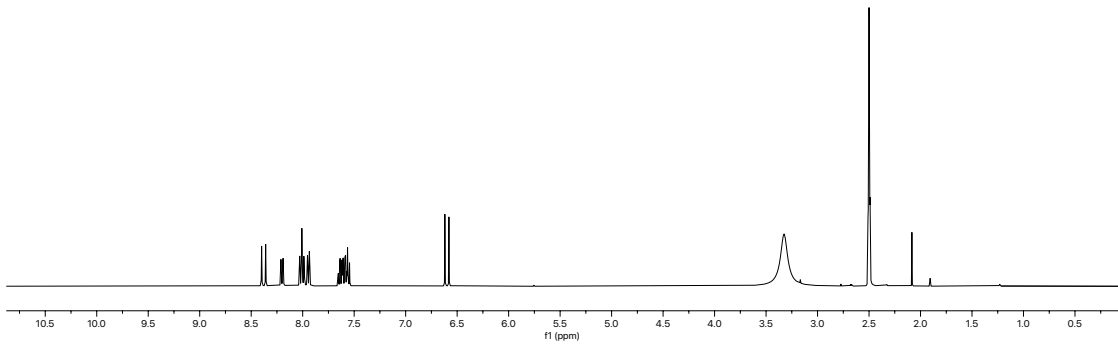


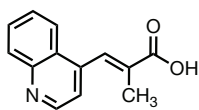
S2.10



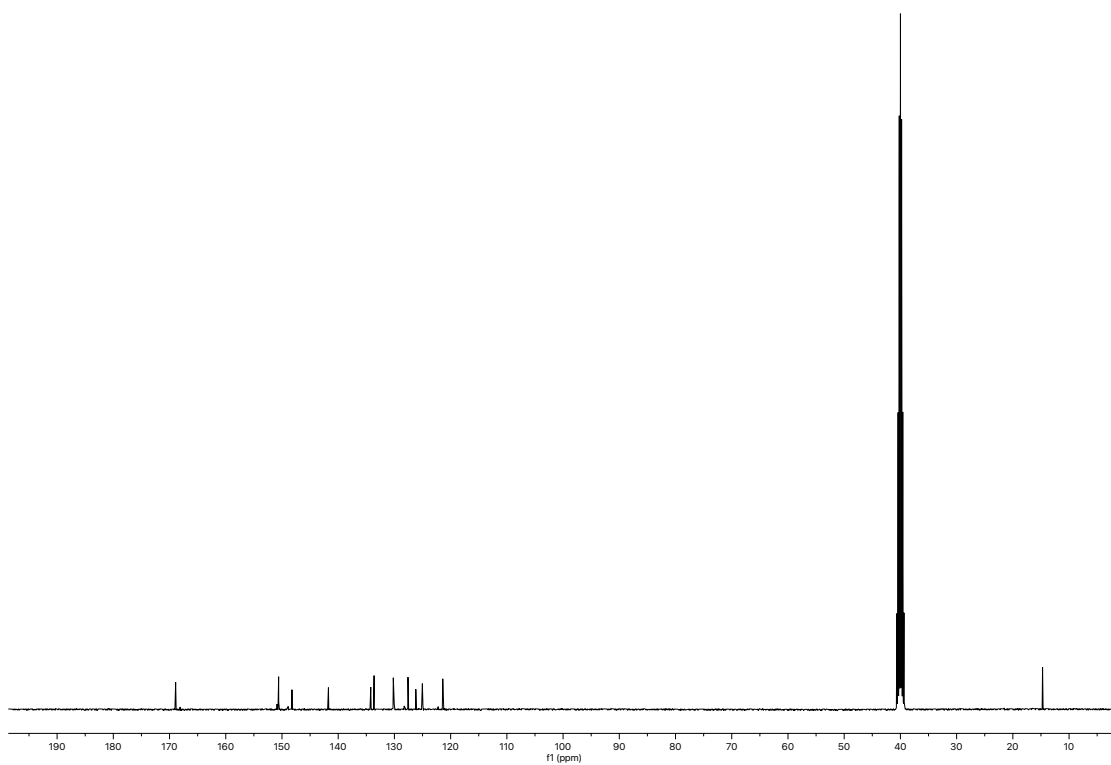
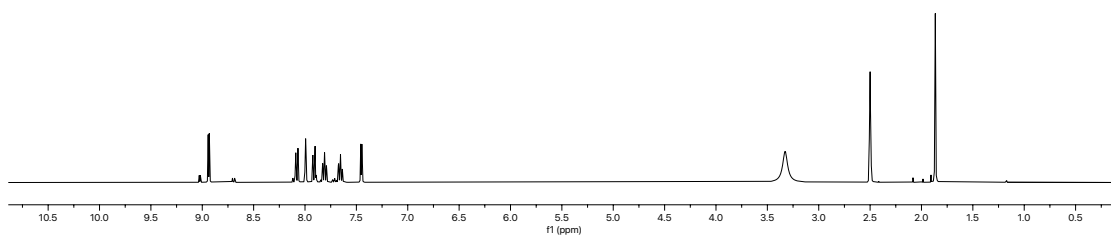


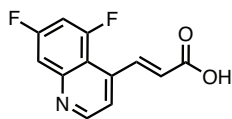
S2.12



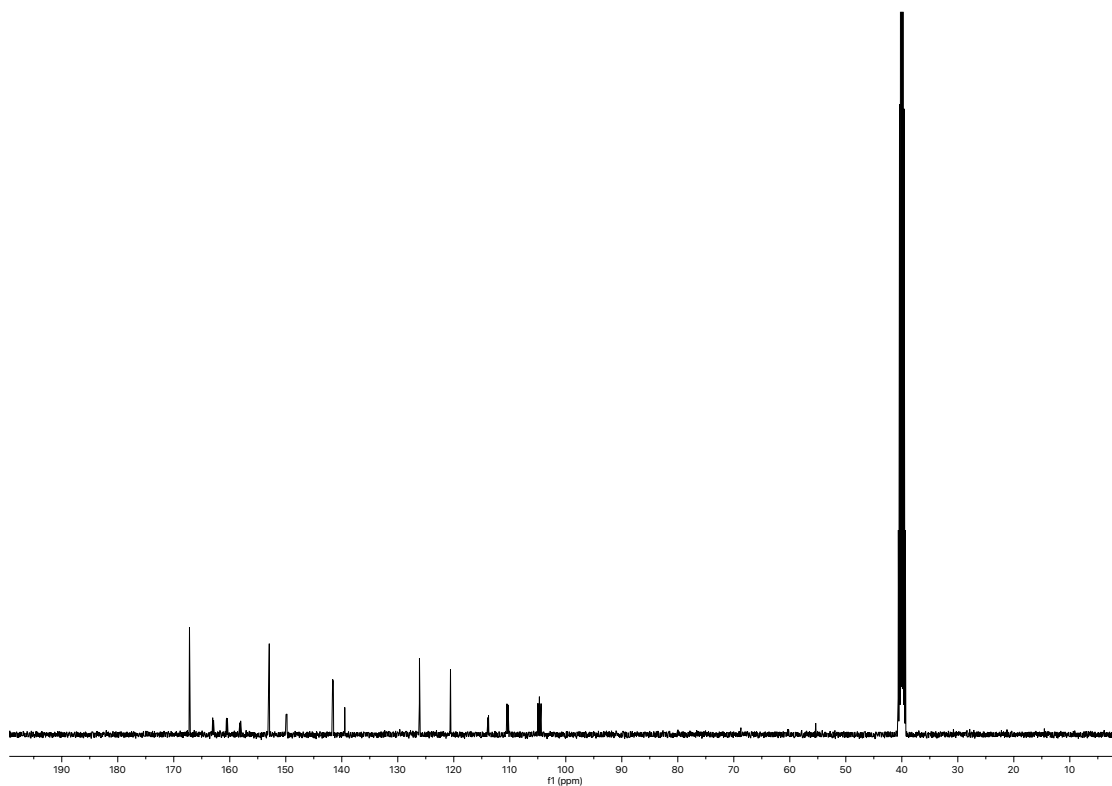
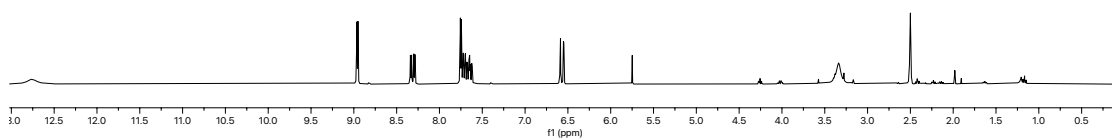


S2.13

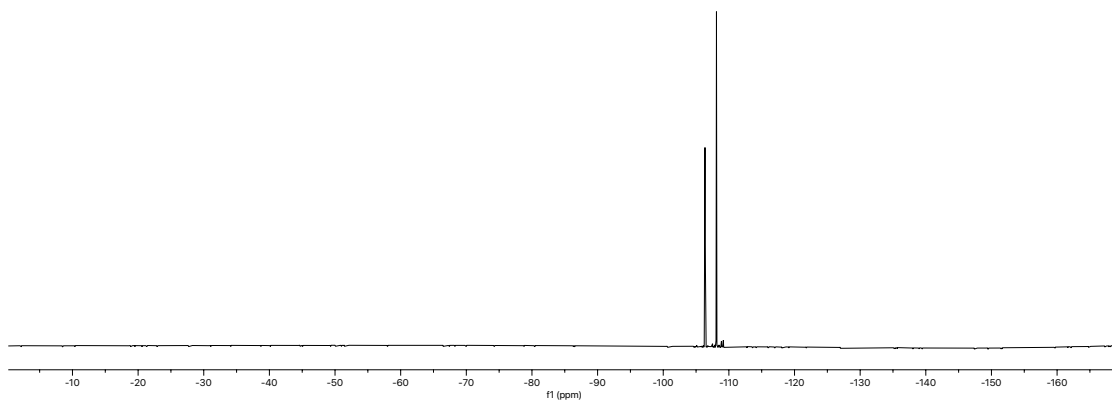




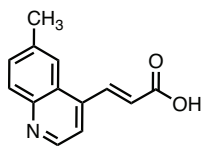
S2.15



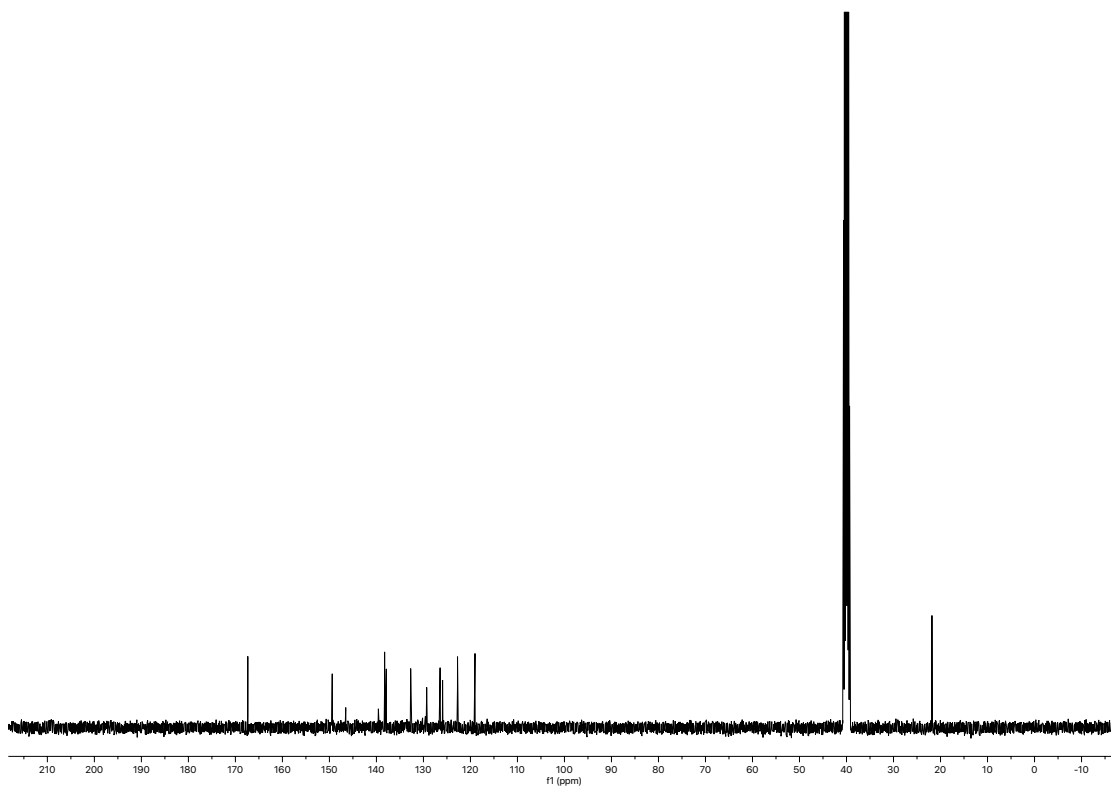
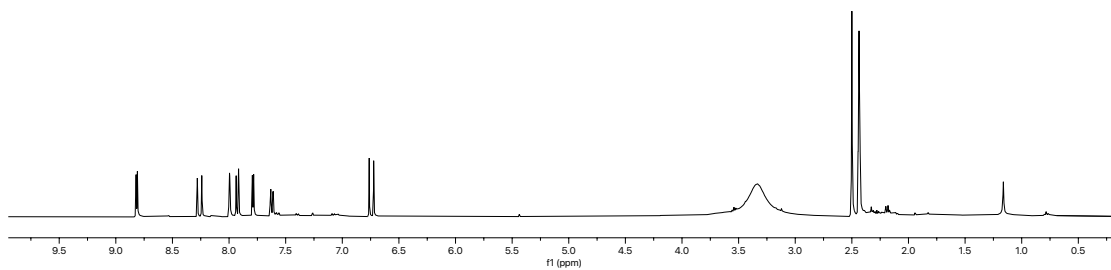


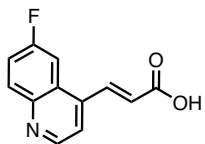




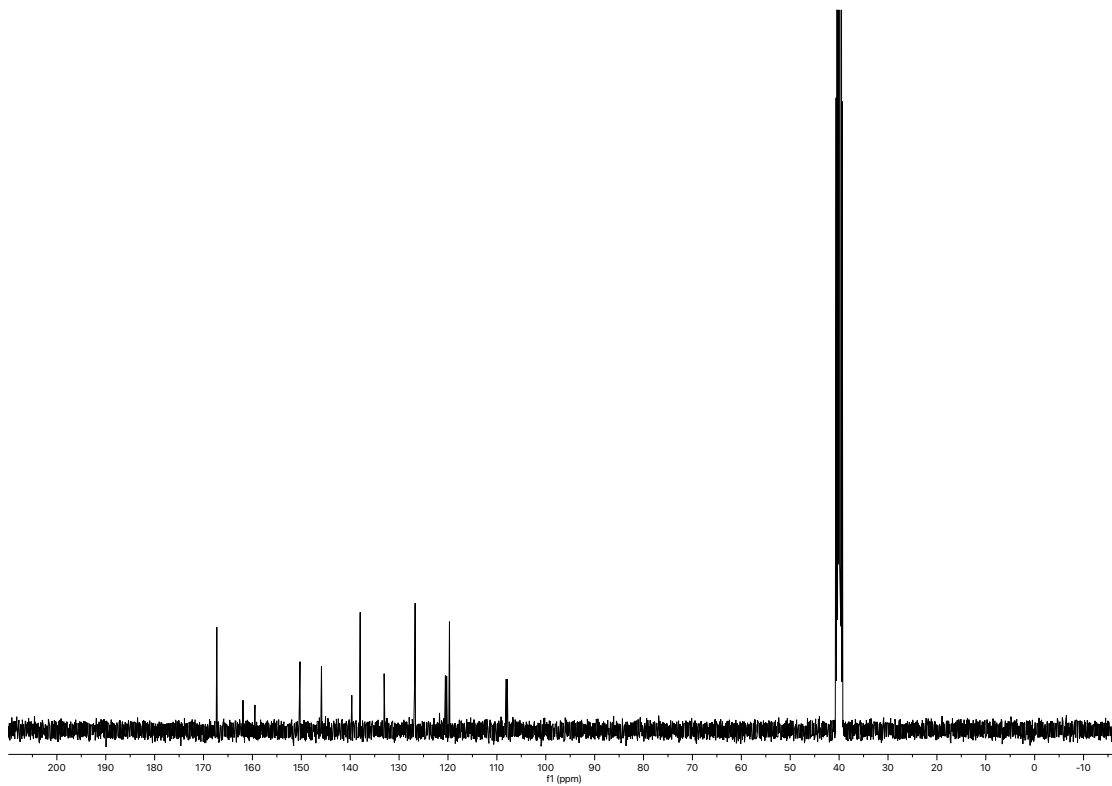
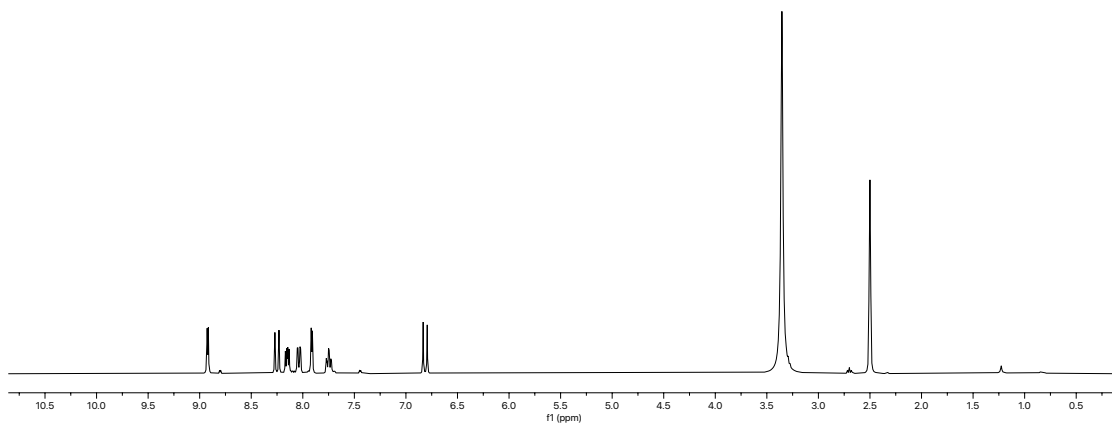


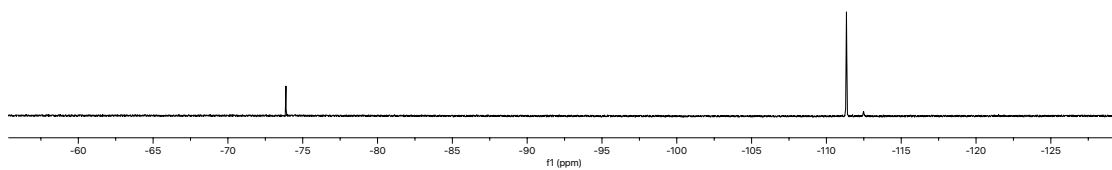
S2.19

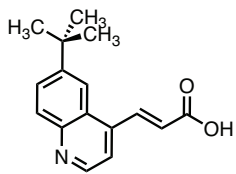




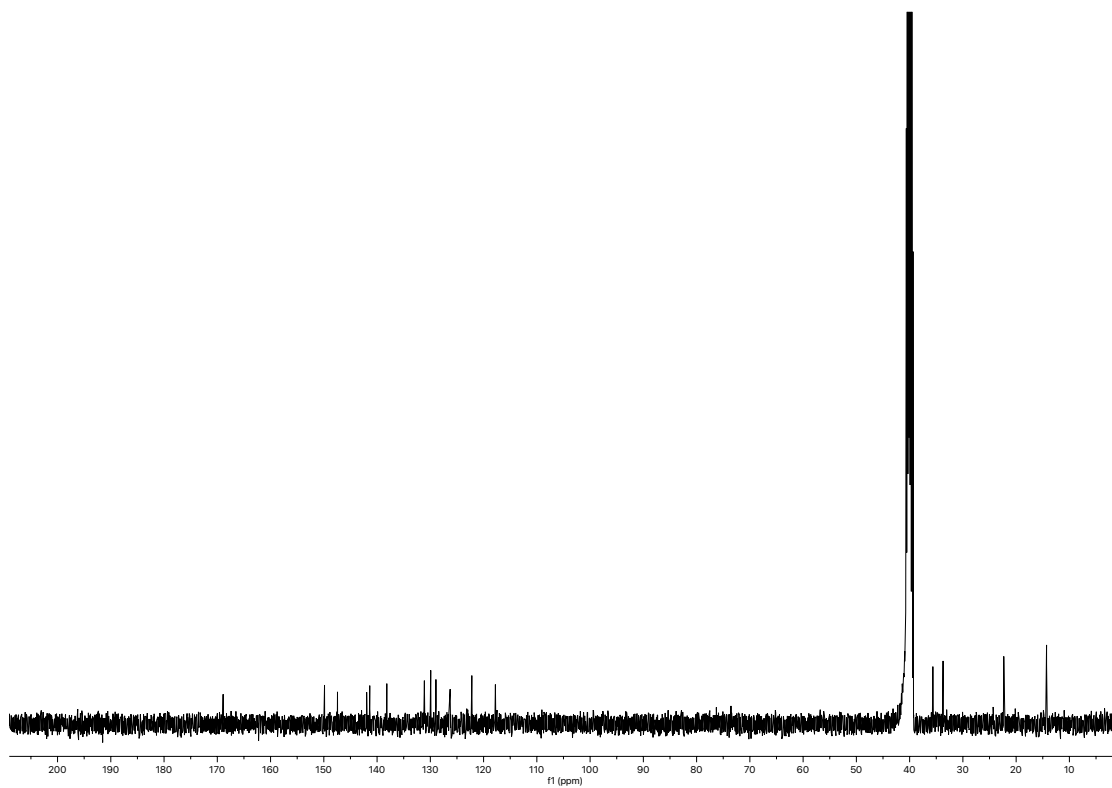
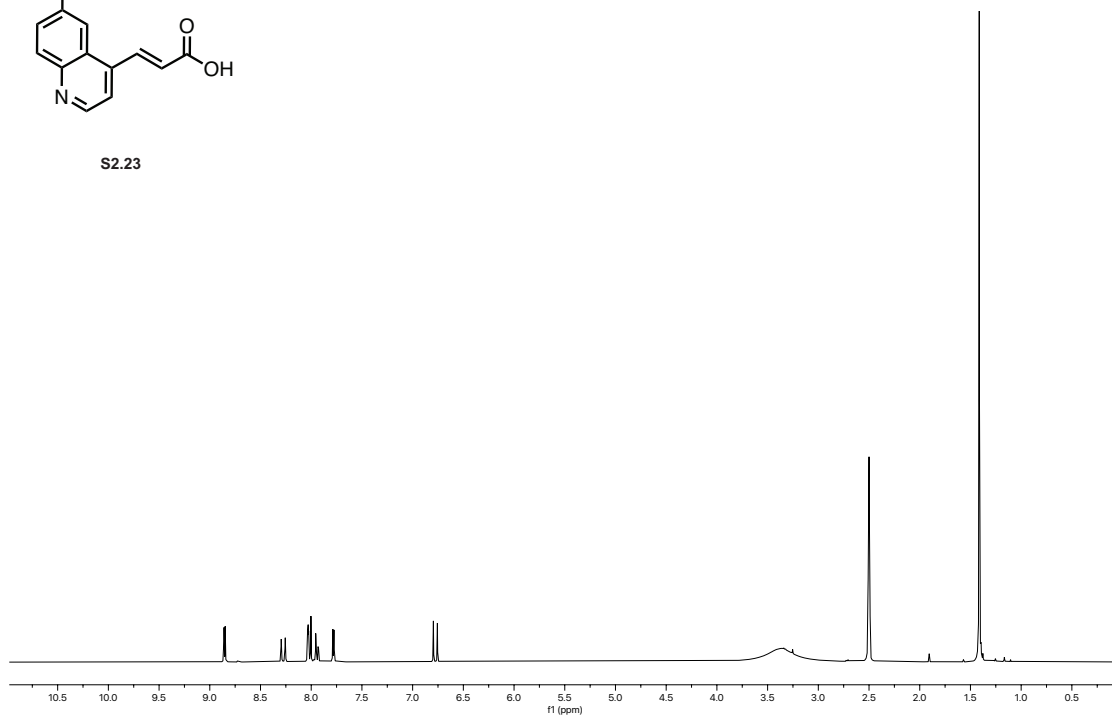
S2.21



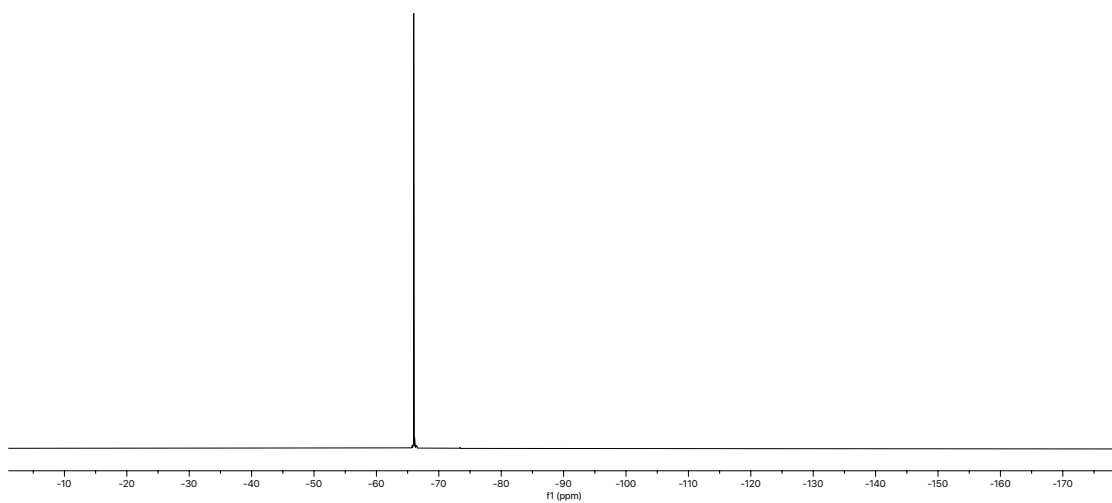




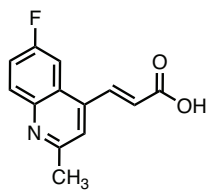
S2.23



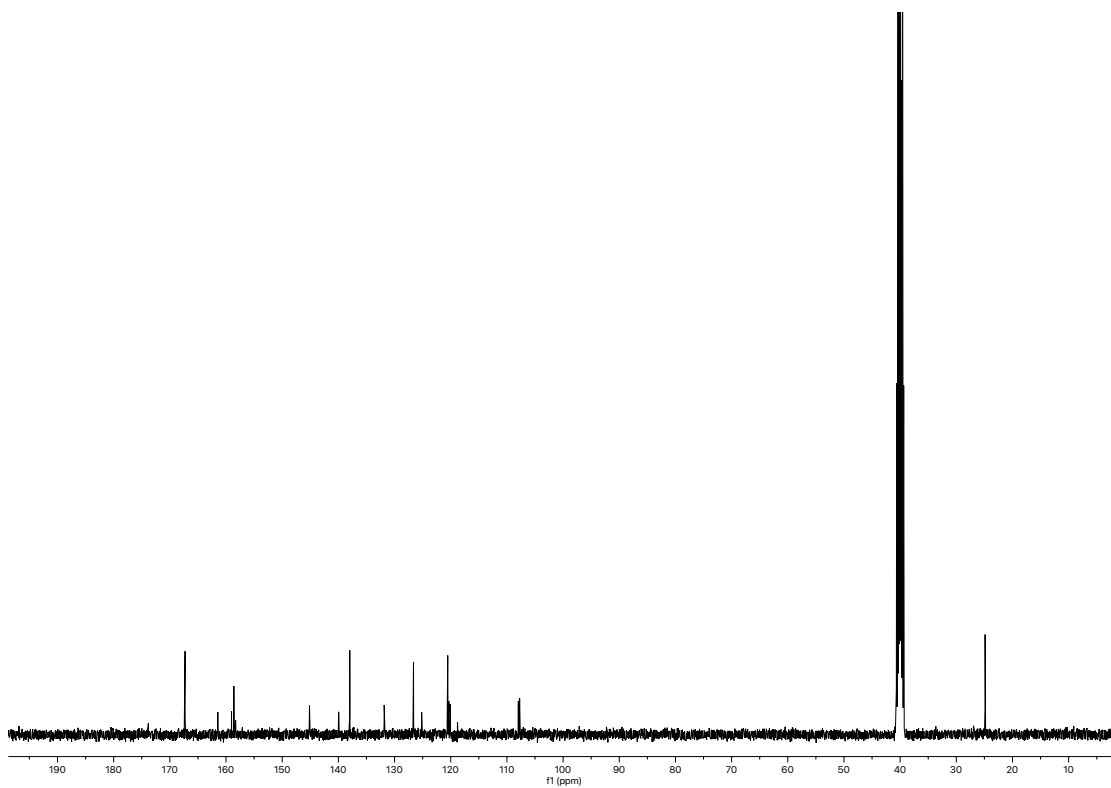
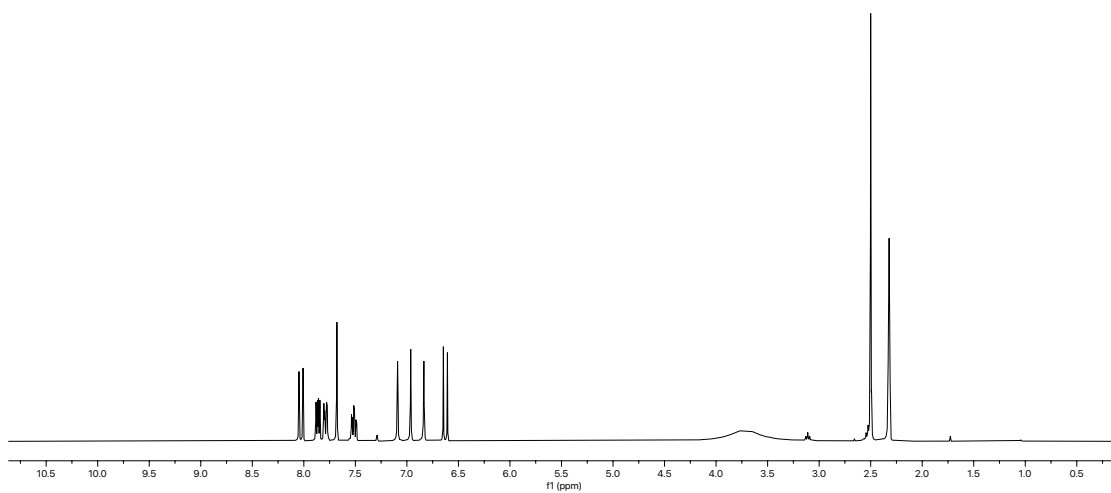


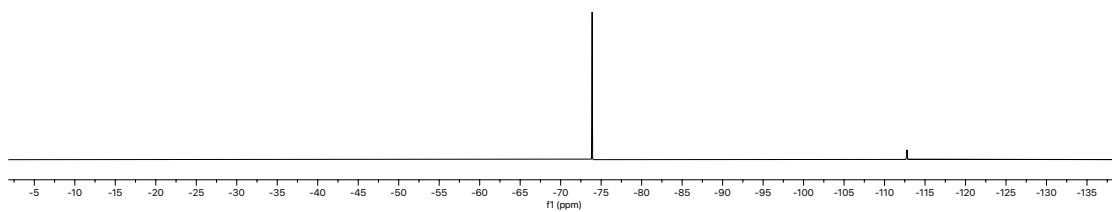


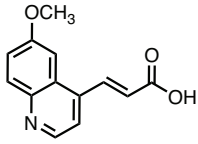




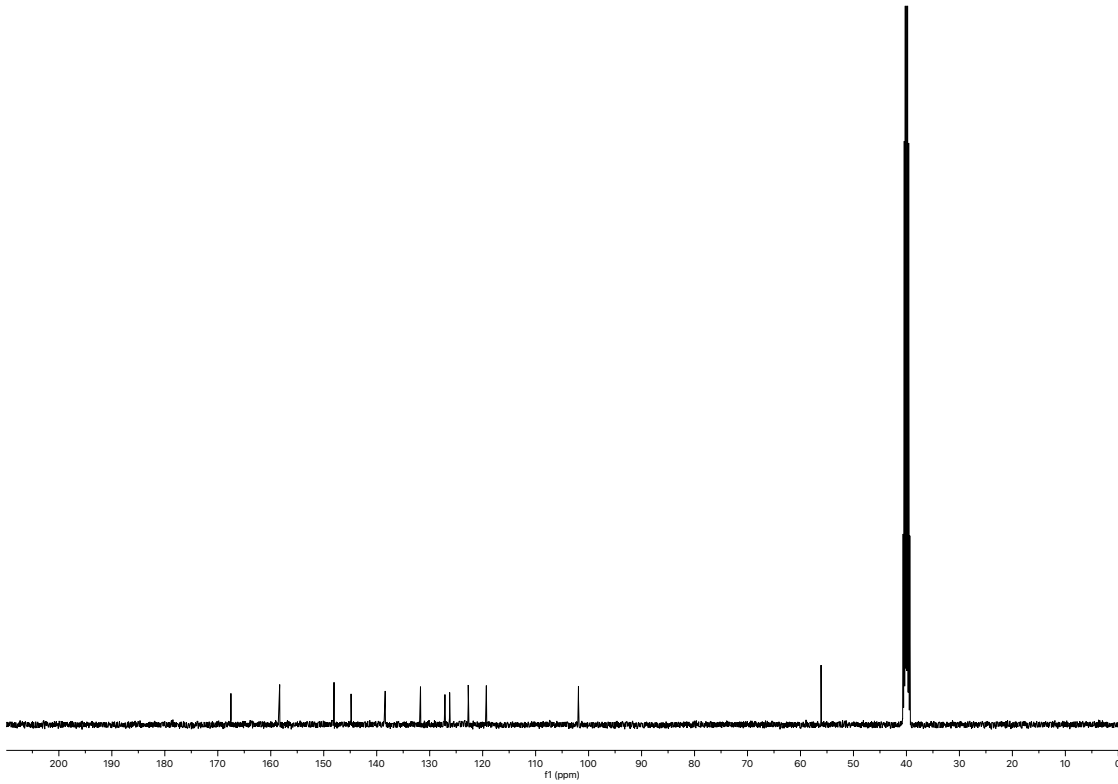
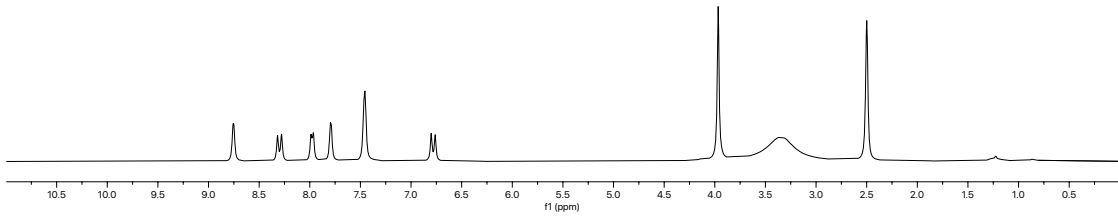
S2.27

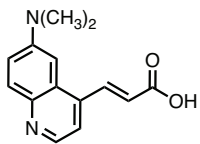




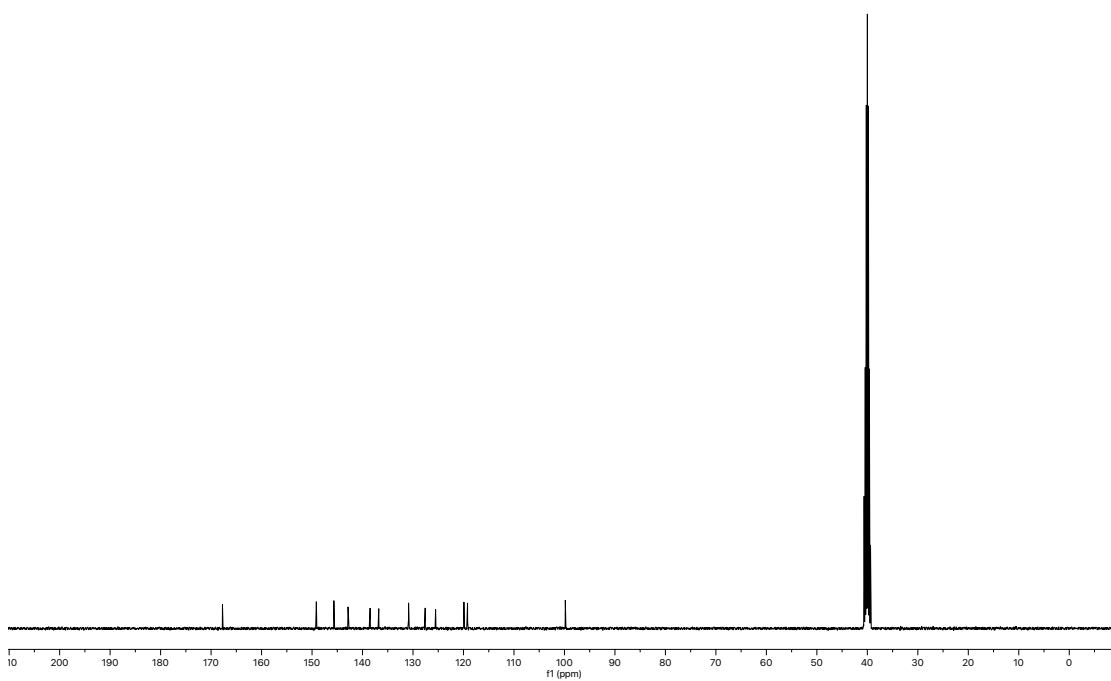
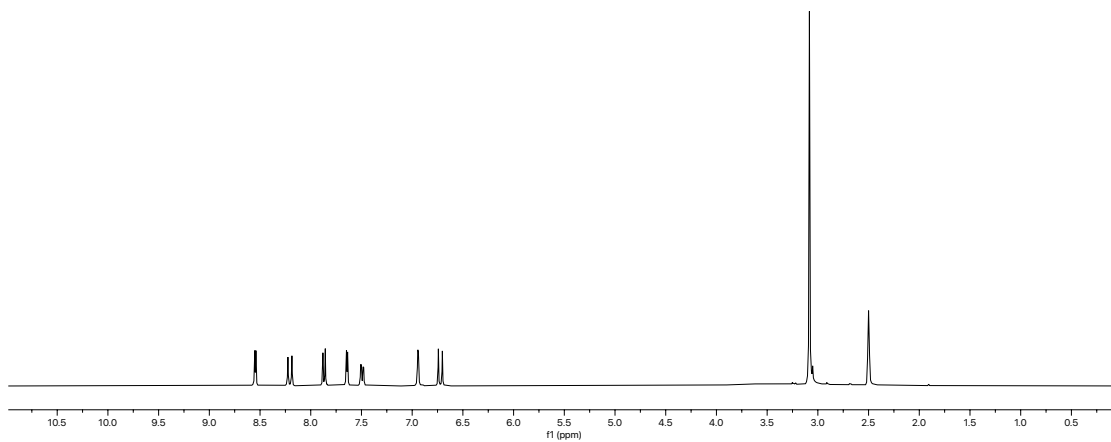


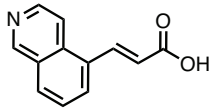
S2.29



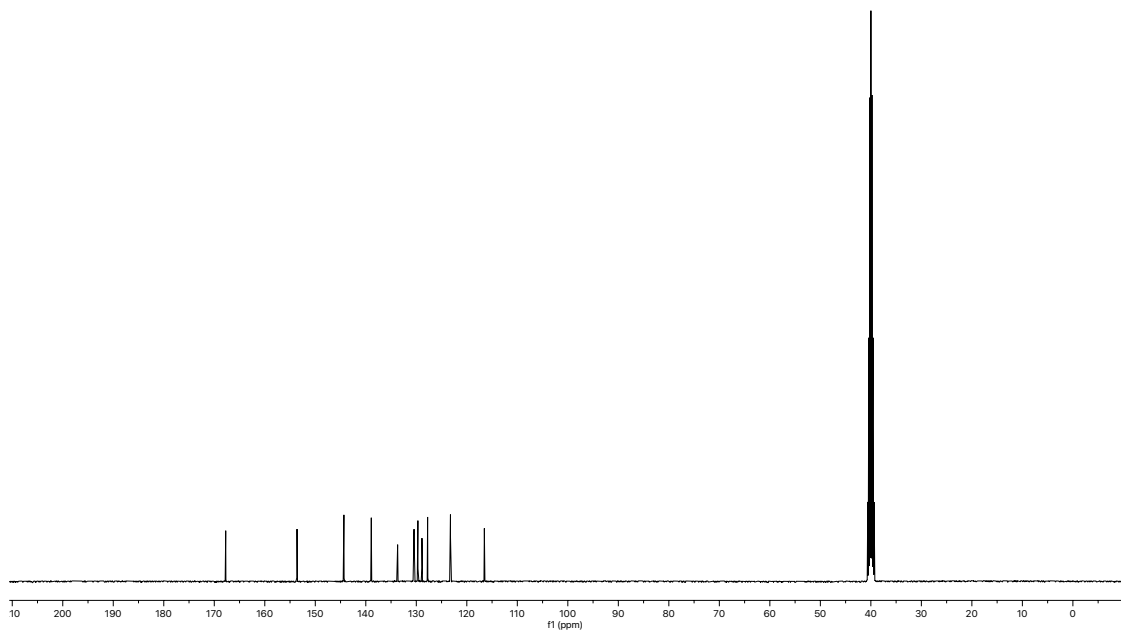
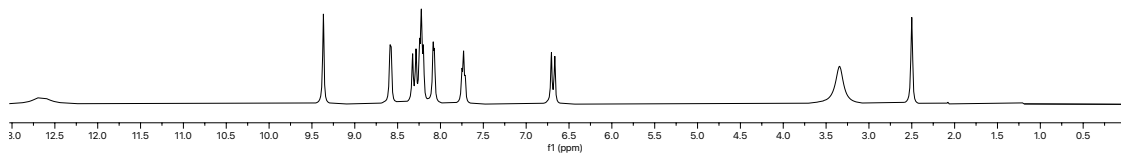


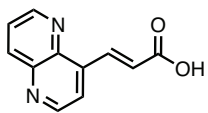
S2.31



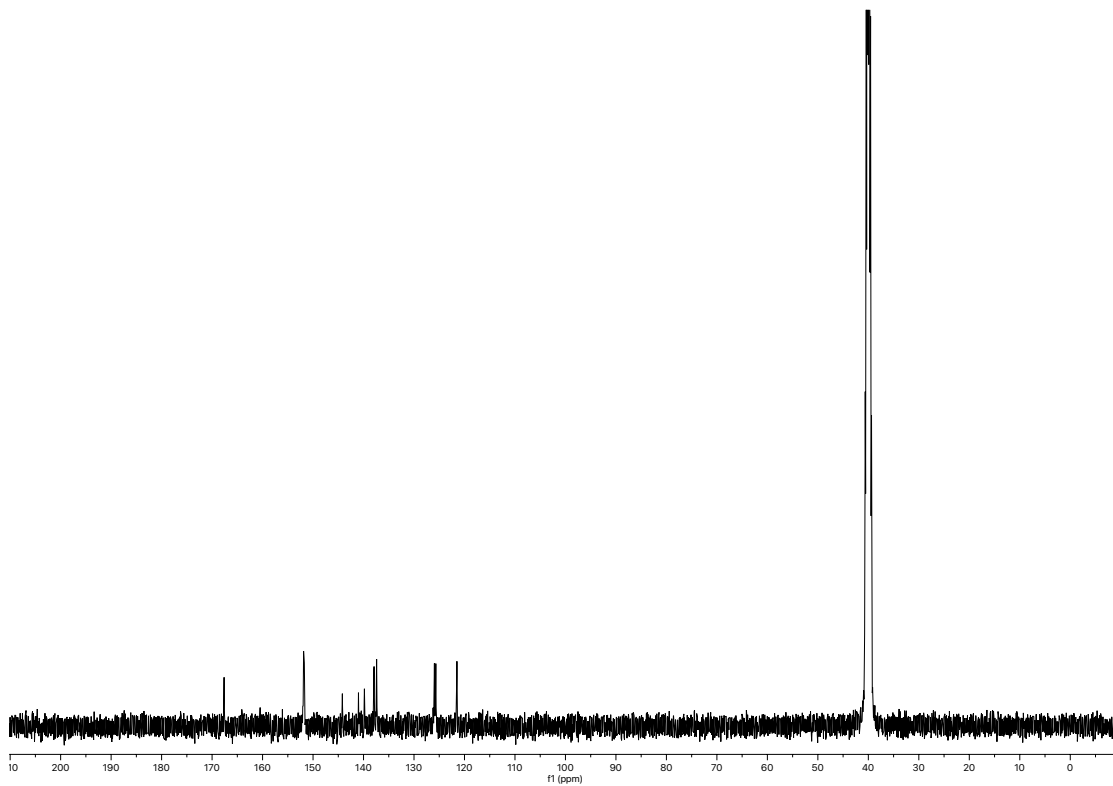
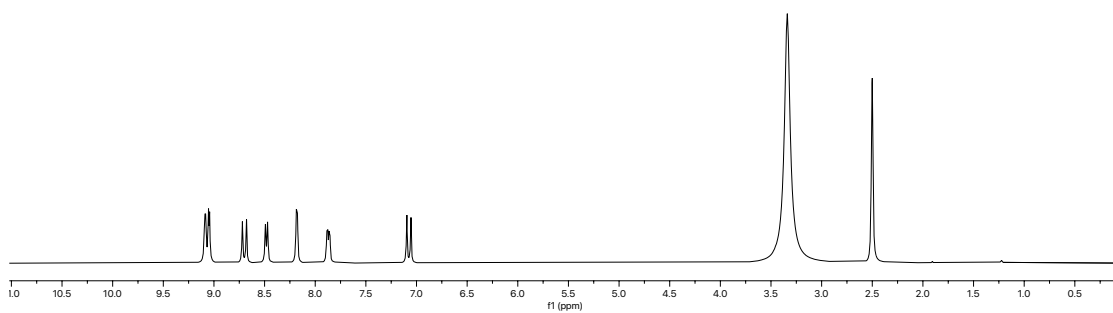


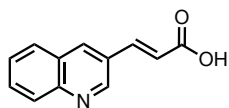
S2.35



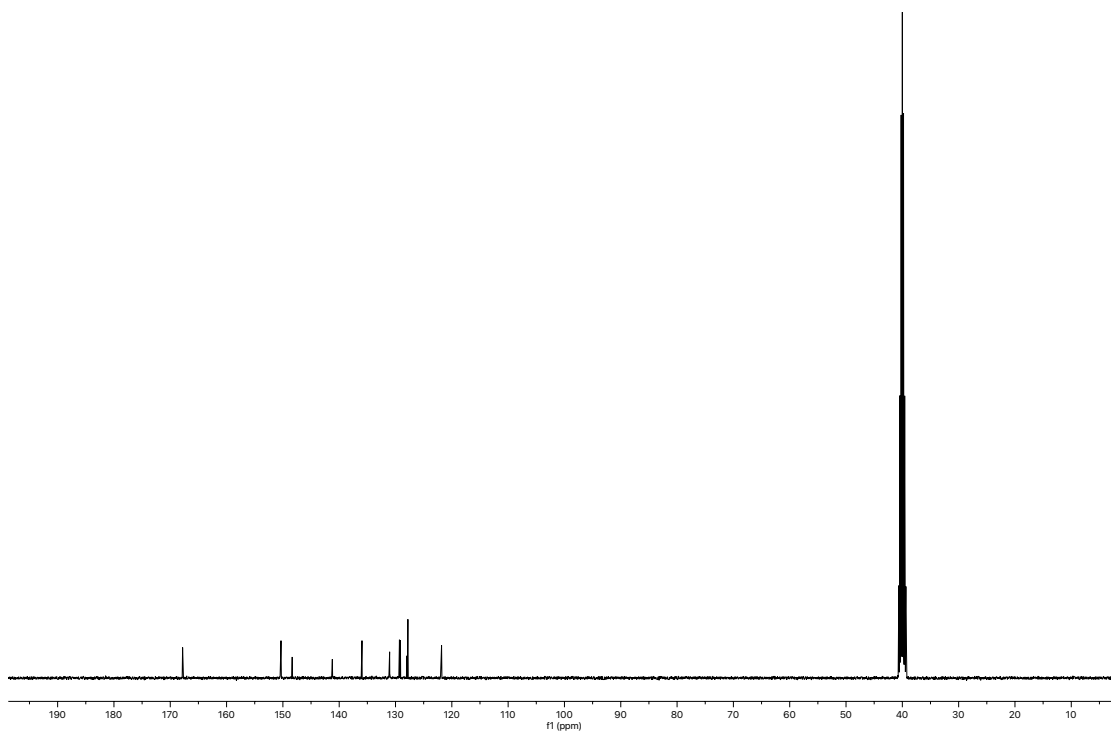
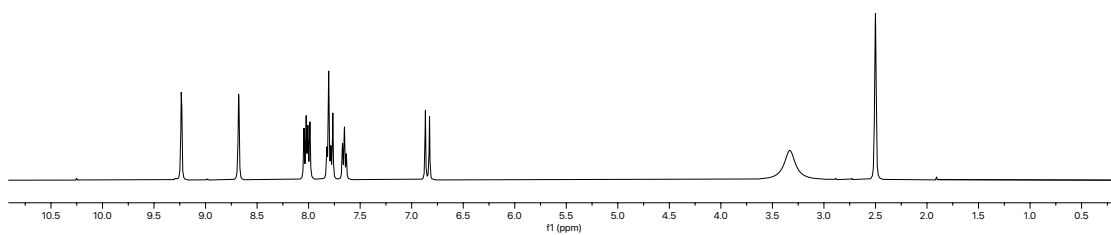


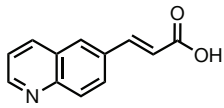
S2.39



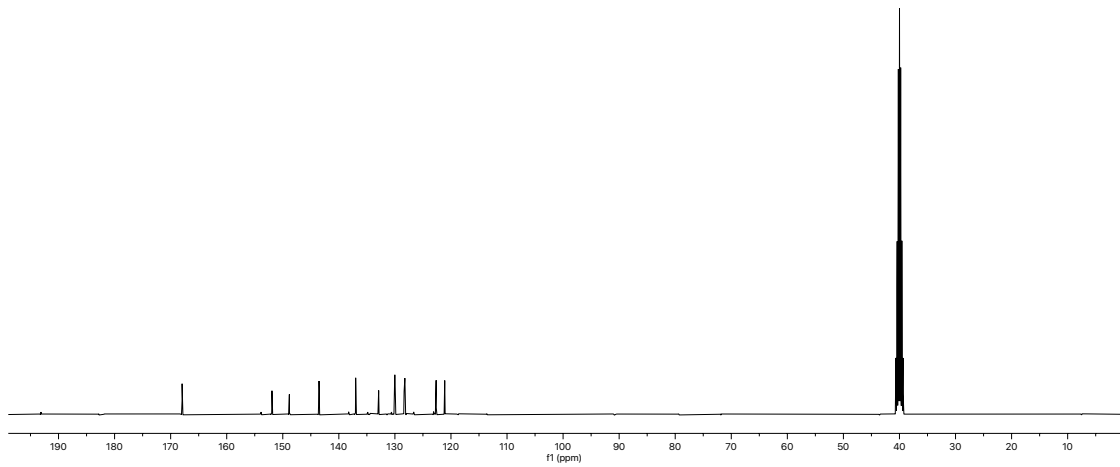
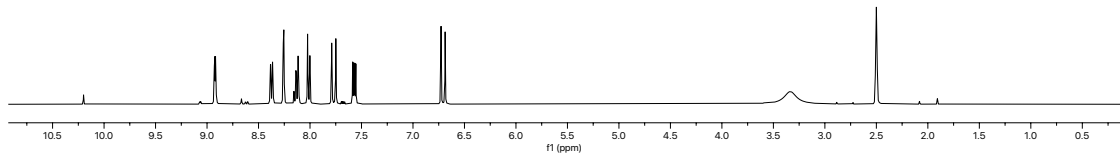


S2.41

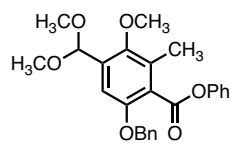




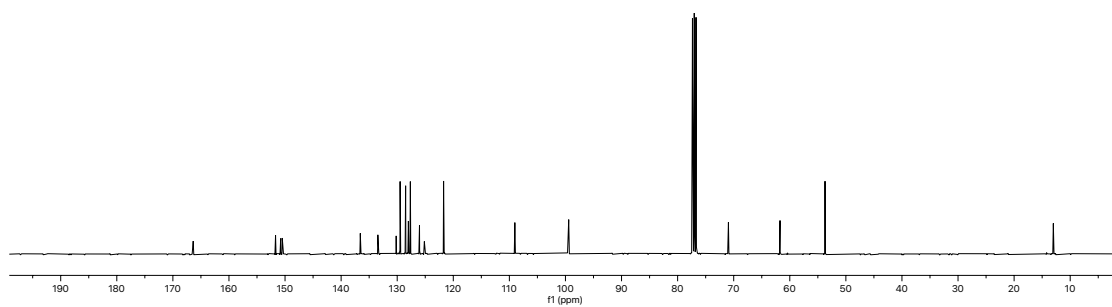
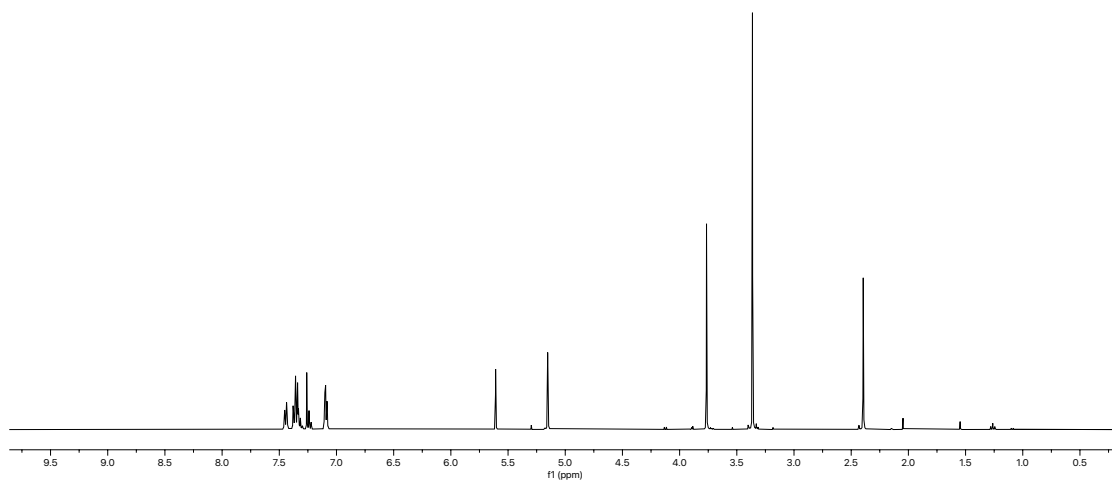
S2.43

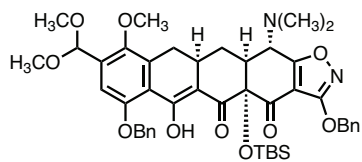




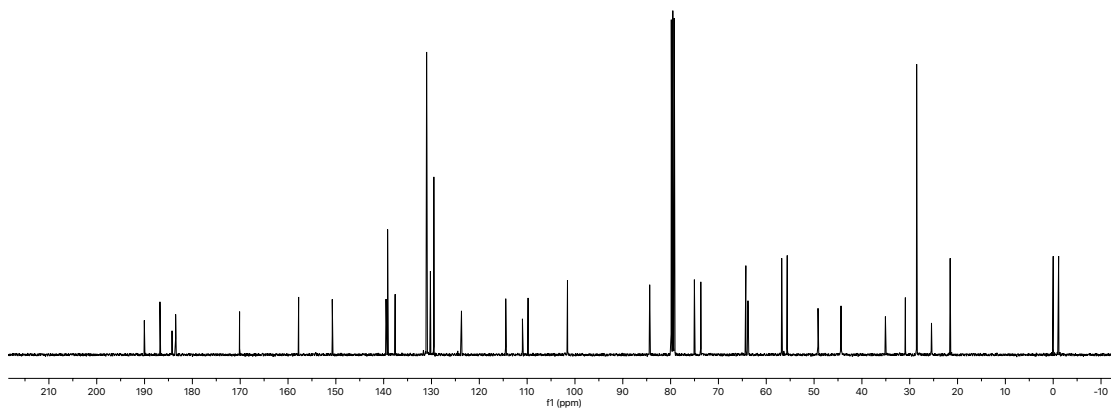
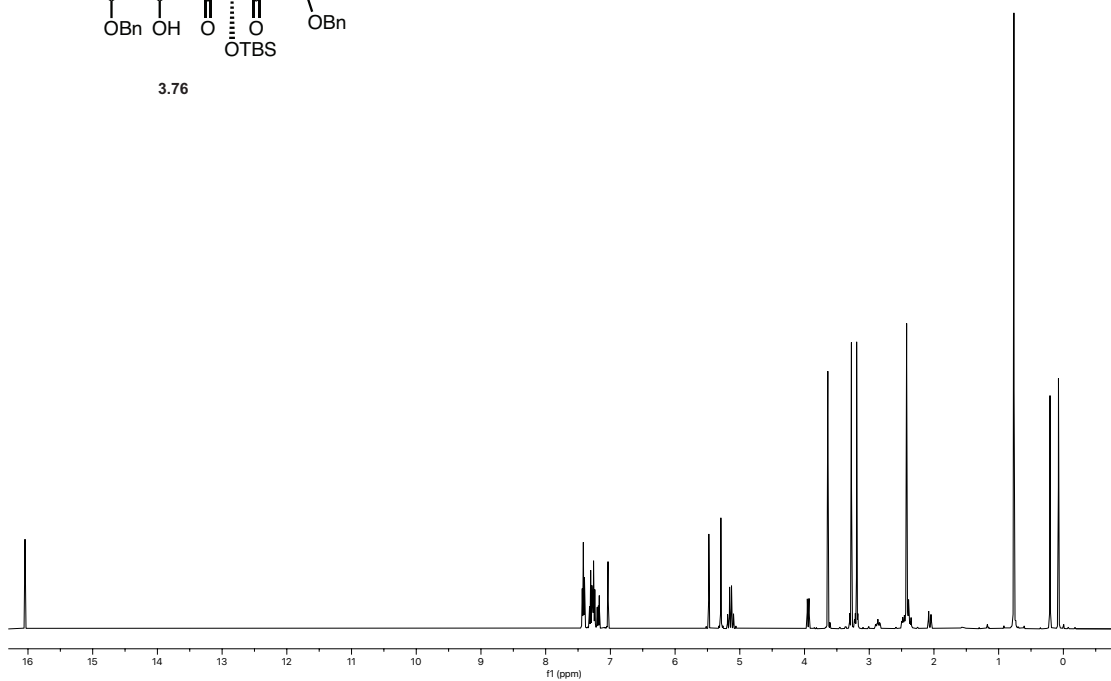


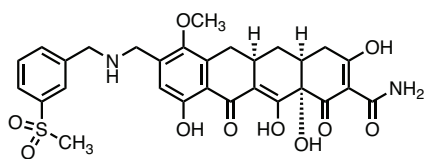
3.75



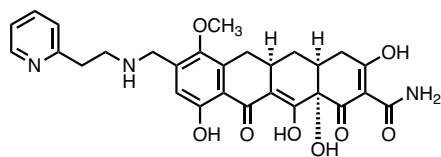
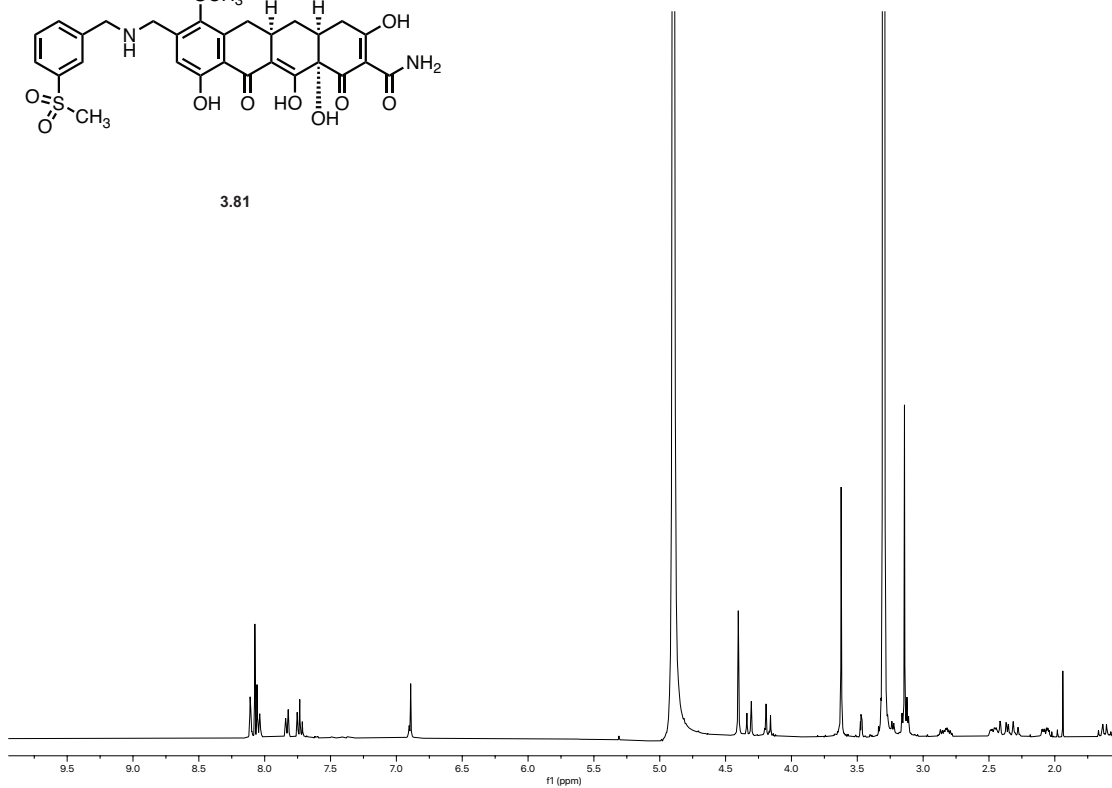


3.76

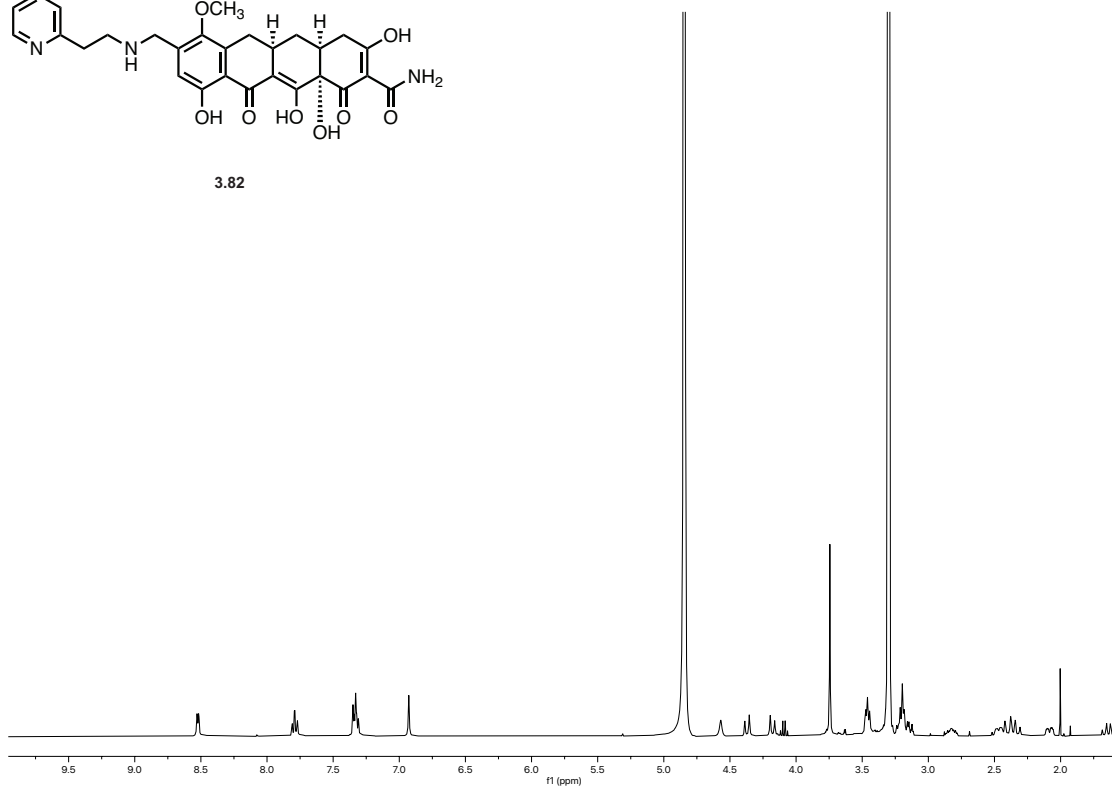


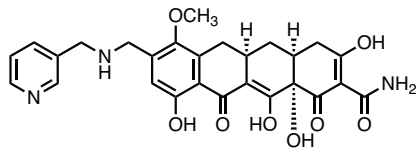


3.81

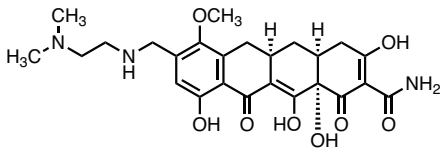
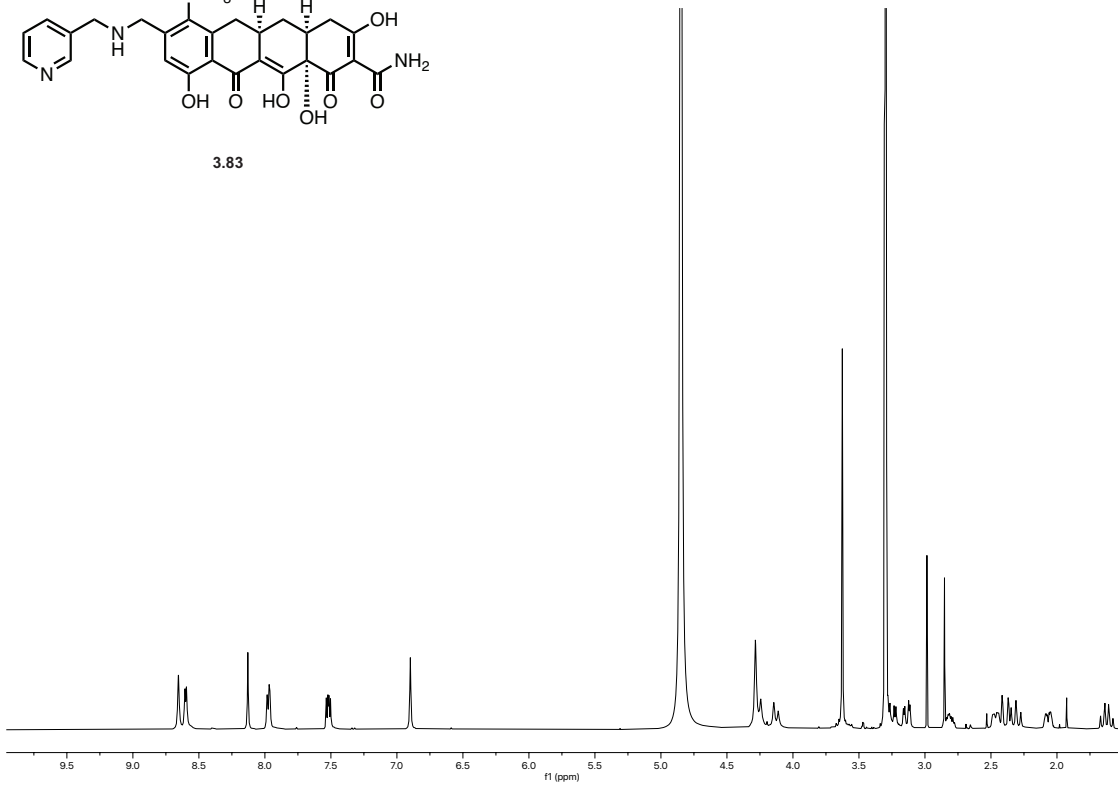


3.82

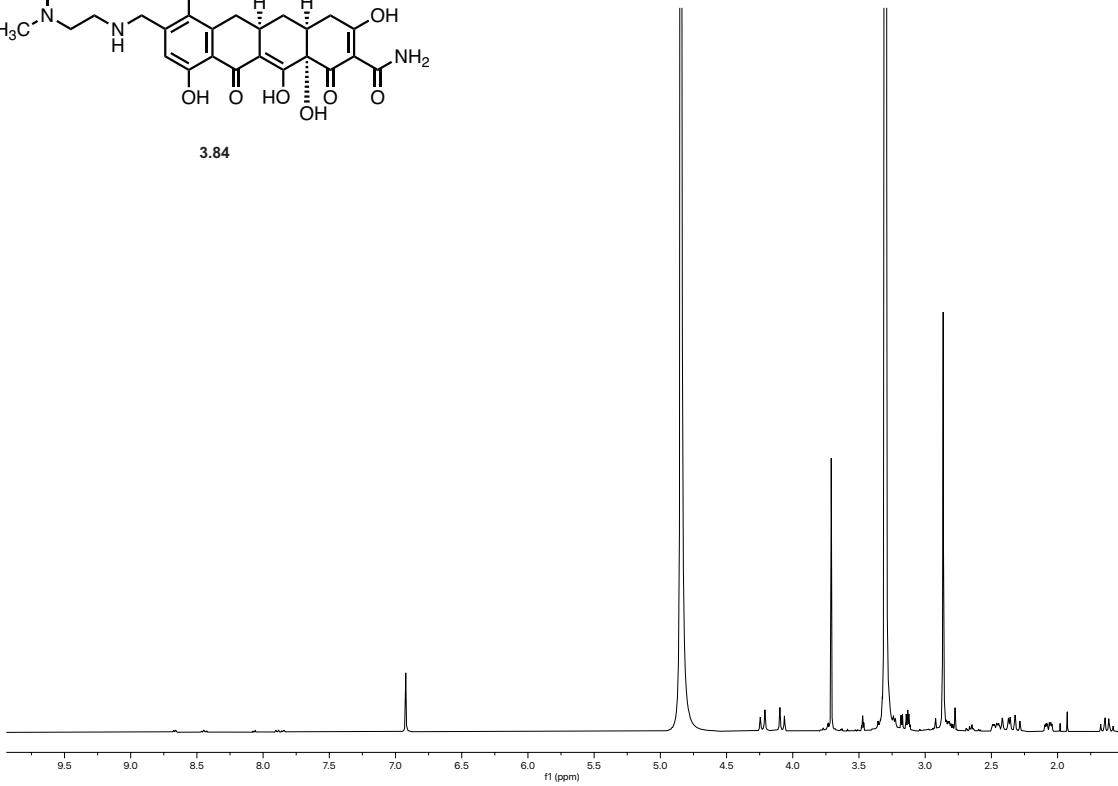


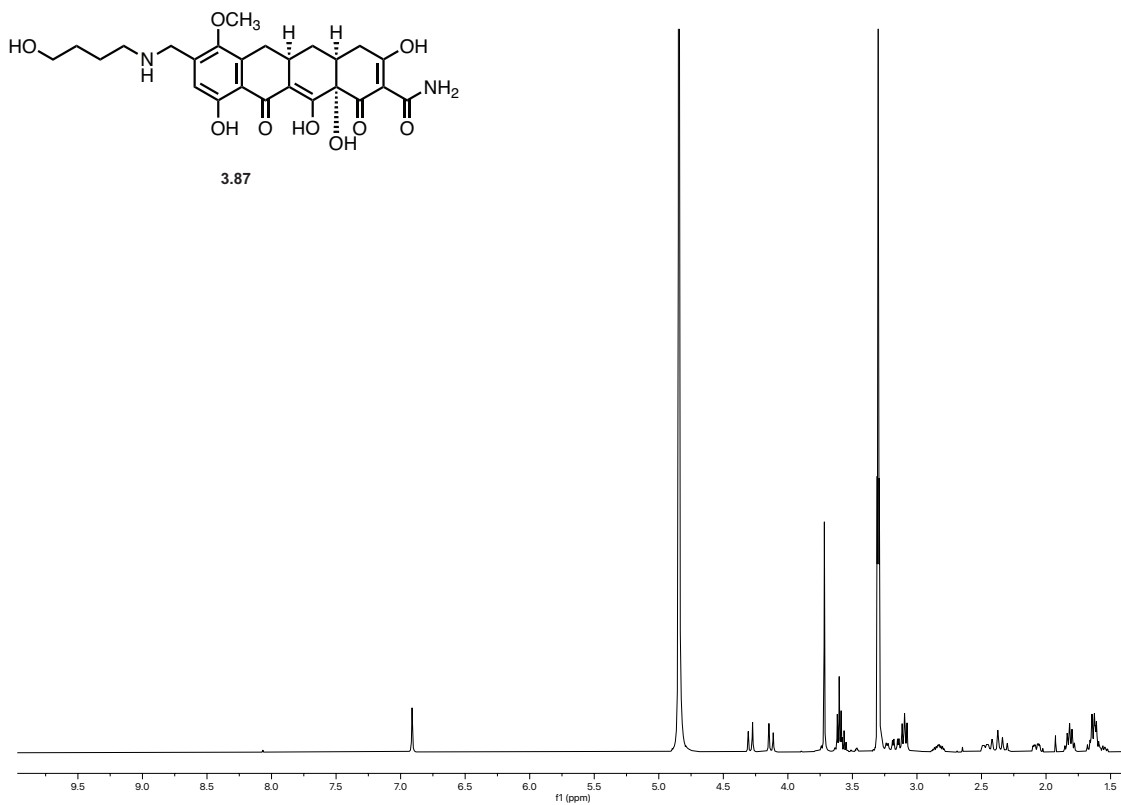
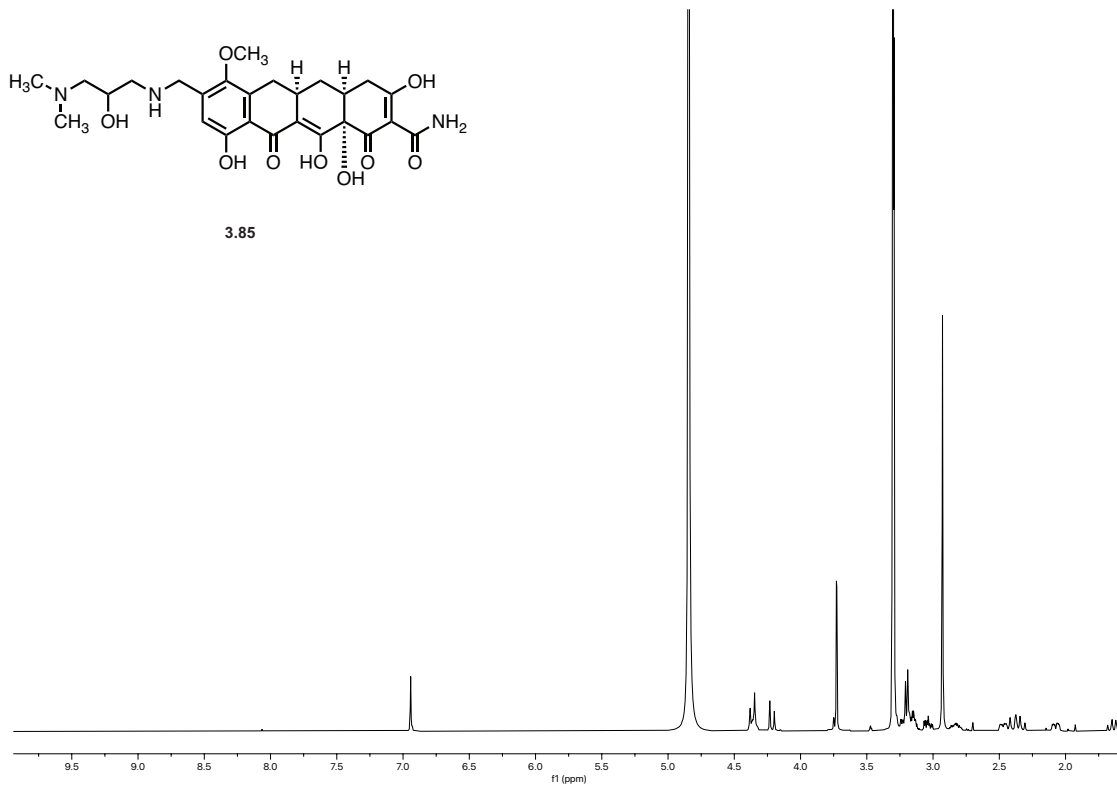


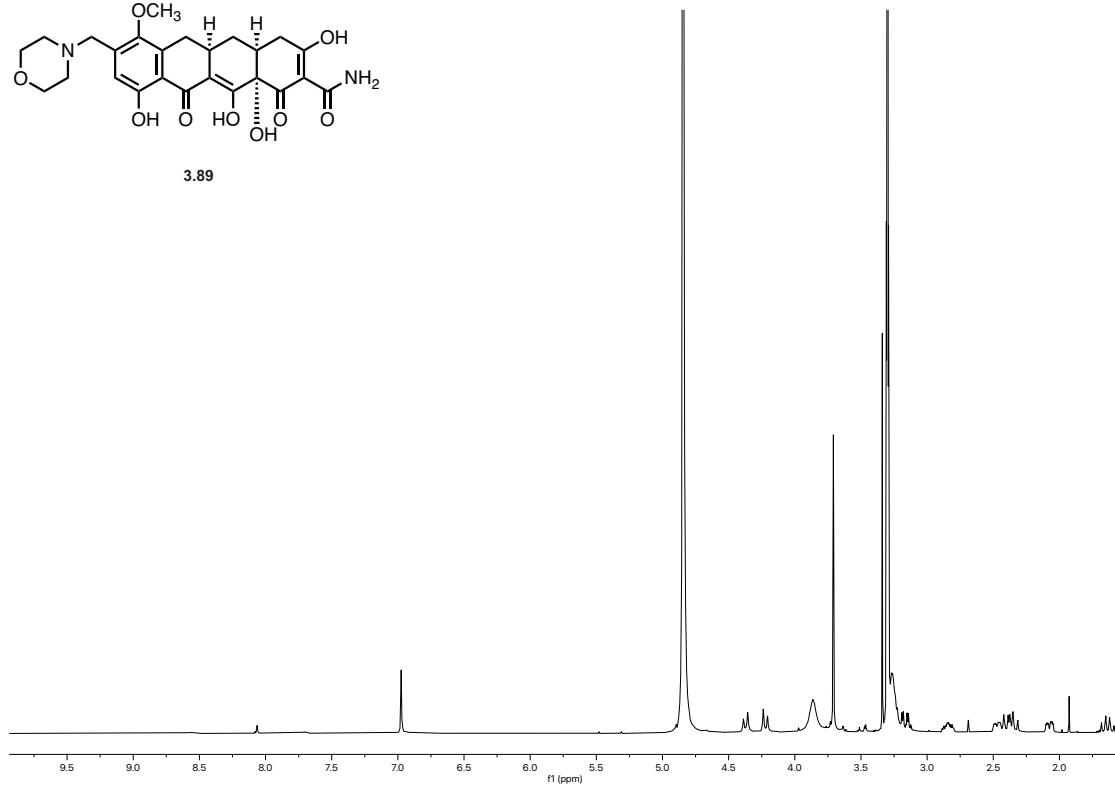
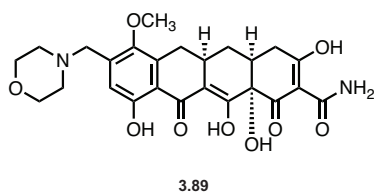
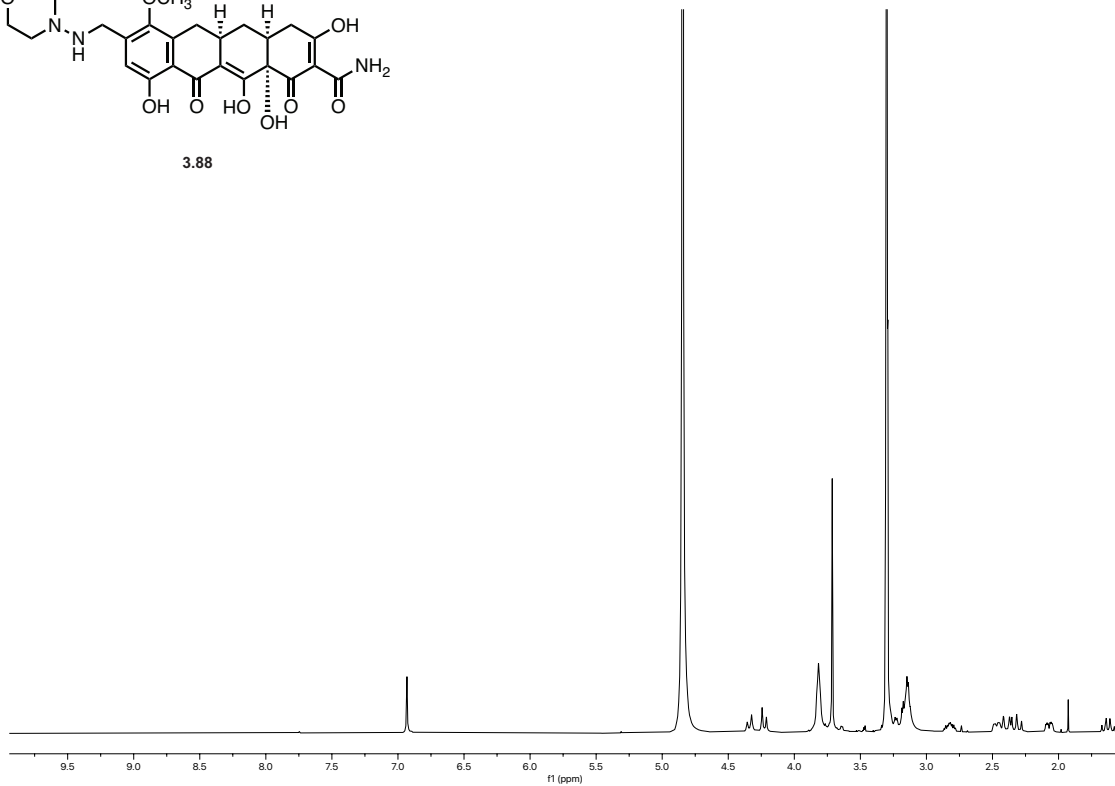
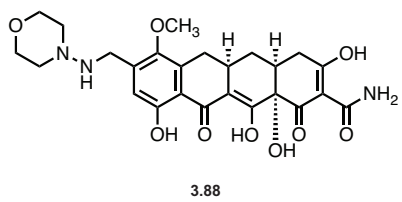
3.83

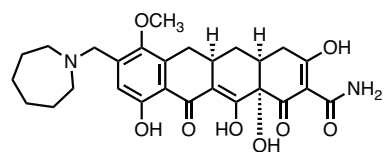


3.84

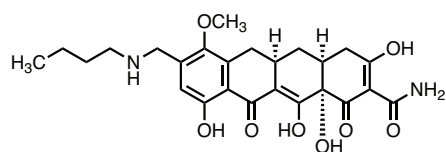
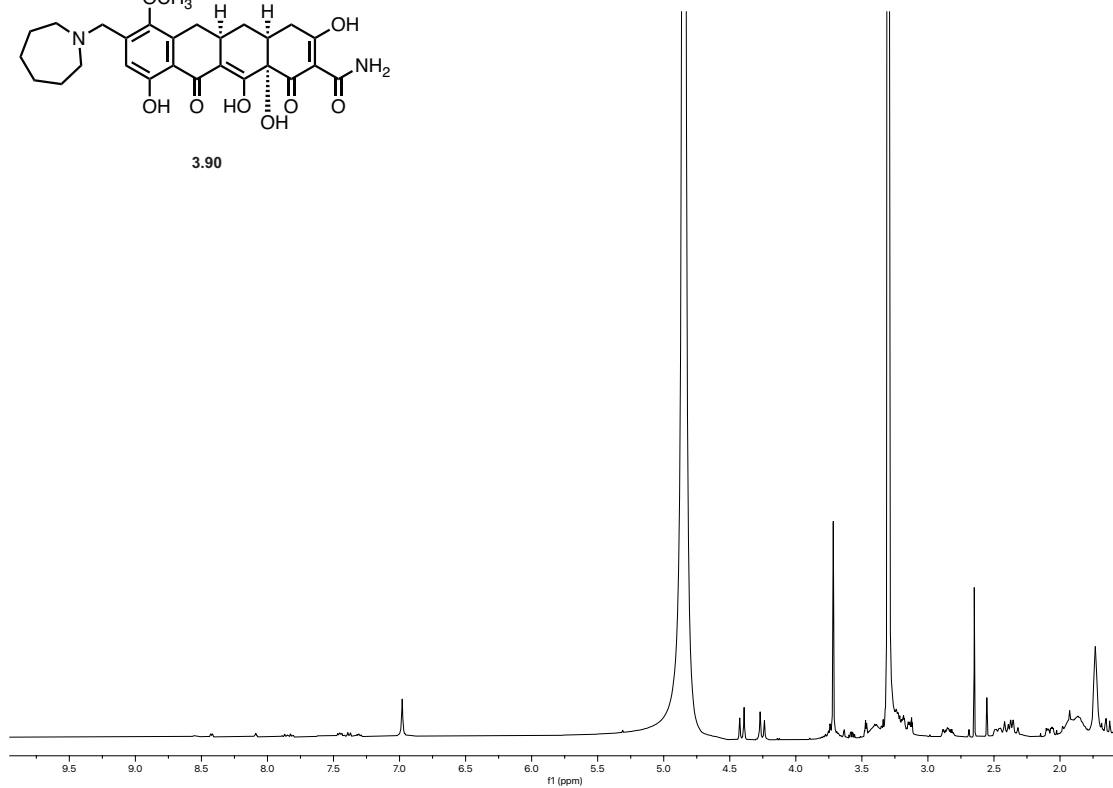




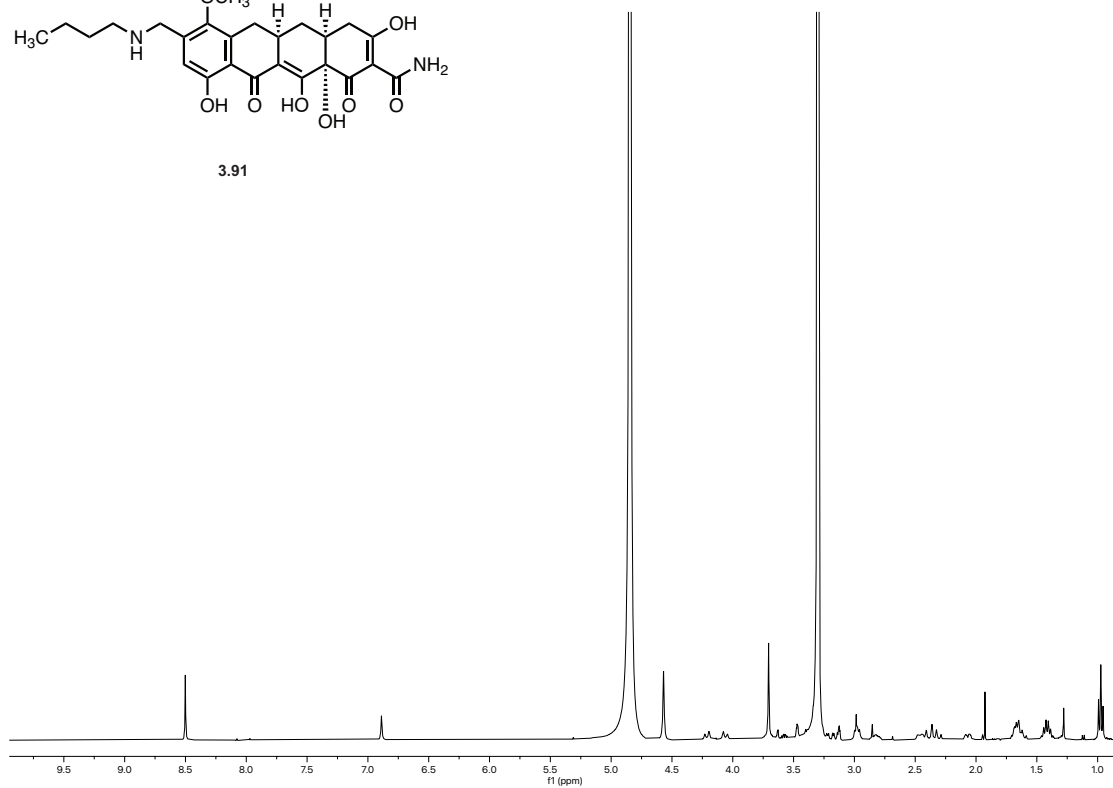


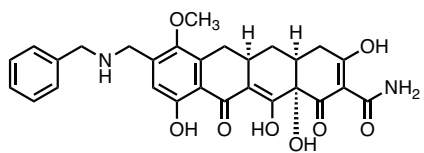


3.90

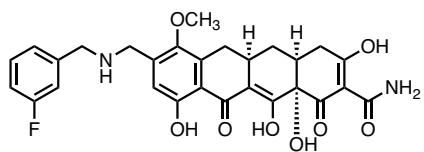
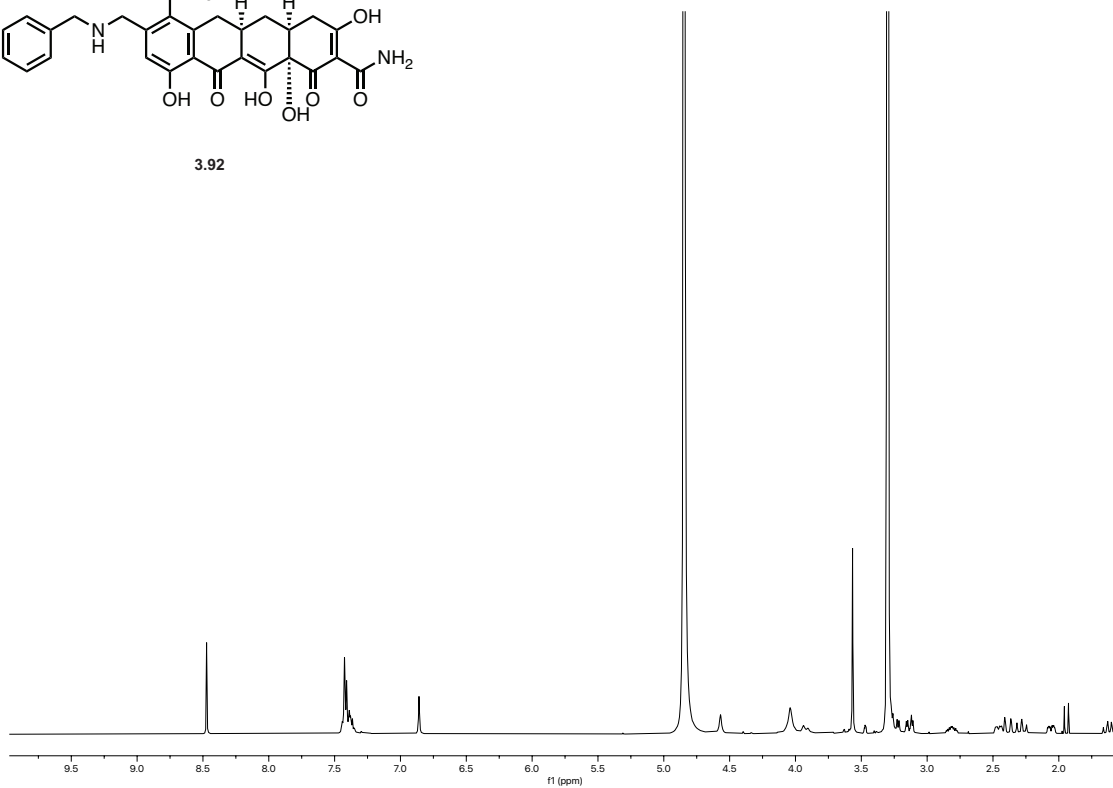


3.91

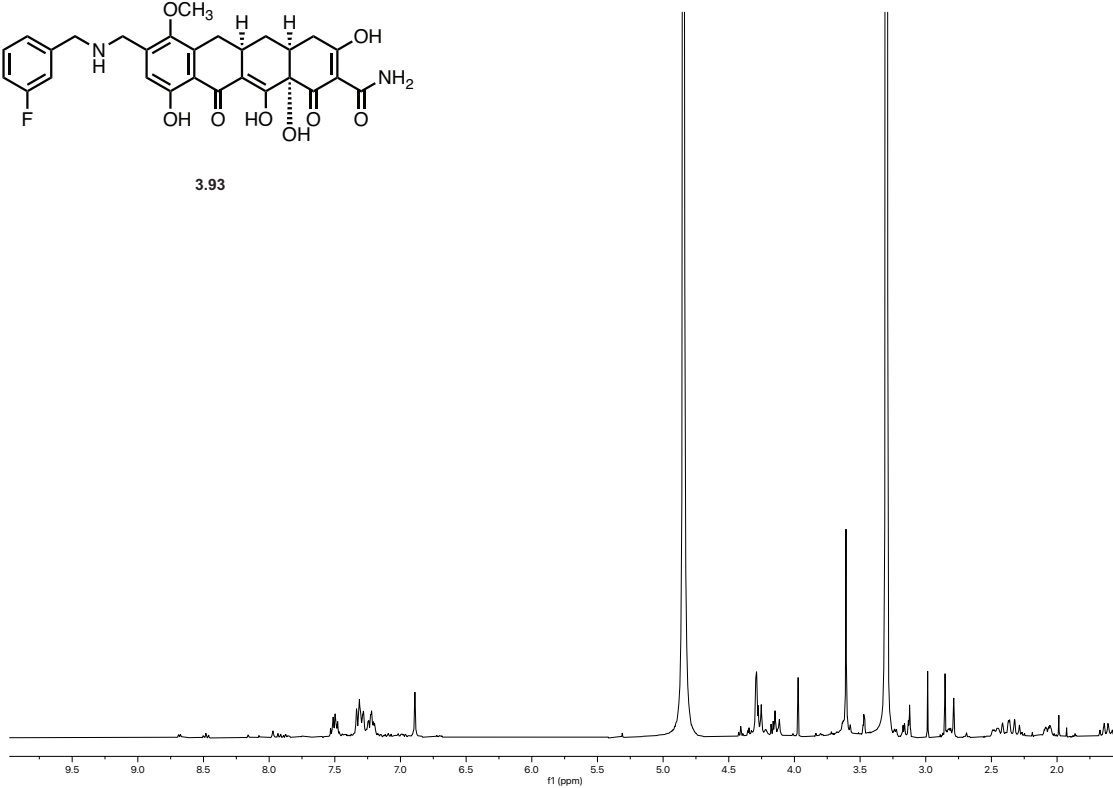




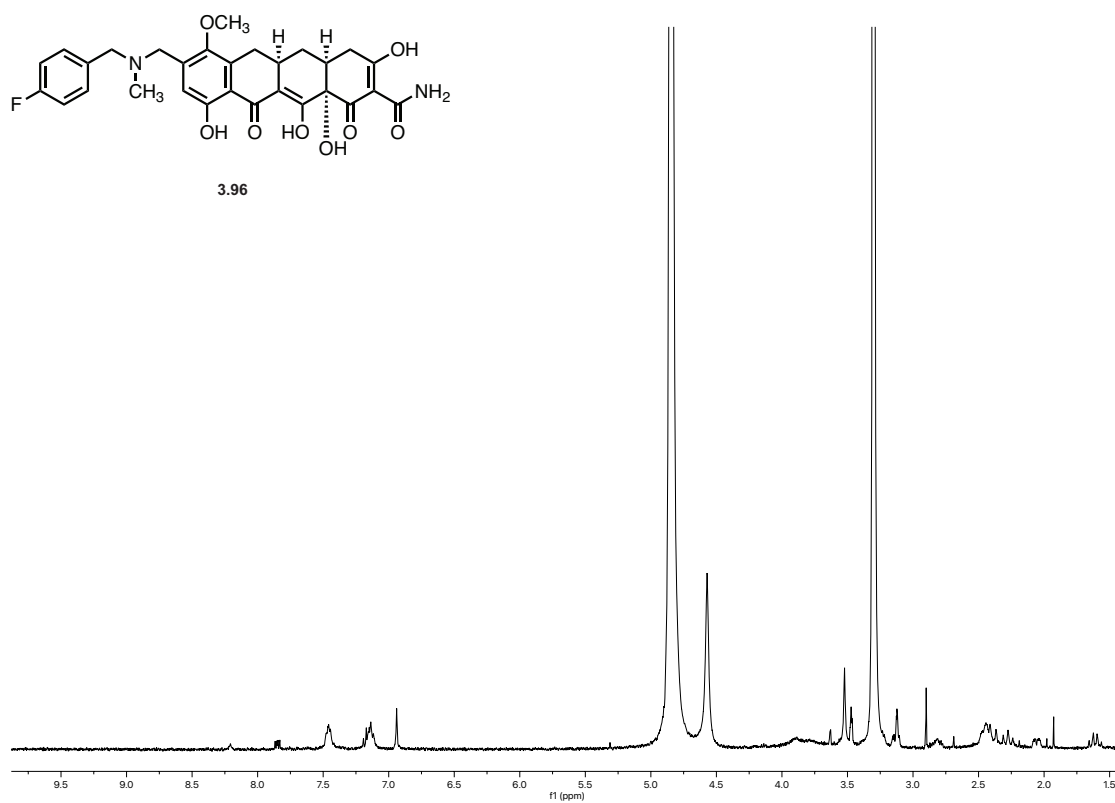
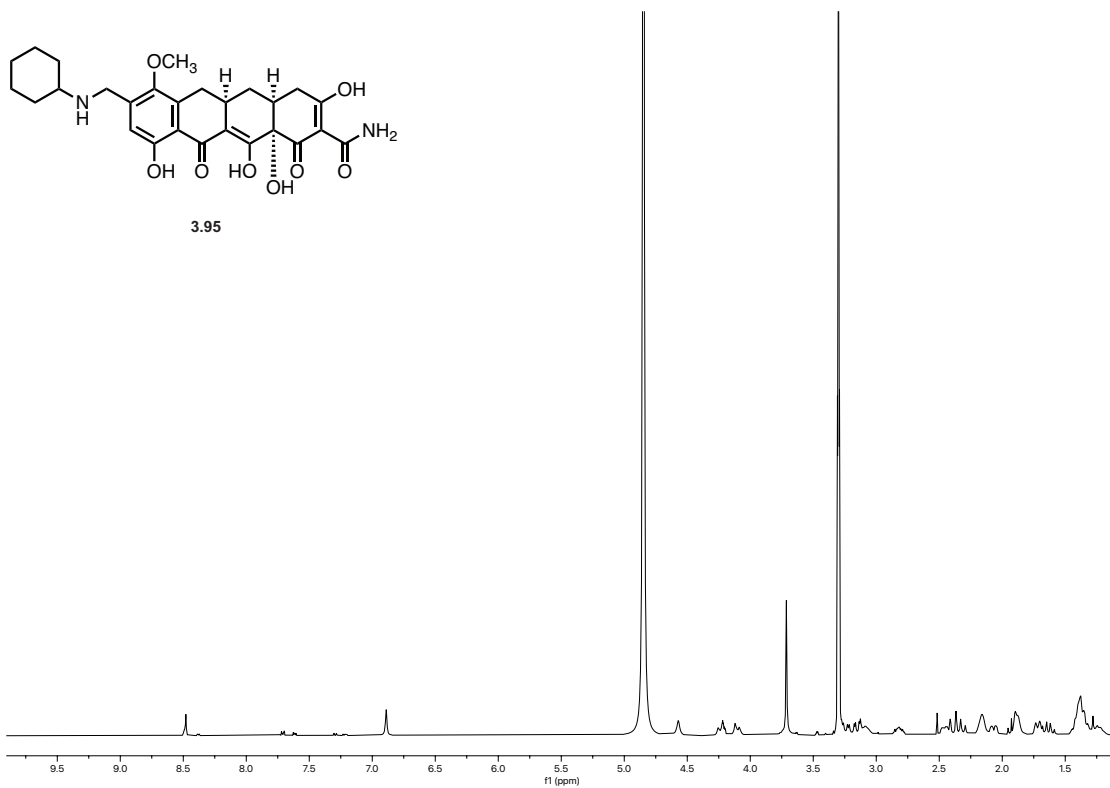
3.92

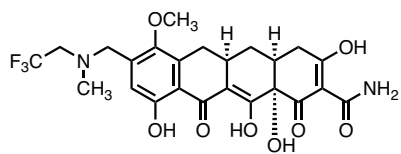


3.93

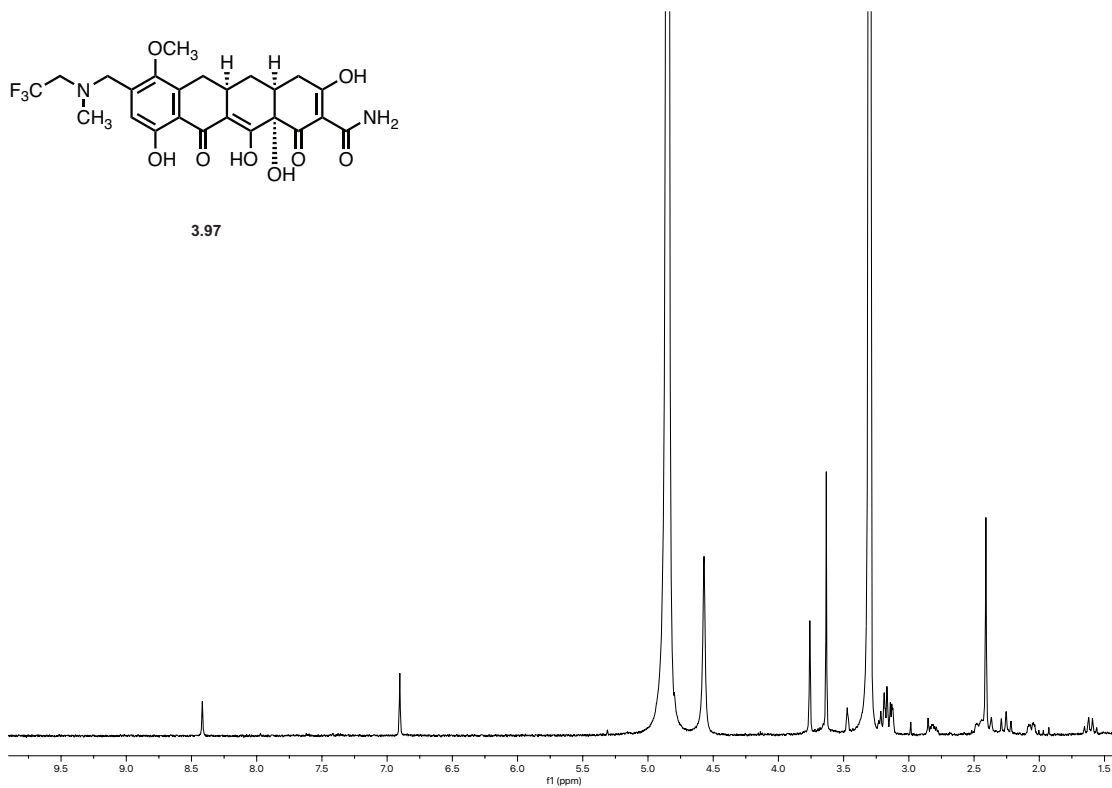


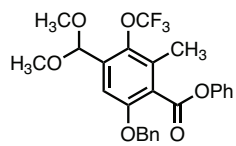




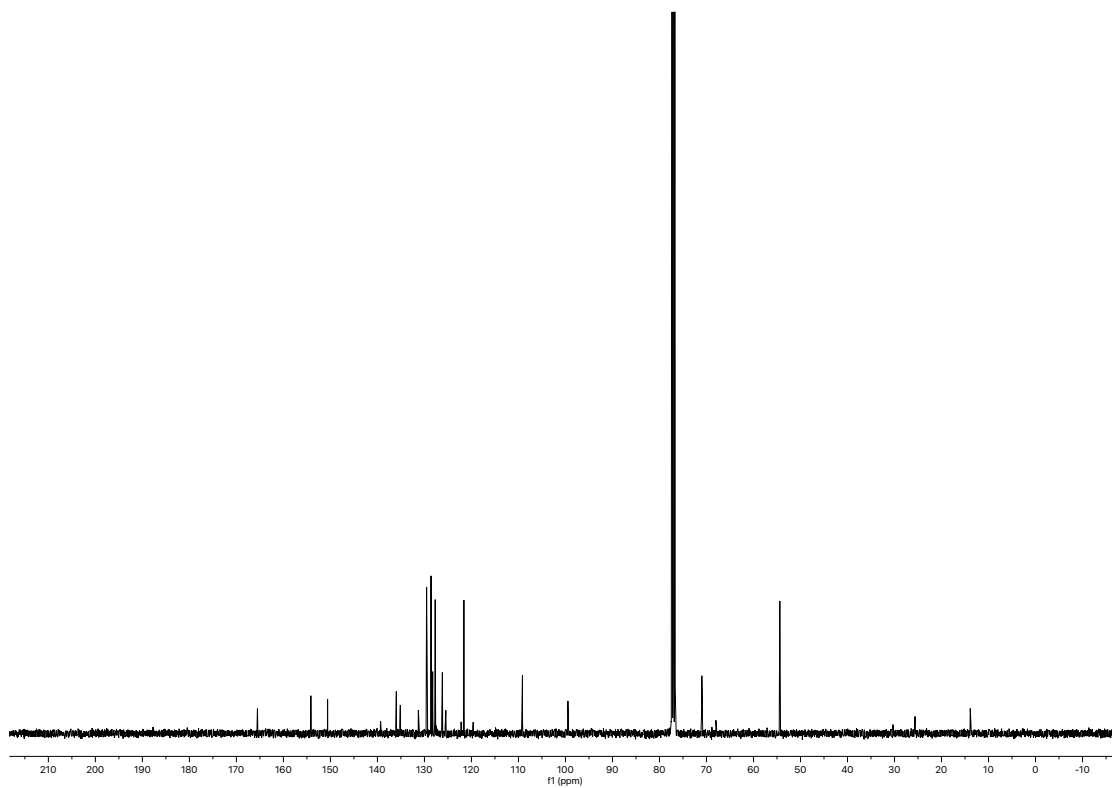
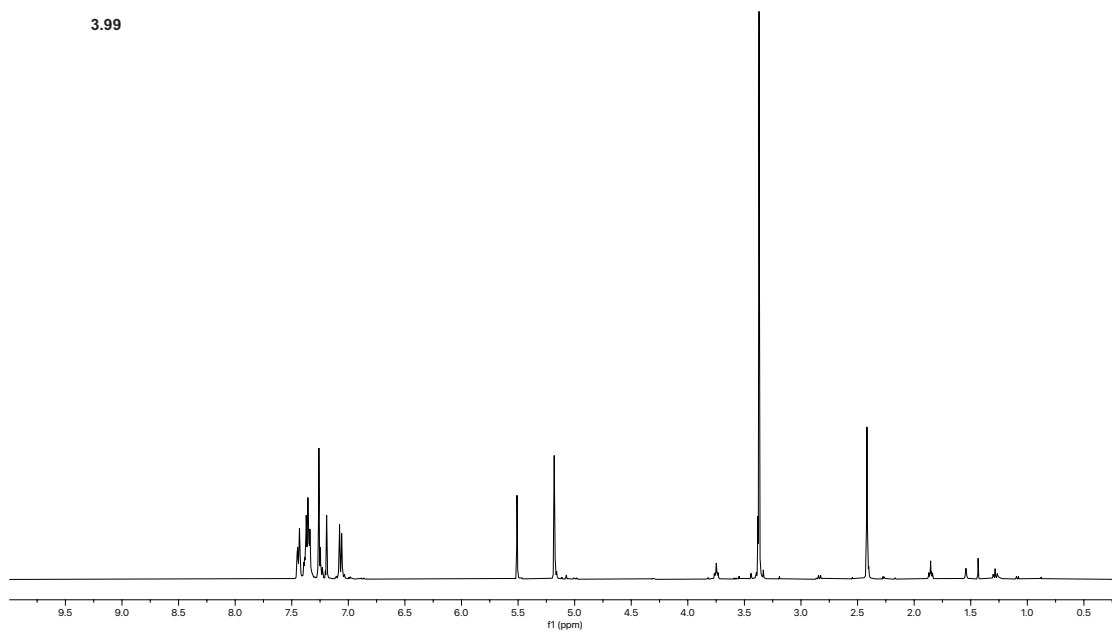


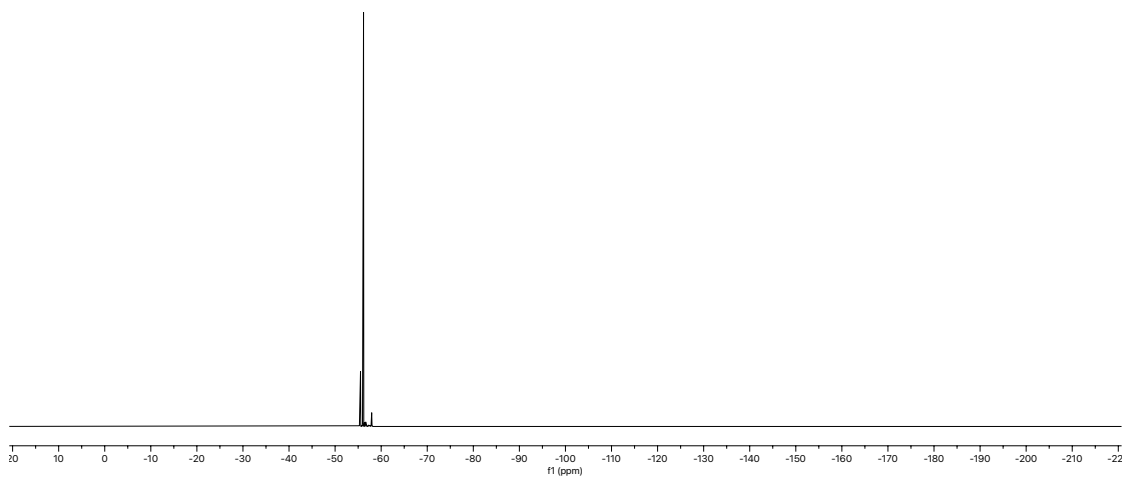
3.97

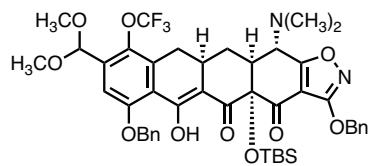




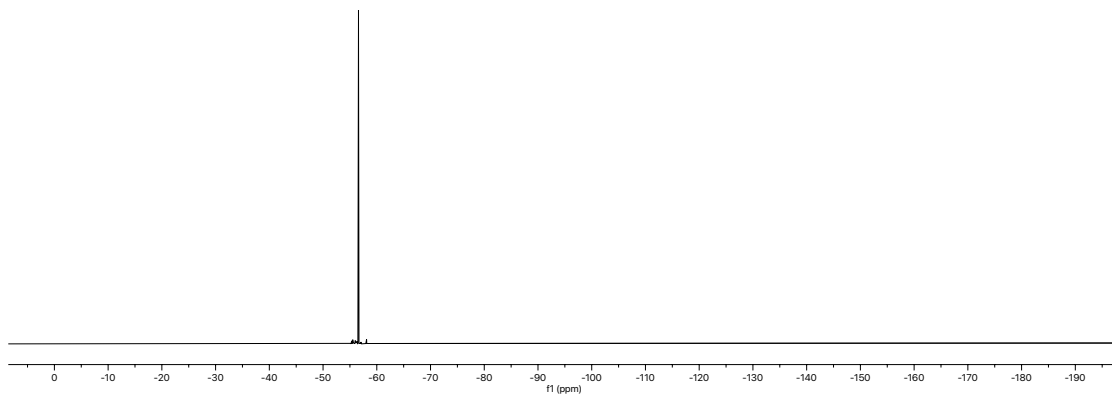
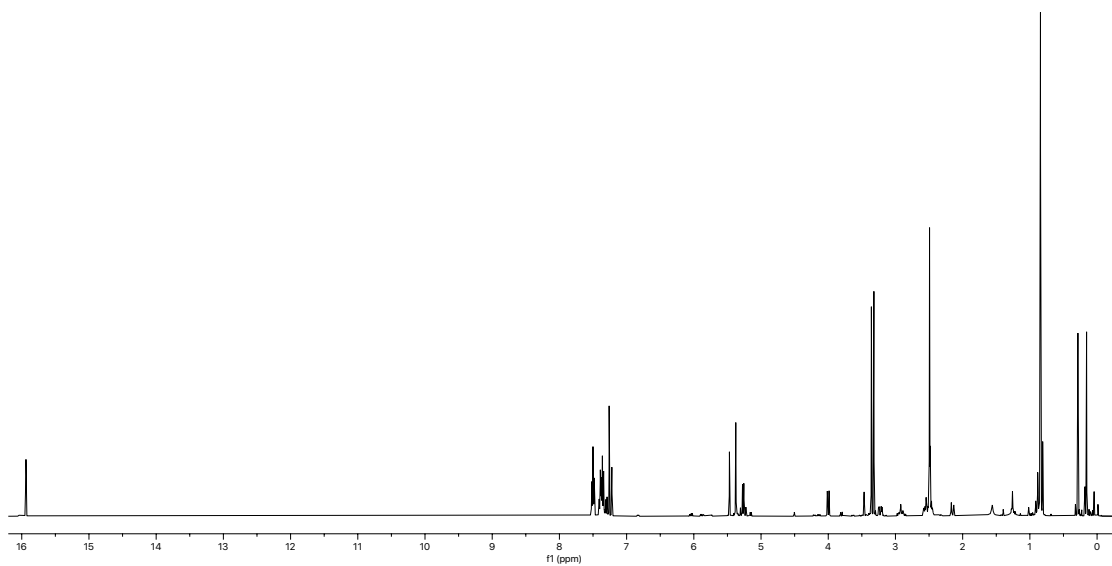
3.99

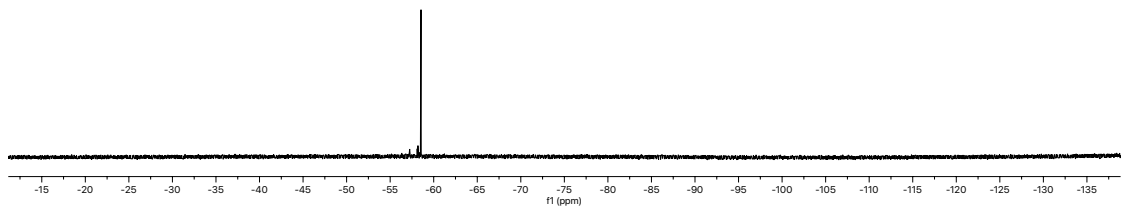
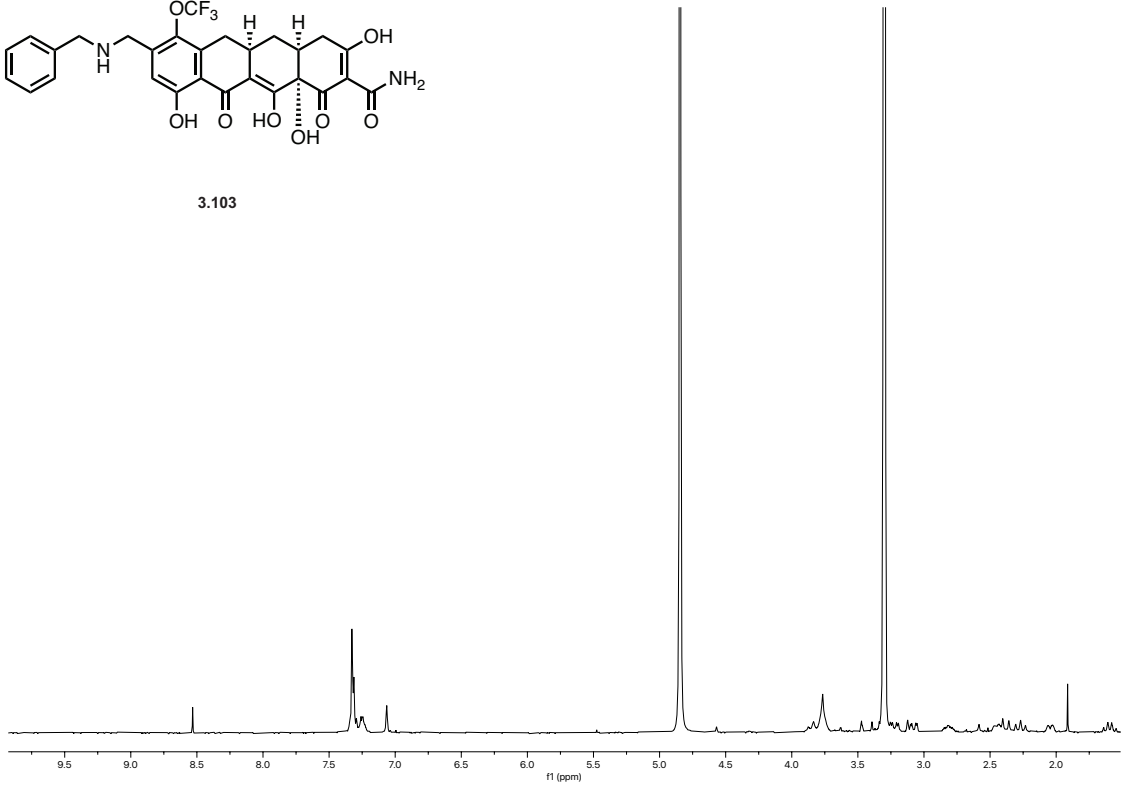
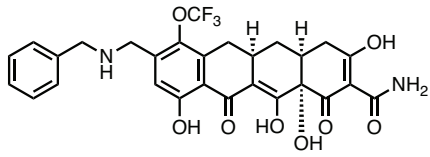


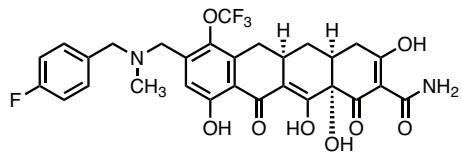




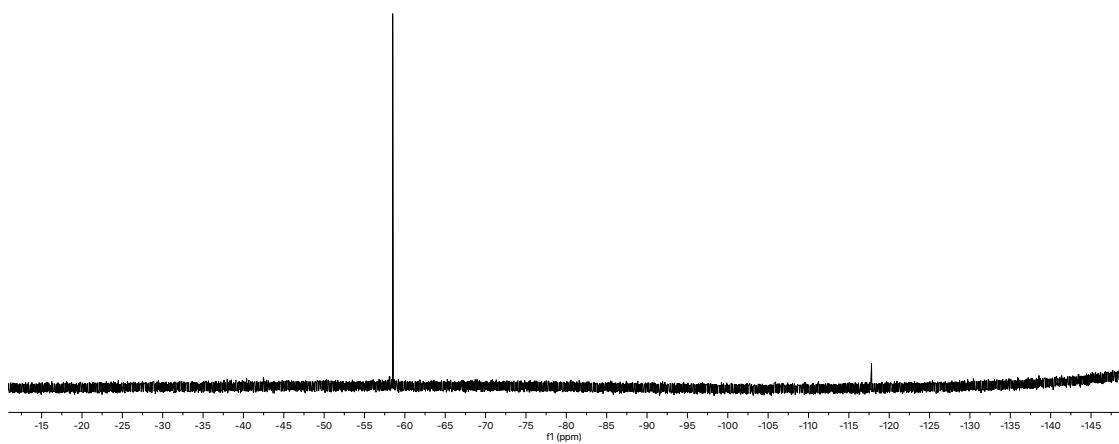
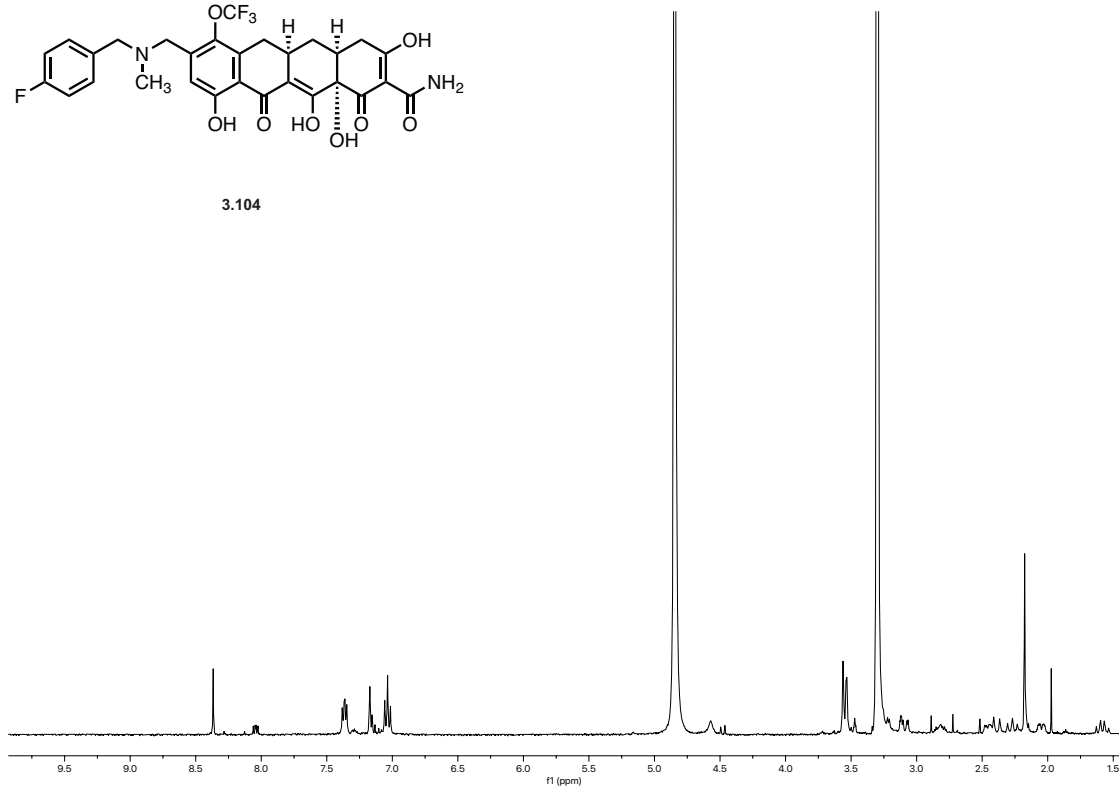
3.100

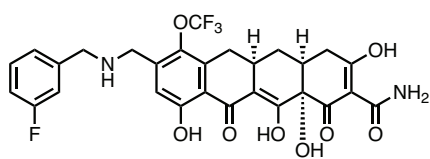






3.104





3.105

